School of Earth and Planetary Sciences

Western Australian Organic & Isotope Geochemistry Centre

Microbial ecosystems of Shark Bay embayments: assessing their functionality and resilience to potential petroleum contamination

Yalimay Mercedes Jiménez de Duarte

ORCID: 0000-0002-4083-8575

This thesis is presented for the Degree of

Doctor of Philosophy in Chemistry

of

Curtin University

July 2020

Declaration

To the best of my knowledge and belief this thesis contains no material previously published by any other person except where due acknowledgment has been made.

This thesis contains no material which has been accepted for the award of any other degree or diploma in any university.

I warrant that I have obtained, where necessary, permission from the copyright owners to use any third-party copyright material reproduced in this thesis, or to use any of my own published work (*e.g.* journal articles) in which copyright is held by another party (*e.g.* publisher, co-author).

I warrant that all research data for this thesis will be stored in a safe location (Curtin R-drive) for at least 5 years after the thesis is published, in line with data storage guidelines at Curtin University.

Yalimay Jiménez

Perth, July 31th 2020

Abstract

Shark Bay (Western Australia), a World Heritage site since 1991, contains treasured ecosystems of geological and ecological significance. In particular, the large Hamelin Pool embayment contains important natural habitats which are host to unique microflora such as microbialites[1], stromatolites, and hypersaline microbial mats. These organisms, biogeochemically correlated with microbial fossils dated to 3.5 billion years ago, are considered modern analogues of early life and continue to flourish in the niche hypersaline setting of Shark Bay ecosystems. The exceptionally high salinities of Shark Bay's embayment such as in Hamelin Pool are being maintained through a limited exchange with open ocean waters by the extensive sea grass barrier in front of Shark Bay and subsequent high evaporation rates of the seawater in the embayments . The high salinities aid in the protection of microbialites by minimising access of predatorial (meta)zoans who would otherwise graze on the microbial communities associated with microbialites.

As the preservation of this natural ecological wonder remains paramount it needs to be protected from anticipated environmental threats. Petroleum hydrocarbon contamination from oil and gas exploration activities and increased shipping traffic in the adjacent Indian Ocean region represents one potential threat. However, there is little specific information on the actual impact that petroleum exposure (PE) might have on the biological structure and function of microbial mats in Hamelin Pool and similar protected hypersaline environments. This PhD project addresses this issue by investigating the ecological responses of non-lithifying smooth and pustular mats - two common microbial mat types of Hamelin Pool - to both short- and long-term PE. A series of laboratory-controlled incubation experiments were performed on viable microbial mats collected from Hamelin Pool. The mats were housed in microcosms and separately subject to zero (control), relatively low and high levels of PE. The biological character of the mats (and a subsequently accumulated biofilm) were monitored through the microcosm incubations by sequencing analysis of environmental 16S rRNA genes (DNA) and reverse transcribed 16S rRNA (cDNA)

[1] "Organosedimentary deposits that have accreted as a result of a benthic microbial community trapping and binding sediment and/or forming the locus of mineral precipitation" (Burne and Moore, 1987).

for the parallel assessment of the total *vs.* living microbial communities in those samples . The functional response of the microbial mats to the petroleum disturbances were investigated using the predictive software PICRUSt2 (Phylogenetic Investigation of Communities by Reconstruction of Unobserved States), using the obtained 16S rRNA datasets. Scanning electron microscope (SEM) imaging analysis was additionally performed on the biofilm to provide complementary physical characterisation.

In **Chapter 2**, microcosms with smooth or pustular mats were separately exposed to petroleum - from a nearby Barrow Island production well - for 30, 60, and 120 days. The impact of this long-term disturbance on the respective microbial mat populations was characterised and compared through 16S rRNA profiling (DNA and cDNA). Both mats lost over two thirds of their microbial diversity by the full 120 days of exposure, although more differences in their respective ecological responses were evident in the early stages of PE. For example, by 30 days of exposure the diversity change in the smooth mats was negligible (<5%) whereas in the pustular mats it was significant (>30%). The greater ecological resistance of the smooth mats was also evident after 60 days of PE. This variation is likely related to the microfabric differences of the mats, with the smooth mats having a less permeable mineral matrix compared to the relatively sandy morphology of the pustular mats. In addition, after 100 days of PE, a uniquely shaped biofilm was formed on the surface of both mats, which was particularly prominent on the exposed pustular mat. Microbial communities were analysed in parallel from different parts of the large three-dimensional structure.

Major changes in the microbial composition (or structure) of both the smooth and pustular mats following PE were observed. Some microorganisms were negatively impacted by the petroleum hydrocarbons, whereas others were stimulated. Those that declined in abundance included Bacteroidetes, Deltaproteobacteria, Planctomycetes, Chloroflexi, Chlorobi, GN04, and Gemmatimonadetes – none of which were detected after 120 days of PE. Conversely, the abundances of cyanobacteria (mainly species of the genus *Halomicronema*), Alpha-and Gammaproteobacteria consistently increased in both mat types. Additional groups (Delta-, Epsilonproteobacteria and Bacteroidetes) also showed a positive response in the hydrocarbon impacted smooth mat. Importantly, the long-term PE resulted in the development of indicator taxa of hydrocarbon degraders in each of the smooth mat, pustular mat and biofilm samples (*e.g.*

Porticoccus hydrocarbonoclasticus, *Nesiotobacter exalbescens*, *Thalassospira*, *Marinobacter* spp., *Halomonas* spp. *Alcanivorax venustensis*, *Coraliomargarita*, *Comamonadaceae*, *Erythrobacteraceae*, *etc*). The increase in 16S rRNA gene transcripts related to known hydrocarbon degraders indirectly suggests an increase in microbial removal of aliphatic (*e.g.*, *n*-alkane, isoprenoid) and aromatic (*e.g.* alkylated- benzenes, naphthalenes and phenanthrenes) compounds from the incident petroleum.

In **Chapter 3** the recovered 16S rRNA genes and reverse-transcribed 16S rRNA transcripts from the **Chapter 2** samples were analysed using PICRUSt2 (Phylogenetic Investigation of Communities by Reconstruction of Unobserved States) to predict the functional response of the two Shark Bay mat types to the PE. The study was focused on processes and pathways related to stress responses and biodegradation of xenobiotics using KEGG (Kyoto Encyclopaedia of Genes and Genomes) classification. After a validation process, reliable functional predictions could be performed using PICRUSt2 in pustular mat samples obtained after 30, 60 and 120 days of exposure). A 'tower-like' biofilm that was only formed on the surface of the PE pustular mat was of particular interest since the unique fabric of this mat type may have promoted the growth of specialised microbial communities capable of building this large three dimensional structure. Moreover, the microcosm in which this biofilm was formed was optically clear, indicative of a potential loss of petroleum due to enhanced microbial degradation. Insights into the tentative metabolic pathways involved would be beneficial for understanding the potential capability of Shark Bay's microbial mats to bioremediate oil spills.

PICRUSt2 predicts gene functions based on the comparison of environmental 16S rRNA genes with closely related 16S rRNA gene sequences that have been sequenced in parallel to functional genes that are present in 20,000 completely sequenced bacterial genomes within the build-in reference database of PICRUSt2. Possibly due to a lack of suitable reference genomes, no reliable predictions of gene functions could be recovered from the more diverse smooth mat microbial communities that were exposed for less than 60 days. PICRUSt2 analysis of the RNA pools from the PE mat samples predicted stress responses (*i.e.,* physiological elasticity, motility, biofilm production, competition for nutrients, *etc*.), as well as survival strategies to be able to cope with the prevailing hypersaline (*i.e*., osmoadaptation) conditions. PE also led to

an increase in the relative abundance of active taxa that possess genes associated with various functions including the detection of contaminants (two-component system); communication between cells (quorum sensing); mobility of microbes (bacterial chemotaxis); and defence mechanisms against microbial attack (*i.e.*, biosynthesis of metabolites or antibiotics and biofilm formation). Significantly, PICRUSt2 analysis also predicted that PE caused an increase in the relative abundance of aromatic hydrocarbon degrading taxa (*i.e.,* cleavage of aromatic rings). This might be related to an increased prominence of PAH degrading taxa such as *Halomicronema* identified in **Chapter 2**. Unfortunately, direct evidence of molecular hydrocarbon biodegradation could not be obtained from the GC-MS characterisation of the petroleum extracted from the water phase (supernatant) of the petroleum-exposed microcosms due to the strong impact of other alteration processes (*i.e.,* experimental loss of gaseous range hydrocarbons due to volatilisation, topping or aqueous solubility). Further organic geochemical analysis with a modified approach will be required to determine the extent and mechanistic pathways of hydrocarbon biodegradation in hypersaline conditions, which remains a matter of some debate.

In **Chapter 4**, incubation experiments with live smooth and pustular mats were conducted to examine their ecological stability under a short-term (pulse) petroleum disturbance (10 days). The response/recovery of the mats was subsequently monitored over a period of one year. Microbial diversity and functional predictions were assessed using the same methodology applied in **Chapters 2** and **3**. Pulse disturbance produced similar microbial responses to the longer-term PE - the microbial community changes and predicted functional responses to stress conditions and degradation of xenobiotics were comparable, but the pulse disturbance revealed additional indicator species related to hydrocarbon degraders (*e.g. Haliea mediterranea, Acinetobacter radioresistens*, *Idiomarina, Rhodovibrio*, and *KSA1*). The comparison of the microbial diversity results from **Chapters 2** and **4**, led to the construction of a conceptual model to systematically estimate the ecological resistance and resilience of microbial mat communities to both short- and long-term disturbances. The model of Hamelin Pool microbial mats showed that the smooth mat microbiome is more resistant to both short- and long-term petroleum disturbances. In contrast, the pustular mat microbiome was neither resistant nor resilient to both short- and long-term disturbances. This result implied that regardless of their initial high microbial diversity and the type of

disturbance (short- or long-term), the microfabric morphology of the mats is critical to protecting the mat microbiomes from anthropogenic damage.

Overall, this study has provided new insights into the ecological stability of smooth and pustular microbial mats in hypersaline marine environments, particularly with respect to petroleum hydrocarbon impacts. The molecular and bioinformatics tool set used in this thesis offers a feasible, low-computer-demand approach to systematically assess the ecological sensitivity of benthic microbial habitats to potential environmental risks. This research also highlights the need for developing experimental designs that can be used for cross-comparison between ecosystems.

Acknowledgements

This PhD project has represented an unforgettable experience that has positively shaped my life. It is the result of the contribution of many people who have supported me in many ways.

Firstly, I would like to express my sincere thanks to my main supervisor Prof. Kliti Grice for providing me with all kinds of opportunities to show the best of me, for allowing me to explore science in many contexts and disciplines, including leadership topics. Thanks to your patience, motivation, persistence, and fairness. I will always recognise and celebrate all your hard work with your students. You constantly show a high level of empathy and make sure your students work in an amenable environment where they can thrive.

I gratefully acknowledge Woodside Petroleum Ltd. and the Australian Research Council for supporting this research and allowing me to explore a topic of environmental interest. I also thanks Curtin University and The Institute for Geoscience Research (TIGeR) for the scholarship and further financial assistance to attend national and international conferences, respectively. Additionally, I thank Elaine Miller from the John de Laeter Centre for her kind assistance with SEM.

Besides my main supervisor, I would like to thank A/Prof. Marco Coolen and Dr. Cornelia Wutcher for introducing me to this captivating topic, which has truly opened my perspective of natural environments and their interactions. Now, I fully enjoy and move between these three fields: Geology, Chemistry, and Biology with easiness. Glad you both pushed me beyond I thought what I was capable of. I truly appreciate your time and guidance to make this research project a real piece of work that now belongs to a big puzzle called science.

This thesis would not be possible without the support of Dr. Paul Greenwood, who kindly volunteered to proofread a big portion of this thesis and provide valuable insights. Paul! I will be always thankful to you! I also extend my gratitude to his son

Darcy Greenwood, for his support during the fieldwork back in 2017 and allow me to spend extra time with his parents some weekends.

This acknowledgment also goes to my lab mates Matthew Campbell and Bettina Schaefer who were key mentors in this journey. I enjoyed so much your fellowship and guidance when I needed it. Many thanks to Peter Hopper and Alex Holman for their patience and always timely technical support. Thanks also to all staff and lecturers from Molecular and Life Sciences school I got the privilege to work with, I have learned a lot (really a lot) during my teaching assistance experience. Thank you so much Harriet and Marcus for your support and pleasant conversations. I thank all other students that I had the opportunity to share at the lab or having a couple of coffee during my studies: Madison, Luis, Ionut, Ekram, Sue, Jaime, Chloe, Darren, Danlei, Charlie, Calum, Nannan, Mattia, Alan, Sohaib, Takashi, you all make me enjoy the ups and downs of this journey.

I also feel so much gratitude for all families and people who helped us when arriving in Australia five years ago. It is a long list but each of you has my admiration. I feel so lucky to have met so many people with big hearts and a real sense of solidarity. To all of you: thank you so much. Special thanks go to Viviana, Jose Miguel, Virgi, Nathy & family, Carlitos, Fabi, Ines, Andres, Marcos, Xiomy & family, Richard, Andrey and all G&G Northbridge crew, you have become my Australian family, *los quiero mucho*, thanks for being there.

I dedicate this work to my husband and my children. It has been a tough but rewarding journey for all of us. *Mi amor*, thanks for depositing your trust in me and support me unconditionally. Thanks for encouraging me to go beyond, my life is fulfilled because of your company and love. You and only you know how far we have gone, and how these times have tested our values, characters, and dreams. Today, everything makes sense, it was all worth it. *Juan* and *Miranda*, you were at all times a motive to keep going, a reason for keeping trying even after failing. You are simply the best children I could have ever asked. You are my life! Thanks for your infinite (truly infinite) patience, for waiting for me so many times, so many hours. Thanks for understanding that *mami* had a dream that is now becoming real.

I also dedicate this work to my parents, grammas, and brother, without your love and dedication early in my life I could not have walked so far. Last but not the least, I dedicate this work to the land where I was born and educated: Venezuela. I hope I can see my people again enjoying the freedom one day I knew. You gave me so much. I hope I can give you back all you offered me. I will find a way, I promise.

Primary publications

The chapters integrating this thesis correspond to papers submitted or in preparation and are listed below.

Chapter 2

Yalimay Jimenez, Kliti Grice, Cornelia Wuchter, Marco J. Coolen. (2020). Responses of hypersaline microbial mats from Shark Bay (Western Australia) to long-term petroleum exposure.
Submitted to *Frontiers in Microbiology (under review)*.

Chapter 3

Yalimay Jimenez, Kliti Grice, and Marco J. Coolen. Functional responses of petroleum-exposed microbial mats from Shark Bay (Western Australia).
In preparation for *PLoS One*.

Chapter 4

Yalimay Jimenez, Kliti Grice, and Marco J. Coolen. Resistance and resilience of microbial mats from Shark Bay to petroleum contamination: comparative assessment to pulse and press disturbances.
In preparation for *Microbiology* Journal.

Statement of contribution of others

The work presented in this thesis was primarily designed, experimentally executed, interpreted and the manuscript were prepared by the first author (Yalimay Jiménez). Contributions by co-authors are described below.

Chapter 2

Kliti Grice conceived the research idea. Yalimay Jiménez, Kliti Grice, Cornelia Wuchter and Marco J.L. Coolen participated in the fieldwork. Yalimay Jiménez designed both experimental setup and sampling schedule. They were supervised and approved by Kliti Grice and Marco Coolen. Yalimay Jiménez performed sampling of the incubation experiments, all molecular biology and work, bioinformatics pipeline, and generated and improved R scripts for all data visualisations. Yalimay Jiménez also executed the physical characterisation of the biofilm by SEM. Yalimay Jiménez, Cornelia Wuchter and Marco J.L. Coolen contributed to statistical analysis. The writing of the manuscript was conducted by Yalimay Jiménez, and reviewed by all the co-authors who also participated in the interpretation of the results. Marco Coolen and Kliti Grice provided the analytical facilities. Financial support was provided by the Australian Research Council #LP150100341, ARC DP (DP15010223), and The Institute for Geoscience Research (TIGeR).

Chapter 3

Yalimay Jiménez and Marco Coolen proposed the use of PICRUSt2 bioinformatic tool, whereas Yalimay Jiménez and Kliti Grice agreed the examination of petroleum by Organic Geochemistry. Yalimay Jiménez performed all chemical lab work and applied all command line (bioinformatics) pipeline, statistical analysis, and data visualisation. The interpretation and writing of the manuscript were performed by Yalimay Jiménez, with contribution of all authors. Financial support was provided by the Australian Research Council #LP150100341, ARC DP (DP15010223), and the Institute for Geoscience Research (TIGeR).

Chapter 4

Kliti Grice conceived the research idea. Yalimay Jiménez, Kliti Grice, Cornelia Wuchter and Marco J.L. Coolen participated in the fieldwork. Yalimay Jiménez designed both experimental setup and sampling schedule. They were supervised and approved by Kliti Grice and Marco Coolen. Yalimay Jiménez performed the sampling of the incubation experiments, all molecular biology and work, bioinformatics pipeline (including PICRUSt), data visualisations, and statistical analysis. The writing of the manuscript was conducted by Yalimay Jiménez and reviewed by all the co-authors who also participated in the interpretation of the results. Marco Coolen and Kliti Grice provided the analytical facilities. Financial support was provided by the Australian Research Council #LP150100341, ARC DP (DP15010223), and The Institute for Geoscience Research (TIGeR).

Secondary publications

The following correspond to conference abstracts based on research conducted during the preparation of this thesis.

Jimenez, Y., Grice, K., Coolen, M. JL., and Scarlett, A. Microbial mats of Shark Bay, Western Australia, and their role in biodegradation of oil spills. "Dorothy Hill Women in Earth Sciences Symposium". November 2019, poster presentation.
** Best student poster award, highly commended (awarded by BHP, Geoscience Centre of Excellence).

Jimenez, Y., Grice, K., Coolen, M. JL., and Scarlett, A. Microbial mats of Shark Bay, Western Australia, and their role in biodegradation of oil spills. "29th International Meeting on Organic Geochemistry". September 2019, poster presentation.

Jimenez, Y., Grice, K., Coolen, M. JL., and Scarlett, A. Shark bay microbial mat community responses to oil contamination a long-term lab-controlled experiment. "Australian Microbial Ecology Conference – AusME 2019". February 2019, poster presentation.

Jimenez, Y., Grice, K., Coolen, M. JL., and Scarlett, A. Lipid profiling in oil-polluted microbial mats from Shark Bay, Australia. "Australian Organic Geochemistry Conference". December 2018, poster presentation.

Jimenez, Y., Grice, K., Coolen, M. JL., and Scarlett, A. Shark Bay microbial mat community responses to oil contamination: a lab-controlled time series experiment. "Australian Geoscience Council Convention 2018". October 2018, oral presentation.

List of Content

CHAPTER 1 1

1.1. OVERVIEW 1

1.2. MICROBIAL ECOLOGY 2

1.3. ECOSYSTEMS' RESPONSES TO DISTURBANCES 2

1.3.1. Biological features for surviving disturbances 4

1.4. MICROBIAL MATS: AN OVERVIEW 5

1.4.1. Formation of microbial mats 6

1.4.2. Microbial mats' microbiome from hypersaline environments 8

1.5. PETROLEUM AS A POLLUTANT AND PROCESSES INVOLVED IN ITS DEGRADATION 10

1.5.1. Petroleum composition 10

1.5.2. Hydrocarbon degradation in petroleum reservoirs 11

1.5.3. Surface petroleum degradation 12

1.6. TECHNIQUES USED FOR MICROBIOLOGICAL ANALYSIS OF MICROBIAL MATS AND CHEMICAL SUSCEPTIBILITY OF PETROLEUM 17

1.6.1. 16S rRNA gene sequencing analyses 17

1.6.2. Complementary DNA 20

1.6.3. Potential functional predictions 21

1.6.4. Gas Chromatography coupled to Mass Spectrometry (GC-MS) 24

1.6.5. Scanning Electronic Microscopy 26

1.7. PETROLEUM BIODEGRADATION UNDER HYPERSALINE CONDITIONS 26

1.7.1. Petroleum degrader's organisms in hypersaline habitats 29

1.8. STUDY SITE: SHARK BAY 30

1.8.1. Nilemah embayment and types of microbial mats observed 32

1.8.2. Nilemah embayment microbiomes: prior studies 34

1.8.3. Microbialites from Shark Bay and early life 37

1.9. ENVIRONMENTAL RISK OF SHARK BAY TO PETROLEUM SPILL 40

1.9.1. Global warming: beyond current threats to Shark Bay 45

1.10. AIMS OF THE THESIS 45

1.11. REFERENCES 48

CHAPTER 2 66

2.1. ABSTRACT 67

2.2. INTRODUCTION 68

2.3. MATERIALS AND METHODS 71

2.3.1. Site description and sampling 71

2.3.2. Microcosm design: simulating field conditions 73

2.3.3. Experimental stage: Microcosm configuration, petroleum exposure and sampling 73

2.3.4. Molecular ecology 75

2.3.5. PCR, library preparation and sequencing 77

2.3.6. Bioinformatics and statistical analysis 78

2.3.7. Scanning electron microscopy imaging 80

2.4. RESULTS 80

2.4.1. Alpha and Beta diversity of the smooth and pustular mat microbiomes 80

2.4.2. Phylum level changes in the taxonomic composition of active bacterial microbiomes in smooth and pustular mats 83

2.4.3. Microbial mat taxa response to petroleum exposure 85

2.4.4. Biofilm development in pustular mat after 120 days of PE and the microbial composition across the three dimensional structure. 88

2.4.5. Active microbiome in the biofilm-related samples of microcosm PS12P. 92

2.5. DISCUSSION 95

2.5.1. Microfabric of microbial mats- a driver for microbiome stress resistance 95

2.5.2. Role of exopolymeric substances (EPS) 96

2.5.3. Microbial community responses to petroleum exposure 97

2.6. CONCLUSIONS 100

2.7. AUTHOR CONTRIBUTIONS 101

2.8. FUNDING 101

2.9. ACKNOWLEDGMENTS 101

2.10. CONFLICT OF INTEREST 102

2.11. DATA ACCESSIBILITY 102

2.12. REFERENCES 103

APPENDIX 2 111

CHAPTER 3 ..... **138**

3.1. ABSTRACT 139

3.2. INTRODUCTION 140

3.3. MATERIAL AND METHODS 143

3.3.1. Dataset from petroleum-exposed incubation experiments 143

3.3.2. Functional prediction by PICRUSt2 and identification of functional markers 143

3.3.3. Petroleum (as pollutant) and petroleum-water interphase samples chemical analysis 145

3.4 RESULTS 147

3.4.1. Prediction validation: NSTI metrics 147

3.4.2. KOs datasets description and data exploration 147

3.4.3. Dominant inferred functional mechanisms under PE conditions 150

3.4.4. Key functional processes abundant under petroleum exposure 153

3.4.5. Organic Geochemistry of petroleum 160

3.5. DISCUSSION 168

3.5.1. Limitations of 16S rRNA-inferred functional predictions 168

3.5.2. Stress response mechanisms 169

3.5.3. Survival strategies 170

3.5.4. Hydrocarbon degradation 173

3.6 CONCLUSIONS 174

3.7. DATA AVAILABILITY 175

3.8. ACKNOWLEDGMENTS 175

3.9. FUNDING 175

3.10. REFERENCES 176

APPENDIX 3 187

CHAPTER 4 ..... **214**

4.1. ABSTRACT 215

4.2. INTRODUCTION 216

4.3. MATERIAL AND METHODS 218

4.3.1. Time-series lab-controlled incubations 218

4.3.2. Molecular microbial ecology 220
4.3.3. Statistical analysis 221
4.3.4. Functional metabolic prediction 221
4.4. RESULTS 222
4.4.1. Microbial community richness and diversity 222
4.4.2. Microbial composition changes upon petroleum exposure 224
4.4.3. Predicted functional responses to petroleum exposure 231
4.5. DISCUSSION 234
4.5.1. Resistance and resilience of microbial mats from Shark Bay 234
4.5.2. Microbial succession upon petroleum exposure 237
4.5.3. Adaptive functional microbial responses to degraded petroleum exposure 239
4.5.4. Limitations and suggested improvements: experimental design and sampling 239
4.6. CONCLUSIONS 240
4.7. FUNDING 241
4.8. ACKNOWLEDGEMENTS 241
4.9. DATA ACCESSIBILITY 241
4.10. REFERENCES 242
APPENDIX 4 247
CHAPTER 5 263
5.1. LABORATORY CONTROLLED INCUBATION EXPERIMENTS IN MICROBIAL ECOLOGY: ADVANTAGES AND LIMITATIONS 264
5.2. METHODS USED FOR MICROBIAL AND FUNCTIONAL DIVERSITY ASSESSMENT: ADVANTAGES AND SETBACKS 265
5.3. RESILIENCE AND RESISTANCE OF SMOOTH AND PUSTULAR MATS EXPOSED TO PETROLEUM 267
5.3.1. Microbial diversity shifts 267
5.3.2. Microfabric as potential major driving factor for ecological resistance 268
5.3.3. Microbial compositional succession 269
5.3.4. Biofilm formation as an adaptive response 269
5.4. SHARK BAY'S MICROBIAL MAT HYDROCARBON BIODEGRADATION CAPABILITIES 269

5.5. IMPLICATIONS FOR CONSERVATION OF SHARK BAY AND OTHER SIMILAR HABITATS 271
5.6. RECOMMENDATIONS FOR FUTURE WORK 271
5.6.1. Experimental design and sampling 271
5.6.2. Omics microbiological analysis 272
5.6.3. Organic geochemical analyses 274
BIBLIOGRAPHY **276**
APPENDIX **314**

List of Figures

Figure 1.1. Diagram showing how microbial ecosystems are assessed or quantified in terms of resilience and resistance using community diversity metrics (Shade et al., 2012a). 3

Figure 1.2. Conceptual model of microbial interactions in a photosynthetic mat, and their role in biogeochemical cycling of C, N, and S across vertical gradients of oxygen and HS^- and availability of photosynthetically active radiation. The narrowing of the wavelengths that escape adsorption with increasing depth is indicated as: blue, B; green, G; yellow, Y; orange, O; and red, R light spectra) (Des Marais, 2003). 6

Figure 1.3. Formation of microbialites. See text for detailed explanation. Image source: partly modified from Dupraz et al. (2009). 7

Figure 1.4. Distribution of halophiles within Bacteria, Archaea and Eukaryota domains. Names in red represent groups which contain, at least, one halophilic organism. Original image from Ciccarelli et al. (2006), and modified by (Edbeib et al., 2016). 8

Figure 1.5. Mechanism of adaptation in hypersaline conditions. (a) Reaction of a non-halophilic organism when exposed to extreme salt concentrations (*i.e.*, osmotic dehydration by releasing H_2O). (b) Halophiles capable to deal with moderate concentration of salts by synthesizing organic solutes. (c) Halophiles facing hypersalinity by equilibrating Cl^- concentration and, therefore, maintaining their cell integrity (Bell, 2012). 9

Figure 1.6. Main types of organic molecules in petroleum. (a) acyclic alkanes; (b) cycloalkanes (naphthalenes); (c) aromatic hydrocarbons; (d) sulfur-rich aromatics. (R means alkyl group). Source: Killops and Killops, 2005. 11

Figure 1.7. Quasi-sequential removal of organic compounds during biodegradation. Source: Head et al., 2003; modified after Wenger et al., 2002, in Larter et al., 2012.....12

Figure 1.8. Weathering processes and their relative timescales. Bars represent the extension of the process over time and its thickness their relative importance (Hook et al., 2017). 13

Figure 1.9. Bacterial aerobic and anaerobic mechanisms for degradation of aliphatic and aromatic organic compounds. Two arrows means that the process

may include additional reactions. Partly modified from Sierra-Garcia and Oliveira (2013). 15

Figure 1.10. 16S ribosomal RNA gene and its variable regions. To visualise its structure, it was divided in six regions: R1 (red) includes V1 and V2; R2 (orange) comprises V3; R3 (yellow) consists of V4; R4 (green) includes V5 and V6; R5 (blue) comprises V7 and V8; and R6 (purple) consists of V9 (Yarza et al., 2014). 18

Figure 1.11. Conserved regions (dark grey) and variable (light green, V1–V9) of 16S rRNA gene and the commonly PCR-amplified regions for next-generation amplicon sequencing-based microbial community profiling (bottom lines) (Jo et al., 2016). 19

Figure 1.12. Diagram showing main steps in the synthesis of second-strand cDNA: (1) primer annealing to produce a single strand of RNA template (after DNA-trace removal); (2) DNA polymerisation, which includes the combination of oligo (dNTPs) primers, random or gene-specific primers and RTase, and will form a cDNA:RNA hybrid; and (3) enzyme deactivation. 21

Figure 1.13. Diagram represents a simplification of PICRUSt workflow and pipeline. Partly modified from Langille et al. (2013) and https://github.com/picrust/picrust2/wiki. 23

Figure 1.14. Flowchart of analytical steps applied for petroleum profiling and detection of environmental markers of biodegradation. Red arrows display a similar path followed in this research. TSEM: Total solvent-extractable materials. SIM: Selected Ion Monitoring, which mode is used for quantitative analysis. GC-TPH: GC analysis of Total Petroleum Hydrocarbons (Fingas, 2015). 25

Figure 1.15. Image depicting experimental setup for simulating an oil spill using microbial mats (numbered plastic container holding the samples) from Ebro Delta, Mediterranean Sea (Llirós et al., 2008). 28

Figure 1.16. Confocal micrographs illustrating oil-degrading bacteria capability of stabilising oil-water emulsions. (A) Hexadecane drops covered by Rhodococcus erythropolis 20S-E1-c (Actinobacteria). (B) Fluorescent oil-degrading bacteria around water-in-oil emulsion. (C) n-hexadecane

drops (black) in presence of Acetinobacter venetianus RAG-1 (Dorobantu et al., 2004). 30

Figure 1.17. Shark Bay region and the location of Nilemah embayment (red square). Image partly modified from Geoscience Australia.....31

Figure 1.18. Hamelin Pool area and the location of microbial mat ecosystems: Nilemah embayment, Garden Point, and Carbla Point, source: Google (left). Biogeomorphic unit scheme and general description at Nilemah embayment. Symbols (microbialites) not at scale. Vertical exaggeration 30X (Morris et al., 2019). Red arrow indicates the sub-unit where samples were collected in this study (right).....33

Figure 1.19. Microbial mats from Nilemah embayment in Hamelin Pool, SB. Smooth (top) and pustular (bottom). Photo credit: Prof Alex Sessions.....34

Figure 1.20. Microbiome of smooth and pustular microbial mats collected in Nilemah embayment. Dot plots show composition and abundance of most abundant (left) and less abundant taxa (right). Mats #1, 2 and 3 were collected in July 2016, while those # 4 and 5 were taken in April 2017. Microbiomes cover Archaea, Bacteria and Eukaryote taxonomical groups using SILVA database (SSU rRNA genes) (Campbell et al., 2020). 36

Figure 1.21. Conceptual models in 3D (left) and outcrop images (right) of different stromatolites facies of the Strelley Pool Chert (Pilbara Craton, Australia). "**a–c**, 'Encrusting/domical laminites'; **d–f**, 'small crested/conical laminites'; **g–i**, 'cuspate swales'; **j–l**, 'large complex cones' (dashed lines in k trace lamina shape and show outlines of intraclast conglomerate piled against the cone at two levels).**m–o**, 'Egg-carton laminites'; **p, q**, 'wavy laminites'; **r–t**, 'iron-rich laminites'. The scale card in b, h and i is 18 cm. The scale card increments in c, e, k, l, n and s are 1 cm. The scale bar in o is about 1 cm. The scale bars in the remaining pictures are about 5 cm" (Allwood et al., 2006).....39

Figure 1.22. Map of Western Australia illustrating the offshore areas nominated for potential petroleum exploration –subjected to Federal Government decision- (top). Shark Bay (red polygon) and the nearby regions with details of current and future use offshore areas (bottom). Map partly

modified, adding information from: https://nopims.dmp.wa.gov.au/Nopims/GISMap/Map. 41
Figure 1.23. Environmental sensitivity index (ESI) of Australian coastline and open sea (deep-sea) zones (DNV, 2011). The arrow indicates Zone WA6 (Shark Bay region). 43
Figure 1.24. Environmental risk index (ERI) of Australian coastline and open sea (deep-sea) zones (DNV, 2011). The arrow indicates Zone WA6 (Shark Bay region). 44
Figure 2.1. Shark Bay area, Western Australia. Red arrow pointing out the sampling area: Nilemah embayment, Hamelin Pool. Modified image from Google Maps (2017) (A). Photo showing the subtidal microbial mat habitats where sampling was conducted. At the time of sampling water depth was about 20-25 cm (B). Photo (close up) exhibiting the sampling points where living microbial mats were collected (white arrows). Note the exposed anoxic layers between pustular and smooth habitats (C).....69
Figure 2.2. Smooth (A) and pustular (B) mat samples from Nilemah embayment collected for lab incubation (Credits: Dr. Alex Sessions – California Institute of Technology, California, USA). Photographs of the microfabrics exhibited by smooth (C) and pustular (D) mats from Hamelin Pool, SB. As previously described in Plet et al. (2018), smooth mats (C) display well-sorted fine grains of minerals and, occasionally fossils, fused by micrite (~40%) (*i.e.*, mud-size carbonate particles). Smooth mats exhibit low porosity and permeability whereas pustular mats (D) are poorly sorted, showing a combination of allochems (*i.e.*, fossils, intraclasts, and ooids) with patches of micrite. Thus, pustular mats have a higher porosity and permeability in comparison to smooth mats. Red lines in panel D simulate paths where fluids (e.g. seawater or other fluids) might percolate (Credits: Images were kindly provided by Dr Chloe Plet –CSIRO, Perth, Australia –, from her research in 2017 at Curtin University). Conceptual model of the local ecosystem sampled, including features observed and parameters measured in the field: Dissolved oxygen (DO) and salinity (NaCl symbol) (E). 72
Figure 2.3. Configuration of the types of controls microcosms and microcosms exposed to petroleum. All controls were subjected to the same conditions

as microcosms exposed to petroleum: 25 °C, artificial light under dial regime (16h light: 8h darkness) plus constant sterile air bubbling. 74

Figure 2.4. Illustration of sampling schedule and nomenclature utilised for both control microcosms and microcosms for petroleum exposure. All microcosms were subsampled at day 0 – initial conditions – (T0). Sampling was repeated after 30 days (T30), 60 days (T60) and 120 days (T120) in all type 1 and type 2 control microcosms. After reaching its maximum incubation time (T30, T60 or T120), type 3 microcosms and microcosms for petroleum exposure were collected as sacrificial samples (marked with an asterisk). Sacrificial samples allowed to analyse a higher amount of sample or duplicate an analysis. NCW: No petroleum Control Water; PCW: Petroleum Control Water; CS#S: Control Sample # Smooth; CS#P: Control Sample # Pustular; PS#S: Petroleum Sample # Smooth; PS#P: Petroleum Sample # Pustular. 76

Figure 2.5. Boxplots of **Shannon index** computed in QIIME2 including DNA and cDNA datasets of pristine mats [labelled as (a) and (b)], controls of microcosms [labelled as (c) – smooth – and (d) – pustular –], petroleum-exposed microcosms and biofilm samples. Centre line in the boxplot represents the median, while box limits are 25th and 75th percentiles. Boxplot whiskers represent 9th and 91st percentiles and outlier values are represented as grey points. PE boxplots group all samples, plus any available duplicates, collected from microcosms exposed to 30, 60 and 120 days. 81

Figure 2.6. Bar plots showing net loss of taxa (as % ASV) when exposed to petroleum for both smooth (left) and pustular mats (right). From left to right each pair of bars show microsoms exposed to petroleum for 30, 60 and 120 days (denoted as T30, 60 and T120). 82

Figure 2.7. Principal Component Analysis (PCA) plots showing microbiome shifts (initial –T0– vs. maximum time of incubation –T30, T60 or T120–) in petroleum incubation experiments in smooth (left) and pustular mat (right) microcosms. 83

Figure 2.8. Relative abundance of the active (cDNA) bacterial microbiomes at phylum level, comparing initial microbial communities (Initial – Day 0) to those evolved after PE for 30, 60 or 120 days) in both smooth (left) and pustular

(right) microbial mat microcosms. See **Table A2.2**, **Table A2.3**, **Table A2.4** and **Table A2.5** for parallel 16S rDNA community data. 84

Figure 2.9. Stacked bar plots showing those active taxa (phylum-class level) that are negatively (absent) or positively affected (emerged or increased its abundance) because of petroleum exposure. Data corresponds to those indicator species statistically determined by ISA and regrouped at a higher taxonomical level. N.B. According to PCA (**Figure 2.7**), no significant changes in the community structure was observed in the smooth microcosms after 30 days of PE. Therefore, this data point for the smooth mat is not shown here.....86

Figure 2.10. Loading plots showing the first 60 species for initial (blue) vs. PE exposed (orange) taxa in both mat types, which strongly influence principal component 1 (PC1) in the PCA plots of **Figure 2.7**. This analysis is based on the communities residing in both DNA and RNA pools. Note the highly weighted species are correlated with previous indicator species detected by ISA. This analysis was used to identify additional indicator organisms associated with degradation of hydrocarbons.....89

Figure 2.11. Heatmap plots depicting microbiome shifts between initial and post petroleum incubated microcosms in both smooth and pustular mats. The right column in each heatmap shows phylum or class taxonomy (legend on the bottom). NB the dotted squares mark the part of the heatmaps that include taxa that increased in abundance due to PE compared to the initials. For this analysis, the raw reads at species level were standardised by total, square root transformed, and then ranked to the 70 more abundant taxa. 90

Figure 2.12. Images of a biofilm developed at the water-column interphase in a pustular mat microcosm exposed to petroleum for 120 days (PS12P T120). Top view of PS12P T120 microcosm and a schematic diagram showing the sampling points (A). Tower-shaped biofilm grown in the middle of the microcosm, denoted with the letter B (B). SEM images showing the microstructure of biofilm wall and a calcium carbonate grain trapped into the net, respectively (C and D). XRD spectra (elemental analysis) of two points in the SEM image D (E and F). 91

Figure 2.13. Relative abundance of the total (DNA) and active (cDNA) bacterial microbiomes at phylum/class level of the biofilm-related samples (*i.e.*, foam, biofilm, and biofilm base) in a pustular mat microcosm exposed to petroleum for 120 days (PS12P T120) (A). Biplot displaying both biofilm-related samples and key variables (species) associated with each sample. These variables are represented by vectors. Note the pattern followed by the samples allowed them to split the plot in four quadrants, showing the driver / indicator species (B). 94

Figure 3.1. Principal Component Analysis (PCA) plot showing total (DNA) and active microbiome (cDNA) distribution of smooth (top left), pustular mats (top right) and biofilm sub-samples (bottom). Initial samples –not subjected to PE– are displayed as black dots, and PE samples as red dots. 149

Figure 3.2. Heatmap showing the relative abundance of predicted KO metabolic pathways (level 3) between initial –as controls– (T0) and petroleum-exposed **smooth mat** after 120 days (PS9S microcosm). (*) Based on PICRUSt2 functional prediction from 16S rRNA data (DNA and cDNA), using KOs responsible for the highest difference between the groups (mainly PC1 in PCA plot - **Figure 3.1**). Data displayed correspond to raw abundance of KOs standardised by total and square root transformed. 151

Figure 3.3. Heatmap showing the relative abundance of predicted KO metabolic pathways (level 3) between initial –as controls– (T0) and petroleum-exposed **pustular mats** after 30, 60 or 120 days (PS10P, PS11P and PS12P microcosms). See legend **Figure 3.2** for details about the source data (*)..... 152

Figure 3.4. Heatmap showing the relative abundance of predicted KO metabolic pathways (level 3) between initial –as controls– (T0) and petroleum-exposed pustular microbial mat **biofilm-related sub-samples** after 120 days (PS12P microcosm). See legend **Figure 3.2** for details about the source data (*). 153

Figure 3.5. Total ion chromatograms of the **saturated fraction** of the petroleum used as a pollutant (Barrow Island #B101; top) and the petroleum-water phase

extracted from smooth (middle) and pustular (bottom) microbial mats at **60 days** of exposure..... 164

Figure 3.6. Total ion chromatograms of the **aromatic fraction** of the petroleum used as a pollutant (Barrow Island #B101; top) and the petroleum-water phase extracted from smooth (middle) and pustular (bottom) microbial mats at **60 days** of exposure..... 165

Figure 3.7. Total ion chromatograms of the **saturated fraction** of the petroleum used as a pollutant (Barrow Island #B101; top) and the petroleum-water phase extracted from smooth (middle) and pustular (bottom) microbial mats at **120 days** of exposure..... 166

Figure 3.8. Total ion chromatograms of the **aromatic fraction** of the petroleum used as a pollutant (Barrow Island #B101; top) and the petroleum-water phase extracted from smooth (middle) and pustular (bottom) microbial mats at **120 days** of exposure..... 167

Figure 4.1. Shark Bay region, showing Nilemah embayment (blue square) (top). Image of Nilemah embayment (close up) and their tidal zones (bottom). Source: Google Maps. 219

Figure 4.2. Incubation tank assemblage for simulating ecosystem conditions following design from **Chapter 2** (top images). Images showing smooth (left bottom) and pustular (right bottom) mat microcosms subjected to chronic PE incubation for 10 days and maintained under lab-conditions up to 1 year..... 220

Figure 4.3. Boxplots of Shannon index computed in QIIME2 including DNA and cDNA datasets of pristine mats (**Chapter 2**), background controls, and PE mats (including T1, T5, T10 and T1y). Centre line in the boxplot represent the median, while box limits indicate 25th and 75th percentiles. Boxplot whiskers represent 9th and 91st percentiles and outlier values are represented as grey points. Data of both smooth and pustular pristine samples was taken from **Chapter 2**..... 223

Figure 4.4. Bar plots showing net loss of active taxa (cDNA) (as % ASV) when exposed to petroleum for both smooth (left) and pustular mats (right). (*) Missing data for smooth mat at 10 days of PE..... 223

Figure 4.5. Relative abundance of the total (DNA) and active (cDNA) bacterial microbiomes at phylum level, comparing initial microbial communities

(Initial – T0) to those evolved after 1 day (T1), 5 days (T5) and 10 days (T10) of PE, and then after 1 year under fresh seawater (T1y) in both smooth (left) and pustular (right) microbial mats microcosms. Smooth mat PE sub-sample at T10 (cDNA) was lost and could not be repeated. 225

Figure 4.6. PCA (Principal Component Analysis) plots showing microbiome shifts in petroleum incubated experiments in smooth (top) and pustular mats (bottom) microcosms. 226

Figure 4.7. Heatmap plot depicting smooth mat microbiome shifts in a time-series petroleum incubated experiment (microcosm SMOC3). The right column shows phylum or class taxonomy (legend on the right). Data displayed correspond to raw reads at species level standardised by total, square root transformed, and then, ranked the 70 more abundant organisms (**). 228

Figure 4.8. Loading plots showing the first 60 species for initial (blue) vs. PE exposed (orange) taxa in both mat types, which strongly influence principal component 1 (PC1) in the PCA plots of Figure 6. This analysis is based on the communities residing in both DNA and RNA pools. Note the highly weighted species are correlated with previously indicator species detected by ISA. This analysis was used to identify additional indicator organisms associated with degradation of hydrocarbons 229

Figure 4.9. Heatmap plot depicting pustular mat microbiome shifts in a time-series petroleum-exposed incubation experiment (microcosm PM OC3). The right column shows phylum or class taxonomy (legend on the right). (**) 230

Figure 4.10. Heatmap showing the relative abundance of predicted KO metabolic pathways (level 3) between initial (T0) and one year after the petroleum contaminant was removed (smooth mat; SM OC3 microcosm). Based on PICRUSt2 functional prediction from 16S rRNA data (DNA and cDNA), using KOs responsible for the highest difference between the groups (mainly PC1 in PCA plot - **Figure A4.7**). Data displayed correspond to raw abundance of KOs standardised by total and square root transformed. 232

Figure 4.11. Heatmap showing the relative abundance of predicted KO metabolic pathways (level 3) between initial (T0) and one year after the petroleum contaminant was removed (pustular mat; PM OC3 microcosm). Based on PICRUSt2 functional prediction from 16S rRNA data (DNA and cDNA), using KOs responsible for the highest difference between the groups (mainly PC1 in PCA plot - **Figure A4.8**). Data displayed correspond to raw abundance of KOs standardised by total and square root transformed. 233

Figure 4.12. Conceptual model of temporal variance of PE smooth and pustular microbial mat communities (% ASVs), to estimate their ecological resistance and resilience to press and pulse disturbances. Red and purple closed circles represent actual data points from lab-controlled incubations discussed in **Chapter 2** and the current study. Dotted lines and question marks refer to uncertainties in the path due to a lack of additional sampled and analysed time points. 235

Figure 4.13. Bacterial taxa that prevailed mainly in both types of microbial mat and irrespective of the level of degradation of the petroleum pollutant used. Bold text: bacteria that were consistently identified in both DNA and RNA pools over the course of the incubation experiment. 238

Figures - Appendix 2

Figure A2.1. Incubation tank assemblage for simulating ecosystem conditions. Image showing the content of each microcosm: an open glass container with a piece of microbial mat and seawater on top (A). Example of internal arrangement of the microcosms in an incubation tank (B). External view of the incubation tank and its components: air pump, air filter, timer and lamp (C). 112

Figure A2.2. Incubation tanks configuration. The top image illustrates the internal array of microcosms in each incubation tank. Photograph on the bottom shows how they were maintained and protected under laboratory conditions. For details of types of microcosms and the nomenclature used see **Figure 2.3** and **Figure 2.4** 113

Figure A2.3. Scheme illustrating the organisation of the different groups of lab-controlled time-series incubation experiments using microbial mats collected from the Nilemah area, Hamelin Pool, Shark Bay (WA). Barrow Island petroleum examined by Two-Dimensional Gas Chromatography/Time-of-Flight Mass Spectrometry (GCxGC ToF-MS) and Gas Chromatography-Mass Spectroscopy (GC-MS) is displayed to show the organic compounds present in the petroleum sample..... 114

Figure A2.4. Rarefaction curves plots of samples collected in both controls and petroleum-incubated smooth and pustular mat microcosms. Petroleum-exposed samples are represented with an asterisk: green for DNA and red for cDNA. 115

Figure A2.5. Rarefaction curves plots of additional biofilm-related samples collected from a 120 day petroleum-exposed pustular microbial mat and compared to initial experimental conditions (T0) and pristine pustular mat (A). Rarefaction curves plot focused on group of samples with less species diversity: Foam (A), Biofilm (late stage –B – & early stage –C –), base of biofilm (D) and pustular microbial mat (PS12P T120 = E) (B). 116

Figure A2.6. Rarefaction curves plots of smooth and pustular microbial mats collected and preserved in its pristine environment. No subjected to lab-controlled conditions..... 117

Figure A2.7. Boxplots of observed OTUs index computed in QIIME2 including DNA and cDNA datasets of pristine mats, control microcosms, petroleum-exposed microcosms and biofilm samples. Centre line in the boxplot represents the median, while box limits are 25th and 75th percentiles. Boxplot whiskers represent 9th and 91st percentiles and outlier values are represented as grey points..... 118

Figure A2.8. Boxplots of Faith's PD (phylogenetic diversity) index computed in QIIME2 including DNA and cDNA datasets of pristine mats, control microcosms, petroleum-exposed microcosms and biofilm samples. Centre line in the boxplot represents the median, while box limits are 25th and 75th percentiles. Boxplot whiskers represent 9th and 91st percentiles and outlier values are represented as grey points. 119

Figure A2.9. Boxplots of Pielou's evenness index computed in QIIME2 including DNA and cDNA datasets of pristine mats, control microcosms,

petroleum-exposed microcosms and biofilm samples. Centre line in the boxplot represents the median, while box limits are 25th and 75th percentiles. Boxplot whiskers represent 9th and 91st percentiles and outlier values are represented as grey points. 120

Figure A2.10. PCA (Principal Component Analysis) plot showing microbiome shifts and clusters of controls and petroleum-exposed microcosms using both smooth (left) and pustular mats (right). 121

Figure A2.11. Photos of controls and petroleum-exposed microcosms after 30-day incubation with Barrow Island – B101 petroleum – both smooth and pustular mats. Images show the visual changes (mainly colour) of petroleum and microbial mats after 30 days of petroleum incubation. 122

Figure A2.12. Photos of controls and petroleum-exposed microcosms after 60-day incubation with Barrow Island – B101 petroleum – both smooth and pustular mats. Images show the visual changes (mainly colour) of petroleum and microbial mats after 60 days of petroleum incubation. 123

Figure A2.13. Photos of controls and petroleum-exposed microcosms after 120-day incubation with Barrow Island – B101 petroleum – both smooth and pustular mats. Photos images the visual changes (mainly colour) of petroleum and microbial mats after 120 days of petroleum incubation. 124

Figure A2.14. Photos of control microcosms: type I –only water – and type II –water and petroleum. 125

Figure A2.15. PCA biplots of initial and petroleum-exposed microcosms for both smooth and pustular mats. The longer vectors (red arrows) represent those organisms which contribution is higher to a particular sample or cluster of samples. Negative correlation of variables are represented for those vectors pointing in the opposite direction. 126

Figure A2.16. Heatmap plot showing microbiome shifts among sub-samples of PS12P microcosm (pustular microbial mat) subjected to Barrow Island (#101) petroleum incubation for 120 days. Sampling points are displayed in **Figure 2.12A-B**. Data displayed corresponds to raw reads at species level, standardised by total, and then square root transformed. 127

Figures - Appendix 3

Figure A3.1. Shark Bay region (source: Google maps), highlighting Nilemah embayment as study site (yellow square) (top). Image of sampling site, depicting intertidal and subtidal environments (bottom). 188

Figure A3.2. Diagram showing the workflow applied to explore and visualise predicted KOs functionalities (PCA and CC plots), and to confirm which of the predicted functions are statistically different as a result of PE..... 189

Figure A3.3. Histograms showing the contribution of each component to explain data variance in PCA plots in smooth and pustular mats microcosms subjected to PE and biofilm subsamples (**Figure 3.1**). Correlation Circle plots (PC1-PC2) representing those variables contributing most (cut off or radius > 0.8) to the clustering of samples (initial vs PE). A list with KOs (genes) clustered in the red circle responsible for PE clustering observed in all three PCA plots in **Figure 3.1** can be found in supplementary **Table A3.4**, **Table A3.5** and **Table A3.6**. 190

Figure A3.4. Extended error bar plot comparing mean proportions ($p < 0.05$) of KOs between initial versus PE samples related to **environmental information processing** in a **smooth mat** microcosm that was exposed to petroleum for 120 days (initials = PS7S $T0^{n=2}$ and PE=PS9S $T120^{n=4}$). Horizontal lines indicate confidence intervals (Tukey's t-test, ANOVA). Software utilised: STAMP, 2015, v.2.1.3. 191

Figure A3.5. Extended error bar plot comparing mean proportions ($p < 0.05$) of KOs between initial versus PE samples related to **environmental information processing** in **pustular mats** microcosms that were exposed to petroleum for 60 and 120 days (initials = PS10P, PS11P and PS12P $T0^{n=6}$ and PE = PS11P T60 and PS12P $T120^{n=6}$). Horizontal lines indicate confidence intervals (Tukey's t-test, ANOVA)..... 192

Figure A3.6. Extended error bar plot comparing mean proportions ($p < 0.05$) of KOs between initial versus PE samples related to **environmental information processing** in **biofilm-related** samples in a pustular mat microcosm after up to 120 days of PE (initials = PS10P, PS11P and

PS12P T0$^{n=6}$ and PE = A, B, C and D T120$^{n=7}$). Horizontal lines indicate confidence intervals (Tukey's t-test, ANOVA)..... 193

Figure A3.7. Extended error bar plot comparing mean proportions ($p < 0.05$) of KOs between initial versus PE samples related to **cellular processes** in a **smooth mat** microcosm after 120 days of PE (initials = PS7S T0$^{n=2}$ and PE=PS9S T120$^{n=4}$). Horizontal lines indicate confidence intervals (Tukey's t-test, ANOVA). Software utilised: STAMP, 2015, v.2.1.3. 194

Figure A3.8. Extended error bar plot comparing mean proportions ($p < 0.05$) of KOs between initial versus PE samples related to **cellular processes** in **pustular mats** microcosms that were exposed to petroleum for 60 and 120 days (initials = PS10P, PS11P and PS12P T0$^{n=6}$ and PE = PS11P T60 and PS12P T120$^{n=6}$). Horizontal lines indicate confidence intervals (Tukey's t-test, ANOVA)..... 194

Figure A3.9. Extended error bar plot comparing mean proportions ($p < 0.05$) of KOs between initial versus PE samples related to **cellular processes** in **biofilm-related** samples in a pustular mat microcosm after 120 days of PE (initials = PS10P, PS11P and PS12P T0$^{n=6}$ and PE = A, B, C and D T120$^{n=7}$). Horizontal lines indicate confidence intervals (Tukey's t-test, ANOVA)..... 195

Figure A3.10. Extended error bar plot comparing mean proportions ($p < 0.05$) of KOs between initial versus PE samples related to **energy metabolism** in a **smooth mat** microcosm after 120 days of PE (initials = PS7S T0$^{n=2}$ and PE=PS9S T120$^{n=4}$). Horizontal lines indicate confidence intervals (Tukey's t-test, ANOVA)..... 195

Figure A3.11. Extended error bar plot comparing mean proportions ($p < 0.05$) of KOs between initial versus PE samples related to **energy metabolism** in **pustular mats** microcosms that were exposed to petroleum for 60 and 120 days (initials = PS10P, PS11P and PS12P T0$^{n=6}$ and PE = PS11P T60 and PS12P T120$^{n=6}$). Horizontal lines indicate confidence intervals (Tukey's t-test, ANOVA)..... 196

Figure A3.12. Extended error bar plot comparing mean proportions ($p < 0.05$) of KOs between initial versus PE samples related to **energy metabolism** in **biofilm-related** samples in a pustular mat microcosm after up to 120

days of PE (initials = PS10P, PS11P and PS12P $T0^{n=6}$ and PE = A, B, C and D $T120^{n=7}$). Horizontal lines indicate confidence intervals (Tukey's t-test, ANOVA)..... 196

Figure A3.13. Extended error bar plot comparing mean proportions ($p < 0.05$) of KOs between initial versus PE samples related to **degradation of xenobiotics** in a **smooth mat** microcosm after 120 days of PE (initials = PS7S $T0^{n=2}$ and PE=PS9S $T120^{n=4}$). Horizontal lines indicate confidence intervals (Tukey's t-test, ANOVA)..... 197

Figure A3.14. Extended error bar plot comparing mean proportions ($p < 0.05$) of KOs between initial versus PE samples related to **degradation of xenobiotics** in **pustular mats** microcosms that were exposed to petroleum for 60 and 120 days (initials = PS10P, PS11P and PS12P $T0^{n=6}$ and PE = PS11P T60 and PS12P $T120^{n=6}$). Horizontal lines indicate confidence intervals (Tukey's t-test, ANOVA)..... 197

Figure A3.15. Extended error bar plot comparing mean proportions ($p < 0.05$) of KOs between initial versus PE samples related to **degradation of xenobiotics** in **biofilm-related** samples in a pustular mat microcosm after up to 120 days of PE (initials = PS10P, PS11P and PS12P $T0^{n=6}$ and PE = A, B, C and D $T120^{n=7}$). Horizontal lines indicate confidence intervals (Tukey's t-test, ANOVA)..... 198

Figure A3.16. Extended error bar plot comparing mean proportions ($p < 0.05$) of KOs between initial versus PE samples related to **biosynthesis of secondary metabolites and antibiotics** in a **smooth mat** microcosm that were exposed to petroleum for 120 days (initials = PS7S $T0^{n=2}$ and PE=PS9S $T120^{n=4}$). Horizontal lines indicate confidence intervals (Tukey's t-test, ANOVA). Software utilised: STAMP, 2015, v.2.1.3..... 198

Figure A3.17. Extended error bar plot comparing mean proportions ($p < 0.05$) of KOs between initial versus PE samples related to **biosynthesis of secondary metabolites and antibiotics** in **pustular mats** microcosms that were exposed to petroleum for 60 and 120 days (initials = PS10P, PS11P and PS12P $T0^{n=6}$ and PE = PS11P T60 and PS12P $T120^{n=6}$). Horizontal lines indicate confidence intervals (Tukey's t-test, ANOVA)..... 199

Figure A3.18. Extended error bar plot comparing mean proportions ($p < 0.05$) of KOs between initial versus PE samples related to **biosynthesis of secondary**

metabolites and antibiotics samples in a pustular mat microcosm after up to 120 days of PE (initials = PS10P, PS11P and PS12P $T0^{n=6}$ and PE = A, B, C and D $T120^{n=7}$). Horizontal lines indicate confidence intervals (Tukey's t-test, ANOVA). 199

Figure A3.19. Total ion chromatograms of the procedural blanks run in parallel during the liquid-liquid extraction. 200

Figure A3.20. Adamantanes ions (m/z 136, 135, 149, 163, 177) assessed in the petroleum utilised as pollutant: Barrow Island #B101. Peaks are identified and described in **Table A3.7** 200

Figure A3.21. Diamantanes ions (m/z 188, 187,201) assessed in the petroleum utilised as pollutant: Barrow Island #B101. Peaks are identified and described in **Table A3.7** 201

Figure A3.22. Alkylnaphthalene ions (m/z 128, 142, 156, 170, 184) assessed in the petroleum utilised as pollutant: Barrow Island #B101. Peaks are identified and described in 202

Figure A3.23. Biphenyl ions (m/z 154, 169,182, 196) assessed in the petroleum utilised as pollutant: Barrow Island #B101. Peaks are identified and described in **Table A3.9**. 203

Figure A3.24. Phenanthrene and anthracene ions (m/z 178, 192, 206, 220 and 234) assessed in the petroleum utilised as pollutant: Barrow Island #B101. Peaks are identified and described in **Table A3.10** 204

Figures - Appendix 4

Figure A4.1. Scheme illustrating the organization of the different groups of lab-controlled time-series incubation experiments using microbial mats collected from the Nilemah area, Hamelin Pool, Shark Bay (WA). Windalia petroleum examined by Two-dimensional Gas Chromatography/Time-of-Flight Mass Spectrometry (GCxGC ToF-MS) and Gas Chromatography-Mass Spectroscopy (GC-MS) are displayed to show the organic compounds present in the petroleum sample..... 248

Figure A4.2. Illustration of sampling schedule and nomenclature utilised for both controls and samples for PE. All samples were subsampled just before

oil pollution (T0), and repeated after 1 day (T1), 5 days (T5), 10 days (T10) and 360 days (1 year) (T1y). 249

Figure A4.3. Diagram showing the workflow followed for microbiological analysis. 250

Figure A4.4. Rarefaction curves of samples collected in both controls and petroleum incubated smooth and pustular mat microcosms incubation experiments, simulating a pulse disturbance..... 251

Figure A4.5. Boxplots of Faith's (top) and Pielou's (bottom) index computed in QIIME2 including DNA and cDNA datasets of pristine mats (**Chapter 2**), controls, and PE mats (including T1, T5, T10 and T1y). Centre line in the boxplot represents the median, while box limits indicate 25th and 75th percentiles. Boxplot whiskers represent 9th and 91st percentiles and outlier values are represented as grey points. Data of pristine smooth and pustular samples was taken from **Chapter 2**..... 252

Figure A4.6. Relative abundance of the total (DNA) and active (cDNA) bacterial microbiomes at phylum level of **control** (untreated) **smooth** and **pustular** mat microcosms. Time-series lab-incubation involved sampling at 0 day (T0 – initial) and after 1 day (T1), 5 days (T5) and 10 days (T10) and 1 year (T1y). Pustular mat PE sub-sample at T1 (DNA) was damaged during nucleic acid extraction. 253

Figure A4.7. PCA (Principal Component Analysis) plot (top) showing the clustering of the **smooth mat** sub-samples collected in the petroleum-exposed SM-OC3 microcosm: initial (T0) vs. 1 year (T1y). Correlation Circle plots (PC1-PC2) (bottom), representing those variables contributing most (cut off or radius > 0.9) to the clustering of samples (initial vs. PE). Only those KOs circled were used for further functional analysis..... 254

Figure A4.8. PCA (Principal Component Analysis) plot (top) showing the clustering of the **pustular mat** sub-samples collected in the petroleum-exposed PM-OC3 microcosm: initial (T0) vs. 1 year (T1y). Correlation Circle plots (PC1-PC2) (bottom), representing those variables contributing most (cut off or radius > 0.9) to the clustering of samples (initial vs. PE). Only those KOs circled were used for further functional analysis. 255

Figure A4.9. Heatmap plot of **smooth mat** microcosms subjected to lab incubation under control (untreated) or petroleum-exposed conditions, comparing

microbiome shifts under pulse (or short-term) and press (long-term) disturbances. The right column depicts phylum or class taxonomy (legend on the bottom). Data displayed correspond to raw reads at species level standardised by total, square root transformed, and then, ranked the 70 more abundant organisms. 256

Figure A4.10. Heatmap plot of **pustular mat** microcosms subjected to lab incubation under control (untreated) or petroleum-exposed conditions, comparing microbiome shifts under pulse (or short-term) and press (long-term) disturbances. The right column depicts phylum or class taxonomy (legend on the bottom). Data displayed correspond to raw reads at species level standardised by total, square root transformed, and then, ranked the 70 more abundant organisms. 257

List of Tables

Table 1.1. Common organic solutes identified in halophiles from hypersaline environments. Partly modified from Edbeib et al. (2016).....9

Table 1.2. Diagnostic ratios used for petroleum fingerprinting based on CEN/TR15522-2 standard (Fingas, 2015). Not a comprehensive list...17

Table 1.3. Annual quantities of oil expected to be spilled for 2011 and projected by 2020. Values do not reflect environmental sensitivity (AMSA, 2012). 42

Table 1.4. Environmental risk index (ERI) projected by 2020 (AMSA, 2012). 44

Table 2.1. Hydrocarbon-degraders identified in petroleum exposure microcosms...99

Table 3.1. Summary of total KOs predicted, retrieved KOs after cut-off and maximum number of metabolic pathways identified..... 150

Table 3.2. Table of predicted KOs (genes) related to **environmental information processing** and their functions across smooth, pustular and biofilm-related samples. Data source: **Figure A3.4**, **Figure A3.5** and **Figure A3.6**. (**) Statistically significant predicted KOs = ++, while those that are not predicted or statistically significant = n.p. Level 3 or category C based on BRITE functional hierarchy. 155

Table 3.3. Table of predicted KOs (genes) related to **cellular processes** and their functions across smooth, pustular and across the tower-shaped biofilm. Data source: **Figure A3.7**, **Figure A3.8** and **Figure A3.9**. (**) in **Table 3.2**. 156

Table 3.4. Table of predicted KOs (genes) related to **energy metabolisms** and their functions across smooth, pustular and biofilm-related samples. Data source: **Figure A3.10**, **Figure A3.11** and **Figure A3.12**. (**) in **Table 3.2**. 157

Table 3.5. Table of predicted KOs (genes) related to **degradation of xenobiotics** and their functions across smooth, pustular and biofilm-related samples. Data source: **Figure A3.13**, **Figure A3.14** and **Figure A3.15**. (**) in **Table 3.2**. 159

Table 3.6. Table of predicted KOs (genes) related to **biosynthesis of secondary metabolites and antibiotics** and their functions across smooth, pustular- and biofilm-related samples. Data source: **Figure A3.16**, **Figure A3.17** and **Figure A3.18**. (**) in **Table 3.2**. 160

Table 3.7. Diagnostic ratios of biodegradation of the petroleum used as a pollutant (Barrow Island #B101) during incubation experiments, control Type 2 (petroleum and water, sample PCW at T60 and T120) and petroleum-exposed microbial mat microcosms (samples PS8S and PS11P at T60, and PS9S and PS12P at T120; sampling schedule is in **Chapter 2**). T0 analysis are not shown as no compounds or impurities were detected. 163

Tables - Appendix 2

Table A2.1. Physicochemical parameters recorded under pristine conditions and the set of microcosms exposed to 120 days of lab incubation with and without petroleum (CS6P T120) and PS12P T120. 129

Table A2.2. Relative abundance of bacterial taxonomy (**phylum level**) of **smooth mat** microcosms subjected to Barrow Island (#101) petroleum exposure. Three experiments were carried out in parallel which lasted 30 days (first table), 60 days (second table) and 120 days (third table). Shown are the differences between total bacteria (DNA) and active bacteria (cDNA). Petroleum-exposed sub-samples are shaded in grey. 130

Table A2.3. Relative abundance of bacterial taxonomy (**class level**) of **smooth mat** microcosms subjected to Barrow Island (#101) petroleum exposure. Three experiments were carried out in parallel which lasted 30 days (first table), 60 days (second table) and 120 days (third table). Shown are the differences between total bacteria (DNA) and active bacteria (cDNA). Petroleum-exposed sub-samples are shaded in grey. 131

Table A2.4. Relative abundance of bacterial taxonomy (**phylum level**) of **pustular mat** microcosms subjected to Barrow Island (#101) petroleum exposure. Three experiments were carried out in parallel which lasted 30 days (first table), 60 days (second table) and 120 days (third table). Shown are the differences between total bacteria (DNA) and active bacteria (cDNA). Petroleum-exposed sub-samples are shaded in grey. 132

Table A2.5. Relative abundance of bacterial taxonomy (**class level**) of **pustular mat** microcosms subjected to Barrow Island (#101) petroleum exposure.

Three experiments were carried out in parallel which lasted 30 days (first table), 60 days (second table) and 120 days (third table). Shown are the differences between total bacteria (DNA) and active bacteria (cDNA). Petroleum-exposed sub-samples are shaded in grey. 133

Table A2.6. Indicator taxa positively affected for petroleum exposure in both smooth vs. pustular mats. Indicator Species Analysis (ISA) was done using the IndicSpecies package in R with significant level alpha <0.05. They represent the statistically significant active indicators using this method. 134

Table A2.7. Relative abundance (%) of microorganisms at phylum level of subsamples of foam, microbial mat and biofilm collected in a pustular mat microcosm after 120 days petroleum exposure (PS12S). Blue bars represent the percentages. 135

Table A2.8. Relative abundance (%) of microorganisms at class level of subsamples of foam, microbial mat and biofilm collected in a pustular mat microcosm after 120 days petroleum exposure (PS12S). Blue bars represent the percentages. 136

Table A2.9. Relative abundance (%) of microorganisms at its maximum level of resolution of subsamples of foam, microbial mat and biofilm collected in a pustular mat microcosm after 120 days petroleum exposure (PS12S). Blue bars represent the percentages. All organisms present up to 90% accumulated abundance are shown. 137

Tables - Appendix 3

Table A3.1. Nearest Sequenced Taxon Index (NSTI) values for **smooth** mats initial and PE microcosms subsamples. 205

Table A3.2. Nearest Sequenced Taxon Index (NSTI) values for **pustular** mats initial and PE microcosms subsamples. 206

Table A3.3. One-way ANOVA p-values of predicted environmental information processing and cellular processes pathways in controls vs. petroleum-exposed microcosms. Data was calculated using KOs that were abundant in the cDNA pool of microcosms subjected to petroleum. 207

Table A3.4. KO (KEGG Orthologs) predicted by PICRUSt2 over 0.80 cutoff for 120 days PE smooth mat microscom subsamples (PS9S T120 – 2 replicates). Data can be explored in KEGG Mapper – Search Pathway using these KOs in the following to link: https://www.genome.jp/kegg/tool/map_pathway1.html (comma should be removed first). 208

Table A3.5. KO (KEGG Orthologs) predicted by PICRUSt2 over 0.8 cutoff for 120 days PE pustular mat microscom subsample (PS9S T120). Data can be explored in KEGG Mapper – Search Pathway using these KOs in the following to link: https://www.genome.jp/kegg/tool/map_pathway1.html (comma should be removed first). 209

Table A3.6. KO (KEGG Orthologs) predicted by PICRUSt over 0.8 cutoff for 120 days petroleum-exposed biofilm-related sub-samples in a pustular mat microscom (PS12P T120). Data can be explored in KEGG Mapper – Search Pathway using these KOs in the following to link: https://www.genome.jp/kegg/tool/map_pathway1.html (comma should be removed first). 210

Table A3.7. Mass spectral features of adamantanes and diamantanes compounds identified in the petroleum utilised as pollutant: Barrow Island #B101. Peaks are displayed in **Figure A3.20** and **Figure A3.21**..... 211

Table A3.8. Mass spectral features of **alkyl naphthalene** compounds identified in the petroleum utilised as pollutant: Barrow Island #B101. Peaks are displayed in the **Figure A3.22**..... 212

Table A3.9. Mass spectral features of **biphenyl, diphenylmethane** and their **alkylated derivatives** compounds identified in the petroleum utilised as pollutant: Barrow Island #B101. Peaks are displayed in **Figure A3.23**. 213

Table A3.10. Mass spectral features of **phenanthrene and anthracene** compounds identified in the petroleum utilised as pollutant: Barrow Island #B101. Peaks are displayed in **Figure A3.24**..... 213

Tables - Appendix 4

Table A4.1. Relative abundance of bacterial taxonomy (**phylum level**) of a **smooth mat control microcosm** under lab-conditions for up to 1 year. Shown are the differences between total bacteria (DNA) and active bacteria (cDNA) communities..... 258

Table A4.2. Relative abundance of bacterial taxonomy (**class level**) of a **smooth mat control microcosm** under lab-conditions for up to 1 year. Shown are the differences between total bacteria (DNA) and active bacteria (cDNA) communities..... 258

Table A4.3. Relative abundance of bacterial taxonomy (**phylum level**) of a **smooth mat microcosm** subjected to **Windalia petroleum** exposure for up to 1 year. Shown are the differences between total bacteria (DNA) and active bacteria (cDNA) communities. Petroleum-exposed sub-samples are represented with a grey shade..... 259

Table A4.4. Relative abundance of bacterial taxonomy (**class level**) of a **smooth mat microcosm** subjected to **Windalia petroleum exposure** for up to 1 year. Shown are the differences between total bacteria (DNA) and active bacteria (cDNA) communities. Petroleum-exposed sub-samples are represented with a grey shade..... 259

Table A4.5. Relative abundance of bacterial taxonomy (**phylum level**) of a **pustular mat control microcosm** under lab-conditions for up to 1 year. Shown are the differences between total bacteria (DNA) and active bacteria (cDNA) communities..... 260

Table A4.6. Relative abundance of bacterial taxonomy (**class level**) of a **pustular mat control microcosm** under lab-conditions for up to 1 year. Shown are the differences between total bacteria (DNA) and active bacteria (cDNA) communities. PM_Control_T0_DNA sub-samples was damaged during DNA elution..... 260

Table A4.7. Relative abundance of bacterial taxonomy (**phylum level**) of a **pustular mat microcosm** subjected to **Windalia petroleum** exposure for up to 1 year. Shown are the differences between total bacteria (DNA) and active bacteria (cDNA) communities. Petroleum-exposed sub-samples are represented with a grey shade..... 261

Table A4.8. Relative abundance of bacterial taxonomy (**class level**) of a **pustular mat microcosm** subjected to **Windalia petroleum exposure** for up to 1 year. Shown are the differences between total bacteria (DNA) and active bacteria (cDNA) communities. Petroleum-exposed sub-samples are represented with a grey shade..... 261

Table A4.9. Nearest Sequenced Taxon Index (NSTI) values for **smooth** mat control and (Windalia) petroleum-exposed microcosm. 262

Table A4.10. Nearest Sequenced Taxon Index (NSTI) values for **pustular** mats control and Windalia petroleum-exposed microcosms..... 262

List of Videos

Video A2.1. Video showing biofilm developed in PS12P microcosm after 100 days petroleum incubation. 128

Abbreviations

DNA: deoxyribonucleic acid

dNTP: deoxyribonucleotide triphosphate

EPS: Exopolymeric substances

HMW: high-molecular-weight

LMW: low-molecular-weight

PE: petroleum exposure(s)

PAHs: Polyaromatic hydrocarbons

rRNA: Ribosomal ribonucleic acid

RTase: Reverse Transcriptase

SB: Shark Bay

KEGG: Kyoto Encyclopedia of Genes and Genomes

KO: KEGG Orthology

BRITE: Hierarchical classifications of biological entities

Chapter 1

INTRODUCTION

1.1. Overview

This chapter provides a general overview of one of the major contemporary topics of microbial ecology: responses of modern ecosystems to petroleum disturbances. It begins with a literature review of ecosystem responses to stress, describing the more relevant terminology, and outlines the microbial features and community properties required to adapt to environmental perturbations. This is followed by an overview of the current state of the knowledge on microbial mats in hypersaline environments, focusing on the unique microbiome of the World heritage listed site Shark Bay. A summary of known microbial mat community responses to petroleum spills and chemical changes shown by the petroleum fractions associated with the degradation by microorganisms are given. Methods and techniques used for the characterisation of environmental microbiomes and petroleum-exposed to physical and chemical degradation processes are then introduced, followed by a description of the study site and potential hazardous commercial and industrial activities that might negatively impact the area under study. Finally, the specific aims of this research project are listed, as well as the approaches and methodologies used to contribute empirical information to help evaluate the real ecological threat of future petroleum spill incidents in the Shark Bay region.

1.2. Microbial ecology

Microbial ecology or environmental microbiology explores the diversity, function, distribution and abundance of microorganisms, their specific interactions and the effect these have on ecosystems. Microbial ecology interacts with a wide range of disciplines and topics, from for example, epidemiology to climate change, and anthropogenic disturbances in microbial ecosystems to evolutionary processes (Barton et al., 2011; Antwis et al., 2017). Microbial communities are highly complex, so modelling approaches have been frequently applied to help explore the behaviour, interaction and response of microbes to certain stimuli (Jessup et al., 2004).

1.3. Ecosystems' responses to disturbances

In microbial ecology several terms are used to describe the behaviour or responses of microbial ecosystems under threat or disturbances. Disturbances are defined as causal incidents that can trigger immediate environmental changes that either directly or indirectly affect microbial communities (Rykiel, 1985; Glasby and Underwood, 1996). Disturbances are often classified according to their temporal or spatial scales. If their duration is relatively discrete, they are considered pulses or short-term, while continuing disturbances are called presses or long-term. Disturbance has also been linked to 'stability' which is defined as "*the tendency of a community to return to a mean condition after a disturbance*" (Pimm, 1984). Stability can be assessed through taxonomical or functional diversity analysis of the microbiome. Stability relates to the two concepts of resilience and resistance (Pimm, 1984). Resistance is defined as 'the degree to which a community is unresponsive to a disturbance', while resilience is 'the rate at which a community returns to a pre-disturbed condition' (Allison and Martiny, 2008). These two terms can be assessed or quantified by using a community diversity metric (**Figure 1.1**). The response of a microbial community to a disturbance can be measured by the diversity index which counts the initial value (y_0) and temporal variance (y_n). Following disturbances (pulse or press) the index can be re-evaluated and compared to, for example, with the initial values. Two hypothetical scenarios can be deduced: (1) the microbial community shifts to a new, alternative stable state or (2) the microbiome returns to the original parameter value. Hence, the 'magnitude of this

change' can be called resistance, while 'the rate of return to y_0' is considered resilience. If the selected diversity index returns to the original natural variance, the ecosystem is described as having 'recovered' (Westman, 1978; Orwin and Wardle, 2004; Suding et al., 2004). However, once an ecosystem reaches an alternative stable state (t_n; **Figure 1.1**) it may be challenging to recover to its initial microbial composition or function (Botton et al., 2006). This was found to be the case for soil microbiomes that had been exposed to both pulse and press disturbances (Shade et al., 2012a). However, the response to pulse disturbances is less well understood for microbial communities in other types of habitats – *i.e.*, aquatic (fresh and marine) and sedimentary environments (Shade et al., 2012a). Comparison between studies and habitats is further complicated by the lack of a common analytical framework or standard samples for data reporting.

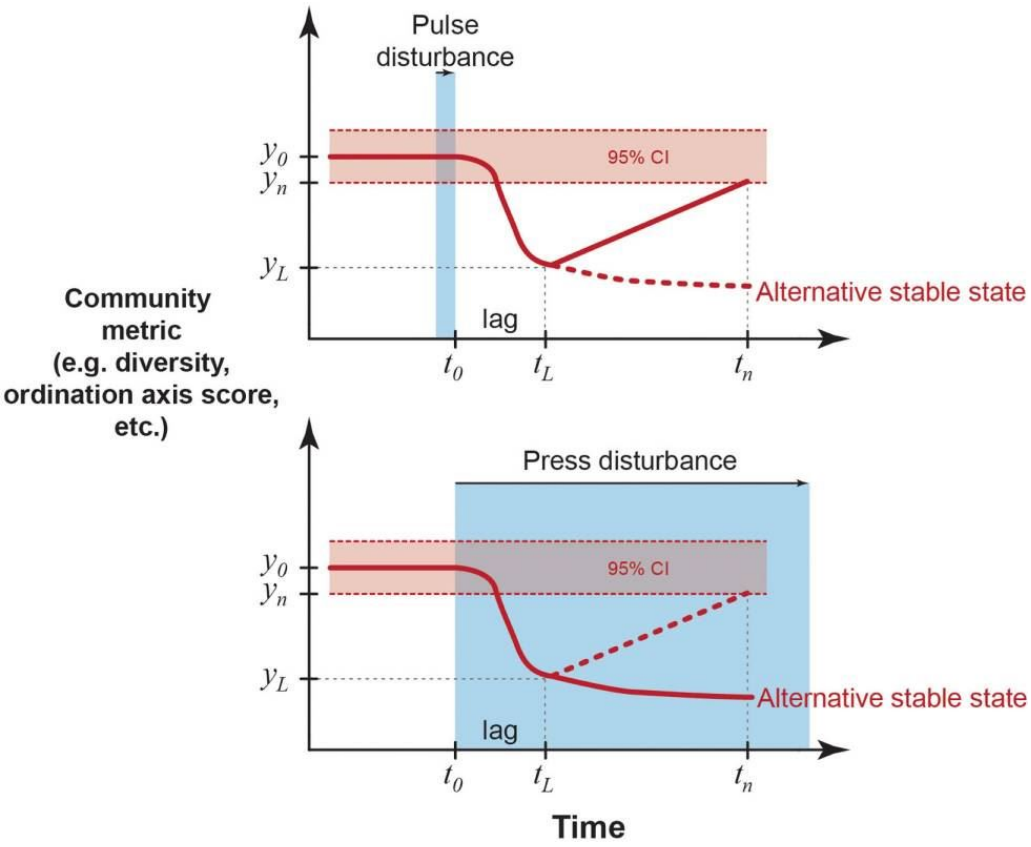

Figure 1.1. Diagram showing how microbial ecosystems are assessed or quantified in terms of resilience and resistance using community diversity metrics (Shade et al., 2012a).

1.3.1. Biological features for surviving disturbances

Disturbed microbial communities need to activate a number of biological processes at either individual (cellular) or community level in order to survive (Shade et al., 2012a). At an individual level, a habitat which contains many microorganisms with flexible physiological properties or metabolic capabilities is expected to be more resistant or resilient (*i.e.*, plasticity; Evans and Hofmann, 2012). Dormancy seems also important to temporarily face disturbances. This strategy allows microorganisms to lower their metabolic activity, which is likely to help preserve part of their microbial diversity (Jones and Lennon, 2010).

At the microbial community level, diversity is a crucial aspect for the stability of a disturbed ecosystem. However, the relationship between resilience and resistance is not always clear at the community level (Shade et al., 2012a). For example, a highly taxonomically diverse community is likely to possess a higher level of functional diversity and redundancy. This will ensure that under hostile conditions, surviving members of the community will increase the possibility of maintaining the functioning of the ecosystem, which is called the 'insurance hypothesis' or buffering effect (Yachi and Loreau, 1999; Shanafelt et al., 2015).

The alpha diversity refers to the average species diversity in a habitat (Willis, 2019). Alpha diversity can be estimated by the total number of species, also known as species richness, using Amplicon Sequence Variants (ASVs). Other indices - *e.g.,* Shannon, Pielou and Faith - provide information on the community composition (including relative abundances), evenness and phylogenetic relationships, respectively (Shannon, 1948; Pielou, 1966; Faith, 1992). Rarefaction is another commonly used technique that allows the calculation of species richness in a given sample, and is useful to verify if additional species can be identified due to higher sequencing depth (Sanders, 1968; Weiss et al., 2017).

Compositional turnover and emergent community networks are other aspects involved in maintaining the stability of microbial communities. Compositional turnover represents the degree of replacement of species between sample categories or along environmental gradients (Wilson and Shmida, 1984) and can be assessed by 'beta diversity'. Differences in microbial communities between samples can be visualised using ordination tools such as Principal Component Analysis (PCA). Whether

microbial communities differ significantly between sample categories can, for example, be determined *via* global or pairwise analysis of similarity (ANOSIM; Lozupone et al., 2007; Chiarucci et al., 2019). Mutualism (cooperation) and antagonism (competition) are considered favourable ecological mechanisms in emergent microbial networks under perturbed conditions (Little et al., 2008). Mutualism will result in a positive correlation or co-occurrence of species whereas a negative correlation between species implies antagonism (Shade et al., 2012b). Network analysis has been demonstrated to be one of the best ways to hypothesise the type of relationship may exist between a group of organisms (Hassani et al., 2018; He et al., 2020)

1.4. Microbial mats: an overview

Microbial mats are ecosystems composed of communities of microorganisms that have colonised solid surfaces or detrital particles at sediment-water interfaces and can be found in a wide range of environments (*e.g.* coastal sediments, deep sea, hydrothermal springs, hypersaline water bodies, dry valleys, gas and petroleum seeps, *etc.*; Des Marais, 2003; Heijs et al., 2005; Ding and Valentine, 2008; Zaikova et al., 2019). Their morphological features, such as lamination, colour, cohesiveness, and microbial composition vary with changes in chemical (*e.g.* pH, salinity, electron acceptor and donors, oxygen levels) and physical (*e.g.* tidal energy, temperature, light, and density) parameters (Franks and Stolz, 2009). Laminated microbial mats usually exhibit a vertical arrangement of the microbial communities that correspond or correlate with different chemical gradients (Pagès et al., 2014). This, in turn, has an impact on their biogeochemical cycles (*e.g.* C, O, N and S), particularly those exposed to a diel regime (Dupraz et al., 2009) (**Figure 1.2**).

In photosynthetic microbial mats, cyanobacteria act as primary producers and nitrogen fixers and thus dominate the upper-layer or aerobic zone (2-3 mm), where light is mainly absorbed and scattered (**Figure 1.2**). Often, their oxygenated photosynthetic activity is associated with carbonate precipitation (Dupraz et al., 2009) responsible for the production of exopolymeric substances (EPS). EPS are mucilaginous materials that coat and bind mineral grains and other particles, offering physical stability, reducing antibiotic penetration, retaining nutrients and enzymes and other benefits

(Czaczyk and Myszka, 2007; Flemming et al., 2007; Pannard et al., 2016). Cyanobacteria produce oxygen and organic carbon ($(CH_2O)_n$) to be utilised by aerobic heterotrophs, thus initiating a chain of interactions between other microbial groups: *e.g.*, anoxygenic phototrophs, anaerobic heterotrophs, fermenters, sulfate reducers and methanogens (Des Marais, 2003; Prieto-Barajas et al., 2018; **Figure 1.2**). SRB oxidise organic matter, reducing sulfate to sulfide (anaerobic respiration) (Canfield and Marais, 1991), which is also involved in the precipitation of calcium carbonate, and therefore assisting in the lithification of mats (Spring et al., 2019). The generation of sulfide by SRB contributes to anoxygenic photosynthesis and aerobic sulfide oxidation. The latter process usually occurs at night when O_2 is consumed by chemolithotrophic bacteria and CO_2 is produced (van Gemerden, 1993).

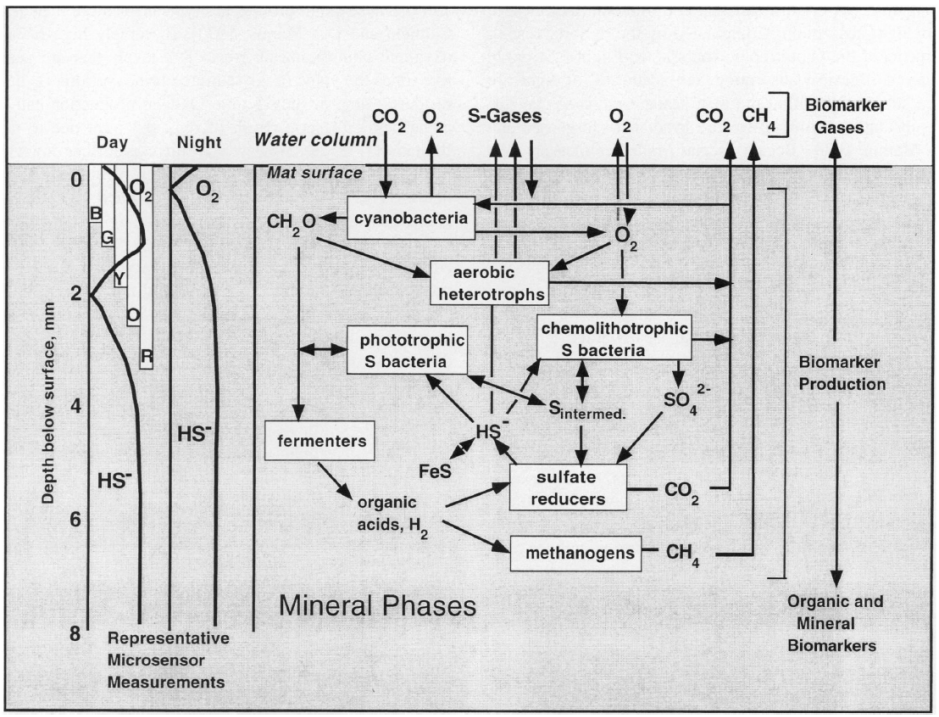

Figure 1.2. Conceptual model of microbial interactions in a photosynthetic mat, and their role in biogeochemical cycling of C, N, and S across vertical gradients of oxygen and HS^- and availability of photosynthetically active radiation. The narrowing of the wavelengths that escape adsorption with increasing depth is indicated as: blue, B; green, G; yellow, Y; orange, O; and red, R light spectra) (Des Marais, 2003).

1.4.1. Formation of microbial mats

Various models have been developed to elucidate how microbial mats may be formed Although, there are several factors involved, the microbial community composition

and the physical structure or fabric of the minerals present, are the key variables shared by these models . Dupraz et al. (2011) summarised the formation of three types of mats in seven steps (**Figure 1.3**): (a) colonisation of mineral particles mainly by Cyanobacteria –Cya– and likely eukaryotic plankton such as diatoms; (b) stabilisation *via* trapping and binding sediments. At this stage, a variety of other bacteria are expected (*i.e.,* sulfate reducing bacteria –SRB, heterotrophic bacteria –Het–, sulfide oxidising bacteria –SOB–, *etc*), forming an interconnected microbial community; (c-d) upward microbial migration due to accumulation of sediments. This stage corresponds to type A mat; (e) biofilm formation after sedimentation diminishes or ceases. This allows anaerobic heterotrophs to produce fine layers of aragonite (as micrite). This step might reflect type B mat features; (f) Colonisation of ooids by cyanobacteria if there is a gap in the trapping and binding processes. It is common to find aragonite precipitated in the bore holes, fusing grains. This characteristic has been found in type C mats.

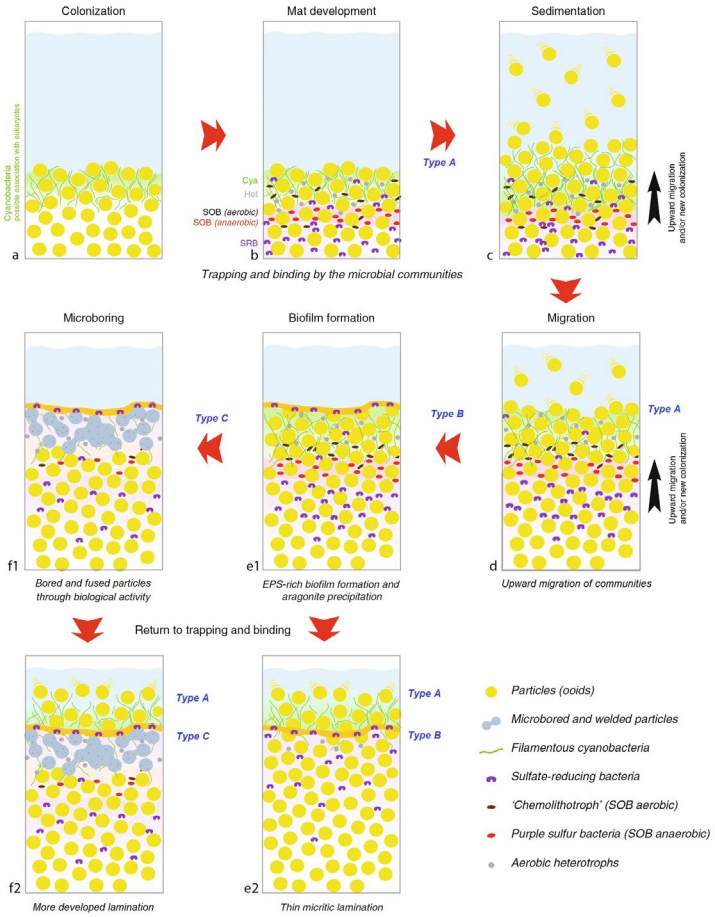

Figure 1.3. Formation of microbialites. See text for detailed explanation. Image source: partly modified from Dupraz et al. (2009).

1.4.2. Microbial mats' microbiome from hypersaline environments

Microbial mats in natural or man-made hypersaline environments display distinctive microbial communities and functional traits (Des Marais, 2003) and are dominated by halophilic (salt-dependent) and halo-tolerant (salt-tolerant) organisms. They are phylogenetically diverse and belong to all three domains of life: Bacteria, Archaea and Eukarya (Gunde-Cimerman et al., 2018; **Figure 1.4**). Halophiles are predominantly found in the archaeal order Halobacteriales. Some of the most common genera are: *Halococcus*, *Haloferax*, *Halobacterium*, *Haloarcula*, *Natromonas*, *Halorubrum*, *Halobaculum*, *Natronobacterium*, *Natronococcus*, *Natrialba* and *Haloterrigena*. Anaerobic archaea, such as methanogens, can be also found in microbial mats or saltern, *e.g. Methanohalophilus halophilus* and *M. muhii*, respectively. The domain Bacteria include many taxonomical groups, *i.e.,* sulfur-oxidizing bacteria, sulfate-reducing bacteria, fermentative bacteria, homoacetogenic bacteria, *etc*. The order Oscillatoriales (phylum Cyanobacteria), family Halomonadaceae (class Gammaproteobacteria) and order Halanaerobiales (phylum Firmicutes) are frequently detected in microbial mats (DasSarma and Arora, 2001). Eukaryotic halophiles that have been reported in saline microbial mats include diatoms such as *Amphora coffeaeformis* and *Nitzschia* and *Navicula* species, protozoa (*e.g. Fabrea salina* and *Porodon utahensis*) (Post et al., 1983) and fungi (*e.g.* the halotolerant yeast *Debaromyces hansenii*) (DasSarma and Arora, 2001).

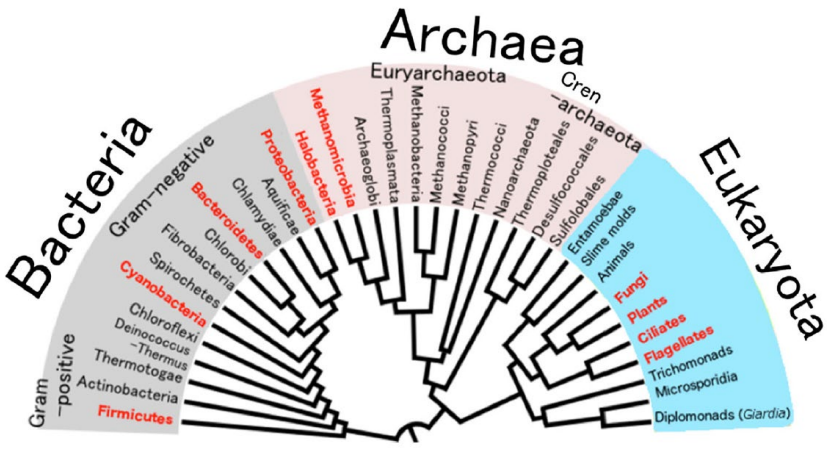

Figure 1.4. Distribution of halophiles within Bacteria, Archaea and Eukaryota domains. Names in red represent groups which contain, at least, one halophilic organism. Original image from Ciccarelli et al. (2006), and modified by (Edbeib et al., 2016).

Halophiles require two major functional adaptations to thrive in hypersaline environments. The first is osmoregulation, a strategy used for balancing the concentration of compatible solutes between the cytoplasm and their outer environment. The solutes can be either K^+ and Cl^- or organic osmotic solutes, *e.g.* glycine betaine, beta-glutamine, beta-glutamate, or trehalose (Oren, 2008; Gunde-Cimerman et al., 2018) (**Figure 1.5**; **Table 1.1**). The second functional adaptation is based on specialised intracellular proteins capable of weakening hydrophobic interactions in the presence of molar salt concentrations to prevent aggregation or loss of function in hypersaline environments (Litchfield, 1998; Ma et al., 2010; Siglioccolo et al., 2011).

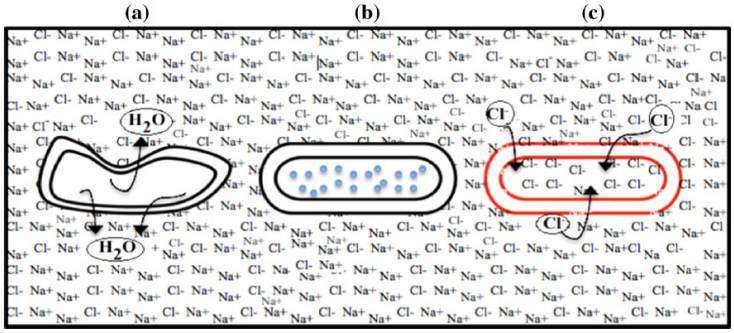

Figure 1.5. Mechanism of adaptation in hypersaline conditions. (a) Reaction of a non-halophilic organism when exposed to extreme salt concentrations (*i.e.,* osmotic dehydration by releasing H_2O). (b) Halophiles capable to deal with moderate concentration of salts by synthesizing organic solutes. (c) Halophiles facing hypersalinity by equilibrating Cl^- concentration and, therefore, maintaining their cell integrity (Bell, 2012).

Table 1.1. Common organic solutes identified in halophiles from hypersaline environments. Partly modified from Edbeib et al. (2016).

Organic solute	Bacteria	References
Betaine	*Actinopolyspora halophila*	Cánovas et al., 1996; Nyyssölä and Leisola, 2001
	Halomonas elongata	
Ectoine	*Methylomicrobium alcaliphilum*	Doronina et al., 2000; Reshetnikov et al., 2011; Shmareva et al., 2018
	M. terricola	
	Methylophaga muralis	
Hydroxyectoine	*Bacillus pasteurii*	Kuhlmann and Bremer, 2002; Bursy et al., 2007
Glutamine and Glutamate	*Halomicronema hongdechloris*	Chen et al., 2019
Sucrose	*Halomonas elongata*	Kindzierski et al., 2017
Glycine betaine	*Halochromatium*	Oren et al., 2013

1.5. Petroleum as a pollutant and processes involved in its degradation

1.5.1. Petroleum composition

Petroleum is a general term used to define a complex mixture of organic compounds which are products of the maturation process of sedimentary organic matter (Peters et al., 2007b). The study of its abundance, composition and origin is studied by organic geochemistry (Kvenvolden, 2006). The chemical composition of petroleum greatly varies depending on its original source and other processes that can occur during migration into the sedimentary basins (Tissot and Welte, 2013) and in the reservoir. It is mainly composed of hydrocarbons of different molecular weights, but also elements, such as oxygen, sulfur, nitrogen and various metals (*i.e.,* Vanadyl, Co and Ni; Selley, 2003; Gad, 2014).

Petroleum mainly consists of aliphatic, aromatic hydrocarbons and polar compounds. The aliphatic fraction (also known as paraffinic or saturate fraction) possesses straight-chain and branched alkane hydrocarbons (*i.e.*, *iso* and *antiso* alkanes), usually between C_5-C_{40} (Tissot and Welte, 2013) (**Figure 1.6**, a and b). The aromatic fraction is composed of either monocyclic (5-6 carbon atoms) or polycyclic molecules (usually up to 6 rings) (Chilingar et al., 2005; Killops and Killops, 2005). The more common aromatic compounds include naphthalenes, phenanthrenes, aromatic steroids and hopanoids, including their alkyl substituents (**Figure 1.6**, c and d). The polar fraction contains a large variety of compounds rich in nitrogen, sulfur and oxygen (NSO). Moreover, some types of petroleum contain certain portions of organic compounds that are difficult to identify by chromatographic techniques due to their structural complexities. They are classified within a fraction called "Unresolved Complex Mixture" (UCM), and their presence is often associated with biodegradation processes, in parallel with a depletion of *n*-alkanes (Killops and Killops, 2005).

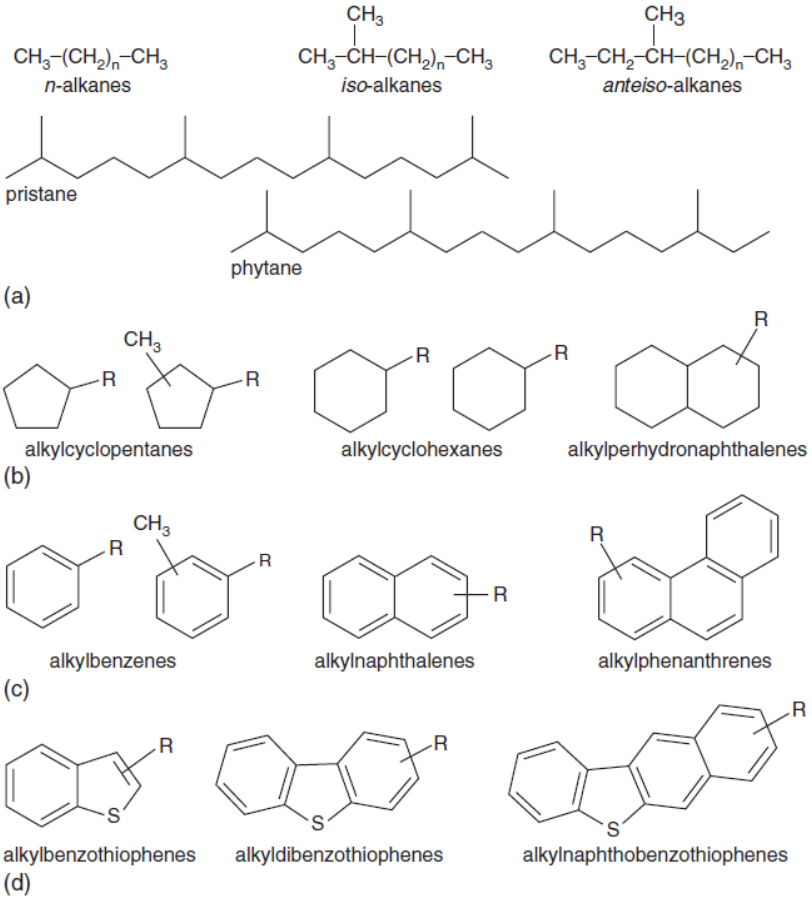

Figure 1.6. Main types of organic molecules in petroleum. (a) acyclic alkanes; (b) cycloalkanes (naphthalenes); (c) aromatic hydrocarbons; (d) sulfur-rich aromatics. (R means alkyl group). Source: Killops and Killops, 2005.

1.5.2. Hydrocarbon degradation in petroleum reservoirs

After the formation of petroleum, its composition can be significantly altered by biodegradation in the reservoir (Peters et al., 2007a). This process consists of anaerobic degradation of its chemical composition by microbes (with essential nutrients) and occurs in reservoirs with temperatures less than 80 °C (Aitken et al., 2004). The effects of biodegradation are important because the process can reduce the quality of the petroleum (Kennicutt, 1988). Biodegradation leads to the quasi-sequential removal of certain compounds in petroleum. For instance, in a slightly biodegraded petroleum low-molecular-weight (LMW) *n*-alkanes are favourably removed, followed by high-molecular-weight (HMW) *n*-alkanes and then later isoprenoids and LMW aromatics (Trolio et al., 1999). Diamondoids (adamantane and diamantane) are known to be greatly resistant to biodegradation (Grice et al., 2000).

Additionally, highly biodegraded samples usually display an unresolved complex mixture (UCM). The susceptibility of certain compound classes to biodegradation led to the biodegradation scale (0 to 10: none to severely biodegraded; Volkman et al., 1984; Larter et al., 2012) (**Figure 1.7**). When biodegradation proceeds the microbial communities produce functionalised metabolites.

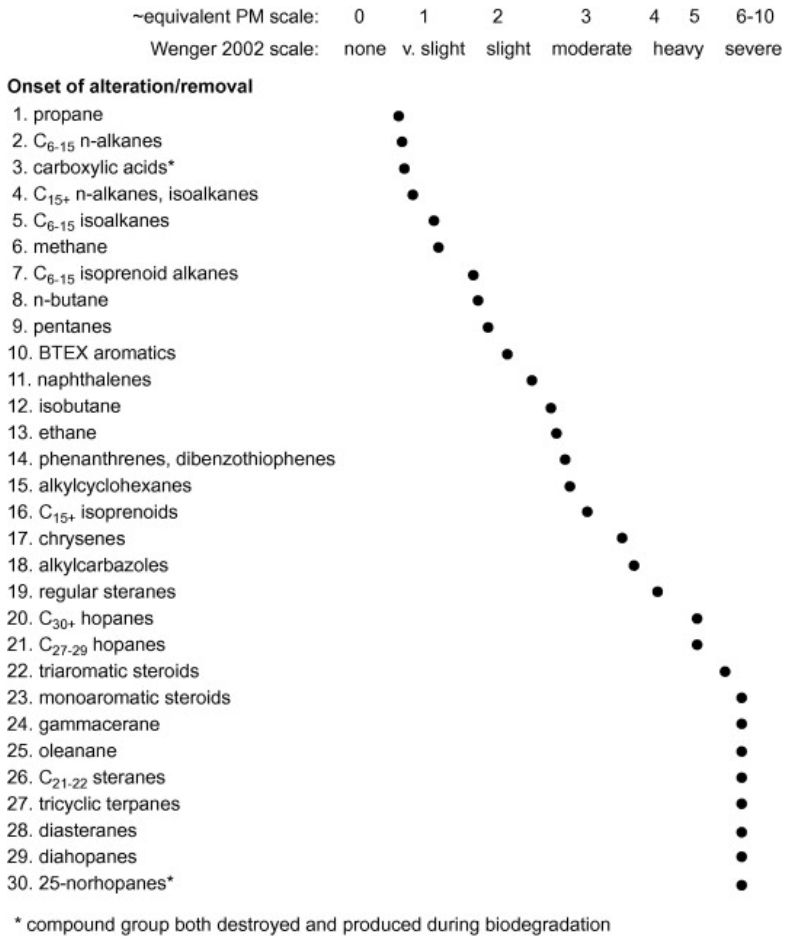

Figure 1.7. Quasi-sequential removal of organic compounds during biodegradation. Source: Head et al., 2003; modified after Wenger et al., 2002, in Larter et al., 2012.

1.5.3. Surface petroleum degradation

1.5.3.1. Abiotic processes

Petroleum is also a common source of terrestrial and marine contamination from pipelines, off-shore platforms, wells, tankers, freighters, and storage facilities (Prince, 2010). Thus, when petroleum is spilled in the environment, *i.e.,* fresh- and marine-waters, soils, and other habitats, the petroleum undergoes processes that lead to chemical changes. The processes affecting the fate of petroleum in nature are

collectively referred to as "weathering", and include: evaporation (usually affecting the relatively more volatile compounds), spreading, dissolution (related to solubility of individual compounds and temperature), emulsification, aggregation, sinking, and oxidation (due to exposure to sunlight – mainly radian energy like UV –, and dependant on photooxidative susceptibilities) (Gagnon et al., 1999; Peters et al., 2007a; Hook et al., 2017; **Figure 1.8**). The extent of their influence over the fate of petroleum varies and depends on many other temporal and local factors (*i.e.* temperature, tidal regime, salinity, *etc.*).

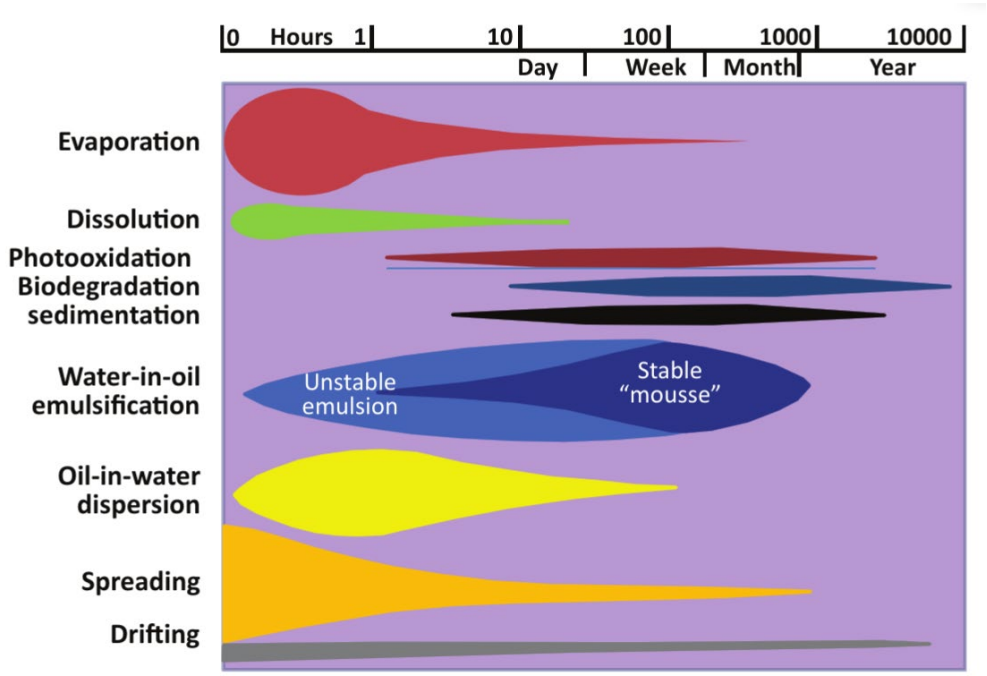

Figure 1.8. Weathering processes and their relative timescales. Bars represent the extension of the process over time and its thickness their relative importance (Hook et al., 2017).

1.5.3.2. Biotic processes

A large variety of microbial communities are capable of using petroleum compounds as sole carbon and energy sources (*i.e.* electron donors), but these compounds can differ in their chemical susceptibility to biodegradation (Kim and Picardal, 2001). Different metabolic processes are required to metabolise the various hydrocarbon fractions of petroleum. Which of these metabolisms are activated depend on factors, such as temperature, salinity, nutrient availability, nature of chemical bonds and their configuration (*e.g.* aliphatic *vs.* aromatic), and the prevalence of aerobic or anaerobic

conditions (Leahy and Colwell, 1990). Although, metabolism of xenobiotics (*i.e.,* toxins or pollutants) is a challenging research area due to the complexity and number of possible reactions that might be involved (Widdel and Musat, 2010), there is still some consensus in regards to general activation mechanisms for degradation of hydrocarbon by aerobic or anaerobic organisms (**Figure 1.9**).

Aliphatic hydrocarbon-degrading aerobic microorganisms usually utilise oxygenases to assist in the oxidation of hydrocarbons. Oxygenases can be divided into two enzyme categories: monoxygenases or dioxygenases, depending on the incorporation of one or two atoms of oxygen into the hydrocarbon structure to form hydroxyl functional groups (*i.e.,* alcohols), respectively (**Figure 1.9**, top sequences A1). Thus, a typical sequence of reactions is triggered to form more stable organic compounds, ending in the production of a carboxylic acid. A final step includes the oxidation of that fatty acid through a *beta*-oxidation process, generating 4-acetyl coenzyme A (α-glucosaminide N-acetyltransferase), which can be either oxidised by citric acid cycle or used for producing new cell material (Widdel and Musat, 2010; Sierra-Garcia and Oliveira, 2013; Madigan et al., 2019).

When degrading polyaromatic aromatic compounds (PAHs), hydrocarbon-degraders microbes may use a variety of different mechanisms to activate those sort of compounds (**Figure 1.9**, top sequences A2). As per aliphatic degradation pathways, monooxygenases and dioxygenases are also involved in the initial activation step for PAH. Examples of these common enzymes are: di-iron multicomponent monooxygenase (SDM), the flavoprotein monooxygenase (FPM) and Rieske non-heme iron oxygenases (RNHO). Activation of the aromatic rings can be also achieved by CoA ligases, producing CoA derivatives that can be then subjected to hydroxylation. Compounds produced as intermediates are further catalysed by other enzymes, called intradiols and extradiols. Although there are still many unknown intermediate steps that require further research, it is thought that these enzymes catabolise aromatic compounds by oxygen chelation, assisting in the cleavage of organic compounds. Once they are fully cleaved, they can then enter into the citric acid cycle or being completely oxidised to CO_2 (Widdel and Musat, 2010; Sierra-Garcia and Oliveira, 2013; Madigan et al., 2019).

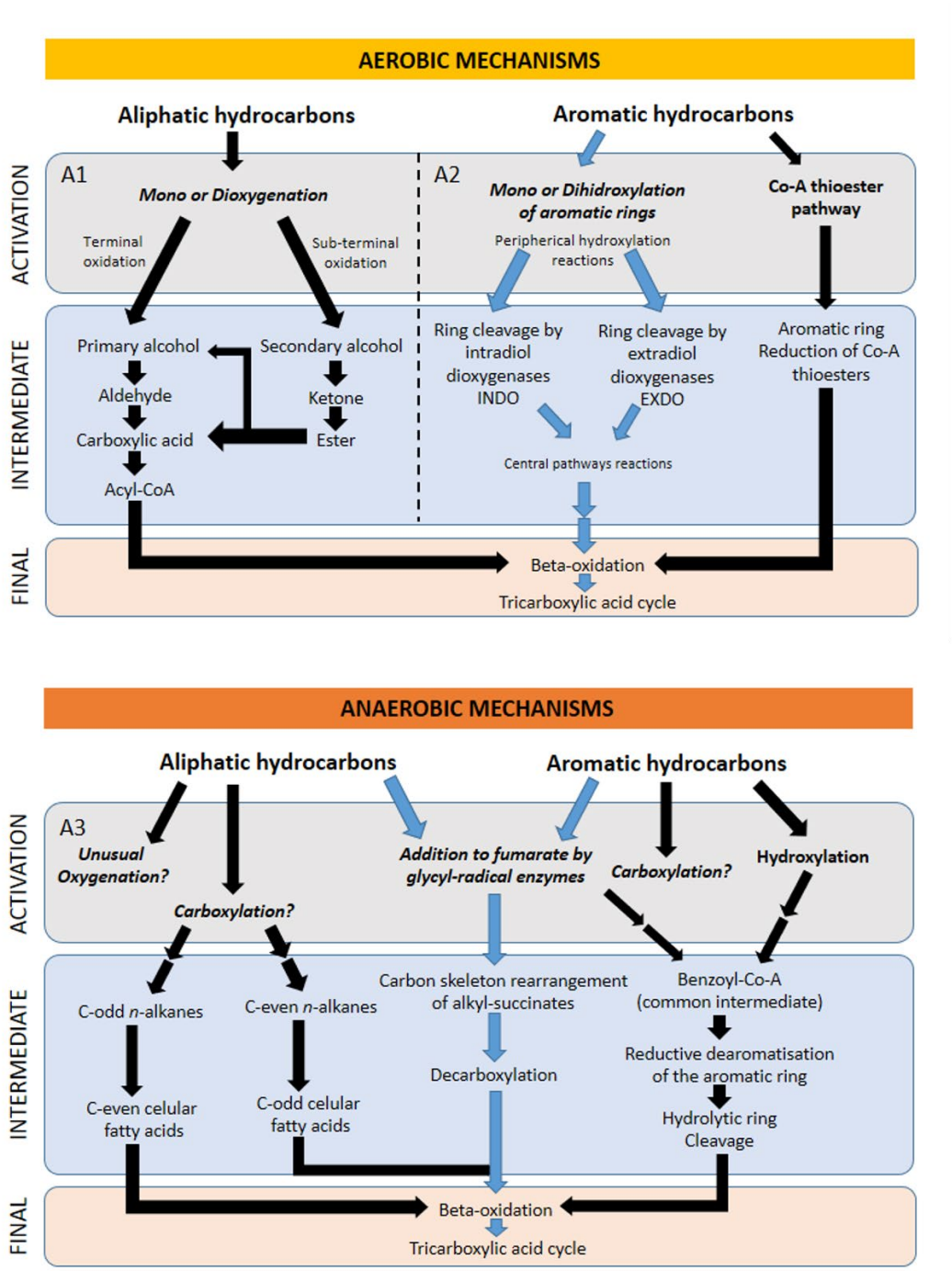

Figure 1.9. Bacterial aerobic and anaerobic mechanisms for degradation of aliphatic and aromatic organic compounds. Two arrows means that the process may include additional reactions. Partly modified from Sierra-Garcia and Oliveira (2013).

Conversely, hydrocarbon degradation by anaerobic microorganisms involves different chemical mechanisms (**Figure 1.9**, bottom sequences A3). Hydrocarbon oxidation under anoxic conditions is usually linked to the reduction of different electron acceptors, *i.e.,* ferric iron, sulfate and nitrate (Madigan et al., 2019). Two mechanisms

are involved in the degradation of aliphatic hydrocarbons: addition of fumarate and carboxylation. The first mechanism activates a subterminal carbon of the alkanes, alicyclic alkanes or alkenes *via* addition of fumarate, from which an intermediate product is generated (*i.e.,* a substituted succinate). This is followed by decarboxylation and the addition of coenzyme A, triggering the beta-oxidation process. The second mechanism includes the conversion of C-even *n*-alkanes into C-odd carboxylic acids, or C-odd *n*-alkanes into C-even fatty acids. Both mechanisms are likely followed by the citric acid cycle. The first mechanism can also be involved in the biodegradation of a variety of aromatic compounds, although ethylbenzene, a typical alkylbenzene, is anaerobically degraded by the oxidation of the methylene carbon. The resulting metabolite is then hydroxylated and dehydrogenated to an aromatic ketone, *i.e.,* acetophenone. This compound is subsequently carboxylated, converted to benzoylCoA, and further altered *via* ring reduction, being later incorporated into the beta-oxidation process and citric acid.

1.5.3.4. Biomarkers proxies as biodegradation indicators

Biomarkers are complex organic compounds with structures which reveal information or elucidate their origin or geologic history. In order to be reliable they need to be chemically stable, abundant, and with unique or common precursors (Peters et al., 2007a). Biomarkers are used to characterise biodegradation processes in reservoirs, but they can be also used to determine the degree of this process in surficial environments. By monitoring selected ions and specific diagnostic ratios. it is usually possible to determine if biodegradation has occurred (George et al., 2002; McIntyre et al., 2007; Bayona et al., 2015). As an example, some of the ratios utilised are listed in **Table 1.2**, which are part of the European CEN/TR15522-2 standard, and an extended list can be found in Fingas (2015). However, caution should be exercised when interpreting them due to the fact they can be affected by other weathering processes (*i.e.,* evaporation, dissolution, *etc.*).

Table 1.2. Diagnostic ratios used for petroleum fingerprinting based on CEN/TR15522-2 standard (Fingas, 2015). Not a comprehensive list.

Diagnostic ion	Diagnostic ratio	Definition
85	C_{17}/Pr	*n*-Heptadecane/Pristane
85	C_{18}/Ph	*n*-Octadecane/Phytane
85	Pr/Ph	Pristane/Phytane
192	4-MD/1-MD	4-Methyldibenzothiophene/1-Methyldibenzothiophene
198	2-MP/1-MP	2-Methylphenanthrene/1-Methylphenanthrene
216	2MF/4-Mpy	2-Methylfluoranthene/4-Methylpyrene
216	B(*a*)F/4-Mpy	Benzo[*a*]fluorene/4-Methylpyrene
216	B(*b* + *c*)F/4-Mpy	Benzo[*b* + *c*]fluorene/4-Methylpyrene
216	2Mpy/4-Mpy	2-Methylpyrene/4-Methylpyrene
216	1Mpy/4-Mpy	1-Methylpyrene/4-Methylpyrene
234	Retene/T-Mphen	Retene/Tetra-Methylphenanthrene

1.6. Techniques used for microbiological analysis of microbial mats and chemical susceptibility of petroleum.

1.6.1. 16S rRNA gene sequencing analyses

Traditionally, the identification and phenotypic characterisation of microorganisms relied on microscopic and cultivation methods (Stolp and Starr, 1981). While biochemical processes and metabolic pathways can be inferred from cultured isolates that grow under different conditions and on different substrates (Lagier et al., 2015), a large number of taxa still appear to be difficult to grow under lab-controlled conditions especially when the goal is to obtain axenic 'pure' cultures (Scheler et al., 2014). Therefore, culture-dependent methods cannot reveal a holistic overview of microbial diversity or activities, especially in complex environmental samples (Austin, 2017). However, bacteria and archaea have important housekeeping genes that evolve at a slow rate and can act as a molecular clock with known rates of evolutionary mutations in their sequences. This was explored by Carl Woese (1977) who tested to what extent evolutionary mutations in the ~1540 base-pair-long 16S rRNA (ribosomal ribonucleic acid) gene could be used to classify prokaryotes down to species level (Woese and Fox, 1977; Lane et al., 1985; Woese, 1987; Woese et al., 1990). This house-keeping gene encodes for 16S ribosomal RNA that binds with ~20 proteins in the cytoplasm to form the small subunit of the ribosome, the cellular organelle that is involved in the biosynthesis of proteins, which is crucial for the survival of cells.

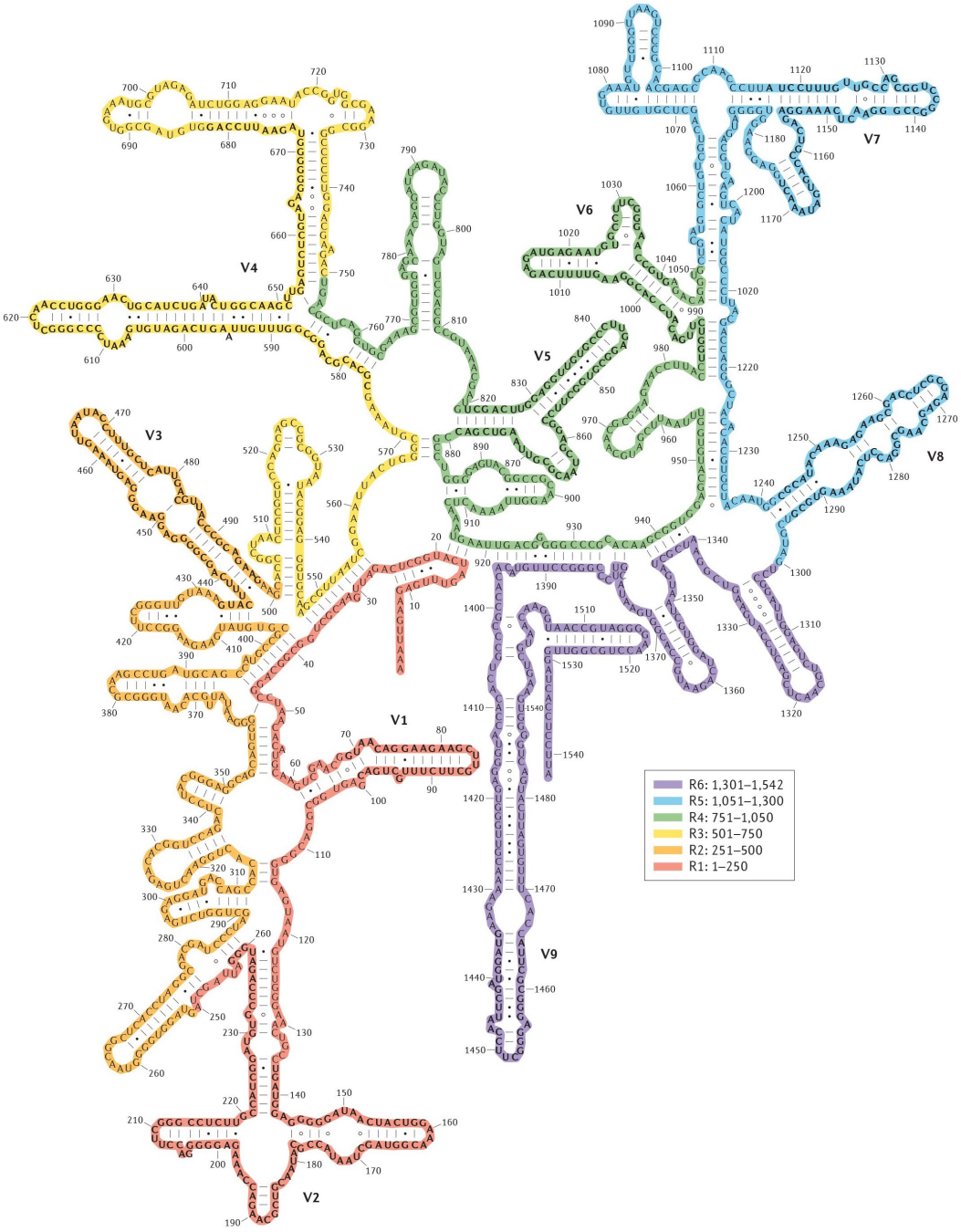

Figure 1.10. 16S ribosomal RNA gene and its variable regions. To visualise its structure, it was divided in six regions: R1 (red) includes V1 and V2; R2 (orange) comprises V3; R3 (yellow) consists of V4; R4 (green) includes V5 and V6; R5 (blue) comprises V7 and V8; and R6 (purple) consists of V9 (Yarza et al., 2014).

The 16S rRNA gene is found in all prokaryotes and has very conserved regions as well as nine faster-evolving hypervariable regions (V1-V9) that enable researchers to study bacterial and archaeal diversity at domain down to species level (**Figure 1.10**). Of those nine hypervariable regions, the ~300 base pairs-long V4 region provides the

highest taxonomic resolution of all variable regions and is the most widely amplified and sequenced section of the 16S rRNA gene to study microbial populations in environmental samples (Kim et al., 2011; Jo et al., 2016; Bukin et al., 2019; **Figure 1.11**). A variety of primers[2] exist to amplify either conserved or hypervariable regions of interest (Jo et al., 2016). A list of the more commonly used primers for targeting bacteria and archaea can be found in Smith and Osborn (2009), Thijs et al. (2017), and Bahram et al. (2019). Nowadays, the 16S rRNA gene has become the most widely sequenced barcoding gene to identify and classify prokaryotes in a wide range of environmental samples without the need to culture these organisms (Clarridge, 2004; Tringe and Hugenholtz, 2008; Kim et al., 2011).

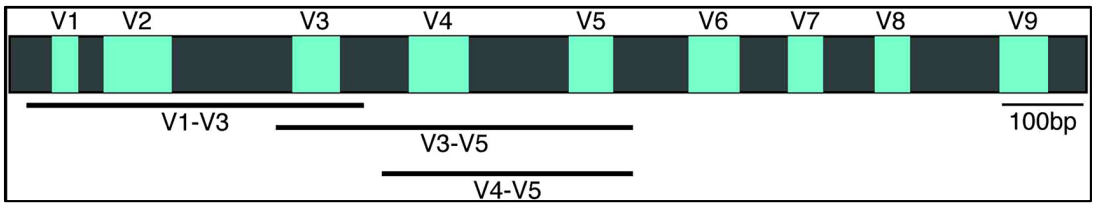

Figure 1.11. Conserved regions (dark grey) and variable (light green, V1–V9) of 16S rRNA gene and the commonly PCR-amplified regions for next-generation amplicon sequencing-based microbial community profiling (bottom lines) (Jo et al., 2016).

The advent of Next-Generation Sequencing (NGS) was one of the innovations that helped to consolidate the use of 16S rRNA gene barcoding as the accepted norm for accurate bacterial and archaeal phylogenetic classification, especially in complex microbial habitats (Tringe and Hugenholtz, 2008; Almeida et al., 2018). The switch from the analysis of small datasets such as sequenced clone libraries to large NGS datasets required the development of bioinformatics pipelines such as Mothur, MAPseq and Quantitative Insights Into Microbial Ecology 2 (QIIME2) (Caporaso et al., 2011; Bolyen et al., 2019; Schloss, 2019). These tools are continuously improving and at the same time evolving to ensure that low quality sequences reads are being removed, and the remaining high quality reads are binned to the corresponding samples, denoised, and taxonomically assigned to sequenced closest relatives available in public sequence reference databases, notably SILVA and Genbank

[2] Short, single-stranded DNA used for the initiation of DNA synthesis (approx. 15-30 base pairs).

(NCBI) (Balvočiūtė and Huson, 2017).

1.6.2. Complementary DNA

Numerous studies have now shown that ancient environmental DNA can be recovered, amplified and sequenced after being preserved for several hundreds of thousands of years (Willerslev et al., 2003; Coolen and Overmann, 2007). Cold and/or anoxic conditions slow down microbial degradation of DNA (*e.g.* Coolen et al., 2004; Coolen and Overmann, 2007) and DNA adsorption to minerals, notably clays, further aids in the long-term preservation of DNA by shielding it from microbial degradation as well as extreme temperature, radiation, humidity changes and exposure to free-radicals or highly potential reactants (Matange et al., 2021). Also in modern environmental samples, it was found that DNA-based analysis contains genomic information of living (actively growing and/or non-growing dormant cells) and dead cells (Li et al., 2017). Therefore, the identification of microbial taxa from environmental DNA does not provide information on whether the source organisms were alive at the time of sampling. In contrast, RNA-based analysis can estimate with more accuracy which members of the environmental microbiome were alive and/or active, since transcription is one of the first levels of cellular responses to a stimulant, and RNA has a much shorter average half-life than DNA (Emerson et al., 2017). Messenger RNA (mRNA), which encodes for proteins involved in physiological processes, only survives for minutes in active cells, and likely only seconds after cell lysis (Keer and Birch, 2003; Moran et al., 2013). Ribosomal RNA transcripts, on the other hand, comprises up to 90% of the total intracellular RNA and are only present in living (including drmant) cells where they function as structural components of ribosomes involved in protein synthesis. rRNA transcripts, which survive only up to several days upon cell death in the environment (Emerson et al., 2017), can be reverse-transcribed to complementary DNA (cDNA) and sequenced, to reveal the identity of the microbial community members that were likely to be alive at the time of sampling. Those that are found to be very abundant in the cDNA dataset, but far less dominant in the in parallel sequenced 16S rRNA gene dataset (DNA pool) were most likely not very abundant in the sample but rather very active. The process of cDNA synthesis is demonstrated in **Figure 1.12**.

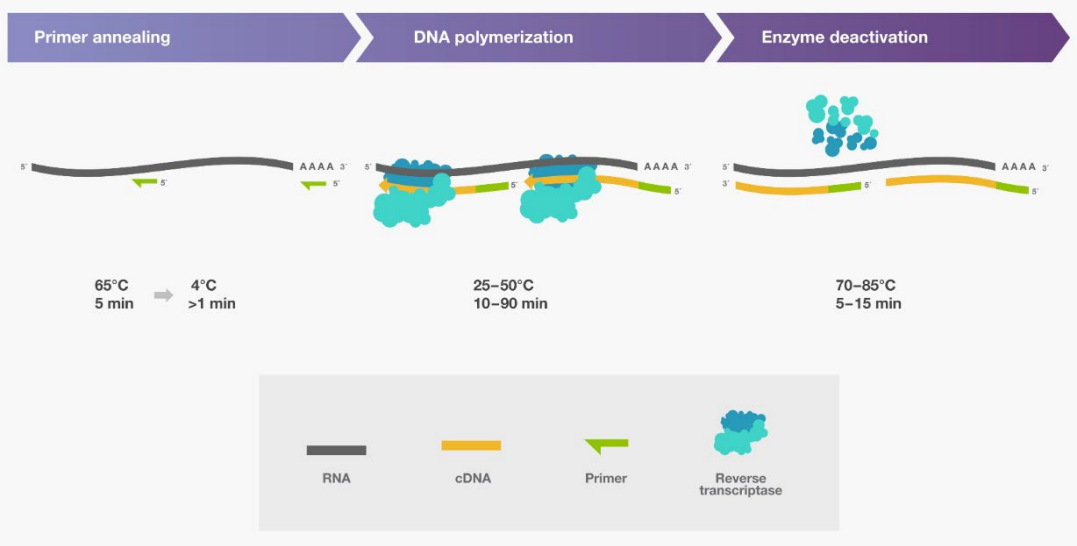

Figure 1.12. Diagram showing main steps in the synthesis of second-strand cDNA[3]: (1) primer annealing to produce a single strand of RNA template (after DNA-trace removal); (2) DNA polymerisation, which includes the combination of oligo (dNTPs[4]) primers, random or gene-specific primers and RTase[5], and will form a cDNA:RNA hybrid; and (3) enzyme deactivation.

1.6.3. Potential functional predictions

Until recently, physiological properties could not be reliably inferred from microbial communities in complex environmental samples based on 16S rRNA gene profiling, unless the sequences were taxonomically closely related to well-described cultivars. Over the last decade, sequencing analysis of environmental metagenomes, single cell genomes, as well as functional metatranscriptomes has generated a wealth of information about the functional potential and capabilities of environmental bacteria and archaea (*e.g.* O'Donnell et al., 2020). However, these NGS approaches are still relatively costly per sample, labour intensive, prone to handling errors, and require the use of demanding bioinformatics pipelines (Hwang et al., 2018; O'Donnell et al., 2020). Several bioinformatics tools (e.g. PICRUSt, Piphillin and Tax4Fun) have been introduced as a cost effective alternative approach to predict approximate functional potential of a community solely based on 16S rRNA gene sequences (Langille et al., 2013; Aßhauer et al., 2015; Iwai et al., 2016). Among them, PICRUSt (Phylogenetic Investigation of Communities by Reconstruction of Unobserved States) has been

[3] Source: https://www.thermofisher.com/au/en/home/life-science/cloning/cloning-learning-center/invitrogen-school-of-molecular-biology/rt-education/reverse-transcription-setup.html
[4] Deoxyribonucleotide triphosphate
[5] Reverse Transcriptase

increasingly used and appears to generate reliable functional predictions if the mapping shows good coverage with the reference genomic databases (Koo et al., 2017b, 2017a).

Last year, an updated version was published as PICRUSt2. This new version can now predict novel phenotypes, using a one order of magnitude larger genome reference database for comparison, and allows the use of customised reference databases (Douglas et al., 2019) . Furthermore, MinPath[6] is now used for inferring pathway abundances, making the predictions more rigorous. PICRUSt2 is compatible with ASVs input files after DADA[7] or deblur denoising steps, which hugely expands its use with current microbiome analysis pipelines (*i.e.,* QIIME2) compared to its previous version[8]. The inference of the potential microbial functions relies on the reconstruction of ancestral states and the weighting method. The algorithm consist of: Alignment of ASVs with reference sequences (step 1), which are then placed into a reference tree for phylogenetic associations – (step 2); followed by hidden state prediction, where gene family copy number of ASVs are predicted (step 3), next their abundance per sample is determined (step 4); and finally their pathway abundances are inferred (step 5) (**Figure 1.13**).

The PICRUSt2 pipeline reveals either stratified (known functions per organism) or unstratified (whole functions of the community) metagenomic predictions. Output files include the metagenome predictions for KEGG[9] orthologs (KO) (Kanehisa and Goto, 2000; Kanehisa et al., 2012), EC (Enzyme Commission), or even, pathways when ECs are regrouped by MetaCyc reactions. For the purpose of this study only KO metagenome predictions will be generated and compared to metagenomes or metatranscriptomes. Thus, depending on the research's interest, different types of metabolism can be selected. Some studies have been focused on energy metabolisms as a whole (*i.e.,* carbon, sulfur or nitrogen), or restricted to more specific pathways, such as: photosynthesis, xylene degradation, PAH degradation, methanogenesis or chemoautotrophic metabolism (*i.e.,* Arnon–Buchanan cycle) (Jeanbille et al., 2016; Hariharan et al., 2017; Koo et al., 2017b; Mukherjee et al., 2017; Roy et al., 2018).

[6] https://omics.informatics.indiana.edu/MinPath/
[7] Divisive Amplicon Denoising Algorithm
[8] https://github.com/picrust/picrust2/wiki
[9] Kyoto Encyclopedia of Genes and Genomes

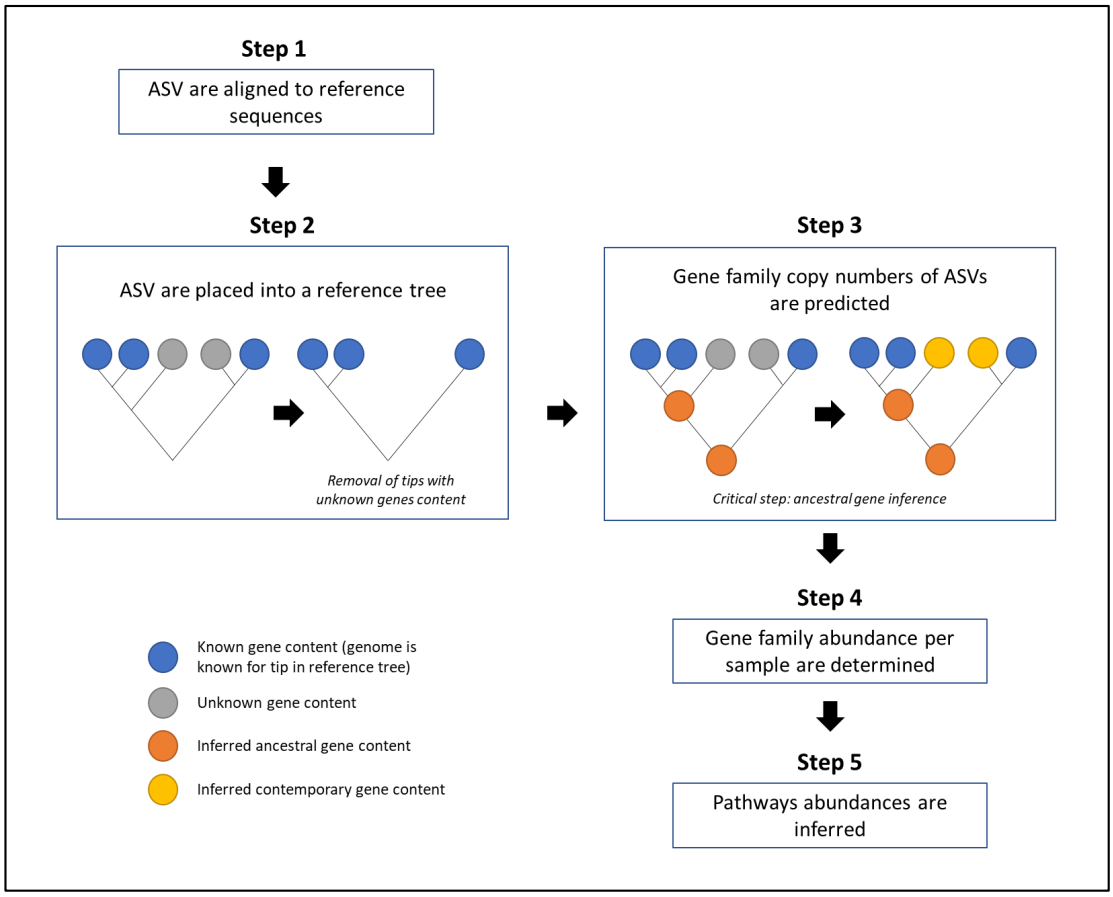

Figure 1.13. Diagram represents a simplification of PICRUSt workflow and pipeline. Partly modified from Langille et al. (2013) and https://github.com/picrust/picrust2/wiki.

Both versions of PICRUSt also generate a validation metric. This 'weighted nearest-sequenced taxon index' (NSTI) quantifies the availability of nearby genome representatives for each microbiome sample (Langille et al., 2013). The NSTI values indicate how well the predicted functionalities in a sample are characterised when compared to the reference genomes. This will then guide the user to discard those samples with speculative interpretations of the predicted functions.

However, this predictive tool does have limitations[10] and it is encouraged to be used under certain guidelines to guarantee that the inferences are meaningful. Two considerations are worth mentioning: (1) the placement of the studied sequences into the reference tree will heavily influence the reliability of the predictions; (2) the

[10] https://github.com/picrust/picrust2/wiki/Key-Limitations

reference genome coverage varies depending on the type of environment. Currently, the well-studied human gut microbiome is better represented in reference genomic databases than microbial communities in extreme environments.

1.6.4. Gas Chromatography coupled to Mass Spectrometry (GC-MS)

The chemical characterisation of petroleum can be performed by a number of analytical techniques. However, a gas chromatograph coupled to Mass Spectrometry (GC-MS) is one of the standard techniques used in forensic petroleum analysis especially when associated with spills (White et al., 2016). GC-MS displaced the stand-alone use of a gas chromatograph fitted with a Flame Ionisation Detector (GC-FID) because of its ability to obtain a mass spectrum of each component (Fingas, 2015). GC-MS is capable of performing rapid scanning, accurately quantifying the presence of volatile and semi-volatile organic compounds, and also possesses a high signal-to-noise output, which is complemented by access to robust, large, and regularly updated mass spectral libraries (Peters et al., 2007a; Fingas, 2015).

Prior to GC-MS analysis, environmental samples need to be separated. Depending on the nature of their matrices, *i.e.,* solid or liquid, the samples will be extracted to obtain the total solvent-extractable materials (TSEMs). A liquid-liquid extraction will be then required for water samples and liquid-solid extraction for sediment or similar matrices (**Figure 1.14**), however, some environmental samples might require other extraction methods to simplify highly complex samples. Routinely it is common to carry out a silica gel chromatography column on a petroleum sample or an extract to obtain a saturate (F1) and aromatic (F2) hydrocarbon fraction eluted with different polarity solvents. Both fractions are then analysed by either GC-FID or GC-MS. If more extensive analysis is required, particularly to separate evaporation and water washing effects comprehensive two-dimensional gas chromatography (GCxGC) is a powerful analysis that has been applied in multiple cases of oil spills and biodegradation (Arey et al., 2005; Reddy et al., 2012; Lima et al., 2019)

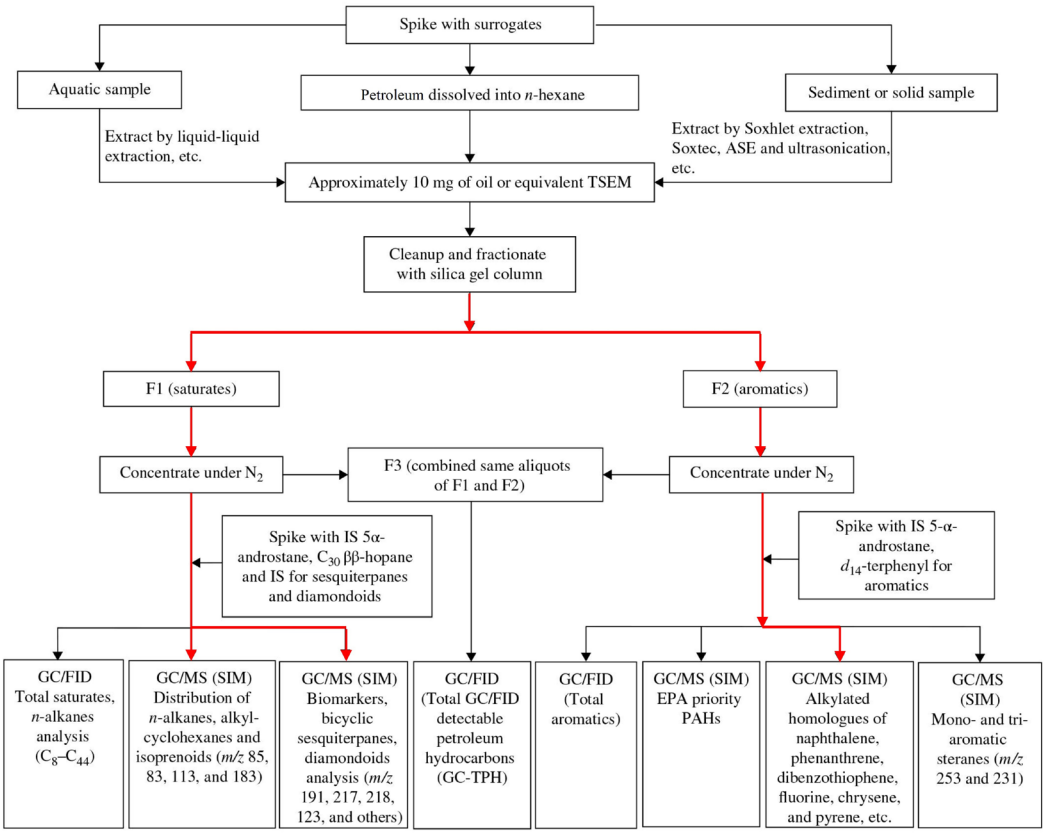

Figure 1.14. Flowchart of analytical steps applied for petroleum profiling and detection of environmental markers of biodegradation. Red arrows display a similar path followed in this research. TSEM: Total solvent-extractable materials. SIM: Selected Ion Monitoring, which mode is used for quantitative analysis. GC-TPH: GC analysis of Total Petroleum Hydrocarbons (Fingas, 2015).

To assess the biodegradation level of a typical petroleum sample various compounds are investigated by GC-MS by their diagnostic ions. These include, *n*-alkanes (*m/z* 85), regular isoprenoids (*m/z* 183), *nor*hopanes (*m/z* 177), hopanes (*m/z* 191) and steranes (*m/z* 217). Typical target ions for the diamondoids are as follows, adamantane and alkyladamantanes (*m/z* 135, 136, 149, 163, and 177) and diamantane and alkyldiamantanes (*m/z* 187, 188, 201) (Grice et al., 2000). For the aromatic fractions the following ions are routinely investigated: naphthalene and alkylnaphthalenes (*m/z* 128, 142, 156, 170, and 184) and phenanthrene and alkylphenanthrenes (*m/z* 178, 192, 206, 220, and 234) (Fisher et al., 1996; Trolio et al., 1999). Based on various observations (see **Figure 1.7**), it is possible to assess the level of biodegradation of a given petroleum sample.

1.6.5. Scanning Electronic Microscopy

Scanning Electronic Microscopy (SEM) can be used to image a wide range of surfaces at micro to sub-nanometre scales (Stokes, 2008). The surface under analysis is targeted by a focused beam of electrons. This interaction produces a variety of signals, which are then captured by detectors (Suga et al., 2014). SEM is extensively used to study crystalline structures, surface topography (morphology), electrical behaviour, and the elemental composition of materials, in which case it is coupled to an X-ray detector (Vernon-Parry, 2000). SEM is a gold-standard approach for characterising biological and geological samples (Black et al., 1999; Golding et al., 2016).

Samples usually do not require extensive preparation, however, in conventional SEM instruments complete dehydration is a prerequisite (Suga et al., 2014). Although, this preparation step may affect the original structure, causing shrinkage or structural distortion, it might be still considered for preliminary examination, particularly when other more sophisticated techniques are not suitable for the type of sample to be analysed (*e.g.* wet-contaminated materials).

1.7. Petroleum biodegradation under hypersaline conditions

Petroleum contamination in hypersaline settings is relatively common. During petroleum drilling, salt is usually added to the oil-based drilling sludge to prevent hydration of the drilled rocks. The production (hypersaline) water pumped from oil-wells is typically discharged in large man-made wetlands (McGenity, 2010; Abed et al., 2014). These events are more likely to happen in arid-, and semi-arid- oil-producing countries, such as Saudi Arabia or Kuwait (Abed et al., 2006; Berthe-Corti and Nachtkamp, 2010; Al-awadhi et al., 2012), and have occurred especially after the Gulf War in 1991 when active oil wells were vandalised (Fowler et al., 1993).

Scientific interest in the environmental impact of these extractive activities (*i.e.,* drilling) has extended the characterisation of microbial communities in hypersaline environments, and their ability to survive or biodegrade petroleum (Fowler et al., 1993). Biodegradation involves microbial-induced decomposition of complex organic matter such as organic pollutants into simpler and potentially less-harmful compounds (Margesin and Schinner, 2001). Degradation of petroleum under hypersaline conditions is still a matter of controversy (McGenity, 2010; Edbeib et al., 2016). While

biodegradation of petroleum has been reported to occur to some extent under hypersaline conditions (Díaz et al., 2000; Yang et al., 2000), other studies have reported a negative correlation between salinity and the degree of petroleum biodegradation (Riis et al., 2003; Kleinsteuber et al., 2006; Qin et al., 2012). These contradictory findings are likely have been caused by the lack of a standard framework for analysis, and variability in the type of analysed samples or environmental conditions, hindering accurate correlation of the results from different studies (Martins and Peixoto, 2012).

Few studies have systematically investigated the effect of petroleum exposure (PE) on extreme environments, such as hypersaline microbial mats, focusing on microbial ecology or organic geochemistry (Benthien et al., 2004; Abed et al., 2006; Bordenave et al., 2007; Llirós et al., 2008; **Figure 1.15**). Experimental constraints, using microcosms or artificial ecosystems (Fahy and McKew, 2010), have been applied to reduce the complexity of hypersaline habitats and simulate natural or field variables under lab conditions. For example, Benthien et al. (2004) exposed pristine (hypersaline) microbial mats from a solar saltern (France) to a sulfur-rich petroleum, monitored the photosynthetic activity and other physicochemical parameters using microsensors, and performed general petroleum profiling using both GC-FID and GC-MS. However, the study did not report microbial community changes, and the assessment of biodegradation was based on relative peaks heights rather than using diagnostic ratios, claiming a total removal of *n*-alkanes (C_{21}-C_{28}) after 100 days of exposure. Abed et al. (2006) also performed biodegradative experiments in microbial mats already exposed to oil spills, using organo-clay complexes as contaminant carriers, and incorporating molecular approaches (*i.e.,* 16S rRNA gene). This study explored the microbial diversity of the samples and found that 15% of bacterial communities belonged to unclassified taxa. Nowadays with the expansion of reference sequence databases, the majority of microbial taxa can now be taxonomically assigned to genus level and microbial interactions can be elucidated more precisely. Unfortunately, gene transcripts are not commonly analysed in parallel and no attempts have been made to predict the functional diversity of the active community. Another attempt to assess the effects of petroleum in hypersaline microbial mats from Salins-de-Giraud (France) was performed by Bordenave et al. (2007). The latter study represents one of the most consistent and systematic studies in comparison to the

aforementioned. The response of microbial mat communities to PE was studied through parallel analysis of 16S rDNA (total microbial community) and 16S rRNA-cDNA (active microbial community) using a mesocosm set up that was monitored for up to one year. However, at the time of this study, two different portions of samples were required to independently extract DNA and RNA. Therefore, the DNA and RNA did not necessarily stem from the same lysed cells and the observed shifts in the total vs active microbial communities were not directly comparable. Furthermore, the conclusions reached in terms of microbial resilience in those habitats were not based on a microbial diversity index, and the discussion was focused only on low-rank taxonomical levels. Thus, there is still a limited understanding of how hypersaline microbial mat communities respond to short- and long-term disturbances at both taxonomic and functional (physiological) levels (Shade et al., 2012a). PE is likely to select for previously unknown microbial taxa in these understudied hypersaline environments. They may utilise novel strategies for the bioremediation of petroleum spills under hypersaline conditions that do not occur in non-hypersaline environments where bioremediation strategies are already in place (Margesin and Schinner, 2001; Edbeib et al., 2016).

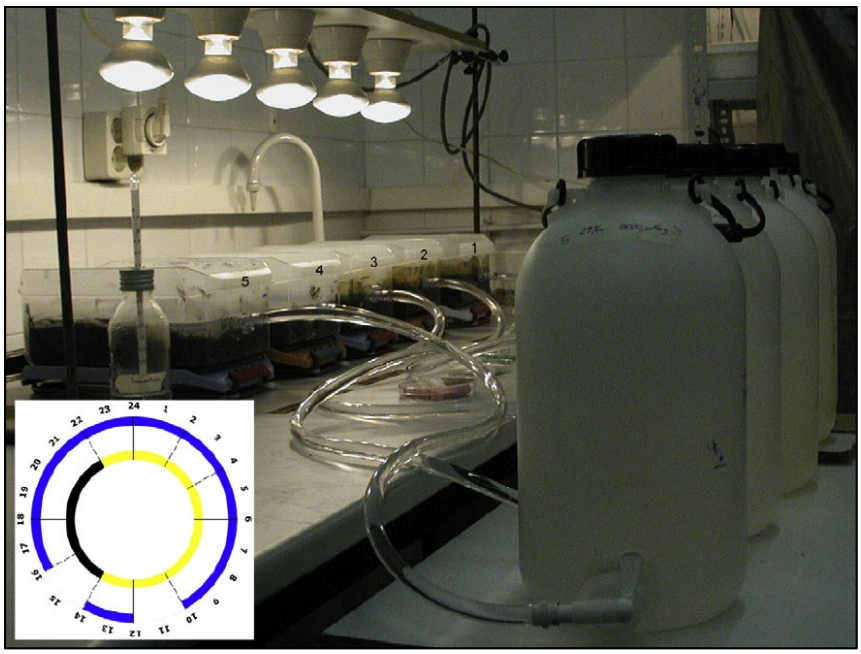

Figure 1.15. Image depicting experimental setup for simulating an oil spill using microbial mats (numbered plastic container holding the samples) from Ebro Delta, Mediterranean Sea (Llirós et al., 2008).

1.7.1. Petroleum degrader's organisms in hypersaline habitats

Microorganisms capable of degrading petroleum under hypersaline conditions have been found in all three kingdoms: Bacteria, Archaea and Eukarya. Commonly known halophilic or halotolerant degraders of hydrocarbons include members of Marinobacter, Alcanivorax, Halomonadaceae, Halobacteriales, Bacillales, Actinobacteria, as well as several fungi and yeasts (Margesin and Schinner, 2001; McGenity, 2010; **Figure 1.16**). To be able to survive under extremely saline conditions, these microorganisms require to uptake organic solutes (as explained in the section 1.4.2 'Microbial mats' microbiome from hypersaline environments'), and simultaneously cope with high concentrations of salt as shown in laboratory enriched cultures (Oren, 2008; Xu et al., 2018). Some studies support, for example, that a microbial consortium is needed to fully degrade xenobiotics rather than one isolated organism (Ghosh et al., 2016; Che and Men, 2019). *Marinobacter* and *Alcanivorax*, members of Gammaproteobacteria clade, have been observed to thrive in up to 20% NaCl, in the presence of alkanes; and they are known for their capacity of producing emulsifiers which activate degrading mechanisms of aliphatic hydrocarbons (McGenity, 2010; Fathepure, 2014). Also, Halomonadaceae comprises at least seven genera associated with the degradation of organic compounds, *i.e.,* *Chromohalobacter*, *Halotalea*, *Zymobacter*, *Halomonas*, *Carnimonas*, *Cobetia*, and *Modicisalibacter* (McGenity, 2010). It is known that some of these microbes use substantial amounts of EPS to break down hydrocarbons as a strategy of adaptation to toxic conditions (Borgne et al., 2008).

Interestingly, several bacterial genera have shown abilities to degrade aromatic compounds, such as 4-hydroxybenzoate (Cuadros-Orellana et al., 2006). Others gram-positive microbes belonging to Firmicutes and Actinobacteria phyla have some oil-degrading strains, such as: genera *Geobacillus* (also thermophilic, order Bacillales) and *Streptomyces albiaxialis*, respectively (Kuznetsov et al., 1992; Chamkha et al., 2008). Certain Archaea have also been shown to be capable of degrading hydrocarbons. For instance, Halobacteriaceae (Halobacteriales) are typically found in hypersaline environments incl. oil reservoirs. In addition, at least three orders within the Fungi Kingdom: Hypocreales, Pleosporales and Micosphaerellales (Obuekwe et al., 2005; Kristanti et al., 2018; Abou Khalil et al., 2021) have been found to be capable of degrading hydrocarbons under hypersaline conditions.

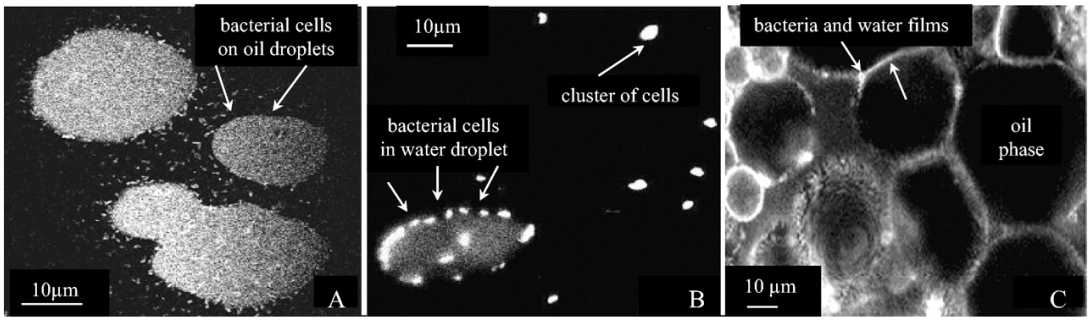

Figure 1.16. Confocal micrographs illustrating oil-degrading bacteria capability of stabilising oil-water emulsions. (A) Hexadecane drops covered by *Rhodococcus erythropolis 20S-E1-c* (Actinobacteria). (B) Fluorescent oil-degrading bacteria around water-in-oil emulsion. (C) *n*-hexadecane drops (black) in presence of *Acetinobacter venetianus* RAG-1 (Dorobantu et al., 2004).

1.8. Study site: Shark Bay

Shark Bay (SB) is located at the most westerly point of Western Australia, approximately 800 km north of Perth (**Figure 1.17**). In December 1991, SB was listed as a World Heritage site for possessing all four of the natural 'outstanding universal values' (OUV): (1) it possesses unique natural beauty and aesthetics; (2) it contains living representatives of early life on Earth (*i.e.,* stromatolites); (3) it is home to unique habitats representing unusual biological and ecological processes, which are also important for understanding the evolution of ancient ecosystems; (4) it contains important natural habitats and threatened species that require conservation in order to protect their biological diversity. SB relies on the Australian Federal Government to safeguard its integrity to guarantee its future preservation. Additionally, any industrial activity that could significantly impact the region is regulated under commonwealth 'Environment Protection and Biodiversity Conservation Act 1999' (EPBC Act) (NESP Earth Systems and Climate Change Hub, 2018).

Shark Bay covers 2.2 million hectares and is characterised by a shallow sea south of the Carnarvon Basin (Playford et al., 2013). It possesses three major arms: Edel Land, Peron, and Nanga peninsulas, which divides the area into three embayments: Henry Freycinet, L'Haridon Bight and Hamelin Pool (**Figure 1.17**). This study investigates samples collected in two ecosystems from Hamelin Pool. Hamelin Pool is an embayment which possesses a restricted water circulation, and limited exchange with

oceanic waters (Suosaari et al., 2016). Faure Sill, a prominent sediment barrier covered by seagrass, is known to be a restriction due to it dissipating tidal current energy coming from the open sea, because of a bottom friction effect. Thus, a progressive wave, from north of the Bay, may last up to 9 hours before reaching the southern area (Burling et al., 2003). Additionally, the combination of this water circulation restriction, low recharge either by precipitation or (riverine and runoff) freshwater input, and a high evaporation rate causes the development of a salinity gradient (halocline), reaching more than 70 PSU in the Nilemah Embayment (Suosaari et al., 2016). Hamelin Pool is home of a diverse range of supratidal-intertidal and subtidal microbial mat habitats, covering 50 km^2 and 570 km^2 of the embayment, respectively (Jahnert and Collins, 2011).

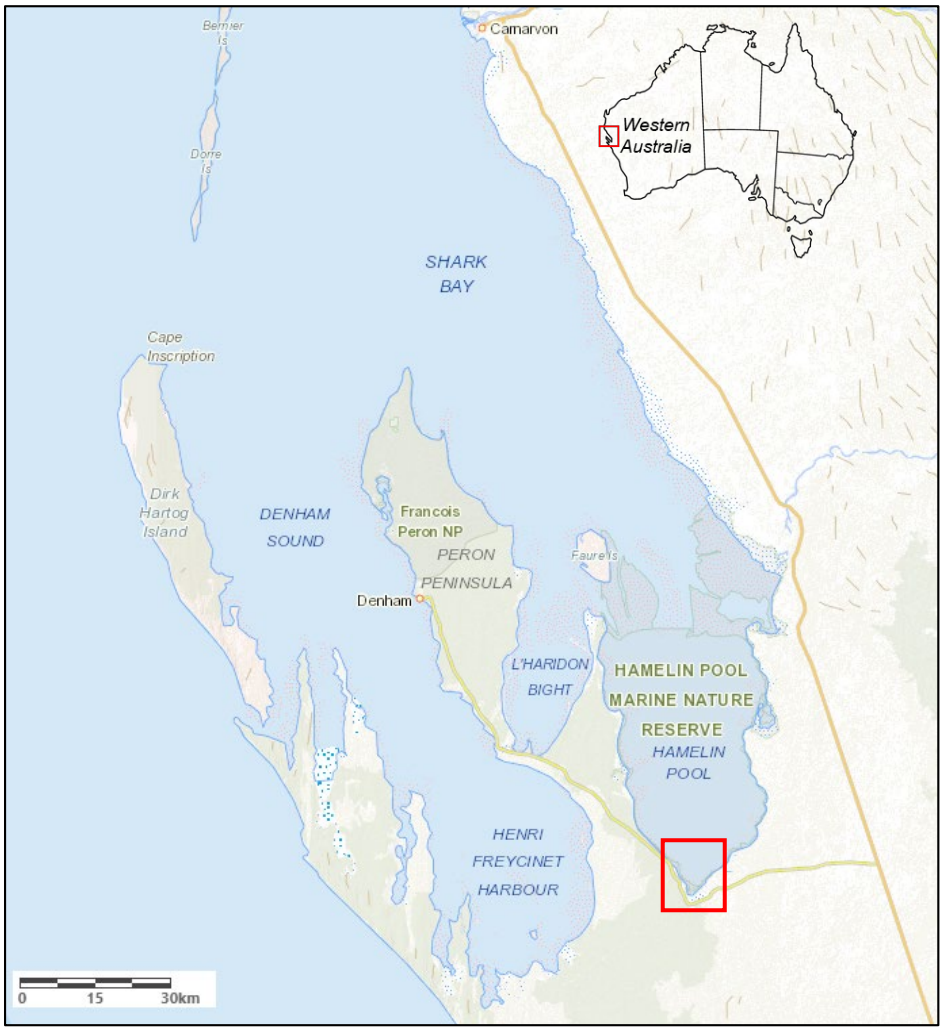

Figure 1.17. Shark Bay region and the location of Nilemah embayment (red square). Image partly modified from Geoscience Australia.

1.8.1. Nilemah embayment and types of microbial mats observed

The Nilemah embayment is characterised as a tidal flat covering an area of 16 km^2, (Jahnert and Collins, 2013). Geomorphologically, the Nilemah embayment consists of several biogeomorphic units (**Figure 1.18**): Supratidal Beach Face Unit (SBFU), mat platform unit (MPU), Transitional Microbial-Mosaic Unit (TMMU), Sand-sheet with Low-elevation Microbialite Unit (SLMU) and Microbial Ridge Swale and Column Unit (MRSCU) (Morris et al., 2019). The MRSCU represents the area where samples have been collected and studied in this research. This unit includes lower intertidal to upper subtidal zones.

Six dominant types of microbial mats have been identified in the Nilemah embayment: smooth, pustular, blister, tufted, colloform and pavement (Jahnert and Collins, 2013). Their location in the biogeomorphic units is based on abiotic factors (*i.e.,* water depth, salinity, light exposure, tide regime, wave energy, *etc*) and these factors likely play a role in the selection of the various members of the microbial mat microbiome (Jahnert and Collins, 2011, 2012). For example, salinity gradient exerts particular pressure against eukaryotic metazoans, known as potential bioturbators, that contributes with the protection of the structures (fabrics) of these types of microbialites (Edgcomb et al., 2014).

For this research project, the more accessible smooth and pustular mat types which possess geologically distinctive macro and micro characteristics were selected. Smooth mats inhabit the MRSCU unit and thrive in the lower intertidal zone with high sediment supply. They exhibit millimetric sub-horizontal well-developed lamination, a smooth and light brown-green surface, a fine-grained carbonate matrix, shell fragments and visible layers of organic matter (**Figure 1.19**, top) (Jahnert and Collins, 2013; Morris et al., 2019). The lamination resembles the structure of 'classic' stromatolites. Pustular mats are more abundant in the upper subtidal zone as low-elevated microbialitic ridges and are exposed to moderate to low sediment deposition. They show brown-green 'gelatinous' pustules, without lamination, patches of micritic (calcium carbonate mud) cement, a mix of poorly sorted bioclastic and mineral grains, and exhibit limited lithification. Micritic cement can be seen inside of the mucilage produced on the top (**Figure 1.19**, bottom) (Jahnert and Collins, 2013; Morris et al., 2019)

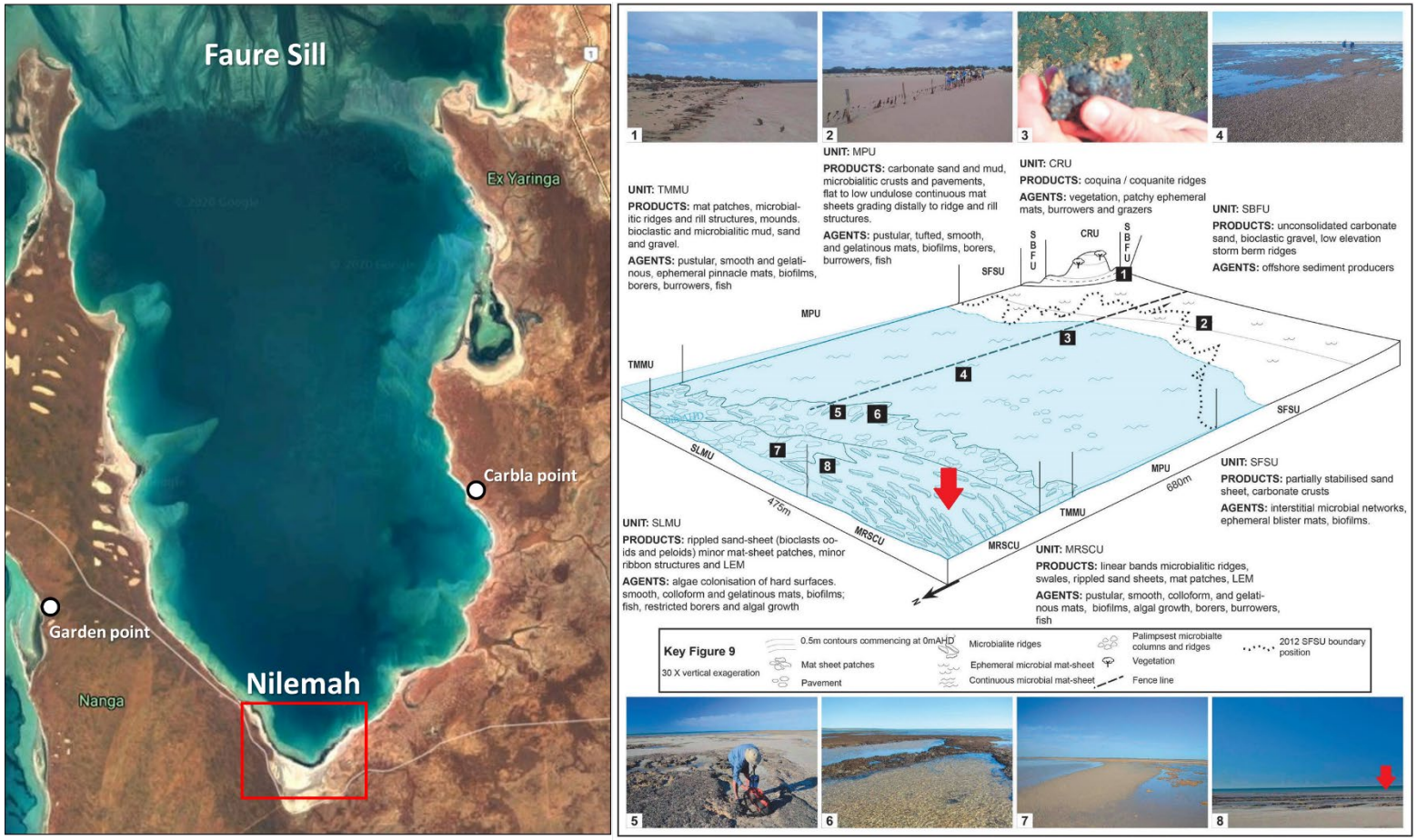

Figure 1.18. Hamelin Pool area and the location of microbial mat ecosystems: Nilemah embayment, Garden Point, and Carbla Point, source: Google (left). Biogeomorphic unit scheme and general description at Nilemah embayment. Symbols (microbialites) not at scale. Vertical exaggeration 30X (Morris et al., 2019). Red arrow indicates the sub-unit where samples were collected in this study (right).

Figure 1.19. Microbial mats from Nilemah embayment in Hamelin Pool, SB. Smooth (top) and pustular (bottom). Photo credit: Prof Alex Sessions.

1.8.2. Nilemah embayment microbiomes: prior studies

Smooth and pustular mat microbiomes from different locations in Hamelin Pool have been previously investigated under pristine conditions by either culture-based or culture-independent techniques (Allen et al., 2009; Wong et al., 2015, 2018; Ruvindy et al., 2016; Babilonia et al., 2018; Campbell et al., 2020). A phylogenetic study based on 16S rRNA carried out at Nilemah embayment showed that both smooth and pustular mat communities possess high microbial diversity. Of the 58 identified bacterial and candidate phyla, 20 have been poorly described, but represented 16%

(smooth) and 10% (pustular) of the total community (Wong et al., 2015). This is also in agreement with another study performed on similar habitats inside Hamelin Pool (Telegraph station) (Allen et al., 2009). In terms of bacterial composition, the upper 2 mm photic zone of the smooth mat was dominated by Cyanobacteria (mainly *Microcoleus* with lower contributions of filamentous *Halomicronema* and sulfide-tolerant *Leptolyngbya*). Proteobacteria and Bacteroidetes were abundant in the surface layer but also deeper in the mat, followed by Chloroflexi, Firmicutes, and Planctomycetes. Similarly, Cyanobacteria, Proteobacteria and Bacteroidetes were highly abundant in the top layer of pustular mats. *Halomicronema* was the more abundant cyanobacterium in this type of mat. Proteobacteria were also dominant below the surface layer.

Recently, the taxonomic and functional diversity of the active microbial communities in smooth and pustular microbial mats from Nilemah embayment was determined based on full length assembled 16S rRNA and functional gene transcripts (mRNA), which showed that bacteria surpass archaeal and eukaryotic communities at a ratio of 90:3:7% respectively (Campbell et al., 2020). However, their bacterial microbial compositions differ between these two types of mats. Smooth mats were dominated by Bacteroidetes, Deltaproteobacteria, Alpha- and Gammaproteobacteria, Spirochaetes and Planctomycetes. Instead, pustular mats showed a higher proportion of Alphaproteobacteria and Planctomycetes as the most dominant taxa, followed by Bacteroidetes, Deltaproteobacteria, Cyanobacteria and Chloroflexi (**Figure 1.20**). In terms of Archaeal and Eukaryotic communities, only a few phyla were represented between the more abundant organisms (**Figure 1.20**, left). Three eukaryotic linages were identified, *i.e.*, Stramenopiles, Rhizaria and Alveolata, while only one archaeal phylum was detected, *i.e.*, Euryarchaeota (Campbell et al., 2020). However, other studies carried out in this area (Nilemah embayment) have also highlighted the importance of either archaea or microbial dark matter as key pieces of these complex microbial ecosystems (Ruvindy et al., 2016; Wong et al., 2020). Interestingly, similar environments in Hamelin Pool (Carbla Point), with a focus on Eukaryotic diversity have been also documented (Edgcomb et al., 2014). The latter study discussed the potential of metazoan as bioturbators that might influence mat fabrics, when these and other organisms (as protists) are in the search for consuming or degrading EPS.

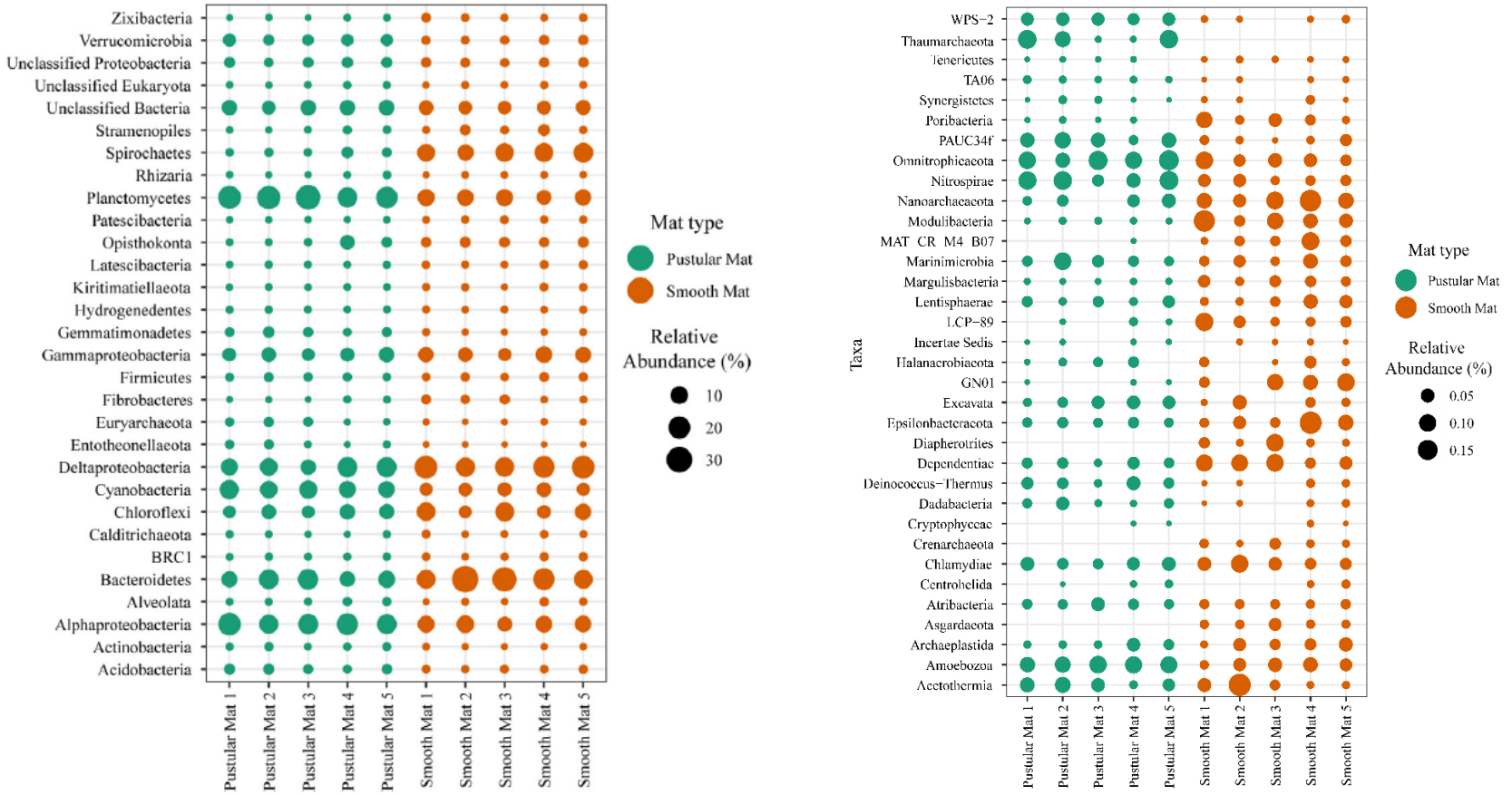

Figure 1.20. Microbiome of smooth and pustular microbial mats collected in Nilemah embayment. Dot plots show composition and abundance of most abundant (left) and less abundant taxa (right). Mats #1, 2 and 3 were collected in July 2016, while those # 4 and 5 were taken in April 2017. Microbiomes cover Archaea, Bacteria and Eukaryote taxonomical groups using SILVA database (SSU rRNA genes) (Campbell et al., 2020).

Shotgun metagenomic and metatranscriptomic analysis have recently revealed the functional genetic potential and active gene expression in samples from the Nilemah embayment (Ruvindy et al., 2016; Wong et al., 2018; Campbell et al., 2020). Smooth and pustular mats were shown to share a high number of pathways involved in carbon and nitrogen fixation, as well as sulfur metabolism. Furthermore, functional annotations related to osmoadaptative traits were identified, which are typical mechanisms to deal with high levels of salinity, including chloride, trehalose and glycine betaine as compatible solutes (Ruvindy et al., 2016). A recent metatrascriptomic survey of pristine pustular and smooth mats of Nilemah Bay recently confirmed that the genes in these pathways were actively transcribed (Campbell et al., 2020). In addition, the latter study confirmed that anoxygenic photosynthesis and the Arnon-Buchanan cycle (chemoautotrophy) are key pathways of the carbon cycle in these mat types. Furthermore, they identified gene transcripts involved in a variety of processes associated with sensing chemical gradients and combating low nutrient conditions (*i.e.,* Ni, Fe) (Campbell et al., 2020).

1.8.3. Microbialites from Shark Bay and early life

Modern stromatolites and microbial mats that are exposed to harsh ecological conditions, such as those found in Shark Bay, have been linked to the history of life on Earth. Ancient rocks poorly preserve relicts of microbial organisms, however, modern analogues offer some clues about the evolution of life (Burns et al., 2009). One of the more distinctive feature is their "physical" morphological similarities (Walter et al., 1976; Horodyski, 1977; Bosak et al., 2009). Modern conically laminated stromatolites are classic counterparts of microbial mats due to their comparable shape, internal structures, and geometrical features (Petroff et al., 2010). The formation' model refers to a biogenic origin: modern specimens seem to grow not only due to the presence of filamentous cyanobacterial communities, which are key in the precipitation of a carbonate matrix, but also to a diverse range of other microbes (Burns et al., 2009). Additionally to this, a hiatus in the sedimentation processes is crucial to allow microbialites flourish (Walter et al., 1976; Brock, 1978; Jones et al., 2002; Burns et al., 2009).

The 'biogenic' model is particularly important because it supports theories about the role of microorganisms in the regulation of ancient global climate and other processes. Microbialites, as self-sustained communities, may be influenced by the oxygenation of the early-Earth atmosphere (Hoehler et al., 2001; Des Marais, 2003), as well as carbon, nitrogen, hydrogen and sulfur biogeochemical cycles (Visscher and Stolz, 2005). For example, mid-Neoproterozoic to Phanerozoic ponds, lakes or oceans might have been as saline as current contemporary environments (Arp et al., 2001; Schinteie and Brocks, 2017). Moreover, unique stromatolites as those found in Pilbara Craton, in Australia (Strelley Pool Chert – SPC) represent a solid evidence of the existence of life as old as 3,430 Myr (Archaean) as abiotic paleoenvironmental models alone cannot explain such a variety of morphotypes (**Figure 1.21**) (Allwood et al., 2006). Genomic analysis of microbial mats from Shark Bay also revealed the presence of hydrogenases, which may be linked to H_2 and methanogenesis, which are critical functional traits for survival and evolution of organisms under anoxic habitats (Wong et al., 2018; Carnevali et al., 2019; Campbell et al., 2020). Thus, by understanding this organo-sedimentary structures and their biotic and abiotic interactions, it will be possible to ecologically and functionally explore their role either in the geologic record of Earth or other extraterrestrial places under extreme conditions (Foster and Mobberley, 2010).

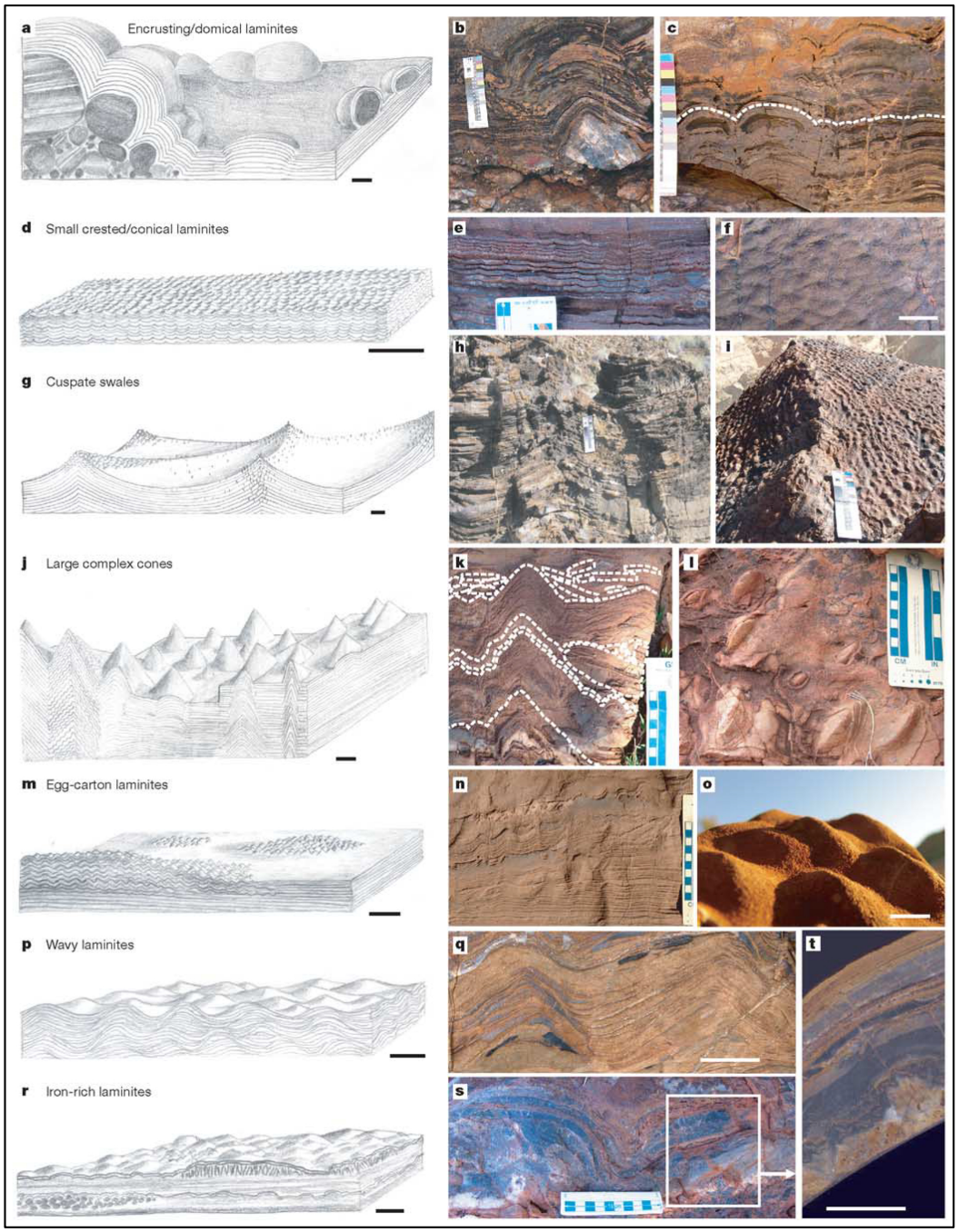

Figure 1.21. Conceptual models in 3D (left) and outcrop images (right) of different stromatolites facies of the Strelley Pool Chert (Pilbara Craton, Australia). "**a–c**, 'Encrusting/domical laminites'; **d–f**, 'small crested/conical laminites'; **g–i**, 'cuspate swales'; **j–l**, 'large complex cones' (dashed lines in k trace lamina shape and show outlines of intraclast conglomerate piled against the cone at two levels).**m–o**, 'Egg-carton laminites'; **p, q**, 'wavy laminites'; **r–t**, 'iron-rich laminites'. The scale card in b, h and i is 18 cm. The scale card increments in c, e, k, l, n and s are 1 cm. The scale bar in o is about 1 cm. The scale bars in the remaining pictures are about 5 cm" (Allwood et al., 2006).

1.9. Environmental risk of Shark Bay to petroleum spill

Most recently (July 2020), petroleum industry stakeholders have nominated two large areas just northwest of the SB region to be considered within the annual offshore petroleum exploration acreage release[11]. The Australian Government has used this consultation process as an initiative for investment and expansion of petroleum exploration across the country, especially in WA, where this industry is flourishing[12]. Their recent proposal for exploration near to SB (May 2020) includes more than 40,000 km^2 offshore areas divided in two blocks: W20-29 and W20-30 (**Figure 1.22**). There is a debate between the parties involved, particularly on how this could impact the environment in the region. Authorities from WA Mines and Petroleum Department and industry analysts claim that: (1) the development of this project might take years to start to operate; (2) areas do not overlap with any maritime protected parks; and (3) the industry have been working for years near to other protected areas following safety environmental plans without major incidents[13]. The Federal Government would need to endorse the nomination before any activities commence. Nevertheless, environmental agencies have raised their concerns since the developments are close to two World Heritage sites: SB and Ningaloo Reef.

In 2011, the Australian Maritime Safety Authority (AMSA) requested the independent consultancy environmental company Det Norske Veritas (DNV, 2011) to estimate the risk of pollution from marine oil spills in Australian ports and waters (Report # PP002916 – Rev 5, 14 December 2011). This request is based on AMSA's 'National Plan to Combat Pollution of the Sea by Oil and Other Noxious and Hazardous Substances' and 'National Maritime Emergency Response Arrangements' (NMERA) (AMSA, 2012). In this report, DNV calculated the frequencies of oil spills in Australia and identified the areas with the highest petroleum spill risks and their main sources, but also projected the potential risks up to 2020.

[11] https://consult.industry.gov.au/offshore-exploration/2020-acreage-release-consultation/
[12] https://www.industry.gov.au/strategies-for-the-future/investing-in-offshore-petroleum-exploration#:~:text=The%20annual%20offshore%20petroleum%20exploration,gas%20exploration%20in%20Australian%20waters
[13] https://www.abc.net.au/news/2020-06-16/world-heritage-sites-skirt-areas-nominated-for-exploration/12359418

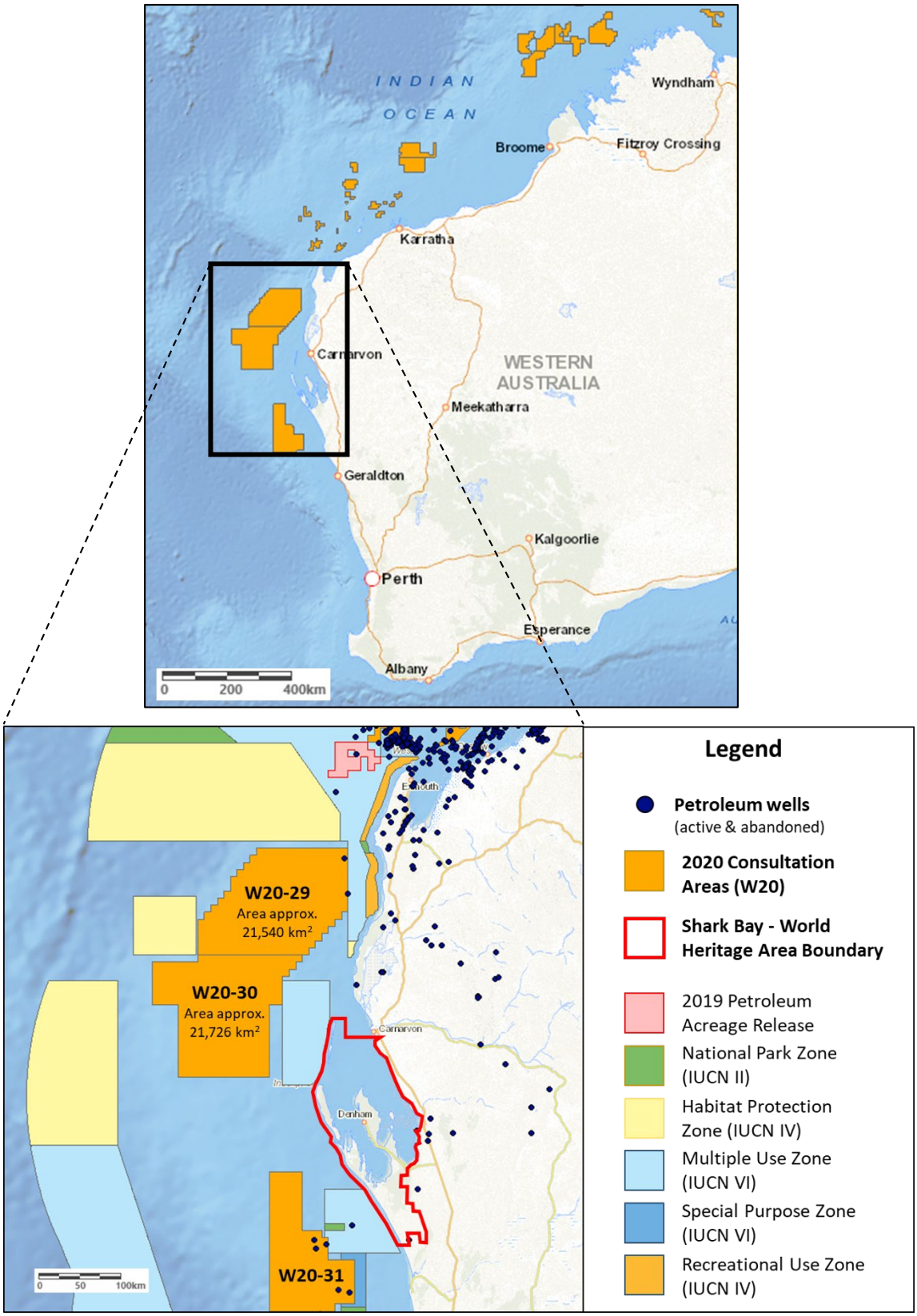

Figure 1.22. Map of Western Australia illustrating the offshore areas nominated for potential petroleum exploration –subjected to Federal Government decision- (top). Shark Bay (red polygon) and the nearby regions with details of current and future use offshore areas (bottom). Map partly modified, adding information from: https://nopims.dmp.wa.gov.au/Nopims/GISMap/Map.

DNV estimated the overall national exceedance frequencies for oil spills (2011). Spills of less than 1 tonne (per year) occur most frequently and are usually shore-based (32%) closely followed by commercial vessels (28%), while trading ships at sea (33%) and offshore production (32%) are responsible for annual oil spills greater than 10,000 tones (**Table 1.3**). This environmental company also calculated the environmental sensitivity index (ESI), which represents the '*average environmental impact of a tonne of oil spilled in a specific location, relative to a spill of the same oil in a defined baseline location*'. ESI is projected to be comparative to the cost of the oil spill. This index includes human-use, biological and physical resources at a ratio of 3:5:2. SB and part of the Carnarvon coastline are the regions with the highest ESI in WA (WA6; **Figure 1.23**).

Table 1.3. Annual quantities of oil expected to be spilled for 2011 and projected by 2020. Values do not reflect environmental sensitivity (AMSA, 2012).

Source	2011		2020	
	Tonnes/year	%	Tonnes/year	%
Trading ships at sea	212	**22.3**	387	**32.2**
Trading ships at port	174	18.3	337	**28.1**
Small commercial vessels	2	0.2	2	0.2
Offshore production	310	**32.7**	217	18.1
Offshore drilling	209	**22.0**	209	17.4
Shore-based	42	4.5	48	4.0
Total	*948*	*100.0*	*1,200*	*100.0*

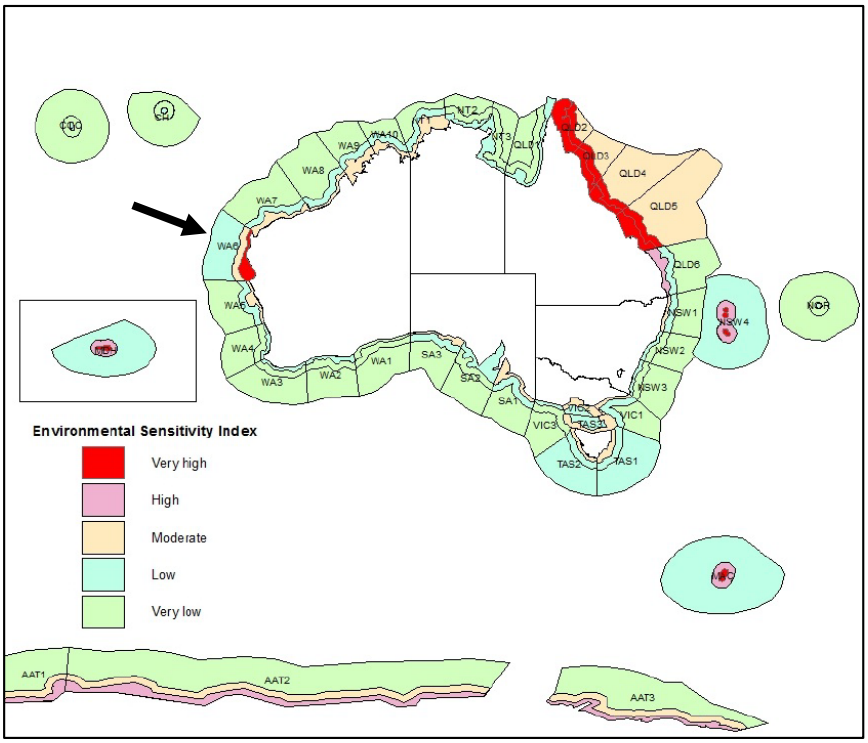

Figure 1.23. Environmental sensitivity index (ESI) of Australian coastline and open sea (deep-sea) zones (DNV, 2011). The arrow indicates Zone WA6 (Shark Bay region).

The contributions of the sources to the oil spill risk were also estimated for 2011 and projected for 2020 (**Table 1.3**). In 2011, offshore production, trading ships at sea and offshore drilling were the most important sources of oil pollution, while trading ships at sea and ships at port were expected to become the most important contributors by 2020. SB has been classified as a 'high' risk area for oil spills due to its environmental sensitivity and close proximity to shipping routes and port facilities (**Figure 1.24**). The overall environmental risk index (ERI) by 2020 was then calculated and expressed in millions of A$ per year (**Table 1.4**), indicating that trading activities (ships at sea and ports) would increase significantly over time. Obviously, these estimations and projections for 2020 were carried out a decade ago. To the best of our knowledge these public reports and figures have not been updated while the WA government has continued stimulating mining and oil investment and activities in the region to boost the Australian economy. Therefore, it is to be expected that the risks have increased, and that previously overlooked risk factors need to be investigated and incorporated in the predictions. A previously overlooked risk factor includes global warming, which will be discussed next.

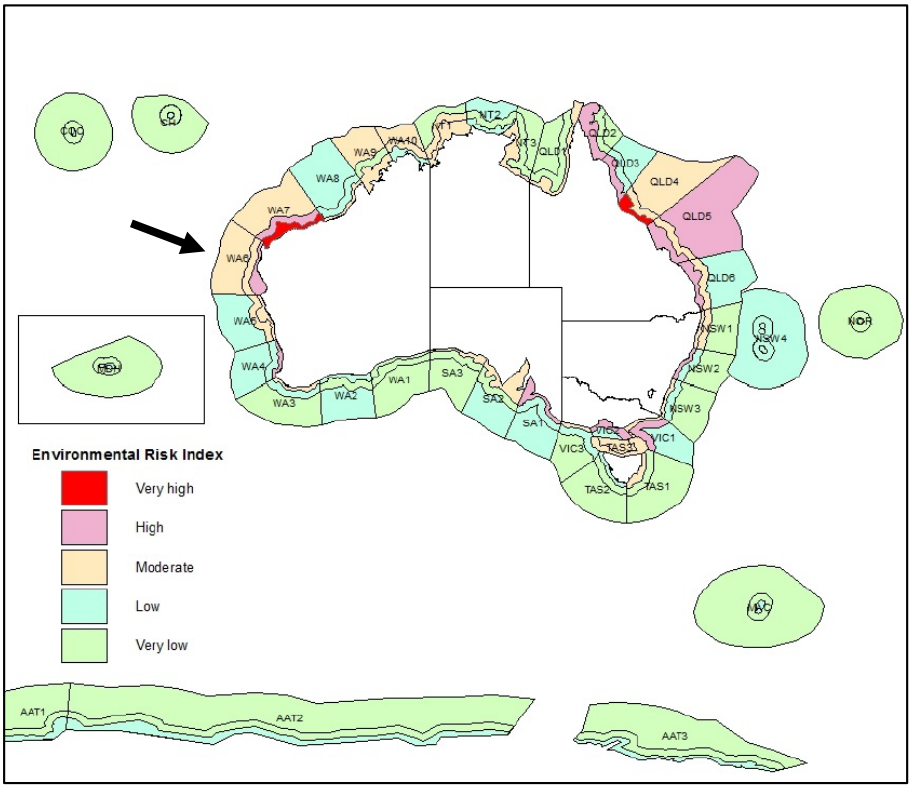

Figure 1.24. Environmental risk index (ERI) of Australian coastline and open sea (deep-sea) zones (DNV, 2011). The arrow indicates Zone WA6 (Shark Bay region).

Table 1.4. Environmental risk index (ERI) projected by 2020 (AMSA, 2012).

Source	ERI (million A$/year)	% increase by 2020
Trading ships at sea	5.0	91
Trading ships at port	10.9	141
Small commercial vessels	0.1	7
Offshore production	0.4	-28%
Offshore drilling	0.2	0
Shore-based	1.2	14

1.9.1. Global warming: beyond current threats to Shark Bay

Extreme marine heat events, storm events, and air temperature are likely to increase in frequency and/or intensity in the context of continuing global warming. This could contribute to a reduction in seagrass expansion in the Wooramel seagrass barrier located in the Faure Sill sediment bank in SB (NESP Earth Systems and Climate Change Hub, 2018). This was evident in 2010-2011 when a marine heatwave in the region resulted in a loss of 900 km^2 of seagrass. If these events continue to increase in frequency and/or intensity, the seagrass meadows could become irreversible damaged. With this natural barrier reduced or lost, the tidal energy from the open ocean may not dissipate with the same forcefulness. In this scenario of global warming combined with increased petroleum exploration and shipping activities in the region, future oil spills that occur offshore, are more likely to reach the southern areas at a higher rate. In addition to global warming, the current balance that maintains SB pristine ecosystems may also be inevitably impacted in the near future by ocean acidification and sea level rise (Reinold et al., 2019). Hence, various organisations have recommended that it will become necessary to: (1) collect existing data and identify knowledge gaps; (2) research the adaptive capacity and/or vulnerability of SB ecosystems to different threats (*i.e.,* thresholds for impact and protection of vital habitats involved in Shark Bay's OUV)[14]; (3) prepare an adaptation strategy plan; and (4) implement the adaptation plan (NESP Earth Systems and Climate Change Hub, 2018).

1.10. Aims of the thesis

The research outlined in this thesis investigates the ecological response of smooth and pustular microbial mats *(i.e.,* microbialites) from the Hamelin Pool embayment of Shark Bay, WA to short- and long-term PE, as well as their capacity to biodegrade petroleum (if any). Analyses were conducted to measure shifts with increasing petroleum impact on their microbial and functional diversity and stress response

[14] "*Were petroleum exploration or production to be permitted within the Area, many of the world heritage values would be adversely affected by the routine impacts of those activities, and there would be the risk of further impacts resulting from accidents. In many cases, especially in marine areas, there are insufficient data to confidently state that a proposal would not have the potential to create a significant impact, particularly with regard to the more intensive and long-term activities such as drilling and production, processing, storage and transport of the product*" (Environmental Protection Authority, 2003).

mechanisms, to ultimately assess the vulnerability of these habitats to potential petroleum spill events. Since this region became a World Heritage site in 1991, several reports have considered the environmental risks to the area, and proposed management plans to tackle the effect of anthropogenic activities and naturogenic change (AMSA, 2012; NESP Earth Systems and Climate Change Hub, 2018; Reinold et al., 2019). Environmental risks are likely to increase in future years since industrial activities in the region, including petroleum (especially natural gas) exploration and extraction, will continue to expand. Therefore, it is imperative that persuasive and systematic evidence of all potential scenarios, including worst-case, becomes publicly available to support current and future environmental protection of this unique region and its natural habitats.

To achieve these aims, an experimental approach was used to simulate the natural environmental setting under lab-controlled conditions. During a time-series incubation experiment, living microbial smooth and pustular mats were exposed to contamination with two different types of petroleum (*i.e.,* an aliphatic-aromatic rich –Barrow Island 6200 #101– and a biodegraded petroleum –Windalia #410– as pollutants). Two types of disturbances were studied: long-term disturbance (up to 120 days) and short-term disturbance (10 days) with a recovery period up to 1 year. Conventional 16S rRNA gene and transcript profiling was performed to identify bacterial and archaeal community responses to PE (total and active microbiome, respectively), while PICRUSt2 was implemented to predict the metabolic capabilities of the petroleum-exposed total *vs.* active mat microbiomes. GC-MS analysis was also used to examine the molecular composition of the original petroleum samples and monitor any subsequent changes in the petroleum over time to determine the susceptibility of certain petroleum hydrocarbons to weathering and/or biodegradation by the two different microbial mats.

Chapter 2 examines the microbial community dynamics of smooth and pustular microbial mats collected from SB subjected to long-term PE. These experiments were performed on extant mats in a series of laboratory-controlled microcosm experiments conducted for up to 120 days. The mats (approx. 350 cm^3) were spiked (0.02% v/v) with regional petroleum from Barrow Island. Control experiments without the addition

of petroleum were conducted in parallel. Sub-samples of biofilm formed under petroleum incubation were also studied by 16S rRNA profiling and Scanning Electron Microscopy (SEM) to elucidate their associated microbiome and tentative structures, respectively.

The purpose of the research in **Chapter 3** was to predict functional mechanisms of the mat microbiomes associated with PE using the 16S rRNA dataset obtained in **Chapter 2**. The approach implemented the newest PICRUSt2 pipeline to predict gene family relative abundances categorised by KEGG mapping. This chapter also provides a brief chemical assessment of the organic fraction extracted from the petroleum-water interphase, to explore the susceptibility of certain petroleum hydrocarbons to biodegradation in SB microbial mats over time. Comparison of the predicted functionalities associated with degradation of hydrocarbons and preliminary chemical diagnostic attempt to enlighten their actual capabilities for biodegradation.

Chapter 4 assessed and compared the adaptive responses and resilience of microbial mats to short-term (10-day pulse) petroleum impact over a recovery period of 1 year. The mats (approx. 60 g wet weight) were subjected to 16.60 % v/v of a regional petroleum from the Windalia Formation. Differences observed between short- (this chapter) and long-term disturbances (**Chapter 2** and **Chapter 3**) were also discussed.

Finally, **Chapter 5** debates the advantages and limitations of laboratory-controlled incubation experiments, as well as the methods applied for microbial and functional diversity assessment. It also discusses the similarities and differences in the ecological responses of both mats to PE, and how they are reflected in their resilience and resistance to disturbances. It briefly examines the potential of these microbial ecosystems to biodegrade hydrocarbons and provides a list of recommendations for improving the experimental design and future work.

1.11. References

Abed, R. M. M., Al-Kharusi, S., Prigent, S., and Headley, T. (2014). Diversity, Distribution and Hydrocarbon Biodegradation Capabilities of Microbial Communities in Oil-Contaminated Cyanobacterial Mats from a Constructed Wetland. *PLoS ONE* 9, e114570. doi:10.1371/journal.pone.0114570.

Abed, R. M. M., Al-Thukair, A., and De Beer, D. (2006). Bacterial diversity of a cyanobacterial mat degrading petroleum compounds at elevated salinities and temperatures: Microbial mats from Saudi Arabia. *FEMS Microbiology Ecology* 57, 290–301. doi:10.1111/j.1574-6941.2006.00113.x.

Abou Khalil, C., Prince, V. L., Prince, R. C., Greer, C. W., Lee, K., Zhang, B., et al. (2021). Occurrence and biodegradation of hydrocarbons at high salinities. *Science of The Total Environment* 762, 143165. doi:10.1016/j.scitotenv.2020.143165.

Aitken, C. M., Jones, D. M., and Larter, S. R. (2004). Anaerobic hydrocarbon biodegradation in deep subsurface oil reservoirs. *Nature* 431, 291–294. doi:10.1038/nature02922.

Al-awadhi, H., Al-mailem, D., Dashti, N., Khanafer, M., and Radwan, S. (2012). Indigenous hydrocarbon-utilizing bacterioflora in oil-polluted habitats in Kuwait, two decades after the greatest man-made oil spill. *Archives of Microbiology; Berlin* 194, 689–705. doi:http://dx.doi.org.dbgw.lis.curtin.edu.au/10.1007/s00203-012-0800-7.

Allen, M. A., Goh, F., Burns, B. P., and Neilan, B. A. (2009). Bacterial, archaeal and eukaryotic diversity of smooth and pustular microbial mat communities in the hypersaline lagoon of Shark Bay. *Geobiology* 7, 82–96. doi:10.1111/j.1472-4669.2008.00187.x.

Allison, S. D., and Martiny, J. B. H. (2008). Resistance, resilience, and redundancy in microbial communities. *PNAS* 105, 11512–11519. doi:10.1073/pnas.0801925105.

Allwood, A. C., Walter, M. R., Kamber, B. S., Marshall, C. P., and Burch, I. W. (2006). Stromatolite reef from the Early Archaean era of Australia. *Nature* 441, 714–718. doi:10.1038/nature04764.

Almeida, A., Mitchell, A. L., Tarkowska, A., and Finn, R. D. (2018). Benchmarking taxonomic assignments based on 16S rRNA gene profiling of the microbiota from commonly sampled environments. *Gigascience* 7. doi:10.1093/gigascience/giy054.

Antwis, R. E., Griffiths, S. M., Harrison, X. A., Aranega-Bou, P., Arce, A., Bettridge, A. S., et al. (2017). Fifty important research questions in microbial ecology. *FEMS Microbiol Ecol* 93. doi:10.1093/femsec/fix044.

Arey, J. S., Nelson, R. K., Xu, L., and Reddy, C. M. (2005). Using Comprehensive Two-Dimensional Gas Chromatography Retention Indices To Estimate Environmental Partitioning Properties for a Complete Set of Diesel Fuel Hydrocarbons. *Anal. Chem.* 77, 7172–7182. doi:10.1021/ac051051n.

Arp, G., Reimer, A., and Reitner, J. (2001). Photosynthesis-Induced Biofilm Calcification and Calcium Concentrations in Phanerozoic Oceans. *Science* 292, 1701–1704. doi:10.1126/science.1057204.

Aßhauer, K. P., Wemheuer, B., Daniel, R., and Meinicke, P. (2015). Tax4Fun: predicting functional profiles from metagenomic 16S rRNA data. *Bioinformatics* 31, 2882–2884. doi:10.1093/bioinformatics/btv287.

Austin, B. (2017). The value of cultures to modern microbiology. *Antonie van Leeuwenhoek* 110, 1247–1256. doi:10.1007/s10482-017-0840-8.

Australian Maritime Safety Authority (AMSA) (2012). Report on the 2011/12 Review of the National Plan to Combat Pollution of the Sea by Oil and Other Hazardous and Noxious Substances and the National Maritime Emergency Response Arragements (2011-2012). Australian Government Available at: https://www.amsa.gov.au/sites/default/files/natplan-review-report.pdf [Accessed June 9, 2020].

Babilonia, J., Conesa, A., Casaburi, G., Pereira, C., Louyakis, A. S., Reid, R. P., et al. (2018). Comparative Metagenomics Provides Insight Into the Ecosystem Functioning of the Shark Bay Stromatolites, Western Australia. *Front. Microbiol.* 9, 1359. doi:10.3389/fmicb.2018.01359.

Bahram, M., Anslan, S., Hildebrand, F., Bork, P., and Tedersoo, L. (2019). Newly designed 16S rRNA metabarcoding primers amplify diverse and novel archaeal taxa from the environment. *Environ Microbiol Rep* 11, 487–494. doi:10.1111/1758-2229.12684.

Balvočiūtė, M., and Huson, D. H. (2017). SILVA, RDP, Greengenes, NCBI and OTT — how do these taxonomies compare? *BMC Genomics* 18, 114. doi:10.1186/s12864-017-3501-4.

Barton, L. L., Northup, D. E., and Northup, D. E. (2011). *Microbial Ecology*. Hoboken, United States: John Wiley & Sons, Incorporated Available at: http://ebookcentral.proquest.com/lib/curtin/detail.action?docID=697468 [Accessed June 27, 2020].

Bayona, J. M., Domínguez, C., and Albaigés, J. (2015). Analytical developments for oil spill fingerprinting. *Trends in Environmental Analytical Chemistry* 5, 26–34. doi:10.1016/j.teac.2015.01.004.

Bell, E. M. ed. (2012). *Life at extremes: environments, organisms and strategies for survival*. Wallingford: CABI doi:10.1079/9781845938147.0000.

Benthien, M., Wieland, A., Oteyza, T. G. de, Grimalt, J. O., and Kühl, M. (2004). Oil-contamination effects on a hypersaline microbial mat community (Camargue,

France) as studied with microsensors and geochemical analysis. *Ophelia* 58, 135–150. doi:10.1080/00785236.2004.10410221.

Berthe-Corti, L., and Nachtkamp, M. (2010). "Bacterial Communities in Hydrocarbon-Contaminated Marine Coastal Environments," in *Handbook of Hydrocarbon and Lipid Microbiology*, ed. K. N. Timmis (Berlin, Heidelberg: Springer), 2349–2359. doi:10.1007/978-3-540-77587-4_171.

Black, K. S., Paterson, D. M., and Davidson, I. R. (1999). Sediment Microfabric of Oil Rig Drill Spoil Heaps: Preliminary Observations Using Low-Temperature Scanning Electron Microscopy. *Environmental Science & Technology* 33, 1983–1990. doi:10.1021/es981091r.

Bolyen, E., Rideout, J. R., Dillon, M. R., Bokulich, N. A., Abnet, C. C., Al-Ghalith, G. A., et al. (2019). Reproducible, interactive, scalable and extensible microbiome data science using QIIME 2. *Nature biotechnology* 37, 852–857.

Bordenave, S., Goñi-Urriza, M. S., Caumette, P., and Duran, R. (2007). Effects of Heavy Fuel Oil on the Bacterial Community Structure of a Pristine Microbial Mat. *Applied and Environmental Microbiology* 73, 6089–6097. doi:10.1128/AEM.01352-07.

Borgne, S. L., Paniagua, D., and Vazquez-Duhalt, R. (2008). Biodegradation of Organic Pollutants by Halophilic Bacteria and Archaea. *MMB* 15, 74–92. doi:10.1159/000121323.

Bosak, T., Liang, B., Sim, M. S., Petroff, A. P., and Hoffman, P. F. (2009). Morphological Record of Oxygenic Photosynthesis in Conical Stromatolites. *Proceedings of the National Academy of Sciences of the United States of America* 106, 10939–10943.

Botton, S., van Heusden, M., Parsons, J. R., Smidt, H., and van Straalen, N. (2006). Resilience of microbial systems towards disturbances. *Critical reviews in microbiology* 32, 101–112.

Brock, T. D. (1978). "Stromatolites: Yellowstone Analogues," in *Thermophilic Microorganisms and Life at High Temperatures* Springer Series in Microbiology., ed. T. D. Brock (New York, NY: Springer), 337–385. doi:10.1007/978-1-4612-6284-8_11.

Bukin, Y. S., Galachyants, Y. P., Morozov, I. V., Bukin, S. V., Zakharenko, A. S., and Zemskaya, T. I. (2019). The effect of 16S rRNA region choice on bacterial community metabarcoding results. *Sci Data* 6. doi:10.1038/sdata.2019.7.

Burling, M. C., Pattiaratchi, C. B., and Ivey, G. N. (2003). The tidal regime of Shark Bay, Western Australia. *Estuarine, Coastal and Shelf Science* 57, 725–735. doi:10.1016/S0272-7714(02)00343-8.

Burns, B. P., Anitori, R., Butterworth, P., Henneberger, R., Goh, F., Allen, M. A., et al. (2009). Modern analogues and the early history of microbial life. *Precambrian Research* 173, 10–18. doi:10.1016/j.precamres.2009.05.006.

Bursy, J., Pierik, A. J., Pica, N., and Bremer, E. (2007). Osmotically induced synthesis of the compatible solute hydroxyectoine is mediated by an evolutionarily conserved ectoine hydroxylase. *J Biol Chem* 282, 31147–31155. doi:10.1074/jbc.M704023200.

Campbell, M. A., Grice, K., Visscher, P. T., Morris, T., Wong, H. L., White, R. A. I., et al. (2020). Functional Gene Expression in Shark Bay Hypersaline Microbial Mats: Adaptive Responses. *Front. Microbiol.* 11. doi:10.3389/fmicb.2020.560336.

Canfield, D. E., and Marais, D. J. D. (1991). Aerobic Sulfate Reduction in Microbial Mats. *Science* 251, 1471–1473.

Cánovas, D., Vargas, C., Csonka, L. N., Ventosa, A., and Nieto, J. J. (1996). Osmoprotectants in Halomonas elongata: high-affinity betaine transport system and choline-betaine pathway. *J Bacteriol* 178, 7221–7226. doi:10.1128/jb.178.24.7221-7226.1996.

Caporaso, J. G., Lauber, C. L., Walters, W. A., Berg-Lyons, D., Lozupone, C. A., Turnbaugh, P. J., et al. (2011). Global patterns of 16S rRNA diversity at a depth of millions of sequences per sample. *Proceedings of the National Academy of Sciences of the United States of America* 108, 4516–4522.

Carnevali, P., Schulz, F., Castelle, C., Kantor, R., Shih, C. C., Sharon, I., et al. (2019). Hydrogen-based metabolism as an ancestral trait in lineages sibling to the Cyanobacteria. *Nature Communications* 10. doi:http://dx.doi.org/10.1038/s41467-018-08246-y.

Chamkha, M., Mnif, S., and Sayadi, S. (2008). Isolation of a thermophilic and halophilic tyrosol-degrading Geobacillus from a Tunisian high-temperature oil field. *FEMS Microbiol Lett* 283, 23–29. doi:10.1111/j.1574-6968.2008.01136.x.

Che, S., and Men, Y. (2019). Synthetic microbial consortia for biosynthesis and biodegradation: promises and challenges. *Journal of Industrial Microbiology and Biotechnology* 46, 1343–1358. doi:10.1007/s10295-019-02211-4.

Chen, M., Hernandez-Prieto, M. A., Loughlin, P. C., Li, Y., and Willows, R. D. (2019). Genome and proteome of the chlorophyll f-producing cyanobacterium Halomicronema hongdechloris: adaptative proteomic shifts under different light conditions. *BMC Genomics* 20, 207. doi:10.1186/s12864-019-5587-3.

Chiarucci, A., Nascimbene, J., Campetella, G., Chelli, S., Dainese, M., Giorgini, D., et al. (2019). Exploring patterns of beta-diversity to test the consistency of biogeographical boundaries: A case study across forest plant communities of Italy. *Ecology and Evolution* 9, 11716–11723. doi:10.1002/ece3.5669.

Chilingar, G. V., Buryakovsky, L. A., Eremenko, N. A., and Gorfunkel, M. V. (2005). *Geology and geochemistry of oil and gas*. Amsterdam: Elsevier.

Ciccarelli, F. D., Doerks, T., Mering, C. von, Creevey, C. J., Snel, B., and Bork, P. (2006). Toward Automatic Reconstruction of a Highly Resolved Tree of Life. *Science* 311, 1283–1287. doi:10.1126/science.1123061.

Clarridge, J. E. (2004). Impact of 16S rRNA Gene Sequence Analysis for Identification of Bacteria on Clinical Microbiology and Infectious Diseases. *Clin Microbiol Rev* 17, 840–862. doi:10.1128/CMR.17.4.840-862.2004.

Coolen, M. J. L., Muyzer, G., Rijpstra, W. I. C., Schouten, S., Volkman, J. K., and Sinninghe Damsté, J. S. (2004). Combined DNA and lipid analyses of sediments reveal changes in Holocene haptophyte and diatom populations in an Antarctic lake. *Earth and Planetary Science Letters* 223, 225–239. doi:10.1016/j.epsl.2004.04.014.

Coolen, M. J. L., and Overmann, J. (2007). 217 000-year-old DNA sequences of green sulfur bacteria in Mediterranean sapropels and their implications for the reconstruction of the paleoenvironment. *Environ. Microbiol.* 9, 238–249. doi:10.1111/j.1462-2920.2006.01134.x.

Cuadros-Orellana, S., Pohlschröder, M., and Durrant, L. R. (2006). Isolation and characterization of halophilic archaea able to grow in aromatic compounds. *International Biodeterioration & Biodegradation* 57, 151–154. doi:10.1016/j.ibiod.2005.04.005.

Czaczyk, K., and Myszka, K. (2007). Biosynthesis of Extracellular Polymeric Substances. Polish J. of Environ. Stud. 16, 799–806.

DasSarma, S., and Arora, P. (2001). Halophiles. *Encyclopedia of Life Sciences*.

Des Marais, D. (2003). Biogeochemistry of Hypersaline Microbial Mats Illustrates the Dynamics of Modern Microbial Ecosystems and the Early Evolution of the Biosphere. *Biological Bulletin* 204, 160–167. doi:10.2307/1543552.

Díaz, M., Grigson, S. J. W., Peppiatt, C. J., and Burgess, J. G. (2000). Isolation and Characterization of Novel Hydrocarbon-Degrading Euryhaline Consortia from Crude Oil and Mangrove Sediments. *Mar. Biotechnol.* 2, 522–532. doi:10.1007/s101260000037.

Ding, H., and Valentine, D. L. (2008). Methanotrophic bacteria occupy benthic microbial mats in shallow marine hydrocarbon seeps, Coal Oil Point, California. *Journal of Geophysical Research: Biogeosciences* 113. doi:10.1029/2007JG000537.

DNV (2011). Assessment of the Risk of Pollution from Marine Oil Spills in Australian Ports and Waters. Det Norske Veritas LTD., UK Available at: https://www.amsa.gov.au/sites/default/files/2011-12-mp-dnv-risk-assessment-final-report-oil-spill.pdf [Accessed May 14, 2020].

Dorobantu, L. S., Yeung, A. K. C., Foght, J. M., and Gray, M. R. (2004). Stabilization of Oil-Water Emulsions by Hydrophobic Bacteria. *Appl. Environ. Microbiol.* 70, 6333–6336. doi:10.1128/AEM.70.10.6333-6336.2004.

Doronina, N. V., Trotsenko, Y. A., and Tourova, T. P. (2000). Methylarcula marina gen. nov., sp. nov. and Methylarcula terricola sp. nov.: novel aerobic, moderately halophilic, facultatively methylotrophic bacteria from coastal saline environments. *Int J Syst Evol Microbiol* 50 Pt 5, 1849–1859. doi:10.1099/00207713-50-5-1849.

Douglas, G. M., Maffei, V. J., Zaneveld, J., Yurgel, S. N., Brown, J. R., Taylor, C. M., et al. (2019). PICRUSt2: An improved and extensible approach for metagenome inference. *BioRxiv; Cold Spring Harbor*. doi:http://dx.doi.org.dbgw.lis.curtin.edu.au/10.1101/672295.

Dupraz, C., Reid, R. P., Braissant, O., Decho, A. W., Norman, R. S., and Visscher, P. T. (2009). Processes of carbonate precipitation in modern microbial mats. *Earth-Science Reviews* 96, 141–162. doi:10.1016/j.earscirev.2008.10.005.

Edbeib, M. F., Wahab, R. A., and Huyop, F. (2016). Halophiles: biology, adaptation, and their role in decontamination of hypersaline environments. *World J Microbiol Biotechnol* 32, 135. doi:10.1007/s11274-016-2081-9.

Edgcomb, V. P., Bernhard, J. M., Summons, R. E., Orsi, W., Beaudoin, D., and Visscher, P. T. (2014). Active eukaryotes in microbialites from Highborne Cay, Bahamas, and Hamelin Pool (Shark Bay), Australia. *The ISME Journal* 8, 418–429. doi:10.1038/ismej.2013.130.

Emerson, J. B., Adams, R. I., Román, C. M. B., Brooks, B., Coil, D. A., Dahlhausen, K., et al. (2017). Schrödinger's microbes: Tools for distinguishing the living from the dead in microbial ecosystems. *Microbiome* 5. doi:10.1186/s40168-017-0285-3.

Environmental Protection Authority (2003). A strategic assessment of the compatibility of petroleum Industry activities with the environmental values and cultural uses of the Shark Bay World Heritage Area. Available at: https://www.epa.wa.gov.au/strategic-assessment-compatibility-petroleum-industry-activities-environmental-values-and-cultural.

Evans, T. G., and Hofmann, G. E. (2012). Defining the limits of physiological plasticity: how gene expression can assess and predict the consequences of ocean change. *Philos Trans R Soc Lond B Biol Sci* 367, 1733–1745. doi:10.1098/rstb.2012.0019.

Fahy, A., and McKew, B. (2010). "Microcosms," in *Handbook of Hydrocarbon and Lipid Microbiology*, ed. K. N. Timmis (Berlin, Heidelberg: Springer Berlin Heidelberg), 3523–3527. doi:10.1007/978-3-540-77587-4_275.

Faith, D. P. (1992). Conservation evaluation and phylogenetic diversity. *Biological conservation* 61, 1–10.

Fathepure, B. Z. (2014). Recent studies in microbial degradation of petroleum hydrocarbons in hypersaline environments. *Front Microbiol* 5. doi:10.3389/fmicb.2014.00173.

Fingas, M. F. (2015). *Handbook of Oil Spill Science and Technology*. Somerset, United States: John Wiley & Sons, Incorporated Available at: http://ebookcentral.proquest.com/lib/curtin/detail.action?docID=1895871 [Accessed July 24, 2020].

Fisher, S. J., Alexander, R., and Kagi, R. I. (1996). Biodegradation of Alkylnaphthalenes in Sediments Adjacent to an Off-Shore Petroleum Production Platform. *Polycyclic Aromatic Compounds* 11, 35–42. doi:10.1080/10406639608544647.

Flemming, H.-C., Neu, T. R., and Wozniak, D. J. (2007). The EPS Matrix: The "House of Biofilm Cells." *Journal of Bacteriology* 189, 7945–7947. doi:10.1128/JB.00858-07.

Foster, J. S., and Mobberley, J. M. (2010). "Past, Present, and Future: Microbial Mats as Models for Astrobiological Research," in *Microbial Mats: Modern and Ancient Microorganisms in Stratified Systems* Cellular Origin, Life in Extreme Habitats and Astrobiology., eds. J. Seckbach and A. Oren (Dordrecht: Springer Netherlands), 563–582. doi:10.1007/978-90-481-3799-2_29.

Fowler, S. W., Readman, J. W., Oregioni, B., Villeneuve, J.-P., and McKay, K. (1993). Petroleum hydrocarbons and trace metals in nearshore Gulf sediments and biota before and after the 1991 war: An assessment of temporal and spatial trends. *Marine Pollution Bulletin* 27, 171–182. doi:10.1016/0025-326X(93)90022-C.

Franks, J., and Stolz, J. F. (2009). Flat laminated microbial mat communities. *Earth-Science Reviews* 96, 163–172. doi:10.1016/j.earscirev.2008.10.004.

Gad, S. (2014). Petroleum Hydrocarbons. *Encyclopedia of Toxicology* 3. doi:10.1016/B978-0-12-386454-3.00899-X.

Gagnon, M. M., Grice, K., and Kagi, R. I. (1999). Biochemical and chemical parameters for aquatic ecosystem health assessments adapted to the Australian oil and gas industy. *The APPEA Journal* 39, 584–599. doi:10.1071/aj98038.

George, S. C., Boreham, C. J., Minifie, S. A., and Teerman, S. C. (2002). The effect of minor to moderate biodegradation on C5 to C9 hydrocarbons in crude oils. *Organic Geochemistry* 33, 1293–1317. doi:10.1016/S0146-6380(02)00117-1.

Ghosh, S., Chowdhury, R., and Bhattacharya, P. (2016). Mixed consortia in bioprocesses: role of microbial interactions. *Applied Microbiology and Biotechnology* 100, 4283–4295. doi:10.1007/s00253-016-7448-1.

Glasby, T. M., and Underwood, A. J. (1996). Sampling to differentiate between pulse and press perturbations. *Environ Monit Assess* 42, 241–252. doi:10.1007/BF00414371.

Golding, C. G., Lamboo, L. L., Beniac, D. R., and Booth, T. F. (2016). The scanning electron microscope in microbiology and diagnosis of infectious disease. *Scientific Reports* 6, 26516. doi:10.1038/srep26516.

Grice, K., Alexander, R., and Kagi, R. I. (2000). Diamondoid hydrocarbon ratios as indicators of biodegradation in Australian crude oils. *Organic Geochemistry* 31, 67–73. doi:10.1016/S0146-6380(99)00137-0.

Gunde-Cimerman, N., Plemenitaš, A., and Oren, A. (2018). Strategies of adaptation of microorganisms of the three domains of life to high salt concentrations. *FEMS Microbiology Reviews; Delft* 42, 353–375. doi:http://dx.doi.org.dbgw.lis.curtin.edu.au/10.1093/femsre/fuy009.

Hariharan, J., Sengupta, A., Grewal, P., and Dick, W. A. (2017). Functional Predictions of Microbial Communities in Soil as Affected by Long-term Tillage Practices. *Agricultural & Environmental Letters* 2, 170031. doi:https://doi.org/10.2134/ael2017.09.0031.

Hassani, M. A., Durán, P., and Hacquard, S. (2018). Microbial interactions within the plant holobiont. *Microbiome* 6. doi:10.1186/s40168-018-0445-0.

He, X., Zhang, Q., Jin, Y., Jiang, L., and Wu, R. (2020). Network mapping of root-microbe interactions in Arabidopsis thaliana. *bioRxiv*, 2020.11.24.397273. doi:10.1101/2020.11.24.397273.

Head, I. M., Jones, D. M., and Larter, S. R. (2003). Biological activity in the deep subsurface and the origin of heavy oil. *Nature* 426, 344–352. doi:10.1038/nature02134.

Heijs, S. K., Sinninghe Damsté, J. S., and Forney, L. J. (2005). Characterization of a deep-sea microbial mat from an active cold seep at the Milano mud volcano in the Eastern Mediterranean Sea. *FEMS Microbiol Ecol* 54, 47–56. doi:10.1016/j.femsec.2005.02.007.

Hoehler, T. M., Bebout, B. M., and Des Marais, D. J. (2001). The role of microbial mats in the production of reduced gases on the early Earth. *Nature* 412, 324–327.

Hook, S., Batley, G., Ross, A., Holloway, M., and Irving, P. (2017). *Oil Spill Monitoring Handbook*. Victoria, Australia: CSIRO Publishing Available at: http://ebookcentral.proquest.com/lib/curtin/detail.action?docID=4723035 [Accessed July 25, 2020].

Horodyski (1977). Lyngbya Mats at Laguna Mormona, Baja California, Mexico: Comparison with Proterozoic Stromatolites. *SEPM JSR* Vol. 47. doi:10.1306/212F732E-2B24-11D7-8648000102C1865D.

Hwang, B., Lee, J. H., and Bang, D. (2018). Single-cell RNA sequencing technologies and bioinformatics pipelines. *Experimental & Molecular Medicine* 50, 1–14. doi:10.1038/s12276-018-0071-8.

Iwai, S., Weinmaier, T., Schmidt, B. L., Albertson, D. G., Poloso, N. J., Dabbagh, K., et al. (2016). Piphillin: Improved Prediction of Metagenomic Content by Direct Inference from Human Microbiomes. *PLoS One* 11. doi:10.1371/journal.pone.0166104.

Jahnert, R. J., and Collins, L. B. (2011). Significance of subtidal microbial deposits in Shark Bay, Australia. *Marine Geology* 286, 106–111. doi:10.1016/j.margeo.2011.05.006.

Jahnert, R. J., and Collins, L. B. (2012). Characteristics, distribution and morphogenesis of subtidal microbial systems in Shark Bay, Australia. *Marine Geology* 303–306, 115–136. doi:10.1016/j.margeo.2012.02.009.

Jahnert, R. J., and Collins, L. B. (2013). Controls on microbial activity and tidal flat evolution in Shark Bay, Western Australia. *Sedimentology* 60, 1071–1099. doi:10.1111/sed.12023.

Jeanbille, M., Gury, J., Duran, R., Tronczynski, J., Ghiglione, J.-F., Agogué, H., et al. (2016). Chronic Polyaromatic Hydrocarbon (PAH) Contamination Is a Marginal Driver for Community Diversity and Prokaryotic Predicted Functioning in Coastal Sediments. *Front. Microbiol.* 7. doi:10.3389/fmicb.2016.01303.

Jessup, C. M., Kassen, R., Forde, S. E., Kerr, B., Buckling, A., Rainey, P. B., et al. (2004). Big questions, small worlds: microbial model systems in ecology. *Trends in Ecology & Evolution* 19, 189–197. doi:10.1016/j.tree.2004.01.008.

Jo, J.-H., Kennedy, E. A., and Kong, H. H. (2016). Research Techniques Made Simple: Bacterial 16S Ribosomal RNA Gene Sequencing in Cutaneous Research. *Journal of Investigative Dermatology* 136, e23–e27. doi:10.1016/j.jid.2016.01.005.

Jones, B., Renaut, R. W., Rosen, M. R., and Ansdell, K. M. (2002). Coniform Stromatolites from Geothermal Systems, North Island, New Zealand. *PALAIOS* 17, 84–103.

Jones, S. E., and Lennon, J. T. (2010). Dormancy contributes to the maintenance of microbial diversity. *Proc Natl Acad Sci U S A* 107, 5881–5886. doi:10.1073/pnas.0912765107.

Kanehisa, M., and Goto, S. (2000). KEGG: kyoto encyclopedia of genes and genomes. *Nucleic Acids Res* 28, 27–30. doi:10.1093/nar/28.1.27.

Kanehisa, M., Goto, S., Sato, Y., Furumichi, M., and Tanabe, M. (2012). KEGG for integration and interpretation of large-scale molecular data sets. *Nucleic Acids Research* 40, D109–D114. doi:10.1093/nar/gkr988.

Keer, J. T., and Birch, L. (2003). Molecular methods for the assessment of bacterial viability. *Journal of Microbiological Methods* 53, 175–183. doi:10.1016/S0167-7012(03)00025-3.

Kennicutt, M. C. (1988). The effect of biodegradation on crude oil bulk and molecular composition. *Oil and Chemical Pollution* 4, 89–112. doi:10.1016/S0269-8579(88)80014-5.

Killops, S., and Killops, V. (2005). *Introduction to Organic Geochemistry | Wiley Online Books*. 2nd ed. Blackwell Publishing Ltd Available at: https://onlinelibrary.wiley.com/doi/book/10.1002/9781118697214 [Accessed April 17, 2021].

Kim, M., Morrison, M., and Yu, Z. (2011). Evaluation of different partial 16S rRNA gene sequence regions for phylogenetic analysis of microbiomes. *Journal of Microbiological Methods* 84, 81–87. doi:10.1016/j.mimet.2010.10.020.

Kim, S., and Picardal, F. (2001). Microbial Growth on Dichlorobiphenyls Chlorinated on Both Rings as a Sole Carbon and Energy Source. *Appl Environ Microbiol* 67, 1953–1955. doi:10.1128/AEM.67.4.1953-1955.2001.

Kindzierski, V., Raschke, S., Knabe, N., Siedler, F., Scheffer, B., Pflüger-Grau, K., et al. (2017). Osmoregulation in the Halophilic Bacterium Halomonas elongata: A Case Study for Integrative Systems Biology. *PLoS One* 12. doi:10.1371/journal.pone.0168818.

Kleinsteuber, S., Riis, V., Fetzer, I., Harms, H., and Müller, S. (2006). Population Dynamics within a Microbial Consortium during Growth on Diesel Fuel in Saline Environments. *Appl. Environ. Microbiol.* 72, 3531–3542. doi:10.1128/AEM.72.5.3531-3542.2006.

Koo, H., Hakim, J. A., Morrow, C. D., Eipers, P. G., Davila, A., Andersen, D. T., et al. (2017a). Comparison of two bioinformatics tools used to characterize the microbial diversity and predictive functional attributes of microbial mats from Lake Obersee, Antarctica. *J Microbiol Methods* 140, 15–22. doi:10.1016/j.mimet.2017.06.017.

Koo, H., Mojib, N., Hakim, J. A., Hawes, I., Tanabe, Y., Andersen, D. T., et al. (2017b). Microbial Communities and Their Predicted Metabolic Functions in Growth Laminae of a Unique Large Conical Mat from Lake Untersee, East Antarctica. *Front. Microbiol.* 8, 1347. doi:10.3389/fmicb.2017.01347.

Kristanti, R. A., Hadibarata, T., Al Farraj, D. A., Elshikh, M. S., and Alkufeidy, R. M. (2018). Biodegradation Mechanism of Phenanthrene by Halophilic Hortaea sp. B15. *Water Air Soil Pollut* 229, 324. doi:10.1007/s11270-018-3969-9.

Kuhlmann, A. U., and Bremer, E. (2002). Osmotically Regulated Synthesis of the Compatible Solute Ectoine in Bacillus pasteurii and Related Bacillus spp. *Appl Environ Microbiol* 68, 772–783. doi:10.1128/AEM.68.2.772-783.2002.

Kuznetsov, V. D., Zaitseva, T. A., Vakulenko, L. V., and Filippova, S. N. (1992). Streptomyces albiaxialis sp. nov. - a new petroleum hydrocarbon-degrading species of thermo- and halotolerant Streptomyces. *Microbiology New York* 61, 62–67.

Kvenvolden, K. A. (2006). Organic geochemistry – A retrospective of its first 70 years. *Organic Geochemistry* 37, 1–11. doi:10.1016/j.orggeochem.2005.09.001.

Lagier, J.-C., Edouard, S., Pagnier, I., Mediannikov, O., Drancourt, M., and Raoult, D. (2015). Current and Past Strategies for Bacterial Culture in Clinical Microbiology. *Clinical Microbiology Reviews* 28, 208–236. doi:10.1128/CMR.00110-14.

Lane, D. J., Pace, B., Olsen, G. J., Stahl, D. A., Sogin, M. L., and Pace, N. R. (1985). Rapid determination of 16S ribosomal RNA sequences for phylogenetic analyses. *Proc Natl Acad Sci U S A* 82, 6955–6959.

Langille, M. G. I., Zaneveld, J., Caporaso, J. G., McDonald, D., Knights, D., Reyes, J. A., et al. (2013). Predictive functional profiling of microbial communities using 16S rRNA marker gene sequences. *Nat Biotechnol* 31, 814–821. doi:10.1038/nbt.2676.

Larter, S., Huang, H., Adams, J., Bennett, B., and Snowdon, L. R. (2012). A practical biodegradation scale for use in reservoir geochemical studies of biodegraded oils. *Organic Geochemistry* 45, 66–76. doi:10.1016/j.orggeochem.2012.01.007.

Leahy, J. G., and Colwell, R. R. (1990). Microbial degradation of hydrocarbons in the environment. *Microbiol Rev* 54, 305–315.

Li, R., Tun, H. M., Link to external site, this link will open in a new window, Jahan, M., Zhang, Z., Kumar, A., et al. (2017). Comparison of DNA-, PMA-, and RNA-based 16S rRNA Illumina sequencing for detection of live bacteria in water. *Scientific Reports (Nature Publisher Group); London* 7, 1–11. doi:http://dx.doi.org.dbgw.lis.curtin.edu.au/10.1038/s41598-017-02516-3.

Lima, M. F. B., Fernandes, G. M., Oliveira, A. H. B., Morais, P. C. V., Marques, E. V., Santos, F. R., et al. (2019). Emerging and traditional organic markers: Baseline study showing the influence of untraditional anthropogenic activities on coastal zones with multiple activities (Ceará coast, Northeast Brazil). *Marine Pollution Bulletin* 139, 256–262. doi:10.1016/j.marpolbul.2018.12.006.

Litchfield, C. D. (1998). Survival strategies for microorganisms in hypersaline environments and their relevance to life on early Mars. *Meteoritics & planetary science* 33, 813–819.

Little, A. E. F., Robinson, C. J., Peterson, S. B., Raffa, K. F., and Handelsman, J. (2008). Rules of Engagement: Interspecies Interactions that Regulate Microbial Communities. *Annual Review of Microbiology* 62, 375–401. doi:10.1146/annurev.micro.030608.101423.

Llirós, M., Gaju, N., de Oteyza, T. G., Grimalt, J. O., Esteve, I., and Martínez-Alonso, M. (2008). Microcosm experiments of oil degradation by microbial mats. II. The changes in microbial species. *Science of The Total Environment* 393, 39–49. doi:10.1016/j.scitotenv.2007.11.034.

Lozupone, C. A., Hamady, M., Kelley, S. T., and Knight, R. (2007). Quantitative and Qualitative β Diversity Measures Lead to Different Insights into Factors That

Structure Microbial Communities. *Appl Environ Microbiol* 73, 1576–1585. doi:10.1128/AEM.01996-06.

Ma, Y., Galinski, E. A., Grant, W. D., Oren, A., and Ventosa, A. (2010). Halophiles 2010: Life in Saline Environments. *Appl Environ Microbiol* 76, 6971–6981. doi:10.1128/AEM.01868-10.

Madigan, M., Bender, K., Buckley, D., Sattley, W. M., and Stahl, D. (2019). *Brock Biology of microorganisms*. 9th ed. Pearson.

Margesin, R., and Schinner, F. (2001). Biodegradation and bioremediation of hydrocarbons in extreme environments. *Applied Microbiology and Biotechnology* 56, 650–663.

Martins, L. F., and Peixoto, R. S. (2012). Biodegradation of petroleum hydrocarbons in hypersaline environments. *Braz J Microbiol* 43, 865–872. doi:10.1590/S1517-83822012000300003.

Matange, K., Tuck, J. M., and Keung, A. J. (2021). DNA stability: a central design consideration for DNA data storage systems. *Nat Commun* 12, 1–9. doi:10.1038/s41467-021-21587-5.

McGenity, T. J. (2010). "Halophilic Hydrocarbon Degraders," in *Handbook of Hydrocarbon and Lipid Microbiology*, ed. K. N. Timmis (Berlin, Heidelberg: Springer), 1939–1951. doi:10.1007/978-3-540-77587-4_142.

McIntyre, C. P., Harvey, P. M., Ferguson, S. H., Wressnig, A. M., Volk, H., George, S. C., et al. (2007). Determining the Extent of Biodegradation of Fuels Using the Diastereomers of Acyclic Isoprenoids. *Environmental Science & Technology* 41, 2452–2458. doi:10.1021/es0621288.

Moran, M. A., Satinsky, B., Gifford, S. M., Luo, H., Rivers, A., Chan, L.-K., et al. (2013). Sizing up metatranscriptomics. *ISME J* 7, 237–243. doi:10.1038/ismej.2012.94.

Morris, T. E., Visscher, P. T., O'Leary, M. J., Fearns, P. R. C. S., and Collins, L. B. (2019). The biogeomorphology of Shark Bay's microbialite coasts. *Earth-Science Reviews*, 102921. doi:10.1016/j.earscirev.2019.102921.

Mukherjee, A., Chettri, B., Langpoklakpam, J. S., Basak, P., Prasad, A., Mukherjee, A. K., et al. (2017). Bioinformatic Approaches Including Predictive Metagenomic Profiling Reveal Characteristics of Bacterial Response to Petroleum Hydrocarbon Contamination in Diverse Environments. *Sci Rep* 7. doi:10.1038/s41598-017-01126-3.

NESP Earth Systems and Climate Change Hub (2018). Climate change and the Shark Bay World Heritage Area: foundations for a climate change adaptation strategy and action plan. Available at: http://nespclimate.com.au/wp-content/uploads/2016/03/SBWHA-CC-workshop-report.pdf [Accessed May 14, 2020].

Nyyssölä, A., and Leisola, M. (2001). Actinopolyspora halophila has two separate pathways for betaine synthesis. *Arch Microbiol* 176, 294–300. doi:10.1007/s002030100325.

Obuekwe, C. O., Badrudeen, A. M., Al-Saleh, E., and Mulder, J. L. (2005). Growth and hydrocarbon degradation by three desert fungi under conditions of simultaneous temperature and salt stress. *International Biodeterioration & Biodegradation* 56, 197–205. doi:10.1016/j.ibiod.2005.05.005.

O'Donnell, S. T., Ross, R. P., and Stanton, C. (2020). The Progress of Multi-Omics Technologies: Determining Function in Lactic Acid Bacteria Using a Systems Level Approach. *Front. Microbiol.* 10. doi:10.3389/fmicb.2019.03084.

Oren, A. (2008). Microbial life at high salt concentrations: phylogenetic and metabolic diversity. *Saline Systems* 4, 2. doi:10.1186/1746-1448-4-2.

Oren, A., Elevi Bardavid, R., Kandel, N., Aizenshtat, Z., and Jehlička, J. (2013). Glycine betaine is the main organic osmotic solute in a stratified microbial community in a hypersaline evaporitic gypsum crust. *Extremophiles* 17, 445–451. doi:10.1007/s00792-013-0522-z.

Orwin, K. H., and Wardle, D. A. (2004). New indices for quantifying the resistance and resilience of soil biota to exogenous disturbances. *Soil Biology and Biochemistry* 36, 1907–1912. doi:10.1016/j.soilbio.2004.04.036.

Pagès, A., Welsh, D. T., Teasdale, P. R., Grice, K., Vacher, M., Bennett, W. W., et al. (2014). Diel fluctuations in solute distributions and biogeochemical cycling in a hypersaline microbial mat from Shark Bay, WA. *Marine Chemistry* 167, 102–112. doi:10.1016/j.marchem.2014.05.003.

Pannard, A., Pédrono, J., Bormans, M., Briand, E., Claquin, P., and Lagadeuc, Y. (2016). Production of exopolymers (EPS) by cyanobacteria: impact on the carbon-to-nutrient ratio of the particulate organic matter. *Aquat Ecol* 50, 29–44. doi:10.1007/s10452-015-9550-3.

Peters, K. E., Walters, C. C., and Moldowan, J. M. (2007a). *The Biomarker Guide: Volume 1, Biomarkers and Isotopes in the Environment and Human History*. Cambridge University Press.

Peters, K. E., Walters, C. C., and Moldowan, J. M. (2007b). *The Biomarker Guide: Volume 2, Biomarkers and Isotopes in Petroleum Systems and Earth History*. Cambridge University Press.

Petroff, A. P., Sim, M. S., Maslov, A., Krupenin, M., Rothman, D. H., and Bosak, T. (2010). Biophysical basis for the geometry of conical stromatolites. *Proceedings of the National Academy of Sciences* 107, 9956–9961. doi:10.1073/pnas.1001973107.

Pielou, E. C. (1966). The measurement of diversity in different types of biological collections. *Journal of Theoretical Biology* 13, 131–144. doi:10.1016/0022-5193(66)90013-0.

Pimm, S. L. (1984). The complexity and stability of ecosystems. *Nature* 307, 321–326. doi:10.1038/307321a0.

Playford, P. E., Cockbain, A. E., Berry, P. F., Roberts, A. P., Haines, P. W., and Brooke, B. P. (2013). The geology of Shark Bay. 299.

Post, F. J., Borowitzka, L. J., Borowitzka, M. A., Mackay, B., and Moulton, T. (1983). The protozoa of a Western Australian hypersaline lagoon. *Hydrobiologia* 105, 95–113. doi:10.1007/BF00025180.

Prieto-Barajas, C. M., Valencia-Cantero, E., and Santoyo, G. (2018). Microbial mat ecosystems: Structure types, functional diversity, and biotechnological application. *Electronic Journal of Biotechnology* 31, 48–56. doi:10.1016/j.ejbt.2017.11.001.

Prince, R. C. (2010). "Bioremediation of Marine Oil Spills," in *Handbook of Hydrocarbon and Lipid Microbiology*, ed. K. N. Timmis (Berlin, Heidelberg: Springer), 2617–2630. doi:10.1007/978-3-540-77587-4_194.

Qin, X., Tang, J. C., Li, D. S., and Zhang, Q. M. (2012). Effect of salinity on the bioremediation of petroleum hydrocarbons in a saline-alkaline soil. *Letters in Applied Microbiology* 55, 210–217. doi:10.1111/j.1472-765X.2012.03280.x.

Reddy, C. M., Arey, J. S., Seewald, J. S., Sylva, S. P., Lemkau, K. L., Nelson, R. K., et al. (2012). Composition and fate of gas and oil released to the water column during the Deepwater Horizon oil spill. *Proceedings of the National Academy of Sciences of the United States of America* 109, 20229–20234.

Reinold, M., Wong, H. L., MacLeod, F. I., Meltzer, J., Thompson, A., and Burns, B. P. (2019). The Vulnerability of Microbial Ecosystems in a Changing Climate: Potential Impact in Shark Bay. *Life* 9, 71.

Reshetnikov, A. S., Khmelenina, V. N., Mustakhimov, I. I., and Trotsenko, Y. A. (2011). Genes and enzymes of ectoine biosynthesis in halotolerant methanotrophs. *Methods Enzymol* 495, 15–30. doi:10.1016/B978-0-12-386905-0.00002-4.

Riis, V., Kleinsteuber, S., and Babel, W. (2003). Influence of high salinities on the degradation of diesel fuel by bacterial consortia. *Canadian Journal of Microbiology/Revue Canadienne de Microbiologie* 49, 713–721.

Roy, A., Sar, P., Sarkar, J., Dutta, A., Sarkar, P., Gupta, A., et al. (2018). Petroleum hydrocarbon rich oil refinery sludge of North-East India harbours anaerobic, fermentative, sulfate-reducing, syntrophic and methanogenic microbial populations. *BMC Microbiology* 18. doi:10.1186/s12866-018-1275-8.

Ruvindy, R., White III, R. A., Neilan, B. A., and Burns, B. P. (2016). Unravelling core microbial metabolisms in the hypersaline microbial mats of Shark Bay using high-throughput metagenomics. *The ISME Journal* 10, 183–196. doi:10.1038/ismej.2015.87.

Rykiel, E. J. (1985). Towards a definition of ecological disturbance. *Australian Journal of Ecology* 10, 361–365. doi:10.1111/j.1442-9993.1985.tb00897.x.

Sanders, H. L. (1968). Marine Benthic Diversity: A Comparative Study. *The American Naturalist* 102, 243–282.

Scheler, O., Glynn, B., and Kurg, A. (2014). Nucleic acid detection technologies and marker molecules in bacterial diagnostics. *Expert Review of Molecular Diagnostics; London* 14, 489–500. doi:http://dx.doi.org.dbgw.lis.curtin.edu.au/10.1586/14737159.2014.908710.

Schinteie, R., and Brocks, J. J. (2017). Paleoecology of Neoproterozoic hypersaline environments: Biomarker evidence for haloarchaea, methanogens, and cyanobacteria. *Geobiology* 15, 641–663. doi:https://doi.org/10.1111/gbi.12245.

Schloss, P. D. (2019). Reintroducing mothur: 10 Years Later. *Applied and Environmental Microbiology* 86. doi:10.1128/AEM.02343-19.

Selley, R. (2003). Petroleum Geology. *Encyclopedia of Physical Science and Technology*, 729–740. doi:10.1016/B0-12-227410-5/00555-X.

Shade, A., Peter, H., Allison, S. D., Baho, D., Berga, M., Buergmann, H., et al. (2012a). Fundamentals of Microbial Community Resistance and Resilience. *Front. Microbiol.* 3. doi:10.3389/fmicb.2012.00417.

Shade, A., Read, J. S., Youngblut, N. D., Fierer, N., Knight, R., Kratz, T. K., et al. (2012b). Lake microbial communities are resilient after a whole-ecosystem disturbance. *ISME J* 6, 2153–2167. doi:10.1038/ismej.2012.56.

Shanafelt, D. W., Dieckmann, U., Jonas, M., Franklin, O., Loreau, M., and Perrings, C. (2015). Biodiversity, productivity, and the spatial insurance hypothesis revisited. *Journal of Theoretical Biology* 380, 426–435. doi:10.1016/j.jtbi.2015.06.017.

Shannon, C. E. (1948). A Mathematical Theory of Communication. *The Belll System Technical Journal* 27, 55.

Shmareva, M. N., Doronina, N. V., Tarlachkov, S. V., Vasilenko, O. V., and Trotsenko, Y. A. (2018). Methylophaga muralis Bur 1, a haloalkaliphilic methylotroph isolated from the Khilganta soda lake (Southern Transbaikalia, Buryat Republic). *Microbiology* 87, 33–46. doi:10.1134/S0026261718010162.

Sierra-Garcia, I. N., and Oliveira, V. M. de (2013). *Microbial Hydrocarbon Degradation: Efforts to Understand Biodegradation in Petroleum Reservoirs.* IntechOpen doi:10.5772/55920.

Siglioccolo, A., Paiardini, A., Piscitelli, M., and Pascarella, S. (2011). Structural adaptation of extreme halophilic proteins through decrease of conserved hydrophobic contact surface. *BMC Structural Biology* 11, 50. doi:10.1186/1472-6807-11-50.

Smith, C. J., and Osborn, A. M. (2009). Advantages and limitations of quantitative PCR (Q-PCR)-based approaches in microbial ecology. *FEMS Microbiol Ecol* 67, 6–20. doi:10.1111/j.1574-6941.2008.00629.x.

Spring, S., Sorokin, D. Y., Verbarg, S., Rohde, M., Woyke, T., and Kyrpides, N. C. (2019). Sulfate-Reducing Bacteria That Produce Exopolymers Thrive in the Calcifying Zone of a Hypersaline Cyanobacterial Mat. *Front. Microbiol.* 10. doi:10.3389/fmicb.2019.00862.

Stokes, D. (2008). *Principles and Practice of Variable Pressure / Environmental Scanning Electron Microscopy (VP-ESEM): Environmental Scanning Electron Microscopy (VP-ESEM)*. New York, United Kingdom: John Wiley & Sons, Incorporated Available at: http://ebookcentral.proquest.com/lib/curtin/detail.action?docID=406511 [Accessed June 27, 2020].

Stolp, H., and Starr, M. P. (1981). "Principles of Isolation, Cultivation, and Conservation of Bacteria," in *The Prokaryotes*, eds. M. P. Starr, H. Stolp, H. G. Trüper, A. Balows, and H. G. Schlegel (Berlin, Heidelberg: Springer Berlin Heidelberg), 135–175. doi:10.1007/978-3-662-13187-9_5.

Suding, K. N., Gross, K. L., and Houseman, G. R. (2004). Alternative states and positive feedbacks in restoration ecology. *Trends in Ecology & Evolution* 19, 46–53. doi:10.1016/j.tree.2003.10.005.

Suga, M., Asahina, S., Sakuda, Y., Kazumori, H., Nishiyama, H., Nokuo, T., et al. (2014). Recent progress in scanning electron microscopy for the characterization of fine structural details of nano materials. *Progress in Solid State Chemistry* 42, 1–21. doi:10.1016/j.progsolidstchem.2014.02.001.

Suosaari, E. P., Reid, R. P., Araujo, T. a. A., Playford, P. E., Holley, D. K., Mcnamara, K. J., et al. (2016). Environmental pressures influencing living Stromatolites in Hamelin Pool, Shark Bay, Western Australia. *PALAIOS* 31, 483–496. doi:10.2110/palo.2016.023.

Thijs, S., Op De Beeck, M., Beckers, B., Truyens, S., Stevens, V., Van Hamme, J. D., et al. (2017). Comparative Evaluation of Four Bacteria-Specific Primer Pairs for 16S rRNA Gene Surveys. *Front. Microbiol.* 8. doi:10.3389/fmicb.2017.00494.

Tissot, B. P., and Welte, D. H. (2013). *Petroleum Formation and Occurrence*. Springer Science & Business Media Available at: https://books.google.com.au/books?hl=en&lr=&id=avLxCAAAQBAJ&oi=fnd&pg=PA3&ots=1J43iXn42F&sig=K8vOdRQoadS_667mES9rV4vU7OE&redir_esc=y#v=onepage&q&f=false [Accessed July 24, 2020].

Tringe, S. G., and Hugenholtz, P. (2008). A renaissance for the pioneering 16S rRNA gene. *Current Opinion in Microbiology* 11, 442–446. doi:10.1016/j.mib.2008.09.011.

Trolio, R., Grice, K., Fisher, S. J., Alexander, R., and Kagi, R. I. (1999). Alkylbiphenyls and alkyldiphenylmethanes as indicators of petroleum biodegradation. *Organic Geochemistry* 30, 1241–1253. doi:10.1016/S0146-6380(99)00099-6.

van Gemerden, H. (1993). Microbial mats: A joint venture. *Marine Geology* 113, 3–25. doi:10.1016/0025-3227(93)90146-M.

Vernon-Parry, K. D. (2000). Scanning electron microscopy: an introduction. *III-Vs Review* 13, 40–44. doi:10.1016/S0961-1290(00)80006-X.

Visscher, P. T., and Stolz, J. F. (2005). Microbial mats as bioreactors: populations, processes, and products. *Palaeogeography, Palaeoclimatology, Palaeoecology* 219, 87–100. doi:10.1016/j.palaeo.2004.10.016.

Volkman, J. K., Alexander, R., Kagi, R. I., Rowland, S. J., and Sheppard, P. N. (1984). Biodegradation of aromatic hydrocarbons in crude oils from the Barrow Sub-basin of Western Australia. *Organic Geochemistry* 6, 619–632. doi:10.1016/0146-6380(84)90084-6.

Walter, M., Bauld, J., and Brock, T. (1976). Microbiology and Morphogenesis of Columnar Stromatolites (Conophyton, Vacerrilla) from Hot Springs in Yellowstone National Park. *Developments in sedimentology* 20, 273–310.

Weiss, S., Xu, Z. Z., Peddada, S., Amir, A., Bittinger, K., Gonzalez, A., et al. (2017). Normalization and microbial differential abundance strategies depend upon data characteristics. *Microbiome* 5, 27. doi:10.1186/s40168-017-0237-y.

Wenger, L. M., Davis, C. L., and Isaksen, G. H. (2002). Multiple Controls on Petroleum Biodegradation and Impact on Oil Quality. *SPE Reservoir Evaluation & Engineering* 5, 375–383. doi:10.2118/80168-PA.

Westman, W. E. (1978). Measuring the Inertia and Resilience of Ecosystems. *BioScience* 28, 705–710. doi:10.2307/1307321.

White, H. K., Conmy, R. N., MacDonald, I. R., and Reddy, C. M. (2016). Methods of Oil Detection in Response to the Deepwater Horizon Oil Spill. *Oceanography* 29, 76–87.

Widdel, F., and Musat, F. (2010). Diversity and common principles in enzymatic activation of hydrocarbons. *Handbook of Hydrocarbon and Lipid Microbiology*, 981–1009.

Willerslev, E., Hansen, A. J., Binladen, J., Brand, T. B., Gilbert, M. T. P., Shapiro, B., et al. (2003). Diverse Plant and Animal Genetic Records from Holocene and Pleistocene Sediments. *Science* 300, 791–795. doi:10.1126/science.1084114.

Willis, A. D. (2019). Rarefaction, Alpha Diversity, and Statistics. *Front. Microbiol.* 10. doi:10.3389/fmicb.2019.02407.

Wilson, M. V., and Shmida, A. (1984). Measuring Beta Diversity with Presence-Absence Data. *The Journal of Ecology* 72, 1055. doi:10.2307/2259551.

Woese, C. R. (1987). Bacterial evolution. *Microbiol Rev* 51, 221–271.

Woese, C. R., and Fox, G. E. (1977). Phylogenetic structure of the prokaryotic domain: The primary kingdoms. *PNAS* 74, 5088–5090. doi:10.1073/pnas.74.11.5088.

Woese, C. R., Kandler, O., and Wheelis, M. L. (1990). Towards a natural system of organisms: proposal for the domains Archaea, Bacteria, and Eucarya. *Proc Natl Acad Sci U S A* 87, 4576–4579.

Wong, H. L., MacLeod, F. I., White, R. A., Visscher, P. T., and Burns, B. P. (2020). Microbial dark matter filling the niche in hypersaline microbial mats. *Microbiome* 8, 135. doi:10.1186/s40168-020-00910-0.

Wong, H. L., Smith, D., Visscher, P. T., and Burns, B. P. (2015). Niche differentiation of bacterial communities at a millimeter scale in Shark Bay microbial mats. *Scientific Reports (Nature Publisher Group); London* 5, 15607. doi:http://dx.doi.org.dbgw.lis.curtin.edu.au/10.1038/srep15607.

Wong, H. L., White, R. A., Visscher, P. T., Charlesworth, J. C., Vázquez-Campos, X., and Burns, B. P. (2018). Disentangling the drivers of functional complexity at the metagenomic level in Shark Bay microbial mat microbiomes. *The ISME Journal* 12, 2619–2639. doi:10.1038/s41396-018-0208-8.

Xu, X., Liu, W., Tian, S., Wang, W., Qi, Q., Jiang, P., et al. (2018). Petroleum Hydrocarbon-Degrading Bacteria for the Remediation of Oil Pollution Under Aerobic Conditions: A Perspective Analysis. *Front. Microbiol.* 9. doi:10.3389/fmicb.2018.02885.

Yachi, S., and Loreau, M. (1999). Biodiversity and ecosystem productivity in a fluctuating environment: The insurance hypothesis. *PNAS* 96, 1463–1468. doi:10.1073/pnas.96.4.1463.

Yang, L., Lai, C.-T., and Shieh, W. K. (2000). Biodegradation of dispersed diesel fuel under high salinity conditions. *Water Research* 34, 3303–3314. doi:10.1016/S0043-1354(00)00072-5.

Yarza, P., Yilmaz, P., Pruesse, E., Glöckner, F. O., Ludwig, W., Schleifer, K., et al. (2014). Uniting the classification of cultured and uncultured bacteria and archaea using 16S rRNA gene sequences. *Nature Reviews. Microbiology; London* 12, 635–45. doi:http://dx.doi.org.dbgw.lis.curtin.edu.au/10.1038/nrmicro3330.

Zaikova, E., Goerlitz, D. S., Tighe, S. W., Wagner, N. Y., Bai, Y., Hall, B. L., et al. (2019). Antarctic Relic Microbial Mat Community Revealed by Metagenomics and Metatranscriptomics. *Front. Ecol. Evol.* 7. doi:10.3389/fevo.2019.00001.

Chapter 2

Responses of hypersaline microbial mats from Shark Bay (Western Australia) to long-term petroleum exposure

Yalimay Jimenez, Kliti Grice, Cornelia Wuchter and Marco J.L. Coolen

Submitted to Frontiers in Microbiology

Specialty Section: Microbiological Chemistry and Geomicrobiology

Impact factor: 4.076

2.1. Abstract

Shark Bay (SB), a World Heritage site, is under threat due to potential petroleum spills from offshore resource industries and shipping activities in the northern regions of Western Australia. Hamelin Pool, the larger embayment of the SB region, sustains a unique diversity of microbial mats. The oceanic currents close to SB could assist the transport of a potential spilled petroleum incident and impact the microbial mats in this region over a significant time frame due to the restricted circulation. Here, we performed a time-series incubation experiment to study the long-term response of SB microbial mats under petroleum exposure (PE). Two of the most common mat types (smooth and pustular mats) were exposed to petroleum for 30, 60 and 120 days and the total vs. active microbial community composition was assessed through environmental 16S rRNA genes and transcript profiling. The smooth mat microbiome appeared to be more resistant than the pustular mat microbiome after 30 days of PE. However, after 120 days of PE over 2/3 of the microbiome disappeared in both mat types compared to the controls. Both mat types yielded a biofilm, albeit different in appearance, as an important PE stress response. The smooth mat developed a transparent, non-rigid and relatively thin layered biofilm whereas the pustular mat developed a massive biofilm that consisted of several 'tower-like' structures of varying heights (up to 5 cm). The dominant microbes that resisted the PE stress belonged to the phyla Cyanobacteria (in particular *Halomicronema excentricum*), Alpha-and Gammaproteobacteria in both mat types, and to Delta-and Epsilonproteobacteria and Bacteroidetes in the smooth mat. PE stimulated oil-utilising bacteria in both mat types, and in particular the biofilm which developed on the pustular mat provided a specific habitat for more diverse hydrocarbon degraders. The different PE stress response of the microbial mats appears to be driven by their unique microfabric differences and the specific mode of life of microbes under PE stress (e.g. physiological elasticity, mobility, EPS producing capability). This research provides new insights into the stress response of microbial mats from SB under long term PE and might be helpful for future ecosystem management plans.

2.2. Introduction

The petroleum industry is one of the most important sectors of the Western Australian (WA) economy, making a valuable contribution to the national GDP. In 2019, the oil and gas sector were valued at $39.7 billion and the production of crude oil and condensate in WA reached 82% of the total Australian production (Department of Mines, Industry Regulation and Safety, DMIRS[15]). Exploration and exploitation activities are developed mainly offshore, especially in the Northwest Shelf and northern areas of WA, where trading routes of petroleum ships at sea occur alongside the WA coast. Some of the most transited shipping routes and ports (*i.e.*, Carnarvon and Exmouth) are close to Shark Bay (SB) a World Heritage site (**Figure 2.1A**). Since 1991, SB or *Gutharraguda* has been recognised as an outstanding natural wonder of the world and was granted national and international protection. However, this region and its marine ecosystems could be impacted by a major petroleum spill from WA's industry. Further, other hydrocarbon pollutants can derive from recreational boats or commercial ships in this region. In fact, the Australian Maritime Safety Authority (AMSA) has reported twenty-seven major petroleum spill incidents across Australia since 1903 (AMSA, 2012). Eight of these spills occurred offshore of WA and the last spill happened in 2012 on Christmas Island. AMSA has projected an increase in the Environmental Risk Index (ERI) between 91 and 141% by 2020 related to petroleum sources from trading ships at sea and ships at ports, respectively.

[15] www.dmp.wa.gov.au

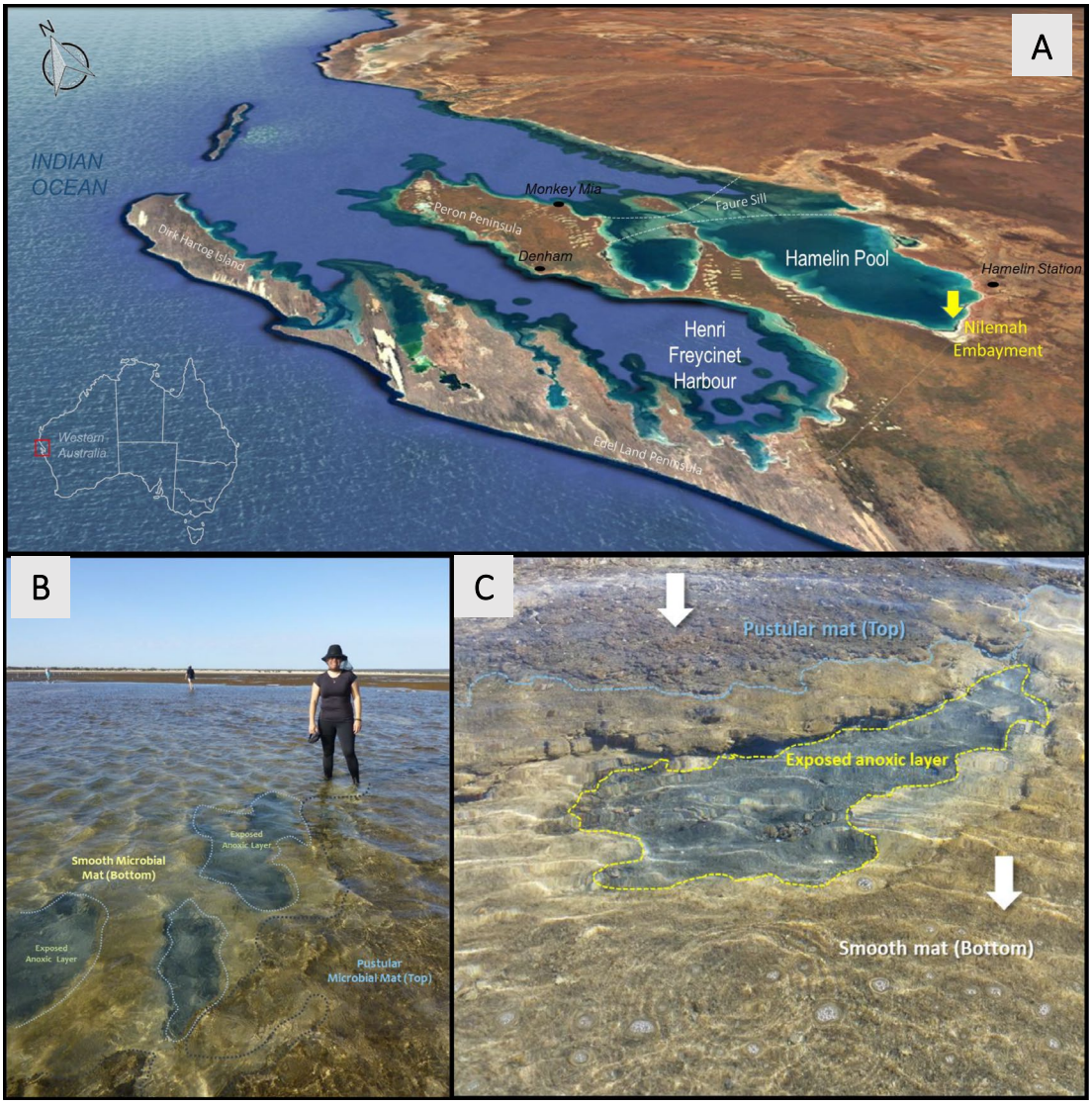

Figure 2.1. Shark Bay area, Western Australia. Red arrow pointing out the sampling area: Nilemah embayment, Hamelin Pool. Modified image from Google Maps (2017) (A). Photo showing the subtidal microbial mat habitats where sampling was conducted. At the time of sampling water depth was about 20-25 cm (B). Photo (close up) exhibiting the sampling points where living microbial mats were collected (white arrows). Note the exposed anoxic layers between pustular and smooth habitats (C).

SB is located in the southern Carnarvon Basin, some 800 km north of Perth, WA. SB contains three main peninsulas: Edel Land, Peron and Nanga, which enclose a shallow saline waterbody called Henri Freycinet Harbour, and two barred basins named L'Haridon Bight and Hamelin Pool, respectively (**Figure 2.1A**) (Playford et al., 2013). Hamelin Pool, being the larger embayment of this region, sustains a unique diversity of microbial mats including extant stromatolites (Jahnert and Collins, 2013; Pagès et al., 2014). Faure Sill, a seagrass bank, creates an underwater barrier restricting

seawater circulation. Furthermore, evaporation exceeding precipitation leads to hypersaline conditions (70 Practical Salinity Unit: PSU). This environment allows microbial mats to flourish, and restricts some predators, which are unable to thrive under these extreme conditions (Playford et al., 2013; Suosaari et al., 2016). Although microbial sedimentary systems are present in different parts of Hamelin Pool's coastline, the Nilemah region, in the southern area of this embayment, exemplifies one of the most hypersaline, accessible and well-developed platforms where microbial mats can thrive (Jahnert and Collins, 2013). Hamelin Pool (SB) is home to a unique assemblage of shallow, pristine microbial mat habitats. Microbial mats are multi-stratified and unlithified organo-sedimentary structures which contain a consortia of bacteria and archaea, thriving by an interconnected network of complex interdependencies (Duran and Goñi-Urriza, 2010; Wong et al., 2016). They are often embedded in an inorganic matrix of shells, carbonates and silicates. Such ecosystems, especially smooth and pustular microbial mats, have been studied previously using multi-disciplinary analyses including microbial, mineral and/or biolipid approaches (Allen et al., 2009; Pagès et al., 2014, 2015; Ruvindy et al., 2016; Plet et al., 2018; Campbell et al., 2020).

The oceanic currents associated with the Indo-Pacific Warm Pool and the Leeuwin currents close to SB could assist the transport of a potential spilled petroleum incident and impact the microbial mats in this region over a significant period of time due to the restricted circulation. Microbial mats exposed to petroleum in hypersaline environments have been investigated in a few studies over the last two decades (Benthien et al., 2004; Abed et al., 2006; Bordenave et al., 2007). They revealed that some microbial taxa (e.g. cyanobacteria, alpha-, delta-, and gamma-proteobacteria) exhibit a remarkable resistance to PE. Furthermore, petroleum contaminated microbial mats select for hydrocarbon-degrading bacteria and are able to biodegrade complex hydrocarbons which is a promising tool for bioremediation purposes (Benthien et al., 2004; De Oteyza et al., 2006; Hernandez-Raquet et al., 2006; Llirós et al., 2008; McGenity et al., 2012; Abed et al., 2014; Fathepure, 2014; Edbeib et al., 2016). Although extensive research has been performed on freshwater and marine environments exposed to petroleum (Berthe-Corti and Nachtkamp, 2010; Dashti et al., 2015), research still needs to be done on microbial responses under hypersaline conditions. Here, we performed microcosm incubation experiments with smooth and

pustular microbial mats from SB, which were exposed to petroleum contamination for up to 120 days. Subsequently, the total vs. active prokaryotic communities were phylogenetically characterised through Illumina MiSeq sequencing of 16S rDNA and reverse transcribed 16S rRNA to investigate microbial stress responses and resistance to long-term PE.

2.3. Materials and methods

2.3.1. Site description and sampling

Smooth and pustular microbial mats dominate intertidal and subtidal areas of the Nilemah area and are the focus of this study (**Figure 2.1B** and **Figure 2.1C**). Both types of living microbial mats were sampled using a sterile spatula in April 2017 (26°27′04.1″ S, 114°05′45.3″ E). Each piece was approximately 20cm x 20cm x 15cm (length x width x depth). Physicochemical parameters were also measured and recorded at the time of sampling for reference to maintain *in situ* environmental conditions during the incubation experiments (**Table A2.1**). Living microbial mats were then transported in glass containers submerged in seawater (**Figure 2.2A** and **Figure 2.2B**), with continuous air bubbling until reaching Western Australian Organic and Isotope Geochemistry Centre (WA-OIGC) facilities at Curtin University, Perth (WA), in less than 48 hours after sampling. Additionally, one core of each pristine smooth and pustular microbial mat (20cm diameter x 15cm depth) and 50 L of hypersaline seawater were also collected in the field (same area where the living microbial mats were collected). The cores were stored at -20°C and used as point of comparison with controls subjected to laboratory conditions, and the hypersaline water (kept in the dark at 4°C) served as aqueous medium for mimicking the original environment.

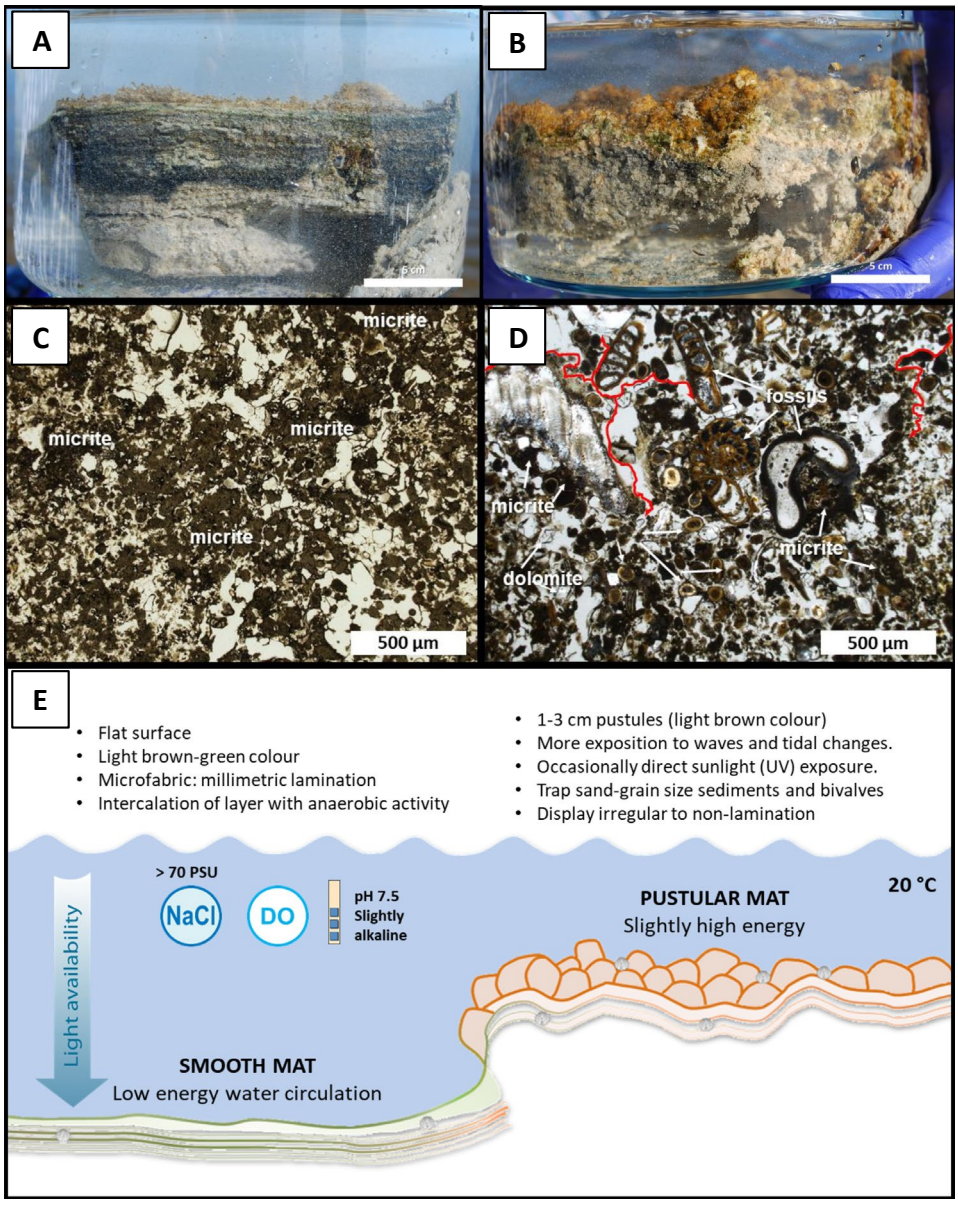

Figure 2.2. Smooth (A) and pustular (B) mat samples from Nilemah embayment collected for lab incubation (Credits: Dr. Alex Sessions – California Institute of Technology, California, USA). Photographs of the microfabrics exhibited by smooth (C) and pustular (D) mats from Hamelin Pool, SB. As previously described in Plet et al. (2018), smooth mats (C) display well-sorted fine grains of minerals and, occasionally fossils, fused by micrite (~40%) (*i.e.*, mud-size carbonate particles). Smooth mats exhibit low porosity and permeability whereas pustular mats (D) are poorly sorted, showing a combination of allochems (*i.e.,* fossils, intraclasts, and ooids) with patches of micrite. Thus, pustular mats have a higher porosity and permeability in comparison to smooth mats. Red lines in panel D simulate paths where fluids (e.g. seawater or other fluids) might percolate (Credits: Images were kindly provided by Dr Chloe Plet –CSIRO, Perth, Australia –, from her research in 2017 at Curtin University). Conceptual model of the local ecosystem sampled, including features observed and parameters measured in the field: Dissolved oxygen (DO) and salinity (NaCl symbol) (E).

2.3.2. Microcosm design: simulating field conditions

The large pieces of living smooth and pustular mats were cut with a pre-cleaned aluminium tube and relocated into individual cylindrical microcosms. The mats in the microcosms were topped up with seawater (**Figure A2.1A**). Each microcosm was filled up to 80% of its water-holding capacity (ca. 600mL). Any loss of water volume due to evaporation was compensated with sterile-filtered MilliQ water over the course of the incubation experiments. Microcosms were individually aerated with 0.22µm-filtered air using a standard aquarium air pump system. The bottom of each microcosm was covered with aluminium foil to ensure artificial light only reached the top surface of the microbial mats (**Figure A2.1B**). The microcosms were then placed in 20L incubation tanks. The incubation tanks were filled with filtered Milli-Q water until reaching approximately half-height of the microcosms and kept at a constant 25°C using an aquarium heater. The external walls of the incubation tanks were covered with a protective non-translucid material to avoid light from the surrounding environment (**Figure A2.1C**). An EcoGlo LED light ('Aqua One', 15W 45cm, model 59092), was used to illuminate the surfaces of the microcosms using a diel cycle set to 8 hour darkness and 16 hour light. The EcoGlo light possesses one blue and two white tubes, which spectral power distributions ranging between 420 and 500 nm (460nm peak) and 420 and 660 nm (with two peaks at 460 nm and 550 nm), respectively (source: Product Information Sheet).

2.3.3. Experimental stage: Microcosm configuration, petroleum exposure and sampling

A total of four incubation tanks (A, B, C and D, **Figure A2.2**) were assembled to group microcosms as controls (A and B) and those that were exposed to petroleum (C and D). There were three types of control microcosms (I, II & III) set for specific purposes (**Figure 2.3**). I and II were placed in tank A, and III in tank B (**Figure A2.2**). Tank A included four microcosms, two type I and two type II divided with a physical barrier. This barrier consisted of a thin, hard plastic wall inserted between type I and II microcosms, which prevented cross-contamination between these microcosms, as it had the same height as the tank. Type I control microcosms were used as experimental blanks for tracking any contamination coming from water replenishment after

evaporation. They were topped up with 600mL of 0.22µm filtered Milli-Q water and were never exposed to the petroleum. Type II control microcosms were essential for following the expected weathering from air bubbling and photochemical changes because of exposure to artificial light irradiance and to assess any microbial community and function changes from PE (**Figure 2.3**). They were also filled up with 600 mL of 0.22 µm- filtered Milli-Q water and 10 mL of petroleum (0.02% v/v) was added. Tank B contained six type III control microcosms. Each microcosm consisted of a piece of microbial mat (approx. 350 cm^3), three with smooth mats and three with pustular mats, and seawater (250 mL). They were never exposed to petroleum and used for tracking any changes in composition due to laboratory incubation conditions. Microcosms used for PE were set up in the same way as the type III control, but they were each exposed to 10mL of petroleum. Three smooth and three pustular microbial mats microcosms were placed in tanks C and D, respectively. The petroleum utilised as a pollutant came from the Barrow Formation (Barrow Sub-basin, labelled as Barrow Island 6200, #101). Barrow Island 6200 is a non-biodegraded paraffinic oil (Trolio et al., 1999; Grice et al., 2000), is very light and displays a high proportion of *n*-alkanes (**Figure A2.3**), considered easy for microorganisms to biodegrade (Volkman et al., 1984).

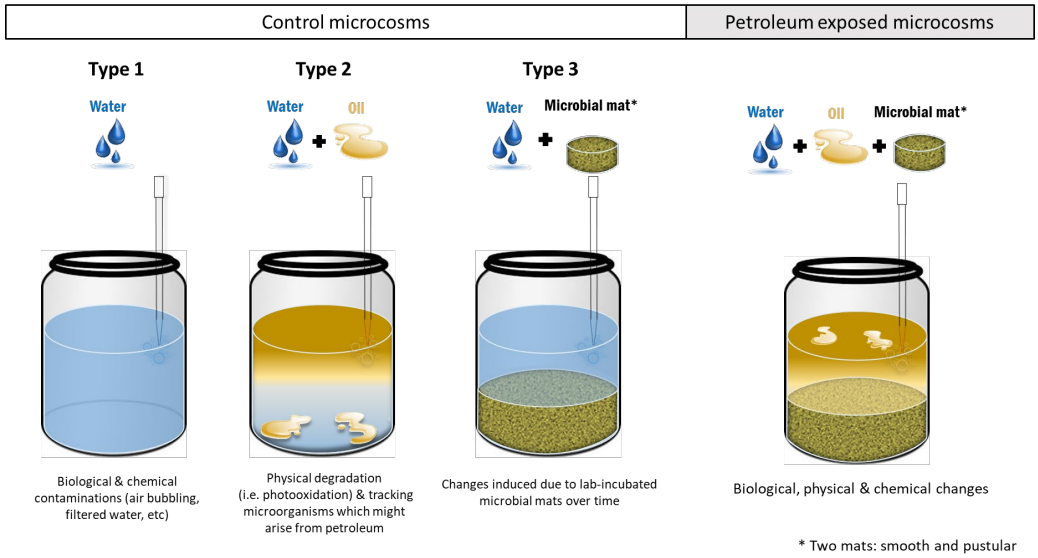

Figure 2.3. Configuration of the types of controls microcosms and microcosms exposed to petroleum. All controls were subjected to the same conditions as microcosms exposed to petroleum: 25 °C, artificial light under dial regime (16h light: 8h darkness) plus constant sterile air bubbling.

Six independent incubation experiments were conducted in parallel, three with each type of microbial mat (smooth and pustular). Each set of incubation experiments consisted of two microcosms: one type III control microcosm and one microcosm for PE. The latter were subjected to either 30 days (T30), 60 days (T60) or 120 days (T120) PE. To increase microbial activation under stress conditions, the petroleum (10 mL) was directly discharged over the microbial mat's surface, removing the seawater from the mats before adding the petroleum. After 4 hours of direct PE, the 250 mL of seawater originally covering the mats was added back to the PE mats. Each microcosm of these three sets of incubation experiments, placed in the tanks B, C and D, was sampled before pollution (day 0 = T0) and after PE (T30, T60 or T120, respectively). Sub-samples of microbial mats were taken from the first 5 mm with a sterile spatula from each microcosm (type III and PE). Therefore, initial microbiomes (T0) were compared to those microbial communities after T30, T60 or T120, in both the controls and PE microcosms. Additionally, type I and II control microcosms (tank A) were also sub-sampled. 4 mL of water or water-petroleum supernatant were collected from each of the experiments. Experimental sampling schedule and nomenclature utilised is shown in **Figure 2.4**. Both microbial mats and water samples were flash frozen using liquid nitrogen and stored at -80°C until further analysis.

2.3.4. Molecular ecology

At T0, T30, T60, and T120 of incubation, sub-samples were obtained from each microcosm inside a HEPA-filtered horizontal laminar flow bench. These sub-samples comprised microbial mats collected from the field (cores collected under pristine conditions), type I controls (local seawater), type II controls (a mixture of petroleum and seawater), type III controls (microbial mats topped with seawater, not exposed to petroleum), PE microbial mats and a biofilm developed in the pustular microbial mats after 120 days of incubation. Also, methodological blanks were incorporated into the pool of samples to determine any contamination through the applied protocol. Prior to sample preparation, all benchtops, instruments and equipment were decontaminated with Thermo Scientific™ RNase AWAY™, and RNase Away-treated vinyl gloves as well as clean lab coveralls were always worn.

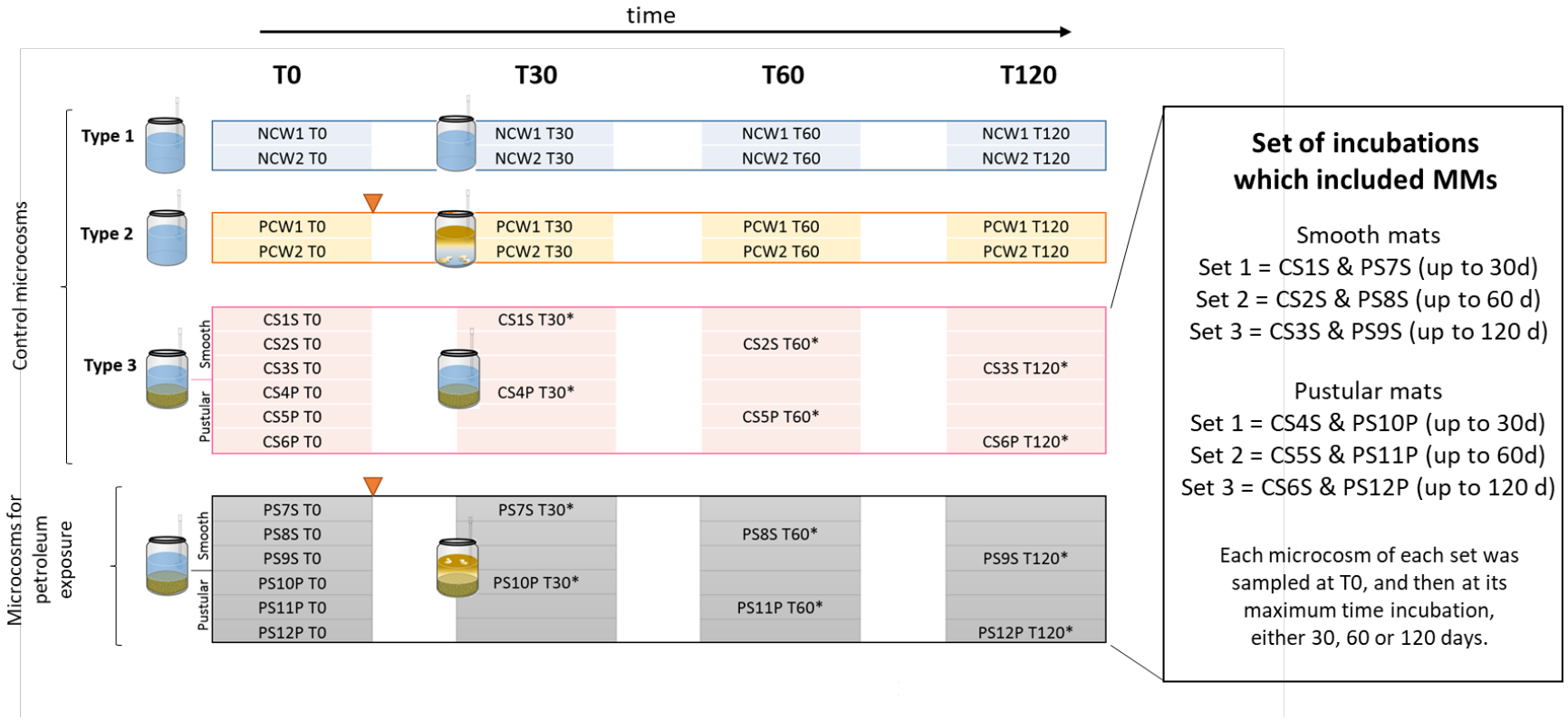

Figure 2.4. Illustration of sampling schedule and nomenclature utilised for both control microcosms and microcosms for petroleum exposure. All microcosms were subsampled at day 0 – initial conditions – (T0). Sampling was repeated after 30 days (T30), 60 days (T60) and 120 days (T120) in all type 1 and type 2 control microcosms. After reaching its maximum incubation time (T30, T60 or T120), type 3 microcosms and microcosms for petroleum exposure were collected as sacrificial samples (marked with an asterisk). Sacrificial samples allowed to analyse a higher amount of sample or duplicate an analysis. NCW: No petroleum Control Water; PCW: Petroleum Control Water; CS#S: Control Sample # Smooth; CS#P: Control Sample # Pustular; PS#S: Petroleum Sample # Smooth; PS#P: Petroleum Sample # Pustular.

RNA and DNA were simultaneously extracted from either mat material or biofilm subsamples using the RNeasy PowerSoil Total RNA Isolation Kit® and DNA elution Accessory Kit® following manufacturer instructions (QIAGEN, Venlo, The Netherlands). The weight of the microbial mat samples varied from 0.5 to 2g, and 0.09 to 0.4g for biofilms. These kits were also used for extracting RNA and DNA from 2mL of the local seawater (type 1 controls) and the petroleum/seawater mixture (type II controls). Prior to extraction, microbial cells in these liquid subsamples were concentrated using Amicon® Ultra 0.5 Centrifugal Filters. Total DNA and RNA were quantified fluorospectrometrically. Quant-IT™ PicoGreen® stained DNA was measured using a VersaFluorTM Fluorometer (BIO-RAD Laboratories), whereas Quant-IT RiboGreen® stained RNA was measured using a Nanodrop 3300 Fluorospectrometer (Thermo Fisher Scientific, Massachusetts, U.S.A).

After quantitation, RNA samples were digested with DNase I and subsequently concentrated using the RNA Clean & ConcentratorTM-5 Kit (Zymo Research, California, U.S.A). The complete removal of traces of DNA during this step was tested by subjecting aliquots of the DNA-free RNA extracts to Polymerase Chain Reaction (PCR) amplification using universal primers targeting the V4 region of bacterial 16S rRNA genes using the PCR protocol described further below. Total pre-cleaned and pre-concentrated RNA samples were transcribed into complementary DNA (cDNA) using the Photoscript II Reverse Transcriptase kit (New England BioLabs, Massachusetts, U.S.A). The resulting cDNA products were stored at -20°C and un-used DNA-free RNA samples at -80°C.

2.3.5. PCR, library preparation and sequencing

Bacterial and archaeal 16S rRNA genes (V4 region) were amplified from the genomic and complementary DNA pools for subsequent library preparation and sequencing to assess the microbial diversity and community composition in the various microcosm samples. The duplication of amplified genes was followed real time using a Realplex quantitative PCR cycler (Eppendorf) and a SYBRGreen assay. The 20µL reaction mixtures contained ~20ng of the DNA or cDNA, TB GreenTM Premix Ex TaqTM (Tli RNaseH Plus) (Takara Bio Inc), PCR water, and 0.2µM final concentration of primers U519fM and U803R (Wuchter et al., 2013). The forward and reverse primers included the Illumina flowcell adapter sequences as well as the pad regions. The reverse primer differed for each amplified DNA or cDNA sample as they included a

unique 12 base Golay barcode sequence to support pooling of samples (Caporaso et al., 2012). Cycling conditions included: initial melting (95°C for 5 min), and 25-35 cycles consisting of a melting step (95°C for 5 sec), annealing (59°C for 34 sec), and primer extension (72°C for 20 sec) which included the photo step. The reactions were stopped at the end of the exponential phase to minimise overamplification and the formation of artefacts. The amount of DNA in each barcoded amplicon was measured using a VersaFluorTM Fluorometer (BIO-RAD Laboratories) following the same protocol mentioned above, then equimolar amounts were pooled.

The pooled library was then concentrated using an Amicon Ultra 0.5 30 KDa Centrifugal Filter and subjected to agarose gel electrophoresis. After imaging of the SYBRgreen- stained gel using a blue light transilluminator (Clare Chemical, Dolores, CO, USA), the desired amplicon was excised from the gel and purified using the Monarch® DNA Gel Extraction Kit (New England Biolabs). The gel-purified library was then concentrated again using an Amicon Ultra 0.5 30 KDa Centrifugal Filter, quantified fluorospectrometrically and sent to the Australian Genomic Research Facility (AGRF). At AGRF, the Illumina HiSeq 2500 platform was used to generate 2x 125 bp paired-end sequence reads. The HiSeq Control Software (HCS) v2.2.68 and Real Time Analysis (RTA) v1.18.66.3 software performed real-time image analysis and base calling on the HiSeq instrument computer. The AGRF Illumina bcl2fastq 2.20.0.422 pipeline was used to generate the sequence data.

2.3.6. Bioinformatics and statistical analysis

Bioinformatics analysis was performed using QIIME 2 version 2019.10 (Quantitative Insights into Microbial Ecology 2[16]) (Bolyen et al., 2019). Briefly, reverse and forward raw sequence reads (*.fastq) were imported, demultiplexed and filtered. DADA2 pipeline was applied for denoising and chimera removal (Callahan et al., 2016). Taxonomy was assigned to ASVs (Amplicon Sequence Variants) against the Greengenes 13_8 99% OTUs reference sequences database, which performance has shown to have better coverage with oceanic biomes (McDonald et al., 2012; Almeida et al., 2018) *via* q2-feature-classifier (Bokulich et al., 2018). Downstream data manipulation and visualisation of taxonomical information was mainly conducted in R Studio[17] using multiple packages. The more relevant included: ggplot2 for stacked

[16] www.qiime2.org
[17] www.rstudio.com

bar plots, and ComplexHeatmap for constructing heatmaps (Gu et al., 2016; Wickham, 2016).

Statistical multivariate analysis for exploring the DNA and cDNA datasets comprised ordination and dimension reduction approaches. The similarity between controls microcosm samples over time (T0 vs. T30, T0 vs. T60 and T0 vs. T120) for both types of microbial mats was assessed by one-way Analysis of Similarities (ANOSIM) using the biostatistics software package Primer-e version 7. To apply this analysis datasets were standardised to relative abundance, square root transformed for down weighing the more abundant species contribution, and a Bray-Curtis similarity matrix was calculated. Obtained *P* and R values indicate significant level of separation between groups of samples (initial *vs.* maximum time of incubation), respectively. Alpha diversity (within-sample diversity) was examined at species level. Rarefaction analysis was performed using the Vegan package (version 2.4-6) in R (Oksanen et al., 2010). Faith's Phylogenetic Diversity, Shannon index, observed OTU (Operational Taxonomic Unit), and Pielou's Evenness metrics were visualised using boxplots (Faith, 1992) for assessing community richness and evenness. These indices were estimated *via* qiime2 diversity core-metrics-phylogenetic command. 5,000 reads sampling depth was set as the cut-off for retaining the most sequences. Beta diversity (between-sample diversity) analysis was performed using the mixOmics R package[18] (Cao et al., 2016). In brief, raw read counts were offset to 1, normalised by Total Sum Scaling (TSS) and then transformed by applying Centered Log Ratio (CLR) transformation. Principal Coordinates Analysis (PCA) plots (PC1 and PC2) were then created for visualising and comparing clusters between initial and post PE microcosms for the different sets of incubations. Using the same R package, biplots and loading plots were also plotted for PC1. They assisted in the identification of those variables, or species, responsible for the identified clusters and their loading weight (or contribution) in the chosen component, respectively. This approach was complemented with the application of Indicator Species Analysis (ISA) by Indicspecies package in R (v. 1.7.8) (Cáceres and Legendre, 2009). ISA endorsed those detected distinctive species that emerged or increased their abundance under stress

[18] http://mixomics.org/mixmc

conditions, *i.e.*, positive effect, and those which were present only under the initial conditions and negatively correlated with PE conditions (negative effect).

2.3.7. Scanning electron microscopy imaging

The micro-internal structure and elemental composition of the biofilm which developed in the pustular mat microcosm incubated with Barrow Island petroleum for 120 days (PS12P T120) was analysed using a variable pressure Zeiss Evo 40XVP scanning electron microscope (SEM), coupled with an Oxford Instruments SiLi X-ray detector for elemental analyses at the John de Laeter Centre[19], Electron Microscopy Facility at Curtin University (Perth, Western Australia). For preparation a small portion of biofilm wall was collected (approx. 5mm x 5mm) with a sterile surgical knife and then dehydrated for further imaging analysis. The dehydration step consisted of rinsing the biofilm sample in a series of ethanol concentrations starting at 50%, increased by 10% increments until reaching 100% ethanol. PCR-grade water was used for dilution of ethanol. To avoid rehydration, the sample was maintained in a glass desiccator until analysis within 24 hours.

2.4. Results

2.4.1. Alpha and Beta diversity of the smooth and pustular mat microbiomes.

In total, 578 amplicon sequence variants (ASVs) were recovered after singleton removal and chimera check using QIIME 2. Rarefaction analysis revealed that the sequence depth was sufficient for all analysed samples (**Figure A2.4**, **Figure A2.5** and **Figure A2.6**). Shannon Index values varied between pristine and control samples, but overall both sample types yielded higher minimum and maximun values (**Figure 2.5**): (a) 6.9 to 8.2 (DNA) and 8.0 to 9.0 (cDNA) in pristine smooth mats; (b) 7.3 to 9.4/9.6 (DNA/cDNA) in pristine pustular mats; (c) 7.2 to 7.9 (DNA) and 7.4 to 9.7 (cDNA) in control smooth mats; and (d) 7.3 to 9.0 (DNA) and 8.3 to 9.5 (cDNA) in control pustular mats. Instead, PE mats resulted in a decrease in the microbial diversity, with the largest changes observed in the pustular mats (5.7-8.0) (

Figure 2.5). This trend was also observed for the OTUs and Faith's PD richness (**Figure A2.7**, **Figure A2.8** and **Figure A2.9**). Furthermore, long term PE resulted in

[19] https://jdlc.curtin.edu.au/

a net loss of ASV and a decline of more than 2/3 of the initial microbial communities in both mat types (**Figure 2.6**).

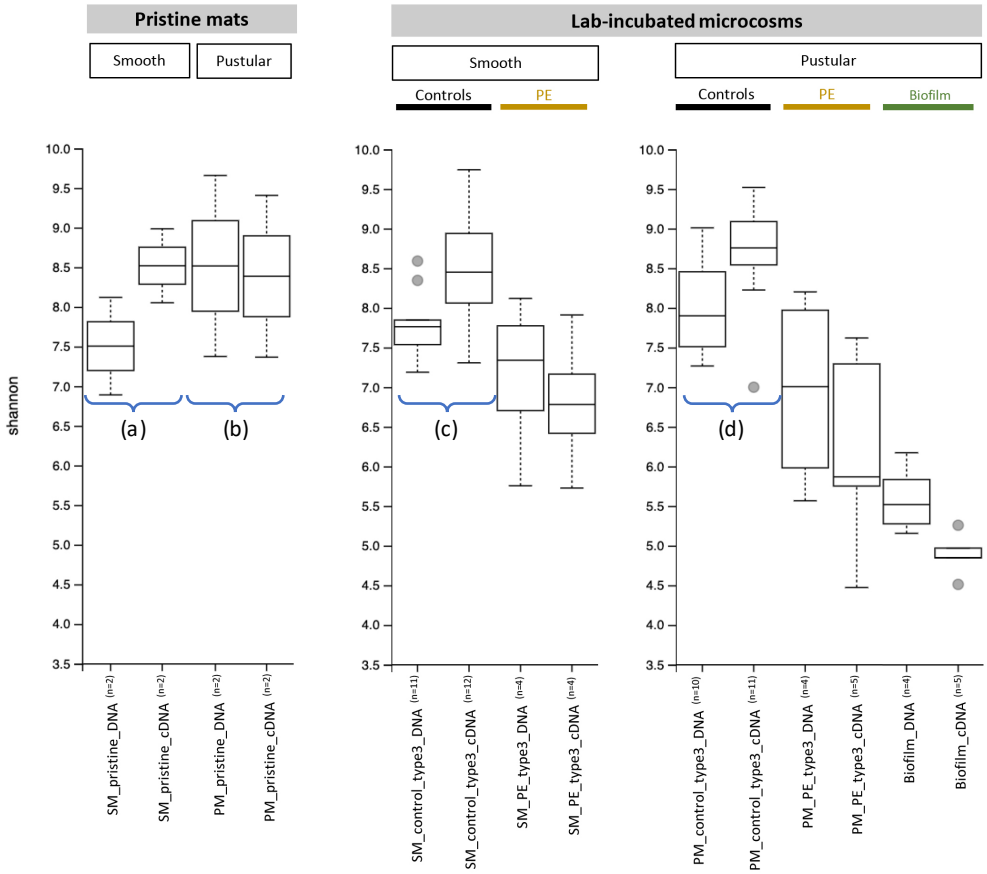

Figure 2.5. Boxplots of **Shannon index** computed in QIIME2 including DNA and cDNA datasets of pristine mats [labelled as (a) and (b)], controls of microcosms [labelled as (c) – smooth – and (d) – pustular –], petroleum-exposed microcosms and biofilm samples. Centre line in the boxplot represents the median, while box limits are 25th and 75th percentiles. Boxplot whiskers represent 9th and 91st percentiles and outlier values are represented as grey points. PE boxplots group all samples, plus any available duplicates, collected from microcosms exposed to 30, 60 and 120 days.

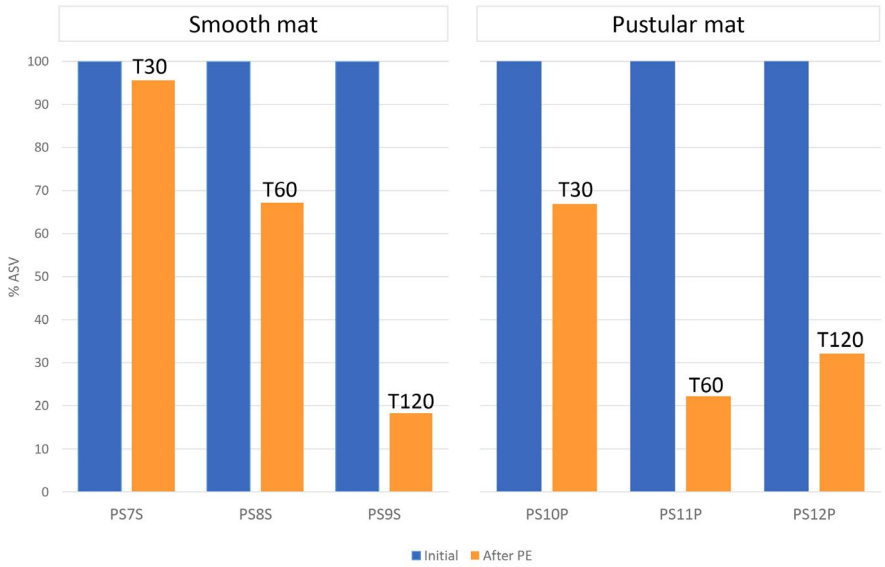

Figure 2.6. Barplots showing net loss of taxa (as % ASV) when exposed to petroleum for both smooth (left) and pustular mats (right). From left to right each pair of bars show microsoms exposed to petroleum for 30, 60 and 120 days (denoted as T30, 60 and T120).

ANOSIM analysis revealed no significant changes in the total and active microbial community (16S rDNA and 16S rRNA/cDNA) when comparing the initial controls (day 0) and control times (day 30, 60 and 120) (R=0.024; p=0.321). This indicates that the untreated communities and their activities did not change substantially under the lab-controlled conditions. However, the microbial communities shifted significantly (p=0.002) when they were exposed to petroleum for both mat types (Smooth mats: R=0.583 and pustular mats: R=0.831).

Microbial community responses were also analysed by PCA, which revealed a distinctive separation between initial and petroleum stressed communities in both mat types (**Figure 2.7**). According to the PCA results, the microbial communities in the smooth mats only started to change after 60 days or 120 days of PE. In contrast, the microbial communities in the pustular mats differed appreciably from the controls after 30 days of PE but did not show notable changes after T60 or T120 of PE. PCA plots including all control microcosms are displayed in the supplementary material (**Figure A2.11**).

2.4.2. Phylum level changes in the taxonomic composition of active bacterial microbiomes in smooth and pustular mats

In total, forty bacterial and three archaeal phyla were identified over the course of the experiment. Proteobacteria, Bacteroidetes, Cyanobacteria, Chloroflexi, Planctomycetes, Spirochaetes, Verrucomicrobia and Firmicutes were the dominant active phyla (*i.e.,* comprising more than 1% of reverse transcribed 16S rRNA) in the initial and PE samples (**Figure 2.8**). In the initial samples Proteobacteria were the dominant phyla comprising 31.9-48.9% in both mat types. This was followed by Bacteroidetes 5.9-17.5%, Chloroflexi 5.3-17.6%., Cyanobacteria 3.9-17.6% and Planctomycetes 0.9-15.0%. Spirochaetes and Verrucomicrobia comprise only up to 2% in the initial smooth and pustular mat samples (**Figure 2.8**, **Table A2.2**, **Table A2.3**, **Table A2.4** and **Table A2.5**).

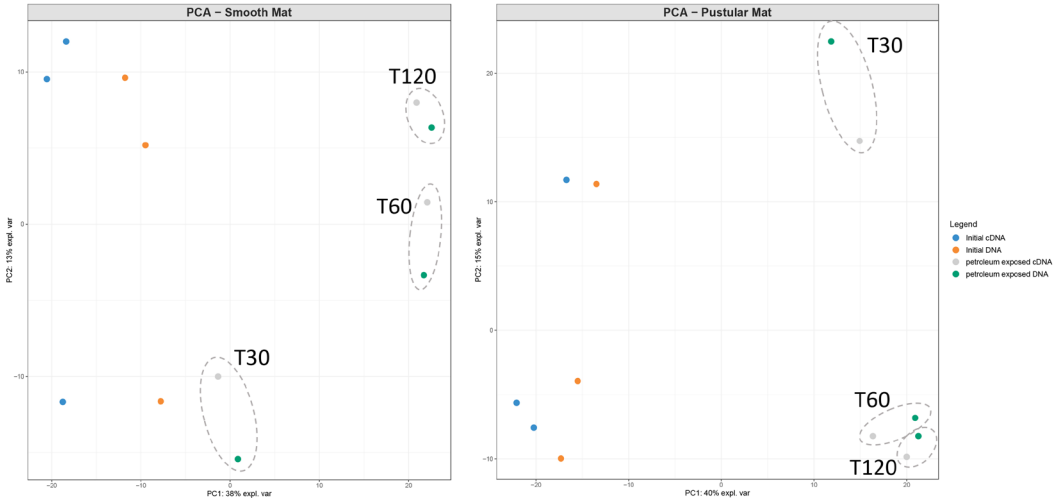

Figure 2.7. Principal Component Analysis (PCA) plots showing microbiome shifts (initial –T0– *vs*. maximum time of incubation –T30, T60 or T120–) in petroleum incubation experiments in smooth (left) and pustular mat (right) microcosms.

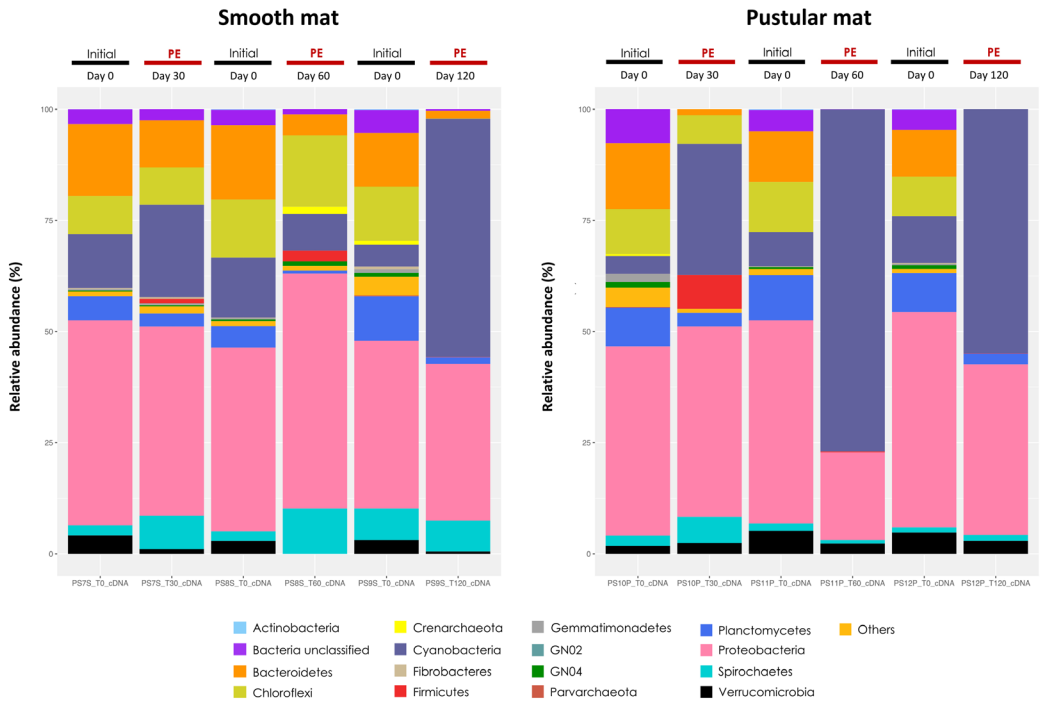

Figure 2.8. Relative abundance of the active (cDNA) bacterial microbiomes at phylum level, comparing initial microbial communities (Initial – Day 0) to those evolved after PE for 30, 60 or 120 days) in both smooth (left) and pustular (right) microbial mat microcosms. See **Table A2.2**, **Table A2.3**, **Table A2.4** and **Table A2.5** for parallel 16S rDNA community data.

Upon PE, the most prominent changes in the active phyla distribution were observed for cyanobacteria in both mat types (**Figure 2.8**). These changes were not observed in the parallel control samples (**Table A2.2**, and **Table A2.4**). In the pustular mat samples active cyanobacteria increased substantially at day 30 and comprised the dominant active phyla at T60 (75%) and T120 (54.9%). In the smooth mat samples active cyanobacteria increased in abundance later and comprised the dominate phyla 120 days after PE (53.6%). Active Bacteroidetes progressively declined in relative abundance in the smooth mat microcosms upon PE, but completely disappeared in the pustular mat after 60 days of PE. Active Chloroflexi disappeared after 60 and 120 days of PE in pustular and smooth mats, respectively. Planctomycetes became less active and/or reached detection limits in both mat types after 60 days of PE. The activity of Spirochaetes was slightly stimulated especially in the smooth mats. The activity of Verrumicrobia, which never represented more than 5% of the active population, was also found to be only slightly affected by PE especially in the pustular mats. Firmicutes were slightly stimulated by PE, they represented between 1 and 5% of the active population at 30 days of PE in both mat microcosms. Physical changes observed

between control (all types) and PE microcosms for smooth and pustular mats can be found in the supplementary material (**Figure A2.11**, **Figure A2.12**, **Figure A2.13** and **Figure A2.14**).

2.4.3. Microbial mat taxa response to petroleum exposure

Exposure of microbial mats to petroleum triggered positive and negative effects on different taxonomic groups (**Figure 2.9**). The negatively affected phyla (ceased or no longer detected) in both types of microbial mats mainly belonged to Deltaproteobacteria (20.2-26.7%), Bacteroidetes (10.6-23.7%) and unclassified Bacteria (9.5-21.1%). In PE smooth mat microcosms, Alphaproteobacteria (15.3-20.3%) and Cyanobacteria (9.9-13.2%) were also greatly affected, followed by a lower proportion of Verrucomicrobia, Planctomycetes and Chlorobi. Instead, in pustular mat PE microcosms, Chloroflexi (12.5-21.3%) and Planctomycetes (8.6-13.2%) largely disappeared once exposed to petroleum, while other microorganisms belonging to Alphaproteobacteria, Gemmatimonadetes and GN04 were also disturbed. At phylum level, PE smooth mat microcosms experienced an increase of Gammaproteobacteria, Cyanobacteria and Alphaproteobacteria, up to 36.7%, 20.2% and 11.7%, respectively. Interestingly, Epsilonproteobacteria represented an active group particularly stimulated under the stressful conditions in this type of mat, ranging between 8.5 to 16.7 % (T60-T120). In contrast, the taxonomical diversity of those positively affected organisms in PE pustular mat microcosms decreased compared to smooth mats. At 30 day of PE, Gammaproteobacteria (57.4%) dominated this group, followed by Cyanobacteria (25.4%), Alphaproteobacteria (14.2%) and Firmicutes (3.0%), whereas after 60 days of exposure Cyanobacteria was the dominant group (> 85%).

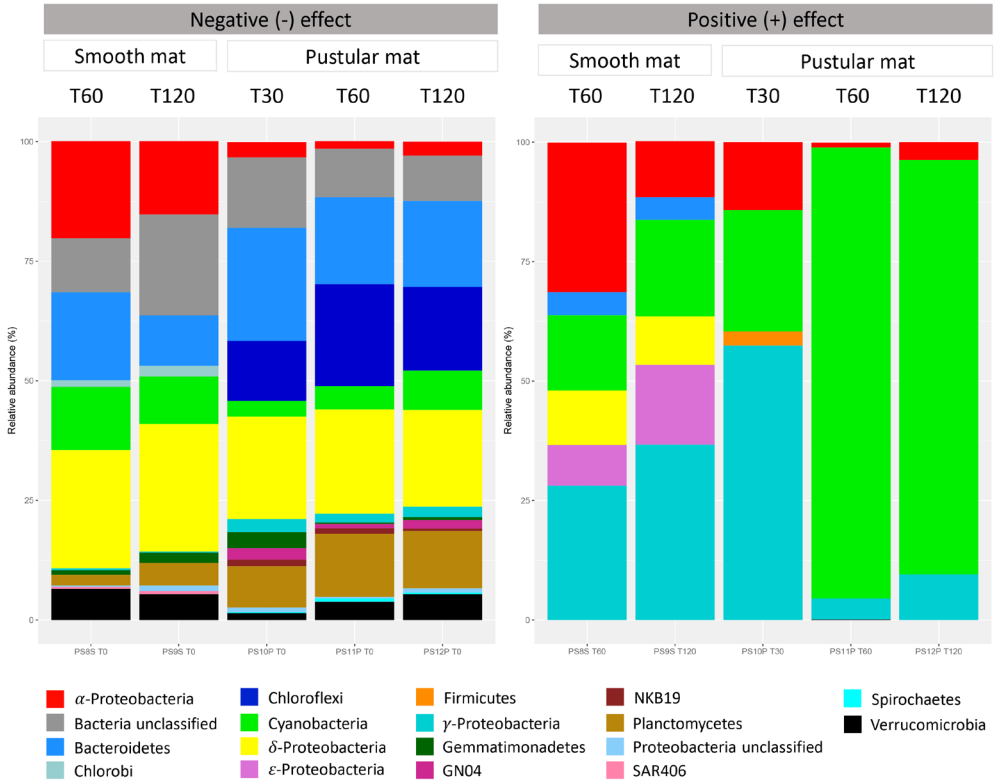

Figure 2.9. Stacked bar plots showing those active taxa (phylum-class level) that are negatively (absent) or positively affected (emerged or increased its abundance) because of petroleum exposure. Data corresponds to those indicator species statistically determined by ISA and regrouped at a higher taxonomical level. N.B. According to PCA (**Figure 2.7**), no significant changes in the community structure was observed in the smooth microcosms after 30 days of PE. Therefore, this data point for the smooth mat is not shown here.

At species level, ISA revealed thirteen taxa with a statistically significant response to PE in the smooth mat microcosms (**Table A2.6**). Combined they comprised between 11.5 and 20.0% of the total active population exposed to petroleum and only 0.2 to 1.0% of the active population in the initial smooth mats. ISA was not performed on smooth mats after only 30 days of PE, since according to PCA these communities did not yet differ significantly from the controls. Thirteen taxa were also identified from the pustular mats that showed a significant response to PE. Combined, these indicator taxa comprised between 9.9 and 79.6% of the total population in the petroleum-exposed pustular mat samples and only 0.9 to 1.7% of the population in the initial pustular mat samples.

Six statistically significant indicator taxa were shared between petroleum-exposed smooth and pustular mats (**Table A2.6**). They represent those taxa which consistently emerged in all PE microcosms regardless of the maximum exposure time. These included Cyanobacteria belonging to genus *Halomicronema*, Alphaproteobacteria (*Thalassospira xiamenensis*) as well as Gammaproteobacteria (Family Alteromonadaceae, *Marinobacter bryozoorum*, *Halothiobacillus hydrothermalis* and *Halomonas*). Indicator taxa that were distinctive to PE smooth mats included *Marinilabilia salmonicolor* (Bacteroidetes), *Nesiotobacter exalbescens* and *Caenispirillum salinarum* (Alphaproteobacteria), sulfate-reducing bacteria of the genera *Desulfovibrio* and *Desulfuromonas* (Deltaproteobacteria), *Helicobacter* (Epsilonproteobacteria), and *Salinivibrio costicola* (Gammaproteobacteria). Indicator taxa that were characteristic to PE pustular mats included the cyanobacterium *Halomicronema excentricum,* one of the more abundant organisms after 60 days of PE. In addition, the Family Cyanobacteriaceae, Family Ruminococcaceae (Firmicutes), *Henriciella* (Alphaproteobacteria), and Gammaproteobacteria: *Marinobacter* and *Porticoccus hydrocarbonoclasticus* were also found in abundance.

Analysis of the loading plots generated in MixOmics yielded additional taxa that helped to differentiate the PE microbial communities from the initial microbiomes (PC1 contribution >0.075 - **Figure 2.10**). They were low in abundance and were only detected in the microcosms exposed to petroleum for 30 days, or emerged later after 60 or 120 days of PE (dotted black square in **Figure 2.11**) (see vectors in biplot plots, supplementary material **Figure A2.15**). Their abundance ranged between 0.1 to 2%. In smooth mat PE microcosms, the indicator species were represented by: *Rhodovibrio* (Alphaproteobacteria), *Halanaerobium hydrogeninformans* (Clostridia) and *Clostridiisalibacter* and *Halocella cellulolsilytica* (Firmicutes) which were especially active at 60 days, *Alcanivorax venustensis* and other *Marinobacter* spp. (Gammaproteobacteria) which increased after 120 days, along with *Spirochaeta* spp. (Spirochaetes) and *Desulfobacter* (Deltaproteobacteria). After 30 days of PE, the pustular mat microcosms also revealed active indicator species (cDNA), all belonging to the order Clostridiales (Firmicutes): *Clostridiisalibacter*, *Clostridium cellobioparum*, *Defluvitalea saccharophila* and *Halocella cellulolsilytica.* Others that emerged after 60 or 120 days, included, *Alcanivorax spp*. (Gammaproteobacteria), *Spirochaeta halophila* (Spirochaetes), *Desulfovibrio* (Deltaproteobacteria),

Salinivibrio costicola, Candidatus *[Marinicellaceae]* (Gammaproteobacteria), *Nesiotobacter exalbescens*, *Caenispirillum salinarum* and *Rhodovibrio* (Alphaproteobacteria), *Coraliomargarita* (Verrucomicrobia) and *Halomicronema hongdechloris* (Cyanobacteria).

2.4.4. Biofilm development in pustular mat after 120 days of PE and the microbial composition across the three dimensional structure.

After 100 days of petroleum incubation, the surface of the pustular microbial mat, PS12P microcosm, was almost fully colonised by a yellowish-green mucilaginous biofilm (**Figure 2.12 A-B**). The biofilm was physically stable, cohesive, and displayed different interconnected tower-like structures. On the centre of the surface, it grew a rigid 5cm high 'tower'-shaped biofilm with an internal water-filled conduit. It was sturdily attached to the surface and continuously connected with other thin-walled biofilms (see **Video A2.1**). The base of the 'tower'-shaped biofilm, which was linked to the microbial mat, was purple brownish in colour. A small (2 x 0.5cm length/width) foamy pellicle was found free floating at the air-water interface. The biofilm continued to develop until the experiment was terminated at 120 days. Preliminary SEM analysis revealed that the biofilm comprised of an interlocking network of organic filamentous material, trapping grains of calcium carbonate (**Figure 2.12 C-D-E-F**). Furthermore, the petroleum-water interface became visibly clearer after 100 days (**Figure A2.13**– PS12P T120 microcosm). A small portion of the water phase was sacrificed to measure and compare the physicochemical parameters with the control microcosms (**Table A2.1**). Five samples were collected for 16S rRNA profiling. The samples included a portion of: foam (A), late-stage biofilm ('tower'-shaped) (B), early-stage biofilm (C), and the base of the late-stage biofilm (D), as well as the top of the pustular mat without biofilm development (E) (**Figure 2.12A** and **Figure 2.12B**).

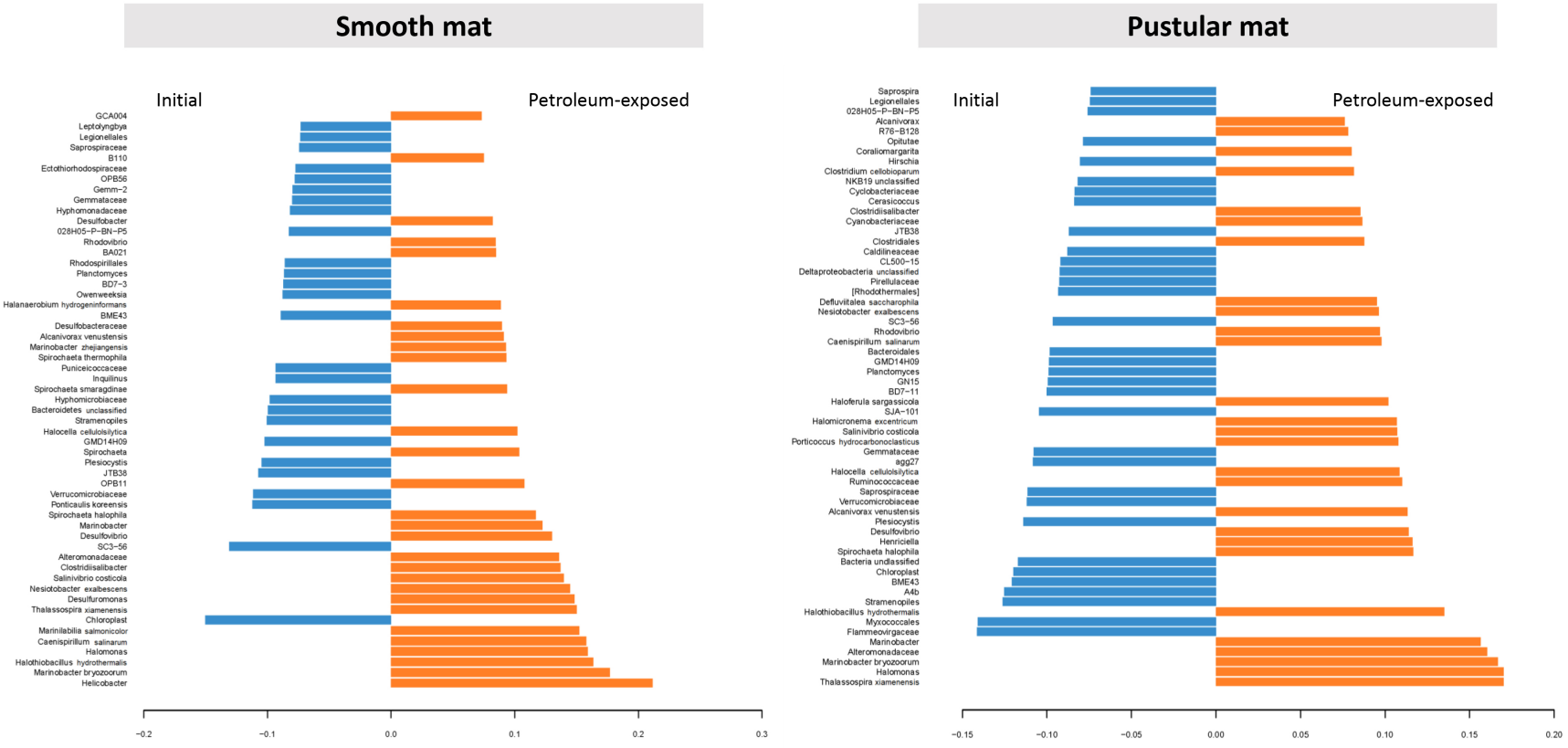

Figure 2.10. Loading plots showing the first 60 species for initial (blue) vs. PE exposed (orange) taxa in both mat types, which strongly influence principal component 1 (PC1) in the PCA plots of **Figure 2.7**. This analysis is based on the communities residing in both DNA and RNA pools. Note the highly weighted species are correlated with previous indicator species detected by ISA. This analysis was used to identify additional indicator organisms associated with degradation of hydrocarbons.

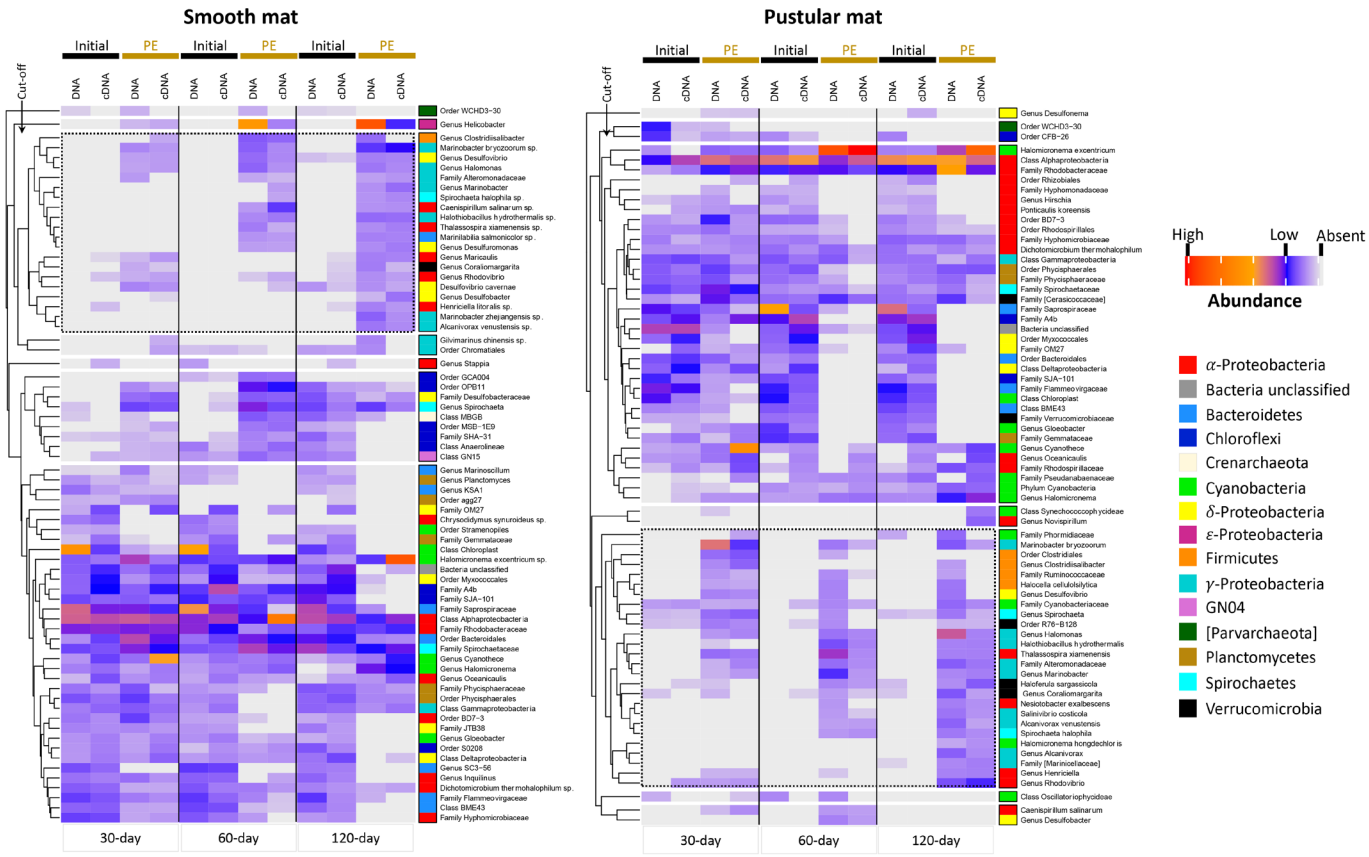

Figure 2.11. Heatmap plots depicting microbiome shifts between initial and post petroleum incubated microcosms in both smooth and pustular mats. The right column in each heatmap shows phylum or class taxonomy (legend on the bottom). NB the dotted squares mark the part of the heatmaps that include taxa that increased in abundance due to PE compared to the initials. For this analysis, the raw reads at species level were standardised by total, square root transformed, and then ranked to the 70 more abundant taxa.

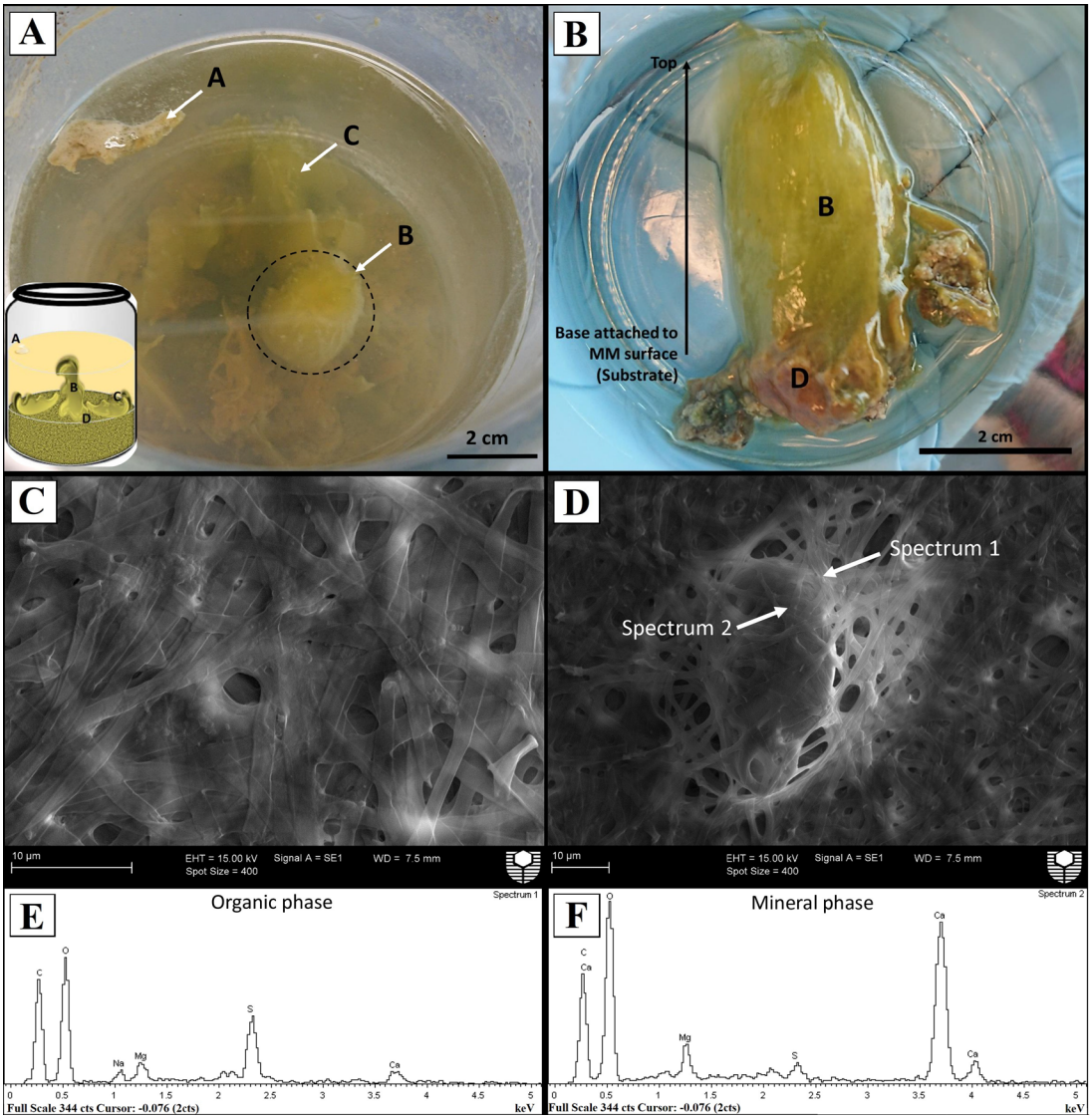

Figure 2.12. Images of a biofilm developed at the water-column interphase in a pustular mat microcosm exposed to petroleum for 120 days (PS12P T120). Top view of PS12P T120 microcosm and a schematic diagram showing the sampling points (A). Tower-shaped biofilm grown in the middle of the microcosm, denoted with the letter B (B). SEM images showing the microstructure of biofilm wall and a calcium carbonate grain trapped into the net, respectively (C and D). XRD spectra (elemental analysis) of two points in the SEM image D (E and F).

Active microbial communities in the biofilm samples, except the foam (A-cDNA), were dominated by Cyanobacteria (mainly Synechococcophycideae) followed by Alpha- and Gammaproteobacteria (**Figure 2.13A**). The microbiome of samples collected at the base of the biofilm and at the top of the pustular mat were similar in composition (**Table A2.7** and **Table A2.8**). Cyanobacteria represented 66.5% of the cDNA pool in sample D (base of the main biofilm 'tower') and 54.9% in sample E (mat without the biofilm), while Proteobacteria comprised respectively 28.9% and 38.4% of the cDNA pool in these samples. Alphaproteobacteria were the most abundant Proteobacteria with 19.9% in sample D and 28.3% in sample E. Planctomycetes (Phycisphaerae subclass) and Verrucomicrobia (Opitutae and Verucomicrobiae sub-classes) did not exceed 3% each. Cyanobacteria (mostly Synechococcophycideae) dominated the community and reached up to 80% in samples collected from the main 'tower' of the biofilm, regardless of its development stage (samples B –late stage- and C –early stage). Alpha- and Gammaproteobacteria were the next two dominant classes, with 10.7% and 4.2% contribution in sample B and 13.4% and 4.5% in sample C. In contrast to mat samples, biofilm samples also contained a variety of other phyla with contribution ≤ 1%: Acidobacteria, Actinobacteria, Bacteroidetes, BCR1, Planctomycetes, Thermi and Verrucomicrobia.

2.4.5. Active microbiome in the biofilm-related samples of microcosm PS12P.

At species level, biofilm-related samples exhibited differences in their microbiomes (**Figure 2.13B**, **Figure A2.16**). Biplot visualisation clearly shows species favoured at each stage of the biofilm development. Sub-samples collected in the main biofilm 'tower' (samples B and C) were dominated by Cyanobacteria (*Halomicronema* and Pseudanabaenacea) (>55% relative abundance) (**Table A2.9**), while *Halomicronema excentricum* was the dominant species in sample D (biofilm base) (55.9%). Unlike samples B, C and D, the free-floating foam (sample A) was mainly composed of *Alcanivorax venustensis* (Gammaproteobacteria) (35.2%) and genus *Halomicronema* (17.1%). The remaining microbial community was comprised of a highly diverse suite of low abundant taxa (0.1% and 1%); many belonging to Alpha- and Gammaproteobacteria, with phylogenetic affiliations to known hydrocarbon degrading species (**Figure A2.16**). **Figure 2.13B** shows that the early stage of biofilm development was characterised by various species belonging to *Cyanothece* (a diazotophic cyanobacteria), *Nesiotobacter exalbescens*, Hyphomicrobiaceae (purple

bacteria), *Coraliomargarita, Marinobacter spp.*, *Thalassospira xiamenensis, Halomicronema hongdechloris*, Phycisphaeraceae and unclassified Gammaproteobacteria. In contrast, the late-stage biofilm can be differentiated by the presence of *Gemmata*, *Halorhodospira*, Caulobacteraceae, Pseudanabaenaceae, *Methylobacterium adhesivum*, *etc*. The foam sample instead holds a very different group of specialised organisms, *i.e*., Oxalobacteraceae and Comamonadaceae (Betaproteobacteria), *Stenotrophomonas* (Gammaproteobacteria), *Rhodococcus globerulus*, *Gilvimarinus chinensis*, *Oceanicaulis*, *Rhizobium daejeonense* and *Halomonas*.

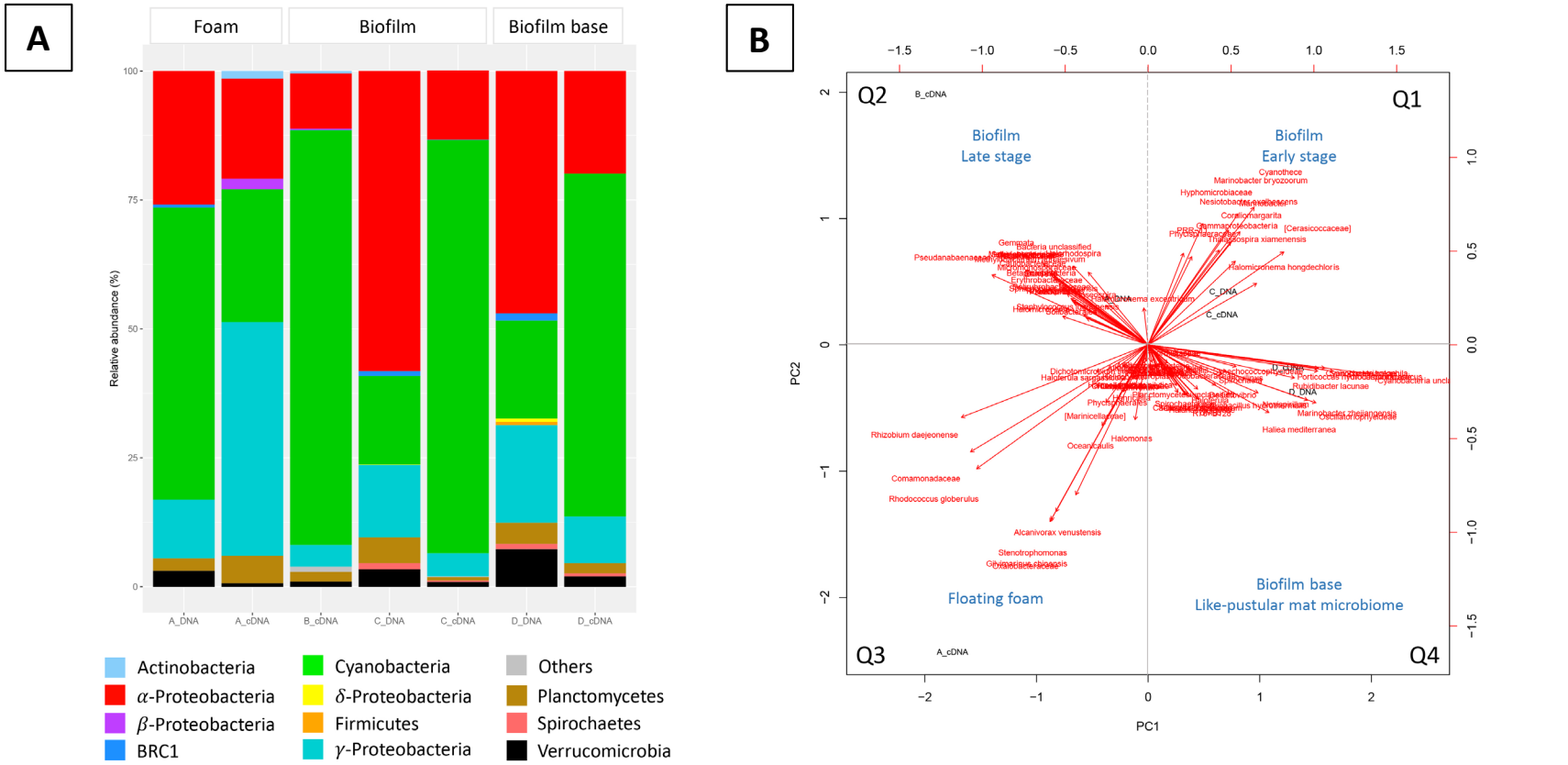

Figure 2.13. Relative abundance of the total (DNA) and active (cDNA) bacterial microbiomes at phylum/class level of the biofilm-related samples (*i.e.*, foam, biofilm, and biofilm base) in a pustular mat microcosm exposed to petroleum for 120 days (PS12P T120) (A). Biplot displaying both biofilm-related samples and key variables (species) associated with each sample. These variables are represented by vectors. Note the pattern followed by the samples allowed them to split the plot in four quadrants, showing the driver / indicator species (B).

2.5. Discussion

The microbial community structure in the pristine smooth and pustular mats revealed a similar distribution when compared to previous 16S rRNA/rDNA studies of SB Nilemah microbial mats (Allen et al., 2009). Both mat types are dominated by Proteobacteria, Bacteroidetes, Planctomycetes, Cyanobacteria, Spirochaetes, and Chloroflexi (**Figure 2.8**). The resident (DNA) community of both mat types shows that the pustular mat has a higher species richness and diversity compared to the smooth mat, but in this study parallel ribosomal transcriptome sequencing revealed that the smooth mats comprised a higher relative abundance of active communities. Recent functional metatranscriptome sequencing performed on both mat types from SB also suggest a higher density of active microbes in the smooth mats (Campbell et al., 2020). This is furthermore in agreement with the concentration profiles of oxygen and hydrogen sulfide in SB microbial mats, consistent with the higher cell densities of aerobic bacteria and thus a more intense cycling of carbon in the surface layers of smooth mats compared to pustular mats (Wong et al., 2015).

2.5.1. Microfabric of microbial mats- a driver for microbiome stress resistance

Smooth and pustular mats showed different responses to long term PE. The microbiome of the smooth mat appears to be more resistant towards environmental stress than that of the pustular mat. The microbiome of the smooth mat was still highly similar (>60%) to the initial composition after 30 days of PE, whereas the species richness of the pustular mat was already severely affected after 30 days. The microfabric of the different mat types may have had a profound effect on their microbiome's resistance towards PE. The smooth mat consists of thin, horizontal and uniform laminations of well-sorted grains of aragonite and small ooids, interbedded with filamentous bacteria and EPS products (Jahnert and Collins, 2013). Smooth mats also contain fused micrite cements and ooids, and thus are more cohesive and compact and therefore exhibit a lower porosity than pustular mats (Plet et al., 2018). Consequently, the micro-layers of the smooth mats are not fully interconnected, impeding or truncating the flux of fluids between the layers thus reducing permeability (**Figure 2.2**). Further, the complex physical transport processes and chemical nanopore interactions occurring in the fine-grained layers of the smooth mats (Essaid et al., 2015) likely serve as a means of prolonged protection of its microbiome

compared to the other mat types. In contrast, pustular mats have a higher abundance of sand-size grains and fewer patches of micrite, resulting in larger and permeable pores that are more interconnected. This structure eases the transport (*i.e.*, advection, diffusion, dispersion) of pollutants into the mat, explaining why the diversity of the microbiome of the pustular mats was negatively impacted by PE earlier than the microbiome of the smooth mats.

2.5.2. Role of exopolymeric substances (EPS)

A massive biofilm was visible on the pustular mat of microcosm PS12P after 120 days of PE (see **Video A2.1**). The biofilm consisted of several 'tower-like' structures of varying heights (up to 5 cm) that were physically bound to the mat's surface and had developed an internal conduit that was filled with water and tiny droplets of petroleum (**Figure 2.12**). In contrast, the smooth mat developed a transparent, non-rigid and relatively thin layered biofilm that was drifting in parallel to the mat's surface. We infer that both mats yielded a biofilm (albeit different in appearance) in response to the PE. Microbial biofilms are well-known to develop in response to environmental stressors or unfavourable ambient conditions (Decho, 2000; Flemming et al., 2016). The pustular mats' ability to produce thicker EPS as a response to desiccation, tidal regime, high temperatures and occasionally strong winds (Jahnert and Collins, 2013; Ruvindy et al., 2016) is especially noticeable as pustules, a feature that is not observed in other types of microbial mats in the Nilemah embayment. The microfabric of the pustular mat seems to be favourable for extensive biofilm formation. A number of studies focused on understanding the effects of physical features of sediments (*i.e.*, particle size, roughness, *etc.*) and chemical conditions (*i.e.,* pH), and their relationship to biofilm adhesion or attachment (Dade et al., 1990; Decho and Gutierrez, 2017; Parker et al., 2018). Notably, large particle sizes have been shown to promote biofilm development (Lagree et al., 2018). Interestingly, smaller pores between 15 and 25nm in diameter minimise biofilm growth, as a consequence of the increase in physicochemical interactions (*i.e.,* intermolecular forces, electrostatic repulsion), which at the same time, are boosted by a higher surface area (Feng et al., 2015). These findings could explain the differences in the pustular and smooth mats' biofilm evolution in our time series PE experiment. The development of a massive biofilm in the smooth mat might be unfavourable as microorganisms are already confined in small pores. Overproduction of EPS could lead to adverse physicochemical conditions

and might destroy the microfabric that allows microhabitats to survive under PE. In contrast, pustular mats possess larger particle sizes and a higher number of pores that are better interconnected. Microorganisms would need to produce a thicker, rigid and continuous biofilm to avoiding negative impact on the more susceptible microbial communities and to reduce the percolation of pollutants in the sedimentary matrix over time.

2.5.3. Microbial community responses to petroleum exposure

Filamentous cyanobacteria of the genus *Halomicronema*, especially *Halomicronema excentricum* were dominant in the smooth and pustular mats after long term PE. Their high % abundances and the identification of filaments by SEM show that they are responsible for the fabric of the massive 'tower like' structure bound by EPS which was identified on the surface of the pustular mat (**Figure 2.11** and **Figure 2.12**). The dominance of cyanobacteria in petroleum polluted microbial mats was reported in previous studies (Diestra et al., 2004; Chaillan et al., 2006). The thin filamentous types, like *Halomicronema excentricum* (Abed et al., 2002), were observed to overgrow microbial populations after petroleum pollution or habitat disturbances (Abed et al., 2006; Hernandez-Raquet et al., 2006). In our study we observed a degradation of the petroleum pollutant most visible in the microcosm with the massive biofilm development. However, despite the dominance of cyanobacteria in petroleum polluted mats, it has been shown that they are incapable of hydrocarbon degradation (Abed and Köster, 2005). Instead, cyanobacteria can indirectly support petroleum degrading microorganisms by providing an EPS matrix for microbial attachment or petroleum emulsification (Musat et al., 2006; Abed, 2010; Stuart et al., 2016). The release of oxygen and simple organic compounds into the matrix stimulates microbial activity (Abed and Köster, 2005; Musat et al., 2006; Abed et al., 2009). Furthermore, diazotroph cyanobacteria can release nitrogen compounds into the EPS matrix that serve as nutrients for the associated microbial communities (Abed, 2010). In this study a member of unicellular diazotroph cyanobacteria (*Cyanothece*) was present in microcosms with and without PE (**Figure 2.11**). *Cyanothece* spp. are known to be highly efficient EPS producers under stressful conditions (Mota et al., 2015) and in this study appeared to be unaffected by the long-term PE. Throughout the PE experiment, *Cyanothece* was likely to be an important source of nitrogen for other microbes living in the mat. In the EPS matrix non-polar hydrocarbons such a benzene,

toluene and xylene can accumulate (Späth et al., 1998) and might provide carbon sources for petroleum-degrading microbial communities. Over the course of the PE experiment a decline in microbial diversity and a shift towards petroleum-degrading bacteria was observed in the top half cm layer of the microbial mats. The diversity of petroleum-stressed indicator species was highest in the smooth mats, but with some overlap between both mat (**Table A2.6**). Both mats shared sequences of Alpha- and Gammaproteobacteria that are known hydrocarbon degraders (**Table 2.1**). For example, members of the detected petroleum-degrading bacteria possess the ability to emulsify hydrocarbons and degrade aliphatic and aromatic compounds (see references in **Table 2.1**).

The detailed analyses of the massive biofilm subsamples from microcosm PS12P (biofilm morphotypes A, B, C and D; **Figure 2.12B**) revealed a distinct low-abundance microbial community structure in the biofilm that differed from the microbial mat (**Figure A2.16**). The biofilm harboured microbes involved in bioremediation of heavy metals, petroleum or wastewater and polysaccharide degradation (**Table 2.1**). The dominance of *Alcanivorax venustensis* on the floating foam (sub-sample A) can be explained by the presence of non-polar hydrocarbons that usually accumulate in the top phase of a water-petroleum column.

Previous studies have shown that petroleum pollution and associated input of organic matter stimulates the microbial sulfur cycle (Abed et al., 2014). PE in our study also selected for taxa putatively involved in sulfur cycling. For example, *Halothiobacillus hydrothermalis*, a chemolithoautotroph using elemental sulfur or sulfur species as electron donors (Sorokin et al., 2014), was an indicator species for both PE mat types and absent in the control samples. Furthermore, sulfate reducing bacteria (SRB) belonging to the class of Deltaproteobacteria (*Desulfovibrio* and *Desulfobacter*), as well as *Desulfuromonas*, which can reduce elemental sulfur to H_2S (Schauder and Kröger, 1993; Kleikemper et al., 2002), were indicator species for the PE smooth mats and were only present at low relative abundance in the non-PE mat microcosms.

Table 2.1. Hydrocarbon-degraders identified in petroleum exposure microcosms.

Mat type or biofilm	Phyla/class	Family, genus or species	Function/ Ecology	References
Pustular and Biofilm	γ-proteobacteria	*Porticoccus hydrocarbonoclasticus*	Obligate Polycyclic Aromatic Hydrocarbon (PAH) degrader and can metabolise n-hexadecane, phenanthrene, pyrene, anthracene and fluorene	(Gutierrez et al., 2012, 2015; Gutierrez, 2019)
Smooth, Pustular and Biofilm	α-proteobacteria	*Nesiotobacter exalbescens*	Toluene degrader Hydrocarbon emulsifier	(Ganesh et al., 2019)
		Thalassospira	Degrade aromatic hydrocarbons - tolerate hydrocarbon polluted sediments	(Zhao et al., 2010; Kappell et al., 2014; Gutierrez et al., 2015; Zhou et al., 2016)
	γ-proteobacteria	*Marinobacter* spp.	Degrading aliphatic and aromatic components	(Huu et al., 1999; Hedlund et al., 2001; Li et al., 2013)
		Halomonas spp.	Degrade a variety of aliphatic and aromatic hydrocarbons under hypersaline conditions	(Oie et al., 2007; McGenity, 2010; Moreno et al., 2011; Gutierrez et al., 2013; Yastrebova et al., 2019)
		Alcanivorax venustensis	Hydrocarbon degrader, capable to grow and metabolise in alkanes and organic acids	(Fernández-Martínez et al., 2003; Liu et al., 2019)
Biofilm	Verrucomicrobia	*Coraliomargarita*	Bioremediation of heavy metals	(Zhou et al., 2019)
	γ-proteobacteria	*Stenotrophomonas*		(Shuona et al., 2017)
	Actinobacteria	*Rhodococcus globerulus*	Petroleum or wastewater degrading bacteria	(Paje et al., 1997)
	α-proteobacteria	*Rhizobium daejeonense*		(Quan et al., 2005)
	α-proteobacteria	*Erythrobacteraceae*		(Ribicic et al., 2018)
	β-proteobacteria	*Comamonadaceae*		(Li et al., 2008)
	Actinobacteria	*Micromonosporaceae*	Polysaccharide degradation	(Yeager et al., 2017)

PE stimulated some genera in the Alphaproteobacteria belonging to the purple non-sulfur bacteria (PNSB). PNSB are metabolically versatile and they are capable of thriving as photoautotrophs, photoheterotrophs or chemoheterotrophs (Bryant and Frigaard, 2006; Hädicke et al., 2011). For example, in both mat types the genus *Rhodovibrio* was present after PE and only at trace levels in the non-exposed controls. The degradation of petroleum components as well as the decay of damaged microbial mat probably releases CO_2 and organic compounds and creates an anoxic or microaerophilic environment that is favourable for PNSB. PE furthermore caused an increase in the relative abundance of the genera *Maricaulis*, *Oceanicaulis* and *Henriciella*, which comprise obligate aerobic and nitrate reducing chemoautotrophs of the family Hyphomonadacea (Alphaproteobacteria) (Quan et al., 2009). All members of these genera are flagellated swarmer cells and *Maricaulis* and *Oceanicaulis* also possess non-motile stalked cells, with the ability to raise themselves from the attached surface. Bacteria capable of swarming and/or stalking would have an advantage over

non-motile bacteria in the PE mats as they will be able to escape the toxic environment (Harshey and Partridge, 2015).

Helicobacter (Epsilonproteobacteria) was a prominent indicator species in the PE smooth mat and was not detected in the control samples nor in any samples of the pustular mat (**Figure 2.11**). *Helicobacter pylori* is the best-known member of this genus for its role in gastrointestinal infectious disease (Kusters et al., 2006). However, members of Epsilonproteobacteria have been repeatedly found in samples from formation and production waters in low-temperature (<50 °C) and low-depth (<80 m) biodegraded or heavy petroleum reservoirs (Grabowski et al., 2005; Pham et al., 2009; Hubert et al., 2012) and other deep-sea environments (Campbell et al., 2006). The metabolic capability of the detected *Helicobacter* is not clear yet but might be similar to *H. pylori*, a microaerophilic H_2 oxidiser (Kuhns et al., 2016). The genus *Helicobacter* possess flagellates and are motile (Lertsethtakarn et al., 2011). For example, the helical shape of the human pathogen *H. pylori* is favourable for penetration of mucoid layers. A flagellated mobility combined with a helical cell shape could be a benefit for successful lodgement on the flat biofilm of the smooth mat.

Both microbial mats established an oil-utilising microbial community on their mat surfaces. However, more than two third of the pristine microbial community disappeared in both mat types and only a small fraction of the original microbes was able to cope with long term PE. In our experiment the ability of microbes to survive and adapt to this environmental stress seems to be determined by their physiological elasticity (*e.g.* adaptation to micro-oxic/anoxic conditions in a decaying environment), their mobility (*e.g.* flagellates allow the cell to position itself along an environmental gradient with more favourable conditions) and especially the form of attachment and growth (*e.g.* capability of massive EPS production to protect cells from chemical exposure).

2.6. Conclusions

To the best of our knowledge this is the first study incubating living smooth and pustular microbial mats from SB under long-term PE. The study explored the microbiome stress responses and identified potential physical drivers explaining microbial succession over time. The results of this research revealed: (1) The smooth mat microbiome displayed a higher microbial resistance under PE, while the pustular

mat microbiome seemed to be more sensitive to hydrocarbons pollutants, likely as a result of differences in their microfabric architecture; (2) EPS production appeared to be an important microbial stress response in both mat types. The pustular mat structure provided a better mode of attachment for EPS-producing bacteria. The extensive EPS formation on pustular mat created a unique habitat for petroleum-degrading bacteria and the EPS structure supported bioremediation processes. (3) While PE stimulated hydrocarbon-degrading bacteria in both mat types over two thirds of the pristine microbial population in the mats disappeared after long-term PE. The more resistant microbes belonged to the phyla Cyanobacteria, Alpha-and Gammaproteobacteria in both mat types, and to Delta-and Epsilonproteobacteria and Bacteroidetes in the smooth mat. Their mode of life (*e.g.* physiological elasticity, mobility, EPS producing capability) has a profound impact on their survival. It still needs to be determined to what degree the different microbial mats might recover after petroleum stress removal. This research provides some insights into the stress resistance of microbial mats from SB under PE and might help for future ecosystem management plans.

2.7. Author contributions

KG proposed the research idea. YJ, KG, CW and MC designed the microcosm's settings and fieldwork. YJ designed microcosms sampling and performed all lab work and bioinformatics pipeline. YJ, CW and MC contributed to statistical analysis. YJ improved R scripts and generated all visualisations and tables. YJ, KG, CW and MC authors contributed to data analysis and writing of the paper.

2.8. Funding

This research was funded by Australian Research Council #LP150100341 and ARC DP (DP15010223). Part of this research was undertaken using Zeiss Evo 40XVP SEM with Oxford Instruments SiLi X-ray detector and Inca software (Manufacturer: Zeiss, Germany) (ARC LE0775553) at the John de Laeter Centre, Curtin University.

2.9. Acknowledgments

The authors would like to acknowledge Bush Heritage and Western Australia Department of Parks and Wildlife for their collaboration with the logistics and issuing all permits necessary to access to this protected area, respectively. WA-OIGC, TIGeR

and Curtin University supported this work with technical and financial assistance. This research was also supported by Graduate Research School at Curtin University, awarding a Curtin International Postgraduate Research Scholarship (CIPRS) to the main author. Yalimay Jimenez is deeply thankful to Bettina Schaefer, Matthew Campbell, Darcy Jack Greenwood, Paul Greenwood, Therese Morris, Peter Hopper and Dr. Alex Holman (WA-OIGC) who provided support either during fieldwork, training, or laboratory activities. In addition, authors thank Ms Elaine Miller (John de Laeter Centre - Electron Microscope Facility Manager) for her kind technical support.

2.10. Conflict of interest

The authors declare that the research was conducted in the absence of any commercial or financial relationships that could be construed as a potential conflict of interest.

2.11. Data accessibility

Raw reads datasets generated for this research can be found in "Shark_Bay_PE_Ecological_Responses" repository at https://github.com/yalimay.

2.12. References

Abed, R. M. M. (2010). Interaction between cyanobacteria and aerobic heterotrophic bacteria in the degradation of hydrocarbons. International Biodeterioration & Biodegradation 64, 58–64. doi:10.1016/j.ibiod.2009.10.008.

Abed, R. M. M., Al-Kharusi, S., Prigent, S., and Headley, T. (2014). Diversity, Distribution and Hydrocarbon Biodegradation Capabilities of Microbial Communities in Oil-Contaminated Cyanobacterial Mats from a Constructed Wetland. PLoS ONE 9, e114570. doi:10.1371/journal.pone.0114570.

Abed, R. M. M., Al-Thukair, A., and De Beer, D. (2006). Bacterial diversity of a cyanobacterial mat degrading petroleum compounds at elevated salinities and temperatures: Microbial mats from Saudi Arabia. FEMS Microbiology Ecology 57, 290–301. doi:10.1111/j.1574-6941.2006.00113.x.

Abed, R. M. M., Dobretsov, S., and Sudesh, K. (2009). Applications of cyanobacteria in biotechnology. Journal of Applied Microbiology 106, 1–12. doi:10.1111/j.1365-2672.2008.03918.x.

Abed, R. M. M., and Köster, J. (2005). The direct role of aerobic heterotrophic bacteria associated with cyanobacteria in the degradation of oil compounds. International Biodeterioration & Biodegradation 55, 29–37. doi:10.1016/j.ibiod.2004.07.001.

Abed, R. M. M., Safi, N. M. D., Köster, J., Beer, D. de, El-Nahhal, Y., Rullkötter, J., et al. (2002). Microbial Diversity of a Heavily Polluted Microbial Mat and Its Community Changes following Degradation of Petroleum Compounds. Appl. Environ. Microbiol. 68, 1674–1683. doi:10.1128/AEM.68.4.1674-1683.2002.

Allen, M. A., Goh, F., Burns, B. P., and Neilan, B. A. (2009). Bacterial, archaeal and eukaryotic diversity of smooth and pustular microbial mat communities in the hypersaline lagoon of Shark Bay. Geobiology 7, 82–96. doi:10.1111/j.1472-4669.2008.00187.x.

Almeida, A., Mitchell, A. L., Tarkowska, A., and Finn, R. D. (2018). Benchmarking taxonomic assignments based on 16S rRNA gene profiling of the microbiota from commonly sampled environments. Gigascience 7. doi:10.1093/gigascience/giy054.

Australian Maritime Safety Authority (AMSA) (2012). Report on the 2011/12 Review of the National Plan to Combat Pollution of the Sea by Oil and Other Hazardous and Noxious Substances and the National Maritime Emergency Response Arragements (2011-2012). Australian Government Available at: https://www.amsa.gov.au/sites/default/files/natplan-review-report.pdf [Accessed June 9, 2020].

Benthien, M., Wieland, A., Oteyza, T. G. de, Grimalt, J. O., and Kühl, M. (2004). Oil-contamination effects on a hypersaline microbial mat community (Camargue, France) as studied with microsensors and geochemical analysis. Ophelia 58, 135–150. doi:10.1080/00785236.2004.10410221.

Berthe-Corti, L., and Nachtkamp, M. (2010). "Bacterial Communities in Hydrocarbon-Contaminated Marine Coastal Environments," in Handbook of

Hydrocarbon and Lipid Microbiology, ed. K. N. Timmis (Berlin, Heidelberg: Springer), 2349–2359. doi:10.1007/978-3-540-77587-4_171.

Bokulich, N. A., Kaehler, B. D., Rideout, J. R., Dillon, M., Bolyen, E., Knight, R., et al. (2018). Optimizing taxonomic classification of marker-gene amplicon sequences with QIIME 2's q2-feature-classifier plugin. Microbiome 6, 90.

Bolyen, E., Rideout, J. R., Dillon, M. R., Bokulich, N. A., Abnet, C. C., Al-Ghalith, G. A., et al. (2019). Reproducible, interactive, scalable and extensible microbiome data science using QIIME 2. Nature biotechnology 37, 852–857.

Bordenave, S., Goñi-Urriza, M. S., Caumette, P., and Duran, R. (2007). Effects of Heavy Fuel Oil on the Bacterial Community Structure of a Pristine Microbial Mat. Applied and Environmental Microbiology 73, 6089–6097. doi:10.1128/AEM.01352-07.

Bryant, D. A., and Frigaard, N.-U. (2006). Prokaryotic photosynthesis and phototrophy illuminated. Trends in Microbiology 14, 488–496. doi:10.1016/j.tim.2006.09.001.

Cáceres, M. D., and Legendre, P. (2009). Associations between species and groups of sites: indices and statistical inference. Ecology 90, 3566–3574. doi:10.1890/08-1823.1.

Callahan, B. J., McMurdie, P. J., Rosen, M. J., Han, A. W., Johnson, A. J. A., and Holmes, S. P. (2016). DADA2: high-resolution sample inference from Illumina amplicon data. Nature methods 13, 581.

Campbell, B. J., Engel, A. S., Porter, M. L., and Takai, K. (2006). The versatile epsilon-proteobacteria: key players in sulphidic habitats. Nature reviews. Microbiology 4, 458–468.

Campbell, M. A., Grice, K., Visscher, P. T., Morris, T., Wong, H. L., White, R. A. I., et al. (2020). Functional Gene Expression in Shark Bay Hypersaline Microbial Mats: Adaptive Responses. Front. Microbiol. 11. doi:10.3389/fmicb.2020.560336.

Cao, K.-A. L., Costello, M.-E., Lakis, V. A., Bartolo, F., Chua, X.-Y., Brazeilles, R., et al. (2016). MixMC: A Multivariate Statistical Framework to Gain Insight into Microbial Communities. PLOS ONE 11, e0160169. doi:10.1371/journal.pone.0160169.

Chaillan, F., Gugger, M., Saliot, A., Couté, A., and Oudot, J. (2006). Role of cyanobacteria in the biodegradation of crude oil by a tropical cyanobacterial mat. Chemosphere 62, 1574–1582. doi:10.1016/j.chemosphere.2005.06.050.

Dade, W. B., Davis, J. D., Nichols, P. D., Nowell, A. R. M., Thistle, D., Trexler, M. B., et al. (1990). Effects of bacterial exopolymer adhesion on the entrainment of sand. Geomicrobiology Journal 8, 1–16. doi:10.1080/01490459009377874.

Dashti, N., Ali, N., Eliyas, M., Khanafer, M., Sorkhoh, N. A., and Radwan, S. S. (2015). Most Hydrocarbonoclastic Bacteria in the Total Environment are Diazotrophic, which Highlights Their Value in the Bioremediation of Hydrocarbon Contaminants. Microbes and environments 30, 70–75. doi:10.1264/jsme2.ME14090.

De Oteyza, T. G., Grimalt, J. O., Llirós, M., and Esteve, I. (2006). Microcosm experiments of oil degradation by microbial mats. Science of The Total Environment 357, 12–24. doi:10.1016/j.scitotenv.2005.04.039.

Decho, A. W. (2000). Microbial biofilms in intertidal systems: an overview. Continental Shelf Research 20, 1257–1273. doi:10.1016/S0278-4343(00)00022-4.

Decho, A. W., and Gutierrez, T. (2017). Microbial Extracellular Polymeric Substances (EPSs) in Ocean Systems. Front Microbiol 8. doi:10.3389/fmicb.2017.00922.

Diestra, E., Solé, A., and Esteve, I. (2004). A comparative study of cyanobacterial diversity in polluted and unpolluted microbial mats by means CLSM. Ophelia 58, 151–156. doi:10.1080/00785236.2004.10410222.

Duran, R., and Goñi-Urriza, M. S. (2010). "Impact of Pollution on Microbial Mats," in Handbook of Hydrocarbon and Lipid Microbiology, ed. K. N. Timmis (Berlin, Heidelberg: Springer), 2339–2348. doi:10.1007/978-3-540-77587-4_170.

Edbeib, M. F., Wahab, R. A., and Huyop, F. (2016). Halophiles: biology, adaptation, and their role in decontamination of hypersaline environments. World J Microbiol Biotechnol 32, 135. doi:10.1007/s11274-016-2081-9.

Essaid, H. I., Bekins, B. A., and Cozzarelli, I. M. (2015). Organic contaminant transport and fate in the subsurface: Evolution of knowledge and understanding. Water Resources Research 51, 4861–4902. doi:10.1002/2015WR017121.

Faith, D. P. (1992). Conservation evaluation and phylogenetic diversity. Biological conservation 61, 1–10.

Fathepure, B. Z. (2014). Recent studies in microbial degradation of petroleum hydrocarbons in hypersaline environments. Front Microbiol 5. doi:10.3389/fmicb.2014.00173.

Feng, G., Cheng, Y., Wang, S.-Y., Borca-Tasciuc, D. A., Worobo, R. W., and Moraru, C. I. (2015). Bacterial attachment and biofilm formation on surfaces are reduced by small-diameter nanoscale pores: how small is small enough? NPJ Biofilms Microbiomes 1, 15022. doi:10.1038/npjbiofilms.2015.22.

Fernández-Martínez, J., Pujalte, M. J., García-Martínez, J., Mata, M., Garay, E., and Rodríguez-Valera, F. (2003). Description of Alcanivorax venustensis sp. nov. and reclassification of Fundibacter jadensis DSM 1 21 78T (Bruns and Berthe-Corti 1999) as Alcanivorax jadensis comb. nov., members of the emended genus Alcanivorax. Int. J. Syst. Evol. Microbiol. 53, 331–338. doi:10.1099/ijs.0.01923-0.

Flemming, H.-C., Wingender, J., Szewzyk, U., Steinberg, P., Rice, S. A., and Kjelleberg, S. (2016). Biofilms: an emergent form of bacterial life. Nature reviews. Microbiology 14, 563–575. doi:http://dx.doi.org.dbgw.lis.curtin.edu.au/10.1038/nrmicro.2016.94.

Ganesh, K. A., Mathew, N. C., K, S., R, K., and G, D. (2019). Genome analysis of deep sea piezotolerant Nesiotobacter exalbescens COD22 and toluene degradation studies under high pressure condition. Scientific Reports 9, 1–14. doi:10.1038/s41598-019-55115-9.

Grabowski, A., Nercessian, O., Fayolle, F., Blanchet, D., and Jeanthon, C. (2005). Microbial diversity in production waters of a low-temperature biodegraded oil reservoir. FEMS Microbiol Ecol 54, 427–443. doi:10.1016/j.resmic.2005.03.009.

Grice, K., Alexander, R., and Kagi, R. I. (2000). Diamondoid hydrocarbon ratios as indicators of biodegradation in Australian crude oils. Organic Geochemistry 31, 67–73. doi:10.1016/S0146-6380(99)00137-0.

Gu, Z., Eils, R., and Schlesner, M. (2016). Complex heatmaps reveal patterns and correlations in multidimensional genomic data. Bioinformatics 32, 2847–2849.

Gutierrez, T. (2019). "Aerobic Hydrocarbon-Degrading Gammaproteobacteria: Porticoccus," in Taxonomy, Genomics and Ecophysiology of Hydrocarbon-Degrading Microbes Handbook of Hydrocarbon and Lipid Microbiology., ed. T. J. McGenity (Cham: Springer International Publishing), 181–189. doi:10.1007/978-3-030-14796-9_32.

Gutierrez, T., Berry, D., Yang, T., Mishamandani, S., McKay, L., Teske, A., et al. (2013). Role of Bacterial Exopolysaccharides (EPS) in the Fate of the Oil Released during the Deepwater Horizon Oil Spill. PLoS ONE 8, e67717. doi:10.1371/journal.pone.0067717.

Gutierrez, T., Biddle, J. F., Teske, A., and Aitken, M. D. (2015). Cultivation-dependent and cultivation-independent characterization of hydrocarbon-degrading bacteria in Guaymas Basin sediments. Front. Microbiol. 6. doi:10.3389/fmicb.2015.00695.

Gutierrez, T., Nichols, P. D., Whitman, W. B., and Aitken, M. D. (2012). Porticoccus hydrocarbonoclasticus sp. nov., an Aromatic Hydrocarbon-Degrading Bacterium Identified in Laboratory Cultures of Marine Phytoplankton. Appl. Environ. Microbiol. 78, 628–637. doi:10.1128/AEM.06398-11.

Hädicke, O., Grammel, H., and Klamt, S. (2011). Metabolic network modeling of redox balancing and biohydrogen production in purple nonsulfur bacteria. BMC Syst Biol 5, 150. doi:10.1186/1752-0509-5-150.

Harshey, R. M., and Partridge, J. D. (2015). Shelter in a swarm. J Mol Biol 427, 3683–3694. doi:10.1016/j.jmb.2015.07.025.

Hedlund, B. P., Geiselbrecht, A. D., and Staley, J. T. (2001). Marinobacter strain NCE312 has a Pseudomonas-like naphthalene dioxygenase. FEMS Microbiol Lett 201, 47–51. doi:10.1111/j.1574-6968.2001.tb10731.x.

Hernandez-Raquet, G., Budzinski, H., Caumette, P., Dabert, P., Ménach, K. L., Muyzer, G., et al. (2006). Molecular diversity studies of bacterial communities of oil polluted microbial mats from the Etang de Berre (France). FEMS Microbiology Ecology; Delft 58, 550–562. doi:http://dx.doi.org.dbgw.lis.curtin.edu.au/10.1111/j.1574-6941.2006.00187.x.

Hubert, C. R. J., Oldenburg, T. B. P., Fustic, M., Gray, N. D., Larter, S. R., Penn, K., et al. (2012). Massive dominance of Epsilonproteobacteria in formation waters from a Canadian oil sands reservoir containing severely biodegraded oil. Environmental Microbiology 14, 387–404. doi:10.1111/j.1462-2920.2011.02521.x.

Huu, N. B., Denner, E. B. M., Ha, D. T. C., Wanner, G., and Stan-Lotter, H. (1999). Marinobacter aquaeolei sp. nov., a halophilic bacterium isolated from a Vietnamese oil-producing well. International Journal of Systematic and Evolutionary Microbiology, 49, 367–375. doi:10.1099/00207713-49-2-367.

Jahnert, R. J., and Collins, L. B. (2013). Controls on microbial activity and tidal flat evolution in Shark Bay, Western Australia. Sedimentology 60, 1071–1099. doi:10.1111/sed.12023.

Kappell, A. D., Wei, Y., Newton, R. J., Van Nostrand, J. D., Zhou, J., McLellan, S. L., et al. (2014). The polycyclic aromatic hydrocarbon degradation potential of Gulf of Mexico native coastal microbial communities after the Deepwater Horizon oil spill. Front Microbiol 5. doi:10.3389/fmicb.2014.00205.

Kleikemper, J., Schroth, M. H., Sigler, W. V., Schmucki, M., Bernasconi, S. M., and Zeyer, J. (2002). Activity and Diversity of Sulfate-Reducing Bacteria in a Petroleum Hydrocarbon-Contaminated Aquifer. Appl. Environ. Microbiol. 68, 1516–1523. doi:10.1128/AEM.68.4.1516-1523.2002.

Kuhns, L. G., Benoit, S. L., Bayyareddy, K., Johnson, D., Orlando, R., Evans, A. L., et al. (2016). Carbon Fixation Driven by Molecular Hydrogen Results in Chemolithoautotrophically Enhanced Growth of Helicobacter pylori. Journal of Bacteriology 198, 1423–1428. doi:10.1128/JB.00041-16.

Kusters, J. G., van Vliet, A. H. M., and Kuipers, E. J. (2006). Pathogenesis of Helicobacter pylori Infection. Clinical Microbiology Reviews 19, 449–490. doi:10.1128/CMR.00054-05.

Lagree, K., Mon, H. H., Mitchell, A. P., and Ducker, W. A. (2018). Impact of surface topography on biofilm formation by Candida albicans. PLOS ONE 13, e0197925. doi:10.1371/journal.pone.0197925.

Lertsethtakarn, P., Ottemann, K. M., and Hendrixson, D. R. (2011). Motility and Chemotaxis in Campylobacter and Helicobacter. Annu. Rev. Microbiol. 65, 389–410. doi:10.1146/annurev-micro-090110-102908.

Li, D., Yang, M., Li, Z., Qi, R., He, J., and Liu, H. (2008). Change of bacterial communities in sediments along Songhua River in Northeastern China after a nitrobenzene pollution event. FEMS Microbiol Ecol 65, 494–503. doi:10.1111/j.1574-6941.2008.00540.x.

Li, R., Zi, X., Wang, X., Zhang, X., Gao, H., and Hu, N. (2013). Marinobacter hydrocarbonoclasticus NY-4, a novel denitrifying, moderately halophilic marine bacterium. SpringerPlus 2, 346. doi:10.1186/2193-1801-2-346.

Liu, J., Zheng, Y., Lin, H., Wang, X., Li, M., Liu, Y., et al. (2019). Proliferation of hydrocarbon-degrading microbes at the bottom of the Mariana Trench. Microbiome 7, 47. doi:10.1186/s40168-019-0652-3.

Llirós, M., Gaju, N., de Oteyza, T. G., Grimalt, J. O., Esteve, I., and Martínez-Alonso, M. (2008). Microcosm experiments of oil degradation by microbial mats. II. The changes in microbial species. Science of The Total Environment 393, 39–49. doi:10.1016/j.scitotenv.2007.11.034.

McDonald, D., Price, M. N., Goodrich, J., Nawrocki, E. P., DeSantis, T. Z., Probst, A., et al. (2012). An improved Greengenes taxonomy with explicit ranks for ecological and evolutionary analyses of bacteria and archaea. The ISME journal 6, 610.

McGenity, T. J. (2010). "Halophilic Hydrocarbon Degraders," in Handbook of Hydrocarbon and Lipid Microbiology, ed. K. N. Timmis (Berlin, Heidelberg: Springer), 1939–1951. doi:10.1007/978-3-540-77587-4_142.

McGenity, T. J., Folwell, B. D., McKew, B. A., and Sanni, G. O. (2012). Marine crude-oil biodegradation: a central role for interspecies interactions. Aquat Biosyst 8, 10. doi:10.1186/2046-9063-8-10.

Moreno, M. de L., Sánchez-Porro, C., Piubeli, F., Frias, L., García, M. T., and Mellado, E. (2011). Cloning, Characterization and Analysis of cat and ben Genes from the Phenol Degrading Halophilic Bacterium Halomonas organivorans. PLoS ONE 6, e21049. doi:10.1371/journal.pone.0021049.

Mota, R., Pereira, S. B., Meazzini, M., Fernandes, R., Santos, A., Evans, C. A., et al. (2015). Effects of heavy metals on Cyanothece sp. CCY 0110 growth, extracellular polymeric substances (EPS) production, ultrastructure and protein profiles. Journal of Proteomics 120, 75–94. doi:10.1016/j.jprot.2015.03.004.

Musat, F., Harder, J., and Widdel, F. (2006). Study of nitrogen fixation in microbial communities of oil-contaminated marine sediment microcosms. Environmental Microbiology 8, 1834–1843. doi:10.1111/j.1462-2920.2006.01069.x.

Oie, C. S. I., Albaugh, C. E., and Peyton, B. M. (2007). Benzoate and salicylate degradation by Halomonas campisalis, an alkaliphilic and moderately halophilic microorganism. Water Research 41, 1235–1242. doi:10.1016/j.watres.2006.12.029.

Oksanen, J., Blanchet, F. G., Kindt, R., Legendre, P., O'hara, R. B., Simpson, G. L., et al. (2010). Vegan: community ecology package. R package version 1.17-4. http://cran. r-project. org>. Acesso em 23, 2010.

Pagès, A., Grice, K., Welsh, D. T., Teasdale, P. T., Van Kranendonk, M. J., and Greenwood, P. (2015). Lipid Biomarker and Isotopic Study of Community Distribution and Biomarker Preservation in a Laminated Microbial Mat from Shark Bay, Western Australia. Microbial Ecology 70, 459–472.

Pagès, A., Welsh, D. T., Teasdale, P. R., Grice, K., Vacher, M., Bennett, W. W., et al. (2014). Diel fluctuations in solute distributions and biogeochemical cycling in a hypersaline microbial mat from Shark Bay, WA. Marine Chemistry 167, 102–112. doi:10.1016/j.marchem.2014.05.003.

Paje, M. L. F., Neilan, B. A., and Couperwhite, l. (1997). A Rhodococcus species that thrives on medium saturated with liquid benzene. Microbiology 143, 2975–2981. doi:10.1099/00221287-143-9-2975.

Parker, S. P., Bowden, W. B., Flinn, M. B., Giles, C. D., Arndt, K. A., Beneš, J. P., et al. (2018). Effect of particle size and heterogeneity on sediment biofilm metabolism and nutrient uptake scaled using two approaches. Ecosphere 9, e02137. doi:10.1002/ecs2.2137.

Pham, V. D., Hnatow, L. L., Zhang, S., Fallon, R. D., Jackson, S. C., Tomb, J.-F., et al. (2009). Characterizing microbial diversity in production water from an Alaskan mesothermic petroleum reservoir with two independent molecular methods. Environmental Microbiology 11, 176–187. doi:10.1111/j.1462-2920.2008.01751.x.

Playford, P. E., Cockbain, A. E., Berry, P. F., Roberts, A. P., Haines, P. W., and Brooke, B. P. (2013). The geology of Shark Bay. 299.

Plet, C., Pagès, A., Holman, A. I., Madden, R. H. C., and Grice, K. (2018). From supratidal to subtidal, an integrated characterisation of Carbla Beach shallow microbial mats (Hamelin Pool, Shark Bay, WA): Lipid biomarkers, stable carbon isotopes and microfabrics. Chemical Geology 493, 338–352. doi:10.1016/j.chemgeo.2018.06.010.

Quan, Z.-X., Bae, H.-S., Baek, J.-H., Chen, W.-F., Im, W.-T., and Lee, S.-T. (2005). Rhizobium daejeonense sp. nov. isolated from a cyanide treatment bioreactor. International Journal of Systematic and Evolutionary Microbiology 55, 2543–2549. doi:10.1099/ijs.0.63667-0.

Quan, Z.-X., Zeng, D.-N., Xiao, Y.-P., Roh, S. W., Nam, Y.-D., Chang, H.-W., et al. (2009). Henriciella marina gen. nov., sp. nov., a novel member of the family Hyphomonadaceae isolated from the East Sea. Journal of microbiology (Seoul, Korea) 47, 156–161. doi:http://dx.doi.org.dbgw.lis.curtin.edu.au/10.1007/s12275-008-0290-0.

Ribicic, D., McFarlin, K. M., Netzer, R., Brakstad, O. G., Winkler, A., Throne-Holst, M., et al. (2018). Oil type and temperature dependent biodegradation dynamics - Combining chemical and microbial community data through multivariate analysis. BMC Microbiology 18, 83. doi:10.1186/s12866-018-1221-9.

Ruvindy, R., White III, R. A., Neilan, B. A., and Burns, B. P. (2016). Unravelling core microbial metabolisms in the hypersaline microbial mats of Shark Bay using high-throughput metagenomics. The ISME Journal 10, 183–196. doi:10.1038/ismej.2015.87.

Schauder, R., and Kröger, A. (1993). Bacterial sulphur respiration. Arch. Microbiol. 159, 491–497. doi:10.1007/BF00249025.

Shuona, C., Hua, Y., Jingjing, C., Hui, P., and Zhi, D. (2017). Physiology and bioprocess of single cell of Stenotrophomonas maltophilia in bioremediation of co-existed benzo[a]pyrene and copper. Journal of Hazardous Materials 321, 9–17. doi:10.1016/j.jhazmat.2016.09.002.

Sorokin, D. Y., Abbas, B., van Zessen, E., and Muyzer, G. (2014). Isolation and characterization of an obligately chemolithoautotrophic Halothiobacillus strain capable of growth on thiocyanate as an energy source. FEMS Microbiol Lett 354, 69–74. doi:10.1111/1574-6968.12432.

Späth, R., Flemming, H.-C., and Wuertz, S. (1998). Sorption properties of biofilms. , ed. T. C. P. Committee Available at: http://search.proquest.com/docview/16543526?rfr_id=info%3Axri%2Fsid%3Aprimo [Accessed May 16, 2020].

Stuart, R. K., Mayali, X., Lee, J. Z., Craig Everroad, R., Hwang, M., Bebout, B. M., et al. (2016). Cyanobacterial reuse of extracellular organic carbon in microbial mats. The ISME Journal 10, 1240–1251. doi:10.1038/ismej.2015.180.

Suosaari, E. P., Reid, R. P., Araujo, T. a. A., Playford, P. E., Holley, D. K., Mcnamara, K. J., et al. (2016). Environmental pressures influencing living Stromatolites in Hamelin Pool, Shark Bay, Western Australia. PALAIOS 31, 483–496. doi:10.2110/palo.2016.023.

Trolio, R., Grice, K., Fisher, S. J., Alexander, R., and Kagi, R. I. (1999). Alkylbiphenyls and alkyldiphenylmethanes as indicators of petroleum biodegradation. Organic Geochemistry 30, 1241–1253. doi:10.1016/S0146-6380(99)00099-6.

Volkman, J. K., Alexander, R., Kagi, R. I., Rowland, S. J., and Sheppard, P. N. (1984). Biodegradation of aromatic hydrocarbons in crude oils from the Barrow Sub-basin of Western Australia. Organic Geochemistry 6, 619–632. doi:10.1016/0146-6380(84)90084-6.

Wickham, H. (2016). ggplot2: elegant graphics for data analysis. Springer.

Wong, H., Ahmed-Cox, A., and Burns, B. (2016). Molecular Ecology of Hypersaline Microbial Mats: Current Insights and New Directions. Microorganisms 4, 6. doi:10.3390/microorganisms4010006.

Wong, H. L., Smith, D., Visscher, P. T., and Burns, B. P. (2015). Niche differentiation of bacterial communities at a millimeter scale in Shark Bay microbial mats. Scientific Reports (Nature Publisher Group); London 5, 15607. doi:http://dx.doi.org.dbgw.lis.curtin.edu.au/10.1038/srep15607.

Yastrebova, O. V., Pyankova, A. A., and Plotnikova, E. G. (2019). Phthalate-Degrading Bacteria Isolated from an Industrial Mining Area and the Processing of Potassium and Magnesium Salts. Appl Biochem Microbiol 55, 397–404. doi:10.1134/S000368381904015X.

Yeager, C. M., Gallegos-Graves, L. V., Dunbar, J., Hesse, C. N., Daligault, H., and Kuske, C. R. (2017). Polysaccharide Degradation Capability of Actinomycetales Soil Isolates from a Semiarid Grassland of the Colorado Plateau. Appl Environ Microbiol 83. doi:10.1128/AEM.03020-16.

Zhao, B., Wang, H., Li, R., and Mao, X. (2010). Thalassospira xianhensis sp. nov., a polycyclic aromatic hydrocarbon-degrading marine bacterium. Int. J. Syst. Evol. Microbiol. 60, 1125–1129. doi:10.1099/ijs.0.013201-0.

Zhou, H., Wang, H., Huang, Y., and Fang, T. (2016). Characterization of pyrene degradation by halophilic Thalassospira sp. strain TSL5-1 isolated from the coastal soil of Yellow Sea, China. International Biodeterioration & Biodegradation 107, 62–69. doi:10.1016/j.ibiod.2015.10.022.

Zhou, L.-Y., Wang, N.-N., Mu, D.-S., Liu, Y., and Du, Z.-J. (2019). Coraliomargarita sinensis sp. nov., isolated from a marine solar saltern. International Journal of Systematic and Evolutionary Microbiology, 69, 701–707. doi:10.1099/ijsem.0.003205.

Appendix 2

SUPPLEMENTARY MATERIAL

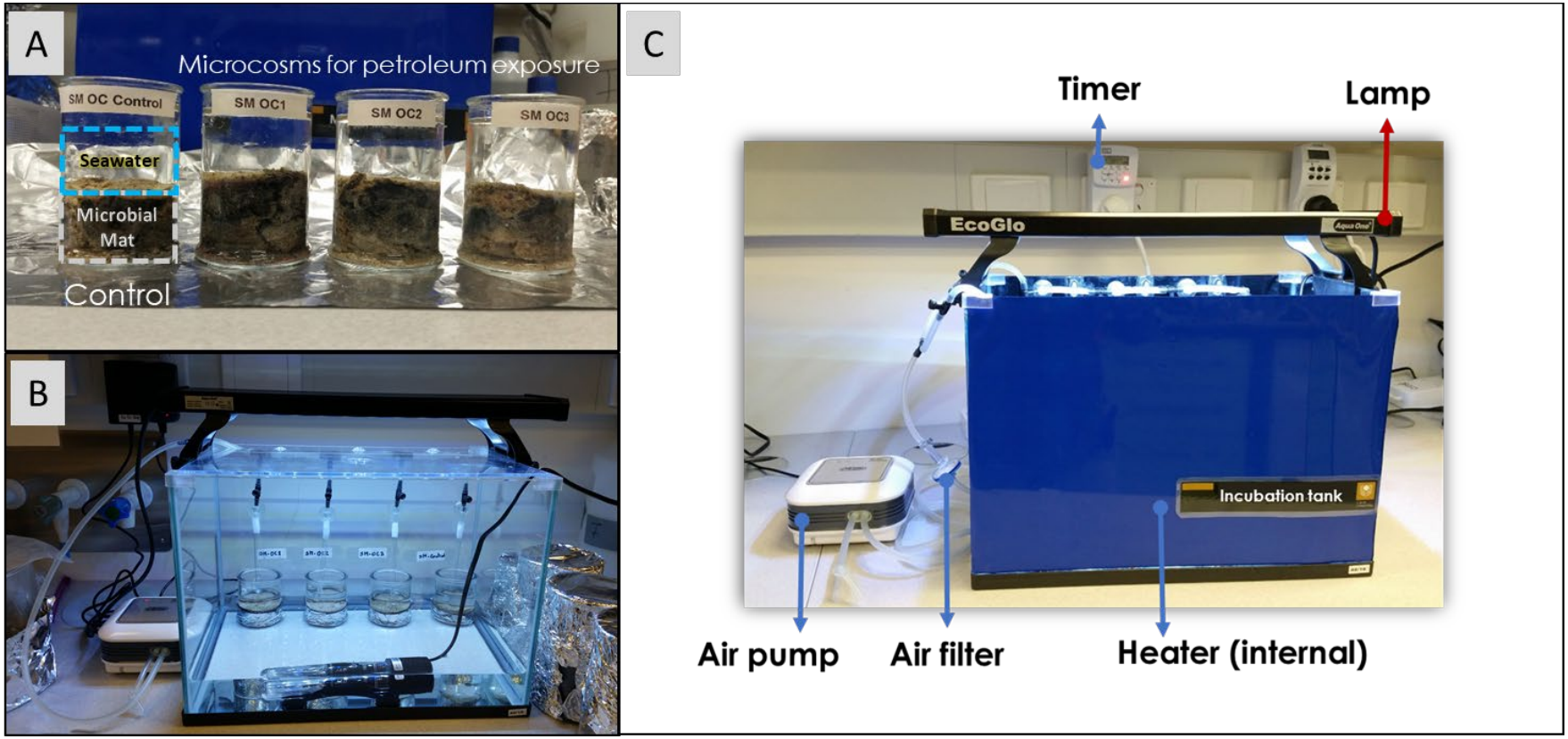

Figure A2.1. Incubation tank assemblage for simulating ecosystem conditions. Image showing the content of each microcosm: an open glass container with a piece of microbial mat and seawater on top (A). Example of internal arrangement of the microcosms in an incubation tank (B). External view of the incubation tank and its components: air pump, air filter, timer and lamp (C).

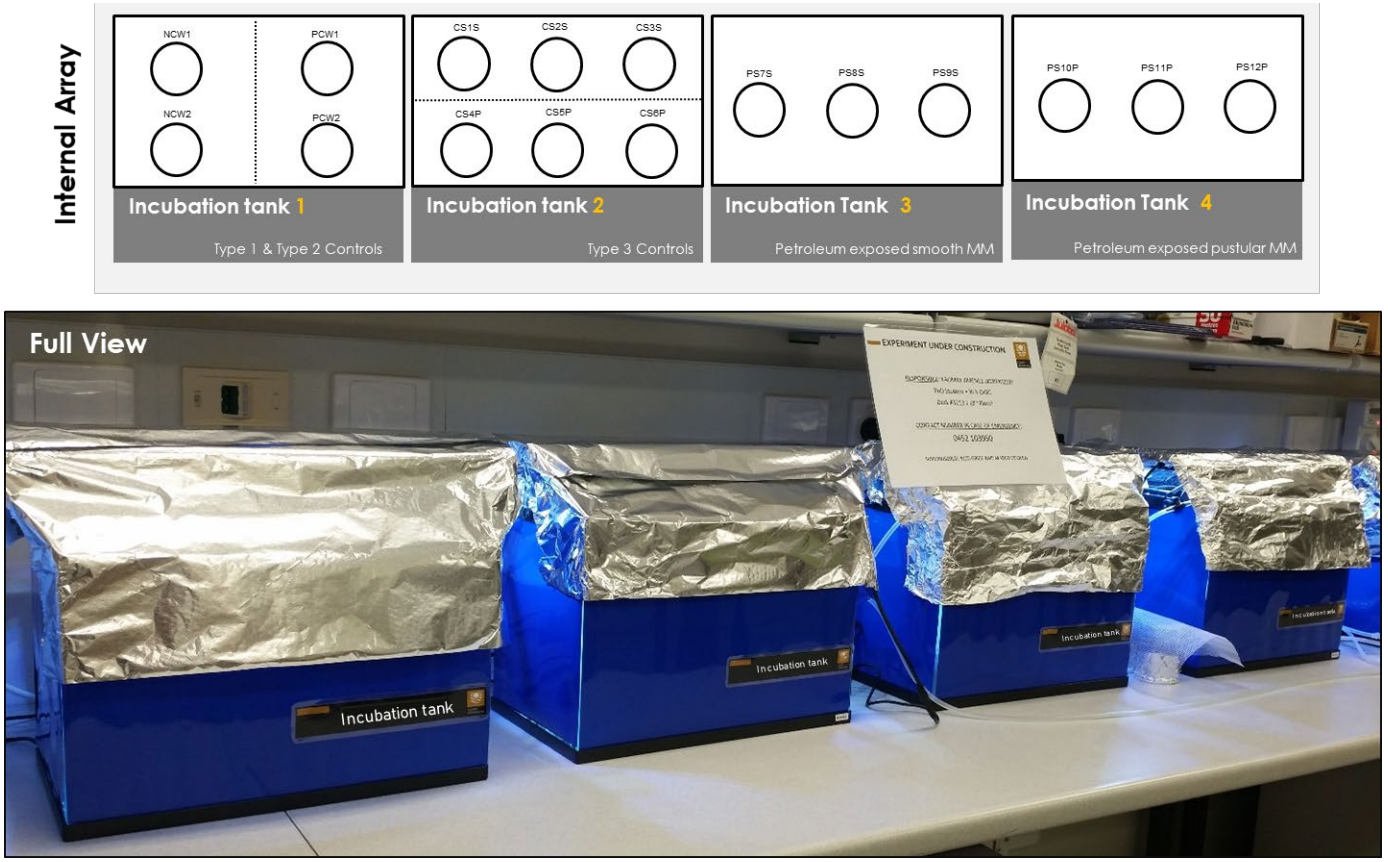

Figure A2.2. Incubation tanks configuration. The top image illustrates the internal array of microcosms in each incubation tank. Photograph on the bottom shows how they were maintained and protected under laboratory conditions. For details of types of microcosms and the nomenclature used see **Figure 2.3** and **Figure 2.4**.

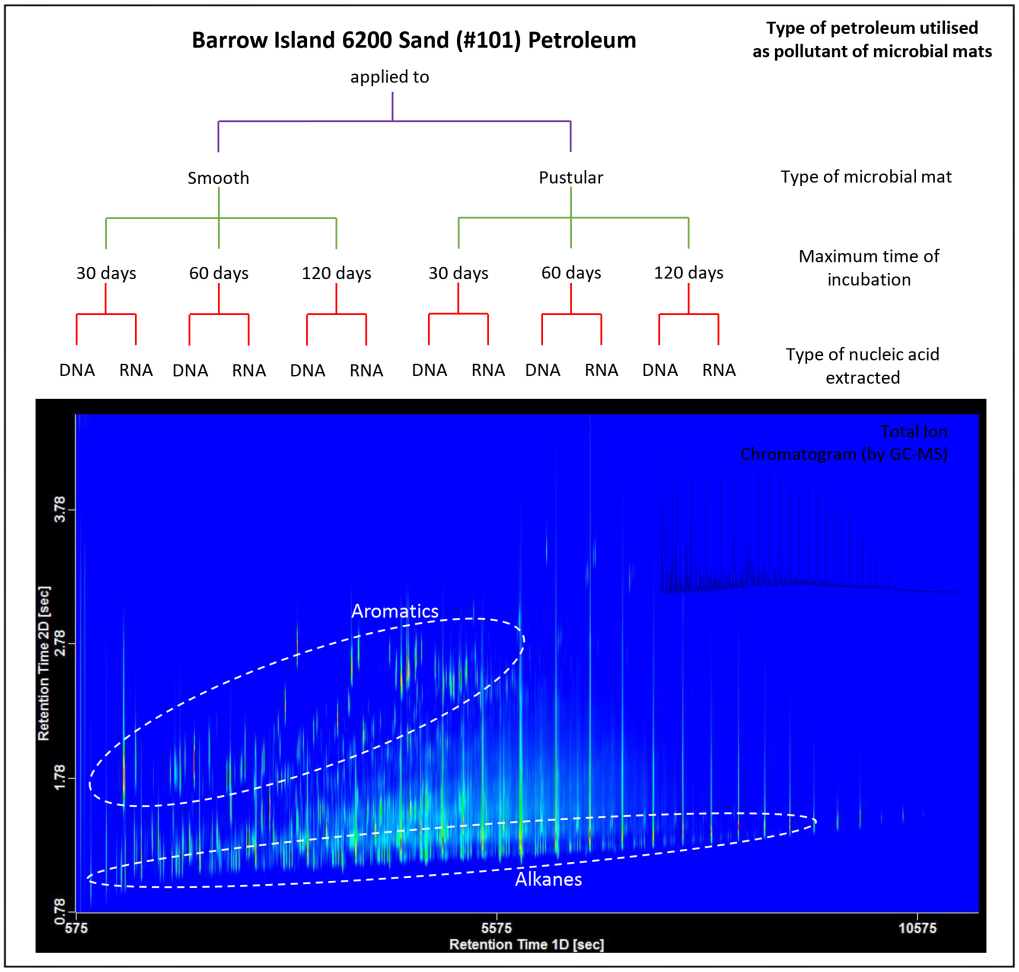

Figure A2.3. Scheme illustrating the organisation of the different groups of lab-controlled time-series incubation experiments using microbial mats collected from the Nilemah area, Hamelin Pool, Shark Bay (WA). Barrow Island petroleum examined by Two-Dimensional Gas Chromatography/Time-of-Flight Mass Spectrometry (GCxGC ToF-MS) and Gas Chromatography-Mass Spectroscopy (GC-MS) is displayed to show the organic compounds present in the petroleum sample.

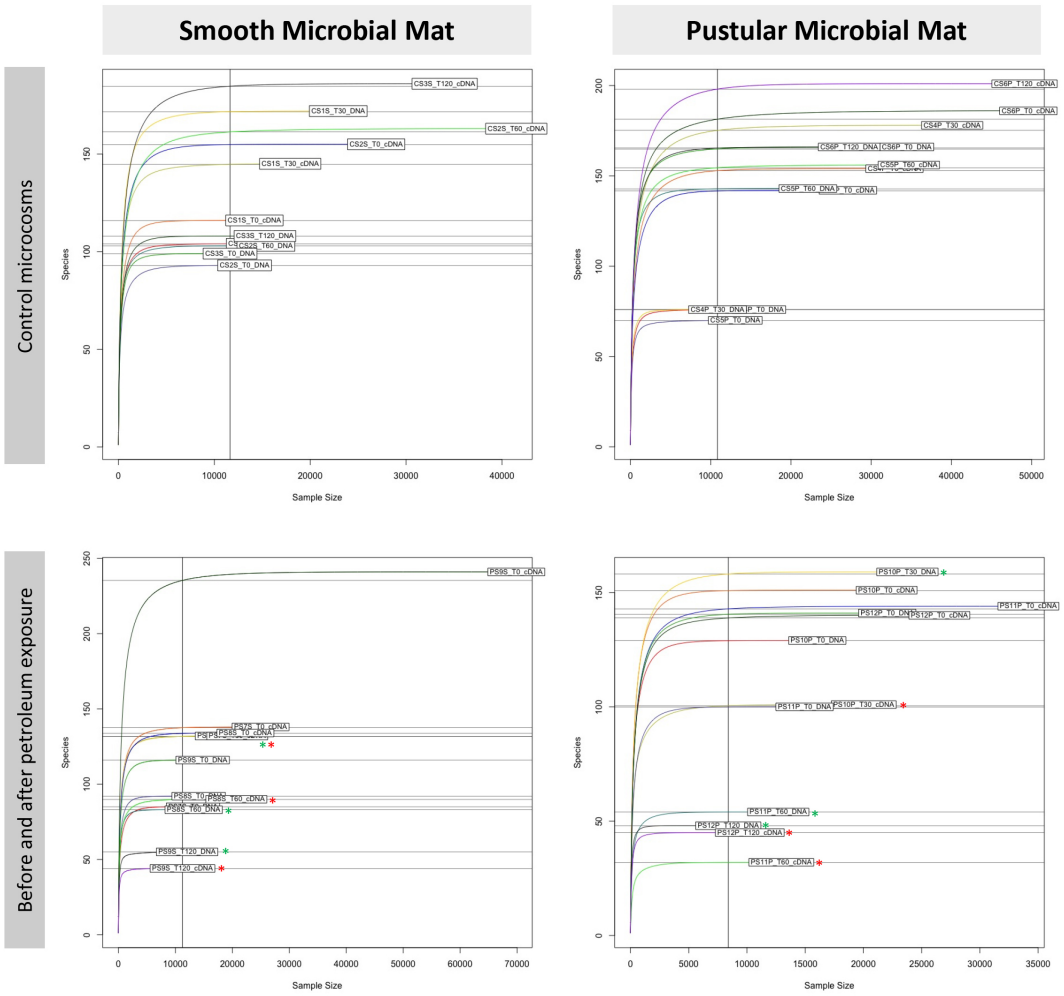

Figure A2.4. Rarefaction curves plots of samples collected in both controls and petroleum-incubated smooth and pustular mat microcosms. Petroleum-exposed samples are represented with an asterisk: green for DNA and red for cDNA.

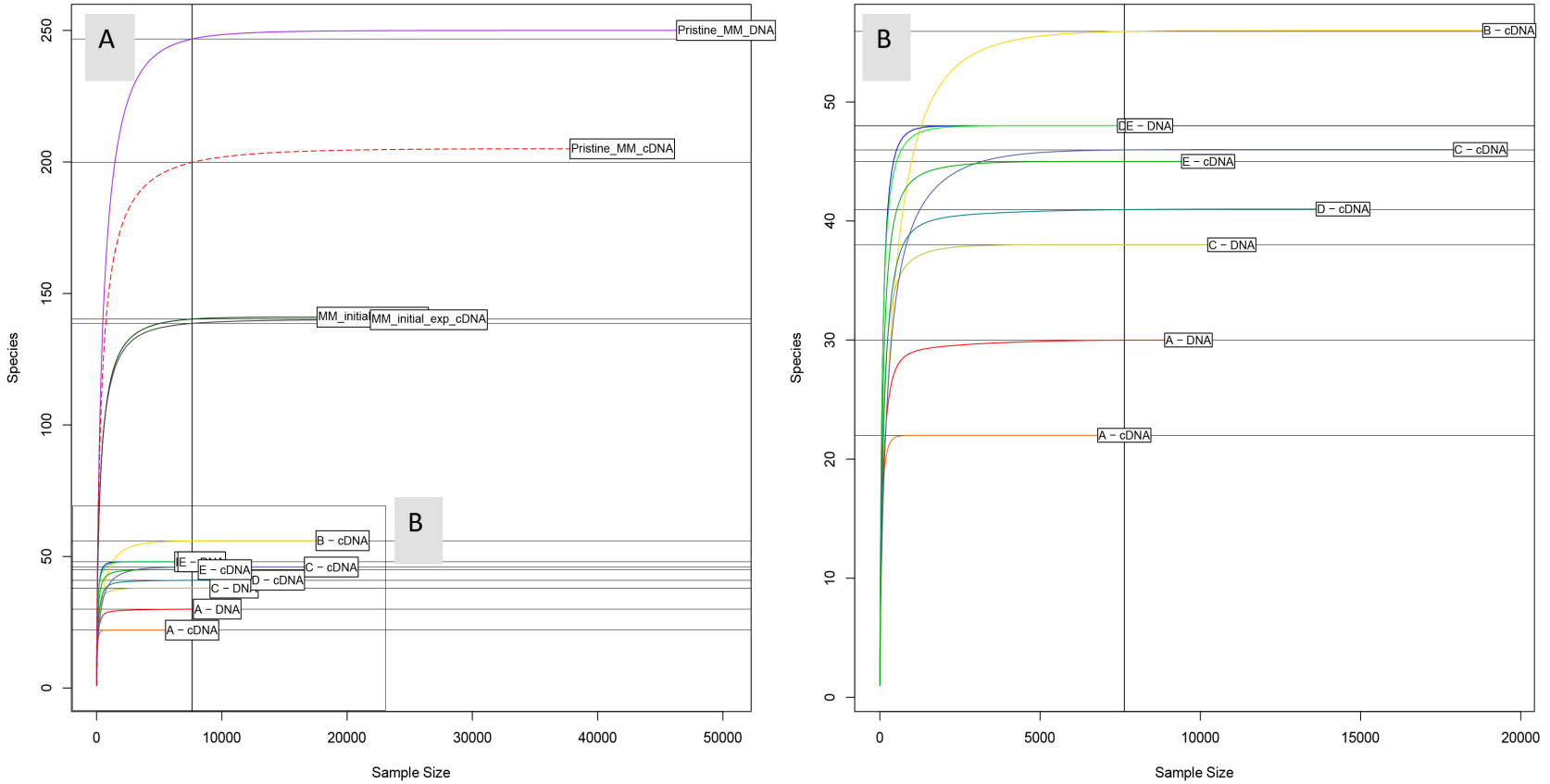

Figure A2.5. Rarefaction curves plots of additional biofilm-related samples collected from a 120 day petroleum-exposed pustular microbial mat and compared to initial experimental conditions (T0) and pristine pustular mat (A). Rarefaction curves plot focused on group of samples with less species diversity: Foam (A), Biofilm (late stage –B – & early stage –C –), base of biofilm (D) and pustular microbial mat (PS12P T120 = E) (B).

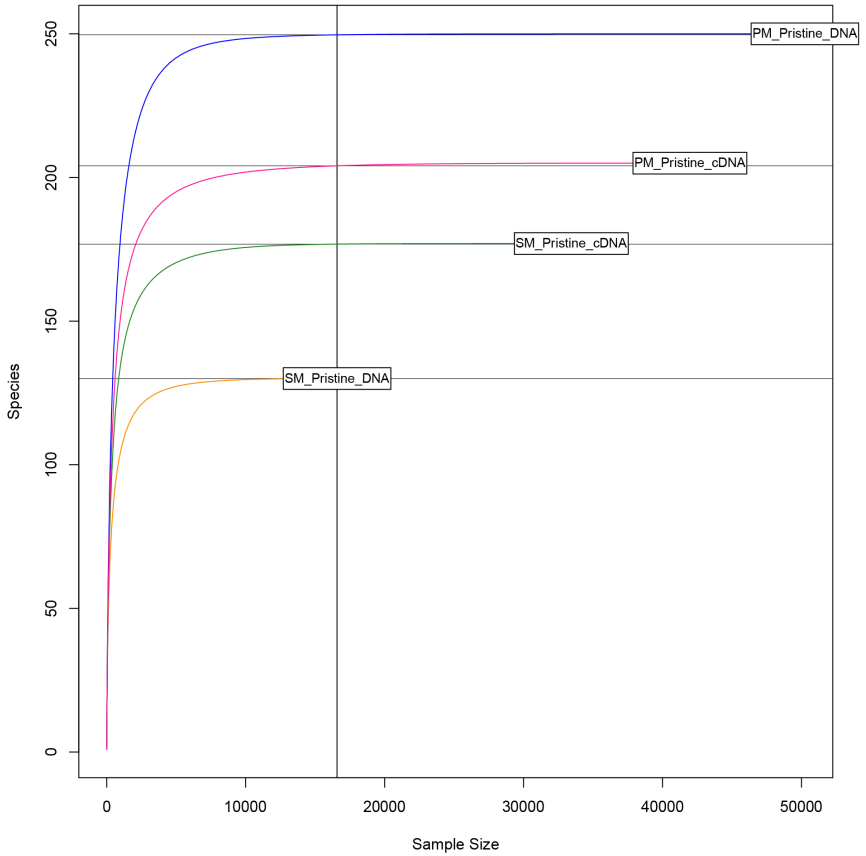

Figure A2.6. Rarefaction curves plots of smooth and pustular microbial mats collected and preserved in its pristine environment. No subjected to lab-controlled conditions.

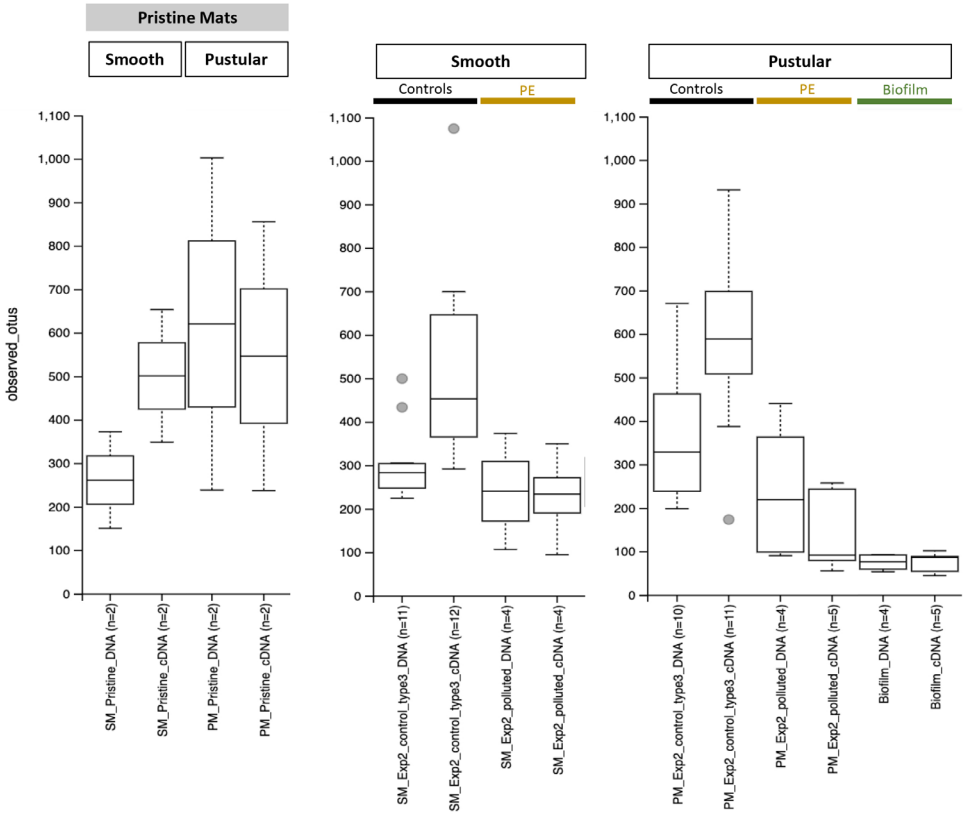

Figure A2.7. Boxplots of observed OTUs index computed in QIIME2 including DNA and cDNA datasets of pristine mats, control microcosms, petroleum-exposed microcosms and biofilm samples. Centre line in the boxplot represents the median, while box limits are 25th and 75th percentiles. Boxplot whiskers represent 9th and 91st percentiles and outlier values are represented as grey points.

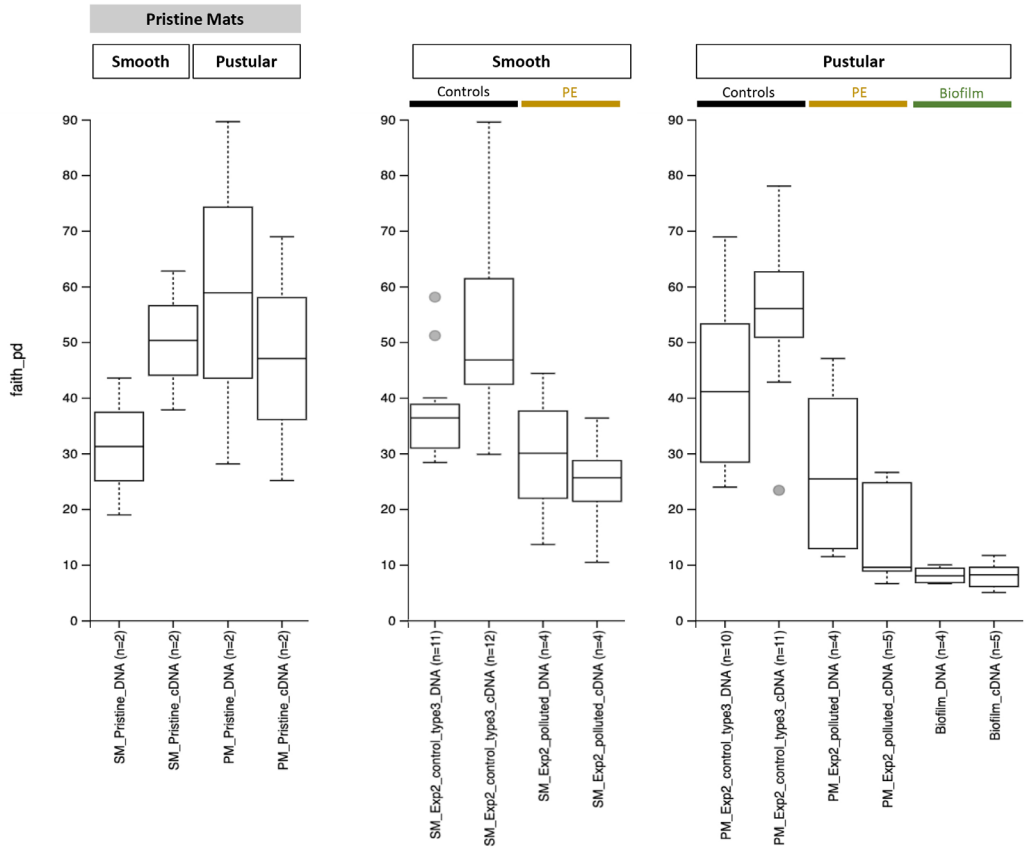

Figure A2.8. Boxplots of Faith's PD (phylogenetic diversity) index computed in QIIME2 including DNA and cDNA datasets of pristine mats, control microcosms, petroleum-exposed microcosms and biofilm samples. Centre line in the boxplot represents the median, while box limits are 25th and 75th percentiles. Boxplot whiskers represent 9th and 91st percentiles and outlier values are represented as grey points.

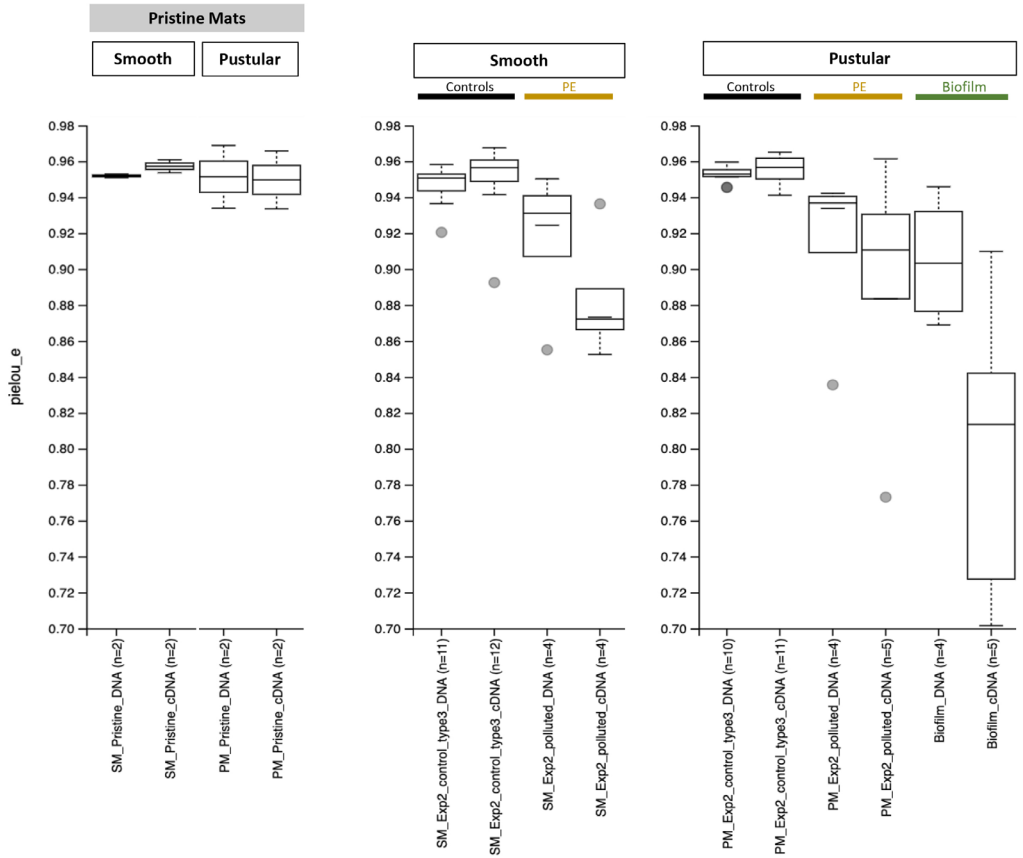

Figure A2.9. Boxplots of Pielou's evenness index computed in QIIME2 including DNA and cDNA datasets of pristine mats, control microcosms, petroleum-exposed microcosms and biofilm samples. Centre line in the boxplot represents the median, while box limits are 25th and 75th percentiles. Boxplot whiskers represent 9th and 91st percentiles and outlier values are represented as grey points.

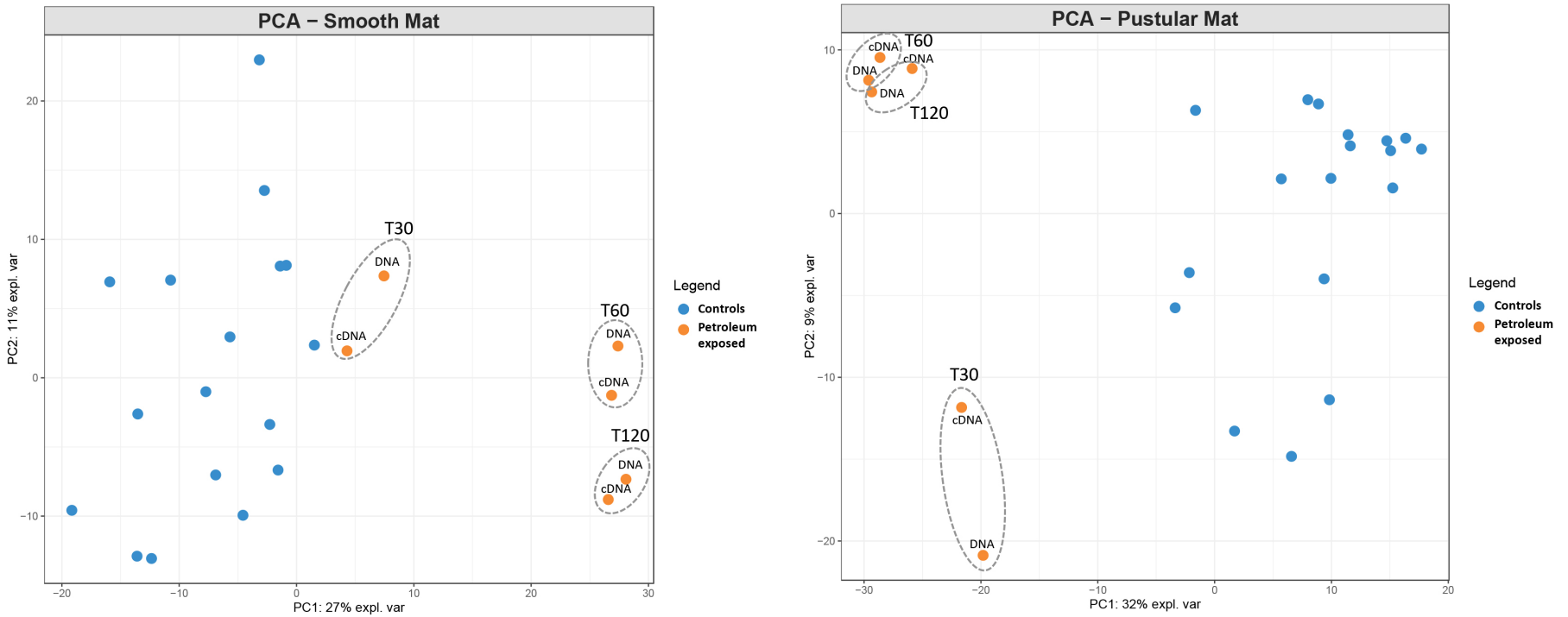

Figure A2.10. PCA (Principal Component Analysis) plot showing microbiome shifts and clusters of controls and petroleum-exposed microcosms using both smooth (left) and pustular mats (right).

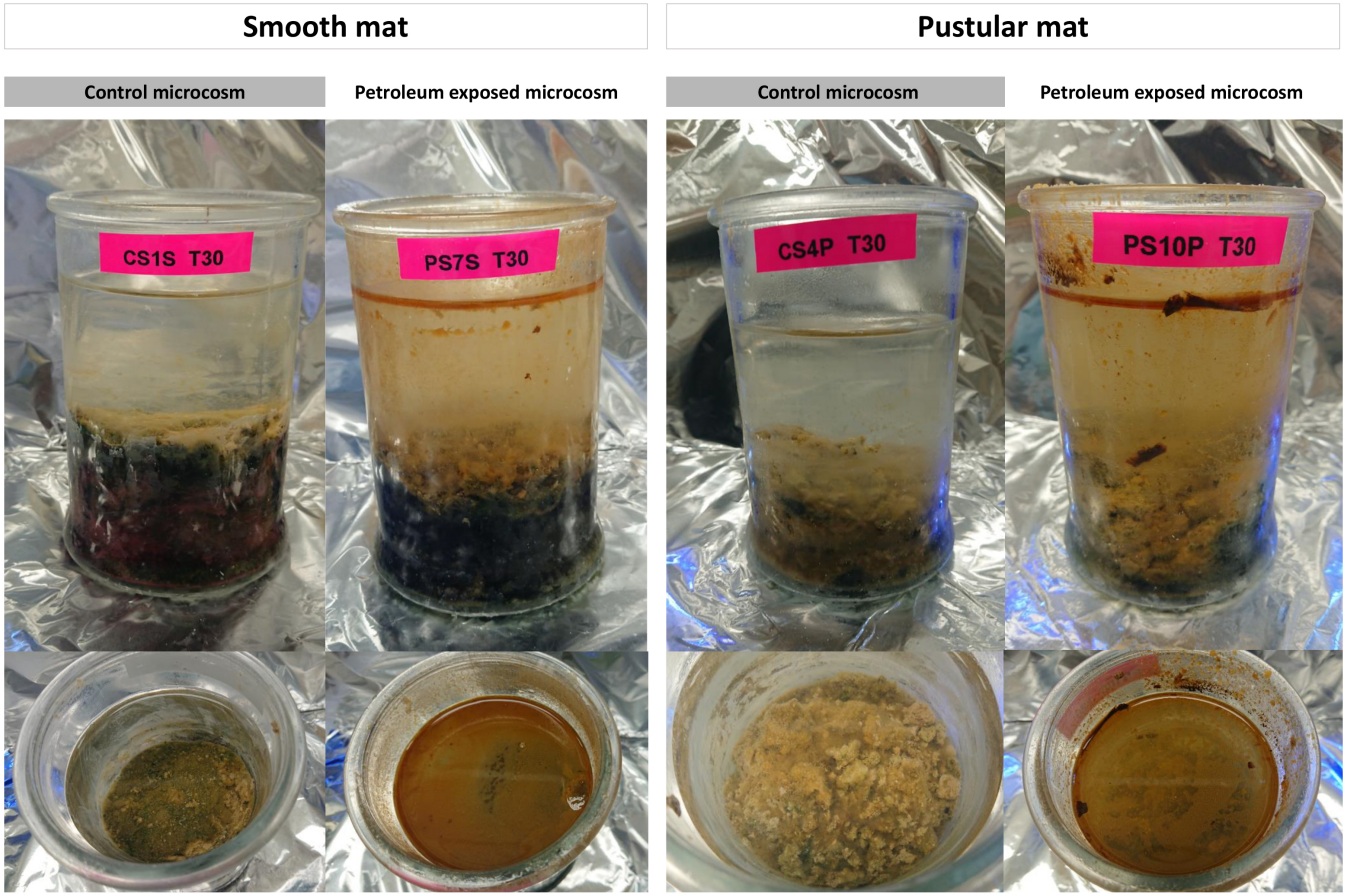

Figure A2.11. Photos of controls and petroleum-exposed microcosms after 30-day incubation with Barrow Island – B101 petroleum – both smooth and pustular mats. Images show the visual changes (mainly colour) of petroleum and microbial mats after 30 days of petroleum incubation.

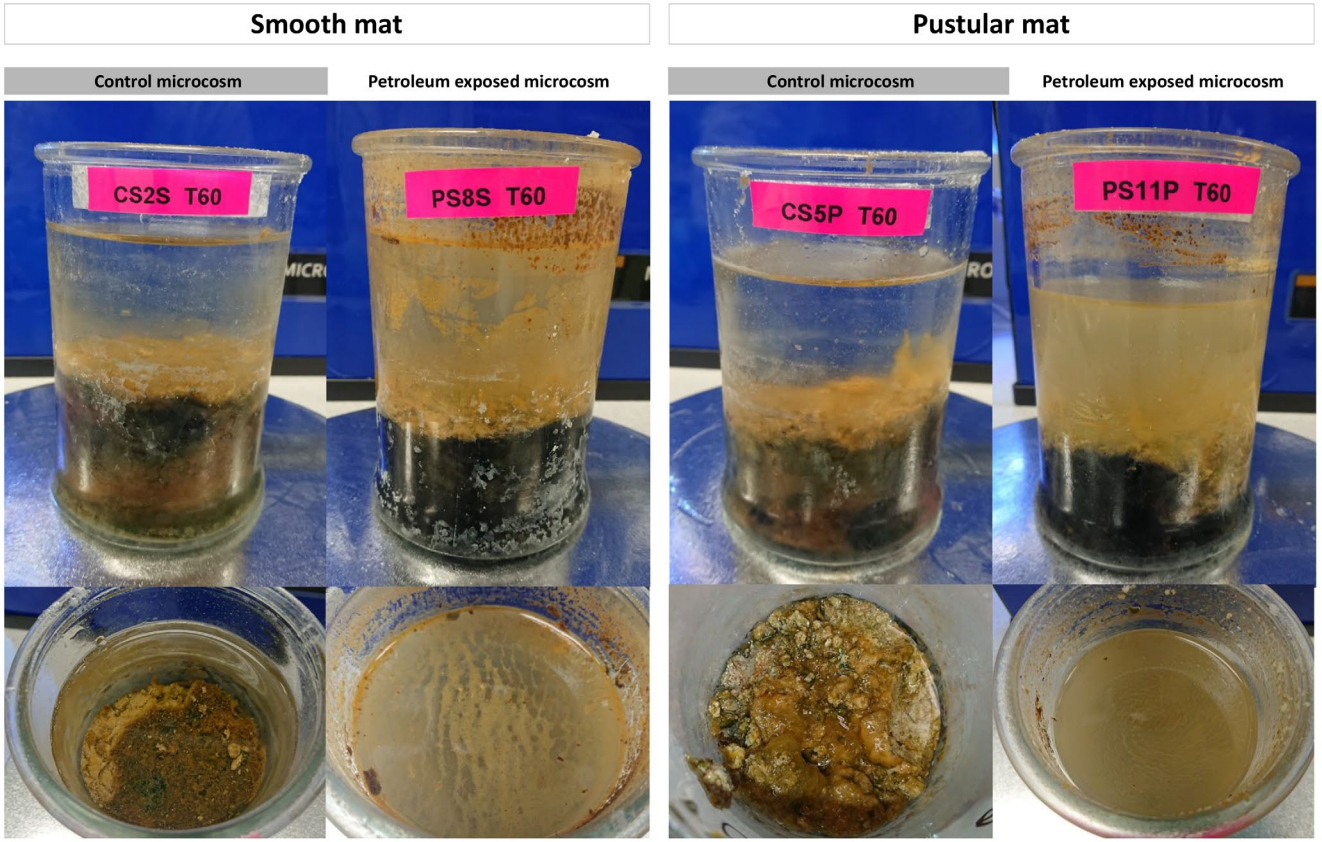

Figure A2.12. Photos of controls and petroleum-exposed microcosms after 60-day incubation with Barrow Island – B101 petroleum – both smooth and pustular mats. Images show the visual changes (mainly colour) of petroleum and microbial mats after 60 days of petroleum incubation.

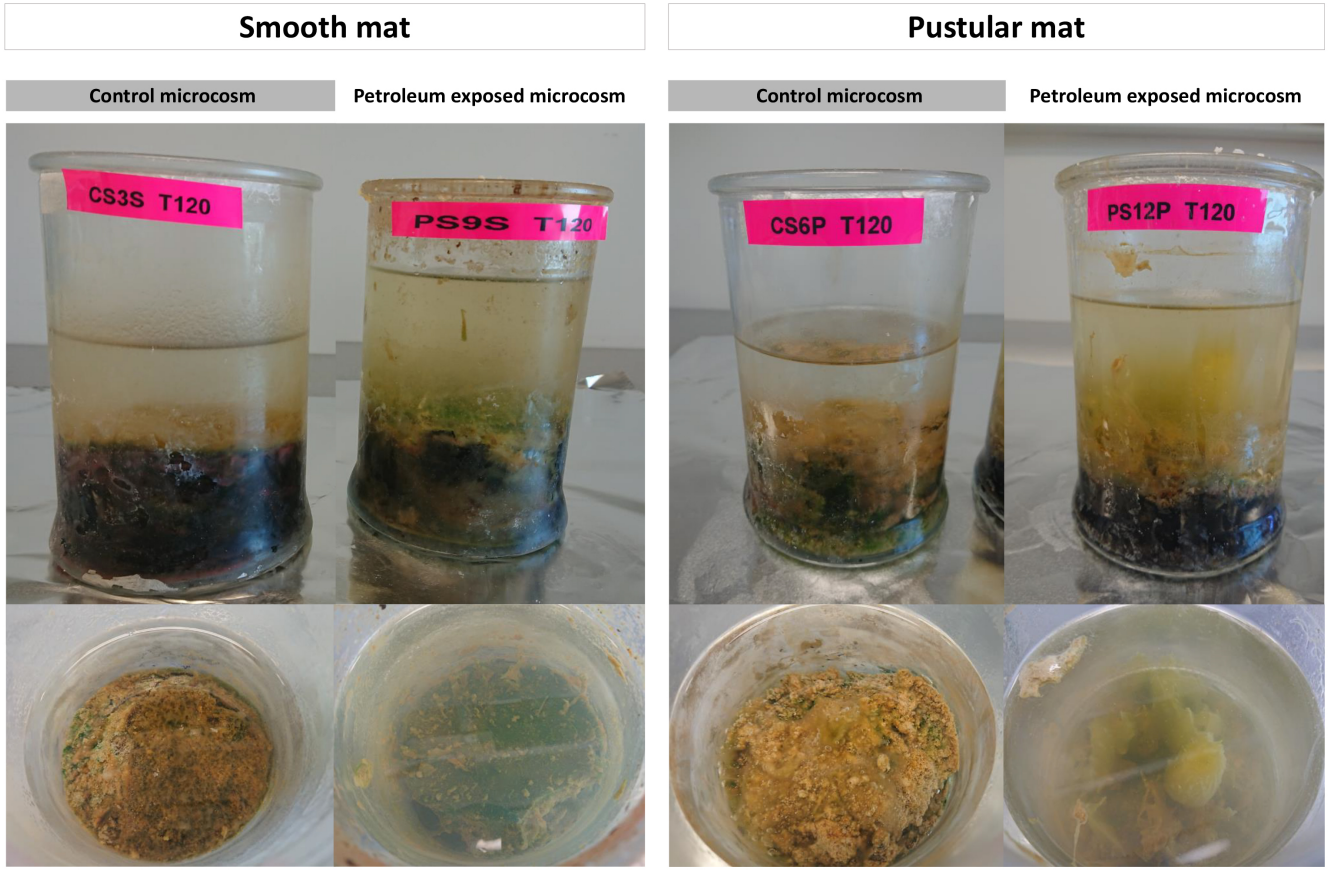

Figure A2.13. Photos of controls and petroleum-exposed microcosms after 120-day incubation with Barrow Island – B101 petroleum – both smooth and pustular mats. Photos images the visual changes (mainly colour) of petroleum and microbial mats after 120 days of petroleum incubation.

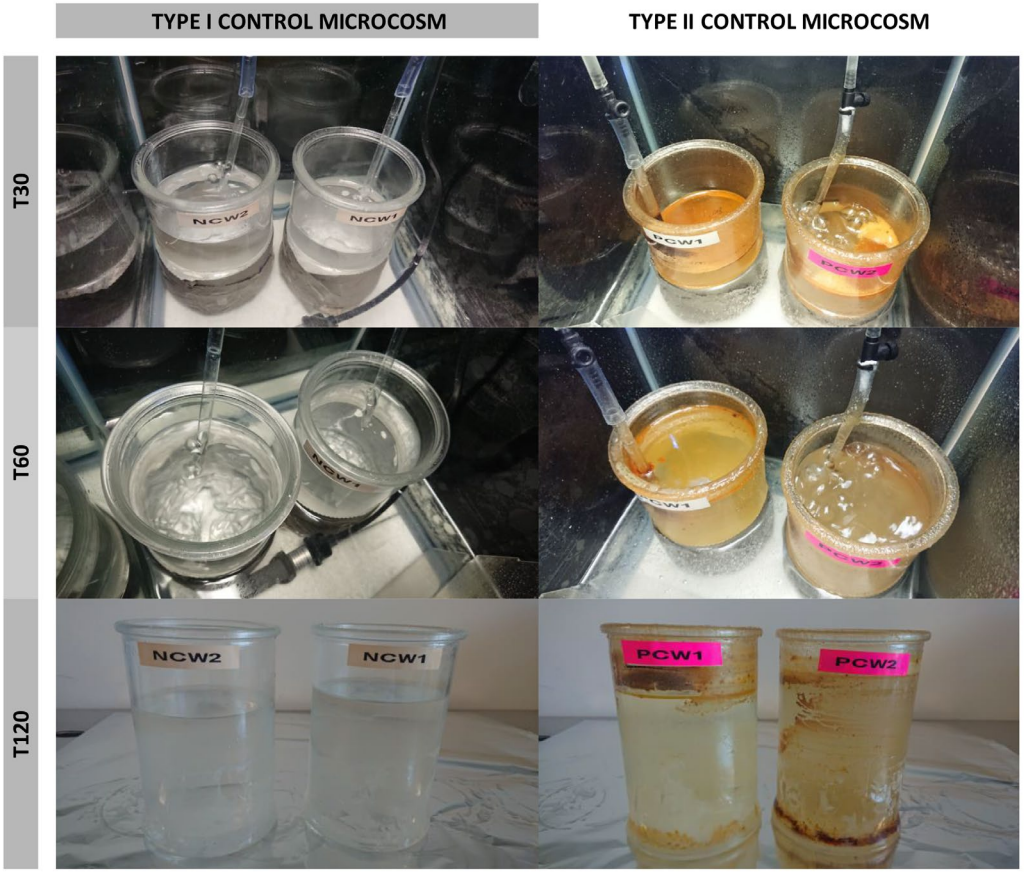

Figure A2.14. Photos of control microcosms: type I –only water – and type II –water and petroleum.

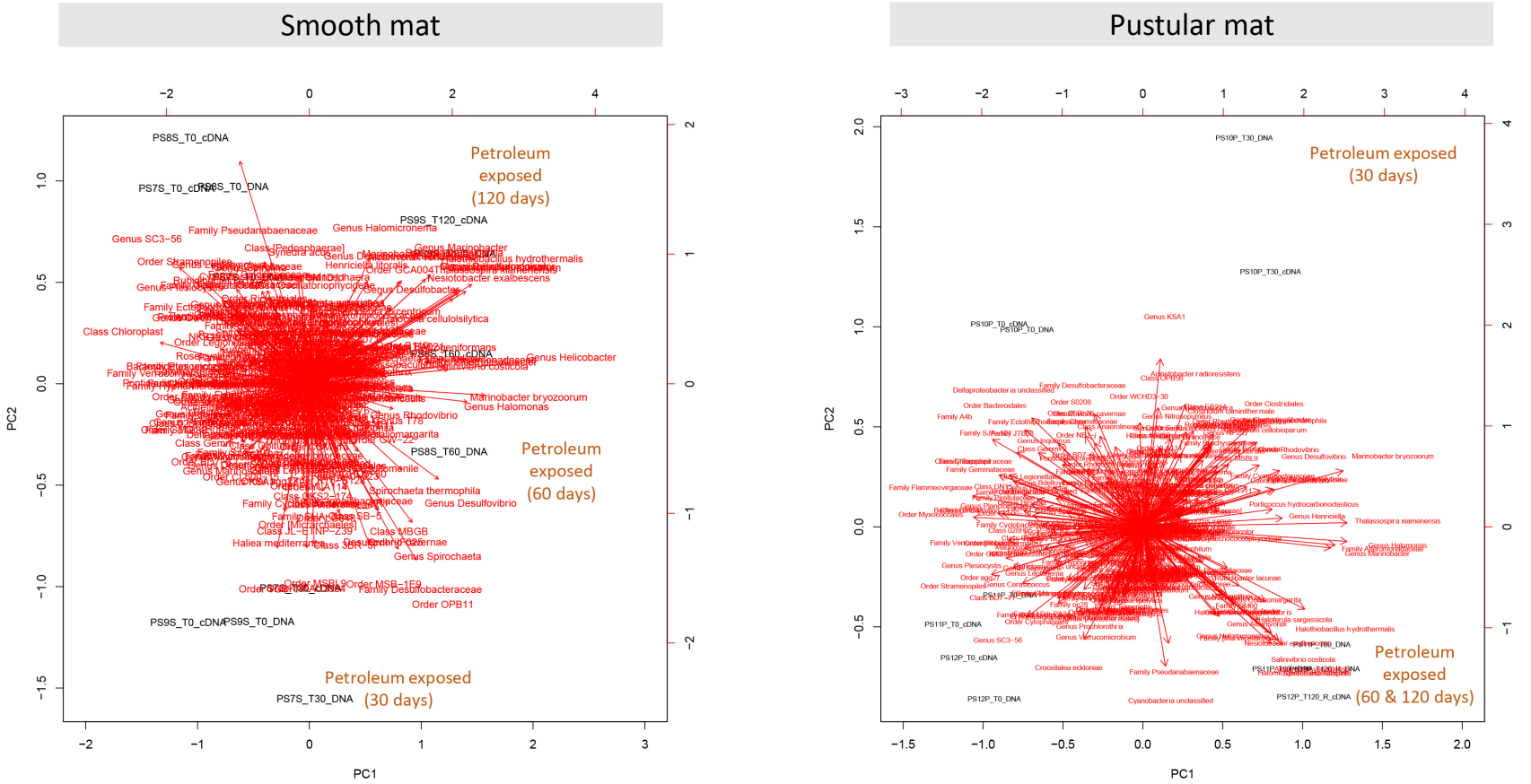

Figure A2.15. PCA biplots of initial and petroleum-exposed microcosms for both smooth and pustular mats. The longer vectors (red arrows) represent those organisms which contribution is higher to a particular sample or cluster of samples. Negative correlation of variables are represented for those vectors pointing in the opposite direction.

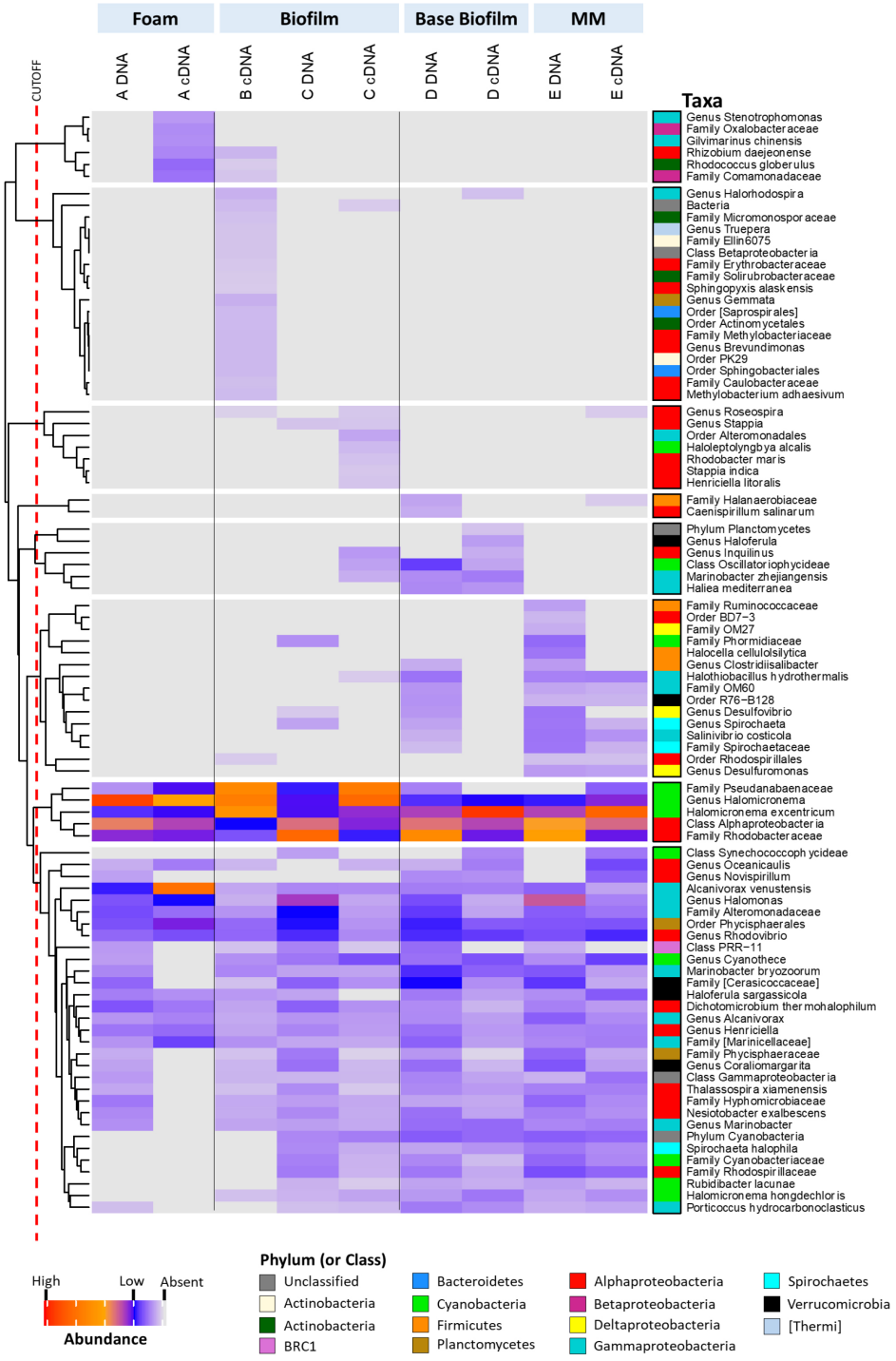

Figure A2.16. Heatmap plot showing microbiome shifts among sub-samples of PS12P microcosm (pustular microbial mat) subjected to Barrow Island (#101) petroleum incubation for 120 days. Sampling points are displayed in **Figure 2.12A-B**. Data displayed corresponds to raw reads at species level, standardised by total, and then square root transformed.

https://youtu.be/usplYzrRhYk

Video A2.1. Video showing biofilm developed in PS12P microcosm after 100 days petroleum incubation.

Table A2.1. Physicochemical parameters recorded under pristine conditions and the set of microcosms exposed to 120 days of lab incubation with and without petroleum (CS6P T120) and PS12P T120.

	Pristine conditions	Lab incubation conditions*	
Parameter	Field	CS6P microcosm control – at 120 days	PS12P microcosm – petroleum exposed – at 120 days
Temperature (°C)	20.32	25.18	25.61
Dissolved oxygen (%)	5.1	66.0	48.8
pH	8.12	7.63	7.07
Conductivity ($\mu S.cm^{-1}$)	45.7	129.0	77.7
Salinity (Practical Salinity Unit)	>70	>70	58.95

*Only measured for CS6P and PS12P microcosms at T120, due to the development of a massive biofilm.

Table A2.2. Relative abundance of bacterial taxonomy (**phylum level**) of **smooth mat** microcosms subjected to Barrow Island (#101) petroleum exposure. Three experiments were carried out in parallel which lasted 30 days (first table), 60 days (second table) and 120 days (third table). Shown are the differences between total bacteria (DNA) and active bacteria (cDNA). Petroleum-exposed sub-samples are shaded in grey.

30-days incubation microcosms

	CONTROLS				BEFORE PETROLEUM EXPOSURE		PETROLEUM EXPOSED	
Taxonomy (Phylum level)	CS1S T0 DNA	CS1S T0 cDNA	CS1S T30 DNA	CS1S T30 cDNA	PS7S T0 DNA	PS7S T0 cDNA	PS7S T30 DNA	PS7S T30 cDNA
Crenarchaeota			0.6		0.1		0.1	
Parvarchaeota	0.6		4.8		0.1		1.4	
Bacteria unclassified	2.4	5.4	3.4	4.6	1.8	3.3	1.3	2.5
Actinobacteria			0.0		0.1	0.0	0.2	
Bacteroidetes	25.8	13.5	21.3	17.5	20.0	16.2	17.8	10.6
Chloroflexi	9.6	15.4	8.7	5.3	6.0	8.5	6.2	8.4
Cyanobacteria	12.7	13.9	4.1	5.4	27.8	12.1	11.0	20.8
Fibrobacteres		0.2	0.4	1.4		0.2	0.7	0.4
Firmicutes			0.1	0.1			1.1	0.9
GN02	0.4		1.9	0.1			0.5	
GN04	1.1	0.9	0.7	1.0		0.3	0.2	0.3
Gemmatimonadetes	0.1	0.2	0.4	0.3		0.3	0.3	0.4
Planctomycetes	8.3	12.4	12.2	7.4	5.8	5.4	8.8	2.9
Proteobacteria	30.5	31.9	24.7	45.6	33.4	46.1	36.1	42.6
Spirochaetes	4.7	2.6	9.0	7.7	2.6	2.3	8.8	7.5
Verrucomicrobia	3.6	2.9	5.1	1.7	2.3	4.1	4.4	1.0
Others	0.2	0.8	2.4	2.0	0.2	1.1	1.0	1.6

60-days incubation microcosms

	CONTROLS				BEFORE PETROLEUM EXPOSURE		PETROLEUM EXPOSED	
Taxonomy (Phylum level)	CS2S T0 DNA	CS2S T0 cDNA	CS2S T60 DNA	CS2S T60 cDNA	PS8S T0 DNA	PS8S T0 cDNA	PS8S T60 DNA	PS8S T60 cDNA
Crenarchaeota							1.9	1.6
Parvarchaeota	0.6	0.0	1.1	0.1			0.3	
Bacteria unclassified	2.5	5.5	1.2	3.6	1.4	3.5	0.4	1.2
Actinobacteria				0.1		0.1		
Bacteroidetes	23.1	13.7	22.1	10.1	26.1	16.7	10.2	4.7
Chloroflexi	7.2	11.8	6.0	9.4	9.3	13.1	15.7	16.0
Cyanobacteria	18.2	8.7	10.3	13.5	25.3	13.5	5.2	8.3
Fibrobacteres	0.3	0.6		0.1		0.1		
Firmicutes							2.9	2.4
GN02	0.0		0.0				0.8	
GN04	0.3	0.8	0.2	0.5	0.6	0.4	1.5	1.1
Gemmatimonadetes	0.1	0.4	0.3	0.3	0.3	0.3		
Planctomycetes	5.6	7.3	8.3	13.8	3.3	4.8	1.4	0.6
Proteobacteria	31.9	41.6	40.8	40.6	29.7	41.4	42.9	52.9
Spirochaetes	7.1	5.2	5.3	3.1	2.2	2.1	14.7	10.2
Verrucomicrobia	2.9	2.0	4.0	3.0	1.6	2.9	0.1	
Others	0.2	2.5	0.4	1.8	0.3	1.1	2.0	1.1

120-days incubation microcosms

	CONTROLS				BEFORE PETROLEUM EXPOSURE		PETROLEUM EXPOSED	
Taxonomy (Phylum level)	CS3S T0 DNA	CS3S T0 cDNA	CS3S T120 DNA	CS3S T120 cDNA	PS9S T0 DNA	PS9S T0 cDNA	PS9S T120 DNA	PS9S T120 cDNA
Crenarchaeota		3.6	0.7	0.3	1.7	0.8	0.3	
Parvarchaeota	0.1	0.0	1.1	0.1	0.2	0.2		
Bacteria unclassified	2.7	1.0	3.1	4.0	1.9	5.2		0.3
Actinobacteria	0.0			0.2		0.1		
Bacteroidetes	27.1	5.9	25.9	11.9	20.5	12.1	3.0	1.8
Chloroflexi	14.1	17.6	13.4	13.4	17.5	12.2	0.4	0.1
Cyanobacteria	11.6	6.5	9.2	8.0	5.3	5.0	9.0	53.6
Fibrobacteres				0.8	0.9	0.6	0.0	
Firmicutes	0.2	2.2	0.0				1.8	0.1
GN02	0.2				1.1	0.1		
GN04	1.5	0.7	1.0	1.4	1.1	0.9		
Gemmatimonadetes	0.2	0.1		0.2	0.6	0.7		
Planctomycetes	4.8	0.9	7.3	14.0	7.9	10.0	1.8	1.4
Proteobacteria	30.7	48.9	31.8	37.6	28.6	37.7	73.8	35.3
Spirochaetes	3.3	10.5	3.3	3.3	10.3	7.1	7.6	7.0
Verrucomicrobia	2.6	0.1	1.7	2.2	1.8	3.1	1.9	0.5
Others	0.9	2.0	1.5	2.6	0.5	4.2	0.5	

Table A2.3. Relative abundance of bacterial taxonomy (**class level**) of **smooth mat** microcosms subjected to Barrow Island (#101) petroleum exposure. Three experiments were carried out in parallel which lasted 30 days (first table), 60 days (second table) and 120 days (third table). Shown are the differences between total bacteria (DNA) and active bacteria (cDNA). Petroleum-exposed sub-samples are shaded in grey.

30-days incubation microcosms

	CONTROLS				BEFORE EXPOSURE		PETROLEUM EXPOSED	
Taxonomy (Class level)	CS1S T0 DNA	CS1S T0 cDNA	CS1S T30 DNA	CS1S T30 cDNA	PS7S T0 DNA	PS7S T0 cDNA	PS7S T30 DNA	PS7S T30 cDNA
Parvarchaea	0.6		4.6		0.1		0.9	
Bacteria undefined	2.4	5.4	3.5	4.6	1.8	3.3	1.3	2.5
BME43	1.9	2.2	0.3	1.0	1.7	1.8	0.4	0.4
Bacteroidia	2.0	1.3	4.0	5.2	0.8	2.6	7.9	4.8
Cytophagia	8.9	4.8	4.5	5.5	5.1	3.7	2.9	0.9
Saprospirae	10.2	3.3	9.5	3.7	9.9	5.3	5.3	3.3
Anaerolineae	9.6	14.6	8.5	4.6	6.0	8.2	6.2	7.9
Chloroplast	6.4	4.3	1.3	1.8	23.1	3.2	0.4	0.1
Oscillatoriophycideae	2.0	3.2	1.3	2.0	1.1	4.0	2.6	17.1
Synechococcophycideae	2.8	3.8	0.6	0.6	2.9	3.4	7.5	2.6
Clostridia			0.1	0.1			1.1	0.9
Phycisphaerae	2.8	3.2	6.4	3.4	3.6	2.1	6.1	1.4
Planctomycetia	3.5	5.1	2.7	0.6	1.0	2.0	0.6	0.1
Alphaproteobacteria	19.9	15.1	12.0	18.7	26.2	31.2	23.4	23.5
Deltaproteobacteria	6.7	11.4	9.1	20.5	4.2	10.6	6.9	11.8
Epsilonproteobacteria							0.2	0.4
Gammaproteobacteria	3.5	5.2	3.4	6.4	2.7	3.9	5.6	7.0
Spirochaetes	4.5	2.3	7.4	5.6	2.6	2.1	8.3	6.4
Opitutae	2.0	1.8	2.3	0.7	1.0	1.6	3.2	0.7
Others (3%)	10.3	12.9	18.7	15.0	6.6	11.1	9.4	8.5

60-days incubation microcosms

	CONTROLS				BEFORE EXPOSURE		PETROLEUM EXPOSED	
Taxonomy (Class level)	CS2S T0 DNA	CS2S T0 cDNA	CS2S T60 DNA	CS2S T60 cDNA	PS8S T0 DNA	PS8S T0 cDNA	PS8S T60 DNA	PS8S T60 cDNA
Parvarchaea	0.6	0.0	1.1	0.2			0.3	
Bacteria undefined	2.5	5.5	1.2	3.6	1.4	3.5	0.5	1.2
BME43	3.4	1.9	3.7	1.4	2.5	2.2	0.2	0.1
Bacteroidia	3.6	2.8	0.8	1.1	1.3	2.6	5.8	4.4
Cytophagia	4.6	3.1	5.2	2.9	6.8	4.4	1.1	0.1
Saprospirae	10.7	4.3	11.5	3.5	14.0	5.3	3.0	0.1
Anaerolineae	6.6	9.4	5.8	8.3	9.3	12.8	15.7	15.7
Chloroplast	13.3	1.9	4.5	1.8	18.4	3.0	0.0	0.0
Oscillatoriophycideae	2.1	3.2	2.4	8.0	1.8	3.1	1.1	1.5
Synechococcophycideae	2.3	2.3	2.5	2.7	4.4	5.5	3.7	6.3
Clostridia							2.9	2.4
Phycisphaerae	3.6	4.1	4.4	7.1	1.5	1.6	0.9	
Planctomycetia	0.7	1.3	2.7	4.1	1.3	2.1		0.6
Alphaproteobacteria	24.1	22.7	32.1	24.0	23.9	25.4	10.8	40.8
Deltaproteobacteria	3.8	12.8	3.6	11.2	3.4	11.9	5.9	6.7
Epsilonproteobacteria							20.6	1.0
Gammaproteobacteria	3.9	5.9	3.6	4.8	2.3	4.0	5.6	4.4
Spirochaetes	6.7	4.0	5.3	2.6	2.2	2.0	13.5	8.8
Opitutae	2.7	1.7	2.8	1.8	1.0	0.6	0.1	
Others (3%)	4.9	13.4	6.9	11.1	4.5	9.9	8.5	6.0

120-days incubation microcosms

	CONTROLS				BEFORE EXPOSURE		PETROLEUM EXPOSED	
Taxonomy (Class level)	CS3S T0 DNA	CS3S T0 cDNA	CS3S T120 DNA	CS3S T120 cDNA	PS9S T0 DNA	PS9S T0 cDNA	PS9S T120 DNA	PS9S T120 cDNA
Parvarchaea	0.1	0.1	0.9	0.1	0.0	0.1		
Bacteria undefined	2.7	1.0	3.1	4.0	1.9	5.2		0.3
BME43	3.0	0.2	3.1	2.4	1.6	0.9		
Bacteroidia	1.3	4.5	4.3	1.9	4.7	3.8	2.0	1.8
Cytophagia	4.4	0.4	5.3	3.5	5.6	2.6	0.3	
Saprospirae	16.5	0.6	12.6	3.3	7.7	3.0	0.7	
Anaerolineae	13.9	17.0	13.3	13.0	17.3	9.8	0.4	0.1
Chloroplast	3.2		3.8	2.5	3.3	1.7		
Oscillatoriophycideae	0.5	1.5	0.5	1.5	0.8	1.5	1.2	3.7
Synechococcophycideae	5.2	4.4	3.5	2.7	0.8	0.9	7.8	49.9
Clostridia	0.2	2.2					1.8	0.1
Phycisphaerae	1.1	0.1	3.0	7.3	5.7	6.0	1.8	1.4
Planctomycetia	3.1	0.8	3.0	4.2	0.9	2.7		
Alphaproteobacteria	22.3	36.3	17.3	16.5	16.5	19.0	12.3	15.9
Deltaproteobacteria	4.8	7.1	8.1	14.7	8.2	13.9	3.2	4.5
Epsilonproteobacteria		1.0					45.7	3.3
Gammaproteobacteria	3.5	4.4	6.2	6.1	3.6	4.5	12.7	11.6
Spirochaetes	2.8	8.3	3.1	2.5	9.6	4.2	7.6	6.9
Opitutae	1.1		1.0	1.0	1.0	1.7	1.9	0.5
Others (3%)	10.4	10.1	8.0	12.9	10.7	18.5	0.8	0.0

Table A2.4. Relative abundance of bacterial taxonomy (**phylum level**) of **pustular mat** microcosms subjected to Barrow Island (#101) petroleum exposure. Three experiments were carried out in parallel which lasted 30 days (first table), 60 days (second table) and 120 days (third table). Shown are the differences between total bacteria (DNA) and active bacteria (cDNA). Petroleum-exposed sub-samples are shaded in grey.

30-days incubation microcosms

	CONTROLS				BEFORE PETROLEUM EXPOSURE		PETROLEUM EXPOSED	
Taxonomy (Phylum level)	CS4P T0 DNA	CS4P T0 cDNA	CS4P T30 DNA	CS4P T30 cDNA	PS10P T0 DNA	PS10P T0 cDNA	PS10P T30 DNA	PS10P T30 cDNA
Crenarchaeota					1.4	0.5	2.1	
Parvarchaeota					4.2	0.2	0.5	
Bacteria unclassified	1.0	4.0	1.8	3.9	7.3	7.6	0.7	
Actinobacteria		0.1		0.1	1.4		0.2	
Bacteroidetes	16.7	9.4	16.6	8.5	17.9	14.9	5.2	1.3
Chloroflexi	1.7	6.5	6.4	8.2	13.0	10.1	2.6	6.4
Cyanobacteria	22.8	14.0	9.7	5.2	8.3	3.9	5.5	29.5
Fibrobacteres		0.2		0.2		0.0		
Firmicutes				0.1			7.1	7.6
GN02			0.3	0.3	0.0		0.0	
GN04		0.6	1.1	1.6	0.8	1.2	0.2	0.0
Gemmatimonadetes		0.2		0.4	1.4	1.8	0.1	
Planctomycetes	3.7	15.0	5.3	13.3	11.1	8.7	7.0	3.1
Proteobacteria	45.7	40.0	47.2	46.6	24.6	42.6	51.8	42.8
Spirochaetes	2.7	3.3	6.6	4.4	3.0	2.3	7.7	5.8
Verrucomicrobia	5.8	4.8	4.9	4.0	3.4	1.8	8.1	2.4
Others		2.0	0.2	3.3	2.1	4.4	1.1	0.9

60-days incubation microcosms

	CONTROLS				BEFORE PETROLEUM EXPOSURE		PETROLEUM EXPOSED	
Taxonomy (Phylum level)	CS5P T0 DNA	CS5P T0 cDNA	CS5P T60 DNA	CS5P T60 cDNA	PS11P T0 DNA	PS11P T0 cDNA	PS11P T60 DNA	PS11P T60 cDNA
Crenarchaeota			0.4					
Parvarchaeota			0.5		0.1			
Bacteria unclassified	1.9	3.0	3.4	6.1	1.7	4.8	0.4	0.1
Actinobacteria		0.1		0.0	0.1	0.1		
Bacteroidetes	26.7	12.8	20.5	10.5	28.1	11.4	0.4	
Chloroflexi	3.0	13.8	7.7	11.6	8.4	11.2		
Cyanobacteria	16.3	17.6	9.8	8.1	12.3	7.7	52.3	76.9
Fibrobacteres						0.0	0.0	
Firmicutes			0.0				2.6	0.2
GN02			1.0	0.1	0.2			
GN04		0.2	1.1	0.7	0.6	0.5		
Gemmatimonadetes		0.0	0.2	0.4	0.1	0.1		
Planctomycetes	1.3	8.2	8.5	9.9	8.8	10.2	0.5	
Proteobacteria	46.6	39.1	34.9	45.4	31.4	45.7	35.1	19.7
Spirochaetes		0.8	2.9	1.4	1.7	1.7	2.2	0.8
Verrucomicrobia	4.2	4.0	7.7	3.7	6.2	5.1	6.1	2.3
Others	0.1	0.5	1.4	2.1	0.3	1.3	0.4	

120-days incubation microcosms

	CONTROLS				BEFORE PETROLEUM EXPOSURE		PETROLEUM EXPOSED	
Taxonomy (Phylum level)	CS6P T0 DNA	CS6P T0 cDNA	CS6P T120 DNA	CS6P T120 cDNA	PS12P T0 DNA	PS12P T0 cDNA	PS12P T120 DNA	PS12P T120 cDNA
Crenarchaeota			0.2		0.4			
Parvarchaeota	0.7	0.1	1.2	0.0				
Bacteria unclassified	3.1	7.0	4.5	4.5	2.2	4.6		
Actinobacteria	0.0	0.1	0.2	0.0	0.0	0.1		
Bacteroidetes	20.8	12.3	25.8	15.3	23.7	10.5	0.1	
Chloroflexi	9.4	9.3	6.8	8.2	9.3	8.9		
Cyanobacteria	8.7	8.7	4.7	15.5	10.1	10.5	17.5	54.9
Fibrobacteres	0.0		0.1	0.2		0.2	0.0	
Firmicutes							2.2	0.1
GN02	0.5	0.0	0.8	0.1	0.5			
GN04	1.0	0.6	0.4	0.3	1.0	0.9		
Gemmatimonadetes	0.3	0.3	0.2	0.3		0.3		
Planctomycetes	8.1	11.7	7.7	9.0	6.2	8.8	3.5	2.4
Proteobacteria	36.9	41.7	37.1	39.3	35.4	48.4	67.0	38.4
Spirochaetes	2.7	1.6	3.4	2.2	2.4	1.2	3.6	1.3
Verrucomicrobia	6.9	5.1	5.0	3.6	7.4	4.8	5.9	2.9
Others	1.0	1.4	2.0	1.5	1.3	0.9	0.3	

Table A2.5. Relative abundance of bacterial taxonomy (**class level**) of **pustular mat** microcosms subjected to Barrow Island (#101) petroleum exposure. Three experiments were carried out in parallel which lasted 30 days (first table), 60 days (second table) and 120 days (third table). Shown are the differences between total bacteria (DNA) and active bacteria (cDNA). Petroleum-exposed sub-samples are shaded in grey.

30-days incubation microcosms

	CONTROLS				BEFORE EXPOSURE		PETROLEUM EXPOSED	
Taxonomy (Class level)	CS4P T0 DNA	CS4P T0 cDNA	CS4P T30 DNA	CS4P T30 cDNA	PS10P T0 DNA	PS10P T0 cDNA	PS10P T30 DNA	PS10P T30 cDNA
Parvarchaea					4.3	0.2	0.5	
Bacteria undefined	1.0	4.0	1.8	4.0	7.3	7.6	0.7	
BME43	3.8	1.7	1.1	0.8	1.0	0.8	0.5	
Bacteroidia	0.4	1.1	2.0	1.6	2.1	3.0	1.8	0.5
Cytophagia	4.5	1.7	6.4	1.8	6.9	5.0	0.7	
Saprospirae	7.9	3.2	5.9	2.7	4.6	3.0	1.6	0.2
Anaerolineae	1.7	6.4	6.4	7.6	12.9	9.6	2.6	6.5
Chloroplast	18.1	1.7	5.3	1.3	5.9	1.7	0.4	0.2
Oscillatoriophycideae	1.8	9.7	2.3	1.8	1.7	1.6	1.7	25.0
Synechococcophycideae	1.7	1.2	0.9	0.4	0.8	0.2	2.4	3.0
Clostridia				0.1			7.1	7.6
Phycisphaerae	2.5	9.1	3.1	7.8	4.3	3.2	6.3	1.9
Planctomycetia	0.6	3.8	1.0	3.2	4.8	2.4	0.4	1.1
Alphaproteobacteria	36.5	23.4	34.9	23.0	10.1	15.2	28.8	28.4
Deltaproteobacteria	5.7	12.3	8.4	18.2	9.0	19.3	5.4	5.9
Epsilonproteobacteria				0.1			0.4	0.3
Gammaproteobacteria	3.2	3.5	3.4	5.1	5.4	7.5	16.8	8.2
Spirochaetes	2.5	2.4	6.4	3.7	2.8	2.0	7.1	5.5
Opitutae	3.1	2.5	3.7	2.5	1.6	0.8	6.5	1.6
Others (3%)	5.1	12.3	7.1	14.5	14.8	16.9	8.5	4.0

60-days incubation microcosms

	CONTROLS				BEFORE EXPOSURE		PETROLEUM EXPOSED	
Taxonomy (Class level)	CS5P T0 DNA	CS5P T0 cDNA	CS5P T60 DNA	CS5P T60 cDNA	PS11P T0 DNA	PS11P T0 cDNA	PS11P T60 DNA	PS11P T60 cDNA
Parvarchaea			0.5		0.1			
Bacteria undefined	1.9	3.0	3.4	6.1	1.7	4.9	0.4	0.1
BME43	5.4	2.8	1.2	1.1	2.0	1.6		
Bacteroidia	0.5	0.7	1.1	0.8	0.7	1.2	0.1	
Cytophagia	7.4	3.6	6.7	3.3	6.0	4.2		
Saprospirae	10.7	3.3	7.7	2.6	17.8	2.3	0.3	
Anaerolineae	3.0	13.7	7.7	11.6	8.4	11.0		
Chloroplast	6.9	2.9	3.6	2.1	4.7	2.3		
Oscillatoriophycideae	1.8	2.5	1.8	2.3	1.6	1.4	1.9	0.6
Synechococcophycideae	4.1	9.2	2.6	2.2	2.2	2.2	50.1	75.6
Clostridia							2.6	0.2
Phycisphaerae	0.1	1.5	3.6	3.9	2.9	3.3	0.5	
Planctomycetia	1.2	4.6	3.2	3.1	5.1	4.0		
Alphaproteobacteria	37.2	23.4	23.2	25.1	21.5	28.4	20.8	14.8
Deltaproteobacteria	5.9	13.7	5.5	15.6	5.8	14.1	2.0	0.5
Epsilonproteobacteria								
Gammaproteobacteria	3.3	1.9	5.5	4.0	3.9	3.0	12.4	4.4
Spirochaetes		0.4	2.2	1.2	1.2	0.8	2.2	0.8
Opitutae	1.0	1.4	3.2	1.6	3.1	3.0	3.7	1.6
Others (3%)	9.7	11.5	17.3	13.6	11.3	12.5	3.1	1.4

120-days incubation microcosms

	CONTROLS				BEFORE EXPOSURE		PETROLEUM EXPOSED	
Taxonomy (Class level)	CS6P T0 DNA	CS6P T0 cDNA	CS6P T120 DNA	CS6P T120 cDNA	PS12P T0 DNA	PS12P T0 cDNA	PS12P T120 DNA	PS12P T120 cDNA
Parvarchaea	0.8	0.1	1.2	0.0				
Bacteria undefined	3.1	7.0	4.5	4.5	2.2	4.6		
BME43	1.8	1.8	2.2	2.0	2.4	1.6		
Bacteroidia	1.3	1.5	2.0	1.6	1.4	1.4		
Cytophagia	5.8	3.7	8.9	5.2	7.6	4.5		
Saprospirae	8.2	3.1	9.2	3.5	10.8	1.7		
Anaerolineae	9.3	9.0	6.8	8.1	9.3	8.9		
Chloroplast	2.9	1.6	2.3	2.8	4.8	4.0		
Oscillatoriophycideae	1.9	3.7	0.6	0.9	0.6	1.5	4.3	3.6
Synechococcophycideae	2.1	1.9	1.2	10.7	2.8	3.6	11.4	49.7
Clostridia							2.2	0.1
Phycisphaerae	4.0	6.4	4.1	3.5	2.0	2.5	3.5	2.4
Planctomycetia	2.5	2.3	3.0	3.3	2.6	2.8		
Alphaproteobacteria	24.2	22.5	24.0	20.7	24.0	28.2	43.8	28.3
Deltaproteobacteria	7.8	13.5	6.8	13.6	7.0	16.0	2.1	0.5
Epsilonproteobacteria		0.0						
Gammaproteobacteria	4.4	5.3	5.7	4.7	4.1	3.7	21.0	9.7
Spirochaetes	2.2	1.1	2.8	1.6	1.7	0.8	3.6	1.3
Opitutae	3.5	3.1	1.4	1.5	3.3	2.3	4.9	0.8
Others (3%)	14.4	12.4	13.5	11.8	13.2	11.9	3.2	3.6

Table A2.6. Indicator taxa positively affected for petroleum exposure in both smooth vs. pustular mats. Indicator Species Analysis (ISA) was done using the IndicSpecies package in R with significant level alpha <0.05. They represent the statistically significant active indicators using this method.

			Smooth						Pustular							
Shared indicator species			PS8S T60		PS9S T120				PS10P T30		PS11P T60		PS12P T120			
Phylum/Class	Family/Genus	Species	DNA	**cDNA**	DNA	**cDNA**	***stat p***	***R value***	DNA	**cDNA**	DNA	**cDNA**	DNA	**cDNA**	***stat p***	***R value***
Cyanobacteria	Genus Halomicronema		1.2	1.8	4.9	4.0	0.874	0.031	0.6	0.7	1.2	1.3	3.6	5.7	0.833	0.018
α-Proteobacteria	Thalassospira	xiamenensis	1.1	0.3	0.8	1.0	1	0.031	1.4	1.1	6.5	0.8	1.0	1.0	1	0.006
γ-Proteobacteria	Family Alteromonadaceae		0.4	0.2	0.5	0.6	1	0.031	0.3	1.0	1.4	0.8	1.8	1.2	1	0.006
γ-Proteobacteria	Marinobacter	bryozoorum	1.7	0.8	2.9	4.2	1	0.031	11.2	3.0	1.2	0.3	2.0	0.5	1	0.006
γ-Proteobacteria	Halothiobacillus	hydrothermalis	0.9	1.1	1.5	1.4	1	0.031	0.1	0.0	2.2	1.0	1.0	1.0	0.913	0.023
γ-Proteobacteria	Halomonas		1.6	0.7	1.2	0.8	1	0.031	0.6	0.9	1.3	0.9	9.0	1.0	1	0.006
Smooth mat indicator species																
Bacteroidetes	Marinilabilia	salmonicolor	0.7	0.6	1.0	1.0	1	0.031	*	*	0.1	*	*	*	**	**
α-Proteobacteria	Nesiotobacter	exalbescens	0.9	0.5	0.5	0.6	1	0.031	*	*	0.6	*	1.0	0.7	**	**
α-Proteobacteria	Caenispirillum	salinarum	0.6	2.8	0.7	0.7	1	0.031	0.2	0.8	0.6	0.5	*	*	**	**
δ-Proteobacteria	Desulfuromonas		0.5	0.5	0.8	1.1	1	0.031	*	*	*	*	0.5	0.5	**	**
δ-Proteobacteria	Desulfovibrio		1.5	0.8	1.0	0.9	0.931	0.031	1.0	0.8	0.9	*	1.2	*	**	**
ε-Proteobacteria	Helicobacter		20.6	1.0	45.7	3.3	1	0.031	0.4	0.3	*	*	*	*	**	**
γ-Proteobacteria	Salinivibrio	costicola	0.8	0.3	0.5	0.3	1	0.031	*	*	0.6	0.1	1.2	0.7	**	**
Pustular mat indicator species																
Cyanobacteria	Family Cyanobacteriaceae		*	*	*	*	**	**	0.3	0.4	0.9	0.4	1.5	0.8	0.844	0.048
Cyanobacteria	Halomicronema	excentricum	2.5	4.5	2.9	45.6	**	**	1.6	1.4	48.0	73.4	7.4	40.4	0.919	0.013
Firmicutes	Family Ruminococcaceae		*	*	0.1	*	**	**	0.6	0.3	0.8	0.0	0.5	0.0	0.913	0.016
α-Proteobacteria	Henriciella		*	0.1	*	*	**	**	0.2	0.3	0.1	0.0	0.9	1.0	0.913	0.022
γ-Proteobacteria	Marinobacter		*	0.5	0.7	1.4	**	**	0.3	0.6	3.2	0.6	0.9	1.0	1	0.006
γ-Proteobacteria	Porticoccus	hydrocarbonoclasticus	*	*	*	*	**	**	0.2	0.3	0.2	0.0	0.3	0.4	0.913	0.022
Verrucomicrobia	Haloferula	sargassicola	*	*	*	*	**	**	0.0	0.0	0.6	0.1	0.0	0.0	0.848	0.049
	% total reads (only statistically significant species)		32.3	**11.5**	62.0	**20.0**			17.6	**9.9**	67.5	**79.6**	29.8	**54.0**		

* Not detected ** Not statistical significant by ISA

Table A2.7. Relative abundance (%) of microorganisms at phylum level of subsamples of foam, microbial mat and biofilm collected in a pustular mat microcosm after 120 days petroleum exposure (PS12S). Blue bars represent the percentages.

Phylum	A_DNA	A_cDNA	B_cDNA	C_DNA	C_cDNA	D_DNA	D_cDNA	E_DNA	E_cDNA
Acidobacteria	0.0	0.0	0.3	0.0	0.0	0.0	0.0	0.0	0.0
Actinobacteria	0.0	1.5	0.5	0.0	0.0	0.0	0.0	0.0	0.0
Bacteria	0.0	0.0	0.2	0.0	0.1	0.0	0.0	0.0	0.0
Bacteroidetes	0.0	0.0	0.4	0.0	0.0	0.0	0.0	0.1	0.0
BRC1	0.6	0.0	0.1	0.9	0.1	1.4	0.0	0.3	0.0
Cyanobacteria	56.6	25.8	80.4	17.2	80.1	19.0	66.5	17.5	54.9
Firmicutes	0.0	0.0	0.0	0.0	0.0	0.7	0.0	2.2	0.1
Planctomycetes	2.4	5.3	1.9	5.0	0.7	4.1	2.0	3.5	2.4
Proteobacteria	37.3	66.8	15.1	72.3	17.9	66.5	28.9	67.0	38.4
Spirochaetes	0.0	0.0	0.0	1.2	0.3	1.0	0.6	3.6	1.3
Thermi	0.0	0.0	0.1	0.0	0.0	0.0	0.0	0.0	0.0
Verrucomicrobia	3.1	0.7	1.0	3.4	0.9	7.3	2.0	5.9	2.9

Table A2.8. Relative abundance (%) of microorganisms at class level of subsamples of foam, microbial mat and biofilm collected in a pustular mat microcosm after 120 days petroleum exposure (PS12S). Blue bars represent the percentages.

Phylum	Class	A_DNA	A_cDNA	B_cDNA	C_DNA	C_cDNA	D_DNA	D_cDNA
Acidobacteria	Chloracidobacteria	0.0	0.0	0.3	0.0	0.0	0.0	0.0
Actinobacteria	Actinobacteria	0.0	1.5	0.4	0.0	0.0	0.0	0.0
Actinobacteria	Thermoleophilia	0.0	0.0	0.1	0.0	0.0	0.0	0.0
Bacteria	unclassified	0.0	0.0	0.2	0.0	0.1	0.0	0.0
Bacteroidetes	Flavobacteriia	0.0	0.0	0.0	0.0	0.0	0.0	0.0
Bacteroidetes	Sphingobacteriia	0.0	0.0	0.2	0.0	0.0	0.0	0.0
Bacteroidetes	Saprospirae	0.0	0.0	0.2	0.0	0.0	0.0	0.0
BRC1	PRR-11	0.6	0.0	0.1	0.9	0.1	1.4	0.0
Cyanobacteria	unclassified	0.0	0.0	0.0	0.8	1.1	1.8	1.5
Cyanobacteria	Chloroplast	0.0	0.0	0.0	0.0	0.0	0.0	0.0
Cyanobacteria	Oscillatoriophycideae	0.5	0.0	0.7	3.1	2.9	5.3	3.0
Cyanobacteria	Synechococcophycideae	56.1	25.8	79.7	13.2	76.0	11.9	62.1
Firmicutes	Clostridia	0.0	0.0	0.0	0.0	0.0	0.7	0.0
Planctomycetes	unclassified	0.0	0.0	0.0	0.0	0.0	0.0	0.1
Planctomycetes	Phycisphaerae	2.4	5.3	1.7	5.0	0.7	4.1	1.9
Planctomycetes	Planctomycetia	0.0	0.0	0.3	0.0	0.0	0.0	0.0
Proteobacteria	Alphaproteobacteria	25.9	19.4	10.7	58.2	13.4	47.0	19.9
Proteobacteria	Betaproteobacteria	0.0	2.0	0.2	0.0	0.0	0.0	0.0
Proteobacteria	Deltaproteobacteria	0.0	0.0	0.0	0.1	0.0	0.6	0.0
Proteobacteria	Gammaproteobacteria	11.4	45.3	4.2	14.0	4.5	18.9	9.0
Spirochaetes	Spirochaetes	0.0	0.0	0.0	1.2	0.3	1.0	0.6
Thermi	Deinococci	0.0	0.0	0.1	0.0	0.0	0.0	0.0
Verrucomicrobia	Opitutae	2.0	0.0	0.4	3.0	0.9	5.5	1.0
Verrucomicrobia	Verruco-5	0.0	0.0	0.1	0.0	0.0	0.7	0.0
Verrucomicrobia	Verrucomicrobiae	1.0	0.7	0.6	0.4	0.0	1.1	1.0

Table A2.9. Relative abundance (%) of microorganisms at its maximum level of resolution of subsamples of foam, microbial mat and biofilm collected in a pustular mat microcosm after 120 days petroleum exposure (PS12S). Blue bars represent the percentages. All organisms present up to 90% accumulated abundance are shown.

Phylum	Class	Order	Family	Genus	Specie	A_DNA	A_cDNA	B_cDNA	C_DNA	C_cDNA	D_DNA	D_cDNA
Cyanobacteria	unclassified					0.0	0.0	0.0	0.8	1.1	1.8	1.4
Cyanobacteria	Synechococcophycideae					0.0	0.0	0.0	0.5	0.0	0.0	0.9
Cyanobacteria	Synechococcophycideae	Pseudanabaenales	Pseudanabaenaceae			0.7	4.4	26.1	3.6	31.2	1.0	0.0
Cyanobacteria	Synechococcophycideae	Pseudanabaenales	Pseudanabaenaceae	Halomicronema		52.4	17.1	30.2	4.5	38.3	3.1	4.1
Cyanobacteria	Synechococcophycideae	Pseudanabaenales	Pseudanabaenaceae	Halomicronema	hongdechloris	0.0	0.0	0.1	0.2	0.4	0.6	1.2
Cyanobacteria	Synechococcophycideae	Pseudanabaenales	Pseudanabaenaceae	Halomicronema	excentricum	3.1	4.3	23.2	4.5	6.0	7.2	55.9
Cyanobacteria	Oscillatoriophycideae	Chroococcales	Cyanobacteriaceae			0.0	0.0	0.0	1.0	0.2	0.9	0.2
Cyanobacteria	Oscillatoriophycideae	Chroococcales	Cyanobacteriaceae	Cyanothece		0.5	0.0	0.7	1.2	2.2	1.3	2.1
Planctomycetes	Phycisphaerae	Phycisphaerales				2.1	5.3	1.5	3.8	0.6	3.5	1.9
Planctomycetes	Phycisphaerae	Proteobacteria	Phycisphaeraceae			0.3	0.0	0.1	1.1	0.0	0.6	0.0
Proteobacteria	Alphaproteobacteria					12.2	7.4	4.0	10.7	5.5	11.1	7.6
Proteobacteria	Alphaproteobacteria	Kiloniellales	Kiloniellaceae	Thalassospira	xiamenensis	0.4	0.0	0.1	0.8	0.1	0.8	0.6
Proteobacteria	Alphaproteobacteria	Rhizobiales	Hyphomicrobiaceae			1.2	0.0	0.3	0.5	0.0	0.0	0.4
Proteobacteria	Alphaproteobacteria	Rhizobiales	Hyphomicrobiaceae	Nesiotobacter	exalbescens	0.8	0.0	0.3	0.8	0.3	1.3	0.4
Proteobacteria	Alphaproteobacteria	Rhizobiales	Hyphomicrobiaceae	Dichotomicrobium	thermohalophilum	2.0	1.2	0.4	1.7	0.7	0.8	0.2
Proteobacteria	Alphaproteobacteria	Rhodobacterales	Rhodobacteraceae			5.8	5.2	2.1	38.4	3.5	25.4	5.0
Proteobacteria	Alphaproteobacteria	Rhodobacterales	Hyphomonadaceae	Oceanicaulis		0.3	1.1	0.2	0.0	0.3	0.3	1.0
Proteobacteria	Alphaproteobacteria	Rhodobacterales	Hyphomonadaceae	Henriciella		1.2	1.5	0.4	0.9	0.5	1.3	0.6
Proteobacteria	Alphaproteobacteria	Rhodospirillales	Rhodospirillaceae			0.0	0.0	0.0	1.1	0.2	1.2	0.3
Proteobacteria	Alphaproteobacteria	Rhodospirillales	Rhodospirillaceae	Rhodovibrio		1.5	2.2	1.6	3.2	0.8	3.2	2.7
Proteobacteria	Alphaproteobacteria	Rhodospirillales	Rhodospirillaceae	Novispirillum		0.5	0.0	0.0	0.0	0.0	0.8	0.7
Proteobacteria	Deltaproteobacteria	Desulfuromonadales	Desulfuromonadaceae	Desulfuromonas		0.0	0.0	0.0	0.0	0.0	0.0	0.0
Proteobacteria	Gammaproteobacteria					0.6	0.0	0.2	0.2	0.2	0.9	0.4
Proteobacteria	Gammaproteobacteria	Alteromonadales	Alteromonadaceae			2.3	1.4	0.6	4.0	0.5	2.8	0.4
Proteobacteria	Gammaproteobacteria	Alteromonadales	Alteromonadaceae	Marinobacter		0.7	0.0	0.4	0.5	0.3	1.4	1.5
Proteobacteria	Gammaproteobacteria	Alteromonadales	Alteromonadaceae	Marinobacter	bryozoorum	0.9	0.0	0.9	0.4	0.4	3.2	1.7
Proteobacteria	Gammaproteobacteria	Alteromonadales	Alteromonadaceae	Porticoccus	hydrocarbonoclasticus	0.2	0.0	0.0	0.1	0.2	1.1	0.8
Proteobacteria	Gammaproteobacteria	Alteromonadales	OM60			0.0	0.0	0.0	0.0	0.0	0.6	0.0
Proteobacteria	Gammaproteobacteria	Chromatiales	Halothiobacillaceae	Halothiobacillus	hydrothermalis	0.0	0.0	0.0	0.0	0.1	1.2	0.0
Proteobacteria	Gammaproteobacteria	[Marinicellales]	[Marinicellaceae]			0.6	2.5	0.7	0.4	0.4	1.7	0.5
Proteobacteria	Gammaproteobacteria	Oceanospirillales	Alcanivoracaceae	Alcanivorax		0.6	0.9	0.3	0.6	0.5	0.8	0.5
Proteobacteria	Gammaproteobacteria	Oceanospirillales	Alcanivoracaceae	Alcanivorax	venustensis	3.6	35.2	0.4	0.8	0.8	1.0	1.0
Proteobacteria	Gammaproteobacteria	Oceanospirillales	Halomonadaceae	Halomonas		2.1	3.9	0.3	6.9	0.4	2.2	0.3
Proteobacteria	Gammaproteobacteria	Vibrionales	Vibrionaceae	Salinivibrio	costicola	0.0	0.0	0.0	0.0	0.0	0.3	0.0
Spirochaetes	Spirochaetes	Spirochaetales	Spirochaetaceae			0.0	0.0	0.0	0.0	0.0	0.2	0.0
Spirochaetes	Spirochaetes	Spirochaetales	Spirochaetaceae	Spirochaeta		0.0	0.0	0.0	0.4	0.0	0.4	0.0
Spirochaetes	Spirochaetes	Spirochaetales	Spirochaetaceae	Spirochaeta	halophila	0.0	0.0	0.0	0.8	0.3	0.4	0.6
Verrucomicrobia	Opitutae	Puniceicoccales	Puniceicoccaceae	Coraliomargarita		0.4	0.0	0.2	1.3	0.2	1.4	0.2
Verrucomicrobia	Opitutae	[Cerasicoccales]	[Cerasicoccaceae]			1.6	0.0	0.1	1.7	0.7	4.0	0.7
Verrucomicrobia	Verrucomicrobiae	Verrucomicrobiales	Verrucomicrobiaceae	Haloferula	sargassicola	1.0	0.7	0.6	0.4	0.0	1.1	0.5

Chapter 3

Functional responses of petroleum-exposed microbial mats from Shark Bay (Western Australia)

Yalimay Jimenez, Kliti Grice, and Marco J.L. Coolen

PLoS One, in preparation

Impact factor: 2.776

3.1. Abstract

The increased shipping activity from mining and petroleum activities offshore of north-western Australia represents a risk for a petroleum spill. Shark Bay is an enclosed coastal environmentally protected area near to the shipping routes in Western Australia, and is therefore vulnerable to petroleum disturbance. Experimental approaches aid to assess and elucidate how habitats might respond to a potential disturbance. The application of high-throughput sequencing techniques in microbial ecological studies has led to a better understanding of the physiological potential and/or activities under disturbances. However, these techniques still are particularly expensive when hundreds of samples are analysed in parallel. 16S rRNA data and the application of PICRUSt2 algorithm offers a lower cost and faster reliable alternative to predict potential functionalities. If required, shotgun metagenomic sequencing can be performed on a smaller selection of samples to confirm the direct presence of functional genes, but this still does no proof that these genes were actively expressed. In the current study, we have applied the more recent PICRUSt2 pipeline on two 16S rRNA datasets (DNA *vs.* cDNA) from a recently performed time-series experiment with petroleum-exposed smooth vs. pustular microbial mats from Shark Bay, to predict the physiological changes of the residing microbial communities resulting from this lab-induced environmental stress. The results of the predicted functional pathways related to biodegradation of xenobiotics were then compared to a brief assessment of the chemical changes observed in the petroleum-water phase samples collected in the original experiment. Overall, PICRUSt2 predicted an increase in the relative abundance of genes encoding for stress adaptive responses in both petroleum-exposed smooth and pustular mats. Motility, biofilm formation (*e.g.* γ-PGA - poly-β-1,6-N-acetyl-D-glucosamine), competition for nutrients or interspecies *via* efflux of antibiotics or metabolites were among the more abundant predicted functional pathways. Predicted genes associated with degradation of aromatic compounds seem to be also abundant in the petroleum-exposed samples, however, the results of the organic geochemical analysis could not confirm that biodegradation of petroleum-exposed mats had occurred during the time series experiment. Our findings reveal that the microbiomes of petroleum-exposed mats have the capacity to adapt to the stress

conditions, and this prediction also elucidate some functionalities which have not been seen previously under pristine conditions.

Keywords: Shark Bay, microbial mats, PICRUSt2, functionalities, biofilm, petroleum biodegradation.

3.2. Introduction

The offshore northern region of Western Australia (WA) is host to various active resources industries. Shipping along this coastline and port activities represent a potential source of pollution in ecosystems. The Australian Maritime Safety Authority (AMSA) (2012) report has predicted in 2020 an increase in petroleum spill frequency by 83% and 94% for ships at sea and ports activities, respectively. These activities represent a threat to the integrity of Shark Bay's ecosystem, a World Heritage site. Shark Bay holds a wide range of microbial mats that require protection due to their World Heritage values[20]. Microbial mats are mainly found in Hamelin Pool, an embayment protected by a natural barrier from the open ocean (**Figure A3.1**).

Microbial mats are a self-sustained, structured and complex consortium of microorganisms that thrive in benthic environments (Des Marais, 2003; Foster and Mobberley, 2010). The two more commonly studied microbial mats from Shark Bay, are smooth and pustular, forms which are recognised for comprising highly diverse microbiomes (Allen et al., 2009; Wong et al., 2015; Babilonia et al., 2018). Metagenomic and metatranscriptomic studies carried out in several intertidal microbial mat ecosystems collected from Hamelin Pool (Shark Bay, WA), have found that they exhibit genes associated with general or 'natural' stress responses, due to osmotic, salinity, UV, heavy metals and oxidative stressors (Babilonia et al., 2018; Campbell et al., 2020).

There is a considerable amount of knowledge about the response mechanisms of microbial habitats (*i.e.*, mainly soils, freshwater, marine sediments) living under natural but stressed environments. In contrast, there is limited recent and comparable experimental data (Benthien et al., 2004; Abed et al., 2006; Bordenave et al., 2007; Llirós et al., 2008), as well as, a limited understanding of how microbial mat

[20] whc.unesco.org/en/list/578

environments react to disturbances such as petroleum exposure (PE) under hypersaline conditions (Duran and Goñi-Urriza, 2010). We recently performed a time series microcosm incubation experiments with smooth and pustular microbial mats from Hamelin Pool and studied the microbial community responses to lab-induced PE contamination that lasted for up to 120 days, using a taxa-centered approach (**Chapter 2**). The total *vs*. active microbial communities in both PE mat types were identified based on Illumina MiSeq sequencing of PCR-amplified environmental 16S rRNA genes and reverse transcribed 16S rRNA. The latter study revealed the diversity and relative abundance of total *vs*. alive microbial communities that were negatively or positively affected, as well as those that remained unaffected by the long-term PE. However, the physiological responses to this long-term PE such as processes involved in the degradation of hydrocarbons and resistance against environmental stress conditions were not investigated.

The physiological potential and/or activities of the various taxa in environmental microbiomes can be elucidated using more advanced shotgun metagenomic and RNA-seq (metatranscriptomic) sequencing approaches (Shakya et al., 2019). However, library preparations and sequencing of environmental metagenomes and metatranscriptomes is still relatively expensive, especially when many samples are involved. In addition, the analysis of the resulting datasets requires advanced bioinformatics skills, and it has been estimated that the costs for the processing and storage of sequence data now outweigh the costs of sequencing (Muir et al., 2016).

While these advanced approaches are instrumental in studying the genomic potential and activities of environmental microbiomes, a few bioinformatics approaches have been developed recently that enable researchers to predict the physiological properties of environmental microbial populations solely based on 16S rRNA gene sequences (Aßhauer et al., 2015; Douglas et al., 2019). Reliable functional predictions solely based on environmental 16S rDNA sequences have become a reality thanks to the parallel sequencing of 16S rRNA operons and functional genes from the same organisms, and thanks to whole genome sequencing of cultivated bacteria, single cell genomics, and sequencing analysis of environmental metagenomic assembled genomes (MAGs) (Alneberg et al., 2018).

For example, Phylogenetic Investigation of Communities by Reconstruction of Unobserved States (PICRUSt2, version 2.3.0) (Louca and Doebeli, 2018; Barbera et al., 2019; Douglas et al., 2019; Czech et al., 2020) has been proven to provide a cost effective alternative to estimate physiological properties of environmental microbiomes. It is also acknowledged that PICRUSt, regardless of its version, has a major caveat that needs to be considered for its applicability: rare environment-specific functions are not likely to be predicted as they depend on existing and appropriated reference genomes[21]. For instance, only those genes enclosed in the Kyoto Encyclopedia of Genes and Genomes (KEGG) orthologs and Enzyme Classification can be predicted (Douglas et al., 2019). For an extended revision of limitations https://github.com/picrust/picrust2/wiki/Key-Limitations. PICRUSt2 (released in July 2019), has addressed these previous limitations and expanded its capabilities, such as the added ability to perform sequence denoising (*i.e.*, Quantitative Insights into Microbial Ecology 2 - QIIME2 pipeline), using a more robust and updated reference genome databases[22] and pathway mappings, as well as, allowing the use of customised reference databases if required (Douglas et al., 2019).

Here, we examined our previously obtained 16S rDNA/16S rRNA datasets from the Hamelin Pool smooth and pustular microbial mats time series incubation experiment (**Chapter 2**), using the latest PICRUSt2 pipeline to predict functional profiles and compared the result between initial (pristine mat microbiomes) and petroleum-exposed microbiomes. Mechanisms related to PE-induced microbial stress response systems (*i.e.*, membrane transport, signal transduction, cellular communication and motility), energy metabolism, biodegradation of xenobiotics, and biosynthesis of secondary metabolites and antibiotics were investigated over the course of incubation, by comparing the abundance of metabolic pathways predicted for both initials *vs.* petroleum-exposed samples. Additionally, we performed some organic geochemical analysis of the petroleum-water interphase of petroleum-exposed samples to determine whether a petroleum biodegradation process was initiated and then compared it with the results of the predicted functional pathways associated with this process.

[21] It affects both PICRUSt approach and current gold-standard sequencing analysis (*i.e.,* 16S rRNA).
[22] Comparatively with the previous version.

3.3. Material and methods

3.3.1. Dataset from petroleum-exposed incubation experiments

Briefly, smooth- and pustular microbial mats from Shark Bay were incubated with petroleum for 30 (T30), 60 (T60) and 120 (T120) days under controlled lab conditions. Pieces of both mat types were placed in microcosms and subjected to artificial light in a diel regime (8 hr dark and 16 hr light), at 25 °C with a constant flux of filtered air. The petroleum additive used in these experiments was from a regional oil well on Barrow Island (#101). Microcosms were subsampled before (T0 "initial") and after PE (T30, T60 or T120). Control microcosms, without petroleum, were incubated in parallel to assess any changes under lab settings. DNA and RNA were extracted from each sub-sample. Complementary DNA was synthesised from RNA extract *via* Photoscript II Reverse Transcriptase. U519fM and U803R primers were used in the PCR amplification of bacterial and archaeal 16S rRNA genes (V4 region). Amplified DNA and cDNA were then barcoded and gel-purified. The pooled barcoded library was then sequenced (MiSeq Illumina) at the Australian Genomic Research Facility (AGRF). Sequenced data was then processed by AGRF Illumina bcl2fastq 2.20.0.422 pipeline. Amplicon Sequence Variant (ASV) x sample abundance matrices were subsequently generated in QIIME 2 (version 2019.10[23]) (Bolyen et al., 2019) as described in detail elsewhere (**Chapter 2**). These ASV abundance matrices formed the template for subsequent function prediction analysis for this study.

3.3.2. Functional prediction by PICRUSt2 and identification of functional markers

DNA-based and RNA-based 16S rRNA sequences datasets processed by QIIME 2 (after demultiplexed and filtered) were analysed through PICRUSt2, version 2.3.0 (Louca and Doebeli, 2018; Barbera et al., 2019; Douglas et al., 2019; Czech et al., 2020) to predict functional gene family abundances of identified taxa in initial conditions samples (T0) and those exposed to petroleum at T30, T60 and T120. This bioinformatics tool allocates functional features in the sample using closed reference 16S rRNA gene sequences. Pre-processed (singleton removed) representative sequences and feature tables obtained after DADA2 denoising step were used as input

[23] www.qiime2.org

data files and initially subjected to the Sequence Placement Approach in PICRUSt2[24]. Weighted Nearest-Sequenced Taxon Index (NSTI) values and KEGG (Kyoto Encyclopaedia of Genes and Genomes) orthologs (KO) metagenomes, as normalised predicted functional abundance table per sample, were obtained as output. PICRUSt2 NSTI values can be used as an indicator of reference genome coverage or the accuracy of the prediction (Langille et al., 2013). By default, the PICRUSt2 algorithm discards those samples over a NSTI cut-off value of 2.00 to avoid speculative interpretations. A higher accuracy prediction (80-85%) is expected for NSTI values <0.06, while those >0.15 may not have well-sequenced reference genomes in public databases for comparison, lowering the accuracy of functional prediction to 20% (Douglas et al., 2019). Therefore, only those samples with NSTI values <0.15 were utilised for this assessment.

Principal Component Analysis (PCA) was performed using the R-package MixOmics[25] and its mix MC framework to explore the data and identify any clustering of predicted KO functions between initial (T0) and PE microbial mats (T30, T60 and T120; Cao et al., 2016). **Figure A3.2** shows the general bioinformatics and biostatistics workflow used. In brief, the KO metagenome dataset was offset to 1, normalized by Total Sum Scaling (TSS) and then transformed by Centered Log Ratio (CLR) before generating PCA plots. Correlation Circle (CC) plots were then created for determining the KOs responsible for the observed variations in PCA plots. Cut-offs in CC plots were set depending on clustering distributions in Principal Component 1 (PC1). This cut-off represents the radius (magnitude) of the variable projection in dimension 1. A larger radius indicates a greater contribution to the clustering observed (González et al., 2012). This cut-off was set to 0.8 for all performed analyses to guarantee retrieving those variables with the higher contribution to PC1 and correlation between them (an angle less than 45°). For detailed understanding of CC plots and their relevance in biological analysis is summarised by González et al. (2012). Those KOs particularly differentiated in PE samples were manually collapsed (or grouped) into Level 2 (or category B) and Level 3 (category C) functions, using

[24] https://github.com/picrust/picrust2
[25] http://mixomics.org/mixmc/

BRITE functional hierarchy[26]. Heatmaps were generated using the R package ComplexHeatmap (Gu et al., 2016) to visualise differences in predicted KOs between the samples. One-way analysis of variance (ANOVA) was then used to verify which level 3 functions differed significantly between initial and PE microbial mats. Pathways and their indicator KOs related to (a) environmental information processing; (b) cellular processes; (c) energy metabolisms; (d) biosynthesis of antibiotics and secondary metabolites; and (e) degradation of xenobiotics were subsequently plotted into comparative abundance graphs using the STAMP software package (*i.e.*, extended error bar plots; Parks et al., 2014). Those statistically differentiated ($p<0.05$) KOs (genes) shared between all types of samples were then retrieved and summarised in tables (type presence or absent).

3.3.3. Petroleum (as pollutant) and petroleum-water interphase samples chemical analysis

The Barrow Island #B101 petroleum sample used in this study (as pollutant) comes from the Carnarvon Basin. Details of the petroleum geology of the Carnarvon Basin have been provided by Crank (1973) and Volkman et al. (1983a). The petroleum reservoirs in the Carnarvon Basin are in marine facies of Cretaceous and Triassic ages and its petroleum geochemistry is presented elsewhere (Alexander et al., 1983; Volkman et al., 1983b, 1984; Armanios et al., 1992; Trolio et al., 1999; Grice et al., 2000). The petroleum sample #B101 was subjected to fractionation and GC-MS analysis. Similarly, petroleum-water interphase samples, from type 2 control samples (PCW1-PCW2 at T0, T60 and T120, Chapter 2) and PE smooth and pustular microbial mats microcosms (PS8S and PS11P at T0-T60, and PS9S and PS12P at T0-T120, **Chapter 2**) were analysed as outlined below.

3.3.3.1. LC separation of petroleum fractions

In a typical separation, the petroleum (5 mg) was subjected to silica gel liquid chromatography (LC). The Barrow Island petroleum sample was dissolved in *n*-hexane (1 mL) and applied to the top of a mini-column (4 cm × 0.4 cm i.d.) of a silica

[26] https://www.genome.jp/kegg/kegg3b.html

gel slurry (activated 120°C overnight). A saturated hydrocarbon fraction was eluted with *n*-hexane (4 mL) and an aromatic fraction was subsequently eluted with *n*-hexane: DCM (7:3, 4 mL) mixture and the polar fraction was eluted with a DCM: methanol (1:1, 4 mL) mixture. The first two fractions were directly collected in sample vials (5 mL) and were made up to 2 mL with *n*-hexane. Gas Chromatography – Mass Spectrometry (GC-MS) analysis was carried out immediately to avoid evaporative loss.

Samples collected from the petroleum-water phase were first subjected to liquid-liquid extraction. An aliquot (8 mL) was extracted with *n*-hexane (3 mL x 2) and DCM (4 mL x 2). Excess solvent was removed gently by a nitrogen gas purge. Elemental sulfur was removed from the extract by adding activated copper powder (1 g) to the extract dissolved in DCM for 72 hours. Residual copper powder and water was removed by passing the extract over anhydrous magnesium sulfate (1 cm, Sigma Aldrich) in a Pasteur pipette. The extract was subsequently separated by a small-scale silica gel liquid chromatography to obtain the saturated, aromatic, and polar fractions as described above for the petroleum sample. Saturated and aromatic fractions were then analysed by GC-MS.The analyses of these fractions will be mainly suitable for those compounds >C10 hydrocarbons and those C10-C15 partially depleted, if any during due to lab work-up fractionation.

3.3.3.2. Gas Chromatography-Mass Spectrometry

The saturated fractions were dissolved in *n*-hexane and analysed by GC-MS using a Hewlett Packard 7890B GC coupled to a 5977B mass spectrometer (DB-1 MSUI column 60 m x 0.25 mm i.d.). The aromatic fractions were dissolved in DCM and analysed using a Hewlett Packard 6890 gas chromatograph (GC) coupled to a 5975 mass spectrometer (DB-5 MSUI column 60 m x 0.25 mm i.d.). In both cases 1 µL of sample was introduced onto a split/splitless injector. The carrier gas used for all GC-MS analyses was helium (ultra-high purity) at a linear velocity of 1mL/min. The GC oven was programmed from 40°C to 325°C at 3°C min-1 and held isothermally at 300°C for 40 min. Samples were analysed in full scan mode. Data acquisition and processing was performed with the ChemStation Data system. Product identification was based on retention time and mass spectral correlations with standard compounds including those that are listed in the NIST mass spectral library.

Selected ions were used to selectively highlight specific classes of hydrocarbon compounds including aliphatics such as *n*-alkanes (*m/z* 85), isoprenoids (*m/z* 183), hopanes (*m/z* 191), *nor*hopanes (*m/z* 177), steranes (*m/z* 217); caged compounds such alkylated adamantanes (*m/z* 135, 136, 149, 163 and 177) and diamantanes (*m/z* 187, 188, and 201); and aromatics such as alkylated naphthalenes (*m/z* 128, 142, 156, 170 and 184), phenanthrenes (*m/z* 178, 192, 206, 220 and 234), and biphenyls (*m/z* 154, 168, 182 and 196). The distributions of these compounds in the Barrow Island petroleum are shown in the supplementary section.

3.4 Results

3.4.1. Prediction validation: NSTI metrics

Microbial functions were predicted from the recovered 16S rRNA genes and transcripts using PICRUSt2 (**Chapter 2**). As part of the PICRUSt2 pipeline, NSTI scores were automatically obtained. In our study, pristine hypersaline smooth and pustular microbial mats which were analysed in parallel to the PE microbial mats, had NSTI values (0.15) near the recommended NSTI limit (*i.e.,* 0.15): $0.13 \pm 0.02^{(n=4)}$ (mean $\pm$ σ) and $0.14 \pm 0.01^{(n=4)}$, respectively. These values are in agreement with other pristine hypersaline environments previously investigated, e.g. Guerrero Negro (Langille et al., 2013). In contrast, all PE pustular mat microbial mats and only smooth microbial mat samples at T120 of PE, yielded lower NSTI values indicative of more confident functional predictions (**Table A3.1**, **Table A3.2**).

3.4.2. KOs datasets description and data exploration

PICRUSt2 analysis yielded a functional orthologs (KEGG Orthology – KO) dataset. The amount of variation in functional diversity between samples was visualised using PCA. PCA of the smooth mat samples (**Figure 3.1**, top left) revealed substantial differences between samples collected before and after PE, with 52% of the variation explained by PC1. Predicted functions differ significantly in those pustular mat microcosms exposed to petroleum for 60 or more days of incubation compared to the initial samples (**Figure 3.1**, top right). We also observed differences in functional

diversity in the various sub-samples of the biofilm which had developed on top of the pustular mat after 100 days of PE. PC1 explained respectively 51% and 57% of the data variance in the pustular mat microcosm and biofilm-related samples (**Figure 3.1**, bottom). Histograms showing the contribution of the remaining PCA components are given in **Figure A3.3**. By using the % of data coverage by PC1 (50-60%) and the observed separation between initial and PE samples' groups allowed us to use Correlation Circle plots for identifying those variables (*i.e.*, KOs) responsible of such a separation and also strongly correlated (≤ 45°) in PE microcosms samples (**Figure A3.3**– red dashed circle, right). These results are in agreement with the observed microbial composition shifts (both DNA and cDNA) between initial and petroleum-exposed samples. Since we have already shown in **Chapter 2** that there was no statistically significant difference between the controls and samples that were incubated in parallel, gene predictions were not further analysed from the control microcosms. Furthermore, the observed decline in microbial diversity with increasing exposure time likely increased the reliability of the fewer predicted gene functions by PICRUSt2.

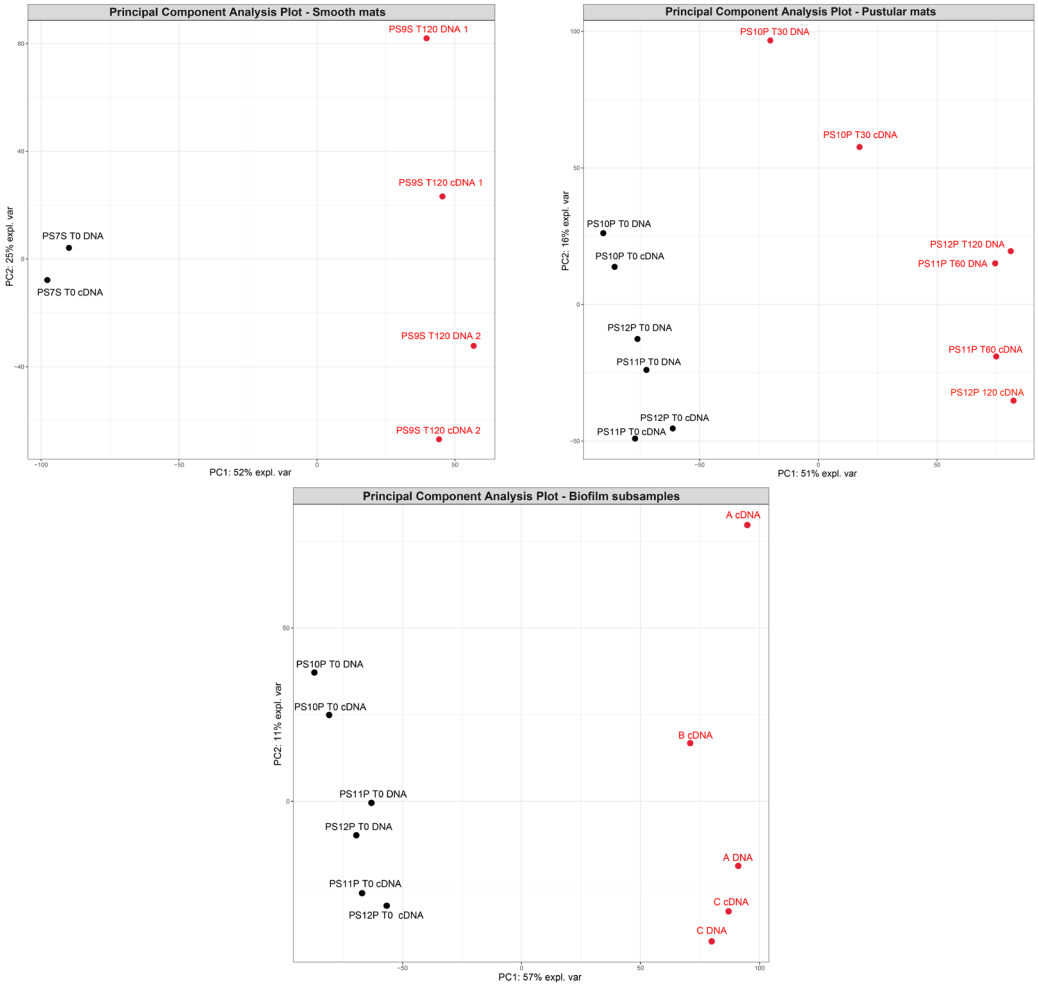

Figure 3.1. Principal Component Analysis (PCA) plot showing total (DNA) and active microbiome (cDNA) distribution of smooth (top left), pustular mats (top right) and biofilm sub-samples (bottom). Initial samples –not subjected to PE– are displayed as black dots, and PE samples as red dots.

A summary of the total number of KOs predicted by PICRUSt2 for all type of samples can be found in **Table 3.1**. In addition, it shows the number of KOs used for subsequent analysis of functions particularly activated under PE and identified those shared between smooth and pustular mats, and between subcategories of the unique tower-like biofilm that was formed only in pustular mats after 120 days of PE. KOs above the 0.8 cut-off (radius) can be found in **Appendix 3**, **Table A3.4**, **Table A3.5** and **Table A3.6**. It should be noted that the actual number of pathways may be fewer since the same KO (*e.g.* gene or enzyme) might be participating in more than one functional mechanism.

Table 3.1. Summary of total KOs predicted, retrieved KOs after cut-off and maximum number of metabolic pathways identified.

	Smooth mats	Pustular mats	Biofilm sub-samples
# samples	2 initials 4 PE samples	6 initials 6 PE samples	6 initials 7 PE samples
Total KOs predicted	5,277	5,562	5,683
KOs after 0.8 cut off	579 (**Table A3.4**)	544 (**Table A3.5**)	545 (**Table A3.6**)
Metabolic pathways identified (max.)	127	115	132

3.4.3. Dominant inferred functional mechanisms under PE conditions

Dominant or main contributing inferred KOs under PE conditions (KOs > 0.8 – PC1) were grouped into the major functional categories (level 3 – KEGG Orthologs) to assess and compare microbial functionalities of microbial mats and biofilm-related samples. Pathways from environmental information processing (*i.e,.* membrane transport and signal transduction) and cellular processes (*i.e.*, cellular community – prokaryotes and cell motility) were abundant in smooth mat samples after PE for 120 days (**Table A3.3**). ABC transporters, Two-Component system (TCS), biofilm formation (type *Vibrio cholerae*) and flagellar assembly mechanisms were particularly dominant in the active microbial community (cDNA) (**Figure 3.2**). These pathways have all been linked to the response system of organisms living under stressed conditions (Ron, 2013).

Metabolic pathways associated with nitrogen metabolism as well as biosynthesis of secondary metabolites and antibiotics seem to predominate in cDNA of PE exposed smooth microbial mats (**Figure 3.2**). Other slightly abundant pathways were those related to amino acid (*i.e.,* glycine, serine and threonine metabolism), nucleotide (*i.e.*, purine metabolism), carbohydrate (pyruvate metabolism) and xenobiotic biodegradation metabolisms (*i.e.*, atrazine degradation) (**Figure 3.2**). Conversely, the most abundant metabolic pathways predicted in pustular microbial mats (cDNA) under PE conditions were related to energy metabolism, mostly photosynthesis – antenna proteins– (**Figure 3.3**). These pathways were closely followed by carbohydrate, nucleotide, amino acid, and cofactors and vitamin metabolisms.

Predicted functions associated with environmental information processing and biosynthesis of antibiotics and/or secondary metabolites were less abundant or perhaps masked by the more abundant mechanisms. Similar mechanistic trends were observed in the predicted functionalities in the subsamples obtained from the tower-shaped biofilm that was formed on the pustular mat after 120 days of PE, except for the additional substantial expression of methane metabolism across all sub-samples (*i.e.*, A, B, C and D; **Figure 3.4**) which was lacking from the other samples obtained during the time series.

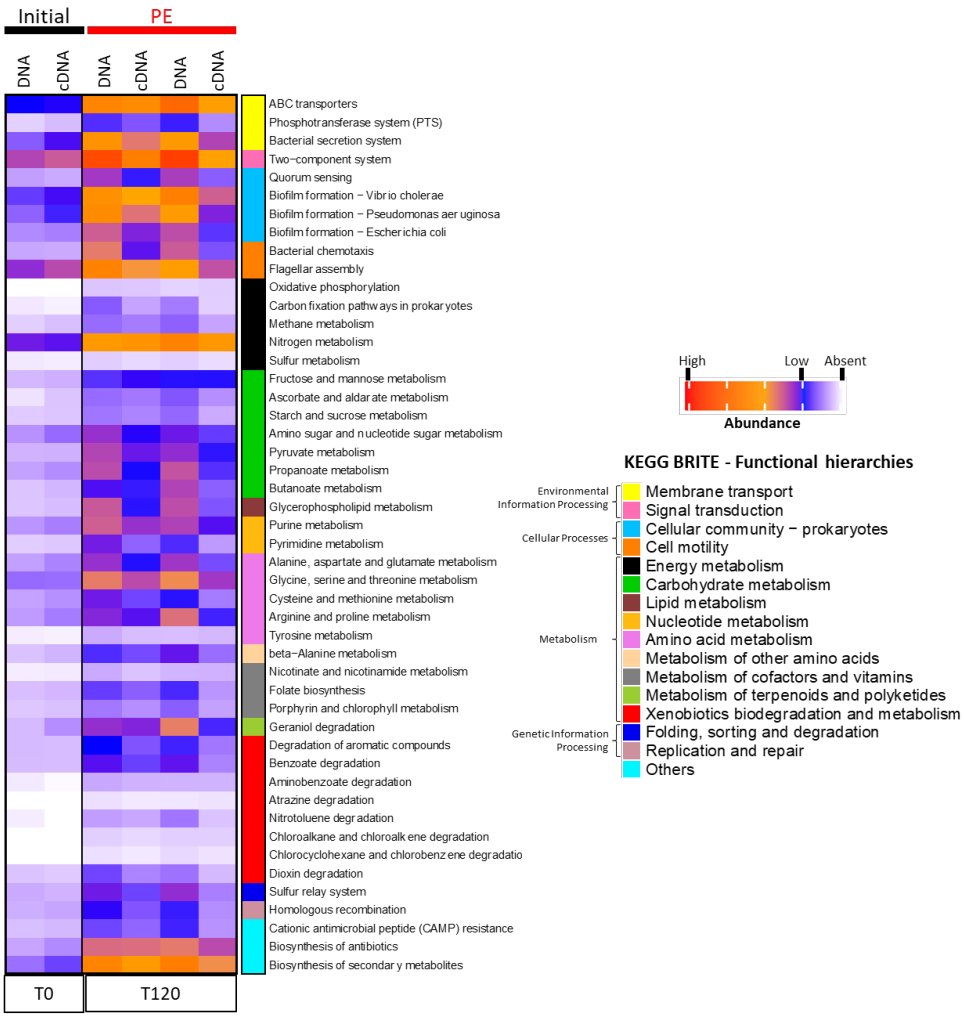

Figure 3.2. Heatmap showing the relative abundance of predicted KO metabolic pathways (level 3) between initial –as controls– (T0) and petroleum-exposed **smooth mat** after 120 days (PS9S microcosm). (*) Based on PICRUSt2 functional prediction from 16S rRNA data (DNA and cDNA), using KOs responsible for the highest difference between the groups (mainly PC1 in PCA plot - **Figure 3.1**). Data displayed correspond to raw abundance of KOs standardised by total and square root transformed.

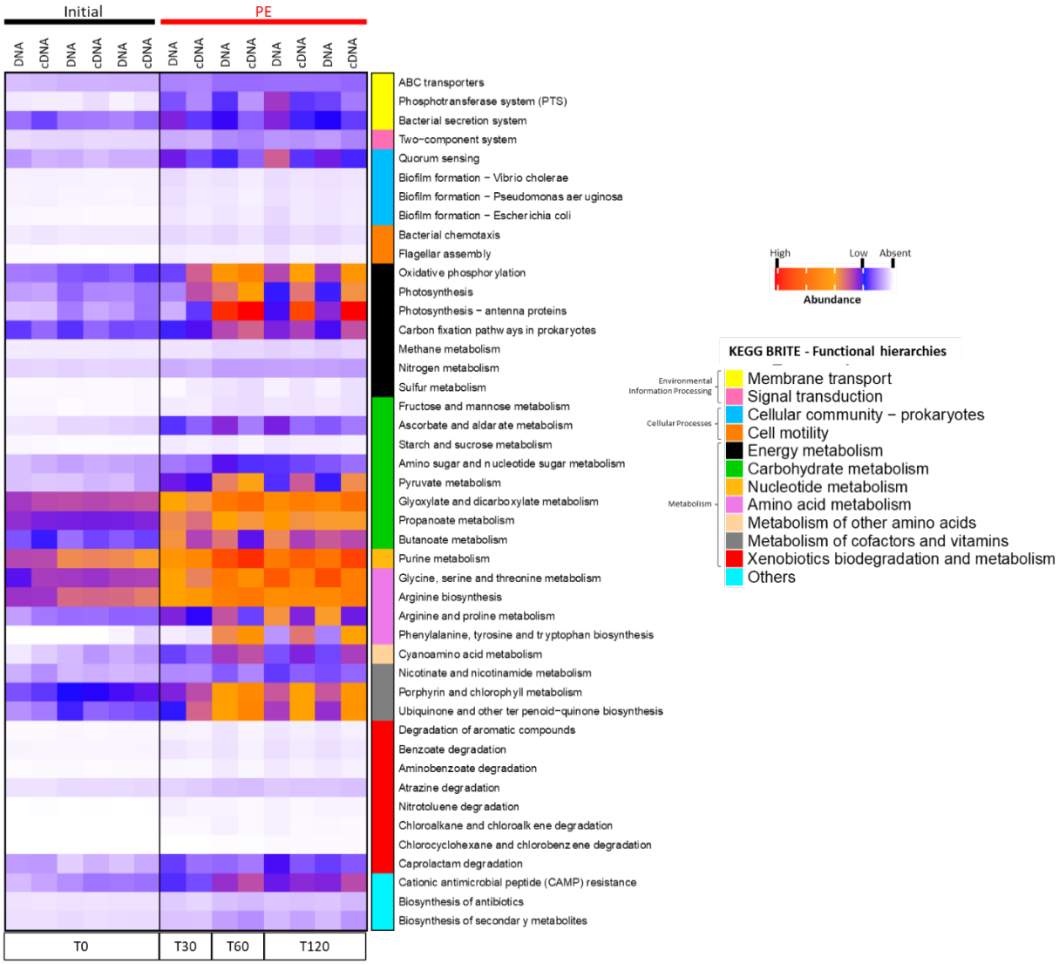

Figure 3.3. Heatmap showing the relative abundance of predicted KO metabolic pathways (level 3) between initial –as controls– (T0) and petroleum-exposed **pustular mats** after 30, 60 or 120 days (PS10P, PS11P and PS12P microcosms). See legend **Figure 3.2** for details about the source data (*).

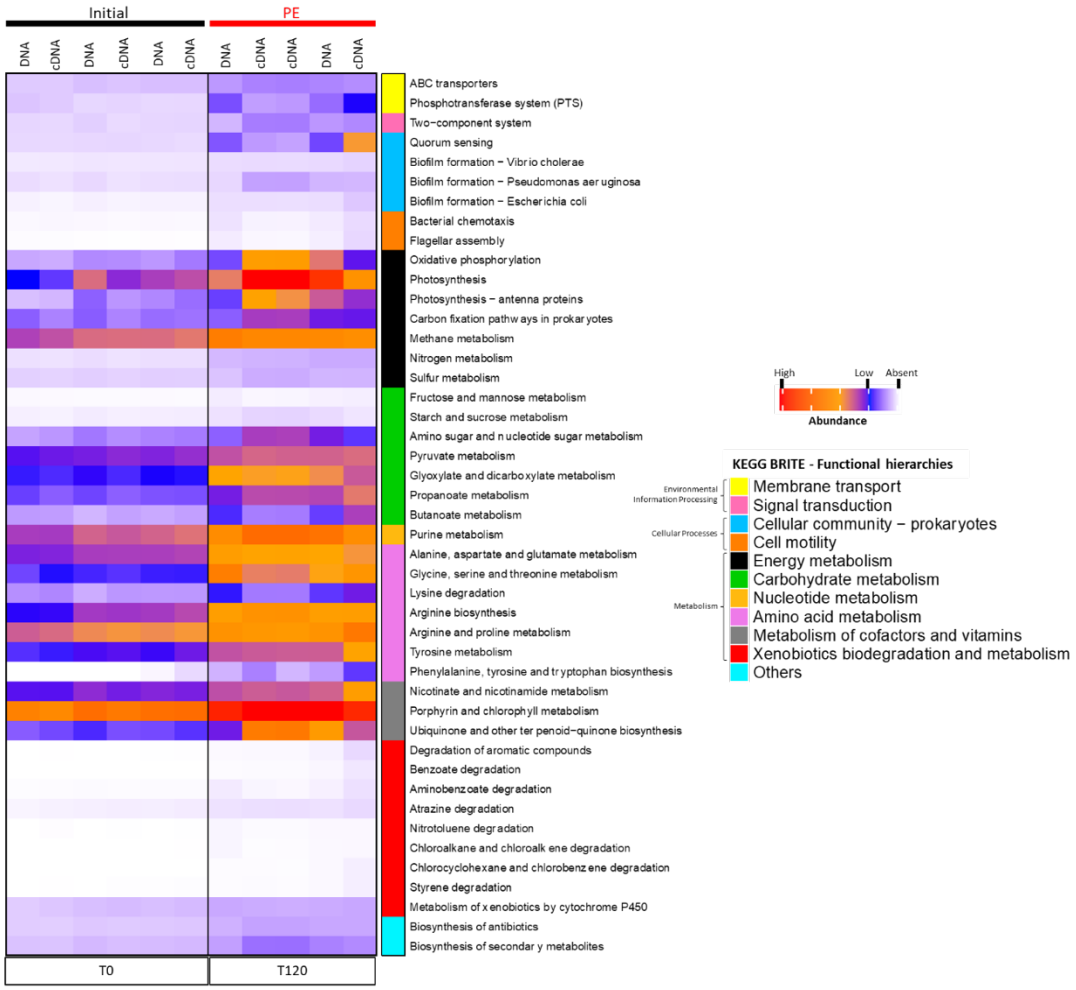

Figure 3.4. Heatmap showing the relative abundance of predicted KO metabolic pathways (level 3) between initial –as controls– (T0) and petroleum-exposed pustular microbial mat **biofilm-related sub-samples** after 120 days (PS12P microcosm). See legend **Figure 3.2** for details about the source data (*).

3.4.4. Key functional processes abundant under petroleum exposure

Microbial ecosystems subjected to stress by PE, usually exhibit a complex and interconnected group of response mechanisms over time (McGenity et al., 2012). To explore the main predicted functional responses of the different microbial mats and biofilm samples the following five major functional mechanisms were evaluated: environmental information processing functional; cellular processes; energy metabolisms; degradation of xenobiotics; and biosynthesis of antibiotics and secondary metabolites.

3.4.4.1 Environmental information processing

Genes involved in environmental information processing comprise ABC transporters, phosphotransferase system (PTS) and TCS (**Table 3.2**). They represent the first part of the sensory system, mainly located in the cell membrane and are responsible for interacting with the external environment and various stimuli (*i.e.*, nutrients, xenobiotics, *etc*) (Bekker et al., 2006). The genes for ABC transporters were predicted in all sample types (smooth and pustular mats, and biofilm). including glutamine (*gln*HPQ), maltose/maltodextrin (*mal*FG), arginine (*aot*P) and multidrug/microcin (*yoj*I) transport systems. All three sample types may harbor active bacteria that possess genes associated with TCS (notably NarL, OmpR and CitB families). Genes associated with adhesion or motility were also predicted to be more abundant in all samples, *i.e.*, pilK and chpB. Predicted arabinose (*ara*FHG), putative amino-acid (*yxe*MNO) and vitamin B12 (*btu*CD) transport systems, and multidrug efflux pump (*mdl*AB and *smd*AB) were more associated with pustular microbial mat and biofilm samples. Predicted PTS genes were mainly more abundant in pustular microbial mat samples, *i.e. ula*AB, *sga*BT, *glv*C, *mal*P, *agl*A, *tre*B and *pts*O.

3.4.4.2 Cellular processes

Genes involved in cellular processes include additional mechanisms involved in sensing and signal transduction (**Table 3.3**). This includes quorum sensing – *i.e.,* cell to cell communication systems–, with gene clusters belonging to this category putatively present in all PE microbial mat samples, comprising: *flh*CD, *lux*R LuxR family regulator and TCS. In contrast, *las*A, *aph*A and *lux*PQU were only identified between the most statistically significant genes predicted in pustular mat samples. Bacterial chemotaxis was represented by two predicted genes - *tar* and *csg*D - shared by all samples. Genes predicted to be involved in biofilm formation (type *Escherichia coli*) were also abundant in each of the smooth mat, pustular mat, and biofilm sub-samples, *i.e.*, *pga*ABCD cluster (biofilm PGA synthesis protein), while biofilm formation *msh*D and *aph*B genes (type *Vibrio Cholerae*) were only predicted in pustular microbial mats.

Table 3.2. Table of predicted KOs (genes) related to **environmental information processing** and their functions across smooth, pustular and biofilm-related samples. Data source: **Figure A3.4**, **Figure A3.5** and **Figure A3.6**. (**) Statistically significant predicted KOs = ++, while those that are not predicted or statistically significant = n.p. Level 3 or category C based on BRITE functional hierarchy.

Level 3	#KO	Function	SM	PM	Biofilm
ABC Transporters	K06073	ABC.VB12.P, *btu*C - vitamin B12 transport system permease protein	n.p.	++	n.p.
	K06074	ABC.VB12.A, *btu*D - vitamin B12 transport system ATP-binding protein [EC:3.6.3.33]	n.p.	++	n.p.
	K06159	*yoj*I - multidrug/microcin transport system ATP-binding/permease protein	++	++	++
	K10025	*aot*P - arginine/ornithine transport system ATP-binding protein [EC:3.6.3.-]	++	++	n.p.
	K10036	*gln*H - glutamine transport system substrate-binding protein	++	++	++
	K10037	*gln*P - glutamine transport system permease protein	++	++	++
	K10038	*gln*Q - glutamine transport system ATP-binding protein [EC:3.6.3.-]	++	++	++
	K10109	malF - maltose/maltodextrin transport system permease protein	++	++	n.p.
	K10110	malG - maltose/maltodextrin transport system permease protein	++	++	++
	K10537	araF - L-arabinose transport system substrate-binding protein	++	++	++
	K10538	araH - L-arabinose transport system permease protein	n.p.	++	++
	K10539	araG - L-arabinose transport system ATP-binding protein [EC:3.6.3.17]	n.p.	++	++
	K16961	yxeM - putative amino-acid transport system substrate-binding protein	n.p.	++	++
	K16962	yxeN - putative amino-acid transport system permease protein	n.p.	++	++
	K16963	yxeO - putative amino-acid transport system ATP-binding protein [EC:3.6.3.-]	n.p.	++	++
	K18889	*mdl*A, *smd*A - ATP-binding cassette, subfamily B, multidrug efflux pump	n.p.	++	n.p.
	K18890	*mdl*B, *smd*B - ATP-binding cassette, subfamily B, multidrug efflux pump	n.p.	++	n.p.
Phosphotransferase system (PTS)	K02750	PTS-Glv-EIIC, *glv*C, *mal*P, *agl*A - PTS system, alpha-glucoside-specific IIC component	n.p.	++	n.p.
	K02779	PTS-Glc-EIIC, *pts*G - PTS system, glucose-specific IIC component	++	++	++
	K02819	PTS-Tre-EIIC, *tre*B - PTS system, trehalose-specific IIC component	n.p.	++	n.p.
	K02822	PTS-Ula-EIIB, *ula*B, *sga*B - PTS system, ascorbate-specific IIB compon.p.nt [EC:2.7.1.194]	n.p.	++	n.p.
	K03475	PTS-Ula-EIIC, *ula*A, *sga*T - PTS system, ascorbate-specific IIC component	n.p.	++	n.p.
	K08485	PTS-HPR.PTSO, *pts*O, *npr* - phosphocarrier protein NPr	n.p.	++	++
Two-Component system (TCS)	K02661	*pil*K - type IV pilus assembly protein PilK	++	++	++
	K03533	*tor*D - TorA specific chaperone	++	++	++
	K06597	*chp*B - chemosensory pili system protein ChpB (putative protein-glutamate methylesterase)	++	++	++
	K07662	*cpx*R - Two-Component system, OmpR family, response regulator CpxR	n.p.	++	n.p.
	K07671	*prr*A - Two-Component system, OmpR family, response regulator PrrA	n.p.	++	n.p.
	K07688	*fim*Z - Two-Component system, NarL family, response regulator, fimbrial Z protein, FimZ	++	++	++
	K07693	*des*R - Two-Component system, NarL family, response regulator DesR	++	++	n.p.
	K07792	*dcu*B - anaerobic C4-dicarboxylate transporter DcuB	n.p.	++	n.p.
	K11637	*cit*S - Two-Component system, CitB family, sensor histidine kinase CitS [EC:2.7.13.3]	++	++	++
	K11638	*cit*T - Two-Component system, CitB family, response regulator CitT	++	++	++
	K16692	*etk*, *wzc* - tyrosine-protein kinase Etk/Wzc [EC:2.7.10.-]	++	++	++
	K19609	*pfe*S, *pir*S - Two-Component system, OmpR family, sensor histidine kinase PfeS [EC:2.7.13.3]	++	++	++
	K19610	*pfe*R, *pir*R - Two-Component system, OmpR family, response regulator PfeR	++	++	++
	K19621	*phc*S - Two-Component system, sensor histidine kinase PhcS [EC:2.7.13.3]	++	++	++

Table 3.3. Table of predicted KOs (genes) related to **cellular processes** and their functions across smooth, pustular and across the tower-shaped biofilm. Data source: **Figure A3.7**, **Figure A3.8** and **Figure A3.9**. (**) in **Table 3.2**.

Level 3	# KO	Function	SM	PM	Biofilm
Quorum Sensing	K02402	*flhC* - flagellar transcriptional activator FlhC	++	++	++
	K02403	*flhD* - flagellar transcriptional activator FlhD	++	++	++
	K10917	*aphA* - PadR family transcriptional regulator, regulatory protein AphA	++	++	++
	K15852	*luxR, vanR* - LuxR family transcriptional regulator, transcriptional activator of the bioluminescence operon	++	++	++
	K08642	*lasA* - LasA protease [EC:3.4.24.-]	n.p.	++	n.p.
	K10910	*luxP* - autoinducer 2-binding periplasmic protein LuxP	n.p.	++	n.p.
	K10909	*luxQ* - Two-Component system, autoinducer 2 sensor kinase/phosphatase LuxQ [EC:2.7.13.3 3.1.3.-]	n.p.	++	n.p.
	K10911	*luxU* - Two-Component system, phosphorelay protein LuxU	n.p.	++	n.p.
Flagellar assembly	K02423	*fliT* - flagellar protein FliT	++	++	++
	K02399	*flgN* - flagella synthesis protein FlgN	++	++	n.p.
	K02414	*fliK* - flagellar hook-length control protein FliK	++	n.p.	n.p.
Bacterial Chemotaxis	K05875	*tar* - methyl-accepting chemotaxis protein II, aspartate sensor receptor	++	++	++
	K04333	*csgD* - LuxR family transcriptional regulator, *csgAB* operon transcriptional regulatory protein	++	++	++
Biofilm formation *Escherichia Coli*	K11931	*pgaB* - poly-beta-1,6-N-acetyl-D-glucosamine N-deacetylase [EC:3.5.1.-]	++	++	++
	K11935	*pgaA* - biofilm PGA synthesis protein PgaA	++	++	++
	K11936	*pgaC* - *ica*A; poly-beta-1,6-N-acetyl-D-glucosamine synthase [EC:2.4.1.-]	++	++	++
	K11937	*pgaD* - biofilm PGA synthesis protein PgaD	++	++	++
	K18968	*adrA* - diguanylate cyclase [EC:2.7.7.65]	++	++	++
Biofilm formation *Vibrio Cholerae*	K10927	*mshD* - MSHA pilin protein MshD	n.p.	++	n.p.
	K10918	*aphB* - LysR family transcriptional regulator, transcriptional activator AphB	n.p.	++	n.p.

Table 3.4. Table of predicted KOs (genes) related to **energy metabolisms** and their functions across smooth, pustular and biofilm-related samples. Data source: **Figure A3.10**, **Figure A3.11** and **Figure A3.12**. (**) in **Table 3.2**.

Level 3	#KO	Function	SM	PM	Biofilm
Photosynthesis	K05376	*cpe*A, *mpe*A; phycoerythrin alpha chain	n.p.	++	++
	K05377	*cpe*B, *mpe*B; phycoerythrin beta chain	n.p.	++	++
	K05378	*cpe*C, *mpe*C; phycoerythrin-associated linker protein	n.p.	++	++
	K05380	*cpe*E; phycoerythrin-associated linker protein	n.p.	++	++
	K05381	*cpe*R; phycoerythrin-associated linker protein	n.p.	++	++
	K05383	*cpe*T; *Cpe*T protein	n.p.	++	++
	K05384	*cpe*U, *mpe*U; bilin biosynthesis protein	n.p.	++	++
	K05385	*cpe*Y; bilin biosynthesis protein	n.p.	++	++
	K05386	*cpe*Z; bilin biosynthesis protein	n.p.	++	++
Oxidative Phophorylation	K00247	*frd*D; fumarate reductase subunit D	n.p.	++	n.p.
	K01535	PMA1, PMA2; H^+-transporting ATPase [EC:3.6.3.6]	++	++	n.p.
	K02262	COX3; cytochrome c oxidase subunit 3	++	++	n.p.
Methan.p. metabolism	K00148	*fdh*A; glutathion.p.-independent formaldehyde dehydrogenase [EC:1.2.1.46]	++	++	++
	K03533	*tor*D; TorA specific chaperon.p.	++	++	++
	K18277	*tmm*; trimethylamin.p. monooxygenase [EC:1.14.13.148]	n.p.	++	n.p.
Nitrogen metabolism	K15576	*nrt*A, *nas*F, *cyn*A; nitrate/nitrite transport system substrate-binding protein	n.p.	n.p.	++
	K15577	*nrt*B, *nas*E, *cyn*B; nitrate/nitrite transport system permease protein	n.p.	n.p.	++
	K15578	*nrt*C, *nas*D; nitrate/nitrite transport system ATP-binding protein [EC:3.6.3.-]	n.p.	n.p.	++
Sulfur metabolism	K05301	*sor*A; sulfite dehydrogenase (cytochrome) subunit A [EC:1.8.2.1]	++	++	++

3.4.4.3. Energy metabolism

Predicted energy metabolism genes relating to photosynthetic, methane, nitrogen and sulfur metabolisms were identified across the sample suite (**Table 3.4**). Genes associated with photosynthesis processes - *i.e.*, cluster *cpe*ABCERTUYZ - were identified in pustular mat and biofilm samples, but not in smooth microbial mats. Oxidative phosphorylation (or respiration) genes were also selectively distributed. For example, *frd*D was identified only in pustular mats, while PMA1, PMA2 and COX3 were present in both smooth and pustular mats. Several methane and sulfur metabolic genes – *i.e.*, *fdh*A, *tor*D and *sor*A - were predicted in all samples, whereas another (*e.g*, *tmm*) was only expected in pustular mat. Genes expressive of a nitrogen metabolism - *i.e.*, *nrt*ABC operon, linked to assimilatory reduction of nitrate pathway (Frías et al., 1997) - were only envisaged abundant in biofilm samples. Nitrogen metabolism genes were only envisaged to be abundant in biofilm samples, belonging to *nrt*ABC operon, which has been linked to assimilatory reduction of nitrate pathway. This metabolism appeared to be more abundant in smooth mat samples at level 3 (**Figure 3.2**), however, after comparing the mean proportions of individual contributions they are only statistically significant in biofilm samples.

3.4.4.4. Degradation of xenobiotic pathways

Seventeen different genes putatively involved in the degradation of organic compounds or xenobiotics were identified (**Table 3.5**). Eight genes predicted common to all samples have been associated with the degradation of i) aromatic compounds - *hpa*D, *bad*H, *bad*I and *dmp*D; ii) chlorocyclohexane and chlorobenzene - *pcp*B; iii) atrazine degradation - *atz*D, iv) aminobenzoate degradation - *van*B; and v) styrene - *dmp*D. Three genes detected in both pustular mat and biofilm samples (but not in smooth mats) have also been attributed to the degradation of vi) benzoate degradation - *ali*B; vii) nitrotoluene degradation - *nfs*A; viii) chlorocyclohexane and chlorobenzene - (*fdh*A). Three additional genes - *hpa*G, *hba*A, and *ali*A - were predicted in both smooth and pustular mats, but not in biofilm samples. Other genes exclusive to smooth mats included *hpa*E, *hpc*C, *bph*H and phenol 2-monooxygenase (enzyme EC:1.14.13.7) was also detected in just the smooth mats.

3.4.4.5. Biosynthesis of secondary metabolites and antibiotics

Genes statistically differentiated in PE samples belonged to a variety of predicted functional mechanisms (**Table 3.6**). Pustular mat and biofilm-related samples showed more predicted genes in overall. Cluster of genes belonging to hydrogen cyanide synthase *i.e.*, *hcn*ABC, a scavenging iron compound, were observed only in pustular microbial mat samples.

Table 3.5. Table of predicted KOs (genes) related to **degradation of xenobiotics** and their functions across smooth, pustular and biofilm-related samples. Data source: **Figure A3.13**, **Figure A3.14** and **Figure A3.15**. (**) in **Table 3.2**.

#KO	Function	SM	PM	Biofilm
K15511	*box*A; benzoyl-CoA 2,3-epoxidase subunit A [EC:1.14.13.208]	++	++	++
K03383	*atz*D; cyanuric acid amidohydrolase [EC:3.5.2.15]	++	++	++
K03391	*pcp*B; pentachlorophenol monooxygenase [EC:1.14.13.50]	++	++	++
K03863	*van*B; vanillate monooxygenase ferredoxin subunit	++	++	++
K07535	*bad*H; 2-hydroxycyclohexane carboxyl-CoA dehydrogenase [EC:1.1.1.-]	++	++	++
K07536	*bad*I; 2-ketocyclohexane carboxyl-CoA hydrolase [EC:3.1.2.-]	++	++	++
K10216	*dmp*D, xylF; 2-hydroxymuconate-semialdehyde hydrolase [EC:3.7.1.9]	++	++	++
K00455	*hpa*D, *hpc*B; 3,4-dihydroxyphenylacetate 2,3-dioxygenase [EC:1.13.11.15]	++	++	++
K00151	*hpa*E, *hpc*C; 5-carboxymethyl-2-hydroxymuconic-semialdehyde dehydrogenase [EC:1.2.1.60]	++	n.p.	n.p.
K05921	*hpa*G; 5-oxopent-3-en.p.-1,2,5-tricarboxylate decarboxylase / 2-hydroxyhepta-2,4-diene-1,7-dioate isomerase [EC:4.1.1.68 5.3.3.-]	++	++	n.p.
K04105	*hba*A; 4-hydroxybenzoate-CoA ligase [EC:6.2.1.27 6.2.1.25]	++	++	n.p.
K04116	*ali*A; cyclohexanecarboxylate-CoA ligase [EC:6.2.1.-]	++	++	n.p.
K04117	*ali*B; cyclohexane carboxyl-CoA dehydrogenase [EC:1.3.99.-]	n.p.	++	++
K10678	*nfs*A; nitroreductase	n.p.	++	++
K00148	*fdh*A; glutathione-independent formaldehyde dehydrogenase [EC:1.2.1.46]	n.p.	++	++
K01502	E3.5.5.7; aliphatic nitrilase	n.p.	n.p.	++
K03380	E1.14.13.7; phenol 2-monooxygenase [EC:1.14.13.7]	++	n.p.	n.p.
K18364	*bph*H, *xyl*J, *tes*E; 2-oxopent-4-enoate/cis-2-oxohex-4-enoate hydratase [EC:4.2.1.80 4.2.1.132]	++	n.p.	n.p.

Table 3.6. Table of predicted KOs (genes) related to **biosynthesis of secondary metabolites and antibiotics** and their functions across smooth, pustular- and biofilm-related samples. Data source: **Figure A3.16**, **Figure A3.17** and **Figure A3.18**. (**) in **Table 3.2**.

#KO	Function	SM	PM	Biofilm
K11258	*ilv*M; acetolactate synthase II small subunit [EC:2.2.1.6]	++	++	++
K15652	*asb*F; 3-dehydroshikimate dehydratase [EC:4.2.1.118]	++	++	++
K00435	*hem*Q; Fe-coproporphyrin III decarboxylase [EC:1.11.1.-]	++	++	++
K05602	*his*N; histidinol-phosphatase [EC:3.1.3.15]	++	++	n.p.
K02362	*ent*D; enterobactin synthetase component D [EC:6.3.2.14 2.7.8.-]	++	++	n.p.
K01757	STR1; strictosidine synthase [EC:4.3.3.2]	++	n.p.	++
K19180	*tll*; dTDP-6-deoxy-L-talose 4-dehydrogenase (NAD+) [EC:1.1.1.339]	++	n.p.	++
K01590	*hdc*, HDC; histidine decarboxylase [EC:4.1.1.22]	n.p.	++	++
K01702	LEU1; 3-isopropylmalate dehydratase [EC:4.2.1.33]	n.p.	++	++
K05369	*peb*A; 15,16-dihydrobiliverdin:ferredoxin oxidoreductase [EC:1.3.7.2]	n.p.	++	++
K05370	*peb*B; phycoerythrobilin:ferredoxin oxidoreductase [EC:1.3.7.3]	n.p.	++	++
K00116	*mqo*; malate dehydrogenase (quinone) [EC:1.1.5.4]	n.p.	++	++
K05358	*qui*A; quinate dehydrogenase (quinone) [EC:1.1.5.8]	n.p.	++	n.p.
K10814	*hcn*A; hydrogen cyanide synthase HcnA [EC:1.4.99.5]	n.p.	++	n.p.
K10815	*hcn*B; hydrogen cyanide synthase HcnB [EC:1.4.99.5]	n.p.	++	n.p.
K10816	*hcn*C; hydrogen cyanide synthase HcnC [EC:1.4.99.5]	n.p.	++	n.p.
K00247	*frd*D; fumarate reductase subunit D	n.p.	++	n.p.
K16792	*aks*D; methanogen homoaconitase large subunit [EC:4.2.1.114]	n.p.	n.p.	++

3.4.5. Organic Geochemistry of petroleum

The saturated and aromatic hydrocarbon distributions of the Barrow Island #B101 petroleum detected by GC and GC-MS analyses are consistent with a non-biodegraded petroleum (**Figure 3.5** top, **Figure 3.6** top). As such it could be assigned a biodegradation level (BL) of 0 based on the biodegradation level index system which has evolved from many petroleum geochemistry studies (*e.g.* Alexander et al., 1983; Volkman et al., 1983b, 1984; Burns et al., 1987; Fisher et al., 1996; Trolio et al., 1999; Grice et al., 2000). For instance, the B101 petroleum contains abundant *n*-alkanes (C_{10} to C_{34}; **Figure 3.5** and **Table 3.7**) including low-molecular-weight (LMW) compounds highly susceptible to biodegradation (thus BL = 0). Other saturated hydrocarbons included regular isoprenoids, pristane (Pr) and phytane (Ph). For #B101,

a Pr/Ph ratio of 3.3 is only consistent with an oxic environment, *i.e.,* marine source and some terrigenous input, not only based on pristane's known oxidative pathway formation but also due to other oils in the basin. This value is largely influenced by the high relative abundance of Pr from tocopherol of plants (Goossens et al., 1984) for the Carnarvon Basin petroleum system (Crank, 1973; Volkman et al., 1983a). The sample also contains low abundances of hopanes dominated by C_{30} αβ hopane (results not shown) indicating minor microbial input (bacteria) and low abundances of C_{27}-C_{29} steranes (results not shown) from algae, land plants and possibly also fungi. The saturated hydrocarbon fraction also contains a series of caged compounds known as diamondoids (adamantanes: **Figure A3.20** and **Table A3.7**; diamantanes: **Figure A3.21** and **Table A3.7**; Grice et al., 2000). The MA/ *n*-C_{11} alkane, MA/A, MDIA/DIA, MAI and MDI for B101 are 0.02, 6.46, 3.70, 64.55 % and 41.32 % (**Table 3.7**) consistent with previously reported data (Grice et al., 2000). Procedural blanks were run in parallel, showing no sign of contamination during extraction and separation steps. Their total ion chromatograms are displayed in **Figure A3.19**. The aromatic hydrocarbons in the B101 petroleum are mainly comprised of LMW aromatic compounds e.g. alkylnaphthalenes, alkylbenzenes, and alkylphenanthrenes (**Figure 3.6** top, **Table 3.7**; **Figure A3.22** and **Table A3.8**, **Figure A3.23** and **Table A3.9**, **Figure A3.24** and **Table A3.10**). Other aromatics detected in relatively low abundance included, retene and several polycyclic aromatic hydrocarbons (PAHs).

The hydrocarbon composition of water samples recovered from both the smooth and pustular mats after 60 and 120 days of PE generally showed little change to the original B101 petroleum (**Figure 3.5**, **Figure 3.6**, **Figure 3.7**, **Figure 3.8**, **Table 3.7**). The main changes relate to the LMW aliphatic hydrocarbons (*i.e.*, *n*-alkanes, Pr and Ph and diamondoids) which showed a decline in relative abundance with increasing time of PE. Evidence for the loss of the LMW compounds can also be inferred from the general decrease in Pr/Ph ratios with time (smooth mats =2.66 day 60 and 0.99 at day 120 and pustular mats = 2.72 day 60 and 1.80 at day 160). Namely, Pr and various stereoisomers are generally more susceptible to biodegradation than Ph (McIntyre et al., 2007). However, since Pr is more volatile than Ph, it is also possible that Pr has been preferentially removed during fractionation and evaporation of subsamples in the lab (Ahmed and George, 2004). The greatest change in Pr/Ph was seen for the

petroleum-water phase of the smooth mat samples. Further investigations are under way to establish the pristane diastereomer ratio (PrDR) and the phytane diastereomer ratio (PhDR) for our samples which might or might not have been impacted by biodegradation (McIntyre et al., 2007). The decline in abundance of these hydrocarbons and loss of alkylnaphthalenes, which are typically the next to be removed after the LMW saturated hydrocarbons, suggests a BL of ~2-3 from the starting #B101 petroleum. However, given that all the LMW compounds have been removed, we cannot exclude weathering processes or the evaporation of components as part of the sample processing conditions for the analysis of lipid biomarkers (*i.e.*, evaporation to dryness). Further evidence for evaporation to dryness is provided below.

At 60 days no *n*-C_{11} alkane nor adamantane and no methyladamantanes were observed in the petroleum-water phases of the pustular and smooth mats and the control. These findings are consistent with evaporation to dryness during sample processing. At 120 days all the diamondoids had been removed from the petroleum-water phases of the pustular and smooth mats. However, the controls were found to contain some methyldiamondoids. The aromatic hydrocarbons are mainly comprised of low- MW aromatic compounds *e.g.* akylbenzenes, alkylnaphthalenes and alkylphenanthrenes. Other aromatics detected in relatively low abundance included, retene and several polycyclic aromatic hydrocarbons (PAHs).

Table 3.7. Diagnostic ratios of biodegradation of the petroleum used as a pollutant (Barrow Island #B101) during incubation experiments, control Type 2 (petroleum and water, sample PCW at T60 and T120) and petroleum-exposed microbial mat microcosms (samples PS8S and PS11P at T60, and PS9S and PS12P at T120; sampling schedule is in **Chapter 2**). T0 analysis are not shown as no compounds or impurities were detected.

		Petroleum	Control Type II	Smooth	Pustular	Control Type II	Smooth	Pustular
Diagnostic ratios		Barrow Island #B101	T60	PS8S T60	PS11P T60	T120	PS9S T120	PS12P T120
Pr/Ph	Pristane/Phytane	3.32	2.80	2.66	2.72	2.64	0.99	1.80
MA/C_{11}[27]	(1MA+2MA)/C_{11}	0.02	-	-	-	-	-	-
MA/A[28]	(1MA+2MA)/A	6.46	-	-	-	-	-	-
MDIA/DIA[29]	1-MD+3-MD+4-MD/DIA	3.70	0.78	0.94	0.79	0.65	-	-
MAI[30]	1-MA/(1-MA+2-MA) %	64.55	-	-	-	-	-	-
MDI[31]	4-MD/(1-MD+3-MD+4-MD) %	41.32	25.70	27.44	34.33	26.79	-	-
DMNs[32]	1,6DMN/1,5 DMN	5.74	3.45	3.98	-.	3.32	3.53	2.88
TMNs[33]	1,3,6 TMN/1,3,7 TMN	1.17	1.24	1.19	1.33	1.27	1.26	1.37
TeMNs[34]	1,3,6,7 TeMN/1,3,5,7 TeMN	2.30	3.23	5.46	4.40	3.83	3.91	3.70
MP[35]	2-MP/9-MP	0.84	0.91	0.99	1.11	0.96	0.97	0.92
	(3-MP + 2-MP)/ (1-MP + 9-MP)	0.82	0.84	0.87	0.95	0.89	0.88	0.83
DMP[36]	1,7-DMP/2,7-DMP	3.53	3.47	3.48	3.66	3.18	3.26	3.54

[27] Saturated fraction, peak areas from *m/z* 135 (Wingert, 1992).
[28] Saturated fraction, peak areas *m/z* 135 and 136 (Wingert, 1992).
[29] Saturated fraction, peak areas *m/z* 187 and 188 (Wingert, 1992).
[30] Saturated fraction, peak areas *m/z* 135 (Chen et al., 1996)
[31] Saturated fraction, peak areas *m/z* 187 (Wingert, 1992).
[32] Aromatic fraction, peak areas *m/z* 156 (Fisher et al., 1996).
[33] Aromatic fraction, peak areas *m/z* 170 (Fisher et al., 1996).
[34] Aromatic fraction, peak areas *m/z* 184 (Fisher et al., 1996).
[35] Aromatic fraction, peak areas *m/z* 192 (Novaković et al., 2012).
[36] Aromatic fraction, peak areas *m/z* 206 (Novaković et al., 2012).

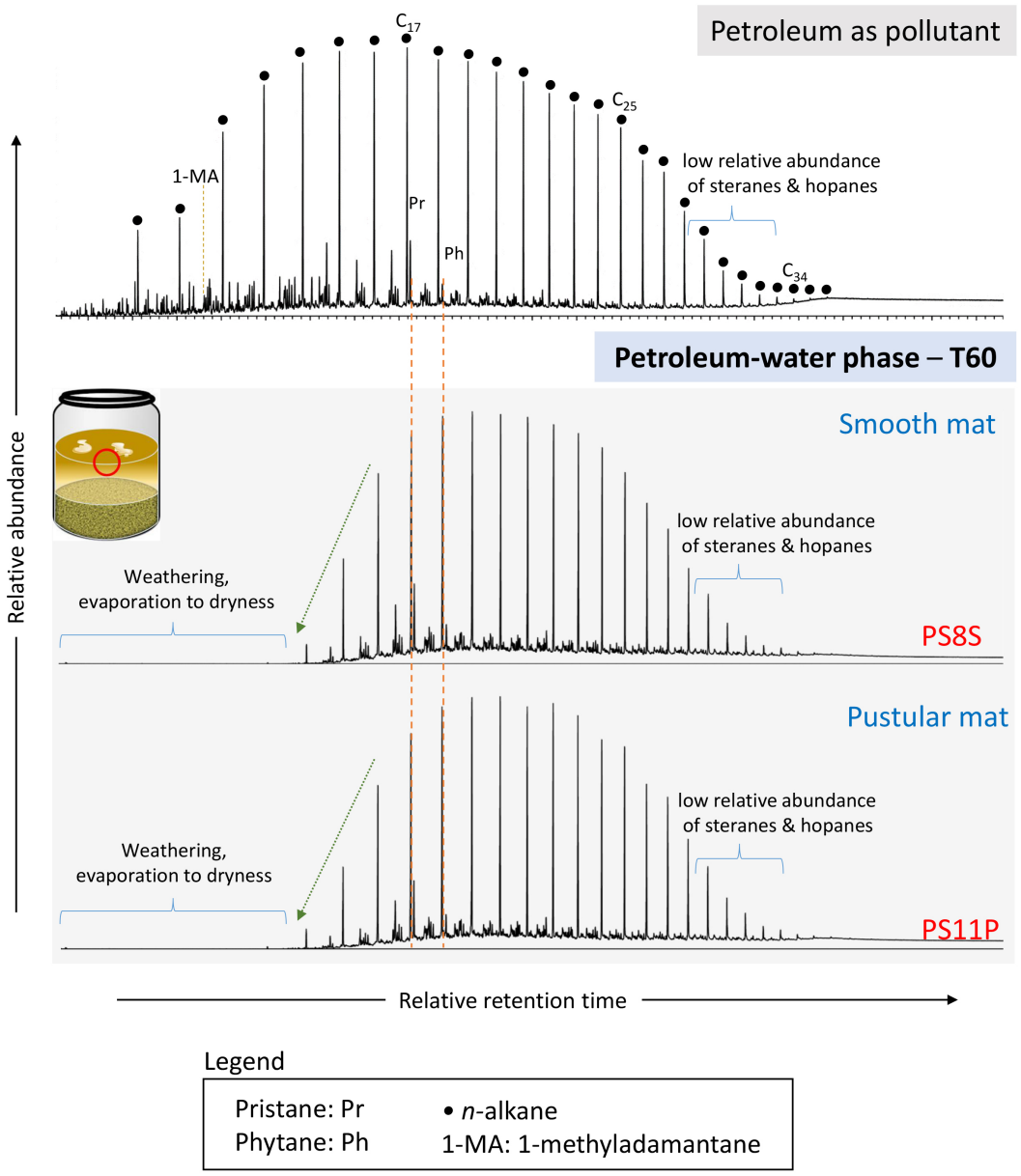

Figure 3.5. Total ion chromatograms of the **saturated fraction** of the petroleum used as a pollutant (Barrow Island #B101; top) and the petroleum-water phase extracted from smooth (middle) and pustular (bottom) microbial mats at **60 days** of exposure.

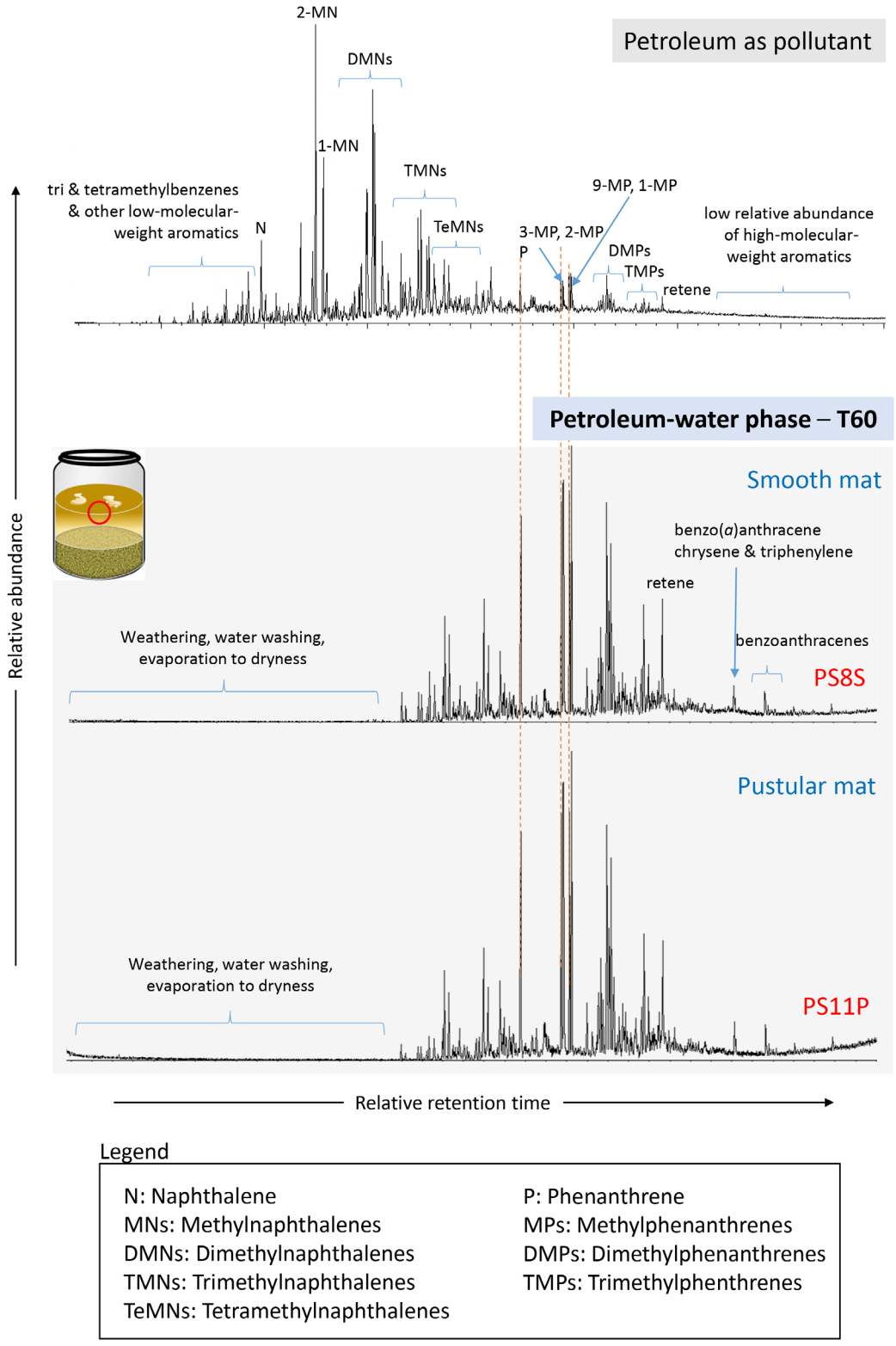

Figure 3.6. Total ion chromatograms of the **aromatic fraction** of the petroleum used as a pollutant (Barrow Island #B101; top) and the petroleum-water phase extracted from smooth (middle) and pustular (bottom) microbial mats at **60 days** of exposure.

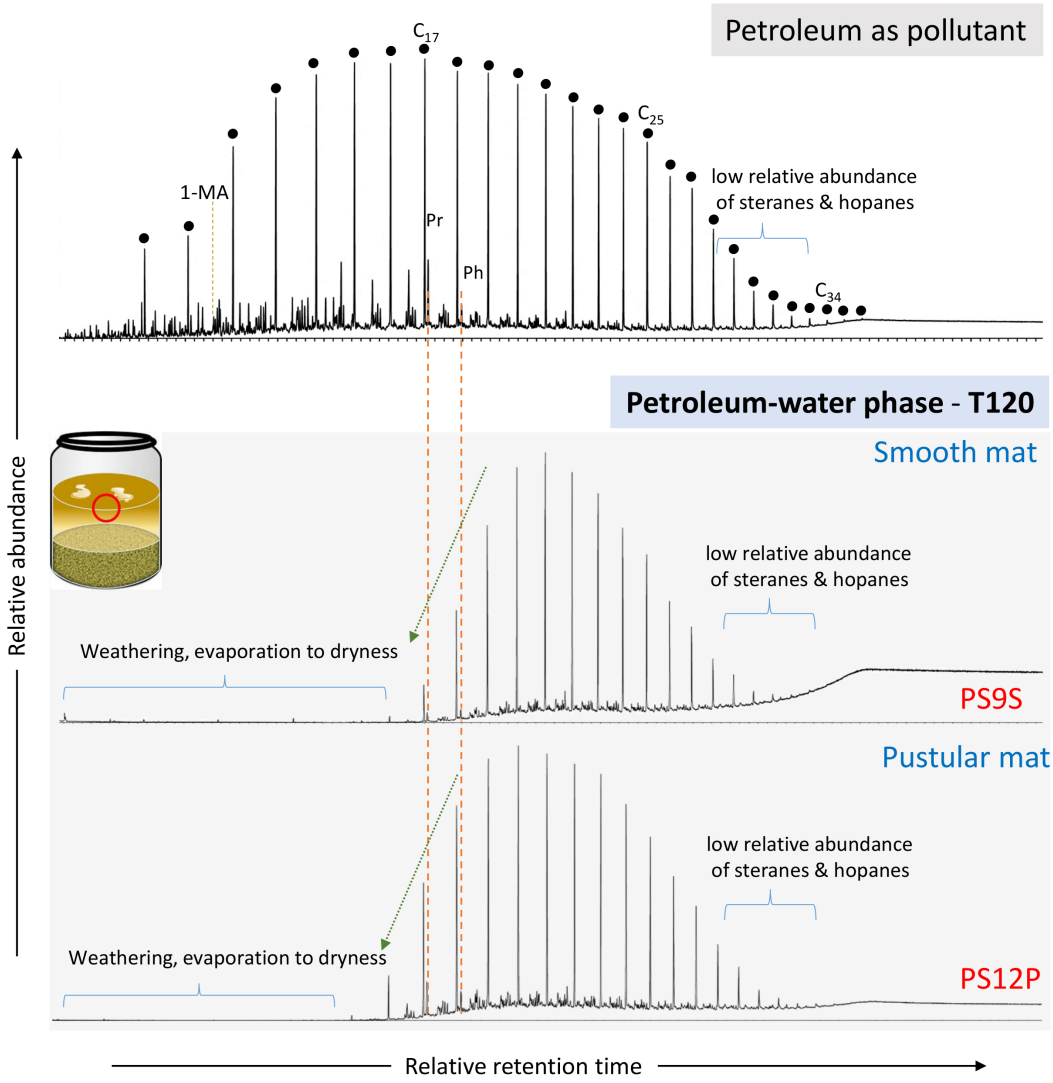

Figure 3.7. Total ion chromatograms of the **saturated fraction** of the petroleum used as a pollutant (Barrow Island #B101; top) and the petroleum-water phase extracted from smooth (middle) and pustular (bottom) microbial mats at **120 days** of exposure.

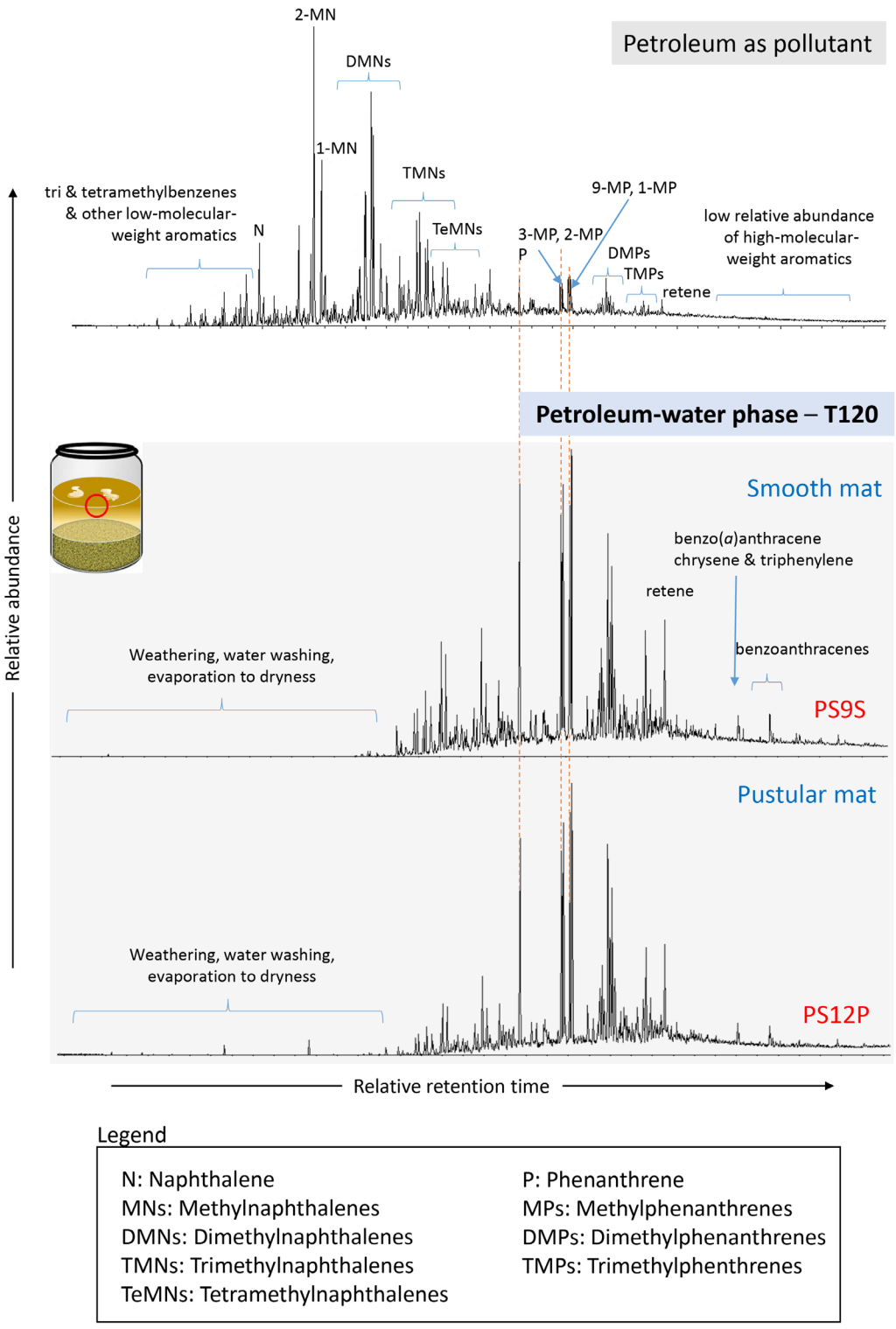

Figure 3.8. Total ion chromatograms of the **aromatic fraction** of the petroleum used as a pollutant (Barrow Island #B101; top) and the petroleum-water phase extracted from smooth (middle) and pustular (bottom) microbial mats at **120 days** of exposure.

3.5. Discussion

3.5.1. Limitations of 16S rRNA-inferred functional predictions

In this study, we acknowledge that PICRUSt2 inferences are only predictions of what functions might potentially be activated under PE, and not an actual reflection of the expressed functional genes. However, over time predictive bioinformatics tools, such as PICRUSt or Taxa4fun (Aßhauer et al., 2015; Douglas et al., 2019), have improved in accuracy and applicability (Koo et al., 2017b, 2017a; Mukherjee et al., 2017; Salerno et al., 2018), especially due to the expansion and refining of genomic reference databases that are being used for taxonomical and functional classification. For example, the recent release of PICRUSt2 in 2019 is now using one order of magnitude more robust sequenced genomes databases than the previous version (PICRUSt1). The criteria to use PICRUSt2 in this study was based on: (1) beta diversity analysis which demonstrated that initial and PE samples displayed a shift in microbial compositions over the course of the incubations (**Chapter 2**). PE likely also resulted in changes in microbial functionalities over the course of incubation. (2) Over 60% of the microbial composition (the reverse transcribed 16S rRNA dataset as input file), including controls (not subjected to PE) and initial smooth and pustular mat microcosms samples, belonged to family, genus and species level. Therefore, an acceptable proportion of the taxa was classified with optimal resolution. (3) A sharp reduction in microbial diversity of PE samples over time, resulted in a higher fraction of organisms that could be identified at genus and species levels. Hence, relatively low weighted NSTI values from PICRUST2 inferences would be expected, due to a good reference genome coverage. (4) The original version of PICRUSt (v1, released in 2014) showed good agreement in some studies (using a reference database from 2013) when compared to more sophisticated approaches (*i.e.*, metagenomics and metatranscriptomics) (Langille et al., 2013; Wilkinson et al., 2018). Therefore, with all new improvements in the latest version (2019), PICRUSt 2 represents an interesting approach for exploring its capability to accurately predict the functional properties of microbial communities in stressed hypersaline habitats such as in Shark Bay, which are under international protection.

3.5.2. Stress response mechanisms

The analysis of significantly abundant genes (level 3 functional categories) predicted by PICRUSt2 suggests substantial differences in the potential functional responses of smooth and pustular microbial mats to PE (**Figure 3.2**, **Figure 3.3** and **Figure 3.4**). Exposure to petroleum likely enriched for microbial taxa that based on close taxonomic affiliation with 16S rRNA genes that are located on sequenced genomes in the build-in PICRUSt 2 database, may possess genes associated with bacterial stress responses. In the smooth microbial mat exposed 120 days to petroleum, these microbes were predicted to be capable of initiating bacterial stress responses to offset these conditions. Bacterial stress response systems are a complex network of mechanisms that sense, respond, and adapt to continuous (or pulse) disturbances or stimuli, by regulating the expression of a large amount of genes and signalling cascade (Ron, 2013). The stress regulatory mechanisms included ABC transporters, bacterial secretion system, Two-Component system, biofilm formation, quorum sensing, bacterial chemotaxis, flagellar assembly and biosynthesis of secondary metabolites or antibiotics (**Figure 3.2**). The mechanisms identified are consistent with the results obtained from a recently reported metagenomic and metatranscriptomic study performed on petroleum spill impacted mats in France (Aubé et al., 2020). **Chapter 2** proposed that the Hamelin Pool smooth mats exhibited more microbial resistance after 30-days of PE compared to pustular microbial mats, due to its highly compacted microfabric (low porosity) that impedes the rapid flux of pollutants into the mats. However, based on the functional predictions outlined above they activated survival and stress response mechanisms to cope with the stressors after a long-term disturbance (T120)

In contrast, the most abundant group of metabolisms predicted for PE pustular mats were related to photosynthetic processes, amino acids, nucleotide- and carbohydrate metabolisms. *Halomicronema* spp. (cyanobacterium), the more dominant taxa in these type of mats, could be playing a fundamental role in increasing oxygenic photosynthetic activity in petroleum-exposed pustular microbial mats (**Chapter 2**), especially those associated with photosynthesis –antenna proteins–, carbon fixation, and porphyrin and chlorophyll metabolisms (**Figure 3.4**). *Halomicronema* spp. are recognised for producing a variety of polysaccharides, cellulose, and disaccharide

trehalose (Chen et al., 2019). These compounds are important constituents of biofilms (Jiao et al., 2010; Donot et al., 2012). Further, 'phycoerythrin', a light-harvesting protein-pigment complex (at 565nm), was found to be dominant (*i.e.*, *cpe*ABCERTUYZ) (**Table 3.2**) (Lichtenberg et al., 2020). This suggests that the carbon cycle in PE pustular mats was entirely driven by photosystem II (PSII), whereas anoxygenic photosynthesis predominated in its pristine counterpart (Campbell et al., 2020).

Pustular microbial mats comprised of a permeable matrix and its microbiome is thus largely exposed to aqueous contaminants (**Chapter 2**). Hence, we hypothesised that the petroleum-exposed pustular mat microbiome utilises a large amount of energy yielding biomass including EPS to help seal the porous fabric, which reduces their exposure to petroleum contaminants as a defence mechanism (Zhou et al., 2015). This was evident from the formation of a dense biofilm in pustular mat microcosm PS12P after 100 days of PE, which could have helped organisms to cope with a less acute PE. This will then promote the development of more specialised (hydrocarbon-degraders) microcolonies, as observed in the biofilm taxonomical analysis (**Chapter 2**), but also to the sorption of nutrients, and to boost synergistic cooperation, competition and enzyme retention (Kostakioti et al., 2013; Flemming et al., 2016).

3.5.3. Survival strategies

Regulatory systems in bacteria control the signalling of molecules or pathways when they detect a chemical or undergo physical changes in their environment by regulating transcription and/or translation processes (Heldin et al., 2016; Bervoets and Charlier, 2019). In this study, a set of gene families (OmpR, NarL and CitB) belonging to a TCS, were predicted in all PE samples. TCS consists of a pair of membrane-bound or periplasmic sensor histidine kinase protein, and a cytoplasmic response regulator protein, which activate gene expression (Bekker et al., 2006; Matson et al., 2017). Some of the predicted TCS genes - *i.e.*, *des*R and *cpx*R - were more abundant, especially in the pustular mats under PE conditions ('sense mechanism'). This is indicative of bacteria that were modulating the effects of temperature and salinity (Jubelin et al., 2005; Krell et al., 2010). Therefore, it seems that both mat microbiomes were not only responding to PE but also may have the potential of displaying osmo-adaptation strategies to cope with hypersalinity (~70 PSU) (**Chapter 2**), as reported

under pristine mat conditions (Campbell et al., 2020). Furthermore, amongst the CitB TCS families, *cit*S (SK) and *cit*T (response regulator) were predicted. These genes support the detection and uptake of environmental citrate or Mg-citrate complexes (Yamamoto et al., 2000). Halophilic bacteria, such a *Marinobacter*, previously identified as an important indicator species of PE microbial mats (**Chapter 2**), has shown to be capable of using citrate as an energy source under aerobic conditions (Huu et al., 1999).

Bacteria in microbial mats under pristine conditions, including those from Shark Bay, generally exhibit a variety of strategies to cope with 'general stress', or 'starvation-stationary conditions' (Ron, 2013; Wong et al., 2015; Ruvindy et al., 2016; Campbell et al., 2020). These strategies include bacterial chemotaxis and biofilm formation. Under extreme stress conditions, such as a chronic exposure to petroleum, different pathways or genes within the same strategies can be similarly expressed. This type of disturbance is called "solvent stress" (Manefield et al., 2017). In our study, we have identified several potential survival pathways that appear to be boosted by PE in all the samples investigated. One of those includes quorum sensing ("talk" strategy), which allows bacteria to respond to external stimuli (Abisado et al., 2018). This kind of responses may include a shift in the cellular density to encourage motion or migration ("move" strategy), which impacts the microbial composition around the cell (Papenfort and Bassler, 2016).

A common receptor of chemotactic response (*i.e.*, methyl-accepting chemotaxis protein –MCP–, *tar*) (**Table 3.3**), and several genes related to flagellar transcriptional activators, synthesis and control were predicted (*i.e.*, *flg*N, *flh*CD, *fli*KT) (Salah Ud-din et al., 2017). PE conditions triggered high signalling activity between motile bacteria in response to low nutrients, light or xenobiotics (Lichtenberg et al., 2020). However, motility is not the only mechanism that might have been stimulated by PE. A bioluminescence transcriptional regulator, *i.e.*, *lux*R, was predicted and statistically representative to all PE mat samples. This gene has been associated with biofilm formation ("fight" strategy) (Papenfort and Bassler, 2016). Predicted lux family genes (*i.e.*, *lux*PQRU) along with *aph*A appear to be more abundant in the pustular microbial mat samples. One of the biofilm formation pathways may have followed the *Vibrio* spp. type mechanism, where quorum sensing inhibits virulence factors and instead

increases biofilm production (Papenfort and Bassler, 2016). Additionally, the *Escherichia coli* type BF pathway was also predicted (*i.e., pga*ABCD gene cluster; **Table 3.3**). This gene cluster participates in the synthesis of the EPS, poly-β-1,6-N-acetyl-D-glucosamine (PNAG or PGA), a biopolymer made from glutamic acid (Echeverz et al., 2017). This might be also related to the predicted increase of the *gln*HPQ genes associated to the uptake of glutamine (**Table 3.2**), a compound necessary to produce glutamate, which is then excreted as γ-PGA (Luo et al., 2016).

Another predicted 'fight strategy' can be associated with competition, preferentially activated in petroleum-exposed pustular mat samples. Competition might be expressed either as exploitative (consumption of resources, *i.e.*, nutrients) or interference (attacking to cause harm; Cornforth and Foster, 2013). One of the predicted *hcn*ABC gene clusters (**Table 3.6**) yields hydrogen cyanide (HCN; Laville et al., 1998). This metabolite is synthesised and excreted by a diverse group of bacteria when scavenging iron, which stimulates microbial growth under nutrient poor conditions (Askeland and Morrison, 1983; Meyer et al., 2002; Zhao et al., 2002; Luque-Almagro et al., 2007). Moreover, this enzyme can also be toxic to bacteria that lack cyanide degrading metabolic pathways. It then becomes a virulence factor, or can be used as a cyanide detoxification medium in wastewater treatment or bioremediation (Cipollone et al., 2008). *Halothiobacillus hydrothermalis*, a chemolithoautotrophic organism, was identified as one of the indicator species of PE conditions (**Chapter 2**), which is able to use thiocyanate (made from HCN) as its main source of energy (Sorokin et al., 2014).

Curiously, response regulator related to β-lactam resistance (*i.e.*, gene *fim*Z) (Hirakawa et al., 2003) (**Table 3.2**) was predicted in both microbial mat and the biofilm sub-sample. β-lactam-sensing proteins are a family of compounds that contain a β-lactam ring (four-membered amide) and mainly inhibit transpeptidases, which interfere with the synthesis of the cellular membrane when bacteria grow and duplicate (Kong et al., 2010; van Bambeke et al., 2017). Thus, the potential activation of *fim*Z suggests that bacteria developed defence mechanisms against microbial attack, which can stimulate biofilm formation (Fisher et al., 2005; Kaplan et al., 2012). This is consistent with PICRUSt2 prediction of multidrug efflux pump genes (*mdl*AB and *yoj*I; **Table 3.2**) in the petroleum-exposed microbial mats. Efflux pumps are proteins

involved in the release of substances from the cell to the surroundings (Webber and Piddock, 2003) and support biofilm formation *via* discharge of quorum quenching, quorum sensing, production of EPS, and efflux of antibiotics or metabolites (Delgado et al., 2005; Alav et al., 2018). Additionally, the efflux of antibiotics or metabolites helps to diminish the effects of oxidative stress generated by aerobic respiration (Poole, 2012), and expected to be high specially in petroleum-exposed pustular microbial mats.

3.5.4. Hydrocarbon degradation

Prior taxonomical analysis of the dataset identified a group of indicator species, which were exclusively abundant under PE conditions (**Chapter 2**). Amongst these indicator species, several potential hydrocarbon degrading genera were detected, namely *Thalassospira*, *Marinobacter*, *Halomonas*, *Porticoccus*, and *Alcanivorax*. They all increased in abundance with increasing PE although their overall relative abundances remained <10%. It has been shown previously that biodegradation of hydrocarbons by halophilic organisms is rather limited, however, it appears there are similarities in the mechanisms used by non-halophilic microbes (Fathepure, 2014). The functions described below that were predicted from the living microbial communities, infer indirectly that biodegradation of hydrocarbons does occur in the microbial mats of Shark Bay under the prevailing hypersaline conditions.

Namely, we predicted a group of genes associated with the catabolism of aromatic hydrocarbons. In both smooth and pustular microbial mat samples the predicted meta-cleavage operon (*hpa*GED) assists in the ring opening of aromatic rings by dioxygenase, dehydrogenase and isomerase enzymes and are associated with the 4-hydroxyphenylacetate (4HPA) degradation pathway (Diaz et al., 2001). Here, we suggest that *Halomonas* spp. as a tentative candidate involved in this degradation pathway, since cultivated *Halomonas* from wastewater have also been shown to contain these genes (Liebgott et al., 2008). *bad*H which is known to be involved in aromatic ring cleavage under anaerobic conditions was another predicted gene present in all PE samples (Hirakawa et al., 2003). Additionally, two other genes - *pcp*B and *van*B - were identified in all PE samples, including the biofilm, which encodes the synthesis of monooxygenase enzymes which typically operate in the early stages of biodegradation. Pentachlorophenol monooxygenase (*pcp*B) has been associated with

the degradation of polychlorinated phenols in environmental samples. Only a selected group of bacteria such as *Sphingomonas* spp. and *Rhodococcus* spp. can degrade these highly toxic compounds (McAllister et al., 1996; Tiirola et al., 2002). The predicted vanillate monooxygenase (*van*B) is a more common enzyme, and catalyses the production of protocatechuate *via* the β-Ketoadipate pathway (Luu et al., 2015), which are fundamental intermediate metabolites of polycyclic aromatic hydrocarbons (PAHs). Intriguingly, it has shown that this enzyme and *Halomonas* are involved in the degradation of plasticisers (Wright et al., 2020). Another interesting finding is the detection of the *atz*D gene, which is associated with the degradation of cyanuric acid to ammonia to support microbial growth (Fruchey et al., 2003).

It was apparent from the functional gene data that the petroleum had been subjected to biodegradation, however, it was not obvious from the petroleum samples obtained from the smooth and pustular mats over 60 and 120 days of exposure that biodegradation had occurred. The presence of alkylnaphthalenes and alkylphenanthrenes argues against biodegradation as these compounds are generally removed at low levels of biodegradation. The progressive loss of the more volatile compounds, such as *n*-C_{10} to *n*-C_{14} alkanes and aromatics ca. C_6-C_9, in most of microcosm experiments tends to point to loss of LMW compounds due to evaporation to dryness (*e.g.* Gagnon et al., 1999; George et al., 2002; Ahmed and George, 2004).

3.6 Conclusions

In this study, we have applied PICRUSt2 pipeline to predict the presence of bacteria that harbor genes involved in stress adaptive responses and the biodegradation pathways of xenobiotics in microbial mats from SB subjected to PE for up to 120 days. Also, a brief analysis of the petroleum-water interphase samples by GC-MS was performed to examine whether biodegradation had started.

(1) Smooth and pustular mats exhibited clear differences in the more abundant predicted functional mechanisms for PE. Predicted functional genes associated with bacterial stress responses of smooth microbial mats were highly abundant, indicating that its microfabric might not the only factor responsible for the resistance of smooth mat microbiomes after prolonged PE. The pustular mat microbiome also displayed adaptive stress responses to PE, but the most abundant predicted genes were associated

with oxygenic photosynthesis and the production of carbohydrates due to the predominance of cyanobacteria in this mat type (*Halomicronema* spp.). (2) Functional pathways associated with motility, biofilm formation, competition for nutrients or interspecies (using virulence factors) were found to be enriched in both PE mat types, as well as potential pathways associated with the degradation of aromatic hydrocarbons. (3) Both microbial mats after 60 and 120 days of PE led to the removal or loss of all the LMW compounds from the original petroleum. Such changes can be attributed to weathering processes, biodegradation (BL 2-3), and experimentally induced evaporation of components. In our case the latter process seems to be the main factor controlling the distribution of petroleum compounds analysed from the water phase in the microcosms.

This study also proposes a simple framework to explore and delimit the variables (*i.e.*, genes, enzymes or proteins) responsible for the observed differences and their classification under KEGG mapper, as a tool for predicting metabolic pathways involved. Additional sequencing analysis of shotgun metagenome and/or functional metatranscriptomes of a select number of samples will verify the accuracy of the functional predictions of the active microbiomes.

3.7. Data availability

Raw reads datasets generated for this research can be found in "Shark_Bay_PE_Funtional_Responses" repository at https://github.com/yalimay.

3.8. Acknowledgments

The authors would like to thanks to Graduate Research School, Western Australian Organic and Isotope Centre (WA-OIGC) and TIGeR Institute at Curtin University for their technical and financial assistance. We also appreciate the advice received from Gavin Douglas (PICRUSt-users forum), Justine Debelius (QIIME forum) and Prof. Lê Cao (mix omics – R software) for assisting in PICRUSt2 analysis.

3.9. Funding

This research was funded by Australian Research Council #LP150100341 and Woodside an ARC DP (DP15010223).

3.10. References

Abed, R. M. M., Al-Thukair, A., and De Beer, D. (2006). Bacterial diversity of a cyanobacterial mat degrading petroleum compounds at elevated salinities and temperatures: Microbial mats from Saudi Arabia. *FEMS Microbiology Ecology* 57, 290–301. doi:10.1111/j.1574-6941.2006.00113.x.

Abisado, R. G., Benomar, S., Klaus, J. R., Dandekar, A. A., and Chandler, J. R. (2018). Bacterial Quorum Sensing and Microbial Community Interactions. *mBio* 9. doi:10.1128/mBio.02331-17.

Ahmed, M., and George, S. C. (2004). Changes in the molecular composition of crude oils during their preparation for GC and GC–MS analyses. *Organic Geochemistry* 35, 137–155. doi:10.1016/j.orggeochem.2003.10.002.

Alav, I., Sutton, J. M., and Rahman, K. M. (2018). Role of bacterial efflux pumps in biofilm formation. *J. Antimicrob. Chemother.* 73, 2003–2020. doi:10.1093/jac/dky042.

Alexander, R., Kagi, R. I., Woodhouse, G. W., and Volkman, J. K. (1983). The geochemistry of some biodegraded Australian Oils. *The APPEA Journal* 23, 53–63. doi:10.1016/S0960-9822(97)70976-X.

Allen, M. A., Goh, F., Burns, B. P., and Neilan, B. A. (2009). Bacterial, archaeal and eukaryotic diversity of smooth and pustular microbial mat communities in the hypersaline lagoon of Shark Bay. *Geobiology* 7, 82–96. doi:10.1111/j.1472-4669.2008.00187.x.

Alneberg, J., Karlsson, C. M. G., Divne, A.-M., Bergin, C., Homa, F., Lindh, M. V., et al. (2018). Genomes from uncultivated prokaryotes: a comparison of metagenome-assembled and single-amplified genomes. *Microbiome* 6. doi:10.1186/s40168-018-0550-0.

Armanios, C., Alexander, R., and Kagi, R. I. (1992). High diahopane and neohopane abundances in a biodegraded crude oil from the Barrow sub-basin of Western Australia. *Organic Geochemistry* 18, 641–645. doi:10.1016/0146-6380(92)90089-G.

Askeland, R. A., and Morrison, S. M. (1983). Cyanide production by Pseudomonas fluorescens and Pseudomonas aeruginosa. *Applied and Environmental Microbiology* 45, 1802–1807. doi:10.1128/AEM.45.6.1802-1807.1983.

Aßhauer, K. P., Wemheuer, B., Daniel, R., and Meinicke, P. (2015). Tax4Fun: predicting functional profiles from metagenomic 16S rRNA data. *Bioinformatics* 31, 2882–2884. doi:10.1093/bioinformatics/btv287.

Aubé, J., Senin, P., Bonin, P., Pringault, O., Jeziorski, C., Bouchez, O., et al. (2020). Meta-omics Provides Insights into the Impact of Hydrocarbon Contamination on Microbial Mat Functioning. *Microb Ecol*. doi:10.1007/s00248-020-01493-x.

Australian Maritime Safety Authority (AMSA) (2012). Report on the 2011/12 Review of the National Plan to Combat Pollution of the Sea by Oil and Other Hazardous and Noxious Substances and the National Maritime Emergency Response Arragements (2011-2012). Australian Government Available at: https://www.amsa.gov.au/sites/default/files/natplan-review-report.pdf [Accessed June 9, 2020].

Babilonia, J., Conesa, A., Casaburi, G., Pereira, C., Louyakis, A. S., Reid, R. P., et al. (2018). Comparative Metagenomics Provides Insight Into the Ecosystem Functioning of the Shark Bay Stromatolites, Western Australia. *Front. Microbiol.* 9, 1359. doi:10.3389/fmicb.2018.01359.

Barbera, P., Kozlov, A. M., Czech, L., Morel, B., Darriba, D., Flouri, T., et al. (2019). EPA-ng: Massively Parallel Evolutionary Placement of Genetic Sequences. *Syst Biol* 68, 365–369. doi:10.1093/sysbio/syy054.

Bekker, M., Teixeira De Mattos, M. J., and Hellingwerf, K. J. (2006). The Role of Two-Component Regulation Systems in the physiology of the Bacterial Cell. *Science Progress* 89, 213–242. doi:10.3184/003685006783238308.

Benthien, M., Wieland, A., Oteyza, T. G. de, Grimalt, J. O., and Kühl, M. (2004). Oil-contamination effects on a hypersaline microbial mat community (Camargue, France) as studied with microsensors and geochemical analysis. *Ophelia* 58, 135–150. doi:10.1080/00785236.2004.10410221.

Bervoets, I., and Charlier, D. (2019). Diversity, versatility and complexity of bacterial gene regulation mechanisms: opportunities and drawbacks for applications in synthetic biology. *FEMS Microbiol Rev* 43, 304–339. doi:10.1093/femsre/fuz001.

Bolyen, E., Rideout, J. R., Dillon, M. R., Bokulich, N. A., Abnet, C. C., Al-Ghalith, G. A., et al. (2019). Reproducible, interactive, scalable and extensible microbiome data science using QIIME 2. *Nature biotechnology* 37, 852–857.

Bordenave, S., Goñi-Urriza, M. S., Caumette, P., and Duran, R. (2007). Effects of Heavy Fuel Oil on the Bacterial Community Structure of a Pristine Microbial Mat. *Applied and Environmental Microbiology* 73, 6089–6097. doi:10.1128/AEM.01352-07.

Burns, B. J., Bostwick, T. R., and Emmett, J. K. (1987). Gippsland terrestrial oils - Recognition of compositional variations due to maturity and biodegradation effects. *The APPEA Journal* 27, 73–85. doi:10.1071/aj86008.

Campbell, M. A., Grice, K., Visscher, P. T., Morris, T., Wong, H. L., White, R. A. I., et al. (2020). Functional Gene Expression in Shark Bay Hypersaline Microbial Mats: Adaptive Responses. Front. Microbiol. 11. doi:10.3389/fmicb.2020.560336.

Cao, K.-A. L., Costello, M.-E., Lakis, V. A., Bartolo, F., Chua, X.-Y., Brazeilles, R., et al. (2016). MixMC: A Multivariate Statistical Framework to Gain Insight

into Microbial Communities. *PLOS ONE* 11, e0160169. doi:10.1371/journal.pone.0160169.

Chen, J., Fu, J., Sheng, G., Liu, D., and Zhang, J. (1996). Diamondoid hydrocarbon ratios: novel maturity indices for highly mature crude oils. *Organic Geochemistry* 25, 179–190. doi:10.1016/S0146-6380(96)00125-8.

Chen, M., Hernandez-Prieto, M. A., Loughlin, P. C., Li, Y., and Willows, R. D. (2019). Genome and proteome of the chlorophyll f-producing cyanobacterium Halomicronema hongdechloris: adaptative proteomic shifts under different light conditions. *BMC Genomics* 20, 207. doi:10.1186/s12864-019-5587-3.

Cipollone, R., Ascenzi, P., Tomao, P., Imperi, F., and Visca, P. (2008). Enzymatic detoxification of cyanide: clues from Pseudomonas aeruginosa Rhodanese. *J. Mol. Microbiol. Biotechnol.* 15, 199–211. doi:10.1159/000121331.

Cornforth, D. M., and Foster, K. R. (2013). Competition sensing: the social side of bacterial stress responses. *Nature reviews. Microbiology* 11, 285–293. doi:http://dx.doi.org.dbgw.lis.curtin.edu.au/10.1038/nrmicro2977.

Crank, K. (1973). Geology of Barrow Island Oil Field. *The APPEA Journal* 13, 49–57. doi:10.1071/aj72008.

Czech, L., Barbera, P., and Stamatakis, A. (2020). Genesis and Gappa: processing, analyzing and visualizing phylogenetic (placement) data. *Bioinformatics*. doi:10.1093/bioinformatics/btaa070.

Delgado, M. A., Vincent, P. A., Farías, R. N., and Salomón, R. A. (2005). YojI of Escherichia coli Functions as a Microcin J25 Efflux Pump. *Journal of Bacteriology* 187, 3465–3470. doi:10.1128/JB.187.10.3465-3470.2005.

Des Marais, D. (2003). Biogeochemistry of Hypersaline Microbial Mats Illustrates the Dynamics of Modern Microbial Ecosystems and the Early Evolution of the Biosphere. *Biological Bulletin* 204, 160–167. doi:10.2307/1543552.

Diaz, E., Ferrandez, A., Prieto, M. A., and Garcia, J. L. (2001). Biodegradation of Aromatic Compounds by Escherichia coli. *Microbiology and Molecular Biology Reviews* 65, 523–569. doi:10.1128/MMBR.65.4.523-569.2001.

Donot, F., Fontana, A., Baccou, J. C., and Schorr-Galindo, S. (2012). Microbial exopolysaccharides: Main examples of synthesis, excretion, genetics and extraction. *Carbohydrate Polymers* 87, 951–962. doi:10.1016/j.carbpol.2011.08.083.

Douglas, G. M., Maffei, V. J., Zaneveld, J., Yurgel, S. N., Brown, J. R., Taylor, C. M., et al. (2019). PICRUSt2: An improved and extensible approach for metagenome inference. *BioRxiv; Cold Spring Harbor*. doi:http://dx.doi.org.dbgw.lis.curtin.edu.au/10.1101/672295.

Duran, R., and Goñi-Urriza, M. S. (2010). "Impact of Pollution on Microbial Mats," in *Handbook of Hydrocarbon and Lipid Microbiology*, ed. K. N. Timmis (Berlin, Heidelberg: Springer), 2339–2348. doi:10.1007/978-3-540-77587-4_170.

Echeverz, M., García, B., Sabalza, A., Valle, J., Gabaldón, T., Solano, C., et al. (2017). Lack of the PGA exopolysaccharide in Salmonella as an adaptive trait for survival in the host. *PLOS Genetics* 13, e1006816. doi:10.1371/journal.pgen.1006816.

Fathepure, B. Z. (2014). Recent studies in microbial degradation of petroleum hydrocarbons in hypersaline environments. *Front Microbiol* 5. doi:10.3389/fmicb.2014.00173.

Fisher, J. F., Meroueh, S. O., and Mobashery, S. (2005). Bacterial Resistance to β-Lactam Antibiotics: Compelling Opportunism, Compelling Opportunity. *Chem. Rev.* 105, 395–424. doi:10.1021/cr030102i.

Fisher, S. J., Alexander, R., and Kagi, R. I. (1996). Biodegradation of Alkylnaphthalenes in Sediments Adjacent to an Off-Shore Petroleum Production Platform. *Polycyclic Aromatic Compounds* 11, 35–42. doi:10.1080/10406639608544647.

Flemming, H.-C., Wingender, J., Szewzyk, U., Steinberg, P., Rice, S. A., and Kjelleberg, S. (2016). Biofilms: an emergent form of bacterial life. *Nature reviews. Microbiology* 14, 563–575. doi:http://dx.doi.org.dbgw.lis.curtin.edu.au/10.1038/nrmicro.2016.94.

Foster, J. S., and Mobberley, J. M. (2010). "Past, Present, and Future: Microbial Mats as Models for Astrobiological Research," in *Microbial Mats: Modern and Ancient Microorganisms in Stratified Systems* Cellular Origin, Life in Extreme Habitats and Astrobiology., eds. J. Seckbach and A. Oren (Dordrecht: Springer Netherlands), 563–582. doi:10.1007/978-90-481-3799-2_29.

Frías, J. E., Flores, E., and Herrero, A. (1997). Nitrate assimilation gene cluster from the heterocyst-forming cyanobacterium Anabaena sp. strain PCC 7120. *J Bacteriol* 179, 477–486.

Fruchey, I., Shapir, N., Sadowsky, M. J., and Wackett, L. P. (2003). On the origins of cyanuric acid hydrolase: purification, substrates, and prevalence of AtzD from Pseudomonas sp. strain ADP. *Appl. Environ. Microbiol.* 69, 3653–3657. doi:10.1128/aem.69.6.3653-3657.2003.

Gagnon, M. M., Grice, K., and Kagi, R. I. (1999). Biochemical and chemical parameters for aquatic ecosystem health assessments adapted to the australian oil and gas industy. *The APPEA Journal* 39, 584–599. doi:10.1071/aj98038.

George, S. C., Boreham, C. J., Minifie, S. A., and Teerman, S. C. (2002). The effect of minor to moderate biodegradation on C5 to C9 hydrocarbons in crude oils. *Organic Geochemistry* 33, 1293–1317. doi:10.1016/S0146-6380(02)00117-1.

González, I., Cao, K.-A. L., Davis, M. J., and Déjean, S. (2012). Visualising associations between paired 'omics' data sets. *BioData Mining* 5, 19. doi:10.1186/1756-0381-5-19.

Goossens, H., de Leeuw, J. W., Schenck, P. A., and Brassell, S. C. (1984). Tocopherols as likely precursors of pristane in ancient sediments and crude oils. *Nature* 312, 440–442. doi:10.1038/312440a0.

Grice, K., Alexander, R., and Kagi, R. I. (2000). Diamondoid hydrocarbon ratios as indicators of biodegradation in Australian crude oils. *Organic Geochemistry* 31, 67–73. doi:10.1016/S0146-6380(99)00137-0.

Gu, Z., Eils, R., and Schlesner, M. (2016). Complex heatmaps reveal patterns and correlations in multidimensional genomic data. *Bioinformatics* 32, 2847–2849.

Heldin, C.-H., Lu, B., Evans, R., and Gutkind, J. S. (2016). Signals and Receptors. *Cold Spring Harb Perspect Biol* 8. doi:10.1101/cshperspect.a005900.

Hirakawa, H., Nishino, K., Yamada, J., Hirata, T., and Yamaguchi, A. (2003). Beta-lactam resistance modulated by the overexpression of response regulators of two-component signal transduction systems in Escherichia coli. *J. Antimicrob. Chemother.* 52, 576–582. doi:10.1093/jac/dkg406.

Huu, N. B., Denner, E. B. M., Ha, D. T. C., Wanner, G., and Stan-Lotter, H. (1999). Marinobacter aquaeolei sp. nov., a halophilic bacterium isolated from a Vietnamese oil-producing well. *International Journal of Systematic and Evolutionary Microbiology,* 49, 367–375. doi:10.1099/00207713-49-2-367.

Jiao, Y., Cody, G. D., Harding, A. K., Wilmes, P., Schrenk, M., Wheeler, K. E., et al. (2010). Characterization of Extracellular Polymeric Substances from Acidophilic Microbial Biofilms. *Appl. Environ. Microbiol.* 76, 2916–2922. doi:10.1128/AEM.02289-09.

Jubelin, G., Vianney, A., Beloin, C., Ghigo, J.-M., Lazzaroni, J.-C., Lejeune, P., et al. (2005). CpxR/OmpR interplay regulates curli gene expression in response to osmolarity in Escherichia coli. *J. Bacteriol.* 187, 2038–2049. doi:10.1128/JB.187.6.2038-2049.2005.

Kaplan, J. B., Izano, E. A., Gopal, P., Karwacki, M. T., Kim, S., Bose, J. L., et al. (2012). Low Levels of β-Lactam Antibiotics Induce Extracellular DNA Release and Biofilm Formation in Staphylococcus aureus. *mBio* 3. doi:10.1128/mBio.00198-12.

Kong, K.-F., Schneper, L., and Mathee, K. (2010). Beta-lactam antibiotics: from antibiosis to resistance and bacteriology. *APMIS* 118, 1–36. doi:10.1111/j.1600-0463.2009.02563.x.

Koo, H., Hakim, J. A., Morrow, C. D., Eipers, P. G., Davila, A., Andersen, D. T., et al. (2017a). Comparison of two bioinformatics tools used to characterize the microbial diversity and predictive functional attributes of microbial mats from

Lake Obersee, Antarctica. *J Microbiol Methods* 140, 15–22. doi:10.1016/j.mimet.2017.06.017.

Koo, H., Mojib, N., Hakim, J. A., Hawes, I., Tanabe, Y., Andersen, D. T., et al. (2017b). Microbial Communities and Their Predicted Metabolic Functions in Growth Laminae of a Unique Large Conical Mat from Lake Untersee, East Antarctica. *Front. Microbiol.* 8, 1347. doi:10.3389/fmicb.2017.01347.

Kostakioti, M., Hadjifrangiskou, M., and Hultgren, S. J. (2013). Bacterial Biofilms: Development, Dispersal, and Therapeutic Strategies in the Dawn of the Postantibiotic Era. *Cold Spring Harb Perspect Med* 3. doi:10.1101/cshperspect.a010306.

Krell, T., Lacal, J., Busch, A., Silva-Jiménez, H., Guazzaroni, M.-E., and Ramos, J. L. (2010). Bacterial Sensor Kinases: Diversity in the Recognition of Environmental Signals. *Annu. Rev. Microbiol.* 64, 539–559. doi:10.1146/annurev.micro.112408.134054.

Langille, M. G. I., Zaneveld, J., Caporaso, J. G., McDonald, D., Knights, D., Reyes, J. A., et al. (2013). Predictive functional profiling of microbial communities using 16S rRNA marker gene sequences. *Nat Biotechnol* 31, 814–821. doi:10.1038/nbt.2676.

Laville, J., Blumer, C., Von Schroetter, C., Gaia, V., Défago, G., Keel, C., et al. (1998). Characterization of the hcnABC Gene Cluster Encoding Hydrogen Cyanide Synthase and Anaerobic Regulation by ANR in the Strictly Aerobic Biocontrol Agent Pseudomonas fluorescens CHA0. *Journal of Bacteriology* 180, 3187–3196. doi:10.1128/JB.180.12.3187-3196.1998.

Lichtenberg, M., Cartaxana, P., and Kühl, M. (2020). Vertical Migration Optimizes Photosynthetic Efficiency of Motile Cyanobacteria in a Coastal Microbial Mat. *Front. Mar. Sci.* 7. doi:10.3389/fmars.2020.00359.

Liebgott, P.-P., Labat, M., Amouric, A., Tholozan, J.-L., and Lorquin, J. (2008). Tyrosol degradation via the homogentisic acid pathway in a newly isolated Halomonas strain from olive processing effluents. *Journal of Applied Microbiology* 105, 2084–2095. doi:10.1111/j.1365-2672.2008.03925.x.

Llirós, M., Gaju, N., de Oteyza, T. G., Grimalt, J. O., Esteve, I., and Martínez-Alonso, M. (2008). Microcosm experiments of oil degradation by microbial mats. II. The changes in microbial species. *Science of The Total Environment* 393, 39–49. doi:10.1016/j.scitotenv.2007.11.034.

Louca, S., and Doebeli, M. (2018). Efficient comparative phylogenetics on large trees. *Bioinformatics* 34, 1053–1055. doi:10.1093/bioinformatics/btx701.

Luo, Z., Guo, Y., Liu, J., Qiu, H., Zhao, M., Zou, W., et al. (2016). Microbial synthesis of poly-γ-glutamic acid: current progress, challenges, and future perspectives. *Biotechnology for Biofuels* 9, 134. doi:10.1186/s13068-016-0537-7.

Luque-Almagro, V. M., Huertas, M. J., Roldán, M. D., Moreno-Vivián, C., Martínez-Luque, M., Blasco, R., et al. (2007). The cyanotrophic bacterium Pseudomonas pseudoalcaligenes CECT5344 responds to cyanide by defence mechanisms against iron deprivation, oxidative damage and nitrogen stress. *Environmental Microbiology* 9, 1541–1549. doi:10.1111/j.1462-2920.2007.01274.x.

Luu, R. A., Kootstra, J. D., Nesteryuk, V., Brunton, C. N., Parales, J. V., Ditty, J. L., et al. (2015). Integration of chemotaxis, transport and catabolism in Pseudomonas putida and identification of the aromatic acid chemoreceptor PcaY. *Molecular Microbiology* 96, 134–147. doi:10.1111/mmi.12929.

Manefield, M., Lee, M., and Koenig, J. (2017). "The Nature and Relevance of Solvent Stress in Microbes and Mechanisms of Tolerance," in *Microbial Ecology of Extreme Environments*, eds. C. Chénard and F. M. Lauro (Cham: Springer International Publishing), 201–213. doi:10.1007/978-3-319-51686-8_9.

Matson, J. S., Livny, J., and DiRita, V. J. (2017). A putative Vibrio cholerae two-component system controls a conserved periplasmic protein in response to the antimicrobial peptide polymyxin B. *PLOS ONE* 12, e0186199. doi:10.1371/journal.pone.0186199.

McAllister, K. A., Lee, H., and Trevors, J. T. (1996). Microbial degradation of pentachlorophenol. *Biodegradation* 7, 1–40. doi:10.1007/BF00056556.

McGenity, T. J., Folwell, B. D., McKew, B. A., and Sanni, G. O. (2012). Marine crude-oil biodegradation: a central role for interspecies interactions. *Aquat Biosyst* 8, 10. doi:10.1186/2046-9063-8-10.

McIntyre, C. P., Harvey, P. M., Ferguson, S. H., Wressnig, A. M., Volk, H., George, S. C., et al. (2007). Determining the Extent of Biodegradation of Fuels Using the Diastereomers of Acyclic Isoprenoids. *Environmental Science & Technology* 41, 2452–2458. doi:10.1021/es0621288.

Meyer, J.-M., Geoffroy, V. A., Baida, N., Gardan, L., Izard, D., Lemanceau, P., et al. (2002). Siderophore Typing, a Powerful Tool for the Identification of Fluorescent and Nonfluorescent Pseudomonads. *Appl. Environ. Microbiol.* 68, 2745–2753. doi:10.1128/AEM.68.6.2745-2753.2002.

Muir, P., Li, S., Lou, S., Wang, D., Spakowicz, D. J., Salichos, L., et al. (2016). The real cost of sequencing: scaling computation to keep pace with data generation. *Genome Biology* 17. doi:10.1186/s13059-016-0917-0.

Mukherjee, A., Chettri, B., Langpoklakpam, J. S., Basak, P., Prasad, A., Mukherjee, A. K., et al. (2017). Bioinformatic Approaches Including Predictive Metagenomic Profiling Reveal Characteristics of Bacterial Response to Petroleum Hydrocarbon Contamination in Diverse Environments. *Sci Rep* 7. doi:10.1038/s41598-017-01126-3.

Novaković, M., Ramadan, M. M. A., Knudsen, T. Š., Antić, M., Beškoski, V., Gojgić-Cvijović, G., et al. (2012). Degradation of methyl-phenanthrene isomers

during bioremediation of soil contaminated by residual fuel oil. *Environ Chem Lett* 10, 287–294. doi:10.1007/s10311-012-0354-6.

Papenfort, K., and Bassler, B. L. (2016). Quorum sensing signal–response systems in Gram-negative bacteria. *Nature Reviews Microbiology* 14, 576–588. doi:10.1038/nrmicro.2016.89.

Parks, D. H., Tyson, G. W., Hugenholtz, P., and Beiko, R. G. (2014). STAMP: statistical analysis of taxonomic and functional profiles. *Bioinformatics* 30, 3123–3124. doi:10.1093/bioinformatics/btu494.

Poole, K. (2012). Bacterial stress responses as determinants of antimicrobial resistance. *J Antimicrob Chemother* 67, 2069–2089. doi:10.1093/jac/dks196.

Ron, E. Z. (2013). "Bacterial Stress Response," in *The Prokaryotes: Prokaryotic Physiology and Biochemistry*, eds. E. Rosenberg, E. F. DeLong, S. Lory, E. Stackebrandt, and F. Thompson (Berlin, Heidelberg: Springer), 589–603. doi:10.1007/978-3-642-30141-4_79.

Ruvindy, R., White III, R. A., Neilan, B. A., and Burns, B. P. (2016). Unravelling core microbial metabolisms in the hypersaline microbial mats of Shark Bay using high-throughput metagenomics. *The ISME Journal* 10, 183–196. doi:10.1038/ismej.2015.87.

Salah Ud-din, A. I., Md, and Roujeinikova, A. (2017). Methyl-accepting chemotaxis proteins: a core sensing element in prokaryotes and archaea. *Cellular and Molecular Life Sciences; Basel* 74, 3293–3303. doi:http://dx.doi.org.dbgw.lis.curtin.edu.au/10.1007/s00018-017-2514-0.

Salerno, J. L., Little, B., Lee, J., and Hamdan, L. J. (2018). Exposure to Crude Oil and Chemical Dispersant May Impact Marine Microbial Biofilm Composition and Steel Corrosion. *Front. Mar. Sci.* 5, 196. doi:10.3389/fmars.2018.00196.

Shakya, M., Lo, C.-C., and Chain, P. S. G. (2019). Advances and Challenges in Metatranscriptomic Analysis. *Front. Genet.* 10. doi:10.3389/fgene.2019.00904.

Sorokin, D. Y., Abbas, B., van Zessen, E., and Muyzer, G. (2014). Isolation and characterization of an obligately chemolithoautotrophic Halothiobacillus strain capable of growth on thiocyanate as an energy source. *FEMS Microbiol Lett* 354, 69–74. doi:10.1111/1574-6968.12432.

Tiirola, M., Wang, H., Paulin, L., and Kulomaa, M. (2002). Evidence for natural horizontal transfer of the pcpB gene in the evolution of polychlorophenol-degrading sphingomonads. *Appl Environ Microbiol* 68, 4495–4501. doi:10.1128/aem.68.9.4495-4501.2002.

Trolio, R., Grice, K., Fisher, S. J., Alexander, R., and Kagi, R. I. (1999). Alkylbiphenyls and alkyldiphenylmethanes as indicators of petroleum

biodegradation. *Organic Geochemistry* 30, 1241–1253. doi:10.1016/S0146-6380(99)00099-6.

van Bambeke, F., Mingeot-Leclercq, M.-P., Glupczynski, Y., and Tulkens, P. M. (2017). "137 - Mechanisms of Action," in *Infectious Diseases (Fourth Edition)*, eds. J. Cohen, W. G. Powderly, and S. M. Opal (Elsevier), 1162-1180.e1. doi:10.1016/B978-0-7020-6285-8.00137-4.

Volkman, J. K., Alexander, R., Kagi, R. I., Noble, R. A., and Woodhouse, C. W. (1983a). A geochemical reconstruction of oil generation in the Barrow Sub-basin of Western Australia. *Geochimica et Cosmochimica Acta* 47, 2091–2105. doi:10.1016/0016-7037(83)90034-0.

Volkman, J. K., Alexander, R., Kagi, R. I., Rowland, S. J., and Sheppard, P. N. (1984). Biodegradation of aromatic hydrocarbons in crude oils from the Barrow Sub-basin of Western Australia. *Organic Geochemistry* 6, 619–632. doi:10.1016/0146-6380(84)90084-6.

Volkman, J. K., Alexander, R., Kagi, R. I., and Woodhouse, G. W. (1983b). Demethylated hopanes in crude oils and their applications in petroleum geochemistry. *Geochimica et Cosmochimica Acta* 47, 785–794. doi:10.1016/0016-7037(83)90112-6.

Webber, M. A., and Piddock, L. J. V. (2003). The importance of efflux pumps in bacterial antibiotic resistance. *J Antimicrob Chemother* 51, 9–11. doi:10.1093/jac/dkg050.

Wilkinson, T. J., Huws, S. A., Edwards, J. E., Kingston-Smith, A. H., Siu-Ting, K., Hughes, M., et al. (2018). CowPI: A Rumen Microbiome Focussed Version of the PICRUSt Functional Inference Software. *Front. Microbiol.* 9. doi:10.3389/fmicb.2018.01095.

Wingert, W. S. (1992). G.c.-m.s. analysis of diamondoid hydrocarbons in Smackover petroleums. *Fuel* 71, 37–43. doi:10.1016/0016-2361(92)90190-Y.

Wong, H. L., Smith, D., Visscher, P. T., and Burns, B. P. (2015). Niche differentiation of bacterial communities at a millimeter scale in Shark Bay microbial mats. *Scientific Reports (Nature Publisher Group); London* 5, 15607. doi:http://dx.doi.org.dbgw.lis.curtin.edu.au/10.1038/srep15607.

Wright, R. J., Bosch, R., Gibson, M. I., and Christie-Oleza, J. A. (2020). Plasticizer Degradation by Marine Bacterial Isolates: A Proteogenomic and Metabolomic Characterization. *Environ. Sci. Technol.* 54, 2244–2256. doi:10.1021/acs.est.9b05228.

Yamamoto, H., Murata, M., and Sekiguchi, J. (2000). The CitST two-component system regulates the expression of the Mg-citrate transporter in Bacillus subtilis. *Molecular Microbiology* 37, 898–912. doi:10.1046/j.1365-2958.2000.02055.x.

Zhao, G., Ceci, P., Ilari, A., Giangiacomo, L., Laue, T. M., Chiancone, E., et al. (2002). Iron and Hydrogen Peroxide Detoxification Properties of DNA-binding Protein from Starved Cells: A Ferritin-like DNA-Binding Protein of Escherichia Coli. *Journal of Biological Chemistry* 277, 27689–27696. doi:10.1074/jbc.M202094200.

Zhou, G., Shi, Q.-S., Huang, X.-M., and Xie, X.-B. (2015). The Three Bacterial Lines of Defense against Antimicrobial Agents. *Int J Mol Sci* 16, 21711–21733. doi:10.3390/ijms160921711.

Appendix 3

SUPPLEMENTARY MATERIAL

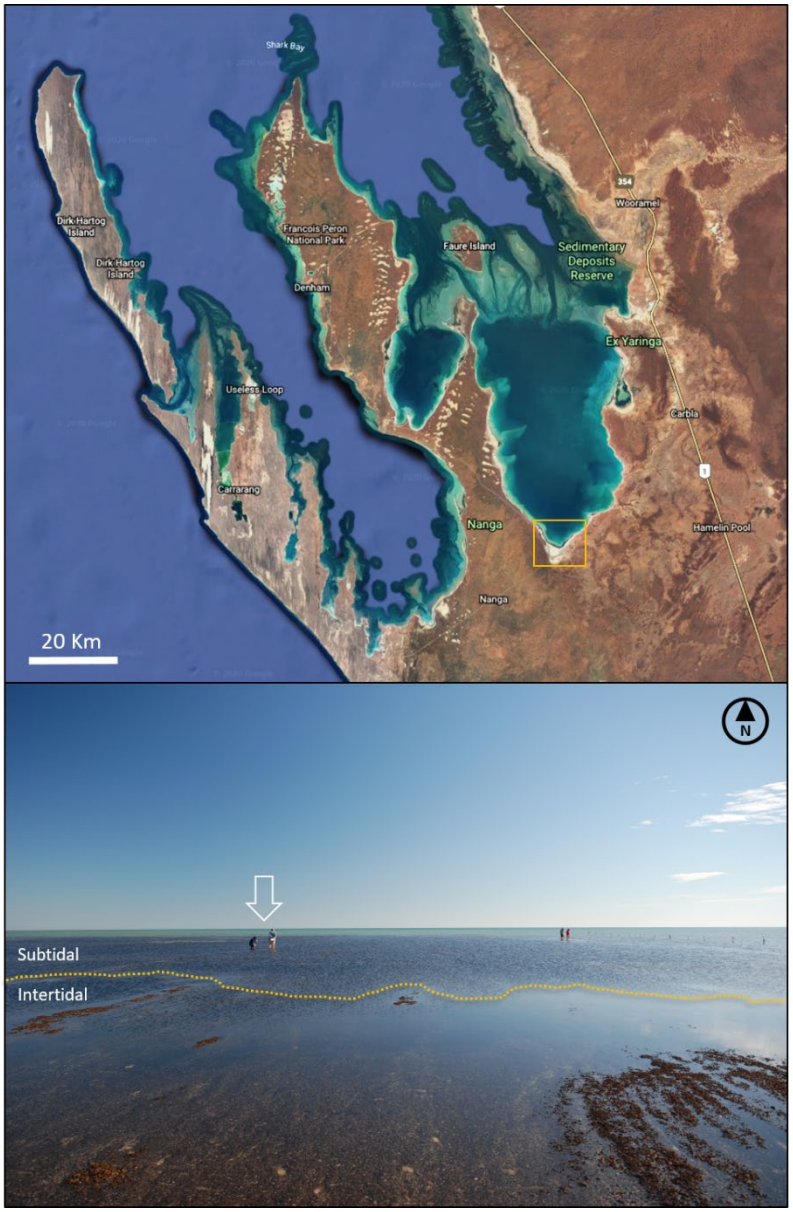

Figure A3.1. Shark Bay region (source: Google maps), highlighting Nilemah embayment as study site (yellow square) (top). Image of sampling site, depicting intertidal and subtidal environments (bottom).

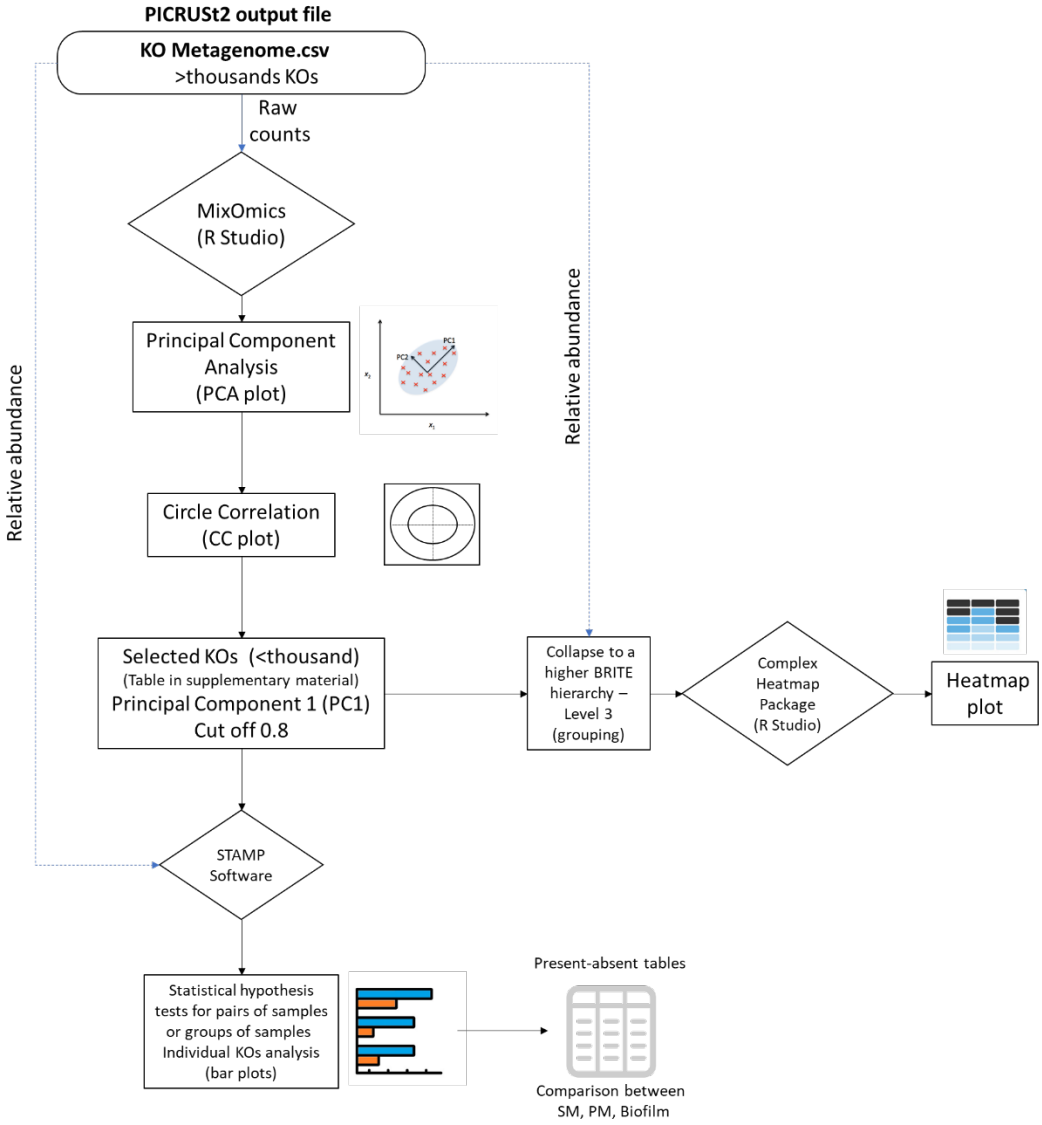

Figure A3.2. Diagram showing the workflow applied to explore and visualise predicted KOs functionalities (PCA and CC plots), and to confirm which of the predicted functions are statistically different as a result of PE.

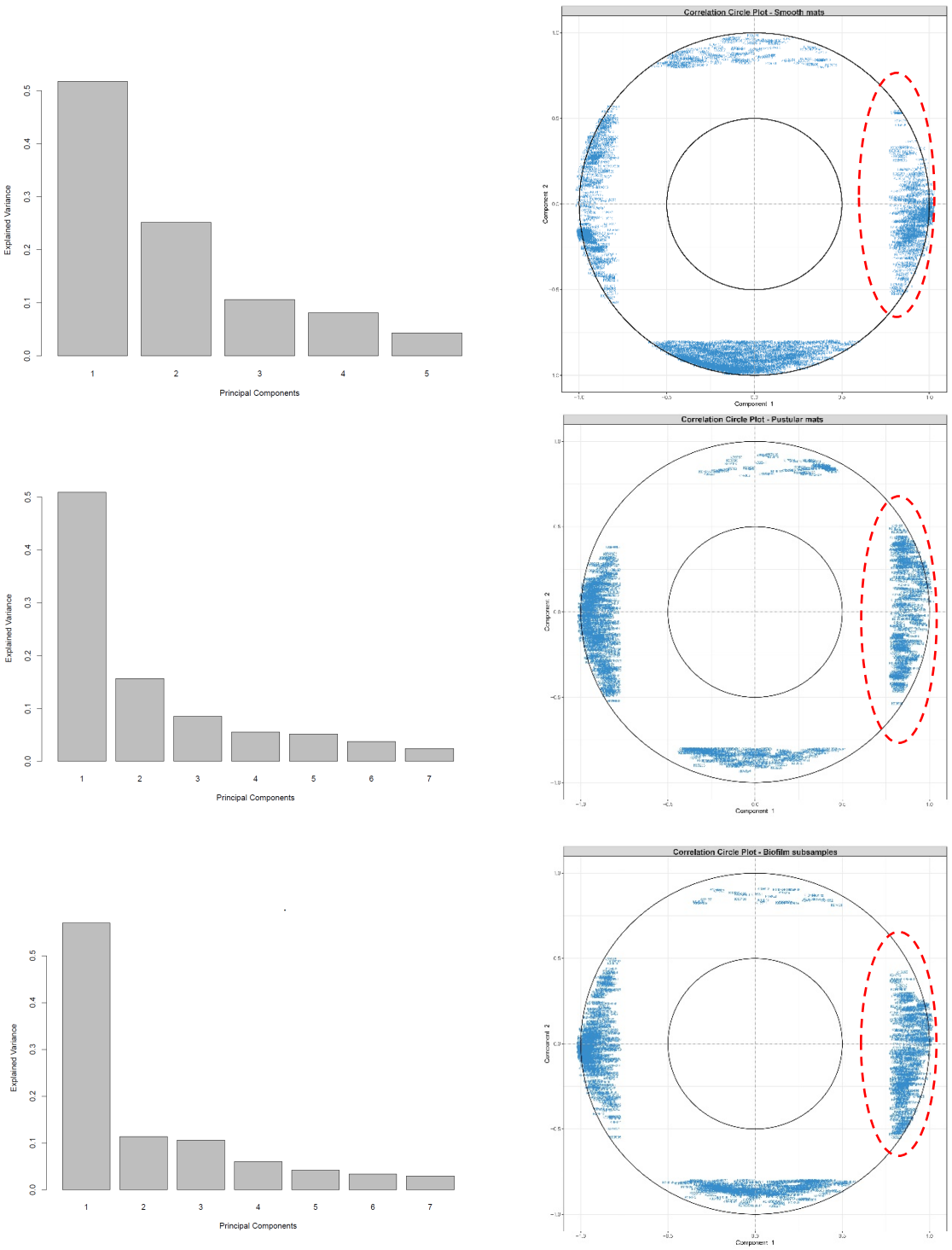

Figure A3.3. Histograms showing the contribution of each component to explain data variance in PCA plots in smooth and pustular mats microcosms subjected to PE and biofilm subsamples (**Figure 3.1**). Correlation Circle plots (PC1-PC2) representing those variables contributing most (cut off or radius > 0.8) to the clustering of samples (initial vs PE). A list with KOs (genes) clustered in the red circle responsible for PE clustering observed in all three PCA plots in **Figure 3.1** can be found in supplementary **Table A3.4**, **Table A3.5** and **Table A3.6**.

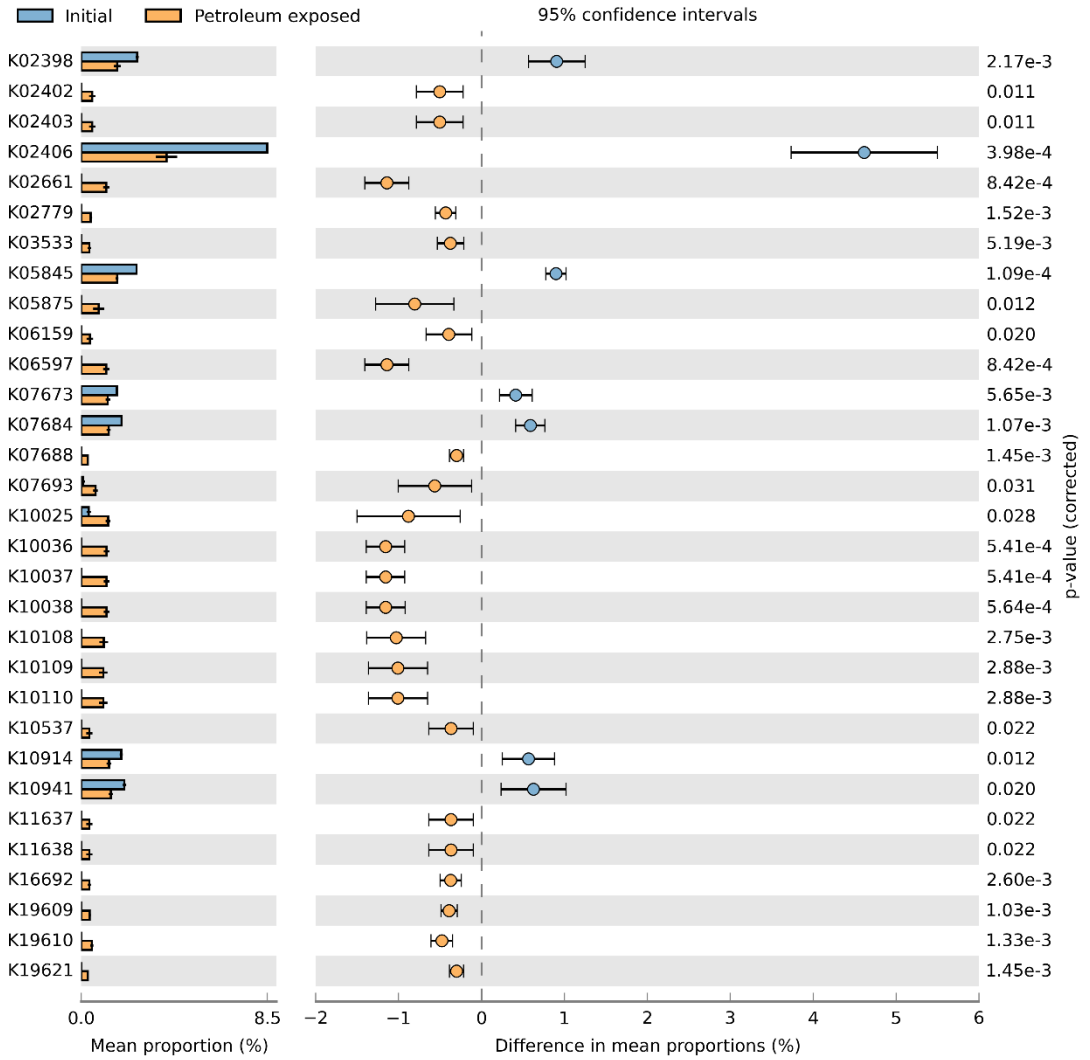

Figure A3.4. Extended error bar plot comparing mean proportions ($p < 0.05$) of KOs between initial versus PE samples related to **environmental information processing** in a **smooth mat** microcosm that was exposed to petroleum for 120 days (initials = PS7S $T0^{n=2}$ and PE=PS9S $T120^{n=4}$). Horizontal lines indicate confidence intervals (Tukey's t-test, ANOVA). Software utilised: STAMP, 2015, v.2.1.3.

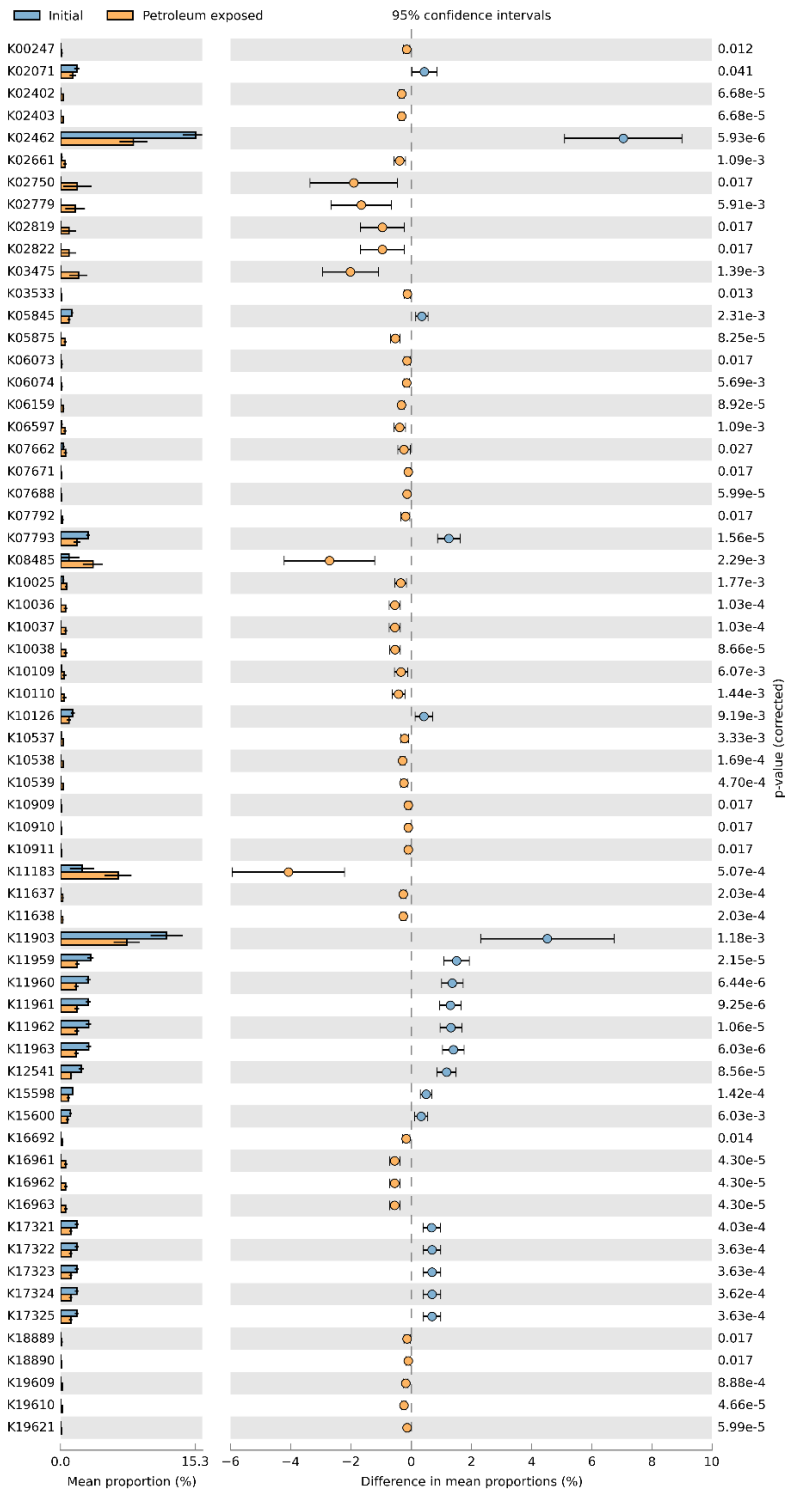

Figure A3.5. Extended error bar plot comparing mean proportions ($p < 0.05$) of KOs between initial versus PE samples related to **environmental information processing** in **pustular mats** microcosms that were exposed to petroleum for 60 and 120 days (initials = PS10P, PS11P and PS12P $T0^{n=6}$ and PE = PS11P T60 and PS12P $T120^{n=6}$). Horizontal lines indicate confidence intervals (Tukey's t-test, ANOVA).

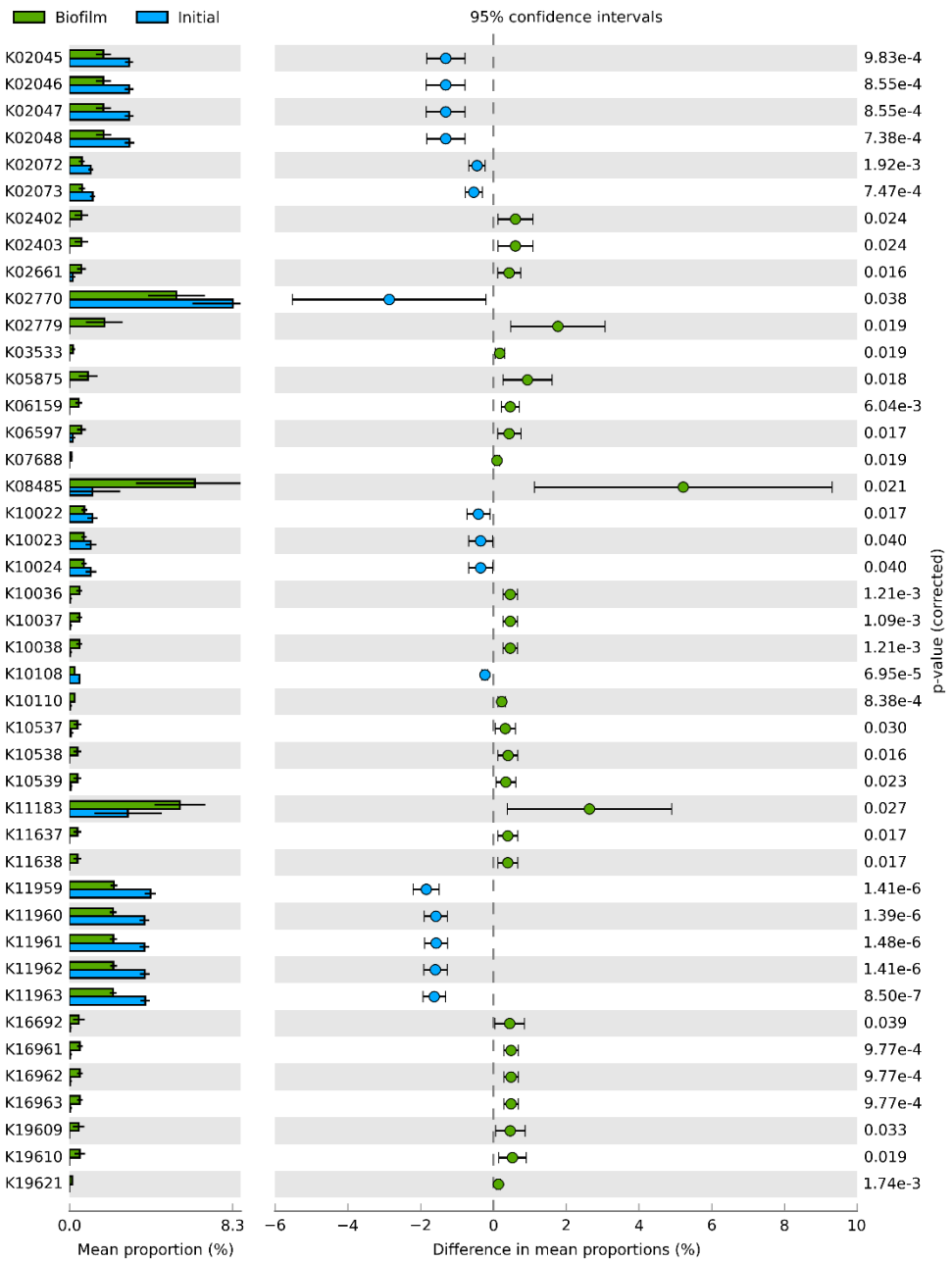

Figure A3.6. Extended error bar plot comparing mean proportions ($p < 0.05$) of KOs between initial versus PE samples related to **environmental information processing** in **biofilm-related** samples in a pustular mat microcosm after up to 120 days of PE (initials = PS10P, PS11P and PS12P $T0^{n=6}$ and PE = A, B, C and D $T120^{n=7}$). Horizontal lines indicate confidence intervals (Tukey's t-test, ANOVA).

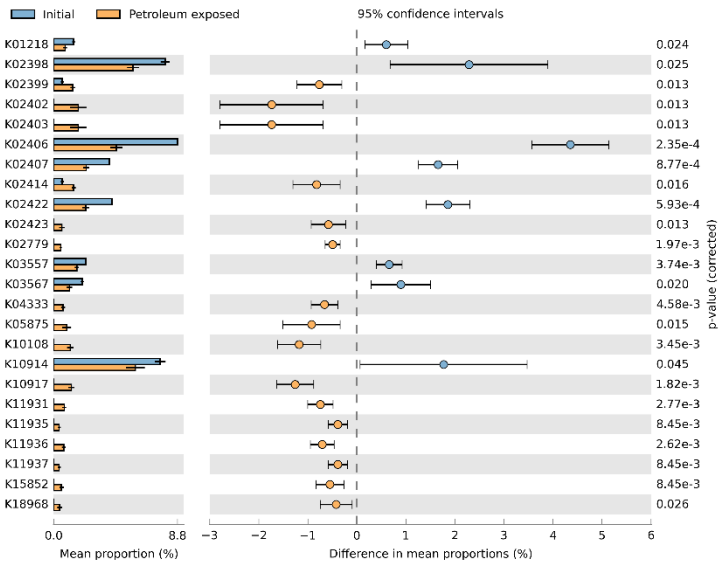

Figure A3.7. Extended error bar plot comparing mean proportions ($p < 0.05$) of KOs between initial versus PE samples related to **cellular processes** in a **smooth mat** microcosm after 120 days of PE (initials = PS7S $T0^{n=2}$ and PE=PS9S $T120^{n=4}$). Horizontal lines indicate confidence intervals (Tukey's t-test, ANOVA). Software utilised: STAMP, 2015, v.2.1.3.

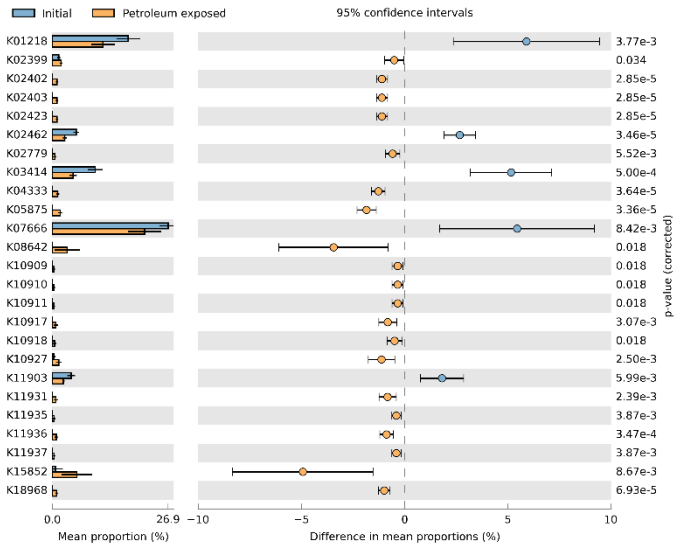

Figure A3.8. Extended error bar plot comparing mean proportions ($p < 0.05$) of KOs between initial versus PE samples related to **cellular processes** in **pustular mats** microcosms that were exposed to petroleum for 60 and 120 days (initials = PS10P, PS11P and PS12P $T0^{n=6}$ and PE = PS11P T60 and PS12P $T120^{n=6}$). Horizontal lines indicate confidence intervals (Tukey's t-test, ANOVA).

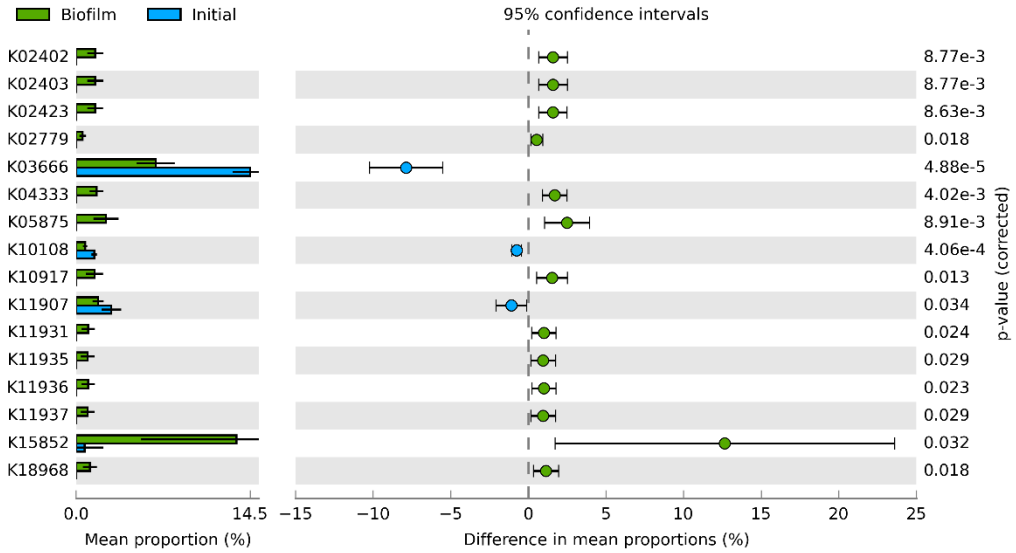

Figure A3.9. Extended error bar plot comparing mean proportions ($p < 0.05$) of KOs between initial versus PE samples related to **cellular processes** in **biofilm-related** samples in a pustular mat microcosm after 120 days of PE (initials = PS10P, PS11P and PS12P $T0^{n=6}$ and PE = A, B, C and D $T120^{n=7}$). Horizontal lines indicate confidence intervals (Tukey's t-test, ANOVA).

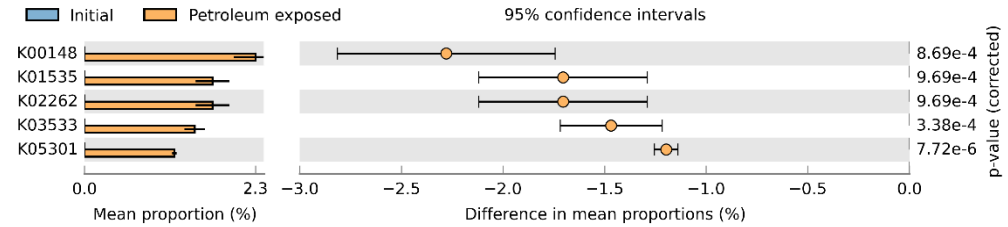

Figure A3.10.Extended error bar plot comparing mean proportions ($p < 0.05$) of KOs between initial versus PE samples related to **energy metabolism** in a **smooth mat** microcosm after 120 days of PE (initials = PS7S $T0^{n=2}$ and PE=PS9S $T120^{n=4}$). Horizontal lines indicate confidence intervals (Tukey's t-test, ANOVA).

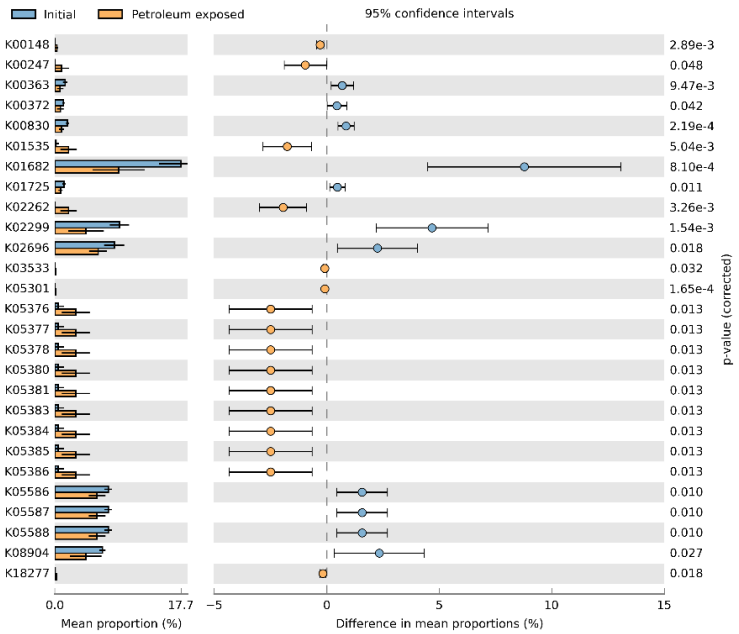

Figure A3.11. Extended error bar plot comparing mean proportions ($p < 0.05$) of KOs between initial versus PE samples related to **energy metabolism** in **pustular mats** microcosms that were exposed to petroleum for 60 and 120 days (initials = PS10P, PS11P and PS12P $T0^{n=6}$ and PE = PS11P T60 and PS12P $T120^{n=6}$). Horizontal lines indicate confidence intervals (Tukey's t-test, ANOVA).

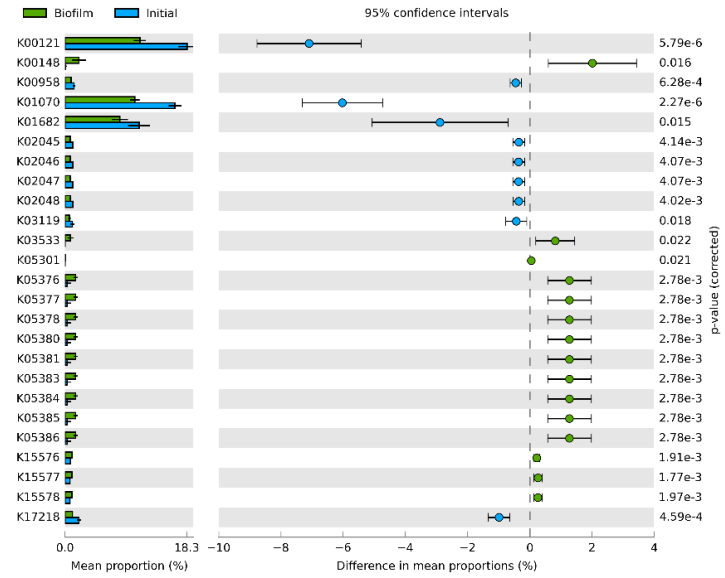

Figure A3.12. Extended error bar plot comparing mean proportions ($p < 0.05$) of KOs between initial versus PE samples related to **energy metabolism** in **biofilm-related** samples in a pustular mat microcosm after up to 120 days of PE (initials = PS10P, PS11P and PS12P $T0^{n=6}$ and PE = A, B, C and D $T120^{n=7}$). Horizontal lines indicate confidence intervals (Tukey's t-test, ANOVA).

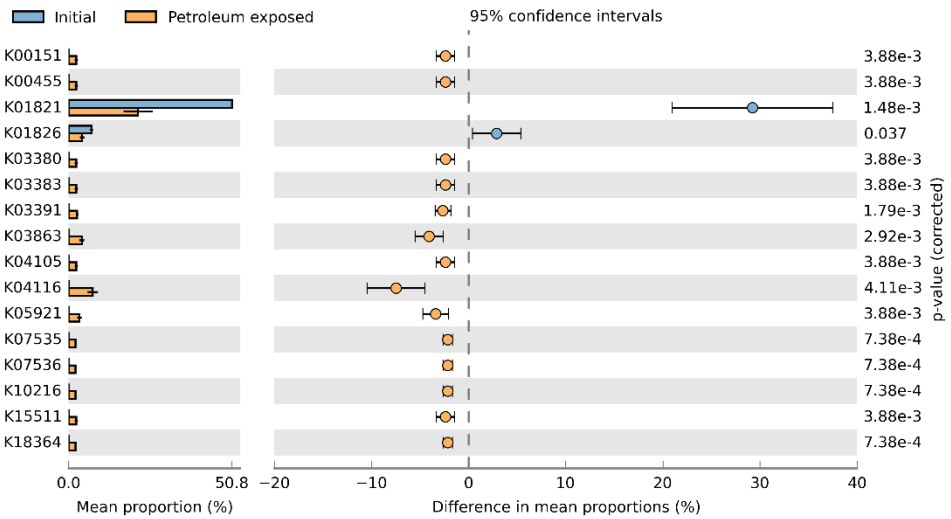

Figure A3.13. Extended error bar plot comparing mean proportions ($p < 0.05$) of KOs between initial versus PE samples related to **degradation of xenobiotics** in a **smooth mat** microcosm after 120 days of PE (initials = PS7S $T0^{n=2}$ and PE=PS9S $T120^{n=4}$). Horizontal lines indicate confidence intervals (Tukey's t-test, ANOVA).

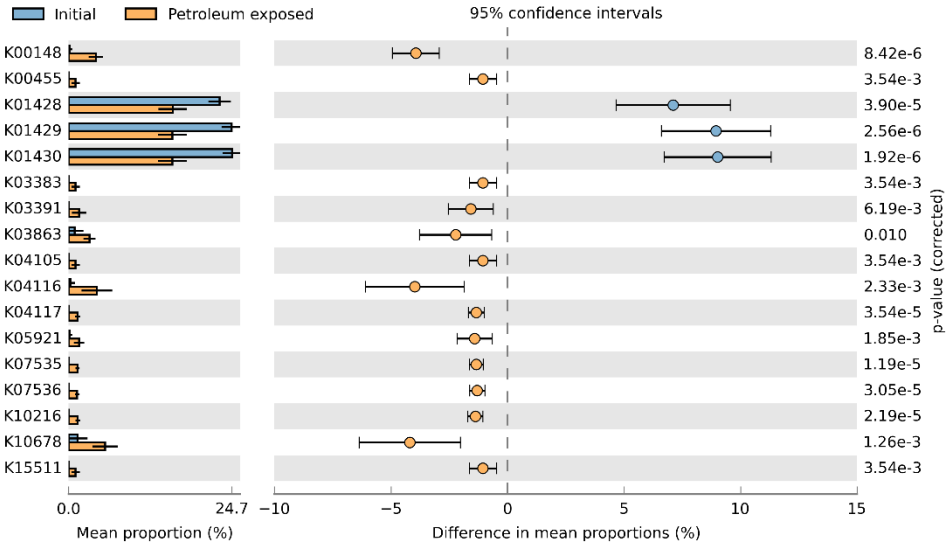

Figure A3.14. Extended error bar plot comparing mean proportions ($p < 0.05$) of KOs between initial versus PE samples related to **degradation of xenobiotics** in **pustular mats** microcosms that were exposed to petroleum for 60 and 120 days (initials = PS10P, PS11P and PS12P $T0^{n=6}$ and PE = PS11P T60 and PS12P $T120^{n=6}$). Horizontal lines indicate confidence intervals (Tukey's t-test, ANOVA).

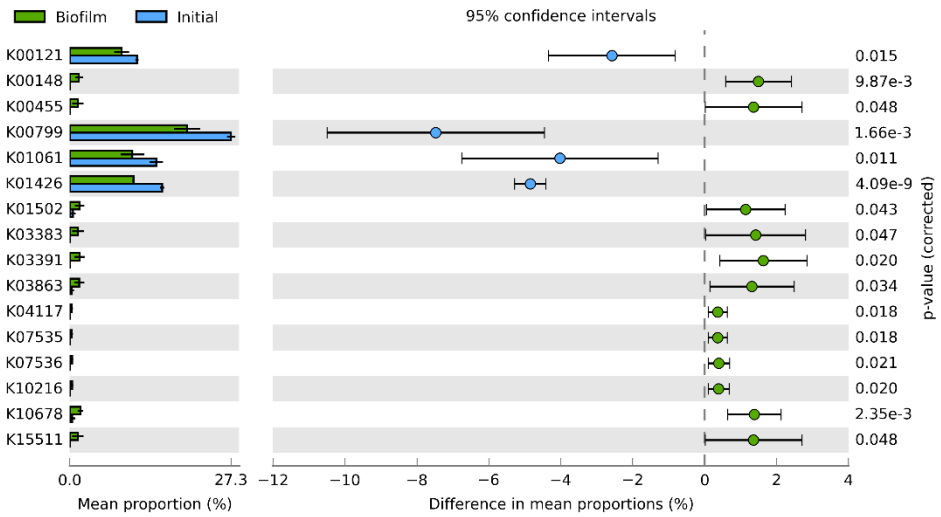

Figure A3.15. Extended error bar plot comparing mean proportions ($p < 0.05$) of KOs between initial versus PE samples related to **degradation of xenobiotics** in **biofilm-related** samples in a pustular mat microcosm after up to 120 days of PE (initials = PS10P, PS11P and PS12P $T0^{n=6}$ and PE = A, B, C and D $T120^{n=7}$). Horizontal lines indicate confidence intervals (Tukey's t-test, ANOVA).

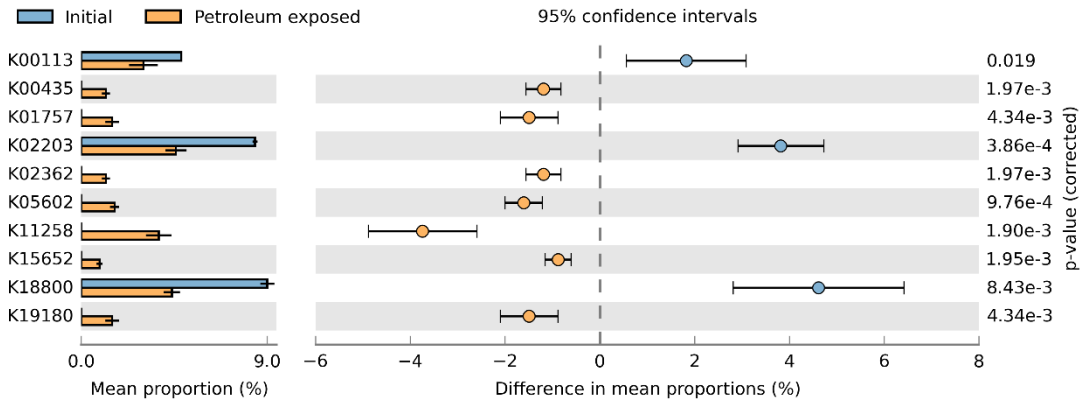

Figure A3.16. Extended error bar plot comparing mean proportions ($p < 0.05$) of KOs between initial versus PE samples related to **biosynthesis of secondary metabolites and antibiotics** in a **smooth mat** microcosm that were exposed to petroleum for 120 days (initials = PS7S $T0^{n=2}$ and PE=PS9S $T120^{n=4}$). Horizontal lines indicate confidence intervals (Tukey's t-test, ANOVA). Software utilised: STAMP, 2015, v.2.1.3.

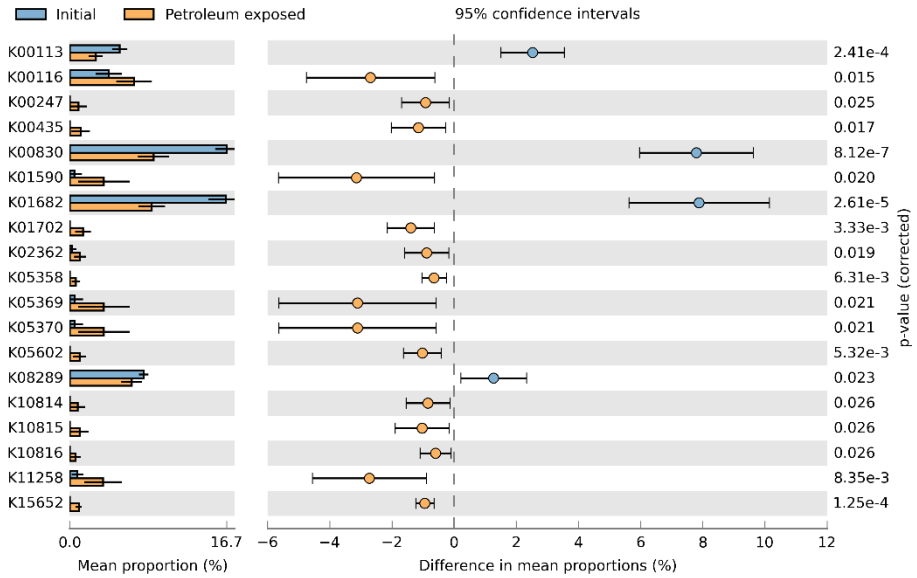

Figure A3.17. Extended error bar plot comparing mean proportions ($p < 0.05$) of KOs between initial versus PE samples related to **biosynthesis of secondary metabolites and antibiotics** in **pustular mats** microcosms that were exposed to petroleum for 60 and 120 days (initials = PS10P, PS11P and PS12P $T0^{n=6}$ and PE = PS11P T60 and PS12P $T120^{n=6}$). Horizontal lines indicate confidence intervals (Tukey's t-test, ANOVA).

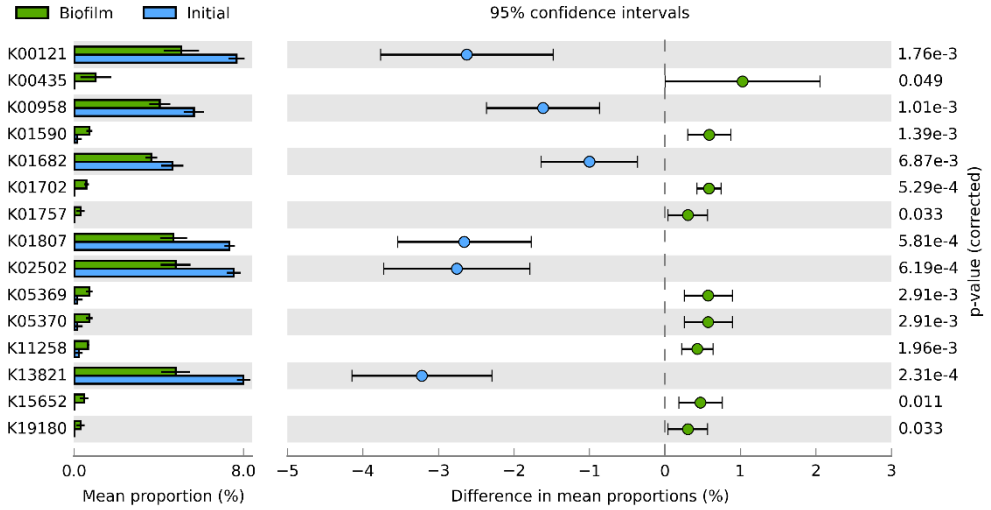

Figure A3.18. Extended error bar plot comparing mean proportions ($p < 0.05$) of KOs between initial versus PE samples related to **biosynthesis of secondary metabolites and antibiotics** samples in a pustular mat microcosm after up to 120 days of PE (initials = PS10P, PS11P and PS12P $T0^{n=6}$ and PE = A, B, C and D $T120^{n=7}$). Horizontal lines indicate confidence intervals (Tukey's t-test, ANOVA).

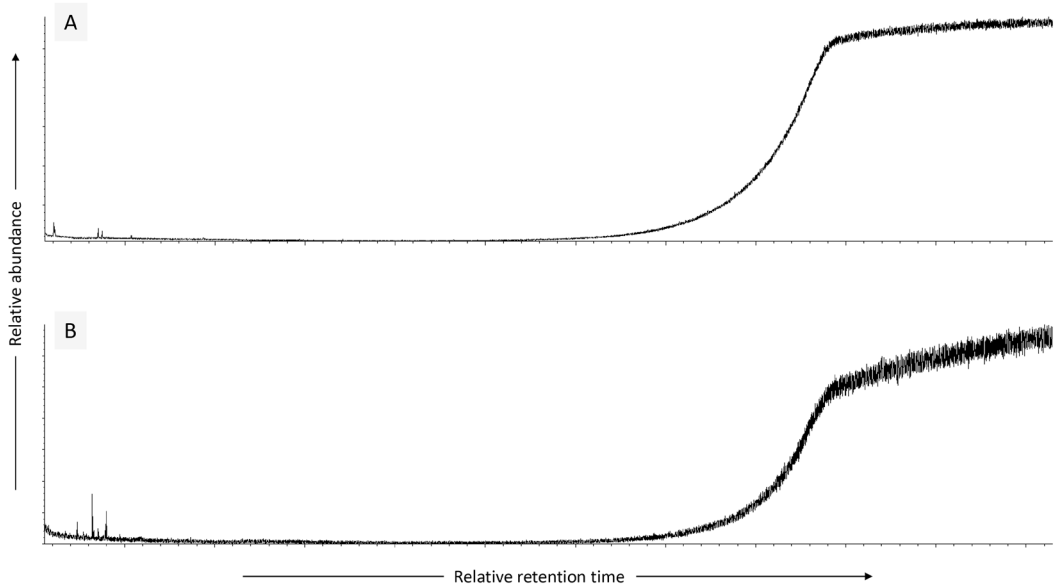

Figure A3.19. Total ion chromatograms of the procedural blanks run in parallel during the liquid-liquid extraction.

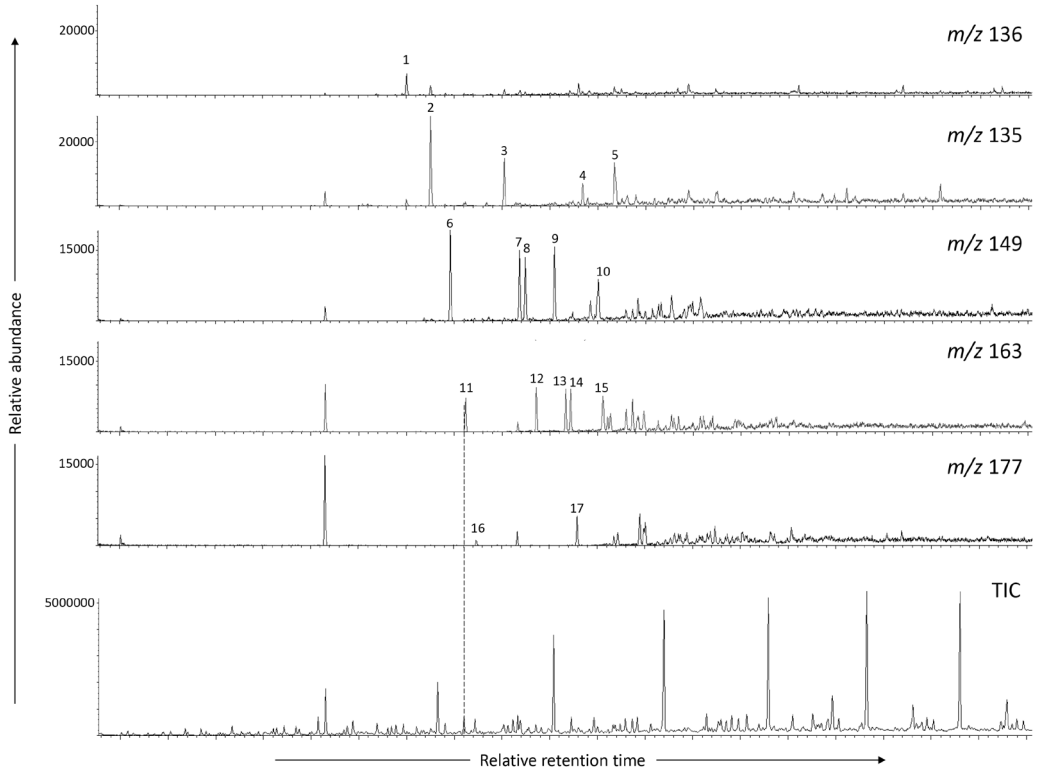

Figure A3.20. Adamantanes ions (*m/z* 136, 135, 149, 163, 177) assessed in the petroleum utilised as pollutant: Barrow Island #B101. Peaks are identified and described in **Table A3.7**.

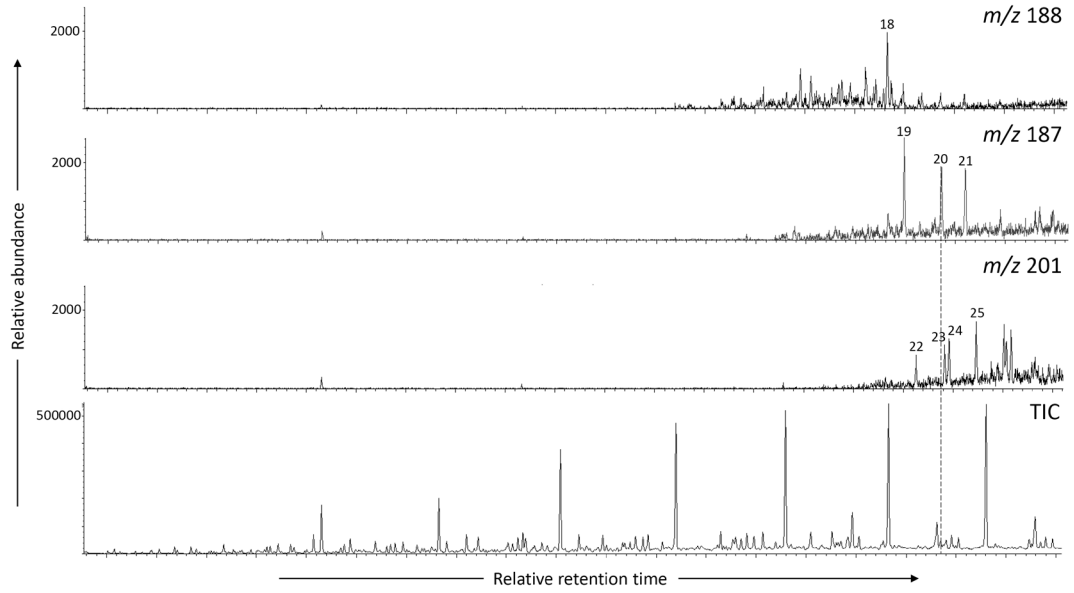

Figure A3.21. Diamantanes ions (*m/z* 188, 187,201) assessed in the petroleum utilised as pollutant: Barrow Island #B101. Peaks are identified and described in **Table A3.7**.

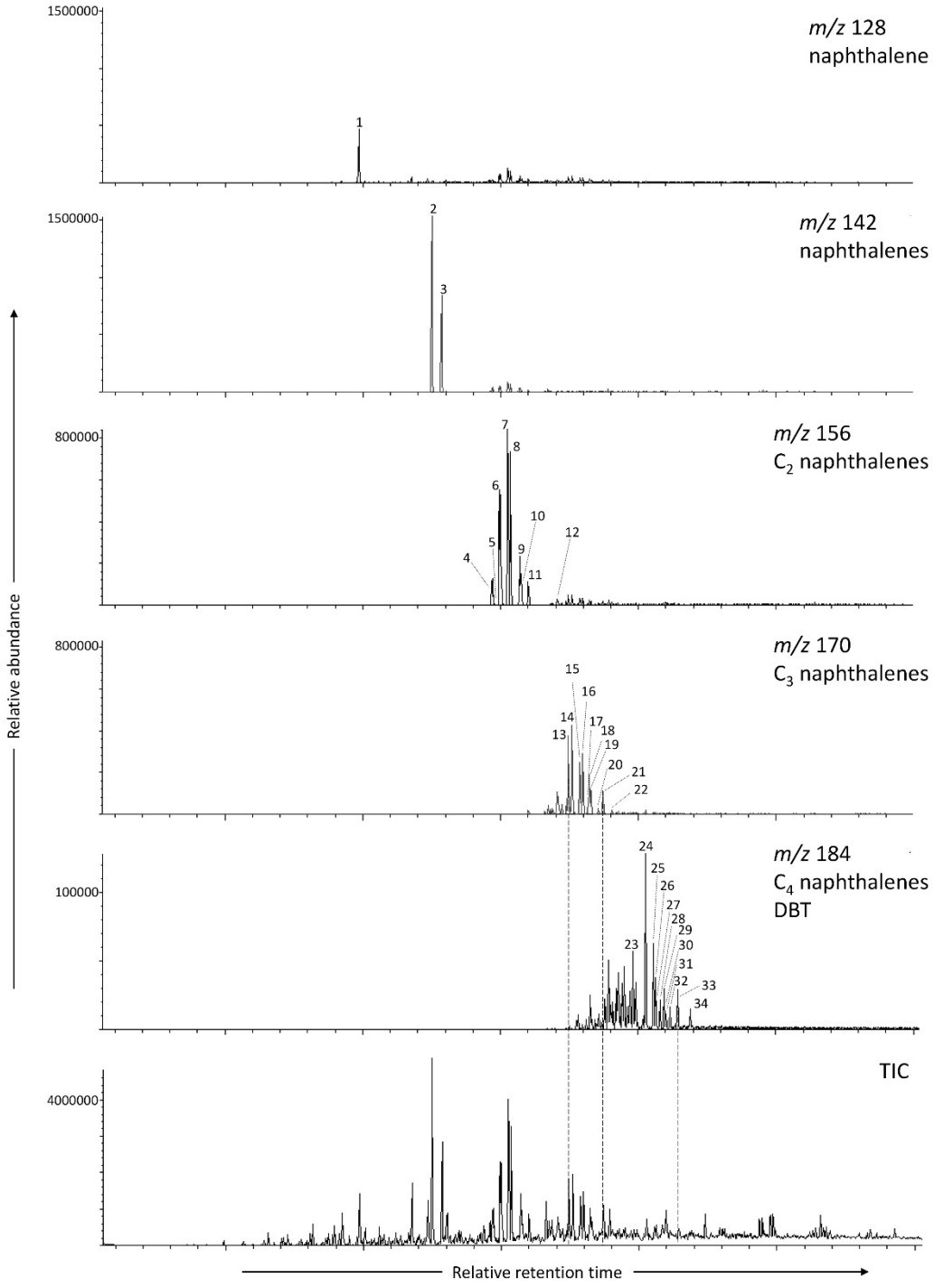

Figure A3.22. Alkylnaphthalene ions (*m/z* 128, 142, 156, 170, 184) assessed in the petroleum utilised as pollutant: Barrow Island #B101. Peaks are identified and described in **Table A3.8**.

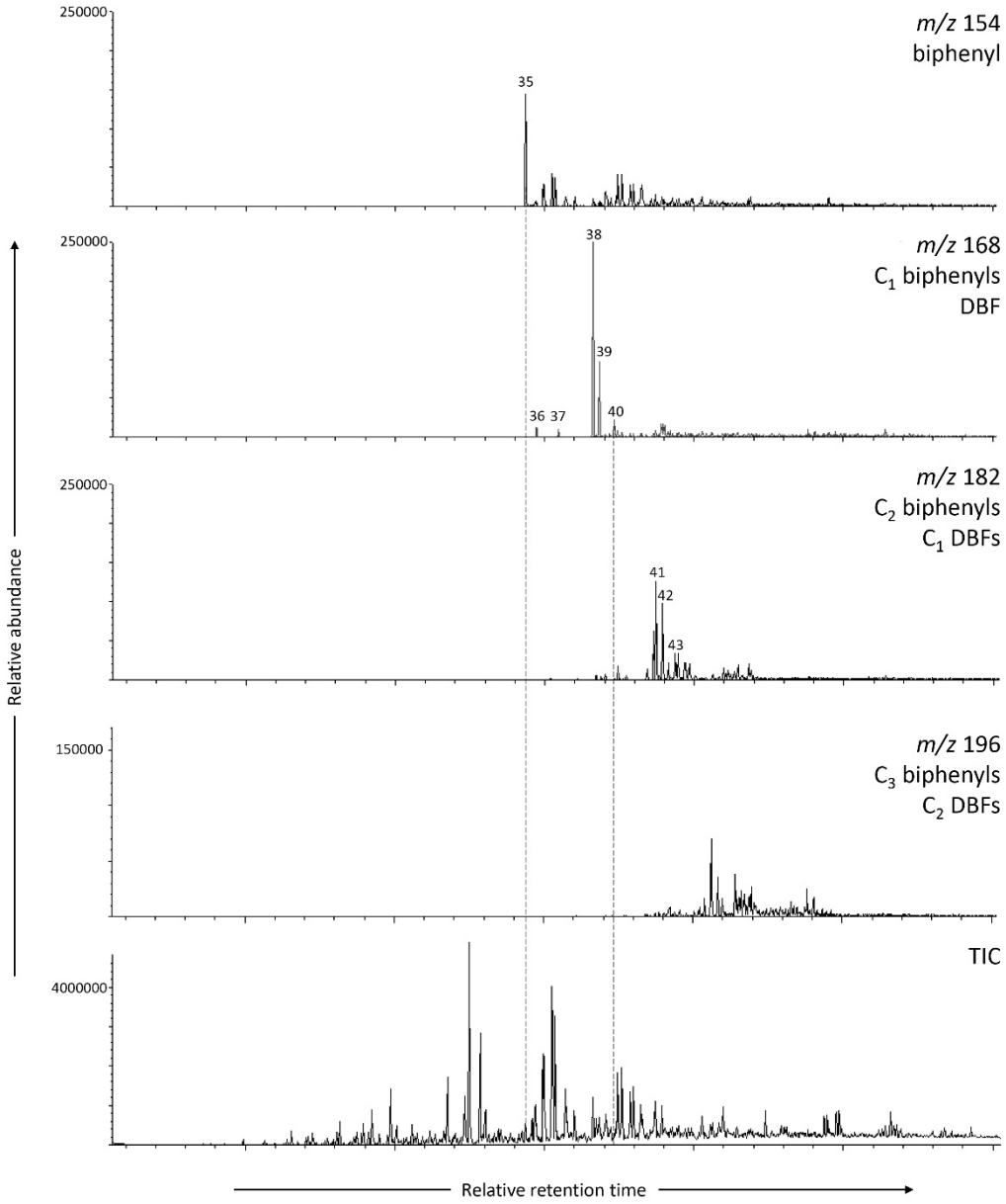

Figure A3.23. Biphenyl ions (*m/z* 154, 169,182, 196) assessed in the petroleum utilised as pollutant: Barrow Island #B101. Peaks are identified and described in **Table A3.9**.

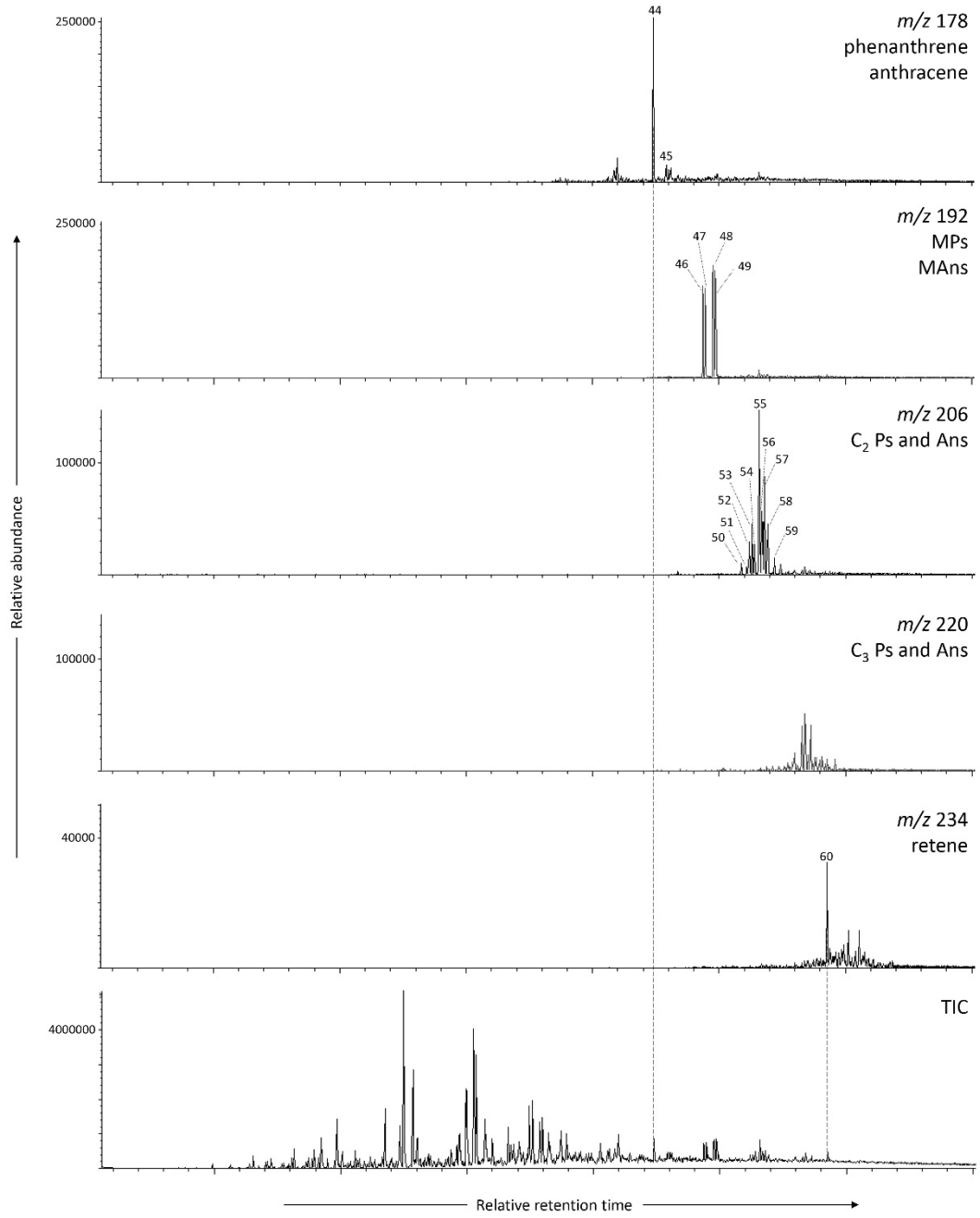

Figure A3.24. Phenanthrene and anthracene ions (*m/z* 178, 192, 206, 220 and 234) assessed in the petroleum utilised as pollutant: Barrow Island #B101. Peaks are identified and described in **Table A3.10**.

Table A3.1. Nearest Sequenced Taxon Index (NSTI) values for **smooth** mats initial and PE microcosms subsamples.

Type of microcosm	Sub-sample ID	Description	NSTI value	Mean ± σ
Petroleum-exposed	PS9S_T120_DNA_1	DNA – 120 days PE smooth MM microcosm	0.08	0.07 ± 0.01
	PS9S_T120_cDNA_1	cDNA – 120 days PE smooth MM microcosm	0.07	
	PS9S_T120_DNA_2	DNA – 120 days PE smooth MM microcosm with EPS forming on the top	0.06	
	PS9S_T120_cDNA_2	cDNA – 120 days PE smooth MM microcosm with EPS forming on the top	0.06	
Initial	PS7S_T0_DNA	DNA – smooth MM control microcosm (T0)	0.12	Not applicable
	PS7S_T0_cDNA	cDNA – smooth MM control microcosm (T0)	0.13	

Table A3.2. Nearest Sequenced Taxon Index (NSTI) values for **pustular** mats initial and PE microcosms subsamples.

Type of microcosm	Sub-sample ID	Description	NSTI value	Mean ± σ
Petroleum-exposed	PS10P_T30_DNA	DNA – 30 days PE pustular MM microcosm	0.09	0.07 ± 0.01
	PS10P_T30_cDNA	cDNA – 30 days PE pustular MM microcosm	0.09	
	PS11P_T60_DNA	DNA – 60 days PE pustular MM microcosm	0.06	
	PS11P_T60_cDNA	cDNA – 60 days PE pustular MM microcosm	0.06	
	PS12P_T120_DNA	DNA – 120 days PE pustular MM microcosm	0.06	
	PS12P_T120_cDNA	cDNA – 120 days PE pustular MM microcosm	0.07	
	D_DNA	DNA – Biofilm base - 120 days PE pustular MM microcosm	0.08	
	D_cDNA	cDNA – Biofilm base - 120 days PE pustular MM microcosm	0.07	
	C_DNA	DNA - Early Stage Biofilm - 120 days PE pustular MM microcosm	0.07	0.08 ± 0.01
	C_cDNA	cDNA - Early Stage Biofilm - 120 days PE pustular MM microcosm	0.08	
	B_cDNA	cDNA - Late Stage Biofilm - 120 days PE pustular MM microcosm	0.08	
	A_DNA	DNA - Foam - 120 days PE pustular MM microcosm	0.09	
	A_cDNA	cDNA - Foam - 120 days PE pustular MM microcosm	0.07	
Initial	PS10P_T0_DNA	DNA - Pustular MM - 0 day	0.15	0.13 ± 0.01
	PS10P_T0_cDNA	cDNA - Pustular MM - 0 day	0.14	
	PS11P_T0_DNA	DNA - Pustular MM - 0 day	0.12	
	PS11P_T0_cDNA	cDNA - Pustular MM - 0 day	0.14	
	PS12P_T0_DNA	DNA - Pustular MM - 0 day	0.12	
	PS12P_T0_cDNA	cDNA - Pustular MM - 0 day	0.13	

Table A3.3. One-way ANOVA p-values of predicted environmental information processing and cellular processes pathways in controls vs. petroleum-exposed microcosms. Data was calculated using KOs that were abundant in the cDNA pool of microcosms subjected to petroleum.

Level 1	Level 2	Level 3	Smooth mat microcosms (T0 vs. T120)	Pustular mat microcosms (T0 vs. T60 &T120)	Biofilm subsamples (PS12P 120) (T0 vs. T120)
Environmental Information Processing	Membrane transport	ABC transporters	0.01	2.1E-08	7.4E-07
		Phosphotransferase system (PTS)	0.03	5.5E-05	no significant
		Bacterial secretion system	0.05	8.9E-04	no significant
	Signal transduction	Two-component system	0.05	1.2E-06	6.2E-05
Cellular Processes	Cellular community - prokaryotes	Quorum sensing	0.04	8.5E-05	2.2E-02
		Biofilm formation - *Vibrio cholerae*	0.03	7.2E-05	2.7E-05
		Biofilm formation - *Pseudomonas aeruginosa*	0.07	2.8E-04	1.5E-03
		Biofilm formation - *Escherichia coli*	0.03	3.7E-05	3.0E-04
	Cell motility	Bacterial chemotaxis	0.05	8.2E-05	5.4E-03
		Flagellar assembly	0.13	6.7E-05	1.1E-02

Table A3.4. KO (KEGG Orthologs) predicted by PICRUSt2 over 0.80 cutoff for 120 days PE smooth mat microscom subsamples (PS9S T120 – 2 replicates). Data can be explored in KEGG Mapper – Search Pathway using these KOs in the following to link: https://www.genome.jp/kegg/tool/map_pathway1.html (comma should be removed first).

KO > 0.80 (Component 1)
K00423, K11909, K11909, K08722, K01150, K10036, K10037, K10038, K09909, K11908, K05602, K02661, K06597, K11258, K02779, K00256, K11936, K18939, K10917, K11931, K12984, K03933, K02560, K11474, K04116, K07518, K08997, K12286, K12287, K03668, K06205, K11923, K18136, K13985, K19610, K05301, K07535, K07536, K07688, K10216, K18364, K18916, K19621, K03863, K17736, K19609, K10108, K10109, K10110, K00158, K13637, K01757, K19180, K01729, K00148, K13938, K03810, K01535, K01884, K02262, K10782, K12049, K18384, K07084, K04333, K05921, K15852, K18030, K00885, K03533, K12700, K17733, K19304, K00151, K00455, K02508, K03380, K03383, K04105, K05818, K08276, K09943, K11935, K11937, K12055, K12537, K12538, K12545, K14974, K15357, K15511, K15540, K16152, K18028, K18289, K18291, K18900, K00435, K01073, K02362, K03391, K07345, K16317, K16692, K18302, K18303, K05834, K10025, K12254, K01210, K01407, K01753, K07964, K10748, K15652, K18786, K03805, K05875, K03674, K02414, K01178, K19355, K06992, K02402, K02403, K02423, K03516, K19585, K01058, K19597, K07693, K08364, K02399, K05997, K00683, K16328, K00032, K17737, K19337, K02521, K01826, K03472, K03112, K19664, K13695, K06899, K02617, K19265, K14260, K03736, K05787, K08363, K01175, K09898, K07097, K07178, K00116, K06603, K03812, K02463, K08485, K07662, K07274, K09891, K03314, K02858, K06879, K19789, K11894, K07689, K07640, K02487, K01825, K08289, K06079, K09860, K07070, K09906, K09908, K09916, K09004, K01002, K01706, K10537, K11441, K11637, K11638, K13522, K13875, K15373, K15735, K16077, K18135, K18336, K18968, K00836, K03776, K03807, K18235, K13694, K01267, K02770, K07039, K06159, K13255, K01218, K06598, K06968, K03735, K02451, K04061, K00635, K10022, K15257, K01959, K00374, K10024, K05591, K00370, K00371, K00373, K03774, K02462, K03981, K02476, K13777, K09926, K07165, K10023, K13778, K07451, K03379, K11907, K06219, K00563, K02072, K10844, K09889, K02073, K10213, K18300, K19168, K03796, K07400, K05845, K06194, K05297, K03680, K07262, K00690, K09902, K03387, K03415, K02395, K07740, K02673, K18850, K08084, K19339, K06972, K03749, K07679, K01141, K06132, K07678, K03449, K11910, K12284, K01654, K07044, K13642, K03611, K07121, K01659, K11891, K13693, K19054, K07235, K10674, K11731, K02398, K03554, K03583, K03580, K08082, K01219, K00131, K05851, K13776, K07181, K02413, K02494, K13053, K10678, K12982, K19416, K12448, K01720, K07250, K18912, K06518, K09918, K09990, K03582, K19058, K15784, K09788, K03656, K08984, K00520, K03577, K16961, K16962, K16963, K02475, K07153, K03528, K10926, K10927, K12285, K12278, K11901, K19000, K18691, K07448, K05605, K03720, K06957, K08295, K02439, K02169, K03690, K12279, K07661, K07287, K09912, K13979, K03567, K13779, K07233, K19294, K11896, K00906, K07236, K07639, K11903, K03597, K02656, K08086, K02203, K06718, K06720, K07122, K05501, K00673, K03181, K11895, K08083, K01580, K02170, K09938, K16291, K09801, K02671, K00362, K03151, K15396, K02674, K03717, K02452, K03586, K09895, K02672, K07248, K03598, K02655, K07237, K03806, K01664, K01821, K02496, K00846, K11905, K06149, K06222, K03683, K06186, K03291, K06183, K11477, K05365, K12297, K05886, K15984, K07673, K03556, K15576, K01779, K02407, K08967, K03298, K10924, K12276, K05020, K00803, K10941, K15461, K07733, K07666, K03599, K03673, K05596, K18901, K11211, K19696, K07014, K00884, K12280, K12281, K12282, K12283, K02404, K02670, K07184, K11893, K18902, K03557, K13634, K10942, K11183, K03803, K10763, K14267, K01584, K09797, K07645, K00113, K07684, K14540, K01045, K09913, K15577, K05526, K07180, K02083, K16844, K07589, K15578, K18649, K04117, K12942, K10914, K07026, K11900, K08224, K12979, K06039, K01573, K18930, K03732, K10974, K06075, K00363, K09786, K03548, K01702, K02406, K03600, K07173, K13775, K02441, K09920, K09914, K18800, K00523, K05832, K05833, K08312, K03616, K01046, K01525, K09858, K02553, K15539, K02024, K02461, K07175, K02676, K07778, K03672, K00210, K08983, K01243, K06447, K03462, K13786, K19163, K02460, K03308, K03184, K09929, K07116, K06895, K08988, K04045, K13041, K00247, K01215, K02344, K02784, K02819, K02822, K03485, K03633, K03645, K03764, K04067, K04770, K05775, K05809, K06078, K06866, K06887, K07186, K07269, K07671, K07751, K08320, K08642, K09161, K09802, K09893, K09894, K09896, K09899, K09900, K09901, K09904, K09917, K10123, K10816, K10909, K10910, K10911, K10913, K11911, K11922, K11926, K12525, K12997, K13638, K15178, K15536, K15723, K16698, K16771, K18657, K18890, K19141, K19227, K19228, K19230, K19236, K07257, K02422, K05540, K11892, K18967, K01455, K18430, K03840, K07320, K03893, K11906, K05541, K06176, K13288, K07506, K02821, K02458

Table A3.5. KO (KEGG Orthologs) predicted by PICRUSt2 over 0.8 cutoff for 120 days PE pustular mat microscom subsample (PS9S T120). Data can be explored in KEGG Mapper – Search Pathway using these KOs in the following to link: https://www.genome.jp/kegg/tool/map_pathway1.html (comma should be removed first).

KO > 0.80 (Component 1)
K13985, K19610, K19610, K11923, K18136, K11936, K03933, K04333, K01178, K01210, K01407, K10748, K18786, K10216, K05301, K07536, K07688, K18916, K19621, K02402, K02403, K02423, K03516, K15652, K06159, K17736, K04117, K19304, K05875, K19609, K19585, K07248, K00836, K07535, K10538, K11441, K13522, K15373, K16077, K18336, K18968, K00032, K17737, K15576, K01753, K06905, K16602, K19156, K07289, K11637, K11638, K13875, K18135, K04033, K00148, K16088, K01002, K15577, K03577, K05997, K15784, K15578, K12500, K00362, K08485, K02575, K11477, K02560, K19707, K11931, K15735, K07274, K19155, K02616, K01118, K03840, K01706, K18303, K01709, K16839, K10974, K05921, K02262, K10782, K12049, K00372, K06718, K06720, K00158, K03707, K16317, K03776, K18939, K02362, K10917, K03810, K19338, K09909, K00661, K07183, K15786, K14540, K15782, K18030, K03893, K10539, K06992, K06079, K19058, K10022, K00455, K02508, K03383, K04105, K05358, K08276, K09943, K11935, K11937, K12055, K12537, K12538, K12545, K14974, K15357, K15511, K15540, K16152, K17733, K18028, K18289, K18900, K01073, K03391, K07345, K18302, K01535, K02779, K05559, K05560, K05561, K05562, K05563, K05564, K07084, K00435, K03647, K06191, K19294, K18291, K18384, K07088, K00247, K07020, K03805, K17735, K07964, K11908, K11909, K16961, K16962, K16963, K11939, K03184, K05845, K07039, K18930, K10038, K09898, K10025, K10036, K10037, K15461, K00116, K01218, K14260, K05886, K01707, K09004, K10537, K03674, K08167, K03862, K07740, K03807, K07223, K15852, K08722, K05541, K11961, K11910, K01578, K15600, K07726, K06205, K03692, K11962, K06219, K06074, K18277, K03774, K09806, K13255, K05596, K15539, K00423, K11811, K03556, K17321, K00370, K11258, K05834, K06923, K07678, K10024, K02462, K09857, K12254, K19158, K19789, K00122, K03112, K07026, K07286, K08289, K15598, K03668, K01428, K08364, K07242, K00374, K00373, K01702, K01826, K00256, K00557, K03580, K02594, K11474, K17322, K17323, K11522, K06955, K03863, K17325, K17324, K19171, K19170, K19172, K00988, K08480, K13938, K06860, K00371, K15785, K01429, K01430, K16692, K16328, K01219, K11525, K04768, K07400, K05787, K06876, K10023, K11954, K01141, K01058, K05778, K16915, K07250, K10674, K09891, K07246, K07283, K01725, K01046, K02399, K10110, K05275, K11960, K08688, K11356, K11958, K02661, K06597, K09928, K18967, K06899, K05777, K05779, K02623, K11955, K11957, K03414, K07494, K02494, K11524, K07190, K13053, K07662, K04116, K12287, K15228, K15229, K01720, K10844, K02521, K09918, K11963, K15268, K11924, K11959, K05978, K11526, K00479, K15257, K03475, K07518, K07086, K19159, K11183, K09940, K09908, K09916, K07070, K06968, K06148, K00885, K12700, K05586, K05587, K05588, K19166, K03611, K11391, K00690, K07262, K03533, K07127, K12256, K03571, K07645, K18473, K13637, K09910, K00884, K00520, K19337, K03812, K09921, K04775, K07793, K05602, K01590, K04708, K15643, K17748, K17749, K17750, K11354, K11355, K06075, K02642, K10678, K07235, K07661, K00004, K00363, K11523, K06879, K02071, K00846, K05795, K03808, K04774, K01406, K02286, K03451, K06598, K00663, K05369, K05370, K05376, K05377, K05378, K05380, K05381, K05383, K05384, K05385, K05386, K06446, K01584, K03394, K06206, K09889, K07639, K03208, K07116, K06946, K10126, K07336, K05501, K10257, K00448, K03472, K17108, K03830, K09902, K08169, K02480, K08904, K07097, K07666, K02168, K02750, K07792, K18218, K03632, K10815, K11750, K11925, K01226, K01232, K01387, K03482, K03658, K03804, K05517, K05880, K06073, K10814, K10918, K15545, K18889, K00113, K05591, K01215, K02344, K02819, K02822, K03485, K03633, K04067, K04770, K05775, K05809, K06078, K06866, K06887, K07269, K07671, K08320, K08642, K08993, K09161, K09802, K09896, K09900, K09901, K09917, K10123, K10816, K10909, K10910, K10911, K11911, K11922, K11926, K12997, K13638, K15178, K15536, K16698, K16771, K18890, K19236, K11894, K05851, K05539, K00830, K15396, K07733, K19168, K00436, K18007, K11903, K09906, K09000, K11777, K07130, K12979, K18850, K02292, K19191, K11145, K13643, K02478, K15383, K12255, K04061, K03610, K11534, K01825, K19141, K12541, K06518, K06145, K03387, K03187, K03608, K19076, K10927, K12285, K12286, K03435, K19120, K19121, K19122, K09127, K19142, K02299, K03554, K09966, K01729, K09834, K01455, K07506, K03609, K11211, K09833, K05928, K08696, K02696, K01682, K02072, K03867, K08697, K08699, K08700, K11520, K08698, K10109

Table A3.6. KO (KEGG Orthologs) predicted by PICRUSt over 0.8 cutoff for 120 days petroleum-exposed biofilm-related sub-samples in a pustular mat microscom (PS12P T120). Data can be explored in KEGG Mapper – Search Pathway using these KOs in the following to link: https://www.genome.jp/kegg/tool/map_pathway1.html (comma should be removed first).

KO > 0.80 (Component 1)
K01702, K10531, K10531, K03896, K15974, K19068, K01753, K02560, K19621, K19610, K03933, K04333, K06159, K13985, K05875, K19609, K00435, K01073, K03391, K06079, K09909, K16317, K07345, K18302, K01178, K01210, K01407, K10748, K11923, K15652, K18136, K18786, K10917, K02423, K02402, K02403, K18303, K03516, K19585, K17737, K06905, K18968, K15576, K13875, K07248, K04033, K13522, K18336, K02575, K00032, K10538, K11441, K17736, K11637, K11638, K15373, K16077, K16602, K18135, K18030, K00148, K18939, K11936, K03383, K17733, K11931, K16088, K00455, K15511, K03556, K19707, K18028, K16692, K15577, K05358, K12537, K12538, K14974, K15357, K18289, K18291, K19058, K11935, K11937, K02508, K04105, K08276, K09943, K12055, K12545, K15540, K16152, K15578, K06992, K03805, K18900, K07084, K19304, K05921, K11909, K01002, K16961, K16962, K16963, K10037, K11908, K10036, K10038, K15852, K03893, K02362, K19155, K11477, K12500, K00256, K15735, K07039, K01709, K08485, K01706, K01535, K11961, K11960, K16839, K11962, K11963, K10110, K02616, K19156, K07518, K14260, K19789, K13053, K07645, K03577, K05997, K07223, K03674, K07262, K11910, K02661, K00362, K06597, K07740, K03807, K05844, K03812, K01590, K09898, K07662, K15643, K17748, K17749, K17750, K00836, K04708, K10974, K10025, K19338, K11959, K05834, K07733, K03840, K05369, K05370, K05376, K05377, K05378, K05380, K05381, K05383, K05384, K05385, K05386, K10674, K11258, K07400, K05845, K14540, K07020, K19168, K03608, K10539, K11954, K08289, K07274, K06191, K03610, K03112, K01725, K15784, K03609, K03647, K06860, K11811, K11356, K11939, K02399, K07678, K09788, K03208, K01046, K06923, K07044, K06718, K05560, K05563, K03776, K05559, K05561, K05562, K05564, K00958, K06720, K07242, K02619, K17108, K11391, K07666, K05886, K08167, K07491, K09928, K05591, K00988, K08480, K05787, K03387, K01218, K07726, K09004, K00936, K07661, K00370, K03810, K07964, K11522, K07070, K09908, K09916, K09891, K19294, K03774, K09940, K00374, K09958, K05275, K07286, K00373, K17893, K06879, K06206, K05501, K11525, K08904, K10023, K10024, K07086, K18930, K00151, K03310, K07235, K07289, K10022, K01058, K05586, K05587, K05588, K00371, K06598, K00121, K02286, K06446, K03863, K08364, K11777, K09918, K07639, K02072, K00221, K01757, K12069, K19180, K05539, K16328, K06899, K02231, K07393, K10537, K19339, K15228, K13255, K15257, K02480, K01807, K15229, K16792, K01959, K00569, K00555, K19597, K01069, K06946, K09913, K10678, K03380, K06183, K02658, K00436, K18007, K07190, K00563, K11312, K09906, K00786, K01414, K11950, K11740, K03668, K02502, K05596, K03321, K01682, K09926, K02770, K00004, K01070, K00520, K02659, K10257, K10109, K06955, K03580, K08299, K00372, K00830, K04117, K07535, K18916, K01219, K09932, K11183, K09780, K02230, K00116, K10831, K03818, K07688, K10216, K09127, K19142, K01426, K09000, K01118, K09834, K06876, K05301, K07536, K09833, K19337, K05928, K08696, K02696, K03867, K08697, K08699, K08700, K11520, K07283, K06149, K08698, K11325, K04037, K04039, K06138, K02692, K02699, K02708, K02710, K02712, K02713, K02719, K08479, K19032, K00082, K09835, K02228, K11894, K02689, K02690, K01428, K19076, K00471, K00514, K01429, K01430, K03666, K00344, K00885, K02779, K03533, K12700, K06205, K02485, K09919, K18473, K13695, K02439, K03808, K02232, K00799, K19164, K08983, K10697, K06219, K17735, K09800, K01502, K03862, K13637, K10108, K15782, K12282, K02549, K07497, K00158, K06986, K02487, K02262, K10782, K12049, K01061, K03502, K13777, K09857, K07146, K02116, K02476, K02073, K01150, K17836, K07347, K00978, K09774, K06148, K13635, K02227, K07395, K01707, K01941, K15786, K00694, K00383, K05541, K02521, K10004, K06181, K07178, K11906, K12059, K07649, K03119, K11145, K00389, K09966, K01584, K10253, K03830, K03090, K07336, K03328, K17218, K02660, K18954, K18300, K14266, K12543, K19166, K00524, K09931, K16915, K12276, K06968, K02048, K00564, K00595, K02224, K12255, K04035, K02233, K03745, K03404, K01729, K06978, K02045, K13821, K11211, K03184, K07183, K07116, K02657, K05818, K03592, K00122, K13778, K02046, K02047, K03457, K09902, K03597, K07346, K08300, K03472, K03435, K10924, K03403, K01825, K16872, K07132, K02552, K02494, K07093, K19355, K00020, K02623, K07000, K03611, K07266, K02706, K02698, K13041, K01175, K07482, K07243, K04772, K11524, K11953, K11907, K02287, K00325, K01674, K18850, K03707, K07250, K03189, K00690

Table A3.7. Mass spectral features of adamantanes and diamantanes compounds identified in the petroleum utilised as pollutant: Barrow Island #B101. Peaks are displayed in **Figure A3.20** and **Figure A3.21**.

	Peak #	Compound	Name abbreviation	Molecular ion
Adamantanes	1	Adamantane	A	136
	2	1-Methyladamantane	1-MA	135
	3	2-Methyladamantane	2-MA	135
	4	1-Ethyladamantane	1-EtA	135
	5	2-Ethyladamantane	2-EtA	135
	6	1,3-Dimethyladamantane	1,3-DMA	149
	7	1,4-Dimethyladamantane (*cis*)	1,4-DMA	149
	8	1,4-Dimethyladamantane (*trans*)	1,4-DMA	149
	9	1,2-Dimethyladamantane	1,2-DMA	149
	10	1-Ethyl,3-methyladamantane	1-Et, 3-MA	149
	11	1,3,5-Trimethyladamantane	1,3,5-TMA	163
	12	1,3,6-Trimethyladamantane	1,3,6-TMA	163
	13	1,3,4-Trimethyladamantane (*cis*)	1,3,4-TMA	163
	14	1,3,4-Trimethyladamantane (*trans*)	1,3,4-TMA	163
	15	1-Ethyl, 3,5-dimethyladamantane	1-Et, 3,5-DMA	163
	16	1,3,5,7-Tetramethyladamantane	1,3,5,7-TeMA	177
	17	1,2,5,7-Tetramethyladamantane	1,2,5,7-TeMA	177
Diamantanes	18	Diamantane	DIA	188
	19	4-Methyldiamantane	4-MDIA	187
	20	1-Methyldiamantane	1-MDIA	187
	21	3-Methyldiamantane	3-MDIA	187
	22	4,9-Dimethyldiamantane	4,9-DMDIA	201
	23	1,4-Dimethyldiamantane + 2,4-dimethyldiamantane	1,4-DMDIA+ 2,4-DMDIA	201
	24	4,8-Dimethyldiamantane	4,8-DMDIA	201
	25	3,4-Dimethyldiamantane	3,4-DMDIA	201

Table A3.8. Mass spectral features of **alkyl naphthalene** compounds identified in the petroleum utilised as pollutant: Barrow Island #B101. Peaks are displayed in the **Figure A3.22**.

Peak #	Compound	Name abbreviation	Molecular ion
1	Naphthalene	N	128
2	2-Methylnaphthalene	2-MN	142
3	1-Methylnaphthalene	1-MN	142
4	2-Ethylnaphthalene	2-EN	156
5	1-Ethylnaphthalene	1-EN	156
6	2,6-Dimethylnaphthalene 2,7-Dimethylnaphthalene	2,6-DMN 2,7-DMN	156
7	1,3-Dimethylnaphthalene 1,7-Dimethylnaphthalene	1,3-DMN 1,7-DMN	156
8	1,6-Dimethylnaphthalene	1,6-DMN	156
9	1,4-Dimethylnaphthalene 2,3-Dimethylnaphthalene	1,4-DMN 2,3-DMN	156
10	1,5-Dimethylnaphthalene	1,5-DMN	156
11	1,2-Dimethylnaphthalene	1,2-DMN	156
12	1,8-Dimethylnaphthalene	1,8-DMN	156
13	1,3,7-Trimethylnaphthalene	1,3,7-TMN	170
14	1,3,6-Trimethylnaphthalene	1,3,6-TMN	170
15	1,4,6-Trimethylnaphthalene 1,3,5-Trimethylnaphthalene	1,4,6-TMN 1,3,5-TMN	170
16	2,3,6-Trimethylnaphthalene	2,3,6-TMN	170
17	1,2,7-Trimethylnaphthalene	1,2,7-TMN	170
18	1,6,7-Trimethylnaphthalene	1,6,7-TMN	170
19	1,2,6-Trimethylnaphthalene	1,2,6-TMN	170
20	1,2,4-Trimethylnaphthalene	1,2,4-TMN	170
21	1,2,5-Trimethylnaphthalene	1,2,5-TMN	170
22	1,4,5-Trimethylnaphthalene	1,4,5-TMN	170
23	1,3,5,7-Tetramethylnaphthalene	1,3,5,7-TeMN	184
24	1,3,6,7-Tetramethylnaphthalene	1,3,6,7-TeMN	184
25	Cadalene	Cadal	198
26	*Iso*cadalene	Isocadal	198
27	1,2,4,7-Tetramethylnaphthalene	1,2,4,7-TeMN	184
28	1,2,5,7-Tetramethylnaphthalene	1,2,5,7-TeMN	184
29	2,3,6,7-Tetramethylnaphthalene	2,3,6,7-TeMN	184
30	1,2,6,7-Tetramethylnaphthalene	1,2,6,7-TeMN	184
31	1,2,37-Tetramethylnaphthalene	1,2,3,7-TeMN	184
32	1,2,3,6-Tetramethylnaphthalene	1,2,3,6-TeMN	184
33	1,2,5,6-Tetramethylnaphthalene 1,2,3,5-Tetramethylnaphthalene	1,2,5,6-TeMN 1,2,3,5-TeMN	184
34	Dibenzothiophene	DBT	184

Table A3.9. Mass spectral features of **biphenyl, diphenylmethane** and their **alkylated derivatives** compounds identified in the petroleum utilised as pollutant: Barrow Island #B101. Peaks are displayed in **Figure A3.23**.

Peak No.	Compound	Name abbreviation	Molecular ion
35	Biphenyl	BP	154
36	2-Methylbiphenyl	2-MBP	168
37	Diphenylmethane	DPM	168
38	3-Methylbiphenyl	3-MBP	168
39	4-Methylbiphenyl	4-MBP	168
40	Dibenzofuran	DBF	168
41	Methyldibenzofuran	MDBF	182
42	Methyldibenzofuran	MDBF	182
43	Methyldibenzofuran	MDBF	182

Table A3.10. Mass spectral features of **phenanthrene and anthracene** compounds identified in the petroleum utilised as pollutant: Barrow Island #B101. Peaks are displayed in **Figure A3.24**.

Peak No.	Compound	Name abbreviation	Molecular ion
44	Phenanthrene	P	178
45	Anthracene	An	178
46	3-Methylphenanthrene	3-MP	192
47	2-Methylphenanthrene	2-MP	192
48	9-Methylphenanthrene 1-Methylanthracene	9-MP 1-MAn	192
49	1-Methylphenanthrene	1-MP	192
50	Unknown		
51	9-Ethylphenanthrene 2-Ethylphenanthrene	9-EP 2-EP	206
52	1-Ethylphenanthrene	1-EP	206
53	3,5-Dimethylphenanthrene 2,6-Dimethylphenanthrene	3,5-DMP 2,6-DMP	206
54	2,7-Dimethylphenanthrene	2,7-DMP	206
55	1,3-Dimethylphenanthrene 3,9-Dimethylphenanthrene 2,10-Dimethylphenanthrene 3,10-Dimethylphenanthrene	1,3-DMP 3,9-DMP	206
56	1,6-Dimethylphenanthrene 2,9-Dimethylphenanthrene 2,5-Dimethylphenanthrene	1,6-DMP 2,9-DMP 2,5-DMP	206
57	1,7-Dimethylphenanthrene	1,7-DMP	206
58	2,3-Dimethylphenanthrene	2,3-DMP	206
59	1,9-Dimethylphenanthrene 4,9-Dimethylphenanthrene	1,9-DMP 4,9-DMP	206
60	Retene	Retene	234

Chapter 4

Resistance and resilience of microbial mats from Shark Bay to petroleum contamination: comparative assessment to pulse and press disturbances

Yalimay Jimenez, Kliti Grice and Marco J.L. Coolen

***Microbiology*, in preparation**

Impact factor: 1.866

4.1. Abstract

Potential petroleum spills caused by the increase of shipping and port activities represent a threat to pristine microbial habitats in Shark Bay, Western Australia. The long-term (acute, press) microbial ecosystem responses associated with widespread smooth- and pustular microbial mats was recently studied using time series microcosm experiments. However, there is no information about the ecological stability of these important microbial mat ecosystems after a short-term or pulse disturbance. Using a comparable microcosm set-up, we have subjected both microbial mat types to a pulse petroleum contamination involving 10 days of acute exposure, followed by a one-year period of recovery. Total *vs*. active microbial community composition were subsequently assessed through 16S rRNA genes and transcript profiling. A comparative assessment of short-term and long-term disturbance responses was conducted to determine whether smooth and pustular mat microbiomes are preferentially unresponsive to both type of disturbances (more resistant) and/or capable to adapt to these disturbances and to maintain their stability over time (more resilient). Three key ecological responses were consistent among both incubation experiments: a shift in their microbial composition and structure, a decline in their microbial diversity, and the activation of potential functionalities associated with stress conditions and degradation of xenobiotics. Differences in the rate of loss of their microbial diversity over time revealed that smooth mats are more resilient and likely more resistant when subjected to pulse disturbances, while pustular mat microbiomes are highly unstable or vulnerable to either short- or long-term disturbances.

Keywords: Resistance, resilience, microbial mats, Shark Bay, pulse, press, disturbances, petroleum spill.

4.2. Introduction

Environmental assessments to potential risks rely on evaluating and understanding the responses of ecosystems to disturbances (Chambers et al., 2019). Resilience and resistance are key concepts to assess the stability of protected ecosystems to environmental threats. Ecosystem resilience is a term introduced to describe the ability of a habitat to adapt to disturbances and maintain its community stability over time. Disturbances can be classified based on their duration (temporal scale) in two types: (1) presses or continuous long-term disturbances, and (2) pulses or short-term events (Glasby and Underwood, 1996; Shade et al., 2012a). These disturbances might cause permanent shifts in their microbial communities (microbiomes) to an alternative, but stable condition known as resistance. However, some microbial communities might return to their pre-disturbance state, known as resilience (Shade et al., 2012a). Furthermore, when assessing ecosystems it is necessary to account for natural 'intrinsic' variability (Chambers et al., 2019). Therefore, to measure if the habitat has shown any sign of 'recovery', the parameter chosen needs to be statistically indistinguishable from the original state or condition (Westman, 1978; Orwin and Wardle, 2004; Suding et al., 2004).

Shark Bay (SB) is located in Western Australia and has been identified as a high environmental risk region due to industrial activities in the local area (Australian Maritime Safety Authority (AMSA), 2012). Shipping and port activities exert an increased risk of a petroleum spill in this protected area due to the proximity of traffic routes and oceanic currents from the north. Shark Bay consists of three important embayments: Henry Freycinet, L'Haridon Bight and Hamelin Pool. Of these, currently Hamelin Pool is naturally protected by a seagrass meadow, however, due to the recent loss (over 30%) of the seagrass (NESP Earth Systems and Climate Change Hub, 2018) the region is at a risk of complete habitat destruction such as microbial mats by a possible petroleum spill event.

Microbial mats are amongst the most widespread habitats in Hamelin Pool. Up to eight zones of microbial mats have been identified in Hamelin Pool. The non-lithifying smooth and pustular microbial mats in this region have been extensively studied during the last decade (Allen et al., 2009; Pagès et al., 2014; Wong et al., 2015, 2016;

Babilonia et al., 2018; Plet et al., 2018; Wong et al., 2018; Campbell et al., 2020). In a recent study a time-series of incubation experiments involving both smooth and pustular mat types from Nilemah Bay have been exposed to a petroleum disturbance (**Chapter 2** and **Chapter 3**). They showed from 16S rRNA gene and transcript profiling that two-thirds of the bacterial components in these mat types were affected by the long-term petroleum exposure (PE).

However, nothing is known about to what extent these mat microbiomes respond to and recover from a pulse PE. Here, we hypothesise that smooth and pustular mats from Shark Bay would not be able to resist a pulse or short-term acute PE, but that these microbial ecosystems will be able to recover to their original state over time. To examine the stability-vulnerability of the mat microbiomes over time, microcosms containing smooth and pustular mats from Nilemah Bay were subjected to chronic PE for 10 days followed by the replacement of most of the petroleum contaminant with sterile seawater. The mats were maintained in the lab in the co-presence of only trace amounts of petroleum for up to one year to allow the microbiomes to recover from this environmental stressor. Changes in total microbial communities (DNA pool) *vs*. active microbial communities (cDNA pool) that occurred during the time-series pulse PE exposure and recovery experiment were characterised through Illumina MiSeq sequencing of 16S rDNA (V4 region). Selected petroleum as a pollutant corresponds to moderately biodegraded petroleum (Windalia #410 from Barrow Sub-basin of the Carnarvon Basin, Western Australia). Its use allowed assessing if oil-biodegrader organisms would still prosper despite more easily assimilated compounds would be in lesser proportion than in the presence of non-degraded petroleum. DNA- and cDNA based datasets were then analysed with PICRUSt2 to predict functional changes associated with environmental information processing (*i.e.,* ABC transporters and Two-Component system), cellular processes (particularly biofilm formation), energy metabolisms, biosynthesis of secondary metabolites, and the potential to degrade xenobiotics.

4.3. Material and methods

4.3.1. Time-series lab-controlled incubations

Samples of smooth and pustular microbial mats used in this study were collected from locations in Nilemah Bay in April 2017 as described in detail recently (**Chapter 2**; **Figure 4.1**). Intact large pieces of living microbial mats were covered with local seawater and transferred into containers and transported to Western Australian Organic and Isotope Geochemistry Centre (WA-OIGC) facilities at Curtin University. Within days after subsampling, these large pieces were divided into smaller pieces (approx. 60 g wet weight) and placed into cylindrical glass microcosms. The mats were covered with ~30 mL seawater prior to incubation (**Figure 4.2**). A total of eight microcosms, four with SMs and four with PMs were placed inside an incubation tank and were exposed to a diel light regime (16 hours light and 8 hours darkness). Each microcosm also received a constant supply of sterile-filtered-air (**Figure 4.2**). See **Chapter 2** for details of the experimental design.

One microcosm was incubated without petroleum and served as a background control. The other microcosm labelled as SMOC3 and PMOC3 received 5 mL (16.6% v/v) of petroleum. The naphthenic-aromatic-rich petroleum contaminant (**Figure A4.1**) was sourced from the largest oil field in WA: Windalia (#410) (Barrow Sub-basin of the Carnarvon Basin). Windalia is a moderately biodegraded level 4 petroleum sample (Volkman et al., 1983a, 1983b). During the first 10 days of petroleum incubation, the mats in the microcosms were in direct contact with the petroleum for a period of 4 hours between 10 am and 2 pm and were separated by the ~30 mL seawater interphase for the remainder of the day. This seawater interphase was transferred using a sterile pipette to a sterile container daily at 10 am and transferred back onto the mats at 2 pm. Samples (1cm x 1 cm x 0.5 cm l x d x h) for DNA and RNA extractions were obtained before (T0), and after 1 day (T1), 5 days (T5), 10 days (T10) of incubation (**Figure A4.2**). After 10 days of incubation, the petroleum-contaminated seawater was removed and replaced with fresh seawater collected in the field (same sampling point – Hamelin Pool, SB). The amount of evaporation was compensated by adding 0.22µm-prefiltered MilliQ water over the course of 1-year incubation (T1y), after which samples were again obtained for DNA and RNA extraction after 1 year of incubation.

The remainder of the mat material was sub-sampled and stored at -80°C for further analyses.

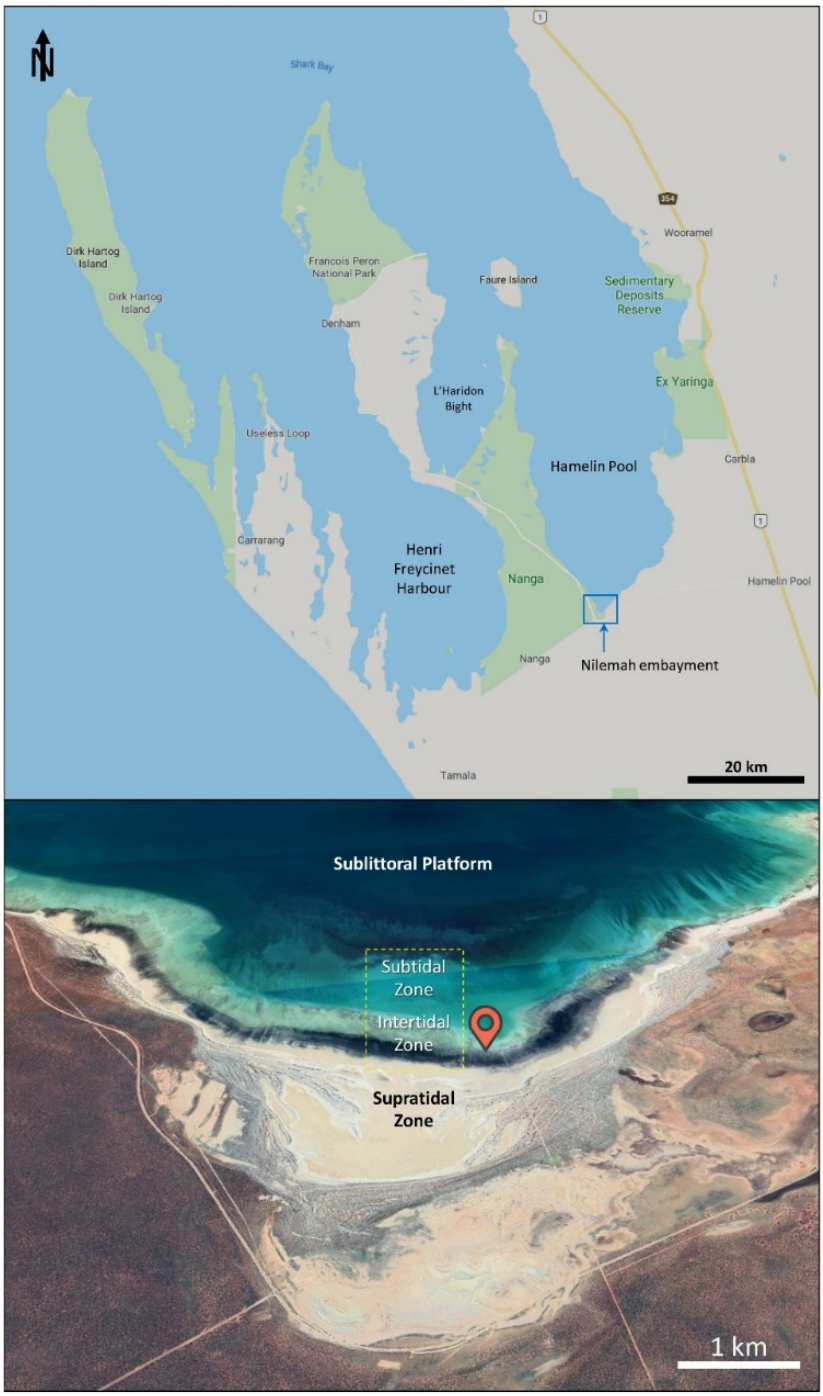

Figure 4.1. Shark Bay region, showing Nilemah embayment (blue square) (top). Image of Nilemah embayment (close up) and their tidal zones (bottom). Source: Google Maps.

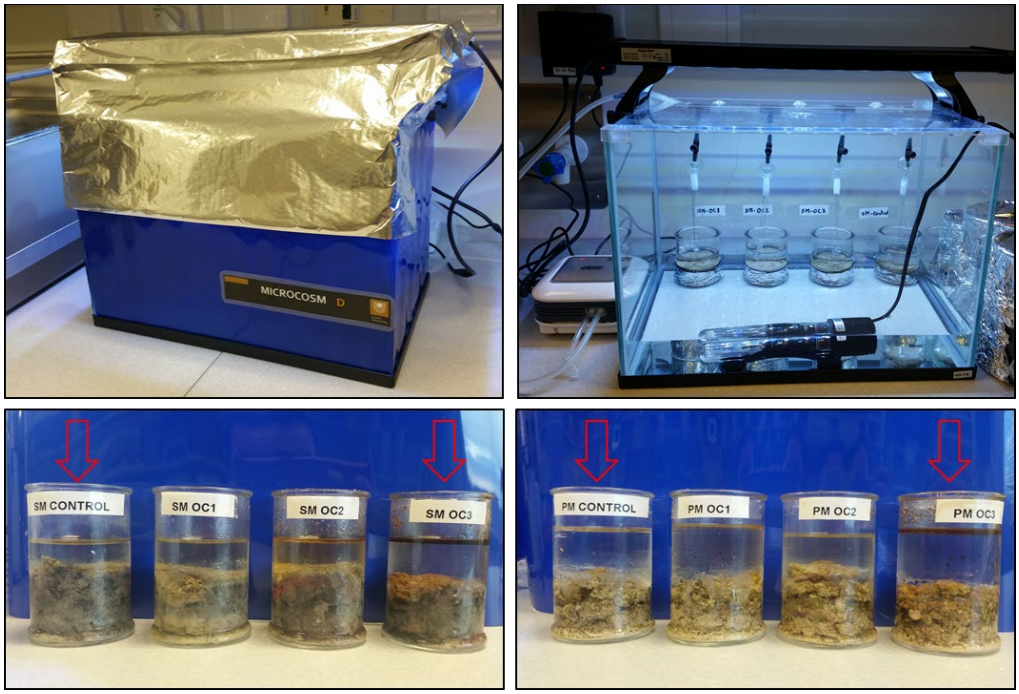

Figure 4.2. Incubation tank assemblage for simulating ecosystem conditions following design from **Chapter 2** (top images). Images showing smooth (left bottom) and pustular (right bottom) mat microcosms subjected to chronic PE incubation for 10 days and maintained under lab-conditions up to 1 year.

4.3.2. Molecular microbial ecology

The same approach used to study microbial community responses to the short-term PE is comparable to the parallel long-term PE experiment, which has been described in detail elsewhere (**Chapter 2**; **Figure A4.3**). Briefly, DNA and RNA were extracted simultaneously from 0.2 g of mat material using the RNeasy PowerSoil total RNA isolation kit and DNA elution Accessory kit QIAGEN, Chadstone Centre, Victoria, Australia). Complementary DNA (cDNA) was generated from extracted RNA samples using Photoscript II Reverse Transcriptase (New England Biolabs, MA, USA). Bacterial and archaeal 16S rRNA genes were PCR amplified from genomic DNA vs. cDNA samples using universal U519fM and U803R primers (Caporaso et al., 2012). Both amplified DNA and cDNA were barcoded and equimolar amounts were pooled (Caporaso et al., 2012). This library was gel-purified and sequenced using a MiSeq Illumina instrument at the Australian Genomic Research Facility (AGRF). AGRF's Illumina bcl2fastq 2.20.0.422 pipeline was applied to the sequenced data and Amplicon Sequence Variant (ASV) abundance per sample was calculated using the

Quantitative Insights into Microbial Ecology 2 (QIIME 2) pipeline (version 2019.10) (Bolyen et al., 2019) as described in detail previously (**Chapter 2**).

4.3.3. Statistical analysis

The biostatistical approaches used to analyse the data have been described in detail in **Chapter 2**. In brief, alpha diversity analysis – at species level – was performed by rarefaction curves using Vegan package in R (Oksanen et al., 2010). [37]Shannon, Faith's PD, observed OTUs, and Pielou's evenness were used to calculate community richness and evenness. Principal Component Analysis (PCA) was generated using the R package MicOmics (Cao et al., 2016) to compare the microbial beta diversity between the samples [38]. MixOmics was also used to create loading plots to determine the highest contribution of variables to the identified clusters (initial vs. PE) (Cao et al., 2016). Where possible, these results were amended with Indicator Species Analysis (ISA) using the IndicSpecies package in R (v. 1.7.8) (Cáceres and Legendre, 2009), to identify taxa that were significantly influenced by PE.

4.3.4. Functional metabolic prediction

The relative abundance of bacterial and archaeal functional gene families of control vs. PE subsamples were predicted from the 16S rRNA genes and transcripts using PICRUSt2 (Phylogenetic Investigation of Communities by Reconstruction of Unobserved States), version 2.3.0. Two datafiles obtained from the QIIME2 pipeline were used as input for PICRUSt2: representative sequences (after removal of singletons) and features tables (after denoising step using DADA2) (Louca and Doebeli, 2018; Barbera et al., 2019; Douglas et al., 2019; Czech et al., 2020). For the purpose of this research, two output files were assessed: KEGG (Kyoto Encyclopedia of Genes and Genomes) orthologs (KO) metagenomes to predict gene functions (Kanehisa et al., 2012, 2014) and Weighted Nearest-Sequenced Taxon Index (NSTI) values to estimate the accuracy of the predictions (Langille et al., 2013; Douglas et al., 2019). Gene predications with NSTI values >2 are considered to be not significant and are automatically discarded by the algorithm. Only samples with NSTI values less than 0.15 are included in the output file (KEGG metagenome). Ideally, values below 0.06

[37] Using https://view.qiime2.org/
[38] Using http://mixomics.org/mixmc (MC framework)

are projected to be highly represented in the reference genomic databases (80-85%) (Langille et al., 2013). PCA was performed in MixOmics to explore functional betadiversity. MixOmics was also used to generate Correlation Circle (CC) plots to identify predicted genes (*i.e.,* KOs) that were positively or negatively correlated with PE. Due to the small number of samples with a good range of NSTI values for each type of microbial mats (*i.e.*, 4 samples), results were only assessed into Level 3 of KEGG Brite Hierarchy[39]. Heatmaps were used to represent the main differences between initial (T0) and the maximum time of incubation (T1y).

4.4. Results

4.4.1. Microbial community richness and diversity

A total of 608 ASVs were identified using the QIIME2 pipeline. 99.6% corresponded to bacteria and 0.4% to archaea. 66.6% of those identified ASVs belonged to family, genus and species levels. According to the plateauing rarefaction curves, the sequence depth was sufficient to cover most of the bacterial and archaeal diversity (**Figure A4.4**). The Shannon index of the active microbial communities in both smooth and pustular mat control samples varied between 6.9 and 9.1. The Shannon index varied between 3.7 and 9.1 in PE mat samples (**Figure 4.3**), with the lowest diversity (as number of ASVs) after one year of incubation (T1y). The reduced diversity was more severe in the pustular mat samples, with a net loss of ASVs of more than 80%, recorded after 10 days of PE with no sign of recovery after 1 year (**Figure 4.4**). Unfortunately, the RNA sample from the smooth mat at 10 days of incubation (T10) was lost and a parallel comparison of the active cDNA community with the pustular mat was not possible. However, based on the results shown in **Figure 4.5** we do not expect major differences in diversity between the missing cDNA and the available parallel DNA sample of this time point (T10). Therefore, it can be inferred that the loss in diversity in the smooth mat microbiome was not as drastic as that of the pustular mats at day 10 of PE. However, after one year of incubation with only trace amounts of petroleum present, the smooth mat only lost 35% of the total ASVs that were initially present,

[39] https://www.genome.jp/kegg/kegg3b.html

while the pustular mat lost ~85% of ASVs. Faith's PD richness and observed OTUs metrics displayed the same trends (**Figure A4.5**).

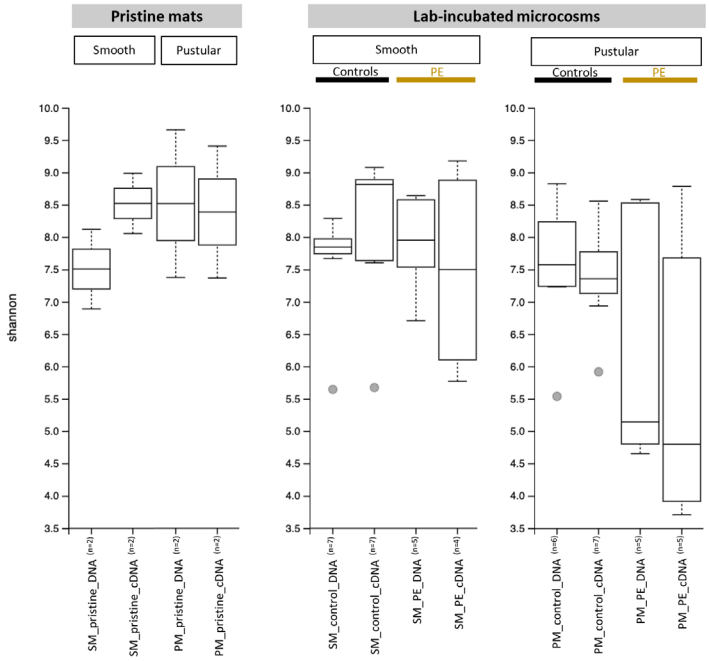

Figure 4.3. Boxplots of Shannon index computed in QIIME2 including DNA and cDNA datasets of pristine mats (**Chapter 2**), background controls, and PE mats (including T1, T5, T10 and T1y). Centre line in the boxplot represent the median, while box limits indicate 25th and 75th percentiles. Boxplot whiskers represent 9th and 91st percentiles and outlier values are represented as grey points. Data of both smooth and pustular pristine samples was taken from **Chapter 2**.

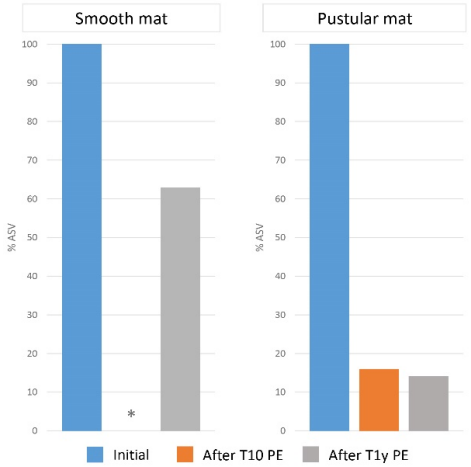

Figure 4.4. Bar plots showing net loss of active taxa (cDNA) (as % ASV) when exposed to petroleum for both smooth (left) and pustular mats (right). (*) Missing data for smooth mat at 10 days of PE.

4.4.2. Microbial composition changes upon petroleum exposure

PCA was performed to analyse the differences in microbial communities between controls and petroleum-exposed smooth and pustular mat samples during the time-series incubation experiment (**Figure 4.6**). PCA revealed that the control samples of the smooth mat shared between 60 and 80% of similarity over the course of incubation, *i.e.,* from day 0 (T0) to 1 year (T1y). These lab controls also clustered with the initial and first three time points after PE (T1, T5 and T10) (**Figure 4.6**, top), with no major changes in their dominant taxa (**Figure A4.9** and **Figure A4.10**). The active (RNA-based) microbial composition in these (control) closely grouping samples was dominated by Proteobacteria (26.2-38.6%) and Bacteroidetes (11.0-17.3%), followed by Spirochaetes, Cyanobacteria, Chloroflexi, and Planctomycetes (**Figure A4.6, Table A4.1** and **Table A4.2**). In contrast, after 1 year of incubation with trace levels of petroleum left in the smooth mat (T1y) (**Figure 4.6**, top), Cyanobacteria (class Synechococcophycideae) (52.3%) predominated over Proteobacteria (25.4%) (**Figure 4.5**). During this period, Deltaproteobacteria were replaced by Gammaproteobacteria while Alphaproteobacteria remained the most abundant class of Proteobacteria in the PE smooth mat. In addition, part of the original taxonomical groups (*i.e.*, Bacteroidetes, Planctomycetes, Spirochaetes, *etc*.) was preserved in the smooth mat (**Table A4.3** and **Table A4.4**).

In contrast, pustular mat control samples only exhibited a high level of similarity ~ 80% during the first 10 days of PE (**Figure 4.6**, bottom). These samples were dominated by Proteobacteria (34.4-35.6%) (mainly Alpha- and Deltaproteobacteria), and Cyanobacteria (class Synechococcophycideae) (12.5-18.6%) (**Figure A4.6**). After 1 year of incubation in the control without PE, the pustular mat revealed an increase in the relative abundance of Cyanobacteria (class Synechococcophycideae) (41.8%), while Alpha- and Deltaproteobacteria became the second most abundant classes (**Table A4.5** and **Table A4.6**). PE caused drastic changes to the pustular mat microbiome (relative to the controls) already had occurred after 10 days of exposure after which the petroleum contaminant was removed, without further significant changes one year later (**Figure 4.6**, bottom). Cyanobacteria (class Synechococcophycideae) and Proteobacteria (classes Alpha- and

Gammaproteobacteria) became the only two detectable phyla at T1y (**Table A4.7** and **Table A4.8**).

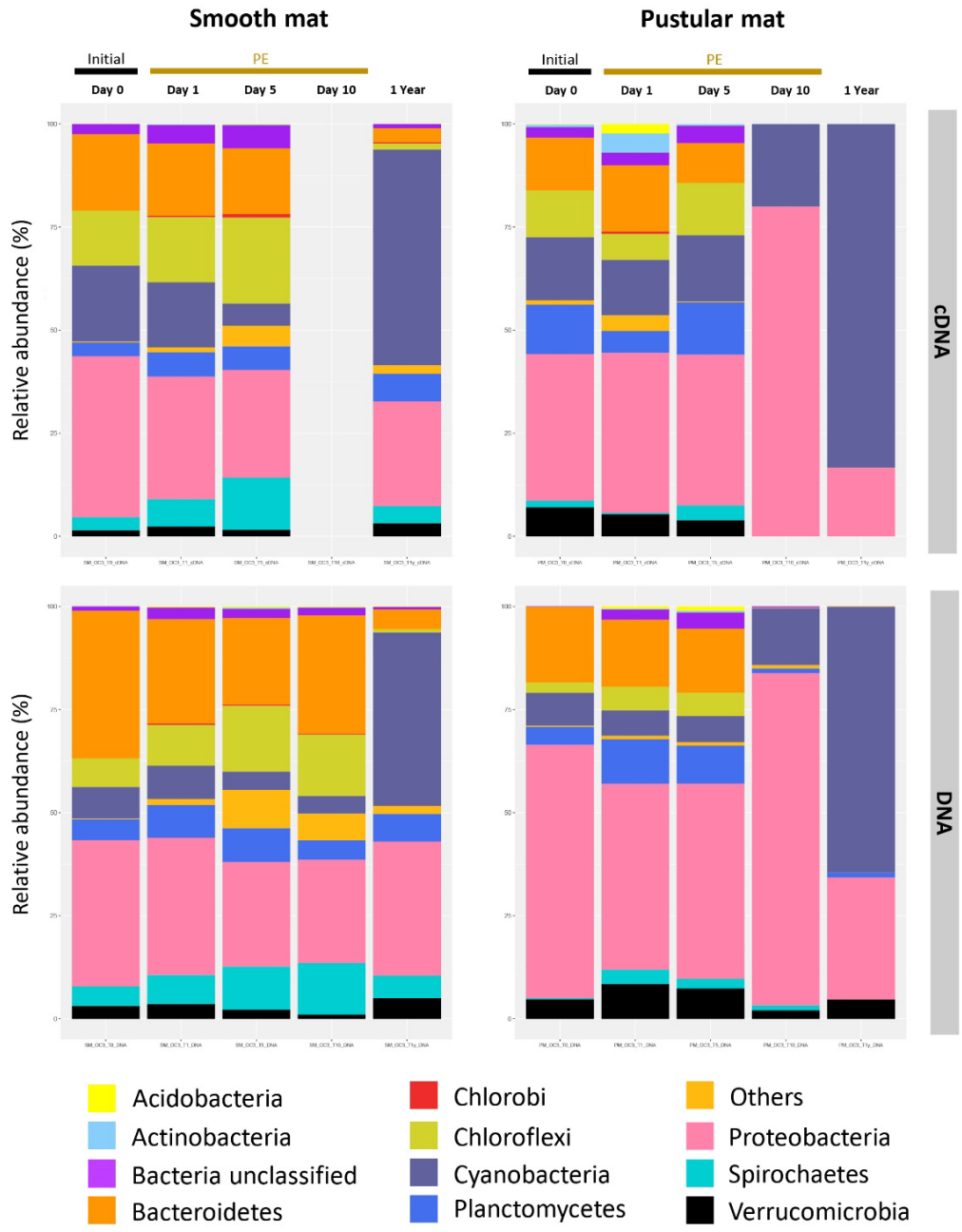

Figure 4.5. Relative abundance of the total (DNA) and active (cDNA) bacterial microbiomes at phylum level, comparing initial microbial communities (Initial – T0) to those evolved after 1 day (T1), 5 days (T5) and 10 days (T10) of PE, and then after 1 year under fresh seawater (T1y) in both smooth (left) and pustular (right) microbial mats microcosms. Smooth mat PE sub-sample at T10 (cDNA) was lost and could not be repeated.

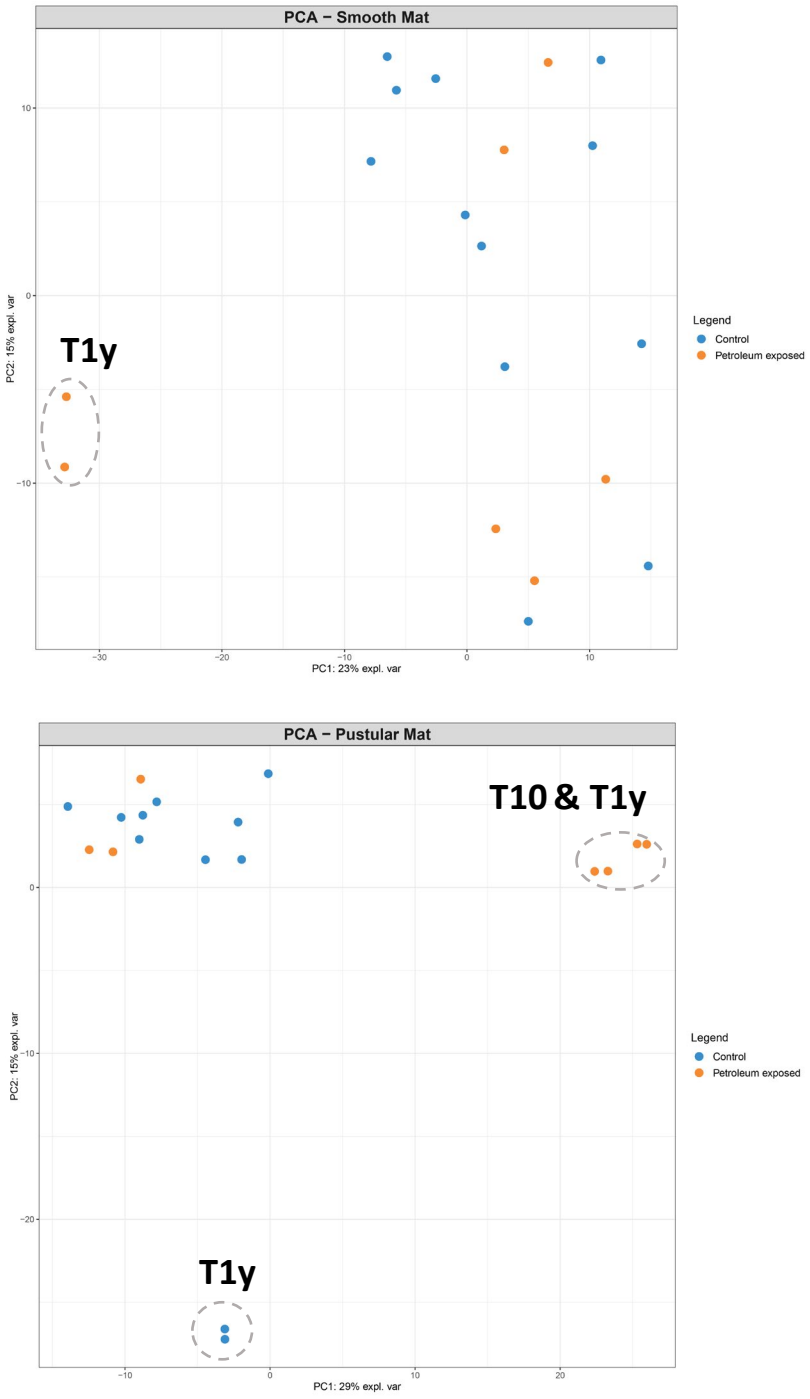

Figure 4.6. PCA (Principal Component Analysis) plots showing microbiome shifts in petroleum incubated experiments in smooth (top) and pustular mats (bottom) microcosms.

Analysis of the microbial composition at species level revealed which members were unaffected (°) over the course of PE as well as those that were positively (+) or negatively affected (-). After 5 days of acute PE, three key species that were not present in the initial samples were detected in the smooth mat (*i.e.*, the genera KSA1 and *Halomonas*, and *Acinetobacter radioresistens*, **Figure 4.7**). One year after the majority of petroleum was removed from the smooth mat, the microbiome revealed a shift towards: (1) a predominance of the cyanobacterium *Halomicronema excentricum* (+); (2) the emergence of certain indicator species, e.g. *Spirochaeta halophila*, *Haliea mediterranea, Marinobacter bryozoorum*, *KSA1*, *Rhodovibrio*, and *Alcanivorax* (+) (**Figure 4.8**); (3) the loss of a wide range of taxonomical groups, e.g. GN02, GN04, Chloroflexi, Crenarchaeota, Deltaproteobacteria, *etc* (-) (**Figure 4.7**); and (4) unaffected members of the microbiome, which interestingly belong to many unclassified classes, orders or families (°).

During the first 10 days of PE, pustular mats revealed a more severe loss (-) in microbial diversity at the species level compared to smooth mats (**Figure 4.9**). Unclassified Alphaproteobacteria dominated the microbial composition, followed by *Halomicronema excentricum* (+). Both loading plots and ISA revealed the presence of species usually associated with hydrocarbon degradation (*i.e.*, *Rhodovibrio*, *Alteromonadaceae*, *Marinobacter bryozoorum*, *Halomonas, etc*) (+). In contrast to petroleum-exposed smooth mat, there were only a few species that remained unaffected (°), which belonged to Rhodobacteraceae, Hyphomicrobiaceae and the class Oscillatoriophycideae. After a recovery lapse of 1 year, the active microbiome was composed of only 15 species (**Figure 4.9**).

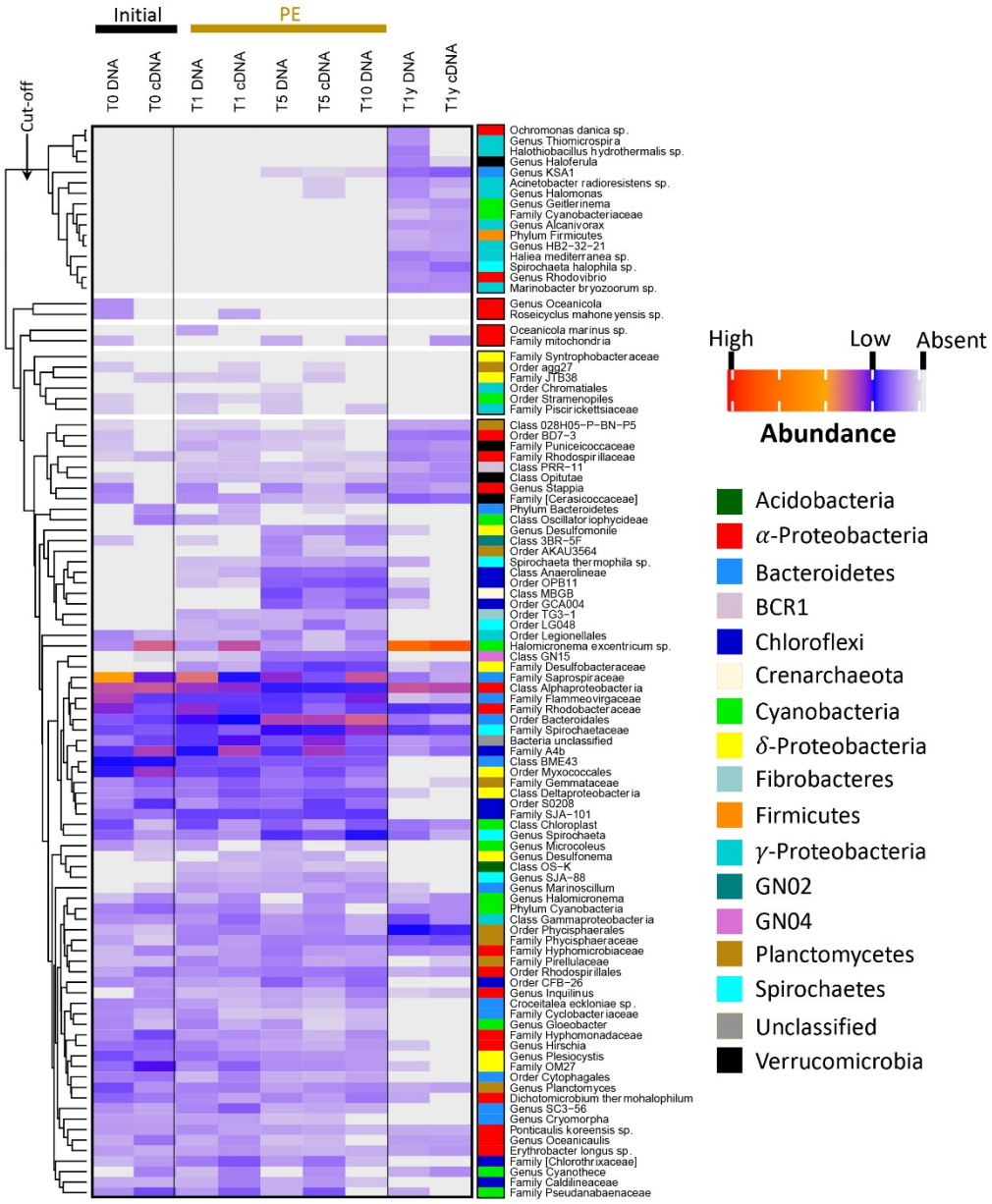

Figure 4.7. Heatmap plot depicting smooth mat microbiome shifts in a time-series petroleum incubated experiment (microcosm SMOC3). The right column shows phylum or class taxonomy (legend on the right). Data displayed correspond to raw reads at species level standardised by total, square root transformed, and then, ranked the 70 more abundant organisms (**).

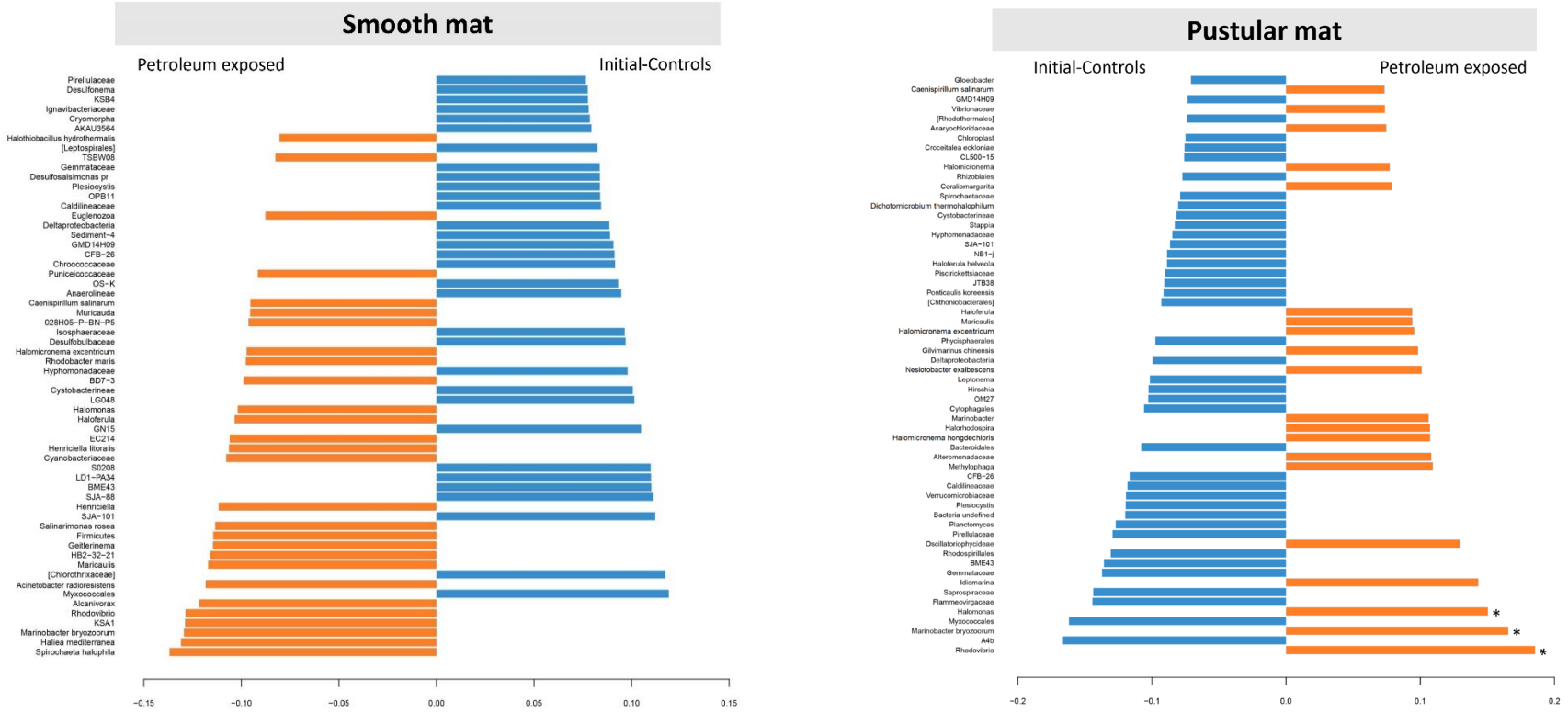

Figure 4.8. Loading plots showing the first 60 species for initial (blue) vs. PE exposed (orange) taxa in both mat types, which strongly influence principal component 1 (PC1) in the PCA plots of Figure 6. This analysis is based on the communities residing in both DNA and RNA pools. Note the highly weighted species are correlated with previously indicator species detected by ISA. This analysis was used to identify additional indicator organisms associated with degradation of hydrocarbons

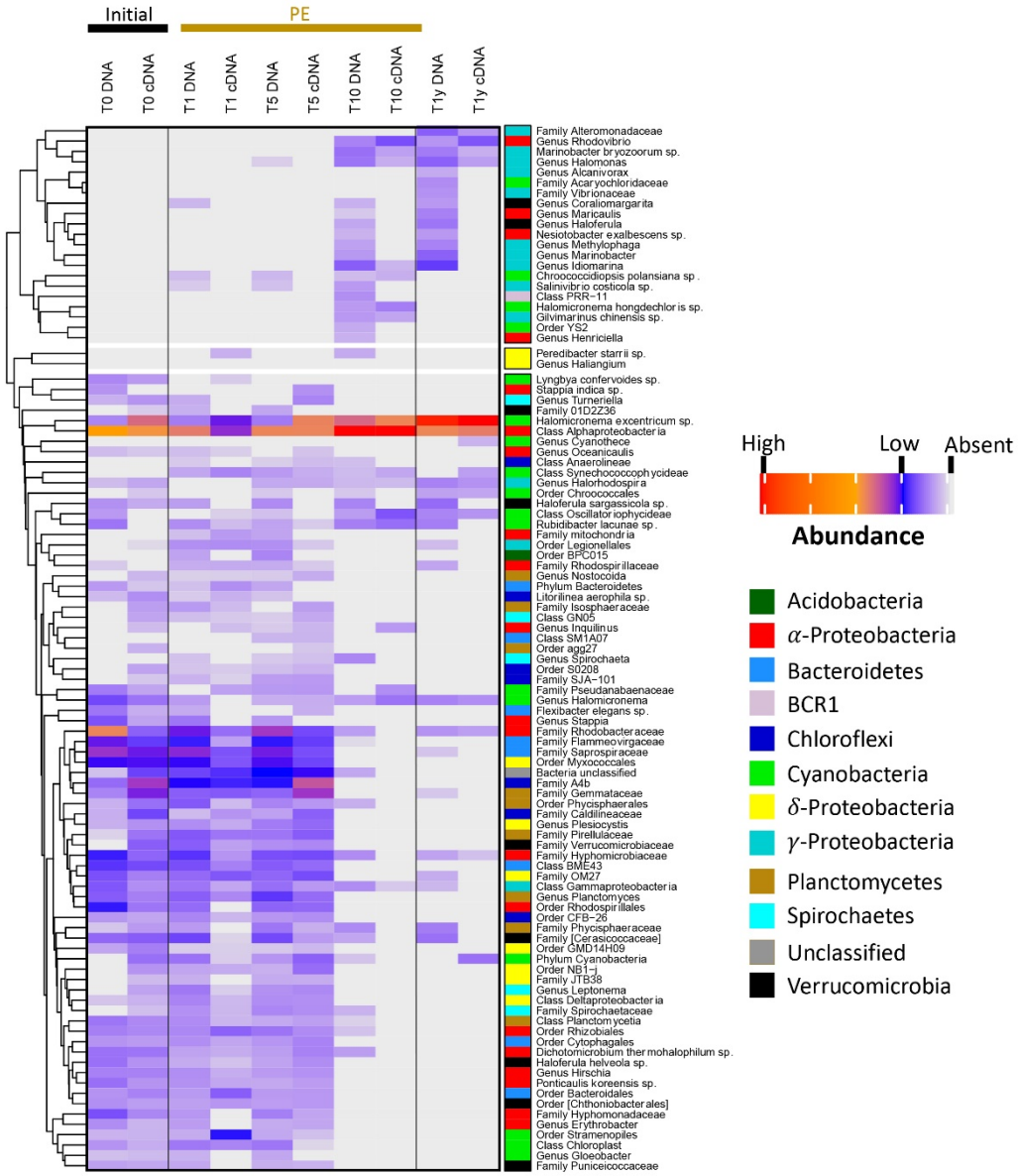

Figure 4.9. Heatmap plot depicting pustular mat microbiome shifts in a time-series petroleum-exposed incubation experiment (microcosm PM OC3). The right column shows phylum or class taxonomy (legend on the right). (**)

4.4.3. Predicted functional responses to petroleum exposure

Functional genes were predicted only from initial (T0) vs. one year (T1y) incubated smooth vs. pustular mat samples, during which the most drastic changes in microbial communities occurred. PICRUSt2 analysis resulted in 5,051 and 4,939 predicted KOs in the smooth and pustular mat microbiomes, respectively. NSTI values are reported in **Table A4.9** and **Table A4.10**. PCA showed that the predicted gene functions in both mat types formed distinct groups between initials and after one year of incubation (**Figure A4.7** and **Figure A4.8**, top). The CC plot with a cut-off set at 0.9 (**Figure A4.7** and **Figure A4.8**, bottom) retrieved a total of 493 and 733 predicted functions (KOs) responsible for the major differences explained by PC1 in respectively smooth and pustular mats. These KOs represented 140 functional (KEGG) pathways for each mat type. The identified pathways were then collapsed to level 3 categories and visualised by heatmaps (**Figure 4.10** and **Figure 4.11**). Due to the small number of samples analysed it was not possible to perform statistical analyses (*i.e.*, ANOVA) to determine with certainty which metabolisms were significantly different between the two sampling time points.

The predicted functional response of both smooth and pustular mats exhibited some metabolic pathways in common (**Figure 4.10** and **Figure 4.11**). Pathways related to environmental information processing (*i.e.*, ABC transporters and Two-component system), cellular processes (particularly biofilm formation), nitrogen metabolism and biosynthesis of secondary metabolites appears to be more abundant under PE conditions in both mat types at T1y. Conversely, smooth- and pustular mats differed in their dominant energy metabolisms. For example, photosynthesis (including antenna protein pathways) and porphyrin and chlorophyll metabolism were predominantly abundant in pustular mats (T1y), while methane metabolism was more pronounced in the smooth mat (T1y). In addition, PICRUSt2 predicted an increase in the relative abundance of genes involved in the degradation of xenobiotics at T1y, especially in the smooth mat (**Figure 4.10**).

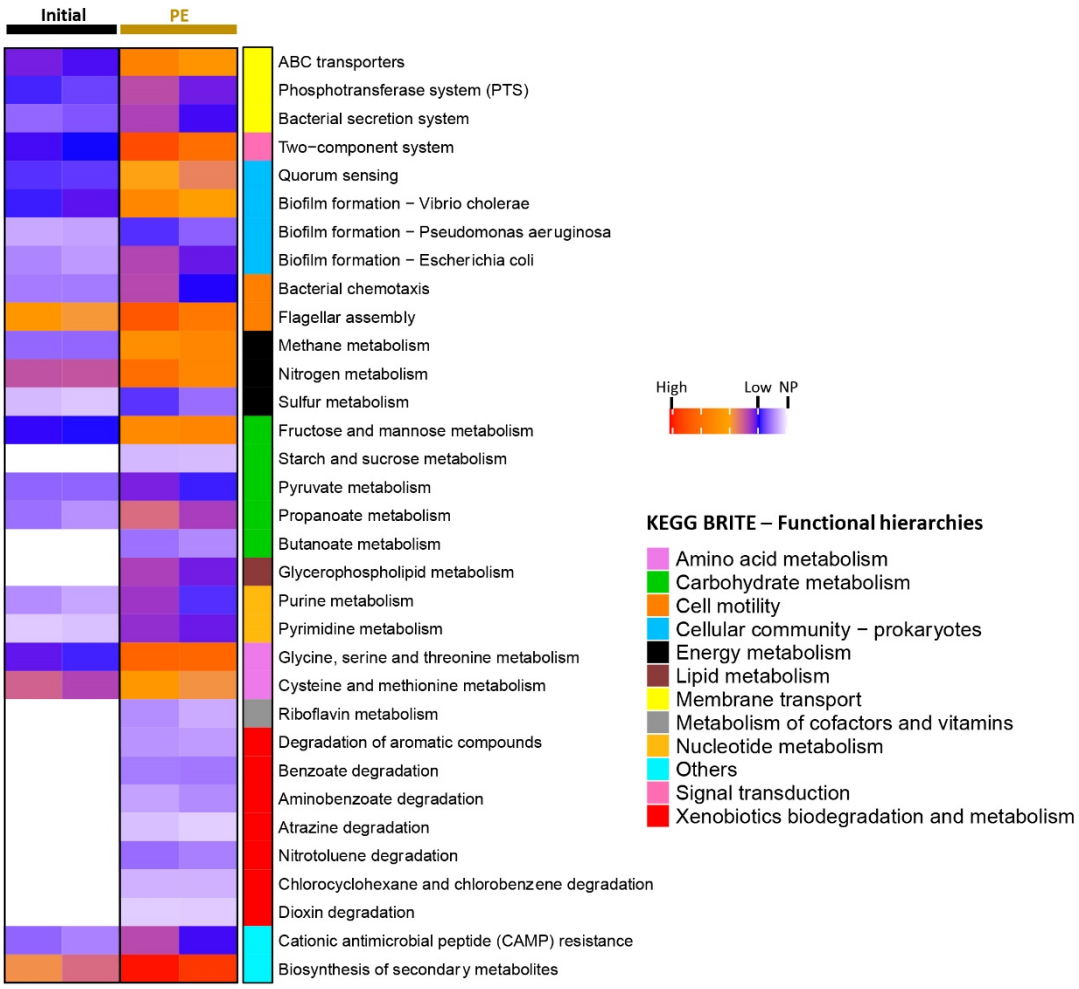

Figure 4.10. Heatmap showing the relative abundance of predicted KO metabolic pathways (level 3) between initial (T0) and one year after the petroleum contaminant was removed (smooth mat; SM OC3 microcosm). Based on PICRUSt2 functional prediction from 16S rRNA data (DNA and cDNA), using KOs responsible for the highest difference between the groups (mainly PC1 in PCA plot - **Figure A4.7**). Data displayed correspond to raw abundance of KOs standardised by total and square root transformed.

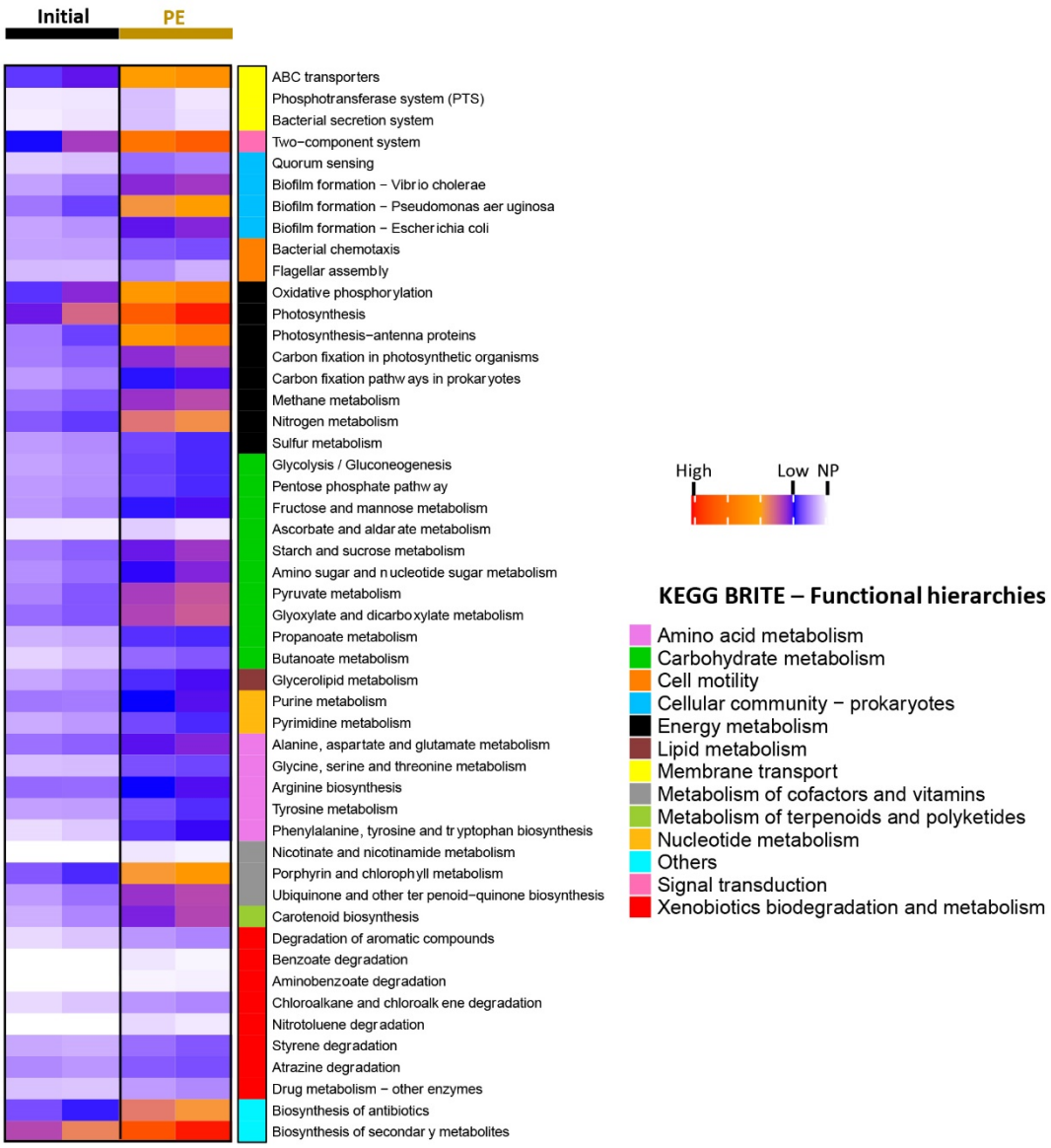

Figure 4.11. Heatmap showing the relative abundance of predicted KO metabolic pathways (level 3) between initial (T0) and one year after the petroleum contaminant was removed (pustular mat; PM OC3 microcosm). Based on PICRUSt2 functional prediction from 16S rRNA data (DNA and cDNA), using KOs responsible for the highest difference between the groups (mainly PC1 in PCA plot - **Figure A4.8**). Data displayed correspond to raw abundance of KOs standardised by total and square root transformed.

4.5. Discussion

Both press (**Chapter 2** and **Chapter 3**) and pulse disturbance experiments (this study) showed that smooth and pustular microbial mat microbiomes from Shark Bay responded in a comparable way to PE. Three critical responses were identified, which will be discussed in detail below: microbial diversity loss as an indicator of resistance and resilience, microbial succession, and an increase in the relative abundance of predicted genes associated with stress conditions and degradation of xenobiotics.

4.5.1. Resistance and resilience of microbial mats from Shark Bay

Our results showed that both pulse- (this Chapter) and press petroleum disturbances (**Chapter 2**) caused a decline in microbial diversity. This loss in microbial diversity increased with time of exposure. Here, we developed a conceptual model to illustrate the resilience and resistance of the smooth and pustular microbial mat communities to PE (**Figure 4.12**). As suggested by Shade et al. (2012), the use of a diversity metric can be applied to assess the stability of the microbial communities subjected to chemical and physical disturbances. We have used the total number of ASV (in %) to evaluate microbial diversity shifts caused by PE. This approach reveals the net change in emerging species that could compensate for the loss of negatively impacted taxa but fails to conceal to what extent the microbial communities returned to the original composition.

For example, the press-disturbed smooth mat microbiome remained largely unaffected during the first 30 days of PE, whereas 70% of the microbial diversity was lost after 4 months of PE (**Chapter 2**) (**Figure 4.12**, panel a-c). In the current pulse disturbance experiment we found that the microbial communities during the first 10 days of PE did not change substantially in the smooth mat. However, the net loss in diversity was only 30% after one year of recovery (**Figure 4.12**, panel d). This shows that the smooth mat microbiome is more resistant to pulse/short-term (~10 days) than press/long-term disturbances (> 30 days). Moreover, they are likely more resilient when exposed to pulse petroleum contaminations than press disturbance. Due to the lack of sampled and analysed time points after the pulse disturbance, it is possible that the microbial diversity would have decreased further (dotted red path with question mark) during the one-year recovery period.

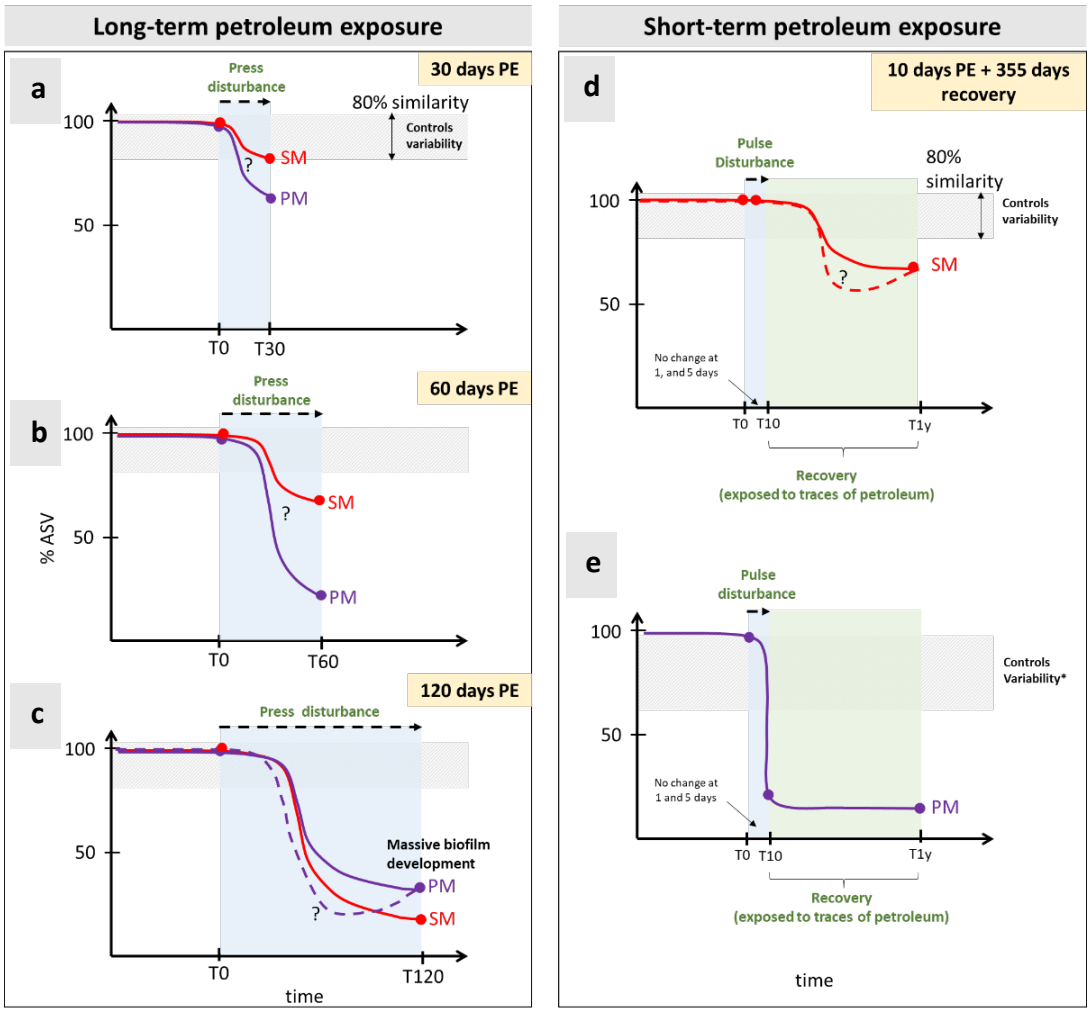

Figure 4.12. Conceptual model of temporal variance of PE smooth and pustular microbial mat communities (% ASVs), to estimate their ecological resistance and resilience to press and pulse disturbances. Red and purple closed circles represent actual data points from lab-controlled incubations discussed in **Chapter 2** and the current study. Dotted lines and question marks refer to uncertainties in the path due to a lack of additional sampled and analysed time points.

In contrast, microbial communities of pustular mats have shown to be highly vulnerable to either pulse or press petroleum disturbances. In Chapter 2, it was found the pustular mats subjected to long-term PE rapidly lost over 33% of its diversity at 30 days of PE and 67% at 60 days (**Figure 4.12**, panel a-c). In one of the pustular mat microcosms, petroleum contamination previously promoted the development of a thick biofilm after 100 days of PE. This caused a net increase in low abundance taxa and in microbial diversity, but the original microbial composition did not recover over the total course of incubation (120 days) (**Chapter 2**). In our current study, we already

detected a sharper drop in the microbial diversity in the pustular mat as soon as 10 days after exposure, which did not improve after one year of recovery (**Figure 4.12**, panel e). Since both pulse and press disturbances resulted in abrupt and rapid microbial diversity declines, the pustular mat microbiome is neither resilient nor resistant these types of disturbances.

When examining the literature, it is difficult to compare our results with other studies in terms of 'ecological' resilience and resistance due to the lack of systematic studies in similar habitats and conditions. Even though environmental disturbances are expected to cause a decline in microbial diversity (Bell et al., 2013; MacDougall et al., 2013), it is most likely incorrect to state that microbiomes are equally vulnerable to both short- and long-term disturbances (Shade et al., 2012a) since the way microbial ecosystems respond to disturbances is highly complex and depends on a variety of factors. For example, the microfabric of the smooth mat possesses a millimetric lamination, and a high proportion of low porosity micrite, which reduces the permeability and infiltration of petroleum contaminant (**Chapter 2**). In contrast, the pustular mat is highly sandy and permeable, which would explain the more severe response of the pustular mat microbiome to pulse petroleum disturbance compared to the better protected smooth mat microbiome.

The insurance hypothesis or buffer effect has been widely accepted between ecologists as a guaranty of recovery and resistance when facing a disturbance (Yachi and Loreau, 1999; Shanafelt et al., 2015). It assumes that multiple species with functional redundancies are present in a biologically diverse ecosystem and that this ecosystem will likely be able to maintain its overall functioning even in case not all species survived a disturbance (Yachi and Loreau, 1999). However, according to the results of this study along with **Chapter 2**, the high microbial diversity in the studied Shark Bay microbial mats was not a guarantee for microbial resilience and resistance. Namely, differences in the type of microfabric might also have contributed to the increased stability of the mat microbiome to PE.

Another factor associated with the microfabric that might have contributed to the increased resistance and resilience of the smooth mat microbiome to PE may be related to a concept known as 'landscape connectivity'. Landscape connectivity traditionally describes the movement of biotic and abiotic resources in a landscape or patches but

can also be applied to the assessment of the stability of environmental microbial communities (Standish et al., 2014; Shackelford et al., 2018). The arrangement or configuration of the biotic and abiotic elements is crucial for recovery, especially when there are nursery (or unaffected) patches to prevent a total collapse of the microbial ecosystem (Shackelford et al., 2018). Mobile bacteria that were negatively affected by the petroleum contamination in our time series experiment may have been able to move through the microfabric and hide in non-contaminated spaces for survival, while the growth of hydrocarbon-degrading taxa contributed to the simultaneous detoxification of contaminated patches.

4.5.2. Microbial succession upon petroleum exposure

The impact of short-term (this study) and long-term (**Chapter 2**) petroleum disturbances resulted in a succession of similar microbial composition and abundance in both smooth and pustular mat over time, regardless of the chemical differences of the petroleum used as contaminants during the lab-incubation experiments. In **Chapter 2**, we utilised a petroleum enriched in *n*-alkanes, which is thought to be easily biodegradable, while in this study we subjected the mats to an already biodegraded petroleum that was depleted in *n*-alkanes and rich in aromatic compounds (**Figure A4.1**). The similarity in microbial community composition in mats exposed with degraded *vs*. undegraded petroleum are remarkably consistent even at species level (**Figure A4.9** and **Figure A4.10**): (1) the cyanobacterium, *Halomicronema excentricum* (+), became the more abundant species, especially during the longest periods of PE in both smooth and pustular mats (T120 and T1y); (2) Unclassified Alphaproteobacteria phyla (+) and Rhodobacteraceae (*) were either highly abundant or unaffected under PE; and (3) low-abundance microorganisms, mostly related to known hydrocarbon degraders emerged in both mat types, under both pulse- and press disturbances and irrespective of the level of degradation of the petroleum contaminant: *Halomonas* spp., *Marinobacter bryozoorum* and Alteromonadaceae (Gammaproteobacteria). Their capacity of biodegrading petroleum has been widely demonstrated (McGenity, 2010; McGenity et al., 2012; Dang and Lovell, 2016; Edbeib et al., 2016). These bacteria have been found in petroleum polluted hypersaline microbial mat habitats (Bordenave et al., 2007) and were previously cultivated from pristine mats from Shark Bay (Allen et al., 2009; Charlesworth et al., 2019). Several

other microorganisms were preferentially identified in smooth or pustular mats and are summarised in **Figure 4.13**.

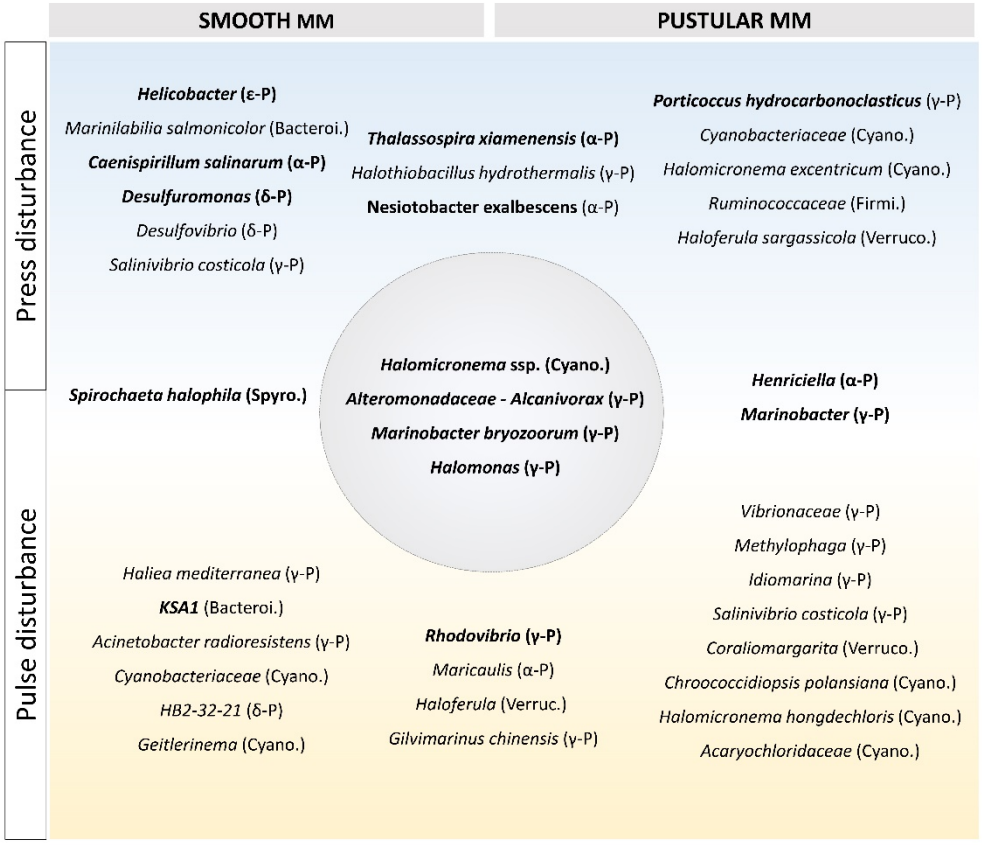

Figure 4.13. Bacterial taxa that prevailed mainly in both types of microbial mat and irrespective of the level of degradation of the petroleum pollutant used. Bold text: bacteria that were consistently identified in both DNA and RNA pools over the course of the incubation experiment.

The pulse disturbance resulted in the development of additional low abundant hydrocarbon-degraders that were not identified previously (Chapter 2). These new organisms might be the result of the differences in the chemical compositions between the petroleum used as a pollutant for pulse and press disturbance experiments. In petroleum-exposed smooth mats (T1y) *Haliea mediterranea, Acinetobacter radioresistens*, *HB2-32-21, Rhodovibrio*, and *KSA1* were members of the active microbial community (cDNA). *Haliea* contains species that can degrade propane, propylene, ethylene, and ethane (Lucena et al., 2010; Suzuki et al., 2012). *Acinetobacter radioresistens* can instead degrade alkanes or aromatic compounds, like

phenanthrene and fluorene (Desouky, 2003; Méndez et al., 2017), and is known for producing emulsifiers that facilitate the initiation of biodegradation of hydrocarbons (Rosenberg et al., 1999). Another interesting finding was the presence of the genus *KSA1*, which has previously been found in soil samples near buried leaking petroleum-pipelines (Su et al., 2019). After ten days of exposure to the degraded petroleum, pustular mats also exhibited lower abundance bacteria associated with petroleum biodegradation, such as *Idiomarina* known to be capable of degrading phenanthrene (Dastgheib et al., 2012) .

4.5.3. Adaptive functional microbial responses to degraded petroleum exposure

One year after most of the petroleum was removed, the pulse disturbed smooth mat still contained active bacteria with predicted genes involved in similar stress adaptation mechanisms as those observed in the smooth mat that was continuously petroleum-exposed for 120 days (**Chapter 3**; **Figure 4.10**). This suggests that one year after exposure to trace amounts of petroleum, the smooth mat microbiome still harboured an active complex network of regulatory systems, such as: ABC transporters, two-component systems, quorum sensing, biofilm formation, flagellar assembly, and biosynthesis of secondary metabolites, as a response to the initial disturbance. The T1y smooth mat also contained predicted pathways associated with hydrocarbon degradation (*e.g.* benzoate, nitrotoluene degradation), and osmoregulation as an adaptation mechanisms to be able to thrive under the prevailing hypersaline conditions (*e.g.* glycine, serine and threonine metabolism; **Figure 4.10**). Comparable microbial mechanisms have been reported in petroleum polluted microbial mats in non-hypersaline environments (Dombrowski et al., 2016; Vasconcellos et al., 2017; Aubé et al., 2020). Although our results along with the findings from **Chapter 3** demonstrated that the smooth mat microbiome contains a degree of functional resistance to long-term PE, it remains to be investigated if they are functionally resilient.

4.5.4. Limitations and suggested improvements: experimental design and sampling

This pilot experimental study allowed us to assess the complexities of simulating a PE under lab-conditions, in term of sample-size constraints and sampling schedule. Since

Shark Bay region is a protected World Heritage site, it was not possible to collect a large number of samples for experimentation. This imposed a sample-size limitation for the design of the experiments, and the sampling schedule needed careful consideration. We were restricted to using small capacity microcosms (approx. 250 mL), yielding a small petroleum-exposed surface area of only 15 cm^2 available for subsampling. A surface area of 1 cm^2 (0.5 cm deep) could be subsampled during maximal five time points without compromising the entire petroleum contaminated surface area. This also compromised the possibility to analyse biological replicates for the assessment of spatial variability in the microbial community composition and predicted functions. Nevertheless, using the same microcosm set-up we observed comparable and consistent trends in microbial community responses between the previous press (**Chapter 2**) *vs*. pulse disturbed smooth and pustular microbial mats from Nilemah Bay. A comparison between those types of experiment can be found in the appendix, *i.e.,* **Figure A4.9** and **Figure A4.10**.

4.6. Conclusions

This study suggests that the microfabric in smooth mat provides a landscape connectivity habitat that enables selected members of the smooth mat microbiome to be more resistant to both pulse and press disturbances and is likely to be more resilient when exposed to short-term hydrocarbon contamination compared to the microbiome of the sandy pustular mats. The pustular mat microbiome was neither resistant nor resilient to both pulse and press disturbances and is therefore considered highly vulnerable to acute PE.

Although the functional responses of both smooth and pustular mats were also analysed and compared (pulse vs. press), due to it was performed using a predictive bioinformatic tool (*i.e.,* PICRUSt2), we can only infer that both microbiome would likely activate a variety of stress responses mechanisms, including degradation of hydrocarbons. In consequence, they might exhibit some degree of resistance.

The results of this preliminary study form the basis for a follow up experiment where functional metatranscriptomes will be mapped to metagenome assembled genomes (MAGs). This will provide a holistic overview of expressed genes and pathways of the key players in these microbial mats under pulse vs. press disturbed conditions. It is also suggested to further investigate how the differences in the petroleum used as a

pollutant could influence the microbial composition in both pulse and press disturbance experiment under the same conditions and PE times. It might be also beneficial to extent the period of petroleum incubation to likely increase the possibility of biodegradation.

4.7. Funding

This study was supported by Woodside and ARC DP (DP150010223) and Australian Research Council (#LP150100341).

4.8. Acknowledgements

We thanks to Bush Heritage and Western Australia Department of Parks and Wildlife for their support during the fieldtrip as well as issuing the permit to collect some samples in Nilemah embayment, respectively. The main author thanks Curtin University for awarding a Curtin International Postgraduate Research Scholarship (CIPRS). Furthermore, we thanks to WA-OIGC and TIGeR Institute and all their technical and financial assistance. We also appreciate the collaboration of Matthew Campbell, Darcy Jack Greenwood and Paul Greenwood during the sample collection, and Peter Hopper and Dr. Alex Holman (WA-OIGC) for the support in the lab.

4.9. Data accessibility

Raw reads datasets generated for this research can be found in "Shark_Bay_PE_Short_Term_Ecological_Responses" repository at https://github.com/yalimay.

4.10. References

Allen, M. A., Goh, F., Burns, B. P., and Neilan, B. A. (2009). Bacterial, archaeal and eukaryotic diversity of smooth and pustular microbial mat communities in the hypersaline lagoon of Shark Bay. *Geobiology* 7, 82–96. doi:10.1111/j.1472-4669.2008.00187.x.

Aubé, J., Senin, P., Bonin, P., Pringault, O., Jeziorski, C., Bouchez, O., et al. (2020). Meta-omics Provides Insights into the Impact of Hydrocarbon Contamination on Microbial Mat Functioning. *Microb Ecol*. doi:10.1007/s00248-020-01493-x.

Australian Maritime Safety Authority (AMSA) (2012). Report on the 2011/12 Review of the National Plan to Combat Pollution of the Sea by Oil and Other Hazardous and Noxious Substances and the National Maritime Emergency Response Arragements (2011-2012). Australian Government Available at: https://www.amsa.gov.au/sites/default/files/natplan-review-report.pdf [Accessed June 9, 2020].

Babilonia, J., Conesa, A., Casaburi, G., Pereira, C., Louyakis, A. S., Reid, R. P., et al. (2018). Comparative Metagenomics Provides Insight Into the Ecosystem Functioning of the Shark Bay Stromatolites, Western Australia. *Front. Microbiol.* 9, 1359. doi:10.3389/fmicb.2018.01359.

Barbera, P., Kozlov, A. M., Czech, L., Morel, B., Darriba, D., Flouri, T., et al. (2019). EPA-ng: Massively Parallel Evolutionary Placement of Genetic Sequences. *Syst Biol* 68, 365–369. doi:10.1093/sysbio/syy054.

Bell, T. H., Yergeau, E., Maynard, C., Juck, D., Whyte, L. G., and Greer, C. W. (2013). Predictable bacterial composition and hydrocarbon degradation in Arctic soils following diesel and nutrient disturbance. *ISME J* 7, 1200–1210. doi:10.1038/ismej.2013.1.

Bolyen, E., Rideout, J. R., Dillon, M. R., Bokulich, N. A., Abnet, C. C., Al-Ghalith, G. A., et al. (2019). Reproducible, interactive, scalable and extensible microbiome data science using QIIME 2. *Nature biotechnology* 37, 852–857.

Bordenave, S., Goñi-Urriza, M. S., Caumette, P., and Duran, R. (2007). Effects of Heavy Fuel Oil on the Bacterial Community Structure of a Pristine Microbial Mat. *Applied and Environmental Microbiology* 73, 6089–6097. doi:10.1128/AEM.01352-07.

Cáceres, M. D., and Legendre, P. (2009). Associations between species and groups of sites: indices and statistical inference. *Ecology* 90, 3566–3574. doi:10.1890/08-1823.1.

Campbell, M. A., Grice, K., Visscher, P. T., Morris, T., Wong, H. L., White, R. A. I., et al. (2020). Functional Gene Expression in Shark Bay Hypersaline Microbial

Mats: Adaptive Responses. Front. Microbiol. 11. doi:10.3389/fmicb.2020.560336.

Cao, K.-A. L., Costello, M.-E., Lakis, V. A., Bartolo, F., Chua, X.-Y., Brazeilles, R., et al. (2016). MixMC: A Multivariate Statistical Framework to Gain Insight into Microbial Communities. *PLOS ONE* 11, e0160169. doi:10.1371/journal.pone.0160169.

Caporaso, J. G., Lauber, C. L., Walters, W. A., Berg-Lyons, D., Huntley, J., Fierer, N., et al. (2012). Ultra-high-throughput microbial community analysis on the Illumina HiSeq and MiSeq platforms. *The ISME Journal* 6, 1621–1624. doi:10.1038/ismej.2012.8.

Chambers, J. C., Allen, C. R., and Cushman, S. A. (2019). Operationalizing Ecological Resilience Concepts for Managing Species and Ecosystems at Risk. *Front. Ecol. Evol.* 7. doi:10.3389/fevo.2019.00241.

Charlesworth, J. C., Watters, C., Wong, H. L., Visscher, P. T., and Burns, B. P. (2019). Isolation of novel quorum-sensing active bacteria from microbial mats in Shark Bay Australia. *FEMS Microbiol Ecol* 95. doi:10.1093/femsec/fiz035.

Czech, L., Barbera, P., and Stamatakis, A. (2020). Genesis and Gappa: processing, analyzing and visualizing phylogenetic (placement) data. *Bioinformatics*. doi:10.1093/bioinformatics/btaa070.

Dang, H., and Lovell, C. R. (2016). Microbial Surface Colonization and Biofilm Development in Marine Environments. *Microbiol. Mol. Biol. Rev.* 80, 91–138. doi:10.1128/MMBR.00037-15.

Dastgheib, S. M. M., Amoozegar, M. A., Khajeh, K., Shavandi, M., and Ventosa, A. (2012). Biodegradation of polycyclic aromatic hydrocarbons by a halophilic microbial consortium. *Applied Microbiology and Biotechnology* 95, 789–798. doi:10.1007/s00253-011-3706-4.

Desouky, A.-E.-H. (2003). Acinetobacter: environmental and biotechnological applications. *African Journal of Biotechnology* 2, 71–74. doi:10.5897/AJB2003.000-1014.

Dombrowski, N., Donaho, J. A., Gutierrez, T., Seitz, K. W., Teske, A. P., and Baker, B. J. (2016). Reconstructing metabolic pathways of hydrocarbon-degrading bacteria from the Deepwater Horizon oil spill. *Nature Microbiology; London* 1, 16057. doi:http://dx.doi.org.dbgw.lis.curtin.edu.au/10.1038/nmicrobiol.2016.57.

Douglas, G. M., Maffei, V. J., Zaneveld, J., Yurgel, S. N., Brown, J. R., Taylor, C. M., et al. (2019). PICRUSt2: An improved and extensible approach for metagenome inference. *BioRxiv; Cold Spring Harbor*. doi:http://dx.doi.org.dbgw.lis.curtin.edu.au/10.1101/672295.

Edbeib, M. F., Wahab, R. A., and Huyop, F. (2016). Halophiles: biology, adaptation, and their role in decontamination of hypersaline environments. *World J Microbiol Biotechnol* 32, 135. doi:10.1007/s11274-016-2081-9.

Glasby, T. M., and Underwood, A. J. (1996). Sampling to differentiate between pulse and press perturbations. *Environ Monit Assess* 42, 241–252. doi:10.1007/BF00414371.

Kanehisa, M., Goto, S., Sato, Y., Furumichi, M., and Tanabe, M. (2012). KEGG for integration and interpretation of large-scale molecular data sets. *Nucleic Acids Research* 40, D109–D114. doi:10.1093/nar/gkr988.

Kanehisa, M., Goto, S., Sato, Y., Kawashima, M., Furumichi, M., and Tanabe, M. (2014). Data, information, knowledge and principle: back to metabolism in KEGG. *Nucleic Acids Research* 42, D199–D205. doi:10.1093/nar/gkt1076.

Langille, M. G. I., Zaneveld, J., Caporaso, J. G., McDonald, D., Knights, D., Reyes, J. A., et al. (2013). Predictive functional profiling of microbial communities using 16S rRNA marker gene sequences. *Nat Biotechnol* 31, 814–821. doi:10.1038/nbt.2676.

Louca, S., and Doebeli, M. (2018). Efficient comparative phylogenetics on large trees. *Bioinformatics* 34, 1053–1055. doi:10.1093/bioinformatics/btx701.

Lucena, T., Pascual, J., Garay, E., Arahal, D. R., Macián, M. C., and Pujalte, M. J. (2010). Haliea mediterranea sp. nov., a marine gammaproteobacterium. *Int. J. Syst. Evol. Microbiol.* 60, 1844–1848. doi:10.1099/ijs.0.017061-0.

MacDougall, A. S., McCann, K. S., Gellner, G., and Turkington, R. (2013). Diversity loss with persistent human disturbance increases vulnerability to ecosystem collapse. *Nature* 494, 86–89. doi:10.1038/nature11869.

McGenity, T. J. (2010). "Halophilic Hydrocarbon Degraders," in *Handbook of Hydrocarbon and Lipid Microbiology*, ed. K. N. Timmis (Berlin, Heidelberg: Springer), 1939–1951. doi:10.1007/978-3-540-77587-4_142.

McGenity, T. J., Folwell, B. D., McKew, B. A., and Sanni, G. O. (2012). Marine crude-oil biodegradation: a central role for interspecies interactions. *Aquat Biosyst* 8, 10. doi:10.1186/2046-9063-8-10.

Méndez, V., Fuentes, S., Morgante, V., Hernández, M., González, M., Moore, E., et al. (2017). Novel hydrocarbonoclastic metal-tolerant Acinetobacter and Pseudomonas strains from Aconcagua river oil-polluted soil. *Journal of soil science and plant nutrition* 17, 1074–1087. doi:10.4067/S0718-95162017000400017.

NESP Earth Systems and Climate Change Hub (2018). Climate change and the Shark Bay World Heritage Area: foundations for a climate change adaptation strategy and action plan. Available at: http://nespclimate.com.au/wp-

content/uploads/2016/03/SBWHA-CC-workshop-report.pdf [Accessed May 14, 2020].

Oksanen, J., Blanchet, F. G., Kindt, R., Legendre, P., O'hara, R. B., Simpson, G. L., et al. (2010). Vegan: community ecology package. R package version 1.17-4. *http://cran. r-project. org>. Acesso em* 23, 2010.

Orwin, K. H., and Wardle, D. A. (2004). New indices for quantifying the resistance and resilience of soil biota to exogenous disturbances. *Soil Biology and Biochemistry* 36, 1907–1912. doi:10.1016/j.soilbio.2004.04.036.

Pagès, A., Welsh, D. T., Teasdale, P. R., Grice, K., Vacher, M., Bennett, W. W., et al. (2014). Diel fluctuations in solute distributions and biogeochemical cycling in a hypersaline microbial mat from Shark Bay, WA. *Marine Chemistry* 167, 102–112. doi:10.1016/j.marchem.2014.05.003.

Plet, C., Pagès, A., Holman, A. I., Madden, R. H. C., and Grice, K. (2018). From supratidal to subtidal, an integrated characterisation of Carbla Beach shallow microbial mats (Hamelin Pool, Shark Bay, WA): Lipid biomarkers, stable carbon isotopes and microfabrics. *Chemical Geology* 493, 338–352. doi:10.1016/j.chemgeo.2018.06.010.

Rosenberg, E., Barkay, T., Navon-Venezia, S., and Ron, E. Z. (1999). "Role of Acinetobacter Bioemulsans in Petroleum Degradation," in *Novel Approaches for Bioremediation of Organic Pollution*, eds. R. Fass, Y. Flashner, and S. Reuveny (Boston, MA: Springer US), 171–180. doi:10.1007/978-1-4615-4749-5_17.

Shackelford, N., Standish, R. J., Lindo, Z., and Starzomski, B. M. (2018). The role of landscape connectivity in resistance, resilience, and recovery of multi-trophic microarthropod communities. *Ecology* 99, 1164–1172. doi:10.1002/ecy.2196.

Shade, A., Peter, H., Allison, S. D., Baho, D., Berga, M., Buergmann, H., et al. (2012). Fundamentals of Microbial Community Resistance and Resilience. *Front. Microbiol.* 3. doi:10.3389/fmicb.2012.00417.

Shanafelt, D. W., Dieckmann, U., Jonas, M., Franklin, O., Loreau, M., and Perrings, C. (2015). Biodiversity, productivity, and the spatial insurance hypothesis revisited. *Journal of Theoretical Biology* 380, 426–435. doi:10.1016/j.jtbi.2015.06.017.

Standish, R. J., Hobbs, R. J., Mayfield, M. M., Bestelmeyer, B. T., Suding, K. N., Battaglia, L. L., et al. (2014). Resilience in ecology: Abstraction, distraction, or where the action is? *Biological Conservation* 177, 43–51. doi:10.1016/j.biocon.2014.06.008.

Su, H., Mi, S., Peng, X., and Han, Y. (2019). The mutual influence between corrosion and the surrounding soil microbial communities of buried petroleum pipelines. *RSC Adv.* 9, 18930–18940. doi:10.1039/C9RA03386F.

Suding, K. N., Gross, K. L., and Houseman, G. R. (2004). Alternative states and positive feedbacks in restoration ecology. *Trends in Ecology & Evolution* 19, 46–53. doi:10.1016/j.tree.2003.10.005.

Suzuki, T., Nakamura, T., and Fuse, H. (2012). Isolation of Two Novel Marine Ethylene-Assimilating Bacteria, Haliea Species ETY-M and ETY-NAG, Containing Particulate Methane Monooxygenase-like Genes. *Microbes Environ* 27, 54–60. doi:10.1264/jsme2.ME11256.

Vasconcellos, S. P., Sierra-Garcia, I. N., Dellagnezze, B. M., Vicentini, R., Midgley, D., Silva, C. C., et al. (2017). Functional and genetic characterization of hydrocarbon biodegrader and exopolymer-producing clones from a petroleum reservoir metagenomic library. *Environmental Technology* 38, 1139–1150. doi:10.1080/09593330.2016.1218940.

Volkman, J. K., Alexander, R., Kagi, R. I., Noble, R. A., and Woodhouse, C. W. (1983a). A geochemical reconstruction of oil generation in the Barrow Sub-basin of Western Australia. *Geochimica et Cosmochimica Acta* 47, 2091–2105. doi:10.1016/0016-7037(83)90034-0.

Volkman, J. K., Alexander, R., Kagi, R. I., and Woodhouse, G. W. (1983b). Demethylated hopanes in crude oils and their applications in petroleum geochemistry. *Geochimica et Cosmochimica Acta* 47, 785–794. doi:10.1016/0016-7037(83)90112-6.

Westman, W. E. (1978). Measuring the Inertia and Resilience of Ecosystems. *BioScience* 28, 705–710. doi:10.2307/1307321.

Wong, H., Ahmed-Cox, A., and Burns, B. (2016). Molecular Ecology of Hypersaline Microbial Mats: Current Insights and New Directions. *Microorganisms* 4, 6. doi:10.3390/microorganisms4010006.

Wong, H. L., Smith, D., Visscher, P. T., and Burns, B. P. (2015). Niche differentiation of bacterial communities at a millimeter scale in Shark Bay microbial mats. *Scientific Reports (Nature Publisher Group); London* 5, 15607. doi:http://dx.doi.org.dbgw.lis.curtin.edu.au/10.1038/srep15607.

Wong, H. L., White, R. A., Visscher, P. T., Charlesworth, J. C., Vázquez-Campos, X., and Burns, B. P. (2018). Disentangling the drivers of functional complexity at the metagenomic level in Shark Bay microbial mat microbiomes. *The ISME Journal* 12, 2619–2639. doi:10.1038/s41396-018-0208-8.

Yachi, S., and Loreau, M. (1999). Biodiversity and ecosystem productivity in a fluctuating environment: The insurance hypothesis. *PNAS* 96, 1463–1468. doi:10.1073/pnas.96.4.1463.

Appendix 4

SUPPLEMENTARY MATERIAL

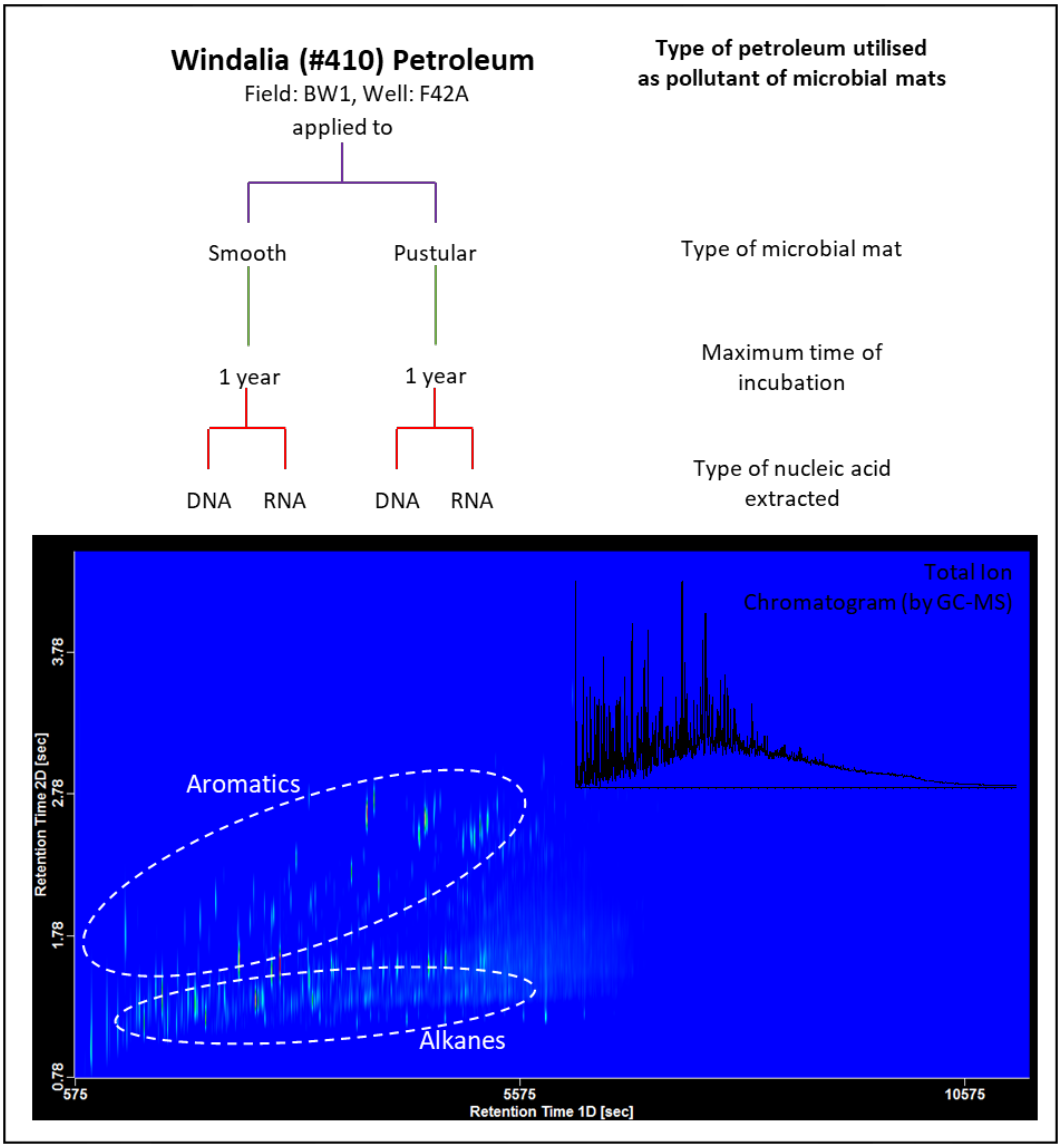

Figure A4.1. Scheme illustrating the organization of the different groups of lab-controlled time-series incubation experiments using microbial mats collected from the Nilemah area, Hamelin Pool, Shark Bay (WA). Windalia petroleum examined by Two-dimensional Gas Chromatography/Time-of-Flight Mass Spectrometry (GCxGC ToF-MS) and Gas Chromatography-Mass Spectroscopy (GC-MS) are displayed to show the organic compounds present in the petroleum sample.

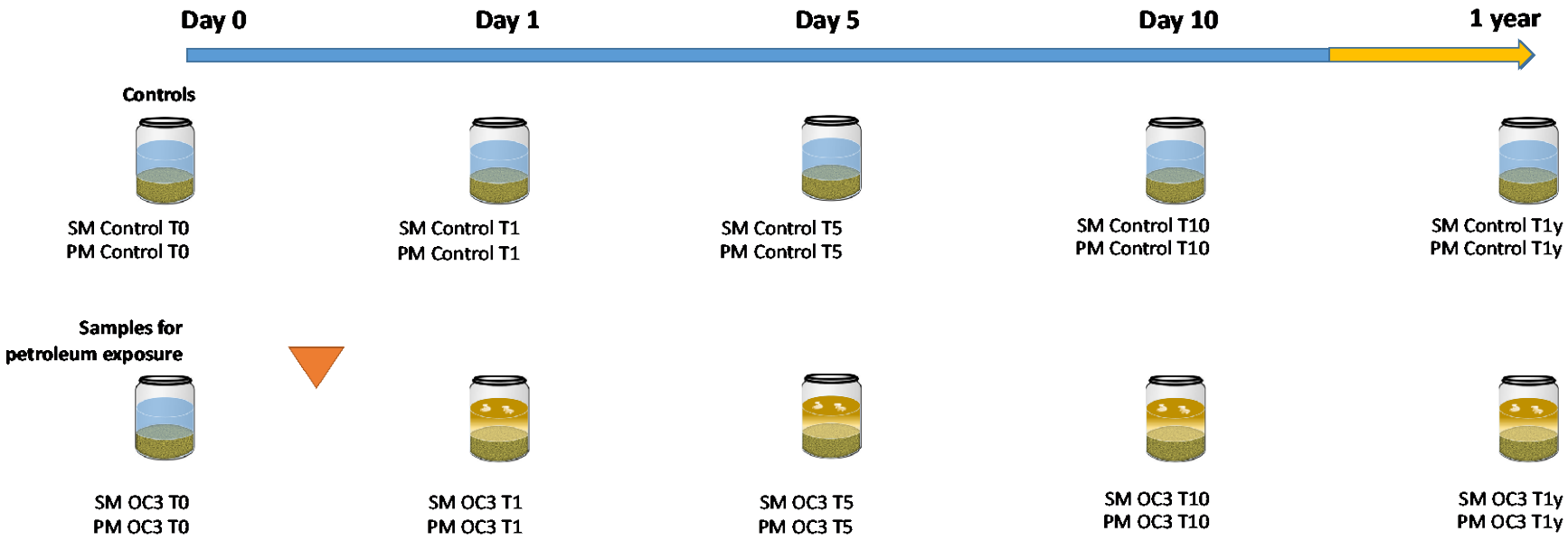

Figure A4.2. Illustration of sampling schedule and nomenclature utilised for both controls and samples for PE. All samples were subsampled just before oil pollution (T0), and repeated after 1 day (T1), 5 days (T5), 10 days (T10) and 360 days (1 year) (T1y).

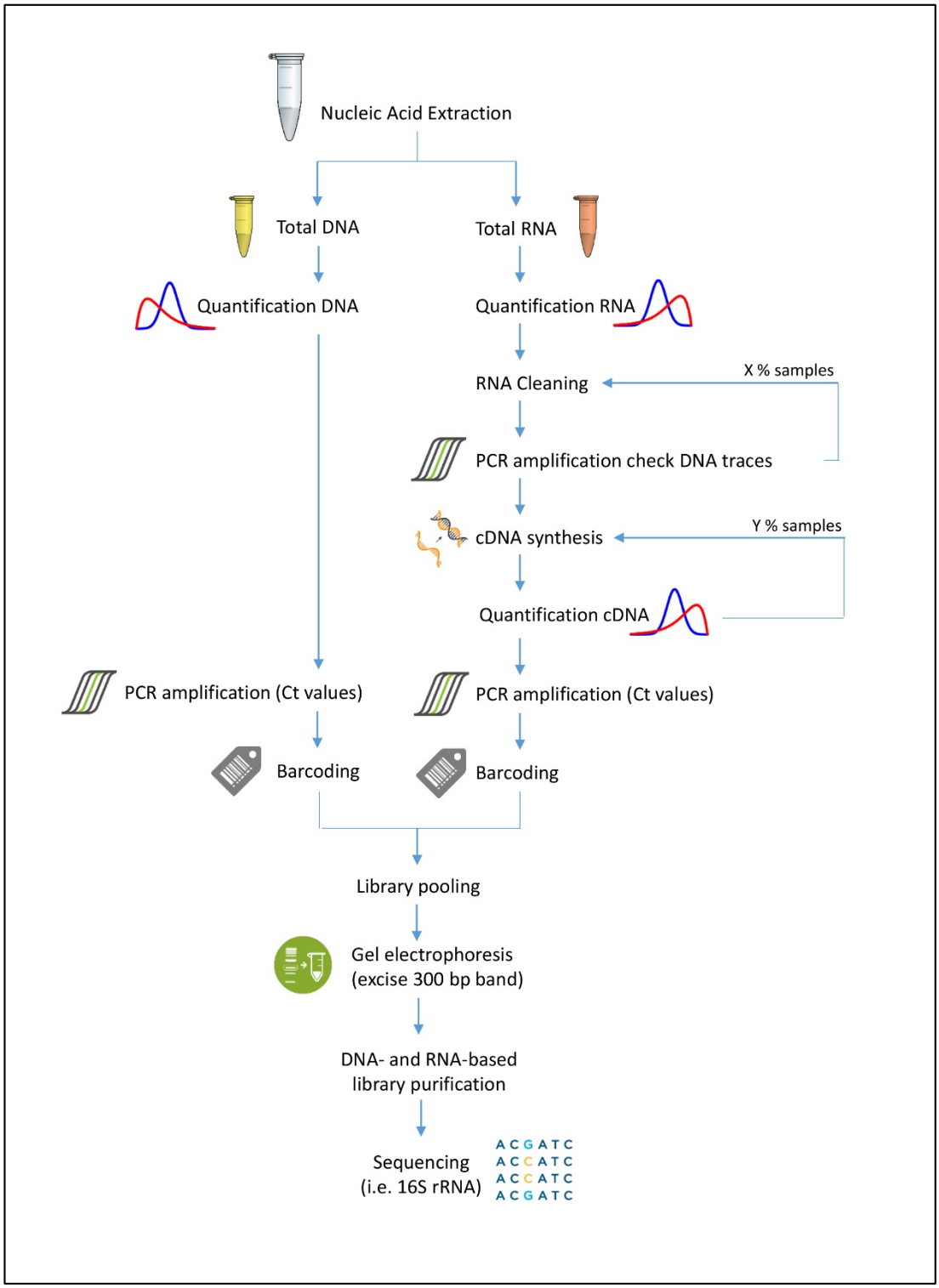

Figure A4.3. Diagram showing the workflow followed for microbiological analysis.

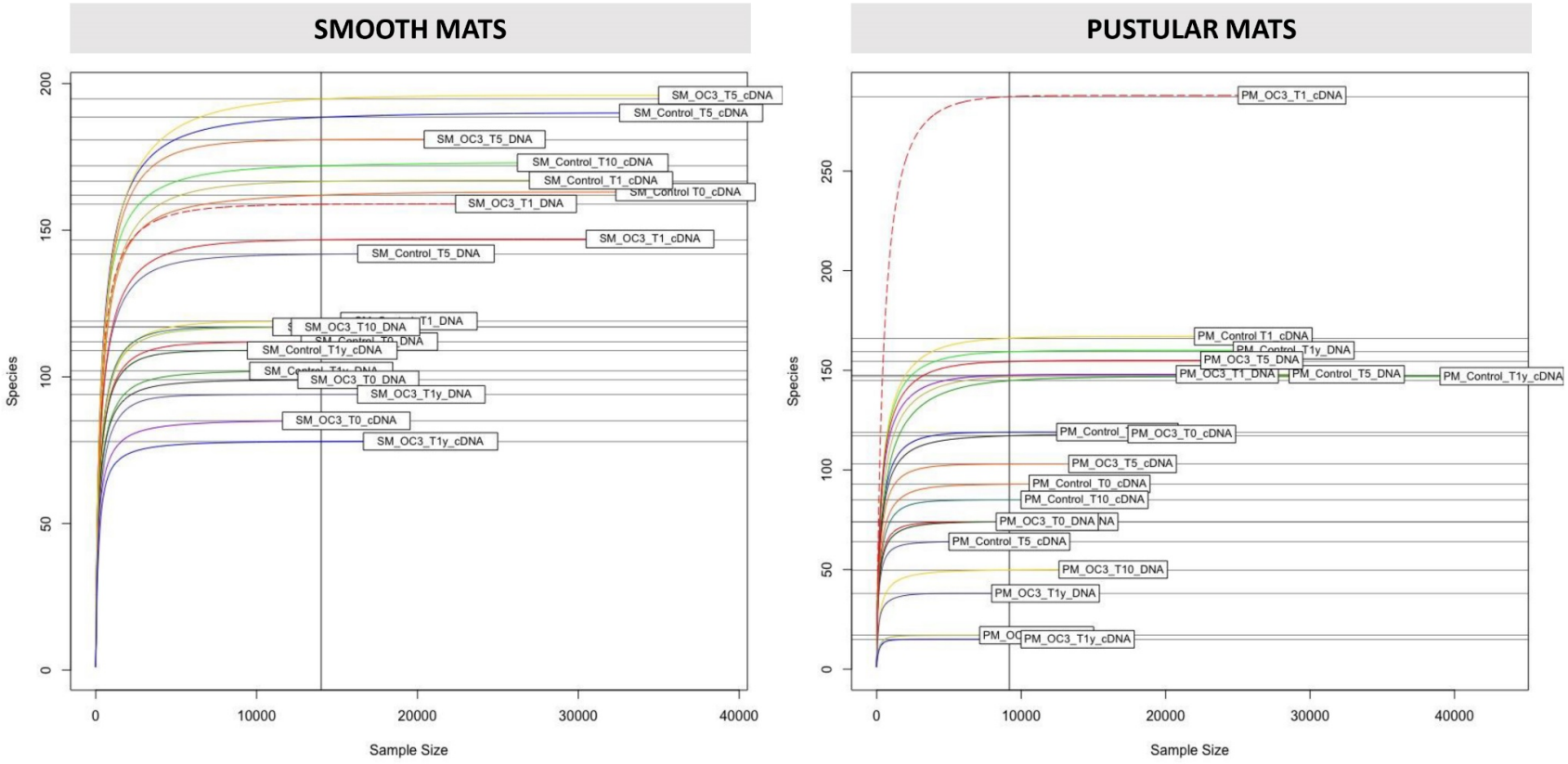

Figure A4.4. Rarefaction curves of samples collected in both controls and petroleum incubated smooth and pustular mat microcosms incubation experiments, simulating a pulse disturbance.

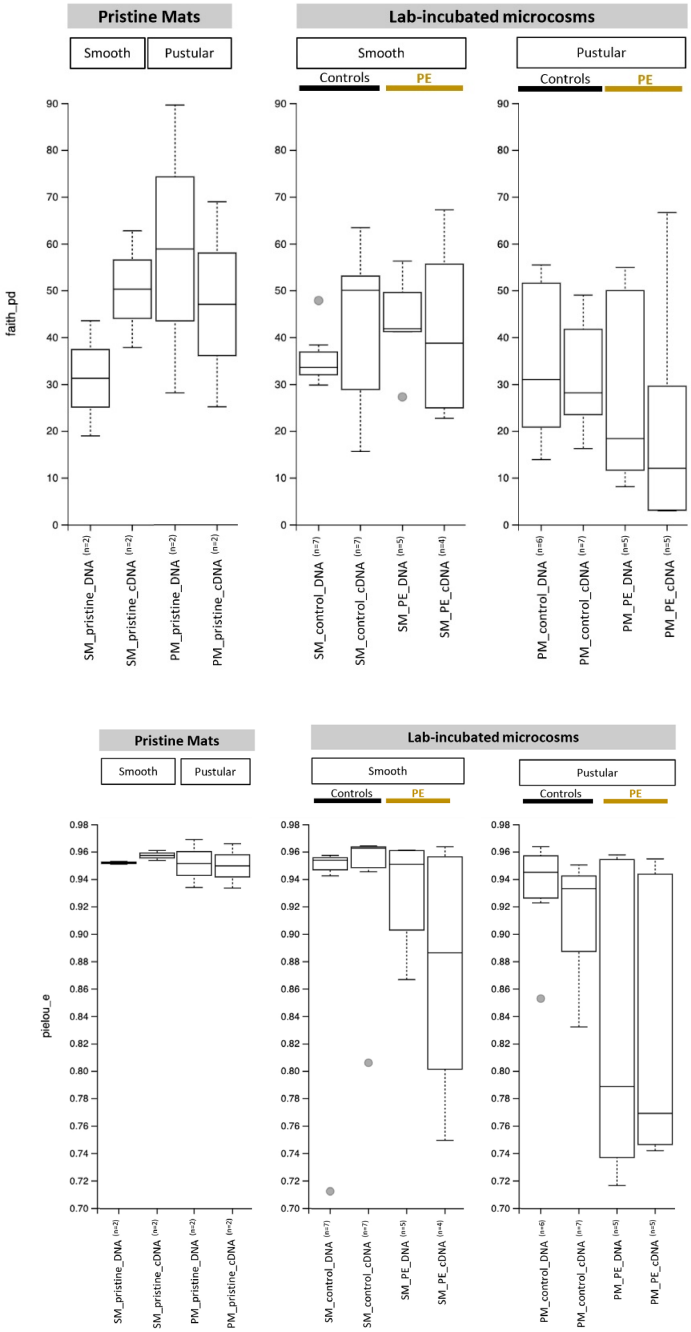

Figure A4.5. Boxplots of Faith's (top) and Pielou's (bottom) index computed in QIIME2 including DNA and cDNA datasets of pristine mats (**Chapter 2**), controls, and PE mats (including T1, T5, T10 and T1y). Centre line in the boxplot represents the median, while box limits indicate 25th and 75th percentiles. Boxplot whiskers represent 9th and 91st percentiles and outlier values are represented as grey points. Data of pristine smooth and pustular samples was taken from **Chapter 2**.

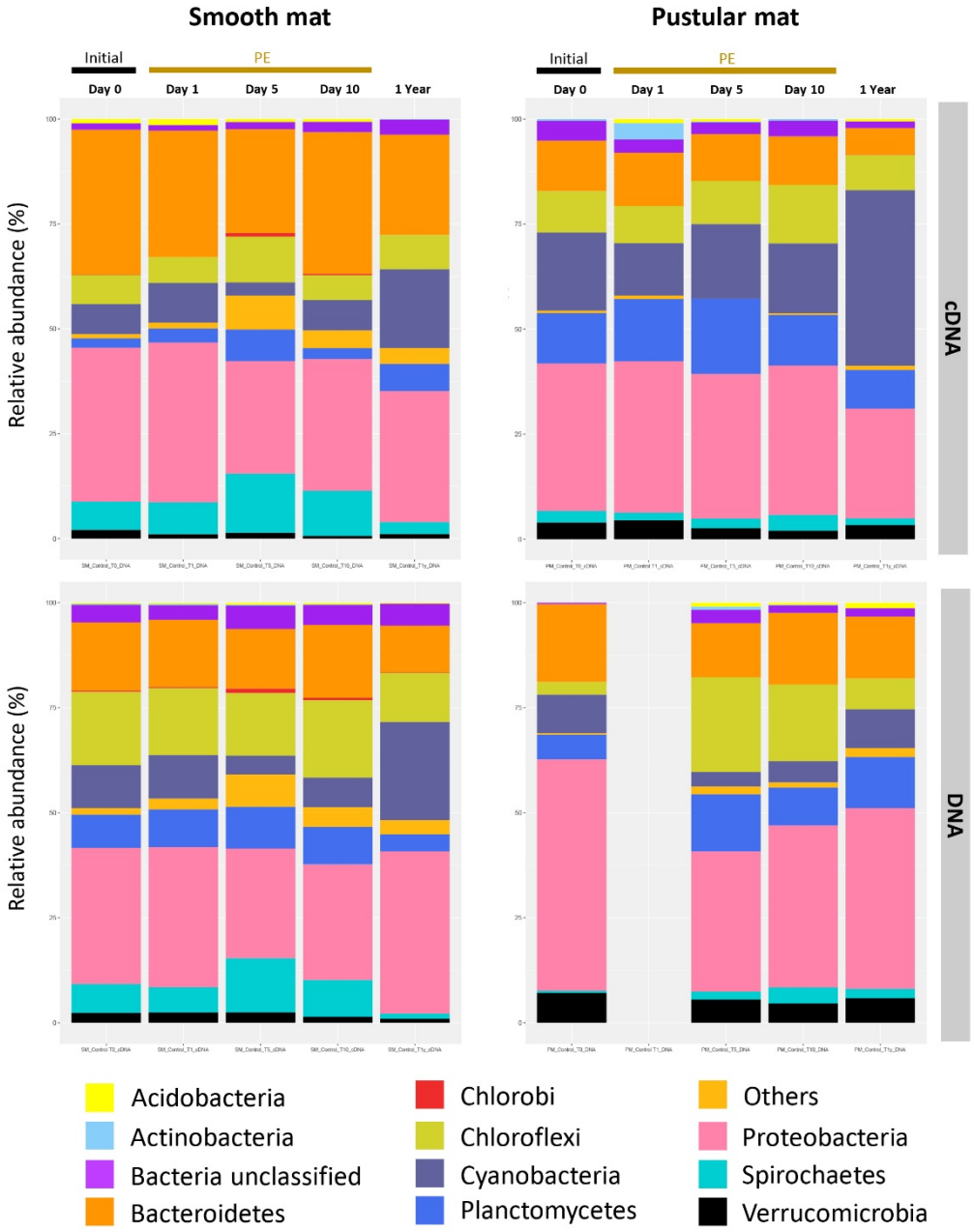

Figure A4.6. Relative abundance of the total (DNA) and active (cDNA) bacterial microbiomes at phylum level of **control** (untreated) **smooth** and **pustular** mat microcosms. Time-series lab-incubation involved sampling at 0 day (T0 – initial) and after 1 day (T1), 5 days (T5) and 10 days (T10) and 1 year (T1y). Pustular mat PE sub-sample at T1 (DNA) was damaged during nucleic acid extraction.

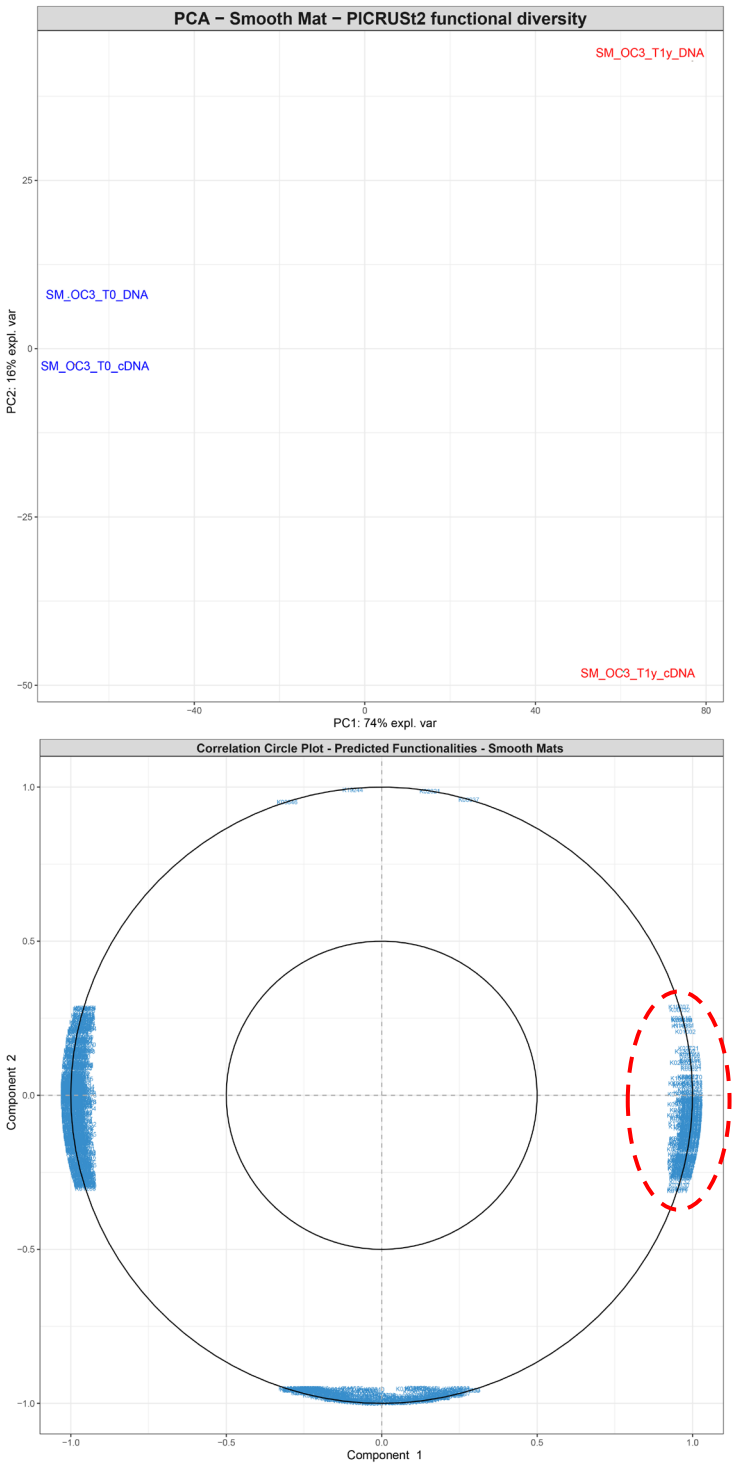

Figure A4.7. PCA (Principal Component Analysis) plot (top) showing the clustering of the **smooth mat** sub-samples collected in the petroleum-exposed SM-OC3 microcosm: initial (T0) *vs*. 1 year (T1y). Correlation Circle plots (PC1-PC2) (bottom), representing those variables contributing most (cut off or radius > 0.9) to the clustering of samples (initial *vs*. PE). Only those KOs circled were used for further functional analysis.

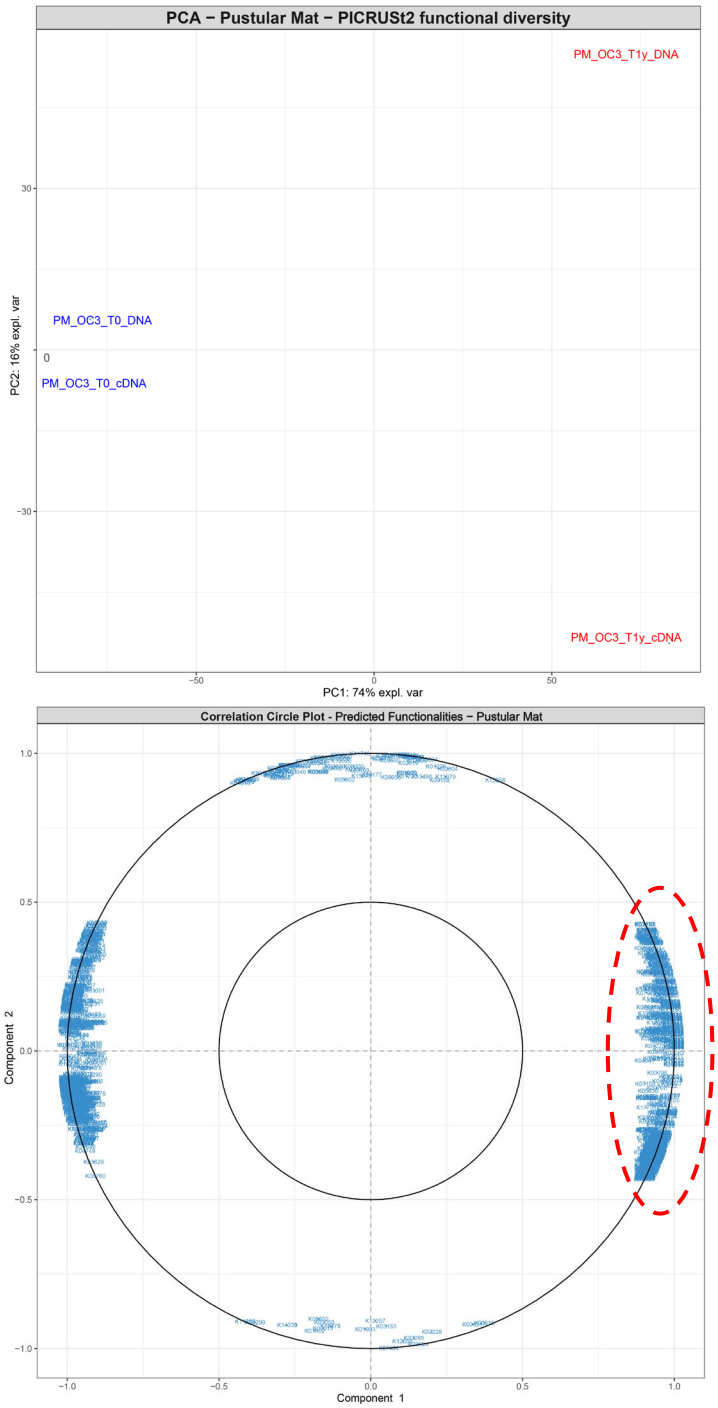

Figure A4.8. PCA (Principal Component Analysis) plot (top) showing the clustering of the **pustular mat** sub-samples collected in the petroleum-exposed PM-OC3 microcosm: initial (T0) *vs.* 1 year (T1y). Correlation Circle plots (PC1-PC2) (bottom), representing those variables contributing most (cut off or radius > 0.9) to the clustering of samples (initial *vs.* PE). Only those KOs circled were used for further functional analysis.

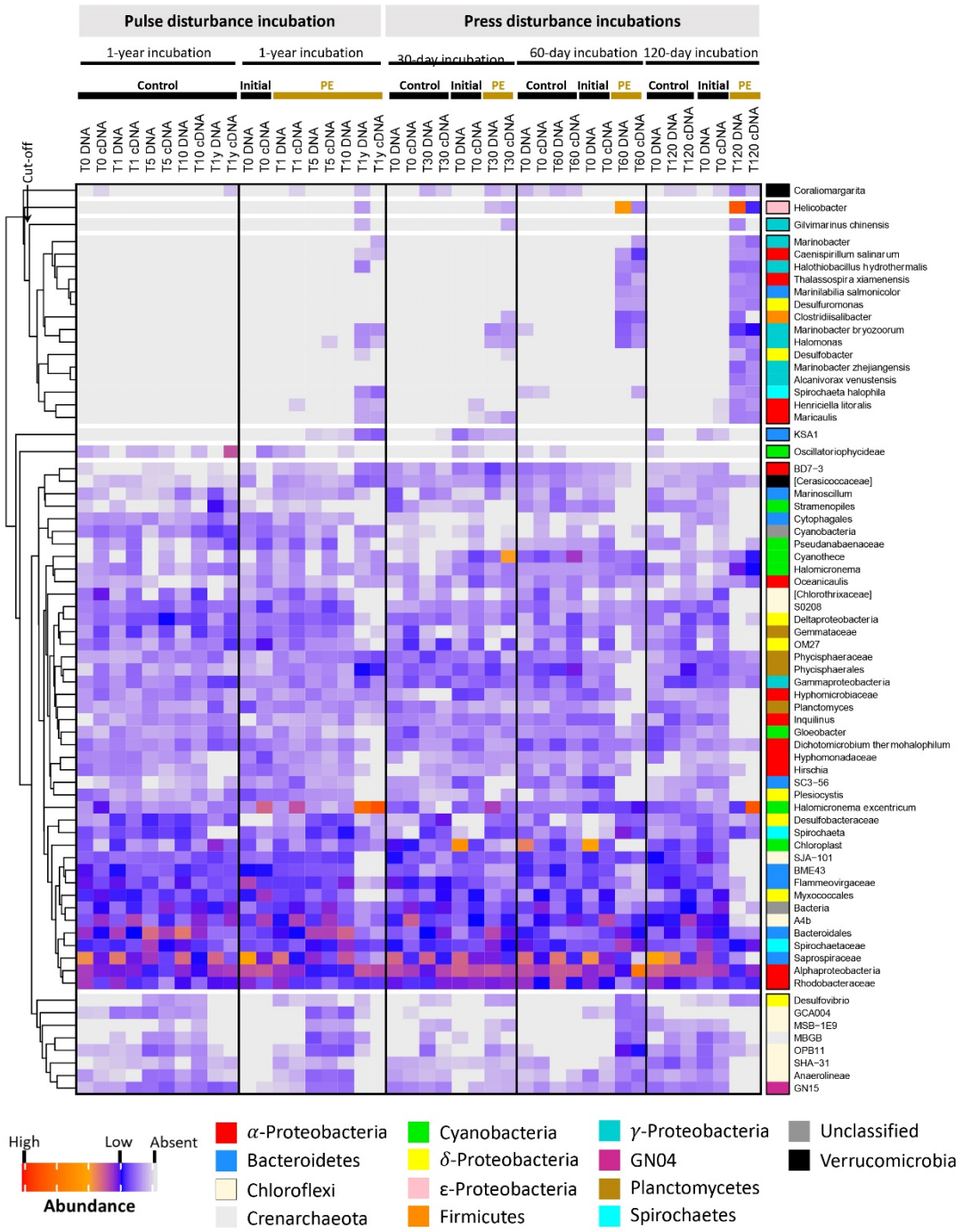

Figure A4.9. Heatmap plot of **smooth mat** microcosms subjected to lab incubation under control (untreated) or petroleum-exposed conditions, comparing microbiome shifts under pulse (or short-term) and press (long-term) disturbances. The right column depicts phylum or class taxonomy (legend on the bottom). Data displayed correspond to raw reads at species level standardised by total, square root transformed, and then, ranked the 70 more abundant organisms.

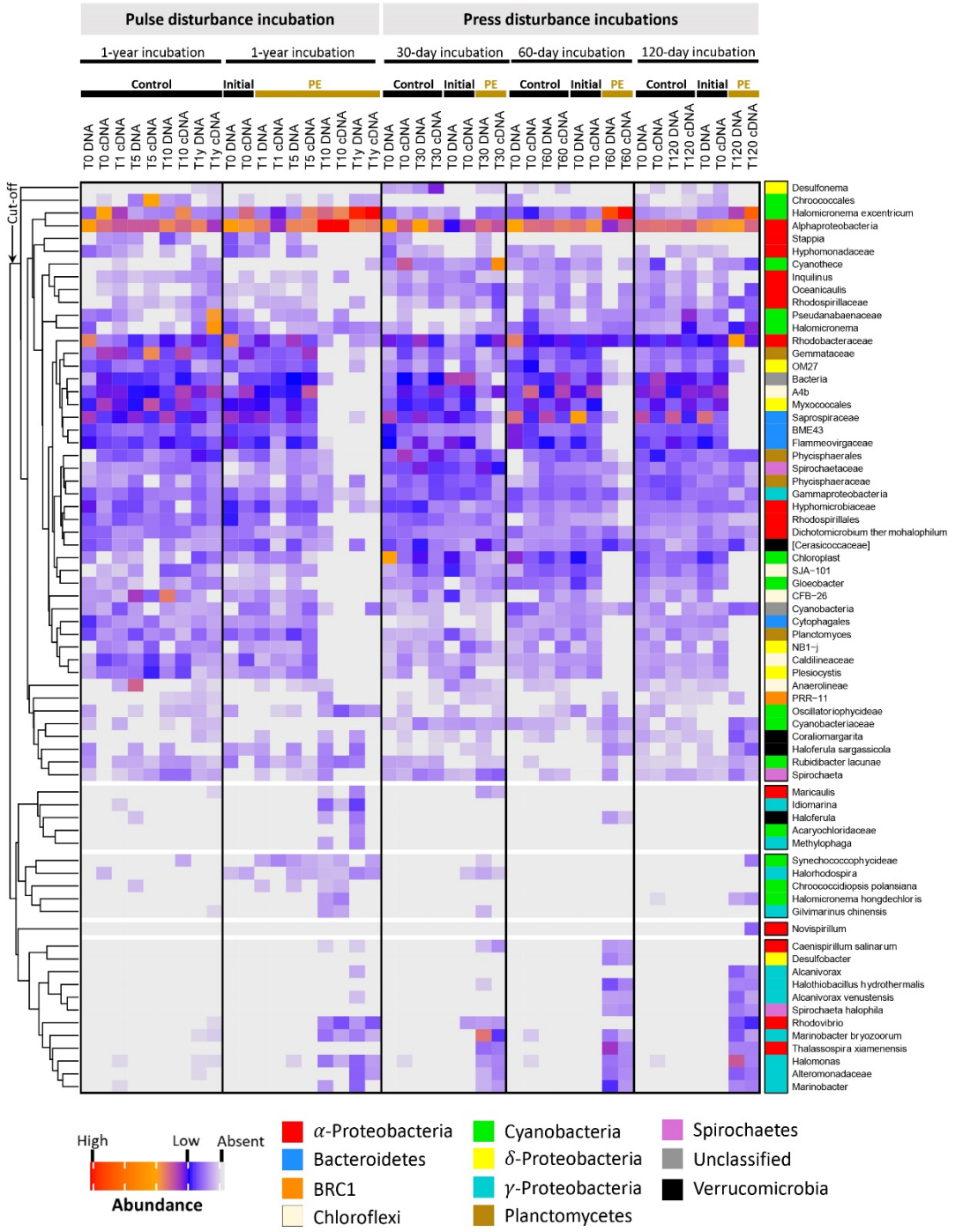

Figure A4.10. Heatmap plot of **pustular mat** microcosms subjected to lab incubation under control (untreated) or petroleum-exposed conditions, comparing microbiome shifts under pulse (or short-term) and press (long-term) disturbances. The right column depicts phylum or class taxonomy (legend on the bottom). Data displayed correspond to raw reads at species level standardised by total, square root transformed, and then, ranked the 70 more abundant organisms.

Table A4.1. Relative abundance of bacterial taxonomy (**phylum level**) of a **smooth mat control microcosm** under lab-conditions for up to 1 year. Shown are the differences between total bacteria (DNA) and active bacteria (cDNA) communities.

Taxonomy (Phylum level)	SM Control T0 DNA	SM Control T0 cDNA	SM Control T1 DNA	SM Control T1 cDNA	SM Control T5 DNA	SM Control T5 cDNA	SM Control T10 DNA	SM Control T10 cDNA	SM Control T1y DNA	SM Control T1y cDNA
Bacteria Unclassified	1.5	4.2	1.3	3.5	1.7	5.6	2.5	4.8	3.7	5.3
Acidobacteria	1.1	0.3	1.4	0.4	0.7	0.4	0.7	0.4		0.2
Actinobacteria		0.3		0.3		0.3		0.1	0.1	
Bacteroidetes	34.5	16.2	30.1	16.0	24.8	14.2	33.8	17.3	23.9	11.0
Chlorobi	0.1	0.3		0.2	0.9	1.0	0.3	0.6		0.2
Chloroflexi	7.0	17.4	6.2	16.0	10.9	14.9	5.9	18.4	8.2	11.8
Cyanobacteria	7.2	10.2	9.4	10.3	3.2	4.5	7.2	7.1	18.8	23.3
Planctomycetes	2.2	8.0	3.3	9.0	7.5	9.9	2.6	8.9	6.5	4.1
Proteobacteria	36.7	32.4	38.1	33.3	26.9	26.2	31.4	27.5	31.3	38.6
Spirochaetes	6.8	6.9	7.6	6.0	14.1	12.9	10.8	8.7	2.9	1.3
Verrucomicrobia	2.0	2.3	1.0	2.5	1.3	2.5	0.6	1.5	1.0	1.0
Others	1.0	1.6	1.4	2.6	8.1	7.6	4.2	4.7	3.8	3.4

Table A4.2. Relative abundance of bacterial taxonomy (**class level**) of a **smooth mat control microcosm** under lab-conditions for up to 1 year. Shown are the differences between total bacteria (DNA) and active bacteria (cDNA) communities.

Taxonomy (Class level)	SM Control T0 DNA	SM Control T0 cDNA	SM Control T1 DNA	SM Control T1 cDNA	SM Control T5 DNA	SM Control T5 cDNA	SM Control T10 DNA	SM Control T10 cDNA	SM Control T1y DNA	SM Control T1y cDNA
Bacteria_Unclassified	1.5	4.2	1.3	3.5	1.7	5.6	2.5	4.8	3.7	5.3
BME43	4.5	1.8	3.8	1.8	1.5	1.7	3.4	2.6	2.0	2.2
Bacteroidia	6.2	4.1	7.1	4.1	10.6	7.1	11.7	6.0	1.3	1.4
Cytophagia	6.9	3.7	6.8	3.8	4.5	1.8	7.0	2.9	7.6	3.0
Saprospirae	13.7	4.9	11.7	4.9	6.7	2.6	10.2	3.9	10.0	2.0
Anaerolineae	5.8	11.8	6.0	14.1	10.9	13.3	5.5	15.0	8.2	10.8
Chloroflexi	1.2	5.6	0.2	1.8		1.5	0.4	3.4		1.0
Oscillatoriophycideae	2.9	1.9	1.8	3.0	1.3	1.3	2.1	2.2	0.2	10.5
Synechococcophycideae	0.9	6.5	2.1	4.6	0.5	1.6	0.9	1.9	3.9	6.8
Phycisphaerae	0.6	2.1	0.9	2.2	3.5	3.7	1.3	3.1	2.0	0.2
Planctomycetia	1.4	5.3	2.3	6.5	3.7	5.8	1.1	5.4	3.6	2.6
Alphaproteobacteria	23.8	16.3	20.7	16.3	13.7	9.1	17.0	11.5	18.1	16.0
Deltaproteobacteria	11.5	13.0	14.9	12.7	12.2	15.5	11.2	13.2	6.6	15.7
Gammaproteobacteria	1.3	3.0	2.3	4.0	0.9	1.3	2.5	2.4	6.4	6.5
Spirochaetes	5.8	4.0	6.3	4.4	11.7	7.7	8.8	5.2	2.3	0.9
Opitutae	0.3	0.2	0.3	0.4	0.3	0.4	0.2	0.2	0.4	0.4
Verrucomicrobiae	0.6	0.9	0.3	1.1	0.3	0.7	0.1	0.4	0.6	0.4
Cyanobacteria_Unclassified	0.9	1.6	1.0	1.5	0.1	0.9	0.6	1.8	2.9	2.3
Chloroplast	2.1	0.1	3.4	0.6	0.9	0.1	2.9	0.7	10.1	2.8
Others (<3%)	8.1	9.2	6.8	8.8	15.1	18.3	10.6	13.3	10.0	9.5

Table A4.3. Relative abundance of bacterial taxonomy (**phylum level**) of a **smooth mat microcosm** subjected to **Windalia petroleum** exposure for up to 1 year. Shown are the differences between total bacteria (DNA) and active bacteria (cDNA) communities. Petroleum-exposed sub-samples are represented with a grey shade.

Taxonomy (Phylum level)	SM OC3 T0 DNA	SM OC3 T0 cDNA	SM OC3 T1 DNA	SM OC3 T1 cDNA	SM OC3 T5 DNA	SM OC3 T5 cDNA	SM OC3 T10 DNA	SM OC3 T10 cDNA	SM OC3 T1y DNA	SM OC3 T1y cDNA
Bacteria Unclassified	1.1	2.5	2.9	4.5	2.2	5.6	1.8		0.6	1.0
Acidobacteria			0.2	0.2	0.3	0.2	0.2		0.1	
Actinobacteria				0.1	0.3	0.2	0.1			
Bacteroidetes	35.8	18.5	25.4	17.5	21.0	16.0	28.7		4.8	3.4
Chlorobi			0.3	0.4	0.3	0.9	0.2			0.3
Chloroflexi	7.0	13.4	9.9	15.8	16.0	20.8	14.9		0.8	1.5
Cyanobacteria	7.6	18.4	8.1	15.8	4.4	5.4	4.3		42.1	52.3
Planctomycetes	5.1	3.3	8.0	5.9	8.2	5.7	4.8		6.7	6.8
Proteobacteria	35.5	39.1	33.3	29.7	25.4	26.2	25.0		32.5	25.4
Spirochaetes	4.7	3.2	7.0	6.6	10.4	12.6	12.5		5.5	4.2
Verrucomicrobia	3.1	1.4	3.6	2.3	2.2	1.5	1.0		5.0	3.1
Others	0.2	0.2	1.5	1.2	9.3	4.9	6.4		1.9	2.0

Table A4.4. Relative abundance of bacterial taxonomy (**class level**) of a **smooth mat microcosm** subjected to **Windalia petroleum exposure** for up to 1 year. Shown are the differences between total bacteria (DNA) and active bacteria (cDNA) communities. Petroleum-exposed sub-samples are represented with a grey shade.

Taxonomy (Class level)	SM OC3 T0 DNA	SM OC3 T0 cDNA	SM OC3 T1 DNA	SM OC3 T1 cDNA	SM OC3 T5 DNA	SM OC3 T5 cDNA	SM OC3 T10 DNA	SM OC3 T10 cDNA	SM OC3 T1y DNA	SM OC3 T1y cDNA
Bacteria_Unclassified	1.1	2.5	2.9	4.5	2.2	5.6	1.8		0.6	1.0
BME43	3.9	3.8	2.3	2.1	2.0	1.9	1.9			
Bacteroidia	1.9	2.6	4.3	3.9	7.5	7.4	9.8		1.3	0.4
Cytophagia	10.3	4.7	5.7	6.0	4.3	3.3	7.0		0.3	0.4
Saprospirae	17.5	5.0	11.3	3.8	5.9	2.1	8.8		1.3	0.4
Anaerolineae	6.7	12.8	8.8	13.8	15.5	19.4	14.7		0.8	1.5
Chloroflexi	0.2	0.5	1.1	2.0	0.5	1.5	0.2			
Oscillatoriophycideae	1.4	2.9	2.2	2.2	0.7	1.1	0.9		1.0	2.0
Synechococcophycideae	2.0	13.6	1.4	11.5	0.9	3.0	1.2		38.7	48.4
Phycisphaerae	0.9	0.2	2.4	1.8	3.6	2.4	2.1		5.7	5.7
Planctomycetia	4.0	3.2	5.3	4.0	4.3	3.1	2.8		0.3	0.6
Alphaproteobacteria	23.5	22.8	21.6	15.9	13.6	10.2	13.6		21.7	19.6
Deltaproteobacteria	9.0	15.1	9.3	10.2	9.7	13.1	9.6		0.9	
Gammaproteobacteria	3.0	1.1	2.0	3.5	1.9	2.4	1.8		9.4	5.0
Spirochaetes	4.1	2.5	4.4	2.6	7.9	6.4	10.6		5.4	4.1
Opitutae	1.0	0.0	1.4	0.9	0.6	0.2	0.5		3.6	3.1
Verrucomicrobiae	1.4	0.6	1.3	0.9	0.6	0.4	0.4		1.4	0.1
Cyanobacteria_Unclassified	1.0	1.6	0.8	1.1	0.2	0.7			0.9	0.8
Chloroplast	2.4	0.2	2.5	0.6	1.9	0.5	2.0		1.4	0.9
Others (<3%)	4.7	4.2	8.9	8.4	16.2	15.0	10.6		5.3	5.3

Table A4.5. Relative abundance of bacterial taxonomy (**phylum level**) of a **pustular mat control microcosm** under lab-conditions for up to 1 year. Shown are the differences between total bacteria (DNA) and active bacteria (cDNA) communities.

Taxonomy (Phylum level)	PM Control T0 DNA	PM Control T0 cDNA	PM Control T1 DNA	PM Control T1 cDNA	PM Control T5 DNA	PM Control T5 cDNA	PM Control T10 DNA	PM Control T10 cDNA	PM Control T1y DNA	PM Control T1y cDNA
Bacteria Unclassified	0.4	4.8		3.2	3.2	2.8	1.8	3.8	2.0	1.6
Acidobacteria				1.0	1.0	0.6	0.5		1.3	0.5
Actinobacteria		0.4		3.9	0.8	0.2	0.1	0.4		
Bacteroidetes	18.5	12.0		12.6	12.9	11.1	17.0	11.6	14.8	6.4
Chlorobi										
Chloroflexi	3.0	9.8		8.9	22.5	10.3	18.3	13.9	7.3	8.4
Cyanobacteria	9.1	18.6		12.5	3.5	17.7	5.1	16.6	9.2	41.8
Planctomycetes	6.0	12.1		14.8	13.6	17.9	9.0	12.1	12.1	9.2
Proteobacteria	55.1	35.1		36.0	33.3	34.4	38.6	35.6	43.1	26.1
Spirochaetes	0.5	2.8		1.8	1.9	2.3	3.8	3.8	2.2	1.6
Verrucomicrobia	7.1	4.0		4.5	5.5	2.6	4.6	2.0	5.9	3.4
Others	0.3	0.6		0.9	1.8		1.2	0.4	2.2	1.0

Table A4.6. Relative abundance of bacterial taxonomy (**class level**) of a **pustular mat control microcosm** under lab-conditions for up to 1 year. Shown are the differences between total bacteria (DNA) and active bacteria (cDNA) communities. PM_Control_T0_DNA sub-samples was damaged during DNA elution.

Taxonomy (Class level)	PM Control T0 DNA	PM Control T0 cDNA	PM Control T1 DNA	PM Control T1 cDNA	PM Control T5 DNA	PM Control T5 cDNA	PM Control T10 DNA	PM Control T10 cDNA	PM Control T1y DNA	PM Control T1y cDNA
Bacteria_Unclassified	0.4	4.7		3.1	3.1	2.8	1.8	3.8	2.0	1.6
BME43	2.9	2.0		1.4	1.2	1.9	1.4	2.8	1.2	0.8
Bacteroidia	0.2	0.7		0.5	0.7	0.5	1.2	1.0	0.8	0.2
Cytophagia	7.9	4.6		3.6	4.0	3.4	6.1	3.9	5.0	2.9
Saprospirae	6.9	2.8		4.5	5.6	3.3	7.2	3.2	4.7	1.1
Anaerolineae	3.0	9.1		8.5	22.4	10.0	18.1	13.9	7.3	8.4
Chloroflexi		0.7		0.4	0.1	0.3	0.1			
Oscillatoriophycideae	2.1	0.1		1.2	2.0	16.9	2.1	2.5	1.8	1.4
Synechococcophycideae	4.7	17.9		8.1	0.6	0.9	1.2	13.6	3.2	37.4
Phycisphaerae	0.3	2.3		2.5	3.9	0.5	2.1	1.6	6.3	3.7
Planctomycetia	5.6	8.8		10.7	8.9	16.5	6.6	9.5	5.2	4.4
Alphaproteobacteria	45.0	18.7		19.9	20.0	15.3	27.8	17.5	28.1	15.7
Betaproteobacteria				2.4						
Deltaproteobacteria	6.9	14.7		11.1	8.6	17.7	8.2	16.0	8.1	6.7
Gammaproteobacteria	3.2	1.6		2.3	4.4	1.3	2.3	2.0	6.2	3.7
Spirochaetes	0.3	0.9		0.7	0.9	1.2	3.0	3.0	2.0	1.5
Opitutae	2.9	1.5		0.9	1.7		1.4	0.3	2.6	1.8
Verrucomicrobiae	3.0	1.6		2.8	2.1	1.7	1.7	0.5	1.6	0.9
Cyanobacteria_Unclassified	0.6	0.3		2.0	0.5		0.6	0.3	0.3	0.4
Chloroplast	1.2	0.0		0.4	0.2		0.6		2.7	1.6
Others (<3%)	2.9	6.8		12.9	9.1	6.0	6.4	4.6	10.9	5.7

Table A4.7. Relative abundance of bacterial taxonomy (**phylum level**) of a **pustular mat microcosm** subjected to **Windalia petroleum** exposure for up to 1 year. Shown are the differences between total bacteria (DNA) and active bacteria (cDNA) communities. Petroleum-exposed sub-samples are represented with a grey shade.

Taxonomy (Phylum level)	PM OC3 T0 DNA	PM OC3 T0 cDNA	PM OC3 T1 DNA	PM OC3 T1 cDNA	PM OC3 T5 DNA	PM OC3 T5 cDNA	PM OC3 T10 DNA	PM OC3 T10 cDNA	PM OC3 T1y DNA	PM OC3 T1y cDNA
Bacteria Unclassified	0.1	2.6	2.5	3.1	4.0	4.2	0.4			
Acidobacteria		0.2	0.6	2.3	1.1					
Actinobacteria		0.6	0.2	4.7	0.4	0.4				
Bacteroidetes	18.3	12.8	16.3	16.0	15.5	9.6			0.1	
Chlorobi				0.6						
Chloroflexi	2.5	11.4	5.7	6.3	5.7	12.7	0.2			
Cyanobacteria	8.0	15.3	6.2	13.5	6.3	16.0	13.7	20.1	64.5	83.4
Planctomycetes	4.4	12.0	10.8	5.3	9.2	12.8	1.1		1.1	
Proteobacteria	61.4	35.5	45.1	38.8	47.3	36.6	80.6	79.9	29.6	16.6
Spirochaetes	0.3	1.6	3.5	0.3	2.4	3.6	1.2			
Verrucomicrobia	4.7	7.0	8.4	5.3	7.3	3.9	2.1		4.7	
Others	0.3	1.1	0.8	3.8	0.9	0.2	0.8			

Table A4.8. Relative abundance of bacterial taxonomy (**class level**) of a **pustular mat microcosm** subjected to **Windalia petroleum exposure** for up to 1 year. Shown are the differences between total bacteria (DNA) and active bacteria (cDNA) communities. Petroleum-exposed sub-samples are represented with a grey shade.

taxonomy	PM OC3 T0 DNA	PM OC3 T0 cDNA	PM OC3 T1 DNA	PM OC3 T1 cDNA	PM OC3 T5 DNA	PM OC3 T5 cDNA	PM OC3 T10 DNA	PM OC3 T10 cDNA	PM OC3 T1y DNA	PM OC3 T1y cDNA
Bacteria_Unclassified	0.1	2.6	2.5	3.1	4.0	4.2	0.4			
BME43	3.0	2.3	2.2	1.0	1.8	1.5				
Bacteroidia	0.7	0.9	0.5	4.0	0.5	0.6				
Cytophagia	7.4	3.8	6.3	2.4	6.3	4.1	0.0			
Saprospirae	6.4	5.0	5.7	4.1	5.1	2.2			0.1	
Anaerolineae	2.5	11.1	5.6	5.3	5.6	12.4	0.1			
Chloroflexi		0.2	0.1	0.5		0.3				
Oscillatoriophycideae	2.6	1.0	1.2	0.8	1.2	0.4	1.8	3.7	2.3	1.3
Synechococcophycideae	4.3	12.1	1.9	6.5	2.5	13.8	11.4	16.4	62.1	80.8
Phycisphaerae	0.4	1.9	2.6	0.2	2.2	0.9	1.1		1.1	
Planctomycetia	4.0	9.4	7.6	4.9	6.7	11.4	0.0		0.1	
Alphaproteobacteria	50.4	24.8	29.7	16.3	31.4	24.6	72.7	78.3	17.0	14.6
Betaproteobacteria				8.9						
Deltaproteobacteria	7.8	8.7	9.7	8.0	10.8	9.7	0.5		0.3	
Gammaproteobacteria	3.1	1.9	5.2	4.9	4.7	2.2	7.5	1.6	12.3	2.0
Spirochaetes	0.0	0.1	1.5	0.2	1.2	1.0	1.1			
Opitutae	2.0	2.5	4.3	0.4	3.5	0.9	0.8		2.0	
Verrucomicrobiae	2.0	3.1	2.8	2.3	2.1	1.8	1.3		2.7	
Cyanobacteria_Unclassified		1.4	1.3	0.1	0.6	1.7	0.1			1.3
Chloroplast	0.9	0.5	1.5	5.3	1.6	0.2				
Others (<3%)	2.4	6.8	7.9	20.8	8.0	6.2	1.2			

Table A4.9. Nearest Sequenced Taxon Index (NSTI) values for **smooth** mat control and (Windalia) petroleum-exposed microcosm.

Type of microcosm	Sub-sample ID	Description	NSTI value
Petroleum-exposed	SM_OC3_T1y_DNA	DNA – 1 year petroleum-exposed smooth microbial mat microcosm	0.09
Petroleum-exposed	SM_OC3_T1y_cDNA	cDNA – 1 year petroleum-exposed smooth microbial mat microcosm	0.09
Control	SM_OC3_T0_DNA	DNA – smooth microbial mat control microcosm (T0)	0.12
Control	SM_OC3_T0_cDNA	cDNA – smooth microbial mat control microcosm (T0)	0.13

Table A4.10. Nearest Sequenced Taxon Index (NSTI) values for **pustular** mats control and Windalia petroleum-exposed microcosms.

Type of microcosm	Sub-sample ID	Description	NSTI value
Petroleum-exposed	PM_OC3_T1y_DNA	DNA – 1 year petroleum-exposed pustular microbial mat microcosm	0.08
Petroleum-exposed	PM_OC3_T1y_cDNA	cDNA – 1 year petroleum-exposed pustular microbial mat microcosm	0.08
Control	PM_OC3_T0_DNA	DNA – pustular microbial mat control microcosm (T0)	0.10
Control	PM_OC3_T0_cDNA	cDNA – pustular microbial mat control microcosm (T0)	0.13

Chapter 5

CONCLUSIONS AND OUTLOOK

"Everything simple is false. Everything complex is unusable" Paul Valéry (1942)

This PhD research project represents the first systematic laboratory study of the likely impacts of petroleum spills on smooth and pustular hypersaline microbial mats of Shark Bay. The unique microbiomes of this World Heritage listed marine site faces an increased risk of hydrocarbon impact due to the rising number of shipping activities in the region. Biogeochemical analysis of the simulation experiments undertaken revealed shifts in the microbial mat communities to short- (pulse) and long-term (press) petroleum hydrocarbon exposure, and an increase in the relative abundances of taxa that likely carried genes that were predicted to be involved in resistance and resilience to such disturbances. A better understanding of the drivers of hydrocarbon resistance in the Shark Bay mats will likely also prove insightful for helping to forecast the response of microbial communities in other similar habitats when exposed to petroleum. The potential of the mat microbiome to biodegrade hydrocarbons was also briefly explored, although further focused work would be needed to quantify their actual capacity to biodegrade hydrocarbon compounds and form active metabolites.

To provide first insights into the resilience of microbial mat microbiomes to short and long-term petroleum exposure (PE), as well as the potential role the key members of these microbiomes play in the degradation of hydrocarbons, this research also introduces an appropriate and new experimental protocol that could be broadly adopted as a feasible and cost-effective analytical framework for similar experiments in the future. The full analytical approach included field collection of viable specimens; a laboratory set-up supporting the growth of the mats; exposing the mats to petroleum; and the combination of well-known taxonomical approaches and recently developed bioinformatic tools to predict the physiological properties of the residing microbial communities.

Several of the noteworthy outcomes of this research are separately detailed under the following sub-headings:

5.1. Laboratory controlled incubation experiments in microbial ecology: advantages and limitations

Experimental approaches constitute a key part of microbial ecology and have been extensively used to study marine coastal habitats for determining both microbial composition and functioning under pristine conditions (Benton et al., 2007; Bolhuis et al., 2014). Experimental datasets are fundamental for simulating and predicting ecological responses when the environment is physically, chemically or biologically disturbed (Benthien et al., 2004; Abed et al., 2006; Bordenave et al., 2007; Llirós et al., 2008; Shade et al., 2012b; Cravo-Laureau and Duran, 2014; Fathepure, 2014). This research relied substantially on a reductionist experimental approach, where important environmental variables (*i.e.*, air supply, light regime and wavelength, salinity and temperature) were controlled under lab conditions in order to reduce the complexities and interdependences between the variables or factors that drive Shark Bay's microbial mat ecosystems. In this regard, the PE was considered to be the most important remaining driving factor controlling the microbial community composition under the designed experimental settings other than the effects of the incubation (*i.e.,* microcosm) isolation itself (**Chapters 2** and **4**).

A robust experimental setup including control microcosms was used for the press disturbance time series experiment (**Chapter 2**) to confirm that: (1) PE was the major cause of the observed changes in the microbial composition; (2) microbial community changes remained stable and were not significantly influenced by the lab conditions; and (3) no chemical and microbial cross-contamination occurred over the course of incubation. In addition, they aided to (4) determine the level of weathering that impacted the composition of petroleum compounds during the time series incubation. Moreover, limiting the sampling points only to initial (T0) and final stages (T30, T60, or T120) was fundamental to preserve the integrity of the mat structure as much as possible given the sample size, to minimise the introduction of any chemical and biological contaminants, and to ensure that enough sample material was available for further analysis. The limited amount of available microbial mat material furthermore forced us to implement a simplified experimental setup and sampling strategy for the pulse incubation experiment (**Chapter 4**). This impacted the ability to obtain and analyse replicate samples. Thus, it would be important to repeat both experimental setups and sampling schemes to evaluate their reproducibility in future studies. However, the results of **Chapters 2** and **4** experiments were highly consistent and comparable (see section 5.3 for details), suggesting that this experimental approach can be successfully applied to monitor microbiome dynamics in environments impacted by petroleum pollutants.

5.2. Methods used for microbial and functional diversity assessment: advantages and setbacks

Microbial (bacterial and archaeal) diversity was investigated in **Chapters 2** and **4**. Amplicon sequencing of the taxonomic marker gene encoding for 16S rRNA remains a widely used approach to characterise the microbial diversity of environmental samples. However, 16S rDNA is located on the microbial genome and genomic DNA can be detected for many days after the cells cease (Selenska and Klingmüller, 1991; Haack et al., 2015) and can even be preserved for hundreds of thousands of years in anoxic and sulfidic sediments (Coolen and Overmann, 2007). 16S rDNA profiling is therefore not suitable to differentiate between live and dead cells (Nielsen et al., 2007). Instead, since gene transcription is among the first levels of cellular response to

stimuli, gene transcripts (RNA) are increasingly being used to target active members of microbial communities (Emerson et al., 2017 and references therein). In this research, amplicon sequencing of environmental 16S rDNA *vs*. reverse transcribed 16S rRNA was used to identify which fraction of the community was alive and active at the time of sampling (**Chapters 2** and **4**). The comparison of DNA- and RNA-based datasets at phylum level revealed that cyanobacteria remained the most important active photoautotrophic communities and were able to resist the stressful PE for the entire duration of both press- and pulse disturbance time series experiments (**Chapters 2** and **4**). Furthermore, at species level, many microorganisms identified in the DNA-based dataset were not detected or were not as abundant as in the cDNA-based dataset. This may be due to the above-described slow decay of environmental DNA, which would have resulted in an overestimation of bacterial richness. A more reliable estimation of bacterial richness comes from the analysis of the living communities through the analysis of 16S rRNA transcripts, which is important to assess ecological resilience and resistance. Although, rRNA occurs in all living microbes including those that are dormant (Blazewicz et al., 2013), a combined analysis of barcoding genes in both DNA and cDNA pools provide a more accurate estimation of changes in the relative abundance of the living microbial population than one based on DNA alone (Blazewicz et al., 2013; Li et al., 2017).

The bioinformatics tool PICRUSt (**Chapters 3** and **4**) (Langille et al., 2013) has so far been used with caution to predict the functional potential of a microbial community based on 16S rRNA gene sequencing data (Jeanbille et al., 2016; Roy et al., 2018; Salerno et al., 2018). The latest improved version (PICRUSt2) offers a 20-fold increase in the build-in bacterial and archaeal genomes database for comparison (Integrated Microbial Genomes – IMG) (Markowitz et al., 2012; Douglas et al., 2020) and was utilised for this thesis to predict functions from the microbial mat 16S rRNA datasets and to generate a model for the ecological 'functional' resilience and resistance of the petroleum-exposed microbial mats. However, applying the PICRUSt2 algorithm to both datasets generated from press and pulse disturbances experiments (**Chapters 3** and **4**), resulted in the removal of those samples which contained a majority of sequences that could not be accurately placed in the reference tree or that did not have good coverage in the reference genomic database (*i.e.*, NSTI > 0.15). The number of

samples with acceptable NSTI values was higher for the press disturbance experiment (**Chapter 3)** so that the predicted functions and functional pathways could be explored in more detail than the pulse disturbance dataset of **Chapter 4**, which only relied on a few samples.

5.3. Resilience and resistance of smooth and pustular mats exposed to petroleum

5.3.1. Microbial diversity shifts

Smooth and pustular mats from Shark Bay contain more than 50 different types of bacterial phyla[40] (Allen et al., 2009). A similarly high microbial diversity was observed in the extreme hypersaline environment in Guerrero Negro (Mexico), which is considered exceptionally diverse compared to the microbial diversity observed in most other non-saline microbial habitats (Harris et al., 2013). High microbial diversity is thought to be a requisite or guarantee to successfully face disturbances, since surviving organisms will likely have functional redundancy capable of maintaining the pre-disturbance functionality when other organisms fail (Yachi and Loreau, 1999). However, this premise can be argued based on the ecological responses observed from the experimental incubations performed in this study. **Chapter 2** describes how smooth and pustular mats responded to 30, 60 or 120 days continuous (press) disturbance to PE. The overall response was a progressive loss of their net microbial diversity over time. However, the rate of the (net) microbial diversity's decline was lower in smooth- than in pustular mats. Pustular mats were capable of developing thick biofilms after 100 days of PE, which likely prevented further loss of its microbial diversity (see section 5.3.4. for more details). The microbial mat microbiome responses to long-term press disturbance were compared to a short-term or pulse disturbance in **Chapter 4**. During this pulse incubation experiments, the same smooth and pustular mats were subjected to 10 days of acute petroleum contamination. Following the removal of the majority of the petroleum, the extent of recovery of the pulse-disturbed mat microbiomes was studied from subsamples taken one year later. The pulse-disturbed pustular mats showed a sharper decline in microbial diversity after

[40] Also confirmed in this study.

10 days of PE and no sign of recovery one year after most of the petroleum contaminant was removed. In contrast, the original microbial composition of the smooth mat did not change during the first 10 days of pulse petroleum disturbance and experienced only 30 % reduction in microbial diversity one year after recovery.

The pattern observed led, for the first time in hypersaline environments, to the development of a conceptual model to assess the ecological resistance and resilience of smooth and pustular mats to PE (**Chapter 4**). The model revealed that: (1) smooth mats are more resistant than pustular mats and likely more resilient after a recovery period, (2) pustular mats are neither resilient nor resistant to acute PE. The model also estimated a threshold before the mat microbiomes reached a new alternative state: smooth mat microbiomes may likely resist petroleum disturbance for as long as 30 days, while pustular mats would be able to deal with this type of disturbance for 5 to 10 days. This implies that the high microbial diversity of the Shark Bay microbial mats does not guarantee microbial stability and should not be used as an indicator of resistance to disturbances.

5.3.2. Microfabric as potential major driving factor for ecological resistance

In **Chapter 2**, it is proposed that differences in the microfabric architecture (Jahnert and Collins, 2013; Plet et al., 2018) play an important role in determining the observed differences in the level of microbial resistance to PE between the smooth and pustular mats. Notably, changes in the permeability of the mineral matrix may cause positive or negative effects to the loss in the microbial diversity of the smooth and pustular mats, respectively. The microfabric of pustular mats is highly permeable, which is expected to enable fast penetration of water-soluble petroleum components into the internal mineral matrix of the pustular mat, and to cause a rapid loss in microbial diversity. In contrast, the microfabric of the smooth mat is more compact and laminated, which may have slowed down penetration of the petroleum contaminants, providing physical refuge to the microbial communities that were present inside its matrix. In macroscale ecology, this phenomenon is associated with a concept called landscape connectivity, or degree of connectivity among spaces or 'landscape elements' (Tischendorf and Fahrig, 2000; Nes and Scheffer, 2005).

5.3.3. Microbial compositional succession

Microbial succession is a commonly described ecological response to disturbances (McGenity et al., 2012). This concept was studied here to understand the initial microbial assembly and stability in extreme environments (*e.g.* hypersaline environments) and whether PE resulted in a shift to new microbial consortia including the emerging of new species that could be linked to biodegradation.

Petroleum exposure re-structured the microbial composition of both types of microbial mats (**Chapters 2** and **4**) and the extent of this change was associated with the duration of the disturbance. A significant finding was that regardless of the type of petroleum utilised as pollutant, and the type of microbial mat, the PE resulted in the enrichment of Cyanobacteria as the main microbial group, followed by Alpha- and Gammaproteobacteria. At species level, PE resulted in the emergence of similar indicator species in both mat types *i.e.*, *Halomonas*, *Marinobacter* spp. and Alteromonadaceae (**Chapter 4**).

5.3.4. Biofilm formation as an adaptive response

Microbial biofilms occur widely in nature, are known to overgrow man-made objects, and can form inside living organisms, including humans (Flemming et al., 2016). There is extensive evidence that biofilms facilitate the survival of microbes under stressed or toxic conditions, *i.e.,* they prolong the persistence of chronic infections (Kostakioti et al., 2013; Kose et al., 2018). In this study, it was found that the development of microbial biofilms was a crucial (ecological) response of pustular mats to PE (**Chapter 2**). This adaptive response likely compensated for the ecological vulnerability of their microbiome to PE, reversing the decline in microbial diversity observed in the 30-day and 60-day petroleum-exposed microcosms (**Chapter 2**). In terms of microbial composition, the formation of this biofilm is strong evidence that it benefited the growth of more specialised organisms not previously detected in the petroleum-exposed mat.

5.4. Shark Bay's microbial mat hydrocarbon biodegradation capabilities

Although the role of microbial mats in the biodegradation of petroleum and other harmful chemical compounds has been previously investigated (Abed et al., 2002,

2006, 2014, 2015; Benthien et al., 2004; Sánchez et al., 2006; Bordenave et al., 2007; Borgne et al., 2008; Llirós et al., 2008, 2008), similar studies are still scarce in hypersaline conditions or environments. As a result, there is still considerable controversy about the extent to which microorganisms are capable of degrading hydrocarbons in hypersaline settings (Martins and Peixoto, 2012). In **Chapters 2** and **4**, it was demonstrated that PE led to a compositional turnover of the original microbial composition leading to the development of several known hydrocarbon-degraders that can preferentially degrade *n*-alkanes, isoprenoids, and aromatic compounds over other organic substrates.

PICRUSt2 analysis predicted that both press- and pulse disturbances associated with PE resulted in an increase in the relative abundance of taxa that possessed genes indicative of stress responses and had the ability to degrade xenobiotics (*i.e.*, hydrocarbons) (**Chapters 3** and **4**). These 16S rRNA-predicted functions found in both mat types overlap with functions described from similar hypersaline environments inferred from extensive shotgun metagenomic and metatranscriptomic profiling (Aubé et al., 2020). Membrane transport and signal transduction represented those metabolic functions mainly expressed in the polluted mats in Aube's study, in particular, those related to ABC transporters and two-component systems (OmpR family). Interestingly, these were among the more abundant predicted functions in our PE microbial mats (**Chapter 3**). and have been previously associated to the modification of microbial physiology as an adaptative response to pollution (Busch et al., 2018; Aubé et al., 2020). PICRUSt2 also emphasised the potential development of taxa that harbor genes involved in the cleavage of aromatic rings, which were not predicted from the control microcosms (**Chapter 3**). However, the rate of petroleum degradation varies, being usually a slow process (Hook et al., 2017) and the initial chemical assessment (**Chapter 3**) performed on saturated and aromatic fractions of the samples collected in the petroleum-water phase from either controls (Type II) or petroleum-exposed microcosms did not yield conclusive evidence for extensive petroleum biodegradation. Some of the widely used biomarkers of biodegradation (*i.e.*, either saturates and LMW aromatics) were likely removed by (typical) physical processes during incubation. Furthermore, a 'concentration effect' might have masked the detection of small chemical changes in the samples.

5.5. Implications for conservation of Shark Bay and other similar habitats

The observed differences in the vulnerability of microbial communities to PE caused by differences in the microfabric between smooth and pustular mats might serve as guidance to forecast the effects of a possible petroleum spill in under-studied hypersaline microbial mat ecosystems elsewhere. In the case of a petroleum spill, microbial communities associated with a predominantly sand-sized highly permeable mineral matrix (similar to a non-lithified-pustular mat) will likely be severely impacted within days after exposure. This requires the removal of any traces of the contaminant in the first five-ten days after the disturbance. Thus, to protect the microbial mats in Shark Bay and to be able to conserve its values as a World Heritage location, this study shows the necessity of maintaining Shark Bay under a high level of protection and even limiting close access of petrol or diesel operated boats in the region. The data used to evaluate the potential of a petroleum spill and its impact in this protected area is rather overdue, since the last publicly open report was published in 2012. Based on the outcomes of this thesis, it is highly recommended to re-assess the environmental risk of the region to possible petroleum spills, including modelling of transport of contaminants and projected physical and chemical changes because of climate change (NESP Earth Systems and Climate Change Hub, 2018; Morris et al., 2019; Reinold et al., 2019).

5.6. Recommendations for future work

To further improve or complement this systematic study there are a number of recommendations and suggested future work that are detailed as follows:

5.6.1. Experimental design and sampling

a) Parallel analysis of fine-scaled physicochemical parameters using microelectrodes: Future time series microcosm experiments should employ micro sensors to monitor scalar irradiance and temporal changes in pH, O_2, hydrogen, methane, and hydrogen sulfide consumption and/or production within the upper few mm of the microbial mats. The measurement of these parameters is key for revealing the dynamic of aerobic and anaerobic processes in microbial mats (*i.e.*, anoxygenic photosynthesis, sulfate reduction and fermentation) (Grötzschel et al., 2002; Pagès et

al., 2014; Nielsen et al., 2015). Using multivariate statistical analysis, it will be possible to determine which communities contribute to these processes while degradation occurs in real time.

b) Modification of salinity and other variables for simulating climate change effects: A recent model tested the stability of microbial mat habitats to changes in salinity, hydrodynamic disturbances, and long-term ocean acidification in the context of climate change (Morris, 2019). However, the model was limited in its ability to predict the responses of some microbial-driven processes (*e.g.* biomineralisation). A similar long-term microcosm experiment and approach as described in this thesis could be used to investigate long-term microbial community responses to elevated levels of salinity, thermal stress, or ocean acidification and to assist in the calibration of model-based predictions of the fate of microbial mats affected by climate change.

c) Time-series sampling: Due to limitations in the amount of microbial mat material that could be sampled from Shark Bay, it was not possible to include more sampling points for the parallel pulse disturbance incubation experiment. Additional time points would have resulted in a completed conceptual model for both press and pulse disturbances. Also, due to the slow growth rate of petroleum degraders, similar microcosm incubation experiments with petroleum-exposed microbial mats should be conducted and monitored for several years to allow the emerging hydrocarbon degraders to remove (the majority of) the petroleum, and to verify whether this results in a full restauration of the original mat microbiomes.

5.6.2. Omics microbiological analysis

a) RNA-sequencing for targeting functional processes and mechanisms of biodegradation: There is a current need to expand our understanding of the diversity of hydrocarbon-degrading bacteria in hypersaline environments, and to elucidate which mechanisms they use for the degradation of hydrocarbons under aerobic as well as anaerobic conditions (Fathepure, 2014). Functional predictions from environmental 16S rRNA genes and transcripts using bioinformatics tools like PICRUSt2 can by no means provide direct proof that biodegradation of petroleum is taking place. We recommend selection of a smaller set of samples where PICRUSt2 predicted a unique diversity of putative petroleum degraders for more in-depth shotgun sequencing of

environmental metagenomes. This will provide taxonomic and functional diversity information based on randomly sequenced environmental functional genes and for the subsequent assembly of environmental metagenomes (MAGs) of the most important members of the mat microbiomes. The parallel sequencing of environmental functional gene transcript using metatranscriptomics and subsequent mapping of the metatranscriptomes to the MAGs (Salazar et al., 2019) will reveal which microbes are actively expressing genes involved in important physiological processes, including those associated with hydrocarbon degradation or the adaptation to elevated salinity (Litchfield, 1998; Edbeib et al., 2016). Further proteomic analysis will provide ultimate proof that the functional gene transcripts have been translated in the respective proteins and enzymes involved in the respective physiological processes (Guazzaroni et al., 2013).

b) Microbial isolation for expanding the identification of hydrocarbon-degraders and unclassified members in understudied hypersaline mat microbiomes: This work confirmed previous studies showing that Shark Bay microbial mats ecosystems exhibit a high microbial diversity. While genomic reference databases are constantly expanding with human gut microorganisms (Zou et al., 2019), microbiomes from other environmental samples (*i.e.,* oceans) (Almeida et al., 2018) are still less represented. This is also true especially for the analysed pristine microbial mat samples from Shark Bay. Many taxa appeared to have not been identified from other environments, as they could only be classified at order, class or even phylum levels through comparison with sequences available in public databases. A loss of microbial diversity in petroleum-exposed mats resulted in a higher relative abundance of taxa that could be identified at family to species level. This shows the potential of the ability to design cultivation media for the selective isolation of bacteria from petroleum-exposed Shark Bay microbial mats to study their stress-responses mechanisms (Bodor et al., 2020). The successful isolation of petroleum degraders from these hypersaline mats could have potential biotechnological applications, particularly in bioremediation (Borgne et al., 2008).

5.6.3. Organic geochemical analyses

a) Determining degree of biodegradation in water: The initial assessment of biodegradation performed on the petroleum-water phase (**Chapter 3**), was shown to be insufficient due to the difficulty of distinguishing between weathering processes and biodegradation. It is recommended to re-analyse the saturated fraction targeting the diastereomers of acyclic isoprenoids. It has been found that the certain diastereomers of *nor*pristane (2,6,10–trimethylpentadecane), phytane (2,6,10,14-tetramethylhexadecane) and pristane (2,6,10,14-tetramethylpentadecane) possesses different biological susceptibilities, and therefore might help to elucidate to what extent biodegradation happen (if any). This method is described in detail in McIntyre *et al.* (2007).

b) Determining degree ofbiodegradation in the microbial mat samples (sediment-water phase) and related metabolites: During the time-series incubation experiments in **Chapter 2**, additional samples of the top centimetre of the microbial mat were collected and preserved to expand the organic analysis (if required) to optimise the use and extraction of information from a holistic point of view. Thus, between 3-5g (wet-weight) of this material, and a small portion of biofilm is available for further analysis. It is suggested to perform an organic extraction on this material to analyse the saturate, aromatic, and polar fractions. The first two fractions can be compared with the results from the petroleum-water phase to assess whether biodegradation was enhanced in the mineral matrix where a higher microbial activity is expected. Also, the chemical analysis of the polar fraction will help to detect metabolites potentially formed during biodegradation.

c) Selection of petroleum samples as pollutant: The selection of type of petroleum samples as pollutant represented a challenge in this research project. It placed a dilemma between facilitating the access to biodegradable compounds and the likelihood of the chemical composition of petroleum traces that might certainly reach the inner coastline of Hamelin Pool. Even though, it would be unlikely for a petroleum rich in low MW hydrocarbons (as B101 and Windalia are) to make it onshore with the volatile fraction still being present, it was necessary to choose relatively easy to biodegraded petroleum types for our studies. With a total available time for both lab

work and data analysis of 2.5 years after submitting the candidacy proposal, it was not possible to extend PE to more than one year. In future experiments, it is recommended to repeat these experiments with more representative less biodegradable petroleum types and to consider longer PE times.

Bibliography

"Every reasonable effort has been made to acknowledge the owners of copyright material. I would be pleased to hear from any copyright owner who has been omitted or incorrectly acknowledged"

A

Abed, R. M. M. (2010). Interaction between cyanobacteria and aerobic heterotrophic bacteria in the degradation of hydrocarbons. International Biodeterioration & Biodegradation 64, 58–64. doi:10.1016/j.ibiod.2009.10.008.

Abed, R. M. M., Al-Kharusi, S., Prigent, S., and Headley, T. (2014). Diversity, Distribution and Hydrocarbon Biodegradation Capabilities of Microbial Communities in Oil-Contaminated Cyanobacterial Mats from a Constructed Wetland. PLoS ONE 9, e114570. doi:10.1371/journal.pone.0114570.

Abed, R. M. M., Al-Thukair, A., and De Beer, D. (2006). Bacterial diversity of a cyanobacterial mat degrading petroleum compounds at elevated salinities and temperatures: Microbial mats from Saudi Arabia. FEMS Microbiology Ecology 57, 290–301. doi:10.1111/j.1574-6941.2006.00113.x.

Abed, R. M. M., Dobretsov, S., and Sudesh, K. (2009). Applications of cyanobacteria in biotechnology. Journal of Applied Microbiology 106, 1–12. doi:10.1111/j.1365-2672.2008.03918.x.

Abed, R. M. M., Klempová, T., Gajdoš, P., and Čertík, M. (2015). Bacterial diversity and fatty acid composition of hypersaline cyanobacterial mats from an inland desert wadi. Journal of Arid Environments 115, 81–89. doi:10.1016/j.jaridenv.2015.01.010.

Abed, R. M. M., and Köster, J. (2005). The direct role of aerobic heterotrophic bacteria associated with cyanobacteria in the degradation of oil compounds. International Biodeterioration & Biodegradation 55, 29–37. doi:10.1016/j.ibiod.2004.07.001.

Abed, R. M. M., Safi, N. M. D., Köster, J., Beer, D. de, El-Nahhal, Y., Rullkötter, J., et al. (2002). Microbial Diversity of a Heavily Polluted Microbial Mat and Its Community Changes following Degradation of Petroleum Compounds. Appl. Environ. Microbiol. 68, 1674–1683. doi:10.1128/AEM.68.4.1674-1683.2002.

Abisado, R. G., Benomar, S., Klaus, J. R., Dandekar, A. A., and Chandler, J. R. (2018). Bacterial Quorum Sensing and Microbial Community Interactions. mBio 9. doi:10.1128/mBio.02331-17.

Abou Khalil, C., Prince, V. L., Prince, R. C., Greer, C. W., Lee, K., Zhang, B., et al. (2021). Occurrence and biodegradation of hydrocarbons at high salinities.

Science of The Total Environment 762, 143165. doi:10.1016/j.scitotenv.2020.143165.

Ahmed, M., and George, S. C. (2004). Changes in the molecular composition of crude oils during their preparation for GC and GC–MS analyses. *Organic Geochemistry* 35, 137–155. doi:10.1016/j.orggeochem.2003.10.002.

Aitken, C. M., Jones, D. M., and Larter, S. R. (2004). Anaerobic hydrocarbon biodegradation in deep subsurface oil reservoirs. Nature 431, 291–294. doi:10.1038/nature02922.

Alav, I., Sutton, J. M., and Rahman, K. M. (2018). Role of bacterial efflux pumps in biofilm formation. J. Antimicrob. Chemother. 73, 2003–2020. doi:10.1093/jac/dky042.

Al-awadhi, H., Al-mailem, D., Dashti, N., Khanafer, M., and Radwan, S. (2012). Indigenous hydrocarbon-utilizing bacterioflora in oil-polluted habitats in Kuwait, two decades after the greatest man-made oil spill. Archives of Microbiology; Berlin 194, 689–705. doi:http://dx.doi.org.dbgw.lis.curtin.edu.au/10.1007/s00203-012-0800-7.

Alexander, R., Kagi, R. I., Woodhouse, G. W., and Volkman, J. K. (1983). The geochemistry of some biodegraded Australian Oils. The APPEA Journal 23, 53–63. doi:10.1016/S0960-9822(97)70976-X.

Allen, M. A., Goh, F., Burns, B. P., and Neilan, B. A. (2009). Bacterial, archaeal and eukaryotic diversity of smooth and pustular microbial mat communities in the hypersaline lagoon of Shark Bay. Geobiology 7, 82–96. doi:10.1111/j.1472-4669.2008.00187.x.

Allison, S. D., and Martiny, J. B. H. (2008). Resistance, resilience, and redundancy in microbial communities. PNAS 105, 11512–11519. doi:10.1073/pnas.0801925105.

Allwood, A. C., Walter, M. R., Kamber, B. S., Marshall, C. P., and Burch, I. W. (2006). Stromatolite reef from the Early Archaean era of Australia. Nature 441, 714–718. doi:10.1038/nature04764.

Almeida, A., Mitchell, A. L., Tarkowska, A., and Finn, R. D. (2018). Benchmarking taxonomic assignments based on 16S rRNA gene profiling of the microbiota from commonly sampled environments. Gigascience 7. doi:10.1093/gigascience/giy054.

Alneberg, J., Karlsson, C. M. G., Divne, A.-M., Bergin, C., Homa, F., Lindh, M. V., et al. (2018). Genomes from uncultivated prokaryotes: a comparison of metagenome-assembled and single-amplified genomes. Microbiome 6. doi:10.1186/s40168-018-0550-0.

Antwis, R. E., Griffiths, S. M., Harrison, X. A., Aranega-Bou, P., Arce, A., Bettridge, A. S., et al. (2017). Fifty important research questions in microbial ecology. FEMS Microbiol Ecol 93. doi:10.1093/femsec/fix044.

Arey, J. S., Nelson, R. K., Xu, L., and Reddy, C. M. (2005). Using Comprehensive Two-Dimensional Gas Chromatography Retention Indices To Estimate Environmental Partitioning Properties for a Complete Set of Diesel Fuel Hydrocarbons. Anal. Chem. 77, 7172–7182. doi:10.1021/ac051051n.

Armanios, C., Alexander, R., and Kagi, R. I. (1992). High diahopane and neohopane abundances in a biodegraded crude oil from the Barrow sub-basin of Western Australia. Organic Geochemistry 18, 641–645. doi:10.1016/0146-6380(92)90089-G.

Arp, G., Reimer, A., and Reitner, J. (2001). Photosynthesis-Induced Biofilm Calcification and Calcium Concentrations in Phanerozoic Oceans. Science 292, 1701–1704. doi:10.1126/science.1057204.

Askeland, R. A., and Morrison, S. M. (1983). Cyanide production by Pseudomonas fluorescens and Pseudomonas aeruginosa. Applied and Environmental Microbiology 45, 1802–1807. doi:10.1128/AEM.45.6.1802-1807.1983.

Aßhauer, K. P., Wemheuer, B., Daniel, R., and Meinicke, P. (2015). Tax4Fun: predicting functional profiles from metagenomic 16S rRNA data. Bioinformatics 31, 2882–2884. doi:10.1093/bioinformatics/btv287.

Aubé, J., Senin, P., Bonin, P., Pringault, O., Jeziorski, C., Bouchez, O., et al. (2020). Meta-omics Provides Insights into the Impact of Hydrocarbon Contamination on Microbial Mat Functioning. Microb Ecol. doi:10.1007/s00248-020-01493-x.

Austin, B. (2017). The value of cultures to modern microbiology. Antonie van Leeuwenhoek 110, 1247–1256. doi:10.1007/s10482-017-0840-8.

Australian Maritime Safety Authority (AMSA) (2012). Report on the 2011/12 Review of the National Plan to Combat Pollution of the Sea by Oil and Other Hazardous and Noxious Substances and the National Maritime Emergency Response Arragements (2011-2012). Australian Government Available at: https://www.amsa.gov.au/sites/default/files/natplan-review-report.pdf [Accessed June 9, 2020].

B

Babilonia, J., Conesa, A., Casaburi, G., Pereira, C., Louyakis, A. S., Reid, R. P., et al. (2018). Comparative Metagenomics Provides Insight Into the Ecosystem

Functioning of the Shark Bay Stromatolites, Western Australia. Front. Microbiol. 9, 1359. doi:10.3389/fmicb.2018.01359.

Bahram, M., Anslan, S., Hildebrand, F., Bork, P., and Tedersoo, L. (2019). Newly designed 16S rRNA metabarcoding primers amplify diverse and novel archaeal taxa from the environment. Environ Microbiol Rep 11, 487–494. doi:10.1111/1758-2229.12684.

Balvočiūtė, M., and Huson, D. H. (2017). SILVA, RDP, Greengenes, NCBI and OTT — how do these taxonomies compare? BMC Genomics 18, 114. doi:10.1186/s12864-017-3501-4.

Barbera, P., Kozlov, A. M., Czech, L., Morel, B., Darriba, D., Flouri, T., et al. (2019). EPA-ng: Massively Parallel Evolutionary Placement of Genetic Sequences. Syst Biol 68, 365–369. doi:10.1093/sysbio/syy054.

Barton, L. L., Northup, D. E., and Northup, D. E. (2011). Microbial Ecology. Hoboken, United States: John Wiley & Sons, Incorporated Available at: http://ebookcentral.proquest.com/lib/curtin/detail.action?docID=697468 [Accessed June 27, 2020].

Bayona, J. M., Domínguez, C., and Albaigés, J. (2015). Analytical developments for oil spill fingerprinting. Trends in Environmental Analytical Chemistry 5, 26–34. doi:10.1016/j.teac.2015.01.004.

Bekker, M., Teixeira De Mattos, M. J., and Hellingwerf, K. J. (2006). The Role of Two-Component Regulation Systems in the physiology of the Bacterial Cell. Science Progress 89, 213–242. doi:10.3184/003685006783238308.

Bell, E. M. ed. (2012). Life at extremes: environments, organisms and strategies for survival. Wallingford: CABI doi:10.1079/9781845938147.0000.

Bell, T. H., Yergeau, E., Maynard, C., Juck, D., Whyte, L. G., and Greer, C. W. (2013). Predictable bacterial composition and hydrocarbon degradation in Arctic soils following diesel and nutrient disturbance. ISME J 7, 1200–1210. doi:10.1038/ismej.2013.1.

Benthien, M., Wieland, A., Oteyza, T. G. de, Grimalt, J. O., and Kühl, M. (2004). Oil-contamination effects on a hypersaline microbial mat community (Camargue, France) as studied with microsensors and geochemical analysis. Ophelia 58, 135–150. doi:10.1080/00785236.2004.10410221.

Benton, T. G., Solan, M., Travis, J. M. J., and Sait, S. M. (2007). Microcosm experiments can inform global ecological problems. Trends in Ecology & Evolution 22, 516–521. doi:10.1016/j.tree.2007.08.003.

Berthe-Corti, L., and Nachtkamp, M. (2010). "Bacterial Communities in Hydrocarbon-Contaminated Marine Coastal Environments," in Handbook

of Hydrocarbon and Lipid Microbiology, ed. K. N. Timmis (Berlin, Heidelberg: Springer), 2349–2359. doi:10.1007/978-3-540-77587-4_171.

Bervoets, I., and Charlier, D. (2019). Diversity, versatility and complexity of bacterial gene regulation mechanisms: opportunities and drawbacks for applications in synthetic biology. FEMS Microbiol Rev 43, 304–339. doi:10.1093/femsre/fuz001.

Black, K. S., Paterson, D. M., and Davidson, I. R. (1999). Sediment Microfabric of Oil Rig Drill Spoil Heaps: Preliminary Observations Using Low-Temperature Scanning Electron Microscopy. Environmental Science & Technology 33, 1983–1990. doi:10.1021/es981091r.

Blazewicz, S. J., Barnard, R. L., Daly, R. A., and Firestone, M. K. (2013). Evaluating rRNA as an indicator of microbial activity in environmental communities: limitations and uses. The ISME Journal; London 7, 2061–8. doi:http://dx.doi.org.dbgw.lis.curtin.edu.au/10.1038/ismej.2013.102.

Bodor, A., Bounedjoum, N., Vincze, G. E., Erdeiné Kis, Á., Laczi, K., Bende, G., et al. (2020). Challenges of unculturable bacteria: environmental perspectives. Rev Environ Sci Biotechnol 19, 1–22. doi:10.1007/s11157-020-09522-4.

Bokulich, N. A., Kaehler, B. D., Rideout, J. R., Dillon, M., Bolyen, E., Knight, R., et al. (2018). Optimizing taxonomic classification of marker-gene amplicon sequences with QIIME 2's q2-feature-classifier plugin. Microbiome 6, 90.

Bolhuis, H., Cretoiu, M., and Stal, L. (2014). Molecular ecology of microbial mats. FEMS Microbiology Ecology. doi:10.1111/1574-6941.12408.

Bolyen, E., Rideout, J. R., Dillon, M. R., Bokulich, N. A., Abnet, C. C., Al-Ghalith, G. A., et al. (2019). Reproducible, interactive, scalable and extensible microbiome data science using QIIME 2. Nature biotechnology 37, 852–857.

Bordenave, S., Goñi-Urriza, M. S., Caumette, P., and Duran, R. (2007). Effects of Heavy Fuel Oil on the Bacterial Community Structure of a Pristine Microbial Mat. Applied and Environmental Microbiology 73, 6089–6097. doi:10.1128/AEM.01352-07.

Borgne, S. L., Paniagua, D., and Vazquez-Duhalt, R. (2008). Biodegradation of Organic Pollutants by Halophilic Bacteria and Archaea. MMB 15, 74–92. doi:10.1159/000121323.

Bosak, T., Liang, B., Sim, M. S., Petroff, A. P., and Hoffman, P. F. (2009). Morphological Record of Oxygenic Photosynthesis in Conical Stromatolites. Proceedings of the National Academy of Sciences of the United States of America 106, 10939–10943.

Botton, S., van Heusden, M., Parsons, J. R., Smidt, H., and van Straalen, N. (2006). Resilience of microbial systems towards disturbances. Critical reviews in microbiology 32, 101–112.

Brock, T. D. (1978). "Stromatolites: Yellowstone Analogues," in Thermophilic Microorganisms and Life at High Temperatures Springer Series in Microbiology., ed. T. D. Brock (New York, NY: Springer), 337–385. doi:10.1007/978-1-4612-6284-8_11.

Bryant, D. A., and Frigaard, N.-U. (2006). Prokaryotic photosynthesis and phototrophy illuminated. Trends in Microbiology 14, 488–496. doi:10.1016/j.tim.2006.09.001.

Bukin, Y. S., Galachyants, Y. P., Morozov, I. V., Bukin, S. V., Zakharenko, A. S., and Zemskaya, T. I. (2019). The effect of 16S rRNA region choice on bacterial community metabarcoding results. Sci Data 6. doi:10.1038/sdata.2019.7.

Burling, M. C., Pattiaratchi, C. B., and Ivey, G. N. (2003). The tidal regime of Shark Bay, Western Australia. Estuarine, Coastal and Shelf Science 57, 725–735. doi:10.1016/S0272-7714(02)00343-8.

Burne, R. V., and Moore, L. S. (1987). Microbialites: Organosedimentary Deposits of Benthic Microbial Communities. PALAIOS 2, 241–254. doi:10.2307/3514674.

Burns, B. J., Bostwick, T. R., and Emmett, J. K. (1987). Gippsland terrestrial oils - Recognition of compositional variations due to maturity and biodegradation effects. The APPEA Journal 27, 73–85. doi:10.1071/aj86008.

Burns, B. P., Anitori, R., Butterworth, P., Henneberger, R., Goh, F., Allen, M. A., et al. (2009). Modern analogues and the early history of microbial life. Precambrian Research 173, 10–18. doi:10.1016/j.precamres.2009.05.006.

Bursy, J., Pierik, A. J., Pica, N., and Bremer, E. (2007). Osmotically induced synthesis of the compatible solute hydroxyectoine is mediated by an evolutionarily conserved ectoine hydroxylase. J Biol Chem 282, 31147–31155. doi:10.1074/jbc.M704023200.

Busch, A., Mesa-Torres, N., and Krell, T. (2018). "The Family of Two-Component Systems That Regulate Hydrocarbon Degradation Pathways," in Cellular Ecophysiology of Microbe, ed. T. Krell (Cham: Springer International Publishing), 1–21. doi:10.1007/978-3-319-20796-4_6-1.

C

Cáceres, M. D., and Legendre, P. (2009). Associations between species and groups of sites: indices and statistical inference. Ecology 90, 3566–3574. doi:10.1890/08-1823.1.

Callahan, B. J., McMurdie, P. J., Rosen, M. J., Han, A. W., Johnson, A. J. A., and Holmes, S. P. (2016). DADA2: high-resolution sample inference from Illumina amplicon data. Nature methods 13, 581.

Campbell, B. J., Engel, A. S., Porter, M. L., and Takai, K. (2006). The versatile epsilon-proteobacteria: key players in sulphidic habitats. Nature reviews. Microbiology 4, 458–468.

Campbell, M. A., Grice, K., Visscher, P. T., Morris, T., Wong, H. L., White, R. A. I., et al. (2020). Functional Gene Expression in Shark Bay Hypersaline Microbial Mats: Adaptive Responses. Front. Microbiol. 11. doi:10.3389/fmicb.2020.560336.

Canfield, D. E., and Marais, D. J. D. (1991). Aerobic Sulfate Reduction in Microbial Mats. Science 251, 1471–1473.

Cánovas, D., Vargas, C., Csonka, L. N., Ventosa, A., and Nieto, J. J. (1996). Osmoprotectants in Halomonas elongata: high-affinity betaine transport system and choline-betaine pathway. J Bacteriol 178, 7221–7226. doi:10.1128/jb.178.24.7221-7226.1996.

Cao, K.-A. L., Costello, M.-E., Lakis, V. A., Bartolo, F., Chua, X.-Y., Brazeilles, R., et al. (2016). MixMC: A Multivariate Statistical Framework to Gain Insight into Microbial Communities. PLOS ONE 11, e0160169. doi:10.1371/journal.pone.0160169.

Caporaso, J. G., Lauber, C. L., Walters, W. A., Berg-Lyons, D., Huntley, J., Fierer, N., et al. (2012). Ultra-high-throughput microbial community analysis on the Illumina HiSeq and MiSeq platforms. The ISME Journal 6, 1621–1624. doi:10.1038/ismej.2012.8.

Caporaso, J. G., Lauber, C. L., Walters, W. A., Berg-Lyons, D., Lozupone, C. A., Turnbaugh, P. J., et al. (2011). Global patterns of 16S rRNA diversity at a depth of millions of sequences per sample. Proceedings of the National Academy of Sciences of the United States of America 108, 4516–4522.

Carnevali, P., Schulz, F., Castelle, C., Kantor, R., Shih, C. C., Sharon, I., et al. (2019). Hydrogen-based metabolism as an ancestral trait in lineages sibling to the Cyanobacteria. Nature Communications 10. doi:http://dx.doi.org/10.1038/s41467-018-08246-y.

Chaillan, F., Gugger, M., Saliot, A., Couté, A., and Oudot, J. (2006). Role of cyanobacteria in the biodegradation of crude oil by a tropical cyanobacterial mat. Chemosphere 62, 1574–1582. doi:10.1016/j.chemosphere.2005.06.050.

Chambers, J. C., Allen, C. R., and Cushman, S. A. (2019). Operationalizing Ecological Resilience Concepts for Managing Species and Ecosystems at Risk. Front. Ecol. Evol. 7. doi:10.3389/fevo.2019.00241.

Chamkha, M., Mnif, S., and Sayadi, S. (2008). Isolation of a thermophilic and halophilic tyrosol-degrading Geobacillus from a Tunisian high-temperature oil field. FEMS Microbiol Lett 283, 23–29. doi:10.1111/j.1574-6968.2008.01136.x.

Charlesworth, J. C., Watters, C., Wong, H. L., Visscher, P. T., and Burns, B. P. (2019). Isolation of novel quorum-sensing active bacteria from microbial mats in Shark Bay Australia. FEMS Microbiol Ecol 95. doi:10.1093/femsec/fiz035.

Che, S., and Men, Y. (2019). Synthetic microbial consortia for biosynthesis and biodegradation: promises and challenges. Journal of Industrial Microbiology and Biotechnology 46, 1343–1358. doi:10.1007/s10295-019-02211-4.

Chen, J., Fu, J., Sheng, G., Liu, D., and Zhang, J. (1996). Diamondoid hydrocarbon ratios: novel maturity indices for highly mature crude oils. Organic Geochemistry 25, 179–190. doi:10.1016/S0146-6380(96)00125-8.

Chen, M., Hernandez-Prieto, M. A., Loughlin, P. C., Li, Y., and Willows, R. D. (2019). Genome and proteome of the chlorophyll f-producing cyanobacterium Halomicronema hongdechloris: adaptative proteomic shifts under different light conditions. BMC Genomics 20, 207. doi:10.1186/s12864-019-5587-3.

Chiarucci, A., Nascimbene, J., Campetella, G., Chelli, S., Dainese, M., Giorgini, D., et al. (2019). Exploring patterns of beta-diversity to test the consistency of biogeographical boundaries: A case study across forest plant communities of Italy. Ecology and Evolution 9, 11716–11723. doi:10.1002/ece3.5669.

Chilingar, G. V., Buryakovsky, L. A., Eremenko, N. A., and Gorfunkel, M. V. (2005). Geology and geochemistry of oil and gas. Amsterdam: Elsevier.

Ciccarelli, F. D., Doerks, T., Mering, C. von, Creevey, C. J., Snel, B., and Bork, P. (2006). Toward Automatic Reconstruction of a Highly Resolved Tree of Life. Science 311, 1283–1287. doi:10.1126/science.1123061.

Cipollone, R., Ascenzi, P., Tomao, P., Imperi, F., and Visca, P. (2008). Enzymatic detoxification of cyanide: clues from Pseudomonas aeruginosa Rhodanese. J. Mol. Microbiol. Biotechnol. 15, 199–211. doi:10.1159/000121331.

Clarridge, J. E. (2004). Impact of 16S rRNA Gene Sequence Analysis for Identification of Bacteria on Clinical Microbiology and Infectious Diseases. Clin Microbiol Rev 17, 840–862. doi:10.1128/CMR.17.4.840-862.2004.

Coolen, M. J. L., Muyzer, G., Rijpstra, W. I. C., Schouten, S., Volkman, J. K., and Sinninghe Damsté, J. S. (2004). Combined DNA and lipid analyses of sediments reveal changes in Holocene haptophyte and diatom populations in an Antarctic lake. Earth and Planetary Science Letters 223, 225–239. doi:10.1016/j.epsl.2004.04.014.

Coolen, M. J. L., and Overmann, J. (2007). 217 000-year-old DNA sequences of green sulfur bacteria in Mediterranean sapropels and their implications for the reconstruction of the paleoenvironment. Environ. Microbiol. 9, 238–249. doi:10.1111/j.1462-2920.2006.01134.x.

Cornforth, D. M., and Foster, K. R. (2013). Competition sensing: the social side of bacterial stress responses. Nature reviews. Microbiology 11, 285–293. doi:http://dx.doi.org.dbgw.lis.curtin.edu.au/10.1038/nrmicro2977.

Crank, K. (1973). Geology of Barrow Island Oil Field. The APPEA Journal 13, 49–57. doi:10.1071/aj72008.

Cravo-Laureau, C., and Duran, R. (2014). Marine coastal sediments microbial hydrocarbon degradation processes: contribution of experimental ecology in the omics'era. Front Microbiol 5. doi:10.3389/fmicb.2014.00039.

Cuadros-Orellana, S., Pohlschröder, M., and Durrant, L. R. (2006). Isolation and characterization of halophilic archaea able to grow in aromatic compounds. International Biodeterioration & Biodegradation 57, 151–154. doi:10.1016/j.ibiod.2005.04.005.

Czaczyk, K., and Myszka, K. (2007). Biosynthesis of Extracellular Polymeric Substances. Polish J. of Environ. Stud. 16, 799–806.

Czech, L., Barbera, P., and Stamatakis, A. (2020). Genesis and Gappa: processing, analyzing and visualizing phylogenetic (placement) data. Bioinformatics. doi:10.1093/bioinformatics/btaa070.

D

Dade, W. B., Davis, J. D., Nichols, P. D., Nowell, A. R. M., Thistle, D., Trexler, M. B., et al. (1990). Effects of bacterial exopolymer adhesion on the entrainment of sand. Geomicrobiology Journal 8, 1–16. doi:10.1080/01490459009377874.

Dang, H., and Lovell, C. R. (2016). Microbial Surface Colonization and Biofilm Development in Marine Environments. Microbiol. Mol. Biol. Rev. 80, 91–138. doi:10.1128/MMBR.00037-15.

Dashti, N., Ali, N., Eliyas, M., Khanafer, M., Sorkhoh, N. A., and Radwan, S. S. (2015). Most Hydrocarbonoclastic Bacteria in the Total Environment are

Diazotrophic, which Highlights Their Value in the Bioremediation of Hydrocarbon Contaminants. Microbes and environments 30, 70–75. doi:10.1264/jsme2.ME14090.

DasSarma, S., and Arora, P. (2001). Halophiles. Encyclopedia of Life Sciences.

Dastgheib, S. M. M., Amoozegar, M. A., Khajeh, K., Shavandi, M., and Ventosa, A. (2012). Biodegradation of polycyclic aromatic hydrocarbons by a halophilic microbial consortium. Applied Microbiology and Biotechnology 95, 789–798. doi:10.1007/s00253-011-3706-4.

De Oteyza, T. G., Grimalt, J. O., Llirós, M., and Esteve, I. (2006). Microcosm experiments of oil degradation by microbial mats. Science of The Total Environment 357, 12–24. doi:10.1016/j.scitotenv.2005.04.039.

Decho, A. W. (2000). Microbial biofilms in intertidal systems: an overview. Continental Shelf Research 20, 1257–1273. doi:10.1016/S0278-4343(00)00022-4.

Decho, A. W., and Gutierrez, T. (2017). Microbial Extracellular Polymeric Substances (EPSs) in Ocean Systems. Front Microbiol 8. doi:10.3389/fmicb.2017.00922.

Delgado, M. A., Vincent, P. A., Farías, R. N., and Salomón, R. A. (2005). YojI of Escherichia coli Functions as a Microcin J25 Efflux Pump. Journal of Bacteriology 187, 3465–3470. doi:10.1128/JB.187.10.3465-3470.2005.

Des Marais, D. (2003). Biogeochemistry of Hypersaline Microbial Mats Illustrates the Dynamics of Modern Microbial Ecosystems and the Early Evolution of the Biosphere. Biological Bulletin 204, 160–167. doi:10.2307/1543552.

Desouky, A.-E.-H. (2003). Acinetobacter: environmental and biotechnological applications. African Journal of Biotechnology 2, 71–74. doi:10.5897/AJB2003.000-1014.

Diaz, E., Ferrandez, A., Prieto, M. A., and Garcia, J. L. (2001). Biodegradation of Aromatic Compounds by Escherichia coli. Microbiology and Molecular Biology Reviews 65, 523–569. doi:10.1128/MMBR.65.4.523-569.2001.

Díaz, M., Grigson, S. J. W., Peppiatt, C. J., and Burgess, J. G. (2000). Isolation and Characterization of Novel Hydrocarbon-Degrading Euryhaline Consortia from Crude Oil and Mangrove Sediments. Mar. Biotechnol. 2, 522–532. doi:10.1007/s101260000037.

Diestra, E., Solé, A., and Esteve, I. (2004). A comparative study of cyanobacterial diversity in polluted and unpolluted microbial mats by means CLSM. Ophelia 58, 151–156. doi:10.1080/00785236.2004.10410222.

Ding, H., and Valentine, D. L. (2008). Methanotrophic bacteria occupy benthic microbial mats in shallow marine hydrocarbon seeps, Coal Oil Point,

California. Journal of Geophysical Research: Biogeosciences 113. doi:10.1029/2007JG000537.

DNV (2011). Assessment of the Risk of Pollution from Marine Oil Spills in Australian Ports and Waters. Det Norske Veritas LTD., UK Available at: https://www.amsa.gov.au/sites/default/files/2011-12-mp-dnv-risk-assessment-final-report-oil-spill.pdf [Accessed May 14, 2020].

Dombrowski, N., Donaho, J. A., Gutierrez, T., Seitz, K. W., Teske, A. P., and Baker, B. J. (2016). Reconstructing metabolic pathways of hydrocarbon-degrading bacteria from the Deepwater Horizon oil spill. Nature Microbiology; London 1, 16057. doi:http://dx.doi.org.dbgw.lis.curtin.edu.au/10.1038/nmicrobiol.2016.57.

Donot, F., Fontana, A., Baccou, J. C., and Schorr-Galindo, S. (2012). Microbial exopolysaccharides: Main examples of synthesis, excretion, genetics and extraction. Carbohydrate Polymers 87, 951–962. doi:10.1016/j.carbpol.2011.08.083.

Dorobantu, L. S., Yeung, A. K. C., Foght, J. M., and Gray, M. R. (2004). Stabilization of Oil-Water Emulsions by Hydrophobic Bacteria. Appl. Environ. Microbiol. 70, 6333–6336. doi:10.1128/AEM.70.10.6333-6336.2004.

Doronina, N. V., Trotsenko, Y. A., and Tourova, T. P. (2000). Methylarcula marina gen. nov., sp. nov. and Methylarcula terricola sp. nov.: novel aerobic, moderately halophilic, facultatively methylotrophic bacteria from coastal saline environments. Int J Syst Evol Microbiol 50 Pt 5, 1849–1859. doi:10.1099/00207713-50-5-1849.

Douglas, G. M., Maffei, V. J., Zaneveld, J. R., Yurgel, S. N., Brown, J. R., Taylor, C. M., et al. (2020). PICRUSt2 for prediction of metagenome functions. Nat Biotechnol 38, 685–688. doi:10.1038/s41587-020-0548-6.

Douglas, G. M., Maffei, V. J., Zaneveld, J., Yurgel, S. N., Brown, J. R., Taylor, C. M., et al. (2019). PICRUSt2: An improved and extensible approach for metagenome inference. BioRxiv; Cold Spring Harbor. doi:http://dx.doi.org.dbgw.lis.curtin.edu.au/10.1101/672295.

Dupraz, C., Reid, R. P., Braissant, O., Decho, A. W., Norman, R. S., and Visscher, P. T. (2009). Processes of carbonate precipitation in modern microbial mats. Earth-Science Reviews 96, 141–162. doi:10.1016/j.earscirev.2008.10.005.

Duran, R., and Goñi-Urriza, M. S. (2010). “Impact of Pollution on Microbial Mats,” in Handbook of Hydrocarbon and Lipid Microbiology, ed. K. N. Timmis (Berlin, Heidelberg: Springer), 2339–2348. doi:10.1007/978-3-540-77587-4_170.

E

Echeverz, M., García, B., Sabalza, A., Valle, J., Gabaldón, T., Solano, C., et al. (2017). Lack of the PGA exopolysaccharide in Salmonella as an adaptive trait for survival in the host. PLOS Genetics 13, e1006816. doi:10.1371/journal.pgen.1006816.

Edbeib, M. F., Wahab, R. A., and Huyop, F. (2016). Halophiles: biology, adaptation, and their role in decontamination of hypersaline environments. World J Microbiol Biotechnol 32, 135. doi:10.1007/s11274-016-2081-9.

Edgcomb, V. P., Bernhard, J. M., Summons, R. E., Orsi, W., Beaudoin, D., and Visscher, P. T. (2014). Active eukaryotes in microbialites from Highborne Cay, Bahamas, and Hamelin Pool (Shark Bay), Australia. The ISME Journal 8, 418–429. doi:10.1038/ismej.2013.130.

Emerson, J. B., Adams, R. I., Román, C. M. B., Brooks, B., Coil, D. A., Dahlhausen, K., et al. (2017). Schrödinger's microbes: Tools for distinguishing the living from the dead in microbial ecosystems. Microbiome 5. doi:10.1186/s40168-017-0285-3.

Environmental Protection Authority (2003). A strategic assessment of the compatibility of petroleum Industry activities with the environmental values and cultural uses of the Shark Bay World Heritage Area. Available at: https://www.epa.wa.gov.au/strategic-assessment-compatibility-petroleum-industry-activities-environmental-values-and-cultural.

Essaid, H. I., Bekins, B. A., and Cozzarelli, I. M. (2015). Organic contaminant transport and fate in the subsurface: Evolution of knowledge and understanding. Water Resources Research 51, 4861–4902. doi:10.1002/2015WR017121.

Evans, T. G., and Hofmann, G. E. (2012). Defining the limits of physiological plasticity: how gene expression can assess and predict the consequences of ocean change. Philos Trans R Soc Lond B Biol Sci 367, 1733–1745. doi:10.1098/rstb.2012.0019.

F

Fahy, A., and McKew, B. (2010). "Microcosms," in Handbook of Hydrocarbon and Lipid Microbiology, ed. K. N. Timmis (Berlin, Heidelberg: Springer Berlin Heidelberg), 3523–3527. doi:10.1007/978-3-540-77587-4_275.

Faith, D. P. (1992). Conservation evaluation and phylogenetic diversity. Biological conservation 61, 1–10.

Fathepure, B. Z. (2014). Recent studies in microbial degradation of petroleum hydrocarbons in hypersaline environments. Front Microbiol 5. doi:10.3389/fmicb.2014.00173.

Feng, G., Cheng, Y., Wang, S.-Y., Borca-Tasciuc, D. A., Worobo, R. W., and Moraru, C. I. (2015). Bacterial attachment and biofilm formation on surfaces are reduced by small-diameter nanoscale pores: how small is small enough? NPJ Biofilms Microbiomes 1, 15022. doi:10.1038/npjbiofilms.2015.22.

Fernández-Martínez, J., Pujalte, M. J., García-Martínez, J., Mata, M., Garay, E., and Rodríguez-Valera, F. (2003). Description of Alcanivorax venustensis sp. nov. and reclassification of Fundibacter jadensis DSM 1 21 78T (Bruns and Berthe-Corti 1999) as Alcanivorax jadensis comb. nov., members of the emended genus Alcanivorax. Int. J. Syst. Evol. Microbiol. 53, 331–338. doi:10.1099/ijs.0.01923-0.

Fingas, M. F. (2015). Handbook of Oil Spill Science and Technology. Somerset, United States: John Wiley & Sons, Incorporated Available at: http://ebookcentral.proquest.com/lib/curtin/detail.action?docID=1895871 [Accessed July 24, 2020].

Fisher, J. F., Meroueh, S. O., and Mobashery, S. (2005). Bacterial Resistance to β-Lactam Antibiotics: Compelling Opportunism, Compelling Opportunity. Chem. Rev. 105, 395–424. doi:10.1021/cr030102i.

Fisher, S. J., Alexander, R., and Kagi, R. I. (1996). Biodegradation of Alkylnaphthalenes in Sediments Adjacent to an Off-Shore Petroleum Production Platform. Polycyclic Aromatic Compounds 11, 35–42. doi:10.1080/10406639608544647.

Flemming, H.-C., Neu, T. R., and Wozniak, D. J. (2007). The EPS Matrix: The "House of Biofilm Cells." Journal of Bacteriology 189, 7945–7947. doi:10.1128/JB.00858-07.

Flemming, H.-C., Wingender, J., Szewzyk, U., Steinberg, P., Rice, S. A., and Kjelleberg, S. (2016). Biofilms: an emergent form of bacterial life. Nature reviews. Microbiology 14, 563–575. doi:http://dx.doi.org.dbgw.lis.curtin.edu.au/10.1038/nrmicro.2016.94.

Foster, J. S., and Mobberley, J. M. (2010). "Past, Present, and Future: Microbial Mats as Models for Astrobiological Research," in Microbial Mats: Modern and Ancient Microorganisms in Stratified Systems Cellular Origin, Life in Extreme Habitats and Astrobiology., eds. J. Seckbach and A. Oren (Dordrecht: Springer Netherlands), 563–582. doi:10.1007/978-90-481-3799-2_29.

Fowler, S. W., Readman, J. W., Oregioni, B., Villeneuve, J.-P., and McKay, K. (1993). Petroleum hydrocarbons and trace metals in nearshore Gulf sediments and biota before and after the 1991 war: An assessment of temporal and spatial

trends. Marine Pollution Bulletin 27, 171–182. doi:10.1016/0025-326X(93)90022-C.

Franks, J., and Stolz, J. F. (2009). Flat laminated microbial mat communities. Earth-Science Reviews 96, 163–172. doi:10.1016/j.earscirev.2008.10.004.

Frías, J. E., Flores, E., and Herrero, A. (1997). Nitrate assimilation gene cluster from the heterocyst-forming cyanobacterium Anabaena sp. strain PCC 7120. J Bacteriol 179, 477–486.

Fruchey, I., Shapir, N., Sadowsky, M. J., and Wackett, L. P. (2003). On the origins of cyanuric acid hydrolase: purification, substrates, and prevalence of AtzD from Pseudomonas sp. strain ADP. Appl. Environ. Microbiol. 69, 3653–3657. doi:10.1128/aem.69.6.3653-3657.2003.

G

Gad, S. (2014). Petroleum Hydrocarbons. Encyclopedia of Toxicology 3. doi:10.1016/B978-0-12-386454-3.00899-X.

Gagnon, M. M., Grice, K., and Kagi, R. I. (1999). Biochemical and chemical parameters for aquatic ecosystem health assessments adapted to the Australian oil and gas industy. The APPEA Journal 39, 584–599. doi:10.1071/aj98038.

Ganesh, K. A., Mathew, N. C., K, S., R, K., and G, D. (2019). Genome analysis of deep sea piezotolerant Nesiotobacter exalbescens COD22 and toluene degradation studies under high pressure condition. Scientific Reports 9, 1–14. doi:10.1038/s41598-019-55115-9.

George, S. C., Boreham, C. J., Minifie, S. A., and Teerman, S. C. (2002). The effect of minor to moderate biodegradation on C5 to C9 hydrocarbons in crude oils. Organic Geochemistry 33, 1293–1317. doi:10.1016/S0146-6380(02)00117-1.

Ghosh, S., Chowdhury, R., and Bhattacharya, P. (2016). Mixed consortia in bioprocesses: role of microbial interactions. Applied Microbiology and Biotechnology 100, 4283–4295. doi:10.1007/s00253-016-7448-1.

Glasby, T. M., and Underwood, A. J. (1996). Sampling to differentiate between pulse and press perturbations. Environ Monit Assess 42, 241–252. doi:10.1007/BF00414371.

Golding, C. G., Lamboo, L. L., Beniac, D. R., and Booth, T. F. (2016). The scanning electron microscope in microbiology and diagnosis of infectious disease. Scientific Reports 6, 26516. doi:10.1038/srep26516.

González, I., Cao, K.-A. L., Davis, M. J., and Déjean, S. (2012). Visualising associations between paired 'omics' data sets. BioData Mining 5, 19. doi:10.1186/1756-0381-5-19.

Goossens, H., de Leeuw, J. W., Schenck, P. A., and Brassell, S. C. (1984). Tocopherols as likely precursors of pristane in ancient sediments and crude oils. Nature 312, 440–442. doi:10.1038/312440a0.

Grabowski, A., Nercessian, O., Fayolle, F., Blanchet, D., and Jeanthon, C. (2005). Microbial diversity in production waters of a low-temperature biodegraded oil reservoir. FEMS Microbiol Ecol 54, 427–443. doi:10.1016/j.resmic.2005.03.009.

Grice, K., Alexander, R., and Kagi, R. I. (2000). Diamondoid hydrocarbon ratios as indicators of biodegradation in Australian crude oils. Organic Geochemistry 31, 67–73. doi:10.1016/S0146-6380(99)00137-0.

Grötzschel, S., Abed, R. M. M., and Beer, D. D. (2002). Metabolic shifts in hypersaline microbial mats upon addition of organic substrates. Environmental Microbiology 4, 683–695. doi:10.1046/j.1462-2920.2002.00356.x.

Gu, Z., Eils, R., and Schlesner, M. (2016). Complex heatmaps reveal patterns and correlations in multidimensional genomic data. Bioinformatics 32, 2847–2849.

Guazzaroni, M.-E., Herbst, F.-A., Lores, I., Tamames, J., Peláez, A. I., López-Cortés, N., et al. (2013). Metaproteogenomic insights beyond bacterial response to naphthalene exposure and bio-stimulation. The ISME Journal 7, 122–136. doi:10.1038/ismej.2012.82.

Gunde-Cimerman, N., Plemenitaš, A., and Oren, A. (2018). Strategies of adaptation of microorganisms of the three domains of life to high salt concentrations. FEMS Microbiology Reviews; Delft 42, 353–375. doi:http://dx.doi.org.dbgw.lis.curtin.edu.au/10.1093/femsre/fuy009.

Gutierrez, T. (2019). "Aerobic Hydrocarbon-Degrading Gammaproteobacteria: Porticoccus," in Taxonomy, Genomics and Ecophysiology of Hydrocarbon-Degrading Microbes Handbook of Hydrocarbon and Lipid Microbiology., ed. T. J. McGenity (Cham: Springer International Publishing), 181–189. doi:10.1007/978-3-030-14796-9_32.

Gutierrez, T., Berry, D., Yang, T., Mishamandani, S., McKay, L., Teske, A., et al. (2013). Role of Bacterial Exopolysaccharides (EPS) in the Fate of the Oil Released during the Deepwater Horizon Oil Spill. PLoS ONE 8, e67717. doi:10.1371/journal.pone.0067717.

Gutierrez, T., Biddle, J. F., Teske, A., and Aitken, M. D. (2015). Cultivation-dependent and cultivation-independent characterization of hydrocarbon-degrading bacteria in Guaymas Basin sediments. Front. Microbiol. 6. doi:10.3389/fmicb.2015.00695.

Gutierrez, T., Nichols, P. D., Whitman, W. B., and Aitken, M. D. (2012). Porticoccus hydrocarbonoclasticus sp. nov., an Aromatic Hydrocarbon-Degrading Bacterium Identified in Laboratory Cultures of Marine Phytoplankton. Appl. Environ. Microbiol. 78, 628–637. doi:10.1128/AEM.06398-11.

H

Haack, S. K., Duris, J. W., Kolpin, D. W., Fogarty, L. R., Johnson, H. E., Gibson, K. E., et al. (2015). Genes Indicative of Zoonotic and Swine Pathogens Are Persistent in Stream Water and Sediment following a Swine Manure Spill. Applied and Environmental Microbiology 81, 3430–3441. doi:10.1128/AEM.04195-14.

Hädicke, O., Grammel, H., and Klamt, S. (2011). Metabolic network modeling of redox balancing and biohydrogen production in purple nonsulfur bacteria. BMC Syst Biol 5, 150. doi:10.1186/1752-0509-5-150.

Hariharan, J., Sengupta, A., Grewal, P., and Dick, W. A. (2017). Functional Predictions of Microbial Communities in Soil as Affected by Long-term Tillage Practices. Agricultural & Environmental Letters 2, 170031. doi:https://doi.org/10.2134/ael2017.09.0031.

Harris, J. K., Caporaso, J. G., Walker, J. J., Spear, J. R., Gold, N. J., Robertson, C. E., et al. (2013). Phylogenetic stratigraphy in the Guerrero Negro hypersaline microbial mat. The ISME Journal 7, 50–60. doi:10.1038/ismej.2012.79.

Harshey, R. M., and Partridge, J. D. (2015). Shelter in a swarm. J Mol Biol 427, 3683–3694. doi:10.1016/j.jmb.2015.07.025.

Hassani, M. A., Durán, P., and Hacquard, S. (2018). Microbial interactions within the plant holobiont. Microbiome 6. doi:10.1186/s40168-018-0445-0.

He, X., Zhang, Q., Jin, Y., Jiang, L., and Wu, R. (2020). Network mapping of root-microbe interactions in Arabidopsis thaliana. bioRxiv, 2020.11.24.397273. doi:10.1101/2020.11.24.397273.

Head, I. M., Jones, D. M., and Larter, S. R. (2003). Biological activity in the deep subsurface and the origin of heavy oil. Nature 426, 344–352. doi:10.1038/nature02134.

Hedlund, B. P., Geiselbrecht, A. D., and Staley, J. T. (2001). Marinobacter strain NCE312 has a Pseudomonas-like naphthalene dioxygenase. FEMS Microbiol Lett 201, 47–51. doi:10.1111/j.1574-6968.2001.tb10731.x.

Heijs, S. K., Sinninghe Damsté, J. S., and Forney, L. J. (2005). Characterization of a deep-sea microbial mat from an active cold seep at the Milano mud volcano in the Eastern Mediterranean Sea. FEMS Microbiol Ecol 54, 47–56. doi:10.1016/j.femsec.2005.02.007.

Heldin, C.-H., Lu, B., Evans, R., and Gutkind, J. S. (2016). Signals and Receptors. Cold Spring Harb Perspect Biol 8. doi:10.1101/cshperspect.a005900.

Hernandez-Raquet, G., Budzinski, H., Caumette, P., Dabert, P., Ménach, K. L., Muyzer, G., et al. (2006). Molecular diversity studies of bacterial communities of oil polluted microbial mats from the Etang de Berre (France). FEMS Microbiology Ecology; Delft 58, 550–562. doi:http://dx.doi.org.dbgw.lis.curtin.edu.au/10.1111/j.1574-6941.2006.00187.x.

Hirakawa, H., Nishino, K., Yamada, J., Hirata, T., and Yamaguchi, A. (2003). Beta-lactam resistance modulated by the overexpression of response regulators of two-component signal transduction systems in Escherichia coli. J. Antimicrob. Chemother. 52, 576–582. doi:10.1093/jac/dkg406.

Hoehler, T. M., Bebout, B. M., and Des Marais, D. J. (2001). The role of microbial mats in the production of reduced gases on the early Earth. Nature 412, 324–327.

Hook, S., Batley, G., Ross, A., Holloway, M., and Irving, P. (2017). Oil Spill Monitoring Handbook. Victoria, Australia: CSIRO Publishing Available at: http://ebookcentral.proquest.com/lib/curtin/detail.action?docID=4723035 [Accessed July 25, 2020].

Horodyski, R. (1977). Lyngbya Mats at Laguna Mormona, Baja California, Mexico: Comparison with Proterozoic Stromatolites. SEPM JSR Vol. 47. doi:10.1306/212F732E-2B24-11D7-8648000102C1865D.

Hubert, C. R. J., Oldenburg, T. B. P., Fustic, M., Gray, N. D., Larter, S. R., Penn, K., et al. (2012). Massive dominance of Epsilonproteobacteria in formation waters from a Canadian oil sands reservoir containing severely biodegraded oil. Environmental Microbiology 14, 387–404. doi:10.1111/j.1462-2920.2011.02521.x.

Huu, N. B., Denner, E. B. M., Ha, D. T. C., Wanner, G., and Stan-Lotter, H. (1999). Marinobacter aquaeolei sp. nov., a halophilic bacterium isolated from a Vietnamese oil-producing well. International Journal of Systematic and Evolutionary Microbiology, 49, 367–375. doi:10.1099/00207713-49-2-367.

Hwang, B., Lee, J. H., and Bang, D. (2018). Single-cell RNA sequencing technologies and bioinformatics pipelines. Experimental & Molecular Medicine 50, 1–14. doi:10.1038/s12276-018-0071-8.

I

Iwai, S., Weinmaier, T., Schmidt, B. L., Albertson, D. G., Poloso, N. J., Dabbagh, K., et al. (2016). Piphillin: Improved Prediction of Metagenomic Content by Direct Inference from Human Microbiomes. PLoS One 11. doi:10.1371/journal.pone.0166104.

J

Jahnert, R. J., and Collins, L. B. (2011). Significance of subtidal microbial deposits in Shark Bay, Australia. Marine Geology 286, 106–111. doi:10.1016/j.margeo.2011.05.006.

Jahnert, R. J., and Collins, L. B. (2012). Characteristics, distribution and morphogenesis of subtidal microbial systems in Shark Bay, Australia. Marine Geology 303–306, 115–136. doi:10.1016/j.margeo.2012.02.009.

Jahnert, R. J., and Collins, L. B. (2013). Controls on microbial activity and tidal flat evolution in Shark Bay, Western Australia. Sedimentology 60, 1071–1099. doi:10.1111/sed.12023.

Jeanbille, M., Gury, J., Duran, R., Tronczynski, J., Ghiglione, J.-F., Agogué, H., et al. (2016). Chronic Polyaromatic Hydrocarbon (PAH) Contamination Is a Marginal Driver for Community Diversity and Prokaryotic Predicted Functioning in Coastal Sediments. Front. Microbiol. 7. doi:10.3389/fmicb.2016.01303.

Jessup, C. M., Kassen, R., Forde, S. E., Kerr, B., Buckling, A., Rainey, P. B., et al. (2004). Big questions, small worlds: microbial model systems in ecology. Trends in Ecology & Evolution 19, 189–197. doi:10.1016/j.tree.2004.01.008.

Jiao, Y., Cody, G. D., Harding, A. K., Wilmes, P., Schrenk, M., Wheeler, K. E., et al. (2010). Characterization of Extracellular Polymeric Substances from Acidophilic Microbial Biofilms. Appl. Environ. Microbiol. 76, 2916–2922. doi:10.1128/AEM.02289-09.

Jo, J.-H., Kennedy, E. A., and Kong, H. H. (2016). Research Techniques Made Simple: Bacterial 16S Ribosomal RNA Gene Sequencing in Cutaneous Research. Journal of Investigative Dermatology 136, e23–e27. doi:10.1016/j.jid.2016.01.005.

Jones, B., Renaut, R. W., Rosen, M. R., and Ansdell, K. M. (2002). Coniform Stromatolites from Geothermal Systems, North Island, New Zealand. PALAIOS 17, 84–103.

Jones, S. E., and Lennon, J. T. (2010). Dormancy contributes to the maintenance of microbial diversity. Proc Natl Acad Sci U S A 107, 5881–5886. doi:10.1073/pnas.0912765107.

Jubelin, G., Vianney, A., Beloin, C., Ghigo, J.-M., Lazzaroni, J.-C., Lejeune, P., et al. (2005). CpxR/OmpR interplay regulates curli gene expression in response to osmolarity in Escherichia coli. J. Bacteriol. 187, 2038–2049. doi:10.1128/JB.187.6.2038-2049.2005.

K

Kanehisa, M., and Goto, S. (2000). KEGG: kyoto encyclopedia of genes and genomes. Nucleic Acids Res 28, 27–30. doi:10.1093/nar/28.1.27.

Kanehisa, M., Goto, S., Sato, Y., Furumichi, M., and Tanabe, M. (2012). KEGG for integration and interpretation of large-scale molecular data sets. Nucleic Acids Research 40, D109–D114. doi:10.1093/nar/gkr988.

Kanehisa, M., Goto, S., Sato, Y., Kawashima, M., Furumichi, M., and Tanabe, M. (2014). Data, information, knowledge and principle: back to metabolism in KEGG. Nucleic Acids Research 42, D199–D205. doi:10.1093/nar/gkt1076.

Kaplan, J. B., Izano, E. A., Gopal, P., Karwacki, M. T., Kim, S., Bose, J. L., et al. (2012). Low Levels of β-Lactam Antibiotics Induce Extracellular DNA Release and Biofilm Formation in Staphylococcus aureus. mBio 3. doi:10.1128/mBio.00198-12.

Kappell, A. D., Wei, Y., Newton, R. J., Van Nostrand, J. D., Zhou, J., McLellan, S. L., et al. (2014). The polycyclic aromatic hydrocarbon degradation potential of Gulf of Mexico native coastal microbial communities after the Deepwater Horizon oil spill. Front Microbiol 5. doi:10.3389/fmicb.2014.00205.

Keer, J. T., and Birch, L. (2003). Molecular methods for the assessment of bacterial viability. Journal of Microbiological Methods 53, 175–183. doi:10.1016/S0167-7012(03)00025-3.

Kennicutt, M. C. (1988). The effect of biodegradation on crude oil bulk and molecular composition. Oil and Chemical Pollution 4, 89–112. doi:10.1016/S0269-8579(88)80014-5.

Killops, S., and Killops, V. (2005). Introduction to Organic Geochemistry | Wiley Online Books. 2nd ed. Blackwell Publishing Ltd Available at: https://onlinelibrary.wiley.com/doi/book/10.1002/9781118697214 [Accessed April 17, 2021].

Kim, M., Morrison, M., and Yu, Z. (2011). Evaluation of different partial 16S rRNA gene sequence regions for phylogenetic analysis of microbiomes. Journal of Microbiological Methods 84, 81–87. doi:10.1016/j.mimet.2010.10.020.

Kim, S., and Picardal, F. (2001). Microbial Growth on Dichlorobiphenyls Chlorinated on Both Rings as a Sole Carbon and Energy Source. Appl Environ Microbiol 67, 1953–1955. doi:10.1128/AEM.67.4.1953-1955.2001.

Kindzierski, V., Raschke, S., Knabe, N., Siedler, F., Scheffer, B., Pflüger-Grau, K., et al. (2017). Osmoregulation in the Halophilic Bacterium Halomonas elongata: A Case Study for Integrative Systems Biology. PLoS One 12. doi:10.1371/journal.pone.0168818.

Kleikemper, J., Schroth, M. H., Sigler, W. V., Schmucki, M., Bernasconi, S. M., and Zeyer, J. (2002). Activity and Diversity of Sulfate-Reducing Bacteria in a Petroleum Hydrocarbon-Contaminated Aquifer. Appl. Environ. Microbiol. 68, 1516–1523. doi:10.1128/AEM.68.4.1516-1523.2002.

Kleinsteuber, S., Riis, V., Fetzer, I., Harms, H., and Müller, S. (2006). Population Dynamics within a Microbial Consortium during Growth on Diesel Fuel in Saline Environments. Appl. Environ. Microbiol. 72, 3531–3542. doi:10.1128/AEM.72.5.3531-3542.2006.

Kong, K.-F., Schneper, L., and Mathee, K. (2010). Beta-lactam antibiotics: from antibiosis to resistance and bacteriology. APMIS 118, 1–36. doi:10.1111/j.1600-0463.2009.02563.x.

Koo, H., Hakim, J. A., Morrow, C. D., Eipers, P. G., Davila, A., Andersen, D. T., et al. (2017a). Comparison of two bioinformatics tools used to characterize the microbial diversity and predictive functional attributes of microbial mats from Lake Obersee, Antarctica. J Microbiol Methods 140, 15–22. doi:10.1016/j.mimet.2017.06.017.

Koo, H., Mojib, N., Hakim, J. A., Hawes, I., Tanabe, Y., Andersen, D. T., et al. (2017b). Microbial Communities and Their Predicted Metabolic Functions in Growth Laminae of a Unique Large Conical Mat from Lake Untersee, East Antarctica. Front. Microbiol. 8, 1347. doi:10.3389/fmicb.2017.01347.

Kose, S. H., Grice, K., Orsi, W. D., Ballal, M., and Coolen, M. J. L. (2018). Metagenomics of pigmented and cholesterol gallstones: the putative role of bacteria. Scientific Reports 8. doi:10.1038/s41598-018-29571-8.

Kostakioti, M., Hadjifrangiskou, M., and Hultgren, S. J. (2013). Bacterial Biofilms: Development, Dispersal, and Therapeutic Strategies in the Dawn of the Postantibiotic Era. Cold Spring Harb Perspect Med 3. doi:10.1101/cshperspect.a010306.

Krell, T., Lacal, J., Busch, A., Silva-Jiménez, H., Guazzaroni, M.-E., and Ramos, J. L. (2010). Bacterial Sensor Kinases: Diversity in the Recognition of

Environmental Signals. Annu. Rev. Microbiol. 64, 539–559. doi:10.1146/annurev.micro.112408.134054.

Kristanti, R. A., Hadibarata, T., Al Farraj, D. A., Elshikh, M. S., and Alkufeidy, R. M. (2018). Biodegradation Mechanism of Phenanthrene by Halophilic Hortaea sp. B15. Water Air Soil Pollut 229, 324. doi:10.1007/s11270-018-3969-9.

Kuhlmann, A. U., and Bremer, E. (2002). Osmotically Regulated Synthesis of the Compatible Solute Ectoine in Bacillus pasteurii and Related Bacillus spp. Appl Environ Microbiol 68, 772–783. doi:10.1128/AEM.68.2.772-783.2002.

Kuhns, L. G., Benoit, S. L., Bayyareddy, K., Johnson, D., Orlando, R., Evans, A. L., et al. (2016). Carbon Fixation Driven by Molecular Hydrogen Results in Chemolithoautotrophically Enhanced Growth of Helicobacter pylori. Journal of Bacteriology 198, 1423–1428. doi:10.1128/JB.00041-16.

Kusters, J. G., van Vliet, A. H. M., and Kuipers, E. J. (2006). Pathogenesis of Helicobacter pylori Infection. Clinical Microbiology Reviews 19, 449–490. doi:10.1128/CMR.00054-05.

Kuznetsov, V. D., Zaitseva, T. A., Vakulenko, L. V., and Filippova, S. N. (1992). Streptomyces albiaxialis sp. nov. - a new petroleum hydrocarbon-degrading species of thermo- and halotolerant Streptomyces. Microbiology New York 61, 62–67.

Kvenvolden, K. A. (2006). Organic geochemistry – A retrospective of its first 70 years. Organic Geochemistry 37, 1–11. doi:10.1016/j.orggeochem.2005.09.001.

L

Lagier, J.-C., Edouard, S., Pagnier, I., Mediannikov, O., Drancourt, M., and Raoult, D. (2015). Current and Past Strategies for Bacterial Culture in Clinical Microbiology. Clinical Microbiology Reviews 28, 208–236. doi:10.1128/CMR.00110-14.

Lagree, K., Mon, H. H., Mitchell, A. P., and Ducker, W. A. (2018). Impact of surface topography on biofilm formation by Candida albicans. PLOS ONE 13, e0197925. doi:10.1371/journal.pone.0197925.

Lane, D. J., Pace, B., Olsen, G. J., Stahl, D. A., Sogin, M. L., and Pace, N. R. (1985). Rapid determination of 16S ribosomal RNA sequences for phylogenetic analyses. Proc Natl Acad Sci U S A 82, 6955–6959.

Langille, M. G. I., Zaneveld, J., Caporaso, J. G., McDonald, D., Knights, D., Reyes, J. A., et al. (2013). Predictive functional profiling of microbial communities using 16S rRNA marker gene sequences. Nat Biotechnol 31, 814–821. doi:10.1038/nbt.2676.

Larter, S., Huang, H., Adams, J., Bennett, B., and Snowdon, L. R. (2012). A practical biodegradation scale for use in reservoir geochemical studies of biodegraded oils. Organic Geochemistry 45, 66–76. doi:10.1016/j.orggeochem.2012.01.007.

Laville, J., Blumer, C., Von Schroetter, C., Gaia, V., Défago, G., Keel, C., et al. (1998). Characterization of the hcnABC Gene Cluster Encoding Hydrogen Cyanide Synthase and Anaerobic Regulation by ANR in the Strictly Aerobic Biocontrol Agent Pseudomonas fluorescens CHA0. Journal of Bacteriology 180, 3187–3196. doi:10.1128/JB.180.12.3187-3196.1998.

Leahy, J. G., and Colwell, R. R. (1990). Microbial degradation of hydrocarbons in the environment. Microbiol Rev 54, 305–315.

Lertsethtakarn, P., Ottemann, K. M., and Hendrixson, D. R. (2011). Motility and Chemotaxis in Campylobacter and Helicobacter. Annu. Rev. Microbiol. 65, 389–410. doi:10.1146/annurev-micro-090110-102908.

Li, D., Yang, M., Li, Z., Qi, R., He, J., and Liu, H. (2008). Change of bacterial communities in sediments along Songhua River in Northeastern China after a nitrobenzene pollution event. FEMS Microbiol Ecol 65, 494–503. doi:10.1111/j.1574-6941.2008.00540.x.

Li, R., Tun, H. M., Link to external site, this link will open in a new window, Jahan, M., Zhang, Z., Kumar, A., et al. (2017). Comparison of DNA-, PMA-, and RNA-based 16S rRNA Illumina sequencing for detection of live bacteria in water. Scientific Reports (Nature Publisher Group); London 7, 1–11. doi:http://dx.doi.org.dbgw.lis.curtin.edu.au/10.1038/s41598-017-02516-3.

Li, R., Zi, X., Wang, X., Zhang, X., Gao, H., and Hu, N. (2013). Marinobacter hydrocarbonoclasticus NY-4, a novel denitrifying, moderately halophilic marine bacterium. SpringerPlus 2, 346. doi:10.1186/2193-1801-2-346.

Lichtenberg, M., Cartaxana, P., and Kühl, M. (2020). Vertical Migration Optimizes Photosynthetic Efficiency of Motile Cyanobacteria in a Coastal Microbial Mat. Front. Mar. Sci. 7. doi:10.3389/fmars.2020.00359.

Liebgott, P.-P., Labat, M., Amouric, A., Tholozan, J.-L., and Lorquin, J. (2008). Tyrosol degradation via the homogentisic acid pathway in a newly isolated Halomonas strain from olive processing effluents. Journal of Applied Microbiology 105, 2084–2095. doi:10.1111/j.1365-2672.2008.03925.x.

Lima, M. F. B., Fernandes, G. M., Oliveira, A. H. B., Morais, P. C. V., Marques, E. V., Santos, F. R., et al. (2019). Emerging and traditional organic markers: Baseline study showing the influence of untraditional anthropogenic activities on coastal zones with multiple activities (Ceará coast, Northeast Brazil). Marine Pollution Bulletin 139, 256–262. doi:10.1016/j.marpolbul.2018.12.006.

Litchfield, C. D. (1998). Survival strategies for microorganisms in hypersaline environments and their relevance to life on early Mars. Meteoritics & planetary science 33, 813–819.

Little, A. E. F., Robinson, C. J., Peterson, S. B., Raffa, K. F., and Handelsman, J. (2008). Rules of Engagement: Interspecies Interactions that Regulate Microbial Communities. Annual Review of Microbiology 62, 375–401. doi:10.1146/annurev.micro.030608.101423.

Liu, J., Zheng, Y., Lin, H., Wang, X., Li, M., Liu, Y., et al. (2019). Proliferation of hydrocarbon-degrading microbes at the bottom of the Mariana Trench. Microbiome 7, 47. doi:10.1186/s40168-019-0652-3.

Llirós, M., Gaju, N., de Oteyza, T. G., Grimalt, J. O., Esteve, I., and Martínez-Alonso, M. (2008). Microcosm experiments of oil degradation by microbial mats. II. The changes in microbial species. Science of The Total Environment 393, 39–49. doi:10.1016/j.scitotenv.2007.11.034.

Louca, S., and Doebeli, M. (2018). Efficient comparative phylogenetics on large trees. Bioinformatics 34, 1053–1055. doi:10.1093/bioinformatics/btx701.

Lozupone, C. A., Hamady, M., Kelley, S. T., and Knight, R. (2007). Quantitative and Qualitative β Diversity Measures Lead to Different Insights into Factors That Structure Microbial Communities. Appl Environ Microbiol 73, 1576–1585. doi:10.1128/AEM.01996-06.

Lucena, T., Pascual, J., Garay, E., Arahal, D. R., Macián, M. C., and Pujalte, M. J. (2010). Haliea mediterranea sp. nov., a marine gammaproteobacterium. Int. J. Syst. Evol. Microbiol. 60, 1844–1848. doi:10.1099/ijs.0.017061-0.

Luo, Z., Guo, Y., Liu, J., Qiu, H., Zhao, M., Zou, W., et al. (2016). Microbial synthesis of poly-γ-glutamic acid: current progress, challenges, and future perspectives. Biotechnology for Biofuels 9, 134. doi:10.1186/s13068-016-0537-7.

Luque-Almagro, V. M., Huertas, M. J., Roldán, M. D., Moreno-Vivián, C., Martínez-Luque, M., Blasco, R., et al. (2007). The cyanotrophic bacterium Pseudomonas pseudoalcaligenes CECT5344 responds to cyanide by defence mechanisms against iron deprivation, oxidative damage and nitrogen stress. Environmental Microbiology 9, 1541–1549. doi:10.1111/j.1462-2920.2007.01274.x.

Luu, R. A., Kootstra, J. D., Nesteryuk, V., Brunton, C. N., Parales, J. V., Ditty, J. L., et al. (2015). Integration of chemotaxis, transport and catabolism in Pseudomonas putida and identification of the aromatic acid chemoreceptor PcaY. Molecular Microbiology 96, 134–147. doi:10.1111/mmi.12929.

M

Ma, Y., Galinski, E. A., Grant, W. D., Oren, A., and Ventosa, A. (2010). Halophiles 2010: Life in Saline Environments. Appl Environ Microbiol 76, 6971–6981. doi:10.1128/AEM.01868-10.

MacDougall, A. S., McCann, K. S., Gellner, G., and Turkington, R. (2013). Diversity loss with persistent human disturbance increases vulnerability to ecosystem collapse. Nature 494, 86–89. doi:10.1038/nature11869.

Madigan, M., Bender, K., Buckley, D., Sattley, W. M., and Stahl, D. (2019). Brock Biology of microorganisms. 9th ed. Pearson.

Manefield, M., Lee, M., and Koenig, J. (2017). "The Nature and Relevance of Solvent Stress in Microbes and Mechanisms of Tolerance," in Microbial Ecology of Extreme Environments, eds. C. Chénard and F. M. Lauro (Cham: Springer International Publishing), 201–213. doi:10.1007/978-3-319-51686-8_9.

Margesin, R., and Schinner, F. (2001). Biodegradation and bioremediation of hydrocarbons in extreme environments. Applied Microbiology and Biotechnology 56, 650–663.

Markowitz, V. M., Chen, I.-M. A., Palaniappan, K., Chu, K., Szeto, E., Grechkin, Y., et al. (2012). IMG: the integrated microbial genomes database and comparative analysis system. Nucleic Acids Research 40, D115–D122. doi:10.1093/nar/gkr1044.

Martins, L. F., and Peixoto, R. S. (2012). Biodegradation of petroleum hydrocarbons in hypersaline environments. Braz J Microbiol 43, 865–872. doi:10.1590/S1517-83822012000300003.

Matange, K., Tuck, J. M., and Keung, A. J. (2021). DNA stability: a central design consideration for DNA data storage systems. Nat Commun 12, 1–9. doi:10.1038/s41467-021-21587-5.

Matson, J. S., Livny, J., and DiRita, V. J. (2017). A putative Vibrio cholerae two-component system controls a conserved periplasmic protein in response to the antimicrobial peptide polymyxin B. PLOS ONE 12, e0186199. doi:10.1371/journal.pone.0186199.

McAllister, K. A., Lee, H., and Trevors, J. T. (1996). Microbial degradation of pentachlorophenol. Biodegradation 7, 1–40. doi:10.1007/BF00056556.

McDonald, D., Price, M. N., Goodrich, J., Nawrocki, E. P., DeSantis, T. Z., Probst, A., et al. (2012). An improved Greengenes taxonomy with explicit ranks for ecological and evolutionary analyses of bacteria and archaea. The ISME journal 6, 610.

McGenity, T. J. (2010). "Halophilic Hydrocarbon Degraders," in Handbook of Hydrocarbon and Lipid Microbiology, ed. K. N. Timmis (Berlin, Heidelberg: Springer), 1939–1951. doi:10.1007/978-3-540-77587-4_142.

McGenity, T. J., Folwell, B. D., McKew, B. A., and Sanni, G. O. (2012). Marine crude-oil biodegradation: a central role for interspecies interactions. Aquat Biosyst 8, 10. doi:10.1186/2046-9063-8-10.

McIntyre, C. P., Harvey, P. M., Ferguson, S. H., Wressnig, A. M., Volk, H., George, S. C., et al. (2007). Determining the Extent of Biodegradation of Fuels Using the Diastereomers of Acyclic Isoprenoids. Environmental Science & Technology 41, 2452–2458. doi:10.1021/es0621288.

Méndez, V., Fuentes, S., Morgante, V., Hernández, M., González, M., Moore, E., et al. (2017). Novel hydrocarbonoclastic metal-tolerant Acinetobacter and Pseudomonas strains from Aconcagua river oil-polluted soil. Journal of soil science and plant nutrition 17, 1074–1087. doi:10.4067/S0718-95162017000400017.

Meyer, J.-M., Geoffroy, V. A., Baida, N., Gardan, L., Izard, D., Lemanceau, P., et al. (2002). Siderophore Typing, a Powerful Tool for the Identification of Fluorescent and Nonfluorescent Pseudomonads. Appl. Environ. Microbiol. 68, 2745–2753. doi:10.1128/AEM.68.6.2745-2753.2002.

Moran, M. A., Satinsky, B., Gifford, S. M., Luo, H., Rivers, A., Chan, L.-K., et al. (2013). Sizing up metatranscriptomics. ISME J 7, 237–243. doi:10.1038/ismej.2012.94.

Moreno, M. de L., Sánchez-Porro, C., Piubeli, F., Frias, L., García, M. T., and Mellado, E. (2011). Cloning, Characterization and Analysis of cat and ben Genes from the Phenol Degrading Halophilic Bacterium Halomonas organivorans. PLoS ONE 6, e21049. doi:10.1371/journal.pone.0021049.

Morris, T. E., Visscher, P. T., O'Leary, M. J., Fearns, P. R. C. S., and Collins, L. B. (2019). The biogeomorphology of Shark Bay's microbialite coasts. Earth-Science Reviews, 102921. doi:10.1016/j.earscirev.2019.102921.

Mota, R., Pereira, S. B., Meazzini, M., Fernandes, R., Santos, A., Evans, C. A., et al. (2015). Effects of heavy metals on Cyanothece sp. CCY 0110 growth, extracellular polymeric substances (EPS) production, ultrastructure and protein profiles. Journal of Proteomics 120, 75–94. doi:10.1016/j.jprot.2015.03.004.

Muir, P., Li, S., Lou, S., Wang, D., Spakowicz, D. J., Salichos, L., et al. (2016). The real cost of sequencing: scaling computation to keep pace with data generation. Genome Biology 17. doi:10.1186/s13059-016-0917-0.

Mukherjee, A., Chettri, B., Langpoklakpam, J. S., Basak, P., Prasad, A., Mukherjee, A. K., et al. (2017). Bioinformatic Approaches Including Predictive Metagenomic Profiling Reveal Characteristics of Bacterial Response to

Petroleum Hydrocarbon Contamination in Diverse Environments. Sci Rep 7. doi:10.1038/s41598-017-01126-3.

Musat, F., Harder, J., and Widdel, F. (2006). Study of nitrogen fixation in microbial communities of oil-contaminated marine sediment microcosms. Environmental Microbiology 8, 1834–1843. doi:10.1111/j.1462-2920.2006.01069.x.

N

Nes, E. H. van, and Scheffer, M. (2005). Implications of Spatial Heterogeneity for Catastrophic Regime Shifts in Ecosystems. Ecology 86, 1797–1807. doi:10.1890/04-0550.

NESP Earth Systems and Climate Change Hub (2018). Climate change and the Shark Bay World Heritage Area: foundations for a climate change adaptation strategy and action plan. Available at: http://nespclimate.com.au/wp-content/uploads/2016/03/SBWHA-CC-workshop-report.pdf [Accessed May 14, 2020].

Nielsen, K. M., Johnsen, P. J., Bensasson, D., and Daffonchio, D. (2007). Release and persistence of extracellular DNA in the environment. Environmental biosafety research 6, 37–53.

Nielsen, M., Revsbech, N. P., and Kühl, M. (2015). Microsensor measurements of hydrogen gas dynamics in cyanobacterial microbial mats. Front. Microbiol. 6. doi:10.3389/fmicb.2015.00726.

Novaković, M., Ramadan, M. M. A., Knudsen, T. Š., Antić, M., Beškoski, V., Gojgić-Cvijović, G., et al. (2012). Degradation of methyl-phenanthrene isomers during bioremediation of soil contaminated by residual fuel oil. Environ Chem Lett 10, 287–294. doi:10.1007/s10311-012-0354-6.

Nyyssölä, A., and Leisola, M. (2001). Actinopolyspora halophila has two separate pathways for betaine synthesis. Arch Microbiol 176, 294–300. doi:10.1007/s002030100325.

O

Obuekwe, C. O., Badrudeen, A. M., Al-Saleh, E., and Mulder, J. L. (2005). Growth and hydrocarbon degradation by three desert fungi under conditions of simultaneous temperature and salt stress. International Biodeterioration & Biodegradation 56, 197–205. doi:10.1016/j.ibiod.2005.05.005.

O'Donnell, S. T., Ross, R. P., and Stanton, C. (2020). The Progress of Multi-Omics Technologies: Determining Function in Lactic Acid Bacteria Using a Systems Level Approach. Front. Microbiol. 10. doi:10.3389/fmicb.2019.03084.

Oie, C. S. I., Albaugh, C. E., and Peyton, B. M. (2007). Benzoate and salicylate degradation by Halomonas campisalis, an alkaliphilic and moderately halophilic microorganism. Water Research 41, 1235–1242. doi:10.1016/j.watres.2006.12.029.

Oksanen, J., Blanchet, F. G., Kindt, R., Legendre, P., O'hara, R. B., Simpson, G. L., et al. (2010). Vegan: community ecology package. R package version 1.17-4. http://cran. r-project. org>. Acesso em 23, 2010.

Oren, A. (2008). Microbial life at high salt concentrations: phylogenetic and metabolic diversity. Saline Systems 4, 2. doi:10.1186/1746-1448-4-2.

Oren, A., Elevi Bardavid, R., Kandel, N., Aizenshtat, Z., and Jehlička, J. (2013). Glycine betaine is the main organic osmotic solute in a stratified microbial community in a hypersaline evaporitic gypsum crust. Extremophiles 17, 445–451. doi:10.1007/s00792-013-0522-z.

Orwin, K. H., and Wardle, D. A. (2004). New indices for quantifying the resistance and resilience of soil biota to exogenous disturbances. Soil Biology and Biochemistry 36, 1907–1912. doi:10.1016/j.soilbio.2004.04.036.

P

Pagès, A., Grice, K., Welsh, D. T., Teasdale, P. T., Van Kranendonk, M. J., and Greenwood, P. (2015). Lipid Biomarker and Isotopic Study of Community Distribution and Biomarker Preservation in a Laminated Microbial Mat from Shark Bay, Western Australia. Microbial Ecology 70, 459–472.

Pagès, A., Welsh, D. T., Teasdale, P. R., Grice, K., Vacher, M., Bennett, W. W., et al. (2014). Diel fluctuations in solute distributions and biogeochemical cycling in a hypersaline microbial mat from Shark Bay, WA. Marine Chemistry 167, 102–112. doi:10.1016/j.marchem.2014.05.003.

Paje, M. L. F., Neilan, B. A., and Couperwhite, l. (1997). A Rhodococcus species that thrives on medium saturated with liquid benzene. Microbiology 143, 2975–2981. doi:10.1099/00221287-143-9-2975.

Pannard, A., Pédrono, J., Bormans, M., Briand, E., Claquin, P., and Lagadeuc, Y. (2016). Production of exopolymers (EPS) by cyanobacteria: impact on the carbon-to-nutrient ratio of the particulate organic matter. Aquat Ecol 50, 29–44. doi:10.1007/s10452-015-9550-3.

Papenfort, K., and Bassler, B. L. (2016). Quorum sensing signal–response systems in Gram-negative bacteria. Nature Reviews Microbiology 14, 576–588. doi:10.1038/nrmicro.2016.89.

Parker, S. P., Bowden, W. B., Flinn, M. B., Giles, C. D., Arndt, K. A., Beneš, J. P., et al. (2018). Effect of particle size and heterogeneity on sediment biofilm metabolism and nutrient uptake scaled using two approaches. Ecosphere 9, e02137. doi:10.1002/ecs2.2137.

Parks, D. H., Tyson, G. W., Hugenholtz, P., and Beiko, R. G. (2014). STAMP: statistical analysis of taxonomic and functional profiles. Bioinformatics 30, 3123–3124. doi:10.1093/bioinformatics/btu494.

Peters, K. E., Walters, C. C., and Moldowan, J. M. (2007a). The Biomarker Guide: Volume 1, Biomarkers and Isotopes in the Environment and Human History. Cambridge University Press.

Peters, K. E., Walters, C. C., and Moldowan, J. M. (2007b). The Biomarker Guide: Volume 2, Biomarkers and Isotopes in Petroleum Systems and Earth History. Cambridge University Press.

Petroff, A. P., Sim, M. S., Maslov, A., Krupenin, M., Rothman, D. H., and Bosak, T. (2010). Biophysical basis for the geometry of conical stromatolites. Proceedings of the National Academy of Sciences 107, 9956–9961. doi:10.1073/pnas.1001973107.

Pham, V. D., Hnatow, L. L., Zhang, S., Fallon, R. D., Jackson, S. C., Tomb, J.-F., et al. (2009). Characterizing microbial diversity in production water from an Alaskan mesothermic petroleum reservoir with two independent molecular methods. Environmental Microbiology 11, 176–187. doi:10.1111/j.1462-2920.2008.01751.x.

Pielou, E. C. (1966). The measurement of diversity in different types of biological collections. Journal of Theoretical Biology 13, 131–144. doi:10.1016/0022-5193(66)90013-0.

Pimm, S. L. (1984). The complexity and stability of ecosystems. Nature 307, 321–326. doi:10.1038/307321a0.

Playford, P. E., Cockbain, A. E., Berry, P. F., Roberts, A. P., Haines, P. W., and Brooke, B. P. (2013). The geology of Shark Bay. 299.

Plet, C., Pagès, A., Holman, A. I., Madden, R. H. C., and Grice, K. (2018). From supratidal to subtidal, an integrated characterisation of Carbla Beach shallow microbial mats (Hamelin Pool, Shark Bay, WA): Lipid biomarkers, stable carbon isotopes and microfabrics. Chemical Geology 493, 338–352. doi:10.1016/j.chemgeo.2018.06.010.

Poole, K. (2012). Bacterial stress responses as determinants of antimicrobial resistance. J Antimicrob Chemother 67, 2069–2089. doi:10.1093/jac/dks196.

Post, F. J., Borowitzka, L. J., Borowitzka, M. A., Mackay, B., and Moulton, T. (1983). The protozoa of a Western Australian hypersaline lagoon. Hydrobiologia 105, 95–113. doi:10.1007/BF00025180.

Prieto-Barajas, C. M., Valencia-Cantero, E., and Santoyo, G. (2018). Microbial mat ecosystems: Structure types, functional diversity, and biotechnological application. Electronic Journal of Biotechnology 31, 48–56. doi:10.1016/j.ejbt.2017.11.001.

Prince, R. C. (2010). "Bioremediation of Marine Oil Spills," in Handbook of Hydrocarbon and Lipid Microbiology, ed. K. N. Timmis (Berlin, Heidelberg: Springer), 2617–2630. doi:10.1007/978-3-540-77587-4_194.

Q

Qin, X., Tang, J. C., Li, D. S., and Zhang, Q. M. (2012). Effect of salinity on the bioremediation of petroleum hydrocarbons in a saline-alkaline soil. Letters in Applied Microbiology 55, 210–217. doi:10.1111/j.1472-765X.2012.03280.x.

Quan, Z.-X., Bae, H.-S., Baek, J.-H., Chen, W.-F., Im, W.-T., and Lee, S.-T. (2005). Rhizobium daejeonense sp. nov. isolated from a cyanide treatment bioreactor. International Journal of Systematic and Evolutionary Microbiology 55, 2543–2549. doi:10.1099/ijs.0.63667-0.

Quan, Z.-X., Zeng, D.-N., Xiao, Y.-P., Roh, S. W., Nam, Y.-D., Chang, H.-W., et al. (2009). Henriciella marina gen. nov., sp. nov., a novel member of the family Hyphomonadaceae isolated from the East Sea. Journal of microbiology (Seoul, Korea) 47, 156–161. doi:http://dx.doi.org.dbgw.lis.curtin.edu.au/10.1007/s12275-008-0290-0.

R

Reddy, C. M., Arey, J. S., Seewald, J. S., Sylva, S. P., Lemkau, K. L., Nelson, R. K., et al. (2012). Composition and fate of gas and oil released to the water column during the Deepwater Horizon oil spill. Proceedings of the National Academy of Sciences of the United States of America 109, 20229–20234.

Reinold, M., Wong, H. L., MacLeod, F. I., Meltzer, J., Thompson, A., and Burns, B. P. (2019). The Vulnerability of Microbial Ecosystems in a Changing Climate: Potential Impact in Shark Bay. Life 9, 71.

Reshetnikov, A. S., Khmelenina, V. N., Mustakhimov, I. I., and Trotsenko, Y. A. (2011). Genes and enzymes of ectoine biosynthesis in halotolerant methanotrophs. Methods Enzymol 495, 15–30. doi:10.1016/B978-0-12-386905-0.00002-4.

Ribicic, D., McFarlin, K. M., Netzer, R., Brakstad, O. G., Winkler, A., Throne-Holst, M., et al. (2018). Oil type and temperature dependent biodegradation dynamics - Combining chemical and microbial community data through multivariate analysis. BMC Microbiology 18, 83. doi:10.1186/s12866-018-1221-9.

Riis, V., Kleinsteuber, S., and Babel, W. (2003). Influence of high salinities on the degradation of diesel fuel by bacterial consortia. Canadian Journal of Microbiology/Revue Canadienne de Microbiologie 49, 713–721.

Ron, E. Z. (2013). "Bacterial Stress Response," in The Prokaryotes: Prokaryotic Physiology and Biochemistry, eds. E. Rosenberg, E. F. DeLong, S. Lory, E. Stackebrandt, and F. Thompson (Berlin, Heidelberg: Springer), 589–603. doi:10.1007/978-3-642-30141-4_79.

Rosenberg, E., Barkay, T., Navon-Venezia, S., and Ron, E. Z. (1999). "Role of Acinetobacter Bioemulsans in Petroleum Degradation," in Novel Approaches for Bioremediation of Organic Pollution, eds. R. Fass, Y. Flashner, and S. Reuveny (Boston, MA: Springer US), 171–180. doi:10.1007/978-1-4615-4749-5_17.

Roy, A., Sar, P., Sarkar, J., Dutta, A., Sarkar, P., Gupta, A., et al. (2018). Petroleum hydrocarbon rich oil refinery sludge of North-East India harbours anaerobic, fermentative, sulfate-reducing, syntrophic and methanogenic microbial populations. BMC Microbiology 18. doi:10.1186/s12866-018-1275-8.

Ruvindy, R., White III, R. A., Neilan, B. A., and Burns, B. P. (2016). Unravelling core microbial metabolisms in the hypersaline microbial mats of Shark Bay using high-throughput metagenomics. The ISME Journal 10, 183–196. doi:10.1038/ismej.2015.87.

Rykiel, E. J. (1985). Towards a definition of ecological disturbance. Australian Journal of Ecology 10, 361–365. doi:10.1111/j.1442-9993.1985.tb00897.x.

S

Salah Ud-din, A. I., Md, and Roujeinikova, A. (2017). Methyl-accepting chemotaxis proteins: a core sensing element in prokaryotes and archaea. Cellular and Molecular Life Sciences; Basel 74, 3293–3303. doi:http://dx.doi.org.dbgw.lis.curtin.edu.au/10.1007/s00018-017-2514-0.

Salazar, G., Paoli, L., Alberti, A., Huerta-Cepas, J., Ruscheweyh, H.-J., Cuenca, M., et al. (2019). Gene Expression Changes and Community Turnover Differentially Shape the Global Ocean Metatranscriptome. Cell 179, 1068-1083.e21. doi:10.1016/j.cell.2019.10.014.

Salerno, J. L., Little, B., Lee, J., and Hamdan, L. J. (2018). Exposure to Crude Oil and Chemical Dispersant May Impact Marine Microbial Biofilm Composition and Steel Corrosion. Front. Mar. Sci. 5, 196. doi:10.3389/fmars.2018.00196.

Sánchez, O., Ferrera, I., Vigués, N., Oteyza, T. G. de, Grimalt, J., and Mas, J. (2006). Role of cyanobacteria in oil biodegradation by microbial mats. International Biodeterioration & Biodegradation 58, 186–195. doi:10.1016/j.ibiod.2006.06.004.

Sanders, H. L. (1968). Marine Benthic Diversity: A Comparative Study. The American Naturalist 102, 243–282.

Schauder, R., and Kröger, A. (1993). Bacterial sulphur respiration. Arch. Microbiol. 159, 491–497. doi:10.1007/BF00249025.

Scheler, O., Glynn, B., and Kurg, A. (2014). Nucleic acid detection technologies and marker molecules in bacterial diagnostics. Expert Review of Molecular Diagnostics; London 14, 489–500. doi:http://dx.doi.org.dbgw.lis.curtin.edu.au/10.1586/14737159.2014.908710.

Schinteie, R., and Brocks, J. J. (2017). Paleoecology of Neoproterozoic hypersaline environments: Biomarker evidence for haloarchaea, methanogens, and cyanobacteria. Geobiology 15, 641–663. doi:https://doi.org/10.1111/gbi.12245.

Schloss, P. D. (2019). Reintroducing mothur: 10 Years Later. Applied and Environmental Microbiology 86. doi:10.1128/AEM.02343-19.

Selenska, S., and Klingmüller, W. (1991). DNA recovery and direct detection of Tn5 sequences from soil. Letters in Applied Microbiology 13, 21–24. doi:10.1111/j.1472-765X.1991.tb00559.x.

Selley, R. (2003). Petroleum Geology. Encyclopedia of Physical Science and Technology, 729–740. doi:10.1016/B0-12-227410-5/00555-X.

Shackelford, N., Standish, R. J., Lindo, Z., and Starzomski, B. M. (2018). The role of landscape connectivity in resistance, resilience, and recovery of multi-trophic microarthropod communities. Ecology 99, 1164–1172. doi:10.1002/ecy.2196.

Shade, A., Peter, H., Allison, S. D., Baho, D., Berga, M., Buergmann, H., et al. (2012a). Fundamentals of Microbial Community Resistance and Resilience. Front. Microbiol. 3. doi:10.3389/fmicb.2012.00417.

Shade, A., Read, J. S., Youngblut, N. D., Fierer, N., Knight, R., Kratz, T. K., et al. (2012b). Lake microbial communities are resilient after a whole-ecosystem disturbance. ISME J 6, 2153–2167. doi:10.1038/ismej.2012.56.

Shakya, M., Lo, C.-C., and Chain, P. S. G. (2019). Advances and Challenges in Metatranscriptomic Analysis. Front. Genet. 10. doi:10.3389/fgene.2019.00904.

Shanafelt, D. W., Dieckmann, U., Jonas, M., Franklin, O., Loreau, M., and Perrings, C. (2015). Biodiversity, productivity, and the spatial insurance hypothesis revisited. Journal of Theoretical Biology 380, 426–435. doi:10.1016/j.jtbi.2015.06.017.

Shannon, C. E. (1948). A Mathematical Theory of Communication. The Belll System Technical Journal 27, 55.

Shmareva, M. N., Doronina, N. V., Tarlachkov, S. V., Vasilenko, O. V., and Trotsenko, Y. A. (2018). Methylophaga muralis Bur 1, a haloalkaliphilic methylotroph isolated from the Khilganta soda lake (Southern Transbaikalia, Buryat Republic). Microbiology 87, 33–46. doi:10.1134/S0026261718010162.

Shuona, C., Hua, Y., Jingjing, C., Hui, P., and Zhi, D. (2017). Physiology and bioprocess of single cell of Stenotrophomonas maltophilia in bioremediation of co-existed benzo[a]pyrene and copper. Journal of Hazardous Materials 321, 9–17. doi:10.1016/j.jhazmat.2016.09.002.

Sierra-Garcia, I. N., and Oliveira, V. M. de (2013). Microbial Hydrocarbon Degradation: Efforts to Understand Biodegradation in Petroleum Reservoirs. IntechOpen doi:10.5772/55920.

Siglioccolo, A., Paiardini, A., Piscitelli, M., and Pascarella, S. (2011). Structural adaptation of extreme halophilic proteins through decrease of conserved hydrophobic contact surface. BMC Structural Biology 11, 50. doi:10.1186/1472-6807-11-50.

Smith, C. J., and Osborn, A. M. (2009). Advantages and limitations of quantitative PCR (Q-PCR)-based approaches in microbial ecology. FEMS Microbiol Ecol 67, 6–20. doi:10.1111/j.1574-6941.2008.00629.x.

Sorokin, D. Y., Abbas, B., van Zessen, E., and Muyzer, G. (2014). Isolation and characterization of an obligately chemolithoautotrophic Halothiobacillus strain capable of growth on thiocyanate as an energy source. FEMS Microbiol Lett 354, 69–74. doi:10.1111/1574-6968.12432.

Späth, R., Flemming, H.-C., and Wuertz, S. (1998). Sorption properties of biofilms. , ed. T. C. P. Committee Available at: http://search.proquest.com/docview/16543526?rfr_id=info%3Axri%2Fsid%3Aprimo [Accessed May 16, 2020].

Spring, S., Sorokin, D. Y., Verbarg, S., Rohde, M., Woyke, T., and Kyrpides, N. C. (2019). Sulfate-Reducing Bacteria That Produce Exopolymers Thrive in the Calcifying Zone of a Hypersaline Cyanobacterial Mat. Front. Microbiol. 10. doi:10.3389/fmicb.2019.00862.

Standish, R. J., Hobbs, R. J., Mayfield, M. M., Bestelmeyer, B. T., Suding, K. N., Battaglia, L. L., et al. (2014). Resilience in ecology: Abstraction, distraction, or where the action is? Biological Conservation 177, 43–51. doi:10.1016/j.biocon.2014.06.008.

Stokes, D. (2008). Principles and Practice of Variable Pressure / Environmental Scanning Electron Microscopy (VP-ESEM): Environmental Scanning Electron Microscopy (VP-ESEM). New York, United Kingdom: John Wiley & Sons, Incorporated Available at: http://ebookcentral.proquest.com/lib/curtin/detail.action?docID=406511 [Accessed June 27, 2020].

Stolp, H., and Starr, M. P. (1981). "Principles of Isolation, Cultivation, and Conservation of Bacteria," in The Prokaryotes, eds. M. P. Starr, H. Stolp, H. G. Trüper, A. Balows, and H. G. Schlegel (Berlin, Heidelberg: Springer Berlin Heidelberg), 135–175. doi:10.1007/978-3-662-13187-9_5.

Stuart, R. K., Mayali, X., Lee, J. Z., Craig Everroad, R., Hwang, M., Bebout, B. M., et al. (2016). Cyanobacterial reuse of extracellular organic carbon in microbial mats. The ISME Journal 10, 1240–1251. doi:10.1038/ismej.2015.180.

Su, H., Mi, S., Peng, X., and Han, Y. (2019). The mutual influence between corrosion and the surrounding soil microbial communities of buried petroleum pipelines. RSC Adv. 9, 18930–18940. doi:10.1039/C9RA03386F.

Suding, K. N., Gross, K. L., and Houseman, G. R. (2004). Alternative states and positive feedbacks in restoration ecology. Trends in Ecology & Evolution 19, 46–53. doi:10.1016/j.tree.2003.10.005.

Suga, M., Asahina, S., Sakuda, Y., Kazumori, H., Nishiyama, H., Nokuo, T., et al. (2014). Recent progress in scanning electron microscopy for the characterization of fine structural details of nano materials. Progress in Solid State Chemistry 42, 1–21. doi:10.1016/j.progsolidstchem.2014.02.001.

Suosaari, E. P., Reid, R. P., Araujo, T. a. A., Playford, P. E., Holley, D. K., Mcnamara, K. J., et al. (2016). Environmental pressures influencing living Stromatolites in Hamelin Pool, Shark Bay, Western Australia. PALAIOS 31, 483–496. doi:10.2110/palo.2016.023.

Suzuki, T., Nakamura, T., and Fuse, H. (2012). Isolation of Two Novel Marine Ethylene-Assimilating Bacteria, Haliea Species ETY-M and ETY-NAG, Containing Particulate Methane Monooxygenase-like Genes. Microbes Environ 27, 54–60. doi:10.1264/jsme2.ME11256.

T

Thijs, S., Op De Beeck, M., Beckers, B., Truyens, S., Stevens, V., Van Hamme, J. D., et al. (2017). Comparative Evaluation of Four Bacteria-Specific Primer Pairs for 16S rRNA Gene Surveys. Front. Microbiol. 8. doi:10.3389/fmicb.2017.00494.

Tiirola, M., Wang, H., Paulin, L., and Kulomaa, M. (2002). Evidence for natural horizontal transfer of the pcpB gene in the evolution of polychlorophenol-degrading sphingomonads. Appl Environ Microbiol 68, 4495–4501. doi:10.1128/aem.68.9.4495-4501.2002.

Tischendorf, L., and Fahrig, L. (2000). On the usage and measurement of landscape connectivity. Oikos 90, 7–19. doi:10.1034/j.1600-0706.2000.900102.x.

Tissot, B. P., and Welte, D. H. (2013). Petroleum Formation and Occurrence. Springer Science & Business Media Available at: https://books.google.com.au/books?hl=en&lr=&id=avLxCAAAQBAJ&oi=fnd&pg=PA3&ots=1J43iXn42F&sig=K8vOdRQoadS_667mES9rV4vU7OE&redir_esc=y#v=onepage&q&f=false [Accessed July 24, 2020].

Tringe, S. G., and Hugenholtz, P. (2008). A renaissance for the pioneering 16S rRNA gene. Current Opinion in Microbiology 11, 442–446. doi:10.1016/j.mib.2008.09.011.

Trolio, R., Grice, K., Fisher, S. J., Alexander, R., and Kagi, R. I. (1999). Alkylbiphenyls and alkyldiphenylmethanes as indicators of petroleum biodegradation. Organic Geochemistry 30, 1241–1253. doi:10.1016/S0146-6380(99)00099-6.

V

van Bambeke, F., Mingeot-Leclercq, M.-P., Glupczynski, Y., and Tulkens, P. M. (2017). “137 - Mechanisms of Action,” in Infectious Diseases (Fourth Edition), eds. J. Cohen, W. G. Powderly, and S. M. Opal (Elsevier), 1162-1180.e1. doi:10.1016/B978-0-7020-6285-8.00137-4.

van Gemerden, H. (1993). Microbial mats: A joint venture. Marine Geology 113, 3–25. doi:10.1016/0025-3227(93)90146-M.

Vasconcellos, S. P., Sierra-Garcia, I. N., Dellagnezze, B. M., Vicentini, R., Midgley, D., Silva, C. C., et al. (2017). Functional and genetic characterization of hydrocarbon biodegrader and exopolymer-producing clones from a petroleum reservoir metagenomic library. Environmental Technology 38, 1139–1150. doi:10.1080/09593330.2016.1218940.

Vernon-Parry, K. D. (2000). Scanning electron microscopy: an introduction. III-Vs Review 13, 40–44. doi:10.1016/S0961-1290(00)80006-X.

Visscher, P. T., and Stolz, J. F. (2005). Microbial mats as bioreactors: populations, processes, and products. Palaeogeography, Palaeoclimatology, Palaeoecology 219, 87–100. doi:10.1016/j.palaeo.2004.10.016.

Volkman, J. K., Alexander, R., Kagi, R. I., Noble, R. A., and Woodhouse, C. W. (1983a). A geochemical reconstruction of oil generation in the Barrow Sub-basin of Western Australia. Geochimica et Cosmochimica Acta 47, 2091–2105. doi:10.1016/0016-7037(83)90034-0.

Volkman, J. K., Alexander, R., Kagi, R. I., Rowland, S. J., and Sheppard, P. N. (1984). Biodegradation of aromatic hydrocarbons in crude oils from the Barrow Sub-basin of Western Australia. Organic Geochemistry 6, 619–632. doi:10.1016/0146-6380(84)90084-6.

Volkman, J. K., Alexander, R., Kagi, R. I., and Woodhouse, G. W. (1983b). Demethylated hopanes in crude oils and their applications in petroleum geochemistry. Geochimica et Cosmochimica Acta 47, 785–794. doi:10.1016/0016-7037(83)90112-6.

W

Walter, M., Bauld, J., and Brock, T. (1976). Microbiology and Morphogenesis of Columnar Stromatolites (Conophyton, Vacerrilla) from Hot Springs in Yellowstone National Park. Developments in sedimentology 20, 273–310.

Webber, M. A., and Piddock, L. J. V. (2003). The importance of efflux pumps in bacterial antibiotic resistance. J Antimicrob Chemother 51, 9–11. doi:10.1093/jac/dkg050.

Weiss, S., Xu, Z. Z., Peddada, S., Amir, A., Bittinger, K., Gonzalez, A., et al. (2017). Normalization and microbial differential abundance strategies depend upon data characteristics. Microbiome 5, 27. doi:10.1186/s40168-017-0237-y.

Wenger, L. M., Davis, C. L., and Isaksen, G. H. (2002). Multiple Controls on Petroleum Biodegradation and Impact on Oil Quality. SPE Reservoir Evaluation & Engineering 5, 375–383. doi:10.2118/80168-PA.

Westman, W. E. (1978). Measuring the Inertia and Resilience of Ecosystems. BioScience 28, 705–710. doi:10.2307/1307321.

White, H. K., Conmy, R. N., MacDonald, I. R., and Reddy, C. M. (2016). Methods of Oil Detection in Response to the Deepwater Horizon Oil Spill. Oceanography 29, 76–87.

Wickham, H. (2016). ggplot2: elegant graphics for data analysis. Springer.

Widdel, F., and Musat, F. (2010). Diversity and common principles in enzymatic activation of hydrocarbons. Handbook of Hydrocarbon and Lipid Microbiology, 981–1009.

Wilkinson, T. J., Huws, S. A., Edwards, J. E., Kingston-Smith, A. H., Siu-Ting, K., Hughes, M., et al. (2018). CowPI: A Rumen Microbiome Focussed Version of the PICRUSt Functional Inference Software. Front. Microbiol. 9. doi:10.3389/fmicb.2018.01095.

Willerslev, E., Hansen, A. J., Binladen, J., Brand, T. B., Gilbert, M. T. P., Shapiro, B., et al. (2003). Diverse Plant and Animal Genetic Records from Holocene and Pleistocene Sediments. Science 300, 791–795. doi:10.1126/science.1084114.

Willis, A. D. (2019). Rarefaction, Alpha Diversity, and Statistics. Front. Microbiol. 10. doi:10.3389/fmicb.2019.02407.

Wilson, M. V., and Shmida, A. (1984). Measuring Beta Diversity with Presence-Absence Data. The Journal of Ecology 72, 1055. doi:10.2307/2259551.

Wingert, W. S. (1992). G.c.-m.s. analysis of diamondoid hydrocarbons in Smackover petroleums. Fuel 71, 37–43. doi:10.1016/0016-2361(92)90190-Y.

Woese, C. R. (1987). Bacterial evolution. Microbiol Rev 51, 221–271.

Woese, C. R., and Fox, G. E. (1977). Phylogenetic structure of the prokaryotic domain: The primary kingdoms. PNAS 74, 5088–5090. doi:10.1073/pnas.74.11.5088.

Woese, C. R., Kandler, O., and Wheelis, M. L. (1990). Towards a natural system of organisms: proposal for the domains Archaea, Bacteria, and Eucarya. Proc Natl Acad Sci U S A 87, 4576–4579.

Wong, H., Ahmed-Cox, A., and Burns, B. (2016). Molecular Ecology of Hypersaline Microbial Mats: Current Insights and New Directions. Microorganisms 4, 6. doi:10.3390/microorganisms4010006.

Wong, H. L., MacLeod, F. I., White, R. A., Visscher, P. T., and Burns, B. P. (2020). Microbial dark matter filling the niche in hypersaline microbial mats. Microbiome 8, 135. doi:10.1186/s40168-020-00910-0.

Wong, H. L., Smith, D., Visscher, P. T., and Burns, B. P. (2015). Niche differentiation of bacterial communities at a millimeter scale in Shark Bay microbial mats. Scientific Reports (Nature Publisher Group); London 5, 15607. doi:http://dx.doi.org.dbgw.lis.curtin.edu.au/10.1038/srep15607.

Wong, H. L., White, R. A., Visscher, P. T., Charlesworth, J. C., Vázquez-Campos, X., and Burns, B. P. (2018). Disentangling the drivers of functional complexity at the metagenomic level in Shark Bay microbial mat microbiomes. The ISME Journal 12, 2619–2639. doi:10.1038/s41396-018-0208-8.

Wright, R. J., Bosch, R., Gibson, M. I., and Christie-Oleza, J. A. (2020). Plasticizer Degradation by Marine Bacterial Isolates: A Proteogenomic and Metabolomic Characterization. Environ. Sci. Technol. 54, 2244–2256. doi:10.1021/acs.est.9b05228.

X

Xu, X., Liu, W., Tian, S., Wang, W., Qi, Q., Jiang, P., et al. (2018). Petroleum Hydrocarbon-Degrading Bacteria for the Remediation of Oil Pollution Under Aerobic Conditions: A Perspective Analysis. Front. Microbiol. 9. doi:10.3389/fmicb.2018.02885.

Y

Yachi, S., and Loreau, M. (1999). Biodiversity and ecosystem productivity in a fluctuating environment: The insurance hypothesis. PNAS 96, 1463–1468. doi:10.1073/pnas.96.4.1463.

Yamamoto, H., Murata, M., and Sekiguchi, J. (2000). The CitST two-component system regulates the expression of the Mg-citrate transporter in Bacillus subtilis. Molecular Microbiology 37, 898–912. doi:10.1046/j.1365-2958.2000.02055.x.

Yang, L., Lai, C.-T., and Shieh, W. K. (2000). Biodegradation of dispersed diesel fuel under high salinity conditions. Water Research 34, 3303–3314. doi:10.1016/S0043-1354(00)00072-5.

Yarza, P., Yilmaz, P., Pruesse, E., Glöckner, F. O., Ludwig, W., Schleifer, K., et al. (2014). Uniting the classification of cultured and uncultured bacteria and archaea using 16S rRNA gene sequences. Nature Reviews. Microbiology; London 12, 635–45. doi:http://dx.doi.org.dbgw.lis.curtin.edu.au/10.1038/nrmicro3330.

Yastrebova, O. V., Pyankova, A. A., and Plotnikova, E. G. (2019). Phthalate-Degrading Bacteria Isolated from an Industrial Mining Area and the Processing of Potassium and Magnesium Salts. Appl Biochem Microbiol 55, 397–404. doi:10.1134/S000368381904015X.

Yeager, C. M., Gallegos-Graves, L. V., Dunbar, J., Hesse, C. N., Daligault, H., and Kuske, C. R. (2017). Polysaccharide Degradation Capability of Actinomycetales Soil Isolates from a Semiarid Grassland of the Colorado Plateau. Appl Environ Microbiol 83. doi:10.1128/AEM.03020-16.

Z

Zaikova, E., Goerlitz, D. S., Tighe, S. W., Wagner, N. Y., Bai, Y., Hall, B. L., et al. (2019). Antarctic Relic Microbial Mat Community Revealed by Metagenomics and Metatranscriptomics. Front. Ecol. Evol. 7. doi:10.3389/fevo.2019.00001.

Zhao, B., Wang, H., Li, R., and Mao, X. (2010). Thalassospira xianhensis sp. nov., a polycyclic aromatic hydrocarbon-degrading marine bacterium. Int. J. Syst. Evol. Microbiol. 60, 1125–1129. doi:10.1099/ijs.0.013201-0.

Zhao, G., Ceci, P., Ilari, A., Giangiacomo, L., Laue, T. M., Chiancone, E., et al. (2002). Iron and Hydrogen Peroxide Detoxification Properties of DNA-binding Protein from Starved Cells: A Ferretin-like DNA-Binding Protein of Escherichia Coli. Journal of Biological Chemistry 277, 27689–27696. doi:10.1074/jbc.M202094200.

Zhou, G., Shi, Q.-S., Huang, X.-M., and Xie, X.-B. (2015). The Three Bacterial Lines of Defense against Antimicrobial Agents. Int J Mol Sci 16, 21711–21733. doi:10.3390/ijms160921711.

Zhou, H., Wang, H., Huang, Y., and Fang, T. (2016). Characterization of pyrene degradation by halophilic Thalassospira sp. strain TSL5-1 isolated from the coastal soil of Yellow Sea, China. International Biodeterioration & Biodegradation 107, 62–69. doi:10.1016/j.ibiod.2015.10.022.

Zhou, L.-Y., Wang, N.-N., Mu, D.-S., Liu, Y., and Du, Z.-J. (2019). Coraliomargarita sinensis sp. nov., isolated from a marine solar saltern. International Journal of Systematic and Evolutionary Microbiology, 69, 701–707. doi:10.1099/ijsem.0.003205.

Zou, Y., Xue, W., Luo, G., Deng, Z., Qin, P., Guo, R., et al. (2019). 1,520 reference genomes from cultivated human gut bacteria enable functional microbiome analyses. Nature Biotechnology 37, 179–185. doi:10.1038/s41587-018-0008-8.

Appendix

Following pages contain documents stating:

- Manuscript submission to Frontier Microbiology (Chapter 2)
- Written permission to use photos taken by Prof. Alex Sessions (Chapter 2)

Your manuscript submission - 571995
1 mensaje

Frontiers Microbiology Editorial Office <microbiology.editorial.office@frontiersin.org> 12 de junio de 2020, 20:24
Responder a: Frontiers Microbiology Editorial Office <microbiology.editorial.office@frontiersin.org>
Para: Yalimay Jimenez <yalimayjimenez@gmail.com>

Dear Ms Jimenez

We are pleased to inform you that we have received the manuscript "Responses of hypersaline microbial mats from Shark Bay (Western Australia) to long-term petroleum exposure" to be considered for publication in Frontiers in Microbiology, section Microbiological Chemistry and Geomicrobiology.

You can access the review forum and track the progress of your manuscript using the following link:
https://www.frontiersin.org//Journal/MySubmission.aspx?stage=100

Your manuscript is now in the initial validation stage to determine its suitability for peer review. Should your manuscript be sent out for peer review, you will receive a notification once we receive the reports from reviewers and the interactive review forum is activated. You will then be able to read the review reports and exchange directly with the reviewers in the interactive review forum as well as submit a revised manuscript, if appropriate.

Best regards,

Your Frontiers in Microbiology team

Frontiers | Editorial Office - Collaborative Peer Review Team
www.frontiersin.org
Avenue du Tribunal Fédéral 34, 1005 Lausanne, Switzerland
Office T 41 21 510 17 25

For technical issues, please contact our IT Helpdesk (support@frontiersin.org) or visit our Frontiers Help Center (zendesk.frontiersin.org/hc/en-us)

----------MANUSCRIPT DETAILS----------
Manuscript title: Responses of hypersaline microbial mats from Shark Bay (Western Australia) to long-term petroleum exposure
Manuscript ID: 571995
Authors: Yalimay Jimenez, Kliti Grice, Cornelia Wuchter and Marco J L Coolen
Journal: Frontiers in Microbiology, section Microbiological Chemistry and Geomicrobiology
Article type: Original Research
Submitted on: 12 Jun 2020

----------ADDITIONAL INFORMATION----------
In order to enable a smooth and efficient review process, please familiarize yourself with the Frontiers review guidelines:
https://www.frontiersin.org/Journal/ReviewGuidelines.aspx?s=678&name=microbiological_chemistry_and_geomicrobiology

To take part in the Resource Identification Initiative please cite antibodies, genetically modified organisms, software tools, data, databases and services using the corresponding catalog number and RRID in the text of your article. Please see here for more information: https://www.frontiersin.org//files/pdf/letter_to_author.pdf

Re: Permission request - Shark Bay microbial mat photos

Alex Sessions <asessions1@gmail.com>
Fri 4/24/2020 5:16 AM
To: Yalimay Jimenez de Duarte <yalimay.jimenezd@postgrad.curtin.edu.au>

Hi Yali,

You are welcome to use the photographs, glad they are useful to you.

cheers,
Alex